AREVA

380-B

TRANSPORT PACKAGE

Safety Analysis Report

Revision 2

AREVA Federal Services LLC

August 2017

TABLE OF CONTENTS

This page left intentionally blank.

1.0 GENERAL INFORMATION

This section presents a general introduction and description of the 380-B package. The 380-B package is used to transport radioactive sealed sources for recovery and management operations. This application seeks authorization of the 380-B package as a Type B(U)–96 shipping container in accordance with the provisions of Title 10, Part 71 of the Code of Federal Regulations [1]. The packaging also meets the requirements of TS-R-1 [2].

The major components comprising the package are discussed in Section 1.2.1, *Packaging*, and illustrated in Figure 1.2-1 through Figure 1.2-5. A glossary of terms is presented in Appendix 1.3.2, *Glossary of Terms and Acronyms*. Detailed drawings of the package design are presented in Appendix 1.3.3, *Packaging General Arrangement Drawings*.

1.1 Introduction

The **Model No. 380-B** package has been developed to transport radioactive sources contained in irradiation devices (shielded devices). Contents may also include shielded source containers. The package may transport shielded devices with isotopes that may be alpha, beta, gamma, and/or neutron emitters. The primary biological shielding is provided by lead shielding in the package. No credit is taken for shielding in the devices. All sources are sealed and encapsulated. The 380-B package provides leaktight containment of the radioactive contents under all NCT and HAC.[1]

The packaging consists of a lead-shielded cask body, lead-shielded closure lid, and upper and lower impact limiters. Shielded devices are placed in the cask body for shipment. The package uses conventional materials and metalworking techniques. When loaded and prepared for transport, the 380-B package is 118.2 inches tall, 100 inches in diameter (over the upper and lower impact limiters), and weighs a maximum of 67,000 lb. The package is designed to be transported singly, with its longitudinal axis vertical, by ground, air, or by water in exclusive use. If shipped by air under TS-R-1 the maximum allowed activity shall be 3,000 A_2.

Since all payloads transported in the 380-B are non-fissile, the criticality safety index does not apply.

An isometric view of the 380-B packaging is shown in Figure 1.1-1. A Cross-section view of the packaging with a generic shielded device and typical blocking/dunnage is shown in Figure 1.1-2.

---

[1] Leaktight is defined as a maximum of 1×10^{-7} reference–cm^3/sec, air leakage per ANSI N14.5–2014 [3].
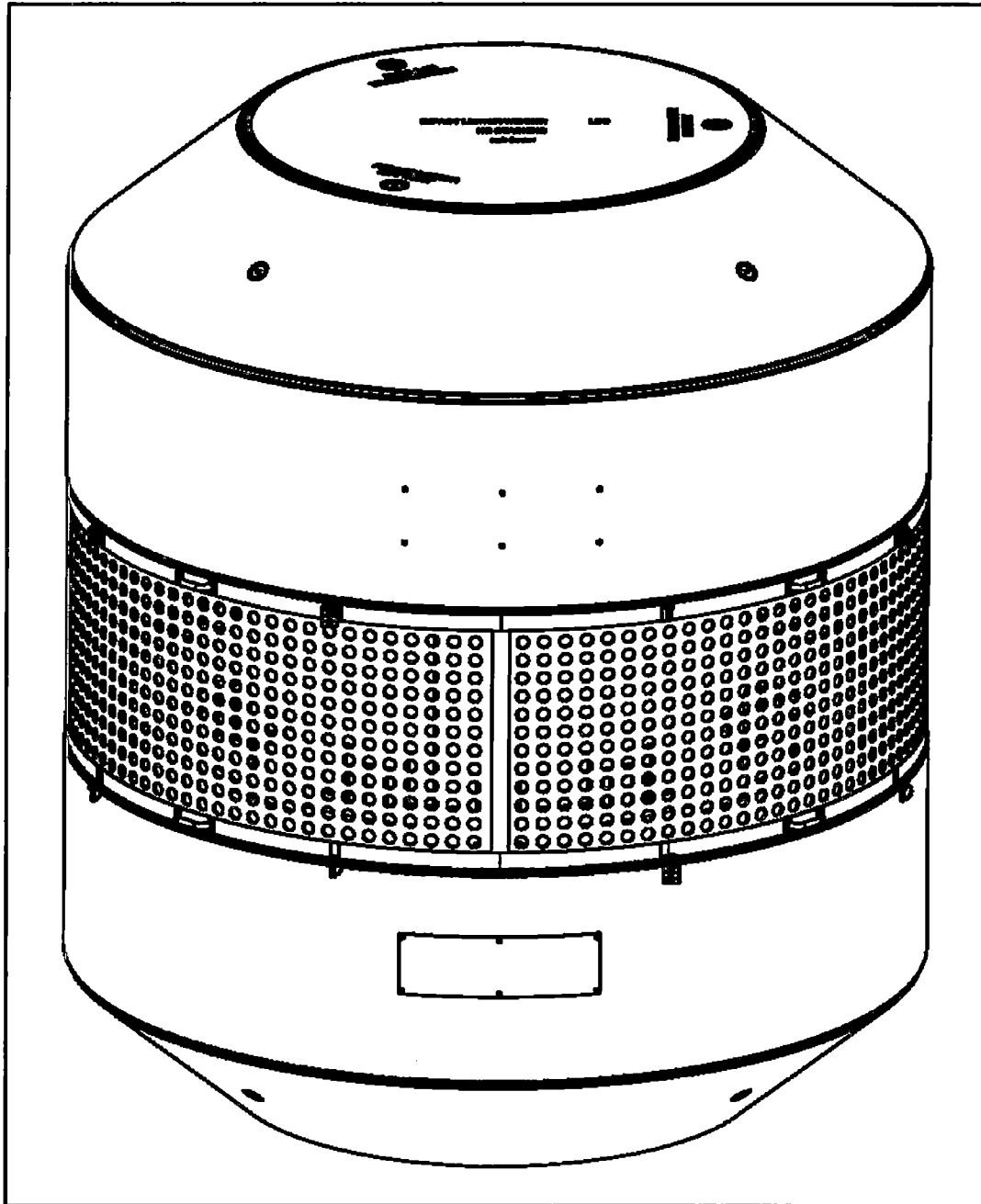
Figure 1.1-1 – 380-B Packaging
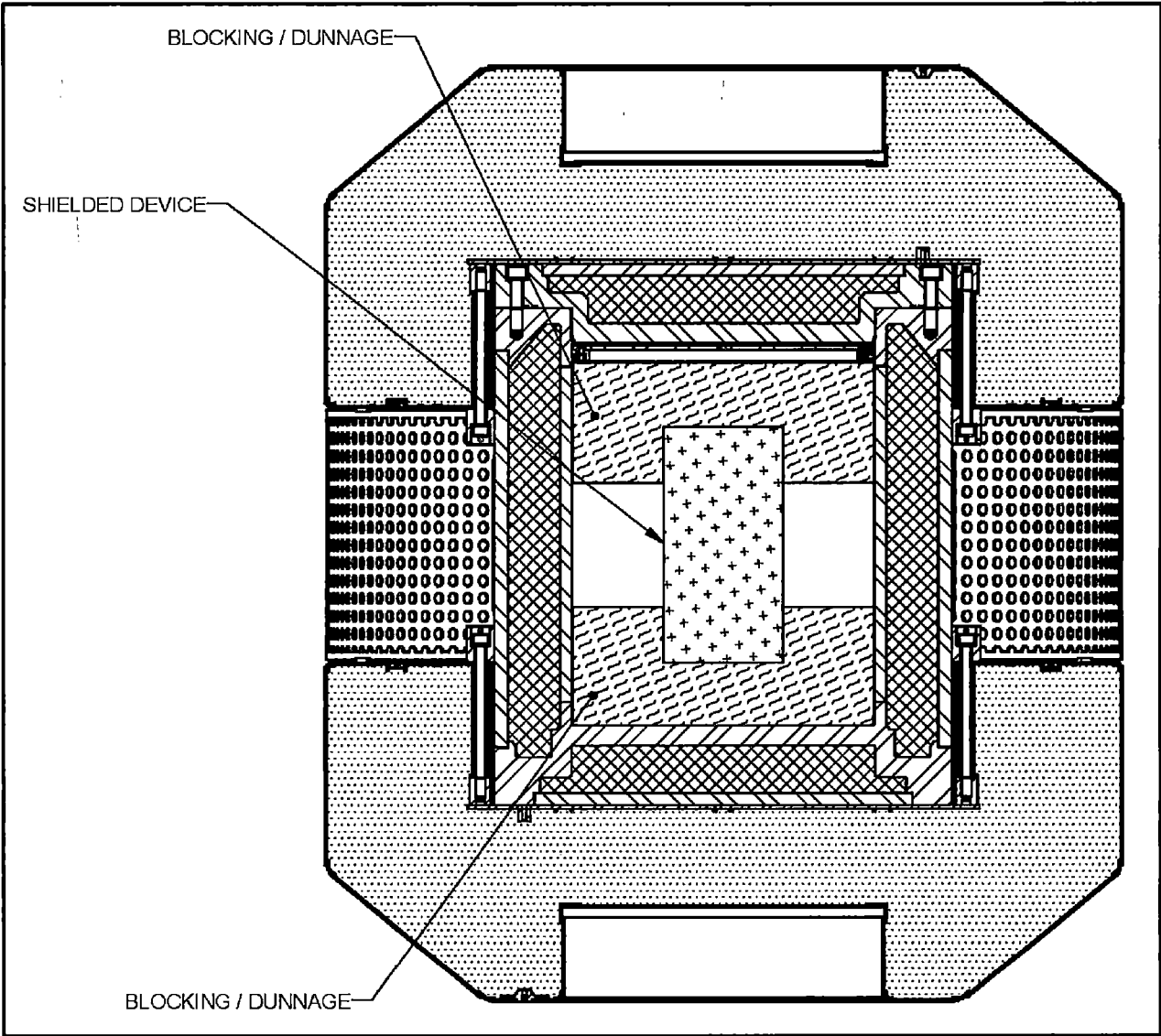
Figure 1.1-2 – 380-B Packaging Cross-section with Shielded Device

1.2 Package Description

This section presents a basic description of the 380-B package components and construction. In the following, drawing references are to the general arrangement drawings provided in Appendix 1.3.3, *Packaging General Arrangement Drawings*.

1.2.1 Packaging

The 380-B package (drawings 1916-02-01-SAR, 1916-02-02-SAR, and 1916-02-03-SAR) consists of a lead-shielded cask body, a lead-shielded closure lid, 36 closure bolts, and upper and lower impact limiters containing polyurethane foam. The package is primarily of welded construction, using Type 304 austenitic stainless steel. These components will now be discussed in detail.

1.2.1.1 Cask Assembly

The 380-B cask assembly consists of a large shielded cask body and bolted closure lid, and is depicted as Assembly A1 on drawing 1916-02-02-SAR. The cask assembly is a right circular cylinder 68-1/8 inches long and 57-1/2 inches in diameter (not including the impact limiter attachment brackets and the thermal shield). The cask body is composed of upper and lower end structures connected by inner and outer shells. Thick lead biological shielding is located between the two shells, and in the lower end structure. The closure lid also has thick lead shielding between the main structure and outer plate. All the structural components of the cask body and lid are constructed of austenitic stainless steel.

The cask body, depicted as Assembly A4 on drawing 1916-02-02-SAR, is comprised of a lower end structure (made from forging or plate) with an integral 2-1/2-inch thick inner plate filled with 6 inches of lead that is covered by a 1-1/2-inch thick bottom outer plate. Concentric inner and outer shells, 1-1/2-inch and 1-3/4-inch thick respectively, form the annulus for a 6-1/2-inch thick lead body shield. The top of the cask body is comprised of an upper end structure (made from forging or plate) that includes an O-ring sealing surface and 36 tapped holes for the lid closure bolts.

The cask lid consists of a main structure (made from forging or plate) with an integral 2-1/2-inch thick inner plate filled with 6 inches of lead that is covered by a 1-1/2-inch thick outer plate, and is depicted as Assembly A3 on drawing 1916-02-02-SAR. The lid has 36 through holes with counter bores to recess and protect the socket head closure bolts. The mating surface of the lid features a step relief located at the bolt circle. This relief prevents any contact from occurring between the lid and the body outside of the bolt circle, thus preventing prying loads from being applied to the closure bolts.

The payload cavity of the cask assembly is 48-1/8 inches long by 38 inches in diameter. The effective cavity size is reduced by the inner cover and mounting brackets. There are mounting brackets welded to the inner wall of the payload cavity. The span between opposite brackets is 37 inches, thereby reducing the opening of the payload cavity by one inch. The payload cavity height to the bottom of the inner cover mounting hardware is 45-3/4 inches.

The cask body end structures and cask lid main structure may be forged from ASTM A182, Type F304 or machined from ASTM A240, Type 304. The inner and outer shells, bottom outer plate, and lid outer plate are made from ASTM A240, Type 304. The inner and outer shells may have

up to two, full penetration longitudinal seam welds. The inner and outer shells are both welded to the upper and lower end structures with complete joint penetration welds prior to lead pour. The bottom outer plate and lid outer plate are also welded to the lower end structure and lid main structure, respectively, with complete joint penetration welds. All butt welds in the containment boundary are full-penetration and either radiograph or ultrasonic inspected.

All lead shielding is made from ASTM B29 lead (in any grade) or optionally, from lead per Federal Specification QQ-L-171E, Grade A or C. The lead shield on the side of the cask body is cast–in–place through the upper end structure. The lead shields in the lower end structure and in the lid are made from lead sheet material that is packed firmly into place prior to completing the outer plate welds.

The socket head closure bolts are made from ASTM A564, Type 630, Condition H1100 precipitation hardened stainless steel with 1-1/2 – 6UNC threads and a 1-5/16-inch diameter shank. The bolts are plated with electroless nickel per SAE-AMS 2404, Revision F, Class 1, or MIL-DTL-26074 Rev. F Class 1 Grade B, and tightened to a torque of 850-950 ft-lb.

The cask body is fitted with a 0.105-inch (12 gauge) Type 304 stainless steel thermal shield between the upper and lower impact limiters. The thermal shield is spaced off the outer cask shell by 0.105-inch (12 gauge) stainless steel strips and three 0.102-0.105-inch (10 AWG) diameter stainless steel wire rings wrapped around the outer shell with 4 inch spacing, as depicted on sheet 4 of drawing 1916-02-02-SAR. The offset thermal shield provides an approximate 1/10 inch air gap between the cask outer shell and environmental conditions.

The upper and lower impact limiters are each attached to the cask body with 12 socket head bolts. The cask body has 24 impact limiter attachment brackets welded to the outer shell, 12 each for the upper and lower impact limiters, which are Type 304 stainless steel. The impact limiter attachment brackets have counter bores to recess and protect the impact limiter attachment bolt heads (see Detail G and Section H-H on sheet 5 of drawing 1916-02-02-SAR). Each impact limiter attachment bracket also has a cross-drilled through hole to facilitate use of a tamper indicating wire and/or security sensor cable. The through hole is positioned such that tamper indicating wire and/or security sensor cable blocks access to the impact limiter attachment bolt.

The closure seal is a 3/8-inch cross-sectional diameter O-ring made of butyl rubber. A vent port, sealed with a butyl sealing washer and threaded brass plug, is located in the top of the cask lid (see Section C-C on sheet 6 of drawing 1916-02-02-SAR). The vent port drill access hole on the lid top surface (containment) is closed using a plug weld that is liquid penetrant inspected on the final pass. A threaded brass cover is used to protect the port plug. The seal test port (not part of containment) is identically configured (see Section D-D on sheet 6 of drawing 1916-02-02-SAR). The butyl material of the containment seal and test seal O-rings, and the vent port and seal test port sealing washers, is made from Rainier Rubber R0405-70, and subject to the tests given in Section 8.1.5.2, *Butyl Rubber O-rings.*.

The 380-B package provides a single level of leaktight containment. The containment boundary of the 380-B package consists of the following elements. Unless noted, all elements are made of ASTM Type 304 stainless steel in various product forms.

- The lower end structure
- The inner shell

- The upper end structure (including lead pour hole plug and welds)

- The containment elastomer O–ring seal (the inner seal in the closure lid)

- The closure lid main structure

- The vent port in the closure lid including elastomer sealing washer and port plug

- The vent port drill access hole plug and weld

The containment boundary is shown in Figure 1.2-1. Detail on the other packaging components is given below, and depicted in Figure 1.2-2 through Figure 1.2-5.

1.2.1.2   Impact Limiters

Impact limiters are attached to each end of the cask assembly, having essentially identical design, and are shown in drawing 1916-02-03-SAR. Each limiter is 100 inches in diameter and 43 inches long overall, with a conical section 16.8 inches long towards the outer end. The impact limiter has a 1/4-inch thick Type 304 stainless steel outer shell and inner cylindrical shell. The inner flat plate of the impact limiter is 1/2-inch thick. The impact limiter contains polyurethane foam that provides energy absorption capability to mitigate impacts from NCT and HAC. The polyurethane foam also provides thermal protection to the cask for the HAC fire, which is important to maintaining the operating temperature limit of the closure lid O-ring seals. The polyurethane foam has a density of 16 pounds per cubic foot (pcf). The polyurethane foam is rigid, closed-cell, and is poured in place.

The top end and inner surface of the impact limiter each feature three, reinforced, 5/8 – 11UNC threads for lifting of the impact limiter only. On the side that mates with the cask, the annular sheet features four plastic melt-out plugs designed to relieve pressure in the HAC fire event. There are four additional plastic melt-out plugs on the tapered outer shell surface.

The impact limiter attachment bolts are made from ASTM A564, Type 630, Condition H1100 precipitation hardened stainless steel with 1-1/4 – 7UNC threads and a 1.1 inch diameter shank. Each impact limiter is attached to the cask assembly with 12 of these bolts. The bolts thread into bosses that are internal to the impact limiter and welded to the 1/2-inch thick inner flat plate. Each threaded boss is accessed via a tube that is welded to the boss and outer sheet that mates with the cask, thereby providing access through the polyurethane foam.

1.2.1.3   Personnel Barrier

A personnel barrier consisting of two equal assemblies of expanded stainless steel sheet and 0.105-inch (12 gauge) stainless steel perimeter strips will be used between the upper and lower impact limiters, and is depicted as Assembly A2 on drawing 1916-02-01-SAR. The personnel barrier will limit access to the cask body such that personnel are prevented from entering the area between the impact limiters. The personnel barrier is necessary to provide acceptable dose rates around the side of the cask body for NCT. The personal barrier will be removable and securable with padlocks and/or pins. The impact limiters feature eight equally spaced mounting brackets for corresponding brackets on each of the personnel barrier assemblies.

1.2.1.4 Inner Cover

The cask assembly includes an inner cover that attaches to the cask body inner shell. The inner cover is comprised of a 1/2-inch thick stainless steel plate with a 2-inch wide by 1-1/2-inch thick reinforcing ring welded to the plate's bottom outer perimeter, and is depicted as Assembly A2 on drawing 1916-02-02-SAR. Optionally, the main two components of the inner cover can made from one piece. The inner cover also serves as an exclusion zone in the NCT shielding evaluation, see Section 5.0, *Shielding Evaluation*, for details.

The inner cover is attached with 1/2-13UNC stainless steel screws that are used in conjunction with rotating retainers that anchor against a shear step welded to the inner shell of the cask assembly. Optionally, there can be any quantity of additional 1/2-13UNC stainless steel screws threaded into the inner cover. One or more threaded holes are provided in the inner cover plate for removal and installation of the inner cover.

1.2.1.5 Gross Weight

The gross weight of the 380-B package, including the cask assembly, impact limiters, payload, and dunnage is 67,000 lb. The empty packaging weight is 55,000 lb. A summary of overall component weights is shown in Table 2.1-2 and discussed in Section 2.1.3, *Weights and Centers of Gravity*.

1.2.1.6 Neutron Moderation and Absorption

Since the 380-B package contains no fissile material, no moderation or absorption of neutrons is necessary to control criticality.

1.2.1.7 Receptacles, Valves, Testing and Sampling Ports

The 380-B package closure lid contains a vent port and a seal test port. There are no valves or receptacles used in the 380-B package.

1.2.1.8 Heat Dissipation

The dissipation of heat from the 380-B package is entirely passive. A thermal shield is used on the cask body to limit the temperature of the lead gamma shield in the HAC fire event. A more detailed description of the package thermal design is given in Chapter 3, *Thermal Evaluation*.

1.2.1.9 Lifting and Tie–down Devices

There are no lifting or tie-down devices that are a structural part of the 380-B package when fully assembled and prepared for transport. There are no provisions to lift the package with the impact limiters installed. The package is secured to the transport vehicle using structures that interface with the surfaces of the upper and lower impact limiters. The package rests directly on a dedicated trailer with designated chocking provisions for the lower impact limiter or on a lower frame that is attached to the vehicle. An upper frame contacts the upper impact limiter and is attached to the vehicle using cables, chains, straps, and/or turnbuckles.

1.2.1.10 Pressure Relief System

There is no pressure relief system in the 380-B package.

1.2.1.11 Shielding

Biological shielding is provided by lead and the thick steel shells of the 380-B package. Hydrogenous neutron shielding is not necessary and none is included in the package design. Details of the shielding are provided in Section 1.2.1.1, *Cask Assembly*. A full assessment of the shielding design is provided in Chapter 5, *Shielding Evaluation*.

1.2.2 Contents

The 380-B package transports shielded devices containing radioactive sources. All sources are sealed and encapsulated. The nuclides that will be transported in the 380-B are listed in Table 1.2-1. The maximum decay heat in the package is 205W. No contents material is fissile.

Shielded devices are units which were designed and manufactured to provide a safe source of radiation for industrial, medical, or research purposes. Shielded devices may also include shielded source containers. Each such device includes a sealed source (or a group of sources), shielding material, and a steel shell to surround the shielding material and provide structure. All shielded devices are placed into the 380-B for shipment and blocked in position using dunnage materials. Blocking/dunnage materials are metallic structures, polyurethane foam, or wood. The blocking/dunnage is used to prevent unwanted motion during normal transport, and does not provide a safety function. All contents materials placed into the cask will be dry, except for the moisture normally present in the wood dunnage which may be used. For this reason, galvanic reactions will not occur. The effect of the wood's moisture content is evaluated in Section 3.3.2, *Maximum Normal Operating Pressure*, and Section 3.4.3.1, *Maximum HAC Pressures*. The effect of radiolysis on the moisture is evaluated in Section 5.5.4, *Gas Generation due to Radiolysis*. A schematic of the contents is provided in Figure 1.2-6.

The details of the device designs may not be known, and the structural performance of the devices in an accident may not be known, therefore no shielding credit is taken for the devices in NCT or HAC.

The maximum total device weight is 10,000 lb and the maximum weight for all dunnage is 2,000 lb. The contents may include more than one device if the combined weight of all devices does not exceed 10,000 lb and the combined activity limits are applied as discussed in Section 7.1.4, *Qualifying the Payload for Transport*. The total contents weight including device(s) and dunnage is 12,000 lb.

1.2.3 Special Requirement for Plutonium

The 380-B package does not contain plutonium.

1.2.4 Operational Features

The 380-B package is of conventional design and is not complex to operate. Operational features are depicted on the drawings provided in Appendix 1.3.3, *Packaging General Arrangement Drawings*. Operating procedures and instructions for loading, unloading, and preparing an empty package for transport are provided in Chapter 7, *Package Operations*.

Table 1.2-1 – Payload Source Nuclides

Nuclide	Maximum Activity
Co-60	7,702 Ci
Cs-137	40,675 Ci
Sr-90	30,606 Ci
Ir-192	33,333 Ci
Ra-226 (no Be)[5]	1,101 Ci
Ra-226Be[5]	4.67 Ci

Notes:

1. Physical form of all nuclides is solid material in a sealed capsule.
2. The maximum decay heat limit for the 380-B package is 205W. The total activity to reach 205W is discussed in Section 5.2.1, *Gamma Source*.
3. The maximum activity listed is the maximum for a single nuclide in the 380-B. For combinations of different nuclides, lower activity limits apply as discussed in Chapter 5, *Shielding Evaluation*.
4. The maximum activity is 16,431 A_2 per Section 5.5.3, *A_2 Calculation*.
5. Non-radioactive impurities may include oxygen, carbon, sulfur, bromine (hydrous), and chlorine (hydrous and anhydrous).
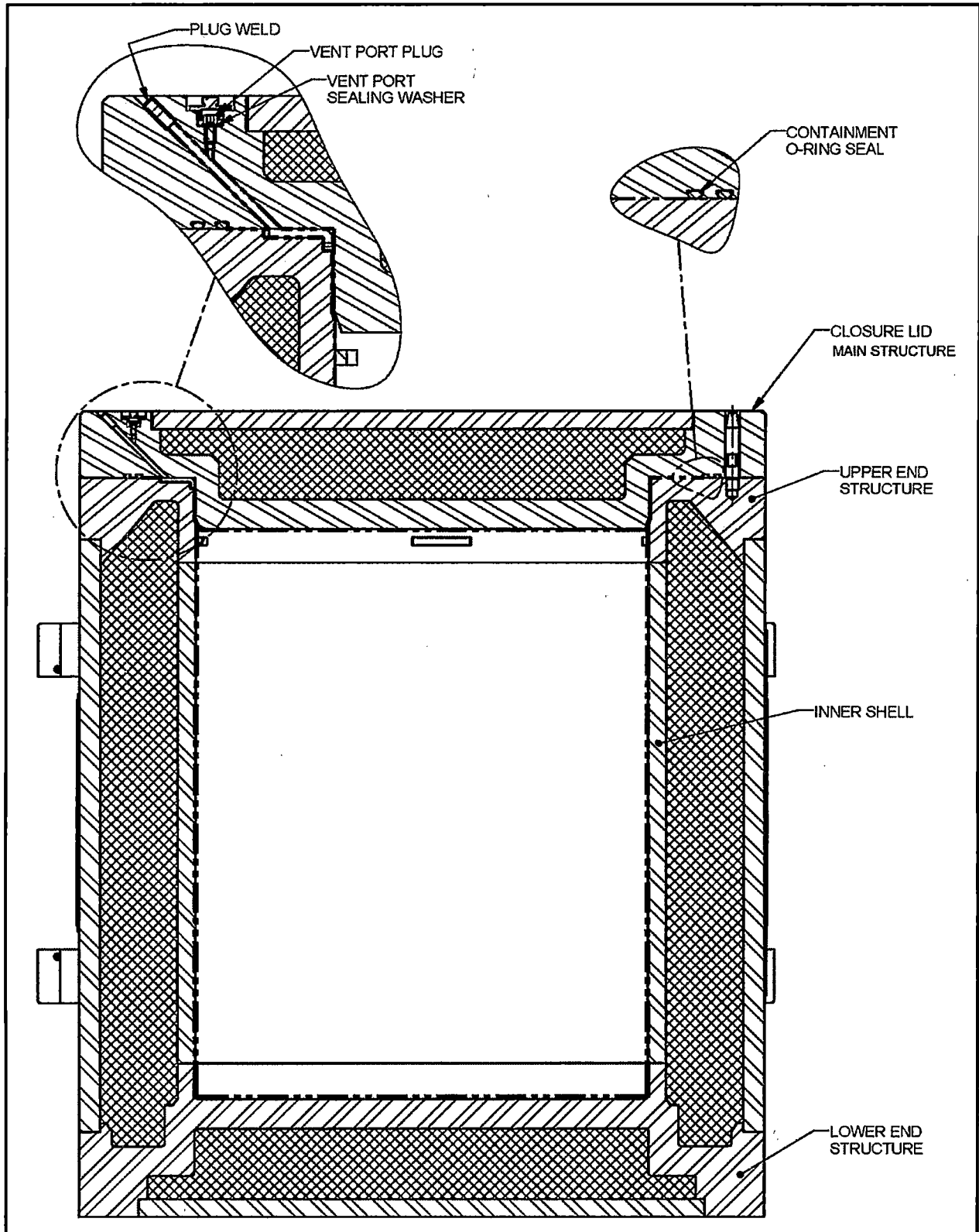
Figure 1.2-1 – 380-B Containment Boundary
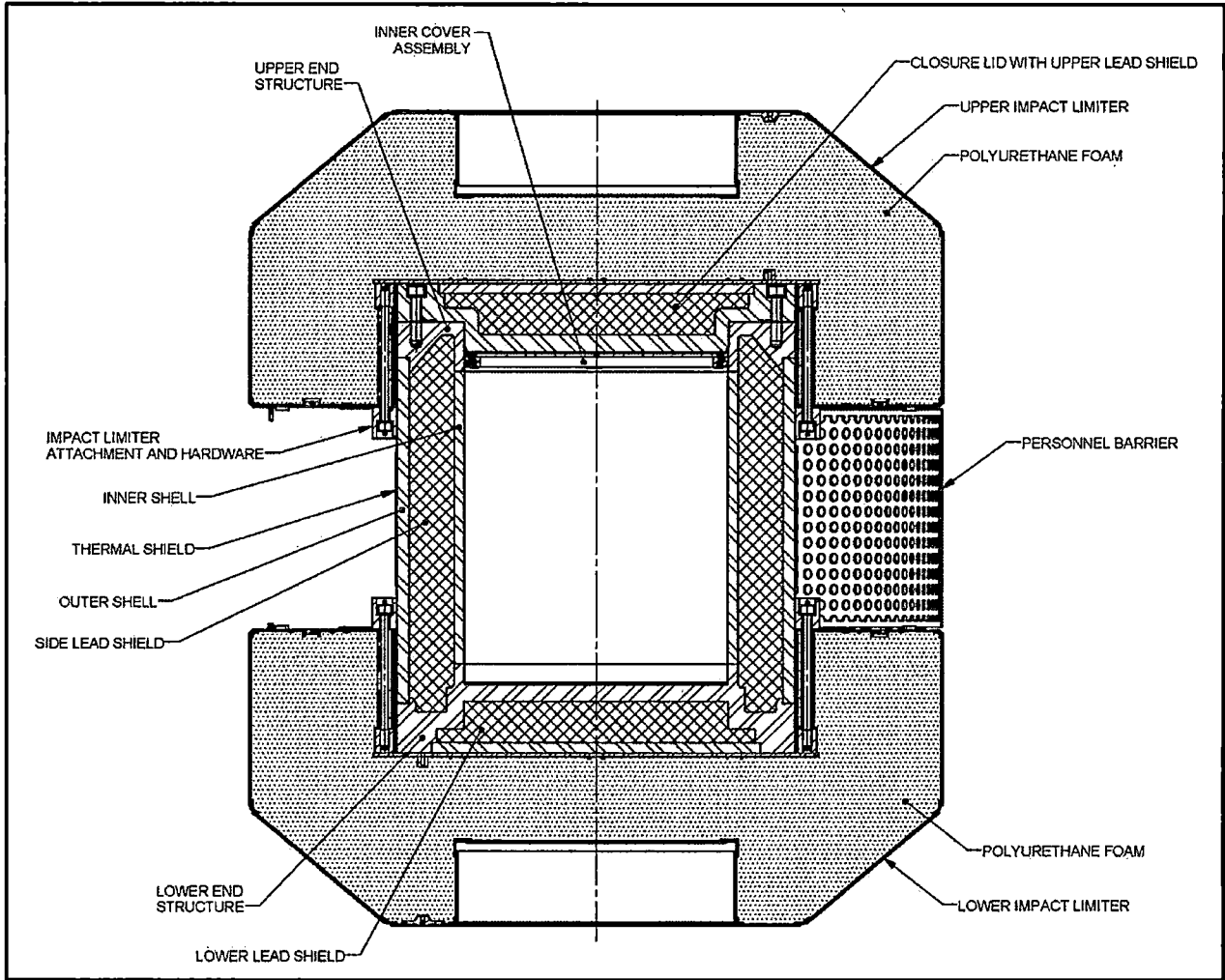
Figure 1.2-2 – 380-B Packaging Cross-Section (Left Personnel Barrier removed for clarity)

Security-Related Information
Figure Withheld Under 10 CFR 2.390.

Figure 1.2-3 – 380-B Packaging Dimensions
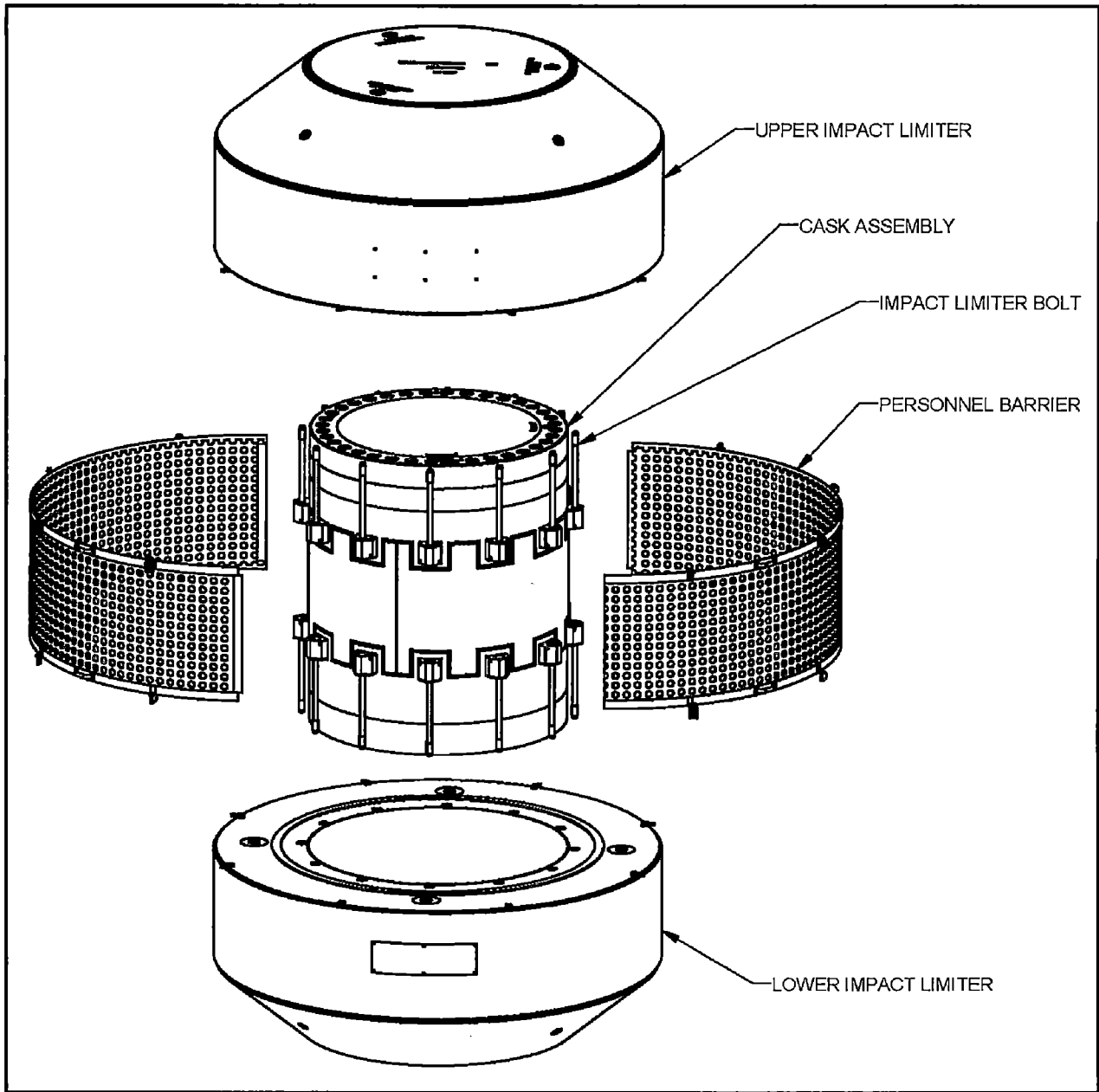
Figure 1.2-4 – 380-B Packaging Exploded View

CLOSURE LID BOLT AND WASHER

CLOSURE LID

INNER COVER ASSEMBLY

ALIGNMENT PIN

CASK BODY

THERMAL SHIELD
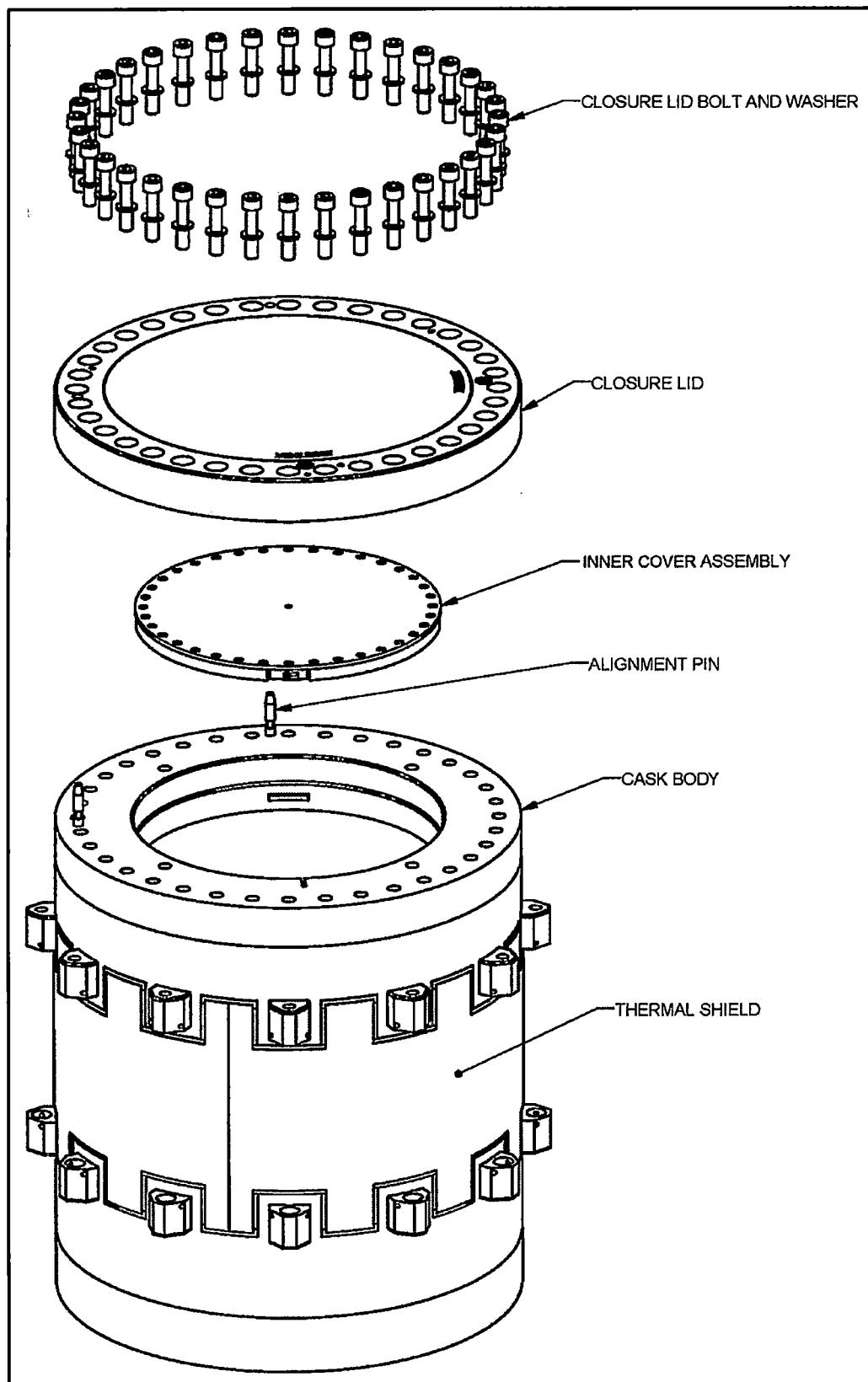
Figure 1.2-5 – 380-B Cask Assembly Exploded View

MIN ½ INCH
AXIAL
CLEARANCE

MIN ½ INCH
TOTAL DIAMETRAL
CLEARANCE

BLOCKING /
DUNNAGE
(CLOSED-TYPE)

SHIELDED
DEVICE

MIN ½ INCH
AXIAL
CLEARANCE

MIN ½ INCH
TOTAL DIAMETRAL
CLEARANCE

BLOCKING /
DUNNAGE
(OPEN-TYPE)

SHIELDED
DEVICE
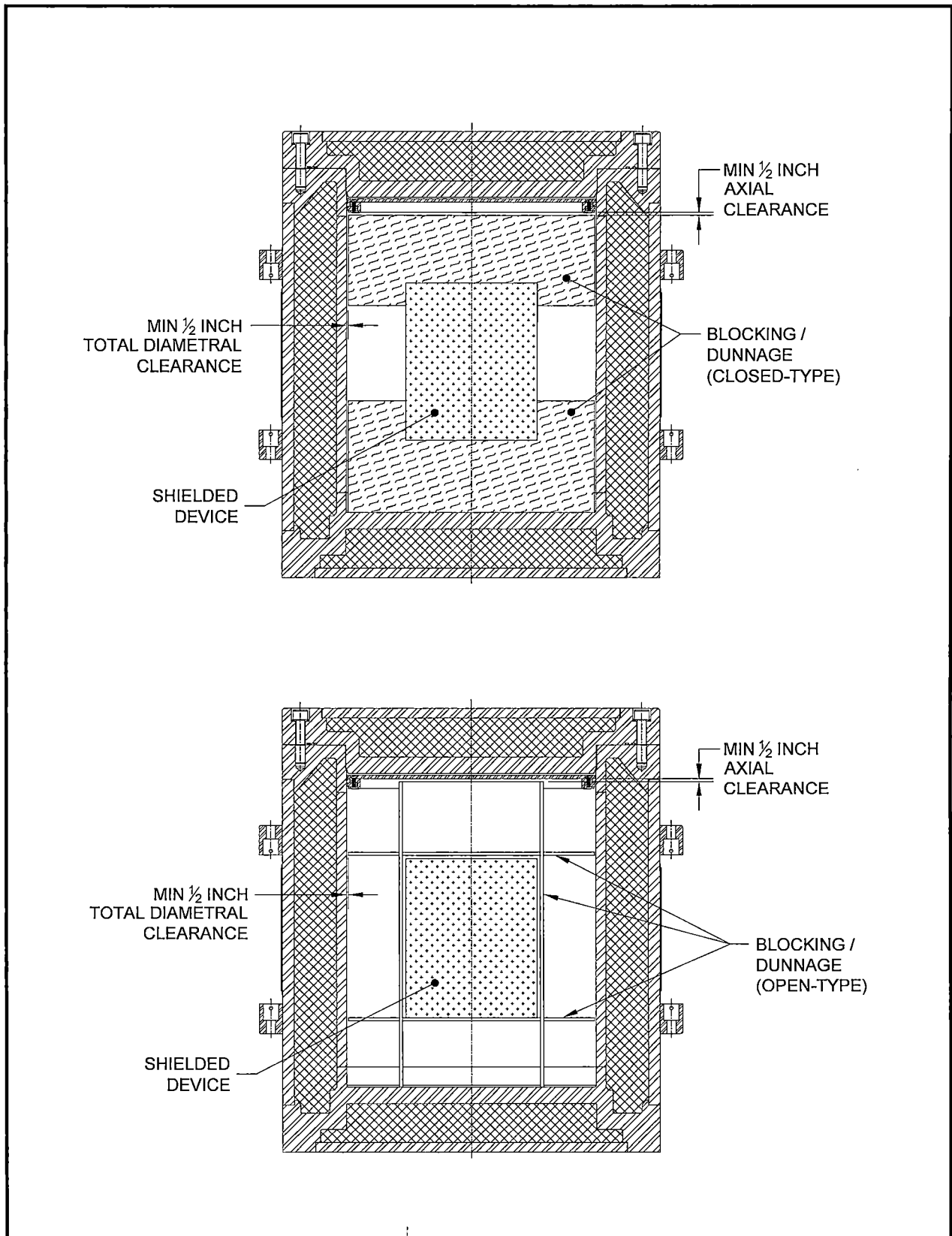
Figure 1.2-6 – 380-B Contents Schematic (Impact Limiters Not Shown)

1.3 Appendices

1.3.1 References

1. Title 10, Code of Federal Regulations, Part 71 (10 CFR 71), *Packaging and Transportation of Radioactive Material*, 01-01-11 Edition.

2. International Atomic Energy Agency, *Regulations for the Safe Transport of Radioactive Material*, TS-R-1, 2009 Edition.

3. ANSI N14.5–2014, *American National Standard for Radioactive Materials – Leakage Tests on Packages for Shipment*, American National Standards Institute (ANSI), Inc.

1.3.2 Glossary of Terms and Acronyms

ANSI – American National Standards Institute.

ASME B&PV Code – American Society of Mechanical Engineers Boiler and Pressure Vessel Code.

ASTM – American Society for Testing and Materials.

AWS – American Welding Society.

Cask Body – 380-B package component consisting of the inner shell, outer shell, upper and lower end structures, side and lower lead shielding.

Closure Lid – 380-B package component consisting of a main structure or body, lid outer plate, and upper lead shield that completes the containment boundary. It contains the vent port, the test port, the containment O–ring seal, and the test O–ring seal.

Closure Lid Main Structure – Part of the closure lid. Massive structural element made from forging or plate material that includes the containment boundary upper plate, closure bolt holes, O-ring grooves, vent port, and test port. May also be referred to as the Closure Lid Body.

Closure Bolts – Fasteners that secure the closure lid to the cask body.

Containment O–ring Seal – Inner elastomeric seal, retained in the closure lid, which forms part of the containment boundary.

HAC – Hypothetical Accident Conditions.

Impact Limiter Attachment Bracket – One of 24 blocks (twelve each end) attached to the outer shell that serves as the attachment point for the impact limiter attachment bolts.

Inner Cover – Assembly of plate and bar, or a single machined plate that attaches to the inner cover shear step on the cask body upper end structure. The inner cover serves as an exclusion zone in the NCT shielding design. May also be referred to as the inner cover plate or assembly.

Inner Cover Shear Step – Plate or bar welded to the payload cavity inner diameter of the cask body upper end structure, or integrally made as part of the upper end structure. Serves an attachment point for the inner cover.

Lower End Structure –	Part of the cask body. Massive structural element made from forging or plate material that connects to both inner and outer cask body shells, contains a cavity for the lower lead shield, and includes the containment boundary lower plate. Interfaces with the lower lead shield, bottom or lower outer plate, and impact limiter. May also be referred to as the Cask Lower End.
MNOP –	Maximum Normal Operating Pressure.
NCT –	Normal Conditions of Transport.
Personnel Barrier –	Assembly of expanded or flattened expanded metal and sheet metal comprised of two halves that is secured to the cask assembly with both upper and lower impact limiters. Prevents access to the cask body in the area between the impact limiters.
Seal Test Port –	Opening located in the closure lid, used to test the leakage rate of the containment O-ring seal. Closed with the seal test port plug that is protected by a dust cover.
Sealed Source –	Sealed capsule containing source material.
Sealing Washers –	Integrated metal and elastomer seals that are used with the vent port and seal test ports.
Shielded Device –	Industrial, medical, or research device for use in irradiating samples. Contains the source, shielding, and surrounding structure.
Test O-ring Seal –	Outer elastomeric O-ring seal, retained in the closure lid, used to allow leakage rate testing of the containment O-ring seal.
Thermal Shield –	Assembly of sheets and wire wraps attached to the outside of the outer shell, forming a thin air gap that inhibits heat transfer into the package during the HAC fire event.
Upper End Structure –	Part of the cask body. Massive structural element made from forging or plate material that connects to both inner and outer cask body shells, and includes the containment O-ring sealing surface and closure bolt threaded holes. Interfaces with the closure lid, and closure bolts. May also be referred to as the Cask Upper End.
Vent Port –	Containment penetration located in the closure lid, which is used to vent the cavity and to introduce helium for leakage rate testing during operations. Closed with the vent port plug, that is protected by a dust cover.

1.3.3 Packaging General Arrangement Drawings

The packaging general arrangement drawings consist of:

- 1916–02–01–SAR, LANS 380-B Package Assembly SAR Drawing, 2 sheets
- 1916–02–02–SAR, LANS 380-B Cask Assembly SAR Drawing, 6 sheets
- 1916–02–03–SAR, LANS 380-B Impact Limiter Assembly SAR Drawing, 4 sheets

This page left intentionally blank.

Security-Related Information
Figure Withheld Under 10 CFR 2.390.

AREVA
February 23, 2016
Records Management

REV	DESCRIPTION		DRAWN	CHECKER	VERIFIED
	NAME/SIGNATURE	DATE			
APPD	N/A	2016			
APPD	K.Regalado/RE78	2/16/16		AREVA Federal Services LLC	
ENGR	N/A			Packaging Projects	
EM		2/22/16		Federal Way, WA 98003	
RE		2/16/16			
TECH CHK	P. Moss / P. Now	2/18/16	DWG TITLE	LANS 380-B PACKAGE ASSEMBLY	
DFTG CHK	P. Moss / P. Now	2/18/16		SAR DRAWING	
DRAWN	P. Pikulin	02/15/16			

AREVA

TOLERANCES UNLESS	SCALE SHOWN	WT. - LBS
FRACTIONS ± 1/2	REV: 0	SHEET 1 OF 2
ANGLES ± 1°	DWG DWG NO.	
	D 1916-02-01-SAR	

Security-Related Information
Figure Withheld Under 10 CFR 2.390.

DWG NO 1916-02-02-SAR REV 2 SH 1

Security-Related Information
Figure Withheld Under 10 CFR 2.390.

2	SEE ECN 1916-02-02-SAR/R1-E1		
1	SEE ECN 1916-02-02-SAR/R0-E1		
REV	DESCRIPTION		
	REVISION HISTORY		

	NAME/SIGNATURE	DATE
APPD		
APPD		
ENGR		
EM		8/18/17
RE		8/18/17
TECH CHG		8/18/17
DFTG CHG		8/18/17
DRAWN	R. Li	8/00/17

AREVA

AREVA Federal Services LLC
Packaging Projects
Federal Way, WA 98003

DWG TITLE LANS 380-B CASK ASSEMBLY
SAR DRAWING

TOLERANCE BLOCK		SCALE SHOWN	WT. - LBS
FRACTIONS ± 1/2		REV 2	SHEET 1 OF 6

DWG SIZE DWG NO.
D   1916-02-02-SAR

1916-02-02-SAR

Security-Related Information
Figure Withheld Under 10 CFR 2.390.

REV. 2   SHEET 2 OF 6
DWG NO.
1916-02-02-SAR

DWG NO. 1916-02-02-SAR REV 2 SH 3

Security-Related Information
Figure Withheld Under 10 CFR 2.390.

REV: 2 SHEET 3 OF 6
DWG NO.
1916-02-02-SAR

DWG NO. 1916-02-02-SAR REV 2 SH 4

Security-Related Information
Figure Withheld Under 10 CFR 2.390.

REV. 2 SHEET 4 OF 6
DWG NO.
1916-02-02-SAR

8   7   6   5   4   3   DWG NO. 1916-02-02-SAR REV 2 SH 5   1

D

C

Security-Related Information
Figure Withheld Under 10 CFR 2.390.

B

A

REV: 2   SHEET 5 OF 6
DWG NO.
1916-02-02-SAR

DWG NO. 1916-02-02-SAR REV 2 SH 6

Security-Related Information
Figure Withheld Under 10 CFR 2.390.

REV: 2 SHEET 6 OF 6
DWG NO.
1916-02-02-SAR

Security-Related Information
Figure Withheld Under 10 CFR 2.390.

1	SEE ECN 1916-02-03-SAR-R0-E1	
REV		DESCRIPTION

REVISION HISTORY

	NAME/SIGNATURE	DATE
APPD		
APPD		
ENGR		
EM		5/22/17
RE		5/22/17
TECH CHG		5/25/17
DFTG CHG		5/25/17
DRAWN	P. PROULX	5-18-17

AREVA

AREVA Federal Services LLC
Packaging Projects
Federal Way, WA 98003

DWG TITLE LANS 380-B IMPACT LIMITER ASSEMBLY
SAR DRAWING

TOLERANCE BLOCK	SCALE SHOWN	WT. - LBS
FRACTIONS ± 1/16 ANGLES ± 1°	REV. 1	SHEET 1 OF 4

DWG SIZE D

DWG NO. 1916-02-03-SAR

DWG NO. 1916-02-03-SAR REV 1 SH 2

Security-Related Information
Figure Withheld Under 10 CFR 2.390.

REV 1 SHEET 2 OF 4
DWG NO.
1916-02-03-SAR

DWG NO 1916-02-03-SAR REV 1 SH 3

Security-Related Information
Figure Withheld Under 10 CFR 2.390.

REV: 1 SHEET 3 OF 4
DWG NO.
1916-02-03-SAR

DWG NO. 1916-02-03-SAR REV 1 SH 4

Security-Related Information
Figure Withheld Under 10 CFR 2.390.

REV: 1 SHEET 4 OF 4
DWG NO.
1916-02-03-SAR

2.0 STRUCTURAL EVALUATION

This section presents evaluations demonstrating that the 380-B package meets all applicable structural criteria. The 380-B package, consisting of a shielded cask body, shielded lid, and upper and lower impact limiters, is evaluated and shown to provide adequate protection for the payloads. Normal conditions of transport and hypothetical accident condition evaluations are performed to address 10 CFR 71 [1] performance requirements. The primary method of performance demonstration is by analysis. Demonstration techniques comply with the methodology presented in NRC Regulatory Guides 7.6 [2] and 7.8 [3]. Performance of the impact limiters under HAC free drop and puncture drop is evaluated by means of half scale physical testing. A discussion of the tests performed is given in Appendix 2.12.2, *Certification Test Plan*, and results of the certification tests are provided in Appendix 2.12.3, *Certification Test Results*.

2.1 Structural Design

2.1.1 Discussion

The 380-B package is designed to provide leaktight containment per [4] for the transport of sealed radioactive sources contained in shielded devices. An isometric view of the package is shown in Figure 1.1-1, with cross-sections of the package shown in Figure 1.1-2. The 380-B package consists of a shielded cask body, a shielded lid, and two impact limiters. The structural components are made from ASTM Type 304 stainless steel, and the shielding material is lead. The payload cavity is 38 inches in diameter and 48.1 inches long. However, the effective payload cavity is 37 inches in diameter and 45.8 inches long due to the presence of an inner cover. Shielding is provided by 6.5 inches of radial lead thickness in the cask wall, 6 inches in the base, and 6 inches in the closure lid. The 380-B containment boundary consists primarily of a 1.5-inch thick Type 304 stainless steel inner shell, a 2.5-inch thick inner baseplate (part of the lower end structure), a 2.5-inch thick inner plate in the closure lid, and an elastomer containment seal. The outer structural shell is 1.75 inches thick. A quantity of 36, 1-1/2-inch diameter, precipitation hardening stainless steel bolts are used to attach the closure lid. The containment seal is a 3/8-inch cross-sectional diameter butyl O-ring seal. A test O-ring seal is used to provide a cavity for helium leak testing of the containment seal. Vent and test ports are located in the closure lid. A thermal shield is attached to the outside of the cask between the impact limiters.

Impact limiters are located at each end of the cask body to mitigate the effects of the free drop impact and the fire event. The impact limiters are essentially identical in design, with a ¼-inch thick ASTM Type 304 stainless steel shell and 16 lb/ft^3 polyurethane foam energy absorbing material. Each limiter is attached using 12, 1-1/4-inch diameter, precipitation hardening stainless steel bolts. A personnel barrier is located between the two impact limiters.

The payload consists of shielded irradiation devices containing sealed sources. After placement in the cask, they are shored in place to restrict motion during transport.

2.1.2 Design Criteria

Proof of performance for the 380-B package is achieved primarily by analysis. Impact limiter performance is demonstrated by half-scale certification testing. The acceptance criteria for analytic

assessments are in accordance with Regulatory Guide 7.6. These design criteria meet the following safety requirements of 10 CFR §71.51:

1. For normal conditions of transport, there shall be no loss or dispersal of radioactive contents, as demonstrated to a sensitivity of 10^{-6} A_2 per hour, no significant increase in external radiation levels, and no substantial reduction in the effectiveness of the packaging.

2. For hypothetical accident conditions, there shall be no escape of radioactive material exceeding a total amount A_2 in one week, and no external radiation dose rate exceeding one rem per hour at one meter from the external surface of the package.

The 380-B package qualifies as a Category I container, which is the highest and most stringent category [5]. Per NUREG/CR-3019 [6] and NUREG/CR-3854 [7], the cask components are classified as follows:

- Containment components are classified as ASME B&PV Code, Section III, Subsection NB [8].

- The non-containment structural components (e.g., outer shell, lid outer plate, bottom outer plate, thermal shield, impact limiter attachment brackets, and impact limiter shells) are classified as ASME B&PV Code, Section III, Subsection NF [9]. Conservatively, the outer shell, lid outer plate, and bottom outer plate, will be analyzed to the requirements of Subsection NB.

The remainder of this section presents the detailed acceptance criteria used for analytic structural assessments of the 380-B package.

2.1.2.1 Containment Structures

A summary of allowable stresses used for containment structures is presented in Table 2.1-1. Containment structures include the inner shell, the upper and lower end structures, and the closure lid main structure. The allowable stresses shown in Table 2.1-1 are consistent with Regulatory Guide 7.6, and the ASME B&PV Code, Section III, Subsection NB, and Appendix F [10]. Peak stresses are further discussed in Section 2.1.2.3.2, *Fatigue Assessment*, and buckling in Section 2.1.2.3.3, *Buckling Assessment*. Closure bolts are evaluated using the guidance of NUREG/CR-6007 [11]. Furthermore, stress intensity in the flanges which could affect compression of the containment O-ring seal is limited to the lesser of the value shown in Table 2.1-1, or the yield strength.

2.1.2.2 Other Structures

Impact limiter structures, including the steel shells and energy-absorbing foam, are expected to permanently deform under NCT and HAC. The impact limiter performance criteria are:

- Limit impact magnitude such that package component stress and deflection criteria are met.

- Prevent "hard" contact of a rigid part of the cask with the ground due to excessive deformation of the foam.

- Maintain attachment to the cask and sufficient structural integrity subsequent to the HAC free drop and puncture drop events so that the containment O-ring seal is protected from excessive temperature in the subsequent HAC fire event.

The performance of the impact limiters is discussed in Sections 2.6, *Normal Conditions of Transport*, and 2.7, *Hypothetical Accident Conditions*. The thermal performance of the packaging is evaluated in Chapter 3, *Thermal Evaluation*.

The packaging has no lifting provisions available for use in the transport configuration. Thus, 10 CFR §71.45(a) does not apply to the 380-B.

Since the 380-B package is not attached to the conveyance using any structural part of the package, tiedown structural criteria are not required.

2.1.2.3 Miscellaneous Structural Failure Modes

2.1.2.3.1 Brittle Fracture

With the exception of the closure bolts, all structural components of the 380-B package are fabricated of austenitic stainless steel. Austenitic stainless steels do not undergo a ductile-to-brittle transition in the temperature range of interest (i.e., down to -40 °F), and thus do not need to be evaluated for brittle fracture. The closure bolts are fabricated from ASTM A564, Type 630, Condition H1100 precipitation hardening stainless steel bolting material. Per Section 5 of NUREG/CR-1815 [12], bolts are not considered as fracture-critical components because multiple load paths exist and bolting systems are generally redundant, as is the case with the 380-B package. Therefore, brittle fracture is not a failure mode of concern.

2.1.2.3.2 Fatigue Assessment

2.1.2.3.2.1 Normal Operating Cycles

Normal operating cycles do not present a fatigue concern for the 380-B package components over its service life. The basis for this conclusion is reached using the six criteria of Article NB-3222.4(d) of the ASME B&PV Code. A summary of the six criteria and their application are discussed below. The service life of the package is 25 years with up to 50 shipments per year for a maximum of 1,250 shipments in the service life.

(1) Atmospheric to Service Pressure Cycle: The total number of atmospheric-to-operating pressure cycles during normal operations does not exceed the number of cycles on the fatigue curve corresponding to a value of $S_a = 3S_m$ for Type 304 stainless steel. From Table 2.6-1 at a bounding temperature of 150 °F (see Section 2.6.1.1, *Summary of Pressures and Temperatures*), the S_m value for Type 304 stainless steel is 20 ksi, which corresponds to an alternating stress value of $S_a = 3S_m = 60$ ksi. The corresponding number of cycles for a value of $S_a = 60$ ksi is greater than 6,000 from Figure I-9.2 and Table I-9.2 of the ASME B&PV Code [13]. The package undergoes one atmospheric-to-operating pressure cycle per shipment, therefore the package will experience 1,250 atmospheric-to-operating pressure cycles in its life. Since the allowable number of cycles is greater than the maximum expected number of cycles, the first criterion is satisfied.

(2) Normal Service Pressure Fluctuation: The specified full range of pressure fluctuations during normal service does not exceed the quantity 1/3 × Design Pressure × (S_a/S_m), where the Design Pressure is 25 psi, S_a is the value obtained from the Type 304 stainless steel design fatigue curve for the total specified number of significant pressure fluctuations (SPF), and S_m is the allowable stress intensity for the material at the service temperature. The total number of service cycles is based on the fill gas extreme temperature range as stated below. Conservatively, two complete

temperature cycles are assumed to occur for each of the 1,250 lifetime shipments for a total quantity of 2,500 pressure fluctuation cycles. From Table I-9.2, $S_a = 80,140$ psi for 2,500 cycles. The value of S_m was defined above as 20 ksi at service temperature. The limiting full range of pressure fluctuation (FRF) becomes:

$$FRF_{LIMIT} = 1/3 \times \text{Design Pressure} \times (S_a/S_m) = 33.4 \text{ psi}$$

Next, the maximum pressure fluctuations in the package will be determined. Of note, the maximum pressure fluctuations will be conservatively assumed to be above the significance level, and therefore the value SPF does not need to be computed. The bulk average fill gas temperature varies between the extremes of $T_1 = -40$ °F and a conservative bounding temperature of $T_2 = 250$ °F. The maximum pressure (conservatively assuming that atmospheric pressure corresponds to -40 °F) is:

$$\frac{P_2}{P_1} = \frac{T_2}{T_1} \Rightarrow P_2 = P_1\left(\frac{T_2}{T_1}\right) = 14.7\left(\frac{250+460}{-40+460}\right) = 24.9 \text{ psia}$$

The resulting pressure fluctuation is FRF = 24.9 − 14.7 = 10.2 psi, which is less than $FRF_{LIMIT} = 33.4$ psi presented above and therefore, the second criterion is satisfied.

(3) Temperature Difference — Startup and Shutdown: The temperature between adjacent points of a package component during normal service does not exceed $1/2(S_a/E\alpha)$, where S_a is the design fatigue curve value taken from Table I-9.2 for the total specified number of temperature difference fluctuations, E is the modulus of elasticity, and α is the mean coefficient of thermal expansion, all evaluated at temperature. The total number of temperature fluctuations will not exceed the number of uses of the package, which is 1,250 as calculated above. It will be conservative to use the value of S_a from Table I-9.2 of the ASME B&PV Code for 2,500 cycles, which is 80,140 psi. From Table 2.6-1 at a bounding temperature of 150 °F, the value of the mean thermal expansion coefficient is $\alpha = 8.75(10^{-6})/$ °F and the modulus of elasticity, $E = 27.8(10^6)$ psi. Therefore, the value of $1/2(S_a/E\alpha)$ = $1/2(80,140/[27.8(10^6)8.75(10^{-6})]) = 165$ °F. Since the package design temperature is 150 °F under ambient conditions of 100 °F, the temperature difference between any two adjacent points cannot approach the 165 °F value. Thus, the third criterion is satisfied.

(4) Temperature Difference — Normal Service: The temperature difference between any two adjacent points does not change during normal service by more than the quantity $1/2(S_a/E\alpha)$, where S_a, E, and α are as defined above. However, normal operating temperatures of the containment boundary are largely determined by the steady heat load, and any changes in temperature due to changes in ambient conditions, warm-up, or cool-down will be relatively slow and even due to the large thermal mass of the package. Therefore, the fourth criterion is satisfied.

(5) Temperature Difference — Dissimilar Materials: The fifth criterion is concerned with dissimilar materials. The containment boundary is constructed of Type 304 stainless steel, and includes a brass vent port plug. The ASTM B16 free-cutting brass used in the vent port plug has a coefficient of thermal expansion which is similar to that of the stainless steel and the temperature of the plug and the surrounding steel is essentially identical. The plug is inspected at each use of the package, and is easily replaced if necessary. Stainless steel closure bolts are used to connect the two parts of the containment vessel. Consideration of the effect of

temperature variation on the stainless steel closure bolts and flanges is included in the closure bolt stress evaluation under criterion six below. Thus, dissimilar materials are not of concern and the fifth criterion is satisfied.

(6) Mechanical Loads: The specified full range of mechanical loads does not result in stresses whose range exceeds the S_a design fatigue curve for the total specified number of load fluctuations. The only repeating mechanical loads will be those associated with tightening of the closure bolts.

The maximum stress intensity developed in the closure bolts during normal operations, given in Section 2.6.1.5, *Closure Bolts*, is bounded by a value of $S_{max} = 50,200$ psi. This stress includes preload stress, thermal stress, and a conservative inclusion of 50% of the applied preload torque as a residual torsion stress. From Table 2.6-1, the allowable stress for the bolting material, S_m, at 150 °F is 73,767 psi. As defined by Table I-9.0 of the ASME B&PV Code, the Maximum Nominal Stress (MNS) of 50,200 psi is less than $2.7S_m$ (i.e., 2.7(73,767) = 199,171 psi). Per NB-3232.3(c), a stress concentration factor of four shall be applied to one-half the value of S_{max}, (i.e., $4(0.5S_{max}) = 4 \times 0.5 \times 50,200 = 100,400$ psi). Per NB-3232.3(d), the alternating stress must be adjusted for the elastic modulus used in the fatigue curves. The modulus at a temperature of 150 °F is $28.05(10^6)$ psi and the modulus used for the fatigue curve in Figure I-9.4 is $30(10^6)$ psi. The adjusted alternating stress is:

$$S_{ALT} = \frac{30}{28.05}100.4 = 107.4 \; ksi$$

From Table I-9.0 for Figure I-9.4, the conservative lower-bound service cycles allowed for a stress of 107.4 ksi is 800. Since closure bolts are tightened twice per package service cycle, the allowable number of package service cycles is half of this value. Therefore the closure bolts should be replaced every 800/2 = 400 service cycles for the package, and the sixth criterion is satisfied.

Summary: The previous discussion verifies that fatigue failure of the packaging containment boundary due to normal operating cycles is not a concern, per Section III, Subsection NB, Article NB-3222.4(d) of the ASME B&PV Code. Therefore the resistance of the 380-B package to fatigue is adequate to ensure a minimum 25 year service life of up to 50 shipments per year.

2.1.2.3.2.2 Normal Vibration Over the Road

Fatigue associated with normal vibration over the road is addressed in Section 2.6.5, *Vibration.*

2.1.2.3.3 Buckling Assessment

Buckling, per Regulatory Guide 7.6, is an unacceptable failure mode for the containment vessel. The intent of this provision is to preclude large deformations that would compromise the validity of linear analysis assumptions and quasi-linear stress allowable limits, as given in Paragraph C.6 of Regulatory Guide 7.6.

Buckling investigations contained herein consider the inner and outer cylindrical shells of the 380-B package. The cylindrical shell buckling analysis is performed using the methodology of ASME B&PV Code Case N-284-4 [14]. Consistent with Regulatory Guide 7.6 philosophy, factors of safety corresponding to ASME B&PV Code, Level A and Level D service conditions are employed. For NCT (Service Level A), the factor of safety is 2.0, and for HAC (Service Level D), the factor of safety is 1.34. Buckling analysis details are provided in Section 2.6.4, *Increased External*

Pressure, Section 2.6.7, *Free Drop* (NCT), Section 2.7.1, *Free Drop* (HAC), and Section 2.7.6, *Immersion – All Packages*.

2.1.3 Weights and Centers of Gravity

The maximum gross weight of the 380-B package is 67,000 lb. The packaging component weights are summarized in Table 2.1-2. The center of gravity (CG) of the package is located 58.9 inches from the bottom outside surface of the external impact limiter. The maximum possible difference between the payload center of gravity, as placed in the payload cavity, and the empty packaging center of gravity, is approximately 5 inches. The resulting shift in the combined center of gravity of the loaded package is less than one inch. Thus, the effect of payload placement on the loaded package center of gravity is negligible.

2.1.4 Identification of Codes and Standards for Package Design

The 380-B package is designated a Category I package. Per the guidance of NUREG/CR-3854, the appropriate design criteria for the containment is Section III, Subsection NB of the ASME B&PV Code. Consequently, the design of the containment boundary is based on the methodology of Regulatory Guide 7.6, and load cases are applied and combined according to Regulatory Guide 7.8. The outer shell, lid outer plate, and bottom outer plate are conservatively included under the NB criteria. The closure bolts are designed using the guidance of NUREG/CR-6007. For other structures such as the thermal shield, impact limiter shells, internal impact limiter components, the criteria is taken from Section III, Subsection NF of the ASME B&PV Code.

Table 2.1-1 – Containment Structure Allowable Stress Limits

Stress Category	NCT	HAC
General Primary Membrane Stress Intensity	S_m	Lesser of: $\quad 2.4S_m$ $0.7S_u$
Local Primary Membrane Stress Intensity	$1.5S_m$	Lesser of: $\quad 3.6S_m$ S_u
Primary Membrane + Bending Stress Intensity	$1.5S_m$	Lesser of: $\quad 3.6S_m$ S_u
Range of Primary + Secondary Stress Intensity	$3.0S_m$	Not Applicable
Pure Shear Stress	$0.6S_m$	$0.42S_u$
Peak	Per Section 2.1.2.3.2, *Fatigue Assessment*	
Buckling	Per Section 2.1.2.3.3, *Buckling Assessment*	
Containment Fasteners: [1]		
Average Tensile Stress Intensity	S_m [2]	Lesser of: $\quad S_y$ $0.7S_u$
Average Tensile + Average Shear + Bending + Residual Torsion Stress Intensity	$1.35S_m$ for $S_u > 100$ ksi	Not Applicable

Notes:

1. Containment fastener stress limits are in accordance with NUREG/CR-6007.
2. S_m is defined as $(2/3)S_y$ as recommended by NUREG/CR-6007.

Table 2.1-2 – 380-B Package Component Weights

Package Component		Weight, lb
Cask Body		38,000
Closure Lid		7,000
Total empty cask assembly		45,000
Impact Limiter	Each: 5,000	10,000
Total empty package		55,000
Contents (maximum)		10,000
Contents Blocking/Dunnage (max)		2,000
Total package (maximum)		**67,000**

2.2 Materials

The 380-B package structural components, including the impact limiter shells, thermal shield, and personnel barrier, are fabricated from Type 304 stainless steel in various product forms. The gamma shielding is made from lead per ASTM B29 (in any grade) or Federal Specification QQ-L-171E, Grade A or C. Polyurethane foam is used for impact energy absorption. Other materials performing a structural function are ASTM B16 UNS C36000 brass alloy (for the test and vent port plugs), and ASTM A564, Type 630, Condition 1100 stainless steel for the closure bolts and impact limiter bolts. The containment O-ring seal is made from butyl rubber. Plastic is used for the fire-consumable vent plugs in the foam cavities. The drawings presented in Appendix 1.3.3, *Packaging General Arrangement Drawings*, delineate the specific materials used for each 380-B package component.

2.2.1 Material Properties and Specifications

Table 2.2-1 through Table 2.2-6 and Figure 2.2-1 present the mechanical properties for the structural materials used in the 380-B package. The density of stainless steel is 0.29 lb/in^3, and Poisson's ratio is 0.31. The density of lead is 0.41 lb/in^3, and Poisson's ratio is 0.45. Data is interpolated or extrapolated from the available data as noted in the tables.

The performance of the 380-B package in free drop and puncture events is partially dependent on the energy-absorbing performance of polyurethane foam. The foam is poured in place within the impact limiter steel shell. Nominally 16 lb/ft^3 polyurethane foam is used. Section 8.1.5.1, *Polyurethane Foam* presents the details of acceptance tests for this material. The nominal, room-temperature crush properties of the polyurethane foam component are given in Table 2.2-6. Properties for both "parallel to rise" and "perpendicular to rise" are given. The "rise" direction is parallel to the force of gravity during solidification, and is oriented to be parallel to the cylindrical axis of the impact limiters.

2.2.2 Chemical, Galvanic, or Other Reactions

The 380-B package weight is supported by the lower impact limiter, whereby the load path includes the polyurethane foam in the impact limiter. The smallest load bearing area of foam is at the bottom, at the small end of the taper, which has an outer diameter of 60 inches and an inner diameter of 40 inches, for an area of 1,571 in^2. The weight of the package, including the maximum 12,000 lb payload, is 67,000 lb. The maximum compressive stress in the foam is therefore 67,000/1,571 = 43 psi. The nominal foam compressive strength in the axial direction (parallel-to-rise of the foam) is 710 psi, from Table 2.2-6. The compressive stress of 43 psi is thus only 1/16th of the foam compressive strength, which demonstrates the normal compressive load is safely in the elastic region where no permanent deformation will occur or accumulate over the package service life.

The materials of construction of the 380-B package will not have significant chemical, galvanic or other reactions in air or water environments. These materials have been previously used, without incident, in radioactive material packages for transport of similar payload materials such as the RH-TRU 72-B (NRC Docket 9212) and the BEA Research Reactor Cask (NRC Docket 9341). The polyurethane foam is fully enveloped by sheets of stainless steel and welded closed. The foam is a rigid, closed-cell (non-water absorbent) material that is free of halogens and chlorides, as discussed in Section 8.1.5.1, *Polyurethane Foam*. The lead gamma shielding in the

shielded devices is fully encased in a steel or stainless steel weldment and cannot be affected by water or atmospheric moisture.

The brass alloy vent port plug is very corrosion resistant. Any damage that could occur to the material is easily detectable since the fitting is handled each time the 380-B package is loaded and unloaded. Similarly, the stainless steel closure bolts can be readily inspected at each use for the presence of corrosion.

The butyl elastomer that is used for the containment O-ring seals contains no corrosives that would react with or adversely affect the 380-B package. This material is organic in nature and noncorrosive to the stainless steel containment boundary of the 380-B package.

A successful RAM packaging history combined with successful use of these fabrication materials in similar industrial environments ensures that the integrity of the 380-B package will not be compromised by any chemical, galvanic or other reactions.

2.2.3 Effects of Radiation on Materials

The radiation associated with the source payload will have no effect on the containment or other safety components comprising the 380-B package. Since loose or unshielded sources are not transported in the 380-B package, exposure of the materials of the packaging to a strong radiation field is not a routine condition of transport. Additionally, materials having safety significance that could be sensitive to radiation dose are either located outside of the package's heavy shielding (e.g., the polyurethane foam in the impact limiters) or subject to annual replacement (e.g., the containment O-ring seal, per Section 8.2.3.4, *Seals*.) For these reasons, there will be no deleterious radiation effects on the packaging, and the requirements of 10 CFR §71.43(d) are met.

Table 2.2-1 – Mechanical Properties of Wrought Type 304 Stainless Steel⑥

Material Specification	Temperature (°F)	① Yield Strength, S_y (psi)	② Ultimate Strength, S_u (psi)	③ Design Stress Intensity, S_m (psi)	④ Elastic Modulus, E ($\times 10^6$ psi)	⑤ Thermal Expansion Coefficient, α ($\times 10^{-6}$ /°F)
ASTM A240 ASTM A249 ASTM A479 Type 304	-40	30,000	75,000	20,000	28.9	8.2
	-20	30,000	75,000	20,000	28.8	8.2
	70	30,000	75,000	20,000	28.3	8.5
	100	30,000	75,000	20,000	28.1	8.6
	200	25,000	71,000	20,000	27.5	8.9
	300	22,400	66,200	20,000	27.0	9.2
	400	20,700	64,000	18,600	26.4	9.5
	500	19,400	63,400	17,500	25.9	9.7
	600	18,400	63,400	16,600	25.3	9.9
	700	17,600	63,400	15,800	24.8	10.0
	800	16,900	62,800	15,200	24.1	10.1

Notes: ① ASME B&PV Code, Section II, Part D, Table Y-1. Value at -40 °F extrapolated using the values at -20 °F and 70 °F.

② ASME B&PV Code, Section II, Part D, Table U. Value at -40 °F extrapolated using the values at -20 °F and 70 °F.

③ ASME B&PV Code, Section II, Part D, Table 2A. Value at -40 °F extrapolated using the values at -20 °F and 70 °F.

④ ASME B&PV Code, Section II, Part D, Table TM-1, Material Group G. Values for -40 °F and -20 °F interpolated from 70 °F and -100 °F. Value at 100 °F interpolated using the values at 70 °F and 200 °F.

⑤ ASME B&PV Code, Section II, Part D, Table TE-1, Material Group 3, Mean Coefficient. Values for -40 °F and -20 °F extrapolated from 100 °F and 200 °F.

⑥ All ASME B&PV Code references from [38].

Table 2.2-2 – Mechanical Properties of Forged Type 304 Stainless Steel⑥

Material Specification	Temperature (°F)	① Yield Strength, S_y (psi)	② Ultimate Strength, S_u (psi)	③ Design Stress Intensity, S_m (psi)	④ Elastic Modulus, E (×10⁶ psi)	⑤ Thermal Expansion Coefficient, α (×10⁻⁶ /°F)
	-40	30,000	70,000	20,000	28.9	8.2
	-20	30,000	70,000	20,000	28.8	8.2
	70	30,000	70,000	20,000	28.3	8.5
	100	30,000	70,000	20,000	28.1	8.6
ASTM A182, Type F304	200	25,000	66,300	20,000	27.5	8.9
	300	22,400	61,800	20,000	27.0	9.2
	400	20,700	59,700	18,600	26.4	9.5
	500	19,400	59,200	17,500	25.9	9.7
	600	18,400	59,200	16,600	25.3	9.9
	700	17,600	59,200	15,800	24.8	10.0
	800	16,900	58,600	15,200	24.1	10.1

Notes: ① ASME B&PV Code, Section II, Part D, Table Y-1. Value at -40 °F extrapolated using the values at -20 °F and 70 °F.

② ASME B&PV Code, Section II, Part D, Table U. Value at -40 °F extrapolated using the values at -20 °F and 70 °F.

③ ASME B&PV Code, Section II, Part D, Table 2A. Value at -40 °F extrapolated using the values at -20 °F and 70 °F.

④ ASME B&PV Code, Section II, Part D, Table TM-1, Material Group G. Values for -40 °F and -20 °F interpolated from 70 °F and -100 °F. Value at 100 °F interpolated using the values at 70 °F and 200 °F.

⑤ ASME B&PV Code, Section II, Part D, Table TE-1, Material Group 3, Mean Coefficient. Values for -40 °F and -20 °F extrapolated from 100 °F and 200 °F.

⑥ All ASME B&PV Code references from [38].

Table 2.2-3 – Mechanical Properties of ASTM A564, Grade 630, Condition H1100 Stainless Steel⑥

Material Specification	Temperature (°F)	① Yield Strength, S_y (psi)	② Ultimate Strength, S_u (psi)	③ Allowable Strength, S_m (psi)	④ Elastic Modulus, E ($\times 10^6$ psi)	⑤ Thermal Expansion Coefficient, α ($\times 10^{-6}$ /°F)
ASTM A564 Grade 630 Condition H1100	-40	115,000	140,000	76,667	29.1	6.2
	-20	115,000	140,000	76,667	29.0	6.2
	70	115,000	140,000	76,667	28.5	6.3
	100	115,000	140,000	76,667	28.3	6.3
	200	106,300	140,000	70,867	27.8	6.4
	300	101,800	140,000	67,867	27.2	6.5
	400	98,300	136,100	65,533	26.7	6.6
	500	95,200	133,400	63,467	26.1	6.7
	600	92,700	131,400	61,800	25.5	6.8
	700	90,300	128,400	60,200	24.9	6.9
	800	86,900	122,500	57,933	24.3	6.9

Notes: ① ASME B&PV Code, Section II, Part D, Table Y-1. Value at -40 °F extrapolated using the values at -20 °F and 70 °F.

② ASME B&PV Code, Section II, Part D, Table U. Value at -40 °F extrapolated using the values at -20 °F and 70 °F.

③ S_m is defined as $(2/3)S_y$ as recommended by NUREG/CR-6007.

④ ASME B&PV Code, Section II, Part D, Table TM-1, for alloy S17400. Values for -40 °F and -20 °F interpolated from 70 °F and -100 °F. Value at 100 °F interpolated using the values at 70 °F and 200 °F.

⑤ ASME B&PV Code, Section II, Part D, Table TE-1, for 17Cr-4Ni-4Cu steels, interpolated between Condition 1075 and Condition 1150, Mean Coefficient. Values for -40 °F and -20 °F extrapolated from 100 °F and 200 °F.

⑥ All ASME B&PV Code references from [38].

Table 2.2-4 – Mechanical Properties of Lead Shielding

Material Specification	Temperature (°F)	① Tensile Yield Strength, S_y (psi)	① Tensile Ultimate Strength, S_u (psi)	① Tensile Proportional Limit (psi)	② Elastic Modulus, E ($\times 10^6$ psi)	② Thermal Expansion Coefficient, ($\times 10^{-6}$ /°F)
ASTM B29 Lead (any grade) or Fed Spec QQ-L-171E, Gr. A or C	-99	----	---	---	2.50	15.3
	70	---	---	---	2.34	16.1
	100	584	1,585	276	2.30	16.2
	175	509	1,158	293	2.20	16.6
	250	498	839	277	2.09	17.0
	325	311	639	189	1.96	17.5
	440	---	----	----	1.74	18.5
	620	---	---	----	1.36	20.4

Notes: ① WADC Technical Report 57-695, ASTIA Document No. 151165, "Determination of the Mechanical Properties of a High Purity Lead and a 0.05% Copper-Lead Alloy," April 1958, by Thomas Tietz, Stanford Research Center, pp. 14, 21, for copperized lead.

② NUREG/CR-0481, SAND77-1872, "An Assessment of Stress-Strain Data Suitable for Finite Element Elastic-Plastic Analysis of Shipping Containers," H. J. Rack and G. A. Knorovsky, Sept. 1978, p. 56 and p. 66.

Table 2.2-5 – Mechanical Properties of Brass Material

Material	Minimum Mechanical Properties
ASTM B16, UNS C36000, Temper H02 (Rod Product Form)	Yield Strength, σ_y = 20,000 psi [43] Ultimate Strength, σ_u = 50,000 psi [43] Modulus of Elasticity, E = 14×10^6 psi [44] Thermal Expansion Coefficient, α = 11.4×10^{-6} /°F [44]

Table 2.2-6 – Nominal Material Properties of 16 lb/ft³ Polyurethane Foam

Property	Direction	Room Temperature Value
Compressive Strength, S (ref. Table 8.1-2 and Table 8.1-3)	Axial (Parallel-to-Rise)	710 psi @ 10% Strain 862 psi @ 40% Strain 3,056 psi @ 70% Strain
	Radial (Perpendicular-to-Rise)	681 psi @ 10% Strain 880 psi @ 40% Strain 3,108 psi @ 70% Strain

FIGURE 11(b) FROM WADC TECHNICAL REPORT 57-695
(Tensile Stress-Strain Curves to 1% Strain at a Strain Rate of 0.005 in/in/minute)
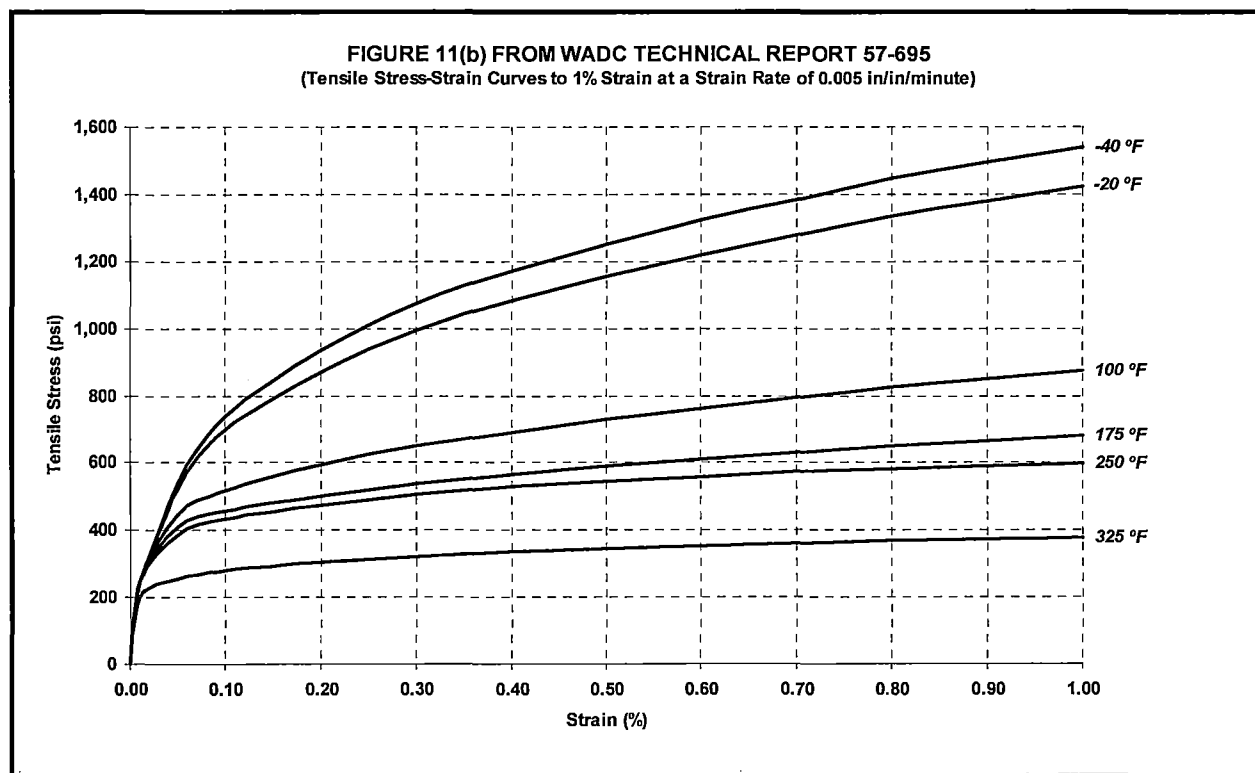
Figure 2.2-1 – Tensile Stress-Strain Curves for Lead Shielding (Source: see note 1 of Table 2.2-4)

2.3 Fabrication and Examination

2.3.1 Fabrication

The 380-B package is fabricated using conventional metal forming and joining techniques. All welding procedures and welding personnel must be qualified in accordance with Section IX of the ASME B&PV Code [15]. Containment boundary welds are full penetration joints. All non-containment joints are fabricated in accordance with the requirements delineated on the drawings in Appendix 1.3.3, *Packaging General Arrangement Drawings*. The containment shell fabrication complies with the tolerance requirements of the ASME B&PV Code, Subsection NE, Article NE-4220 [16]. Article NE-4220 is selected because the package cylindrical shells are verified for HAC buckling performance using the ASME B&PV Code Case N-284-4. This Code Case is for Section III, Division 1, Class MC construction, and is based on the fabrication requirements of NE-4222, as stated in Section 1120 of the Code Case. Therefore, it is appropriate to fabricate the 380-B package using shell tolerances from NE-4220, rather than NB-4220.

The polyurethane foam and butyl rubber O-rings are procured using written procedures. See Section 8.1.5, *Component and Material Tests*, for details of the fabrication and performance requirements of these components.

2.3.2 Examination

Each of the materials performing a significant safety function must meet the ASTM specifications delineated on the drawings in Appendix 1.3.3, *Packaging General Arrangement Drawings*. Safety-significant materials not having an ASTM designation are controlled by means of written procedures whose requirements are summarized in Section 8.1.5, *Component and Material Tests*.

Forgings are subject to ultrasonic and liquid penetrant inspection per the ASME B&PV Code, Subsection NB, Article NB-2540 [17].

All welds are subject to visual examination per AWS D1.6 [19]. The weld between the inner containment shell and the lower end structure, and the longitudinal weld(s) in the inner and outer shell, are examined by radiographic inspection in accordance with the ASME B&PV Code, Subsection NB, Article NB-5000, and Section V, Article 2 [20]. The welds between the inner containment shell and upper end structure, and the welds between the outer shell and either end structure, are examined by ultrasonic inspection in accordance with the ASME B&PV Code, Subsection NB, Article NB-5000, and Section V, Article 4 [21]. All welds made on the cask body and lid, excluding seal welds and tack welds, are liquid penetrant inspected on the final pass in accordance with the ASME B&PV Code, Subsection NB, Article NB-5000, and Section V, Article 6 [22]. All other welds, including the impact limiter attachment lugs to the cask body, the personnel barrier, the inner cover, and all impact limiter shell welds, excluding seal welds and tack welds, are liquid penetrant inspected on the final pass in accordance with the ASME B&PV Code, Subsection NF, Article NF-5000, and Section V, Article 6 [23]. Three structurally important impact limiter shell groove welds are examined by ultrasonic inspection in accordance with the ASME B&PV Code, Subsection NF, Article NF-5000, and Section V, Article 4 [24].

Each 380-B package will also be subjected to the following tests:

- An internal pressure test, in which the containment boundary is pressurized to 125% of the design pressure per the ASME B&PV Code, Subsection NB, Article NB-6220 [25], or 150%

of the MNOP, per 10 CFR §71.85(b), whichever is greater. The pressure test requirements are described in Section 8.1.3.2, *Containment Boundary Pressure Testing*.

- Containment boundary leakage rate test, which includes helium leakage rate tests of the containment boundary, the main containment O-ring seal, and the vent port containment O-ring seal. The leakage rate test requirements are described in Section 8.1.4, *Fabrication Leakage Rate Tests*.

- A test to ensure the integrity of the lead gamma shielding. The gamma test requirements are described in Section 8.1.6, *Shielding Integrity Test*.

2.4   General Standards for All Packages

This section defines the general standards for all packages. The 380-B package meets all requirements delineated for this section.

2.4.1   Minimum Package Size

The minimum dimension of the 380-B package is 100 inches (the diameter of the impact limiters/personnel barrier). Thus, the 4-in. minimum requirement of 10 CFR §71.43(a) is satisfied.

2.4.2   Tamper-Indicating Feature

A tamper-indicating seal is made by passing an electronic security monitor cable through holes which are cross-drilled in the impact limiter attachment lugs. The cable crosses the upper impact limiter attachment bolt heads. The bolt heads cannot be accessed without interrupting the current in the cable, which is monitored remotely to detect any tampering. In addition, damage to the cable provides physical evidence of possible tampering, irrespective of the active monitoring of the current. As an option, a tamper-indicating lockwire shall be placed across at least one of the upper impact limiter attachment brackets. Thus, the requirement of 10 CFR §71.43(b) is satisfied.

2.4.3   Positive Closure

The 380-B package cannot be opened unintentionally. The upper impact limiter, which is attached using 12, 1-1/4-inch diameter bolts, blocks access to the closure bolts and to the vent port. Thus, the requirements of 10 CFR §71.43(c) are satisfied.

2.4.4   Materials

The requirements of 10 CFR §71.43(d) are discussed in Section 2.2, *Materials*.

2.4.5   Valves

The containment boundary of the 380-B package does not contain any valves. The closure lid contains one vent port which penetrates the containment boundary and which is closed with a brass port plug. The vent port is closed and tested during pre-shipment leak testing of the 380-B package. The port is protected from inadvertent use or from tampering by the impact limiter as described above. Thus, the requirements of 10 CFR §71.43(e) are satisfied.

2.4.6   Package Design

As shown in Chapter 2.0, *Structural Evaluation*, Chapter 3.0, *Thermal Evaluation*, and Chapter 5.0, *Shielding Evaluation*, the structural, thermal, and shielding requirements, respectively, of 10 CFR §71.43(f) are satisfied for the 380-B package.

2.4.7   External Temperatures

As shown in Table 3.3-1 from Section 3.3, *Thermal Evaluation for Normal Conditions of Transport*, the maximum accessible surface temperature with maximum internal decay heat load and no insolation is bounded by 185 °F. This satisfies the limit of 10 CFR §71.43(g) for exclusive use shipments.

2.4.8 Venting

The 380-B package does not include any features intended to allow continuous venting of the containment boundary during transport. Thus, the requirements of 10 CFR §71.43(h) are satisfied.

2.5   Lifting and Tie–down Standards for All Packages

2.5.1   Lifting Devices

Because the payloads transported in the 380-B are self-shielded, they can be loaded into the packaging without the need to move the cask body from the conveyance. Thus, the 380-B is not normally removed from the conveyance. In addition, the packaging has no lifting provisions available for use in the transport configuration. Thus, 10 CFR §71.45(a) does not apply to the 380-B.

2.5.2   Tie–down Devices

During transport, the 380-B package rests on a dedicated trailer, and is held down by means of a steel frame which rests on top of the upper impact limiter. The steel tiedown frame is attached by chains or equivalent to the conveyance, so that a nominal downward load is applied to keep the 380-B package in place. In this configuration, the package contacts only the conveyance on the bottom and the steel frame on the top, and therefore has no integral tie–down devices which are a structural part of the package. Therefore, per 10 CFR §71.45(b)(1), no evaluation of tie–down devices is required.

The threaded holes used for lifting the upper impact limiter are covered by mechanical means, such as a set screw, during transport. Thus, 10 CFR §71.45(b)(2) is satisfied.
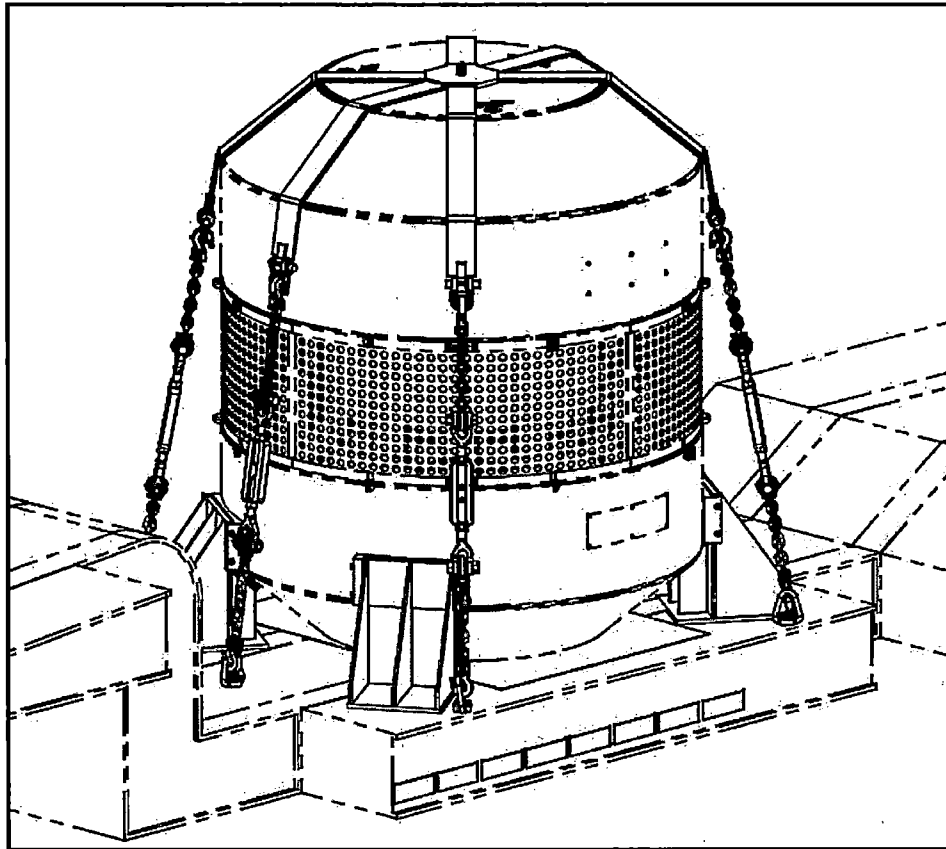
Figure 2.5-1 – 380-B Package Restraint System

2.6 Normal Conditions of Transport

When subjected to normal conditions of transport (NCT) as specified in 10 CFR §71.71, the 380-B package meets the performance requirements specified in Subpart E of 10 CFR 71. This is demonstrated in the following subsections where each NCT condition is addressed and shown to meet the applicable design criteria. Load combinations used in this section are consistent with Regulatory Guide 7.8. Margins of safety are summarized in Table 2.6-3.

2.6.1 Heat

The normal heat condition, as defined in 10 CFR §71.71(c)(1), is evaluated in Section 3.0, *Thermal Evaluation*. The bounding temperatures and pressures for use in structural analyses are summarized in the following section. Material properties and stress limits, consistent with the design criteria shown in Table 2.1-1, are summarized for the relevant bounding temperatures in Table 2.6-1.

2.6.1.1 Summary of Pressures and Temperatures

The bounding maximum temperatures for the 100 °F ambient NCT condition of the 380-B package are presented in Table 3.1-1 of Chapter 3, *Thermal Evaluation*. All components of the cask body are bounded by a temperature of 150 °F in that condition. The bulk average polyurethane foam in the impact limiter is bounded by a temperature of 150 °F.

The initial pressure in the package at assembly is ambient, i.e., 14.7 psia. As determined in Section 3.3.2, *Maximum Normal Operating Pressure*, the maximum normal operating pressure (MNOP) can be conservatively defined to be 10 psig. The design pressure of the 380-B package is 25 psig, which is significantly higher than the MNOP. The maximum NCT pressure is presented in Table 3.1-2.

2.6.1.2 Differential Thermal Expansion

2.6.1.2.1 Contents

The 380-B packaging does not include a lodgment, basket, or other internal structure. The 380-B payload consists of shielded devices that are located within the payload cavity by means of non-structural dunnage/blocking. Thus, differential thermal expansion is not of concern.

2.6.1.2.2 Lead

Due to different thermal expansion coefficients, the lead gamma shielding creates a stress in the inner shell under NCT hot conditions. An upper bound interface pressure between the lead and the inner shell is now determined, and applied as a pressure load to the finite element model as shown in Appendix 2.12.4, *Stress Analysis Finite Element Models*, and to the buckling analysis as shown in Appendix 2.12.6, *Cask Shell Buckling Evaluations*. First, note that the lead and the cask inner and outer shells are all in contact, and are stress-free, at the point of solidification of the lead at 620 °F. As the cask and lead cool, the lead contracts more than the stainless steel, and an interface pressure develops between the lead and the inner shell. This interface pressure is a function of the amount of interference between the lead and inner shell, and of the yield point of the lead at the NCT temperature. Due to the effects of material creep, the interface pressure will diminish over a relatively short period of time, thus reducing the resulting inner shell stresses.

However, the effects of lead creep are conservatively neglected. The amount of interference between the lead and the inner shell depends upon the free state radii of these components, both at their respective NCT temperatures. The free state outer radius of the inner shell at the NCT hot temperature is:

$$r_{ioh} = r_{io}[1 + \alpha_{s100}(T_{sh} - 70)] = 20.505 \, inches$$

where the outer free state radius of the inner shell at room temperature, r_{io} = 20.5 inches, the lower bound NCT hot case temperature of the shell, T_{sh} = 100 °F, and the coefficient of thermal expansion of the inner shell material at 100 °F is α_{s100} = 8.6(10^{-6})/°F from Table 2.6-2. Note that the NCT hot condition includes a 100 °F ambient with insolation, therefore the inner shell and lead temperatures will be at least 100 °F. The interface pressure calculation is conservative for lower bound temperatures, since the lead will contract more and apply a larger pressure. Therefore, 100 °F will be used for this calculation.

To determine the free state radii of the lead under NCT temperatures, it is necessary to start with the radii of the steel shells at the lead solidification point at 620 °F, at which point all of the components are in stress free contact. The radii of the lead/steel interfaces at 620 °F are:

$$r_{Li620} = r_{io620} = r_{io}[1 + \alpha_{s620}(620 - 70)] = 20.612 \, inches$$

$$r_{Lo620} = r_{oi620} = r_{oi}[1 + \alpha_{s620}(620 - 70)] = 27.147 \, inches$$

where r_{Li620} & r_{io620} represent the inner lead-steel interface radius, and r_{Lo620} & r_{oi620} represents the outer lead-steel interface radius at 620 °F. In these equations, the room temperature outer radius of the inner shell, r_{io} = 20.5 inches, the inner radius of the outer shell, r_{oi} = 27.0 inches, and the thermal expansion coefficient of the shells at 620 °F, α_{s620} = 9.9(10^{-6})/°F from Table 2.6-2. These values are then used to find the free state lead dimensions at the NCT temperature of lead as follows. Note that two thermal expansion terms are used (first contracting the lead from 620 °F to 70 °F, then expanding it from 70 °F to the hot lead temperature), since the thermal expansion coefficients given in Table 2.6-2 are based on 70 °F. The NCT hot case temperature of the lead is given a conservative lower bound of T_{Lh} = 100 °F as discussed above.

$$r_{Lih} = r_{Li620}[1 + \alpha_{L620}(70 - 620) + \alpha_{L100}(T_{Lh} - 70)] = 20.391 \, inches$$

$$r_{Loh} = r_{Lo620}[1 + \alpha_{L620}(70 - 620) + \alpha_{L100}(T_{Lh} - 70)] = 26.855 \, inches$$

where r_{Lih} is the free state inner radius of the lead, and r_{Loh} is the outer radius, at NCT. From Table 2.6-2, the thermal expansion coefficient of the lead from 620 °F to 70 °F, α_{L620} = 20.4(10^{-6})/°F, and from 70 °F to T_{Lh}, the corresponding coefficient is α_{L100} = 16.2(10^{-6})/°F. Next, the interference between the inner shell and the lead will be found. Since the lead has a relatively low yield stress, the interface pressure between the inner shell and the lead will be governed by the lead yield stress, which in turn depends on the location of the lead stress state on the lead stress-strain curve. The hoop strain in the lead is equal to u/r, where u represents the radial displacement of the inner surface, and r is the inner radius of the lead. The interface pressure can be conservatively maximized by assuming that the cask inner shell is rigid, and therefore all of the radial interference is taken by the lead. The radial interference is:

$$u = r_{ioh} - r_{Lih} = 0.115 \, inches$$

The maximum lead strain is then:

$$\varepsilon_{Lh} = \frac{u}{r_{Lih}}(100) = 0.564\%$$

Stress-strain curves for lead at various temperatures are reproduced in Figure 2.2-1. The hoop stress at a temperature of 100 °F, corresponding to a maximum strain of 0.564% may be conservatively bounded by a value of $\sigma_{Lh} = 800$ psi. It may be observed from the figure that the actual stress would be somewhat lower. The maximum sustainable interface pressure can be backed out of the equation for hoop stress in a thick walled cylinder, Table 32, Case 1a [26], as:

$$p_h = \frac{\sigma_{Lh}}{\dfrac{r_{Loh}^2 + r_{Lih}^2}{r_{Loh}^2 - r_{Lih}^2}} = 215 \, psi$$

A conservative upper bound external pressure of 225 psi, applied to the inner shell, represents the worst case lead contraction loading for the NCT hot condition.

2.6.1.3 Stress Calculations

2.6.1.3.1 Stresses Due to Pressure Loading

The finite element model described in Appendix 2.12.4, *Stress Analysis Finite Element Models,* is loaded with the internal maximum design pressure of 25 psi, without thermal loading, and gives the result discussed in Section 2.12.4.4.1, *Case No. 1, Design Pressure Only,* and shown in Figure 2.12.4-5. The maximum overall stress intensity which results from the model, which bounds both the primary membrane and membrane plus bending stress, is 14,333 psi, located near a stress concentration caused by the bolt preload. Since this value is less than the lowest (primary membrane) stress allowable, as shown in Section 2.6.1.4, *Comparison with Allowable Stresses,* it is not necessary to identify the individual stress components.

2.6.1.3.2 Stresses Due to Thermal Loading

The same finite element model is loaded with 25 psi internal pressure and the lead contraction pressure determined in Section 2.6.1.2.2, *Lead,* and gives the result discussed in Section 2.12.4.4.2, Case No. 2, *Lead Shrinkage Pressure,* and shown in Figure 2.12.4-7. Since the 380-B package has a simple pressure vessel design, having relatively modest temperature gradients of less than 10 °F (see Figure 3.3-2), thermal stresses due to self-constraint of the steel structure under NCT temperatures will not be significant, and are not specifically evaluated. The maximum overall stress intensity due to pressure and lead shrinkage loading is 14,139 psi. As for the pressure loading case, this stress is located near a stress concentration caused by the bolt preload. Since this value is less than the lowest (primary membrane) stress allowable, as shown in Section 2.6.1.4, *Comparison with Allowable Stresses,* it is not necessary to identify the individual stress components.

2.6.1.4 Comparison with Allowable Stresses

As stated in Section 2.6.1.3.1, *Stresses Due to Pressure Loading*, the maximum pressure stress is conservatively compared to the lowest (primary membrane) stress allowable, which is S_m per Table 2.1-1. At the bounding temperature of 150 °F given in Section 2.6.1.1, *Summary of Pressures and Temperatures*, the value of S_m for Type 304 is 20,000 psi from Table 2.6-1. The margin of safety is:

$$MS = \frac{20,000}{14,333} - 1 = +0.40$$

From Table 2.1-1, the limit on the range of primary plus secondary stress intensity is $3S_m$. For the range of stress intensity of 14,139 psi given in Section 2.6.1.3.2, *Stresses Due to Thermal Loading*, the margin of safety is:

$$MS = \frac{(3)20,000}{14,139} - 1 = +3.24$$

Thus, the margin of safety for the NCT warm condition is sufficient.

2.6.1.5 Closure Bolts

Thirty-six closure bolts attach the closure lid to the cask body. The closure lid is sized such that support against lateral loads (in the plane of the lid) is obtained from the fit between the lid and the cask body, thus preventing any shear loading of the closure bolts. In addition, the lid is prepared with a step located on the bolt circle which extends to the outer edge of the lid. The step prevents any bolt prying or significant bolt bending from occurring as a result of lid deformation. The design pressure is set at 25 psig.

The closure bolts are tightened to 900 ± 50 ft-lb of torque, or a maximum of 950 ft-lb. From Section 4.2 of NUREG/CR-6007 [11], the maximum non-prying tensile force per bolt due to the preload, Fa_max, is found from:

$$Fa\_max = \frac{Q\max}{(K)(Db)} = 50,667 \; lb$$

where Qmax = 950 × 12 = 11,400 in-lb is the maximum bolt torque, K = 0.15 is the nut factor for a lubricated bolt (approximately equal to the average of the values for lubricated surfaces in Table 4.1 of [11]), and Db = 1.5 inches is the nominal diameter of the closure bolt. The maximum residual torsion is 50% of the applied torsion, or:

$$Mtr = 0.5(Q\max) = 5,700 \; in - lb$$

From Section 4.4 of [11], the maximum non-prying tensile force per bolt, Fa_max, due to pressure loads are:

$$Fa\_max = \frac{\pi D \lg^2 (Pli - Plo)}{4Nb} = 1,782 \; lb$$

where Dlg = 47.50 inches is the diameter of the pressure boundary, i.e., the inner (containment) O-ring seal, Pli = 25 psig + 14.7 psia = 39.7 psia is the internal pressure, Plo = 3.5 psia is the NCT cold external reduced pressure as required by 10 CFR §71.71(3), and Nb = 36 is the

quantity of closure bolts. From this evaluation, it is clear that the preload force is governing over the pressure force.

Even though the temperatures of the closure lid and bolts are the same, a thermally induced loading is applied to the closure bolts due to the difference in thermal expansion coefficient between the ASTM A564 closure bolts and the Type 304 stainless steel closure lid. From Section 4.5 of [11], the maximum non-prying tensile force due to thermal expansion effects is:

$$Fa = \frac{\pi}{4} Dbs^2 (Eb)[al(Tl) - ab(Tb)] = 7,259\ lb$$

where the thermal expansion coefficient of the closure lid material, al = $8.75(10^{-6})$ in/in/°F from Table 2.6-1, the modulus of elasticity of the bolt, Eb = $28.05(10^6)$ psi, and the thermal expansion coefficient of the bolt, ab = $6.35(10^{-6})$ in/in/°F, from Table 2.6-1. The diameter of the bolt shank, which governs the elastic behavior of the bolt, is Dbs = 1.31 inches. The change in temperature of both components, Tl = Tb = (150 – 70) = 80 °F, where the bounding temperature of the components is 150 °F, and the ambient temperature is 70 °F.

The combined bolt load due to preload and thermal expansion is equal to 50,667 + 7,259 = 57,926 lb. The corresponding average axial bolt stress is:

$$Sba = 1.2732 \frac{(57,926)}{Dbs^2} = 42,976\ psi$$

where the load term in the numerator is the sum of the preload and thermal loads. The thread stress diameter is equal to Dba = Db – 0.9743(p) = 1.34 inches, where Db is 1.5 inches and the pitch, p, is 0.167 for the 1-1/2-6 UNC bolt. However, since the shank diameter, Dbs = 1.31 inches is smaller than the thread stress diameter, the shank diameter governs the stress calculation. The residual torsional stress is:

$$Sbt = \frac{5.093(Mtr)}{Dbs^3} = 12,913\ psi$$

From Table 6.1 of [11], for NCT the allowable average tensile stress is $S_m = (2/3)S_y$, which, using the yield strength value from Table 2.6-1 is equal to 73,767 psi at the NCT hot temperature of 150 °F. The margin of safety is:

$$MS_{Sba} = \frac{73,767}{Sba} - 1 = +0.72$$

Combining the axial and residual torsional shear stresses, the maximum closure bolt stress intensity is:

$$Sbi = \sqrt{Sba^2 + 4Sbt^2} = 50,139\ psi$$

As noted at the beginning of this section, bolt shear or prying loads are precluded by the design of the closure lid. From Table 6.1 of [11], the allowable stress intensity is $1.35S_m$ for cases where S_y is greater than 100 ksi. The margin of safety is:

$$MS_{Sbi} = \frac{1.35(73,767)}{Sbi} - 1 = +0.99$$

Thus, the closure bolts are not of concern for the NCT hot condition, including the reduced external pressure load case.

2.6.2 Cold

For the cold condition, a -40 °F steady state ambient temperature is utilized per Regulatory Guide 7.8 [3], with zero insolation and zero decay heat. This results in a uniform temperature of -40 °F throughout the cask.

In Section 2.6.1, *Heat*, the interface pressure between the cask inner shell and the lead gamma shielding was evaluated at the NCT hot condition. Since the lead will contract further at lower temperatures, that analysis is now repeated for the NCT cold condition to determine the maximum overall interface pressure. Note that the entire strain history of the lead is assumed to occur at a temperature of -40 °F, which conservatively maximizes interface pressure. All of the strain actually occurs at temperatures warmer than -40 °F, where the yield stress is lower.

The amount of interference between the lead and the inner shell depends upon the free state radii of these components, both at -40 °F. The free state outer radius of the inner shell at -40 °F is:

$$r_{ioc} = r_{io}[1 + \alpha_{s-40}(-40 - 70)] = 20.482 \, inches$$

where the outer free state radius of the inner shell at room temperature, $r_{io} = 20.5$ inches, and the coefficient of thermal expansion of the shell at -40 °F, $\alpha_{s-40} = 8.2(10^{-6})$/°F from Table 2.6-2.

To determine the free state radii of the lead at -40 °F, it is necessary to start with the radii of the steel shells at the lead solidification point at 620 °F, at which point all of the components are in stress free contact. The radii of the lead/steel interfaces at 620 °F were found above. The value $r_{Li620} = 20.612$ inches represents the inner radius of the lead and $r_{Lo620} = 27.147$ inches represents the outer lead radius. These values are then used to find the free state lead dimensions at the cold temperature of -40 °F as follows. Note that two thermal expansion terms are used (first contracting the lead from 620 °F to 70 °F, then contracting it further from 70 °F to -40 °F), since the thermal expansion coefficients given in Table 2.6-2 are based on 70 °F.

$$r_{Lic} = r_{Li620}[1 + \alpha_{L620}(70 - 620) + \alpha_{L-40}(-40 - 70)] = 20.344 \, inches$$

$$r_{Loc} = r_{Lo620}[1 + \alpha_{L620}(70 - 620) + \alpha_{L-40}(-40 - 70)] = 26.795 \, inches$$

where r_{Lic} is the free state inner radius of the lead, and r_{Loc} is the outer radius, at -40 °F. From Table 2.6-2, the thermal expansion coefficient of the lead from 620 °F to 70 °F, $\alpha_{L620} = 20.4(10^{-6})$/°F, and from 70 °F to -40 °F, $\alpha_{L-40} = 15.6(10^{-6})$/°F. Since the lead has a relatively low yield stress, the interface pressure between the inner shell and the lead will be governed by the lead yield stress, which in turn depends on the location of the lead stress state on the lead stress-strain curve. The hoop strain in the lead is equal to u/r, where u represents the radial displacement of the inner surface, and r is the inner radius of the lead. The interface pressure can be conservatively maximized by assuming that the inner shell is rigid, and therefore all of the radial interference is taken by the lead. The radial interference is:

$$u = r_{ioc} - r_{Lic} = 0.138 \, inches$$

The maximum lead strain is then:

$$\varepsilon_{Lh} = \frac{u}{r_{Lic}}(100) = 0.678\%$$

Stress-strain curves for lead at various temperatures are reproduced in Figure 2.2-1. From the curve representing a lead temperature of -40 °F, the maximum lead stress corresponding to a strain of 0.678% is bounded by $\sigma_{Lc} = 1,400$ psi. The maximum sustainable interface pressure can be backed out of the equation for hoop stress in a thick walled cylinder, Table 32, Case 1a [26], as:

$$p_c = \frac{\sigma_{Lc}}{\dfrac{r_{Loc}^2 + r_{Lic}^2}{r_{Loc}^2 - r_{Lic}^2}} = 376 \; psi$$

Using this external pressure, the inner shell membrane stress is:

$$\sigma_i = \frac{p_c r_{avg}}{t} = 4,951 \; psi$$

where r_{avg} is the minimum average inner shell radius, 19.75 inches, and t is the wall thickness of 1.5 inches. From Table 2.1-1, the allowable stress is S_m. From Table 2.6-1, $S_m = 20,000$ psi at 150 °F, which also applies to -40 °F. The margin of safety is:

$$MS = \frac{20,000}{4,951} - 1 = +3.04$$

The maximum external pressure p_c is also used in the shell buckling evaluation.

Since the coefficient of thermal expansion of the closure lid material is slightly larger than that of the bolting material, a reduction in closure bolt preload will occur at the NCT cold condition. Using the terminology of [11], the reduction in preload is:

$$Fa = \frac{\pi}{4} Dbs^2 (Eb)[al(Tl) - ab(Tb)] = -8,629 \; lb$$

where the bolt shank diameter, Dbs = 1.31 inches, the bolt modulus of elasticity, Eb = 29.1(10⁶) psi and the coefficient of thermal expansion of the bolt material, ab = 6.2(10⁻⁶) in/in/°F from Table 2.6-1, the coefficient of thermal expansion of the lid material, al = 8.2(10⁻⁶) in/in/°F from Table 2.6-1, and Tl = Tb = -40 – 70 = –110 °F. The minimum bolt preload torque is 900 ft-lb minus 50 ft-lb, or Qmin = 10,200 in-lb. The minimum room temperature bolt preload force is:

$$Fa\_min = \frac{Q\min}{K(Db)} = 45,333 \; lb$$

where Db is 1.5 inches and K = 0.15 as stated above. Thus, the residual preload at the NCT minimum temperature of -40 °F is 45,333 – 8,629 = 36,704 lb, or a reduction of 19%. This is adequate to maintain the compression of the containment O-ring under the NCT cold condition.

Therefore, the NCT cold condition is not of concern.

2.6.3   Reduced External Pressure

The effect of reduced external pressure of 3.5 psia, per 10 CFR §71.71(c)(3), is considered negligible for the 380-B package compared to other design loadings. This conclusion is based on

the NCT structural analyses presented in Section 2.6.1, *Heat*, demonstrating the structural integrity for a 25 psig internal design pressure. Based on the Maximum Normal Operating Pressure (MNOP) of 10 psig, the reduced external pressure conditions would cause a pressure of 21.2 psig. Therefore, the 25 psig internal design pressure analysis is conservatively bounding for the reduced external pressure case.

2.6.4 Increased External Pressure

The effect of an increased external pressure of 20 psia, per 10 CFR §71.71(c)(4), is acceptable for the 380-B package. Consistent with Regulatory Guide 7.8 [3], this loading corresponds to a minimum ambient temperature of -20 °F, no insolation, no decay heat, and minimum internal pressure. Conservatively, a minimum ambient temperature of -40 °F is used. Additionally, the fabrication stress resulting from the shrinking of the radial lead shield of p_c = 376 psi (see Section 2.6.2, *Cold*) is included as a radial pressure on the outside of the inner shell. Conservatively, the inner shell is evaluated neglecting the outer shell, even though the external pressure would be applied to the much stronger outer shell rather than the inner shell. As an additional conservatism, an external pressure of p_o = 21.7 psig will be applied which equals the external pressure required for the HAC immersion condition per 10 CFR §71.73(c)(6) and thus bounds the pressure required in this evaluation. The combined external pressure (lead shrinkage plus immersion) on the shell side is therefore p_{ext} = p_c + p_o = 397.7 psig.

Since the cask is closed under ambient conditions, the internal pressure in the cask at a temperature of -40 °F is

$$p_i = p_{amb} \frac{(-40 + 460)}{(70 + 460)} = 11.6 \ psia$$

where p_{amb} is 14.7 psia. Therefore the net equivalent differential gas pressure on the shell side is p_{ds} = 397.7 + (14.7 − 11.6) = 400.8 psi. An upper bound value of p_{ds} = 410 psi is used. The net differential gas pressure on the cask ends is p_{de} = 21.7 + (14.7 − 11.6) = 24.8 psi.

The compressive hoop stress is:

$$\sigma_\theta = p_{ds} \frac{r_{avg}}{t} = 5,398 \ psi$$

where the mean inner shell radius, r_{avg} = 19.75 inches, and the thickness, t = 1.5 inches. The compressive axial stress, obtained by supporting the pressure load from the entire cask cross section over the inner shell cross section, is:

$$\sigma_\phi = \frac{p_{de} \pi r_{cask}^2}{2 \pi r_{avg} t} = 346 \ psi$$

where r_{cask} = 57.5/2 = 28.75 inches. Using Mohr's circle, the maximum shear stress is:

$$\sigma_{\phi\theta} = \frac{1}{2}(\sigma_\theta - \sigma_\phi) = 2,526 \ psi$$

The maximum stress intensity is twice this value, or SI = 5,052 psi. From Table 2.6-1, the allowable membrane stress intensity for the inner shell is 20,000 psi. The margin of safety is:

$$MS = \frac{20{,}000}{5{,}052} - 1 = +2.96$$

The effect of the pressure on the flat bottom plate is evaluated using Table 24, Case 10b of [26]. The evaluation assumes a fixed edge, uniformly loaded plate. The bottom plate is bounding since its diameter is larger than the inner plate of the closure lid. Conservatively, the dead weight of the lower lead shield and the self-weight of the plate are added to the pressure. The lead is 6 inches thick, and the plate is 2.5 inches thick. The total applied pressure is:

$$p_{end} = 6.0(0.41) + 2.5(0.29) + 21.7 = 24.9 \ psi$$

where 0.41 and 0.29 are the densities of lead and stainless steel, respectively. The maximum bending moment at the edge of the plate is:

$$M = \frac{qa^2}{8} = 1{,}123.6 \ in - lb/in$$

where the radius, a = 38.0/2 = 19.0 inches. The stress is:

$$\sigma = \frac{6M}{t^2} = 1{,}078.6 \ psi$$

where the plate thickness, t = 2.5 inches. The allowable membrane plus bending stress for NCT, from Table 2.1-1, is 1.5S_m, which, from Table 2.6-1, is equal to 30,000 psi at 150 °F, which also applies to -40 °F. The margin of safety is:

$$MS = \frac{30{,}000}{1{,}078.6} - 1 = +26.8$$

The possibility of buckling of the inner shell due to external pressure is evaluated using [14]. Consistent with Regulatory Guide 7.6 [2], a factor of safety corresponding to ASME B&PV Code, Service Level A is employed. In this case, the applicable factor of safety is 2.00 for normal conditions, as specified in [14]. All interaction check values, including the maximum value of 0.4500, are less than unity, as required. Thus, the increased external pressure load case of 10 CFR §71.71(c)(4) is not of concern. The detailed buckling analysis is presented in Appendix 2.12.6, *Cask Shell Buckling Evaluations*.

2.6.5 Vibration

The effects of vibration normally incident to transport are shown to be insignificant. Draft ANSI Standard N14.23 [27] identifies peak truck trailer vibration inputs. Table 2 of [27] shows peak vibration accelerations of a trailer bed as a function of package and tiedown system natural frequency. For the frequency range 0 to 5 Hz, and conservatively assuming a light package, Table 2 gives peak accelerations (99% level) of 2g in the vertical direction, and 0.1g in both the lateral and longitudinal directions. All other frequency ranges give significantly lower vertical acceleration levels. Due to cask symmetry, the vertical load of ±2g governs the ±0.1g in the lateral and longitudinal directions.

Design fatigue curves are taken from Figure I-9.2 and Table I-9.2 of [13] for the Type 304 stainless steel cask material, from which the allowable amplitude, S_a, of the alternating stress component (1/2 of the alternating stress range) as a function of number of loading cycles may be

obtained. Table I-9.2 extends the fatigue allowable data to the endurance limit, which is used in the fatigue assessment of transportation vibration. The allowable amplitude, S_a, from Table I-9.2 for Type 304 stainless steel cask material at 10^{11} cycles is 13,600 psi. This value is adjusted based on the ratio of room temperature elastic modulus of $28.3(10)^6$ psi, which is the basis for Table I-9.2, and the elastic modulus at NCT maximum temperature, as follows:

$$S_a = 13,600 \left[\frac{27.8(10^6)}{28.3(10^6)} \right] = 13,360 \, \text{psi}$$

where $27.8 (10^6)$ psi is the elastic modulus at the bounding temperature of all cask components of 150 °F from Table 2.6-1.

The 380-B package is transported vertically. In this orientation, the closure lid experiences the ±2g loading transverse to the plane of the lid. A bounding stress value for a 2g load can be obtained from the upper cover plate. Although this is not a containment component, the stress in the plate will bound the stress in the thicker, lower containment plate of the lid. This is because while the mass of the plate increases with the first power of thickness, the bending stiffness increases as t^2, thus a thinner plate will have the higher stress under the same inertia load.

The thickness of the closure plate is 1.5 inches. Since the density of stainless steel is 0.29 lb/in^3, the unit weight of the plate is $0.29 \times 1.5 = 0.435$ psi. The radius, a = 22.75 inches. Under a load of 2g, the maximum bending moment in the plate (at the center) is found from Table 24, Case 10a of [26], and is:

$$M = 2K_M q a^2 = 92.9 \, in - lb/in$$

where the factor 2 is the vibrational load, and $K_M = 0.20625$ for $r_o = 0$ from [26]. The stress in the closure lid is:

$$\sigma = \frac{6M}{t^2} = 247.7 \, psi$$

where the thickness of the upper closure plate, t = 1.5 inches. For the allowable amplitude, S_a, found above, equal to 13,360 psi, the margin of safety against fatigue due to vibration is:

$$MS = \frac{13,360}{247.7} - 1 = +52.9$$

Therefore, fatigue of the 380-B package due to transportation vibration is not of concern.

2.6.6 Water Spray

The materials of construction used in the 380-B package are not affected by the water spray test identified in 10 CFR §71.71(c)(6). The exterior surfaces of the packaging are predominantly Type 304 stainless steel that is not compromised by exposure to water for 1-hour. This test was not performed and is unnecessary due to the materials of construction.

2.6.7 Free Drop

Section 10 CFR §71.71(c)(7) specifies a free drop from a height of 1 ft for a package weight more than 33,100 lb. The governing orientations of top end, bottom end, and side are evaluated

for the NCT free drop event. The choice of governing orientations is discussed in further detail in Appendix 2.12.2, *Certification Test Plan*. NCT free drop impacts are developed in Appendix 2.12.5, *Free Drop Impact Evaluation*. A value of 35g is chosen to bound the calculated impact magnitude for all NCT drop orientations.

A personnel barrier is used to restrict access to the space between the two impact limiters. The personnel barrier is made in two halves. Each half section is attached at each axial edge to the adjacent impact limiter at four bracket locations (total of eight fastenings per half-barrier). The attachment fasteners include padlocks and/or wire lock pins, and the attachment brackets are welded to the personnel barrier and to the impact limiter shell. The barrier and related components are made of ductile, Type 304 stainless steel. The only free drop orientation which could present the potential for damage to the personnel barrier is the side drop. According to Table 2.12.5-10, the maximum deformation of the impact limiter outer diameter (and thus the personnel barrier) in the NCT side drop is 2.1 inches. Based on the geometry of a circle, this radial deformation corresponds to a width of approximately 28 inches. Because the attachment locations are distributed equally around the 100-inch impact limiter diameter, they are separated by approximately 39 inches. Thus, even if the NCT free drop side orientation impact caused the loss of two, or even four of the attachments, there will exist at least four more attachments on the affected half-barrier to maintain the position of the personnel barrier on the package. Thus, the personnel barrier will remain effective for all NCT.

Cask body stresses are analyzed for the NCT free drop using the same finite element model identified in Section 2.6.1.3, *Stress Calculations*, and which is also used for evaluation of the HAC free drop event. A full discussion of the model and the calculation results is given in Appendix 2.12.4, *Stress Analysis Finite Element Models*. The model is loaded by a global, quasi-static acceleration field consistent with an impact of 35g. The cask stress analysis for NCT is identical with the analysis for HAC, except for the acceleration value and allowable stresses.

Each stress calculated from the quasi-static model is increased by the dynamic load factor (DLF), equal to 1.15, as calculated in Section 2.7.1.5, *Dynamic Load Factor*.

As discussed in Section 2.7.1.4, *Oblique Drop*, cask stresses are governed by those resulting from the end and side drop orientations. The stress analyses for NCT free drop are given in Sections 2.6.7.1, *NCT Bottom Down End Drop*, 2.6.7.2, *NCT Top Down End Drop* and 2.6.7.3, *NCT Side Drop*.

2.6.7.1 NCT Bottom Down End Drop

From Section 2.12.4.4.3, *Case No. 3, NCT Bottom-Down End Drop*, the maximum linearized membrane stress intensity resulting from the bottom-down impact of 35g is 4,359 psi, located at the center of the bottom outer plate, as shown in Figure 2.12.4-11. From Table 2.1-1, the limit on primary membrane stress is S_m. At the bounding temperature of 150 °F, the value of S_m for Type 304 is 20,000 psi from Table 2.6-1. The margin of safety is:

$$MS = \frac{20,000}{(1.15)4,359} - 1 = +2.99$$

The maximum linearized primary membrane plus bending stress intensity is 16,420 psi, located at the outer edge of the bottom outer plate as shown in Figure 2.12.4-12. From Table 2.1-1, the

limit on primary membrane plus bending stress is $1.5S_m$. At the bounding temperature of 150 °F, the value of S_m for Type 304 is 30,000 psi from Table 2.6-1. The margin of safety is:

$$MS = \frac{30,000}{(1.15)16,420} - 1 = +0.59$$

From Section 2.12.4.4.10, *Case No. 3b, NCT Bottom-Down End Drop with Cold Lead Shrinkage Pressure*, the maximum linearized membrane stress intensity resulting from the bottom-down impact of 35g is 4,531 psi, located at the center of the bottom outer plate, as shown in Figure 2.12.4-52. From Table 2.1-1, the limit on primary membrane stress is S_m. At the bounding temperature of 150 °F, the value of S_m for Type 304 is 20,000 psi from Table 2.6-1. The margin of safety is:

$$MS = \frac{20,000}{(1.15)4,531} - 1 = +2.84$$

The maximum linearized primary membrane plus bending stress intensity is 16,580 psi, located at the outer edge of the bottom outer plate as shown in Figure 2.12.4-53. From Table 2.1-1, the limit on primary membrane plus bending stress is $1.5S_m$. At the bounding temperature of 150 °F, the value of S_m for Type 304 is 30,000 psi from Table 2.6-1. The margin of safety is:

$$MS = \frac{30,000}{(1.15)16,580} - 1 = +0.57$$

The NCT membrane plus bending plus secondary stress allowable is 60,000 psi. The lead shrinkage pressure applied to the outside surface of the inner shell creates a self-limiting, strain-controlled, fabrication stress that must meet the NCT membrane plus bending plus secondary stress allowable. The inner shell, where the lead shrinkage pressure is applied, is not an area of high stress as shown in the stress plots. Therefore, no comparison to the NCT membrane plus bending plus secondary stress allowable is necessary.

Buckling of the cask shells will be evaluated using ASME B&PV Code Case N-284-4 [14]. Since the only difference between the NCT and HAC free drops is the impact magnitude and the applied factor of safety, it is possible to determine the bounding case. The cask shells are subject to buckling loads in the end drop orientation. Due to its much greater stiffness compared to the inner shell, the cask outer shell will carry most of the axial loading. Thus, the outer shell is conservatively assumed to carry the entire axial load without assistance from the inner shell. Thermal stress is not included as discussed in Section 2.6.1.3.2, *Stresses Due to Thermal Loading*. No other stresses are applied for the end drop buckling evaluation.

Since the HAC end drop is evaluated for an impact of 100g and the NCT for 35g, and the factor of safety required by Code Case N-284-4 is 1.34 for HAC and 2.00 for NCT, the equivalent loading for the two cases is:

$$\text{HAC: } 100 \times 1.34 = 134, \text{ NCT: } 35 \times 2.00 = 70$$

Thus, the HAC free drop case bounds the NCT case. The HAC buckling evaluation is presented in Section 2.7.1.2, *End Drop*.

The inner cover is located at the top of the cask cavity by retainers that clamp four shear steps which are welded to the cask inner shell. The weight of the inner cover is:

$$W_{SP} = \frac{\pi}{4}\left(37.75^2 \times 2 - 33.75^2 \times 1.5\right)(0.29) = 260 \; lb$$

where the ring's outer diameter is 37.75 inches, the inner diameter of the perimeter stiffener ring is 33.75 inches, the plate is ½ inches thick, and the stiffener ring is 1.5 inches thick. The four shear steps are 4.97 inches long, and have ¼-inch groove welds on both long sides attaching them to the cask inner shell wall (the groove welds on the short ends are conservatively neglected). The shear area is:

$$A = 4 \times 4.97 \times 0.25 \times 2 = 9.94 \; in^2$$

In an end drop, the inner cover is supported by the shear steps. The shear stress in the shear step attachment groove welds at 35g is:

$$\tau = \frac{260 \times 35}{9.94} = 915.5 \; psi$$

From Table 2.1-1, the allowable for pure shear stress is $0.6S_m$, which for Type 304 stainless steel at 150 °F is equal to $0.6 \times 20,000 = 12,000$ psi. The margin of safety is:

$$MS = \frac{12,000}{(1.15)915.5} - 1 = +10.4$$

As shown, all cask body margins of safety for the NCT bottom down end drop condition are positive.

2.6.7.2   NCT Top Down End Drop

From Section 2.12.4.4.5, *Case No. 5, NCT Top-Down End Drop*, the maximum linearized membrane stress intensity resulting from the top-down impact of 35g is 5,873 psi, located at the center of the lid outer plate, as shown in Figure 2.12.4-24. From Table 2.1-1, the limit on primary membrane stress is S_m. At the bounding temperature of 150 °F, the value of S_m for Type 304 is 20,000 psi from Table 2.6-1. The margin of safety is:

$$MS = \frac{20,000}{(1.15)5,873} - 1 = +1.96$$

The maximum linearized primary membrane plus bending stress intensity is 16,170 psi, located at the center of the lid outer plate as shown in Figure 2.12.4-24. From Table 2.1-1, the limit on primary membrane plus bending stress is $1.5S_m$. At the bounding temperature of 150 °F, the value of S_m for Type 304 is 30,000 psi from Table 2.6-1. The margin of safety is:

$$MS = \frac{30,000}{(1.15)16,170} - 1 = +0.61$$

From Section 2.12.4.4.11, *Case No. 5b, NCT Top-Down End Drop with Cold Lead Shrinkage Pressure*, the maximum linearized membrane stress intensity resulting from the top-down impact of 35g is 5,859 psi, located at the center of the lid outer plate, as shown in Figure 2.12.4-58. From Table 2.1-1, the limit on primary membrane stress is S_m. At the bounding temperature of 150 °F, the value of S_m for Type 304 is 20,000 psi from Table 2.6-1. The margin of safety is:

$$MS = \frac{20,000}{(1.15)5,859} - 1 = + 1.97$$

The maximum linearized primary membrane plus bending stress intensity is 16,180 psi, located at the center of the lid outer plate as shown in Figure 2.12.4-58. From Table 2.1-1, the limit on primary membrane plus bending stress is $1.5S_m$. At the bounding temperature of 150 °F, the value of S_m for Type 304 is 30,000 psi from Table 2.6-1. The margin of safety is:

$$MS = \frac{30,000}{(1.15)16,180} - 1 = + 0.61$$

The NCT membrane plus bending plus secondary stress allowable is 60,000 psi. The lead shrinkage pressure applied to the outside surface of the inner shell creates a self-limiting, strain-controlled, fabrication stress that must meet the NCT membrane plus bending plus secondary stress allowable. The inner shell, where the lead shrinkage pressure is applied, is not an area of high stress as shown in the stress plots. Therefore, no comparison to the NCT membrane plus bending plus secondary stress allowable is necessary.

Since both impact limiters have essentially identical construction, they have the same impact response, and the buckling evaluation for the bottom down end drop summarized in Section 2.6.7.1, *NCT Bottom Down End Drop*, applies equally to the top down end drop.

In the top-down orientation, the NCT non-prying closure bolt load is calculated according to Section 4.6 of [11] using:

$$Fa = \frac{1.34\sin(xi)(DLF)(ai)(Wl + Wc)}{Nb} = 28,466 \; lb$$

where the impact angle, $xi = 90°$ for the end drop impact, the dynamic load factor, $DLF = 1.15$, the bounding NCT free drop impact magnitude, $ai = 35g$, the weight of the lid is bounded by $Wl = 7,000$ lb from Table 2.1-2, and the weight of the contents, $Wc = 12,000$ lb from Table 2.1-2, and the quantity of bolts, $Nb = 36$. Note that no support for the lid is assumed from the inner surface of the impact limiter.

The applied bolt load due to the design pressure, found in Section 2.6.1.5, *Closure Bolts*, is 1,782 lb. The sum of the NCT free drop load plus the load due to the design pressure is equal to $28,466 + 1,782 = 30,248$ lb. This value is however much less than the sum of preload and thermal expansion load, equal to 57,926 lb from Section 2.6.1.5, *Closure Bolts*. Therefore, the bolt load in the NCT free drop event is governed by the preload plus thermal load, and the margins of safety calculated in Section 2.6.1.5, *Closure Bolts* are not affected by the NCT free drop event.

In the top down free drop, the inner cover will be loaded by the contents of the cask, which could overload the attachment of the inner cover to the cask. However, the nominal gap between the top of the inner cover and the inner surface of the closure lid is ¼ inches. Thus, the maximum translation of the inner cover in the top down free drop is only ¼ inches, and the inner cover will remain capable of excluding a payload radioactive source (should it become loose inside the cask cavity) from locating in the corner between the side wall and closure lid. See Section 5.3.1, *Configuration of Source and Shielding*, for more discussion relative to the shielding evaluation.

As shown, all cask body margins of safety for the NCT top down end drop condition are positive.

2.6.7.3 NCT Side Drop

The NCT side free drop is evaluated using the same finite element model which was used for the end drop case. The quasi-static acceleration of 35g also applies to the side drop, since it bounds the calculated side drop impact as shown in Table 2.12.5-10. The side drop orientation is governing over the slapdown orientation as discussed in Section 2.7.1.4, *Oblique Drop*.

From Section 2.12.4.4.7, *Case No. 7, NCT Side Drop*, the maximum linearized primary membrane stress intensity resulting from the side drop impact of 35g is 11,500 psi, located at the bottom of the outer shell, as shown in Figure 2.12.4-39. From Table 2.1-1, the limit on primary membrane stress is S_m. At the bounding temperature of 150 °F, the value of S_m for Type 304 is 20,000 psi from Table 2.6-1. The margin of safety is:

$$MS = \frac{20,000}{(1.15)11,500} - 1 = +0.51$$

The maximum linearized primary membrane plus bending stress intensity is 19,780 psi, located at the bottom of the outer shell, as shown in Figure 2.12.4-39. From Table 2.1-1, the limit on primary membrane plus bending stress is $1.5 S_m$. At the bounding temperature of 150 °F, the value of S_m for Type 304 is 30,000 psi from Table 2.6-1. The margin of safety is:

$$MS = \frac{30,000}{(1.15)19,780} - 1 = +0.32$$

From Section 2.12.4.4.12, *Case No. 7b, NCT Side Drop with Cold Lead Shrinkage Pressure*, the maximum linearized primary membrane stress intensity resulting from the side drop impact of 35g is 11,550 psi, located at the bottom of the outer shell, as shown in Figure 2.12.4-65. From Table 2.1-1, the limit on primary membrane stress is S_m. At the bounding temperature of 150 °F, the value of S_m for Type 304 is 20,000 psi from Table 2.6-1. The margin of safety is:

$$MS = \frac{20,000}{(1.15)11,550} - 1 = +0.51$$

The maximum linearized primary membrane plus bending stress intensity is 19,960 psi, located at the bottom of the outer shell, as shown in Figure 2.12.4-65. From Table 2.1-1, the limit on primary membrane plus bending stress is $1.5 S_m$. At the bounding temperature of 150 °F, the value of S_m for Type 304 is 30,000 psi from Table 2.6-1. The margin of safety is:

$$MS = \frac{30,000}{(1.15)19,960} - 1 = +0.31$$

The NCT membrane plus bending plus secondary stress allowable is 60,000 psi. The lead shrinkage pressure applied to the outside surface of the inner shell creates a self-limiting, strain-controlled, fabrication stress that must meet the NCT membrane plus bending plus secondary stress allowable. The inner shell, where the lead shrinkage pressure is applied, is not an area of high stress as shown in the stress plots. Therefore, no comparison to the NCT membrane plus bending plus secondary stress allowable is necessary.

As shown, the cask body margins of safety for the NCT side drop condition are positive.

2.6.8 Corner Drop

The 380-B package is not required to be evaluated for the corner drop condition, since 10 CFR §71.71(c)(8) applies only to rectangular fiberboard or wood packages weighing less than 110 lb or to cylindrical fiberboard or wood packages weighing less than 220 lb. The weight of the 380-B package exceeds these limits and therefore does not need to be evaluated for the NCT corner drop.

2.6.9 Compression

Section 10 CFR §71.71(c)(9) specifies, for packages weighing up to 11,000 lb, a compression loading equal to the greater of the equivalent of five times the package weight or 2 lb/in^2 over the package projected area. The 380-B weight exceeds this limit, and therefore does not need to be evaluated for compression.

2.6.10 Penetration

The impact of a 1.25-inch diameter, hemispherical ended, 13-lb steel bar, per 10 CFR §71.71(c)(10), dropped vertically from a height of 40 inches, would not have a significant effect on the 380-B package. Slight denting of the thermal shield on the outside of the cask could occur, but the bar could not penetrate or rip into the shield, and could not harm the impact limiters or impact limiter attachments. The minimum material thickness to prevent penetration for the specified test may be calculated using [33]:

$$t = \frac{E^{2/3}}{672D} = 0.015 \ inches$$

where E = 43.3 ft-lb is the potential energy of the 13-lb penetration bar for a 40-inch drop, and D = 1.25 inches is the penetration bar diameter. The impact limiter outer shell is 0.25-inch thick, and the cask thermal shield is 0.105-inch thick. Therefore, this test is unnecessary and was not performed.

Table 2.6-1 – Summary of NCT Design Parameters

Parameter	Containment (Type 304, Wrought or Forged)	Closure Bolts (A564, Grade 630, Condition H1100)
NCT Hot Bounding Temperature, °F	150	150
Coefficient of Thermal Expansion, α, (in/in/°F)	8.75×10^{-6}	6.35×10^{-6}
Elastic Modulus, psi	27.8×10^{6}	28.05×10^{6}
Design Stress, S_m, psi	20,000	73,767
Yield Stress, S_y, psi	27,500	110,650
Primary Membrane Stress Intensity (P_m), psi	$S_m = 20,000$	n/a*
Primary Membrane + Bending Stress Intensity ($P_m + P_b$), psi	$1.5 S_m = 30,000$	n/a*
Primary Membrane + Bending + Secondary Stress Intensity ($P_m + P_b + Q$), psi	$3.0 S_m = 60,000$	n/a*
NCT Cold Bounding Temperature, °F	-40	-40
Coefficient of Thermal Expansion, α, (in/in/°F)	8.2×10^{-6}	6.2×10^{-6}
Elastic Modulus, psi	28.9×10^{6}	29.1×10^{6}

* Bolting allowable stresses are discussed in the sections where they are used.

Table 2.6-2 – Summary of Thermal Expansion Coefficients, /°F

	-40 °F	100 °F	620 °F
Type 304 Stainless Steel	8.2×10^{-6}	8.6×10^{-6}	9.9×10^{-6}
Lead Shielding	15.6×10^{-6}	16.2×10^{-6}	20.4×10^{-6}

Table 2.6-3 – Summary of Margins of Safety for NCT

Component	Loading Condition	Minimum Margin of Safety
Heat, Section 2.6.1.4	Pressure, membrane	+0.40
	Pressure, membrane + bending	+3.24
Closure Bolts, Section 2.6.1.5	Preload + thermal	+0.72
	Axial + shear	+0.99
Cold, Section 2.6.2	Lead shrinkage pressure, membrane	+3.04
Increased External Pressure, Section 2.6.4	Inner shell, membrane	+2.96
	Bottom outer plate, membrane + bending	+26.8
	Inner shell buckling (Code Case N-284-4)	+0.4500*
Vibration, Section 2.6.5	Lid outer plate, fatigue	+52.9
Free drop, Section 2.6.7	Bottom down, membrane	+2.84
	Bottom down, membrane + bending	+0.57
	Inner cover step, shear	+10.4
	Top down, membrane	+1.96
	Top down, membrane + bending	+0.61
	Side down, membrane	+0.51
	Side down, membrane + bending	+0.31

*Maximum check value must be less than unity, see Appendix 2.12.6, *Cask Shell Buckling Evaluations*.

This page left intentionally blank.

2.7 Hypothetical Accident Conditions

When subjected to the hypothetical accident conditions as specified in 10 CFR §71.73 [1], the 380-B package meets the performance requirements specified in Subpart E of 10 CFR 71. This is demonstrated in the following subsections, where each accident condition is addressed and the cask shown to meet the applicable design criteria. The method of demonstration is primarily by analysis. The loads specified in 10 CFR §71.73 are applied sequentially, per Regulatory Guide 7.8 [3]. Resulting stresses are maintained below the limits established by Regulatory Guide 7.6 [2]. Dynamic testing of impact limiter performance is discussed in Section 2.12.3, *Certification Test Results*. A summary of cumulative damage is provided in Section 2.7.8, *Summary of Damage*.

2.7.1 Free Drop

Subpart F of 10 CFR 71 requires that a 30 ft free drop be considered. The free drop is to occur onto a flat, essentially unyielding, horizontal surface, and the cask is to strike the surface in an orientation for which maximum damage is expected. Several impact orientations and bounding ambient environments are considered. In order to minimize the number of specific analyses that must be performed, the worst case maximum cold drop impact loads are conservatively applied to the cask using material properties and allowables corresponding to maximum (warm) Normal Conditions of Transport (NCT) temperatures.

2.7.1.1 Impact Forces and Deformations

In Section 2.1.2.2, *Other Structures*, the design criteria of the impact limiters of the 380-B Package includes the requirement to limit the free drop impact such that cask component stress and deflection criteria are met. The impact and deformation response of the impact limiters is evaluated and discussed in Appendix 2.12.5, *Free Drop Impact Evaluation*. This appendix also includes a benchmark comparison of the analysis results to the results obtained from the half-scale certification testing of the impact limiters. The tests are discussed in Appendix 2.12.2, *Certification Test Plan*, and the results are reported in Appendix 2.12.3, *Certification Test Results*. The analysis results in Appendix 2.12.5, *Free Drop Impact Evaluation,* contributed to informing the choice of physical test orientations. The governing half-scale test results (i.e., cold accelerations and warm deformations) were all lower than originally predicted. The maximum equivalent full scale HAC impact occurred in the end impact orientation with cold foam, and was equal to 78g. (Half-scale impacts are converted to full scale by multiplying them by 0.5.) The analytically predicted maximum impact, assuming a lower-bound cold temperature of -40 °F, was 92.8g. The equivalent full scale certification test results are summarized and compared to the analytically predicted values in Table 2.7-1. All of the calculations in this section utilize a bounding HAC impact of 100g, which is higher than the maximum result obtained from either test or analysis for any orientation. Although no NCT tests were performed, the same conservative prediction techniques were used to set the bounding NCT impact at 35g, as described in Section 2.6.7, *Free Drop*.

The second design criterion of the impact limiters is to prevent "hard" contact of a rigid part of the cask with the ground due to excessive deformation of the foam. The horizontal side and center of

gravity (C.G.) over corner orientations were performed during certification testing (Test D2 and Test D3, see Appendix 2.12.3, *Certification Test Results*). These test orientations have the greatest potential for exceeding the crush capacity of the impact limiters, and were performed with the energy absorbing foam at the equivalent maximum NCT hot case temperature. In both cases, the impact limiter did not experience hard, or uncushioned impact. The maximum equivalent full scale crush distance in the certification test occurred in the C.G.-over-corner orientation, and amounted to 11.9 inches, or 60% of the available crush distance. (Half-scale impact limiter deformations are converted to full scale by multiplying them by 2.0.) The maximum predicted crush in the HAC free drop, assuming the bounding NCT warm foam temperature of 160 °F (conservatively higher than the actual bounding temperature of 150 °F) and minimum as-poured foam strength is 15.8 inches, or 80% of the available crush distance. Not only is the majority of the foam in the limiter at a lower value of strain than this maximum value, the value is well within the range in which strain energy absorption is effective.

The final requirement is that the impact limiter structures and attachments to the cask maintain sufficient integrity subsequent to the HAC free drop and puncture drop events so that the containment O–ring seal is protected from excessive temperature in the subsequent HAC fire event. As documented in Appendix 2.12.3, *Certification Test Results*, the impact limiter attachment bolts and lugs hold the impact limiters in the original position on the cask body during the free drop and puncture drop series. No separation between the impact limiters and cask body occurred, and essentially no deformation of the attachment bolts occurred in the certification tests. In addition, the worst–case damage to the impact limiter shells as a result of the puncture tests is fully accounted for in the thermal model, as discussed in Chapter 3, *Thermal Evaluation*.

It is noted that unexpected impact limiter shell damage occurred during the D2 free drop, performed at the NCT warm temperature in the C.G.-over-corner orientation. As shown in Figure 2.12.3-29, Figure 2.12.3-30, and Figure 2.12.3-31, the impact limiter shell split open along a butt joint weld seam located on the top flat annulus of the impact limiter. This seam was designed as a complete joint penetration (CJP) weld, but from Figure 2.12.3-31, it appears that the actual penetration depth was less than 50% of the material thickness. Since the split occurred only at the seam itself and since the seam was significantly underwelded, it is clear that the failure was related only to the faulty weld and that the strength of the base material was not exceeded. In other words, the failure would not have occurred in the absence of the joint or in the presence of a correctly welded CJP joint. The weld failure was judged an unacceptable condition due to its possible consequences in the HAC fire event, and to prevent its occurrence on production packaging, three design enhancements were made, as shown in Zone A-C/3 on sheet 4 of SAR drawing 1916-02-03-SAR:

1. The weld symbol requires fusion to the backing bar, which will ensure complete joint penetration.

2. Three joints near the weld failure in the impact limiter shells must be ultrasonically inspected as shown in flag note 5.

3. A reinforcing ring is used over the subject weld joint. The reinforcing ring consists of a ¼-inch thick, 2-inch wide ring which spans the weld joint, and is attached on the ID and OD using a continuous full-thickness fillet weld.

Test D2 was not repeated with the design enhancements in place. However, the reinforcing ring (without the improved weld symbol nor the ultrasonic inspection) was added to each half-scale impact limiter used in the side drop test (D3) as shown in Figure 2.12.3-35 and Figure 2.12.3-36. As shown in Figure 2.12.3-48 and Figure 2.12.3-49, the region of the subject weld, covered by the reinforcing ring, underwent significant deformation in the side drop impact, without failure or any signs of cracking or other material distress. These test results, along with incorporation of all three design enhancements in the production packagings, indicate that the performance of the subject weld joint is not of concern.

For these reasons, the performance of the impact limiters is considered acceptable.

2.7.1.2   End Drop

The HAC end orientation free drop is evaluated using a combination of computer and manual calculations using an acceleration of 100g as discussed in Section 2.7.1.1, *Impact Forces and Deformations*. Stresses in the cask body are evaluated using the finite element model described in Appendix 2.12.4, *Stress Analysis Finite Element Models*. Both bottom down and top down impact orientations are considered. Including manual calculations, four analyses of the HAC end drop are performed:

- Cask body stress
- Closure bolt stress
- Lead slump evaluation
- Buckling evaluation

Cask Body Stress. From Section 2.12.4.4.4, *Case No. 4, HAC Bottom-Down End Drop*, the maximum linearized primary membrane stress intensity resulting from the bottom-down impact of 100g is 12,110 psi, located at the center of the bottom outer plate, as shown in Figure 2.12.4-17. From Table 2.1-1, the limit on primary membrane stress is the lesser of $2.4S_m$ and $0.7S_u$, which for Type 304 forged material is $0.7S_u = 47,705$ psi at 150 °F. Applying the DLF of 1.15 from Section 2.7.1.5, *Dynamic Load Factor*, the margin of safety is:

$$MS = \frac{47,705}{(1.15)12,110} - 1 = +2.43$$

The maximum linearized membrane plus bending stress intensity is 45,240 psi, and occurs at the outside edge of the bottom outer plate as shown in Figure 2.12.4-18. The allowable membrane plus bending stress, from Table 2.1-1, is the lesser of $3.6S_m$ or S_u, which for Type 304 forged material is $S_u = 68,150$ psi at 150 °F. The margin of safety is:

$$MS = \frac{68,150}{(1.15)45,240} - 1 = +0.31$$

For stress specifically in the containment boundary, the maximum linearized membrane stress is 8,638 psi at the edge of the inner cavity bottom plate, as shown in Figure 2.12.4-20. The HAC membrane stress allowable is 47,705 psi. Applying the DLF of 1.15, the margin of safety is:

$$MS = \frac{47,705}{1.15(8,638)} - 1 = +3.80$$

The maximum linearized membrane plus bending stress in the containment boundary is 42,680 psi at the center of the cavity bottom plate, as shown in Figure 2.12.4-19. The HAC membrane plus bending stress allowable is 68,150 psi. Applying the DLF of 1.15, the margin of safety is:

$$MS = \frac{68,150}{1.15(42,680)} - 1 = +0.39$$

From Section 2.12.4.4.6, *Case No. 6, HAC Top-Down End Drop*, the maximum linearized primary membrane stress intensity resulting from the top-down impact of 100g is 14,690 psi, located at the center of the closure lid outer plate, as shown in Figure 2.12.4-31. The limit on primary membrane stress is identified above as 47,705 psi. The margin of safety is:

$$MS = \frac{47,705}{(1.15)14,690} - 1 = +1.82$$

The maximum linearized membrane plus bending stress intensity is 41,690 psi, also located at the center of the closure lid outer plate, as shown in Figure 2.12.4-31. The limit on membrane plus bending stress is identified above as 68,150 psi. The margin of safety is:

$$MS = \frac{68,150}{(1.15)41,690} - 1 = +0.42$$

For stress specifically in the containment boundary, the maximum linearized membrane stress is 8,573 psi at the bottom outside edge of the closure lid bottom plate, as shown in Figure 2.12.4-34. The HAC membrane stress allowable is 47,705 psi. Applying the DLF of 1.15, the margin of safety is:

$$MS = \frac{47,705}{1.15(8,573)} - 1 = +3.84$$

The maximum linearized membrane plus bending stress in the containment boundary is 40,260 psi at the bottom center of the closure lid bottom plate, as shown in Figure 2.12.4-33. The HAC membrane plus bending stress allowable is 68,150 psi. Applying the DLF of 1.15, the margin of safety is:

$$MS = \frac{68,150}{1.15(40,260)} - 1 = +0.47$$

As shown, all cask body margins of safety for the HAC end free drop condition are positive.

Closure Bolt Stress. In the top-down orientation, the HAC non-prying closure bolt load is calculated according to Section 4.6 of [11] using:

$$Fa = \frac{1.34\sin(xi)(DLF)(ai)(Wl + Wc)}{Nb} = 81,331\ lb$$

where the impact angle, xi = 90° for the end drop impact, the dynamic load factor, DLF = 1.15, the bounding HAC free drop impact magnitude is 100g, the weight of the lid is bounded by Wl =

7,000 lb, and the weight of the contents, Wc = 12,000 lb (10,000 lb maximum device weight plus up to 2,000 lb of dunnage), and the quantity of bolts, Nb = 36. Note that no support for the lid is assumed from the inner surface of the impact limiter. In addition, per Section 2.12.4.4.6, *Case No. 6, HAC Top-Down End Drop*, the gap between the closure lid and the cask body, created by the 0.06-inch step in the lid surface at the bolt circle, does not close as a result of lid deflection. Therefore, the lid step prevents prying loads on the closure bolts.

The sum of all applied loads (the HAC free drop load of 81,331 lb plus the load due to the design pressure, equal to 1,782 lb as determined in Section 2.6.1.5, *Closure Bolts*) is equal to Fa = 81,331 + 1,782 = 83,113 lb. This value exceeds the preload of 50,667 lb. The average tensile stress is:

$$Sba = 1.2732 \frac{Fa}{Dbs^2} = 61,663 \; psi$$

where the value of Dbs, the reduced shank diameter of the bolts, is 1.31 inches. From Table 2.1-1, the allowable average tensile stress intensity for HAC is the lesser of $0.7S_u$ or S_y. From Table 2.2-3, the governing value is $0.7S_u = 98,000$ psi at 150 °F. The margin of safety is:

$$MS = \frac{98,000}{61,663} - 1 = +0.59$$

Thus, the margin of safety of the closure lid bolts for the HAC end free drop condition is positive.

Lead Slump. In the end drop, impact forces act on the lead gamma shield which have the potential to cause a reconfiguration of the lead in the direction of impact. The lead could experience flow strains causing a gap to appear at the upper surface of the lead. The maximum amount of gap will correspond to the greatest force parallel to the cask axis, which occurs in the end free drop case. The gap will be greatest for the cold, -40 °F case, since the thermal shrinkage of the lead relative to the steel will be greatest, as well as having the greatest impact load. The HAC end free drop impact is bounded by 100g and is the same whether the impact is on the top or the bottom of the cask. Of note, since the closure lid lead shield and the bottom lead shield are installed manually, using small scraps and lead wool hammered into place to fill all cavities, lead slump cannot occur. The following analysis applies only to the side cavity in which lead is poured in the molten state. As shown below, the lead material does not reach its minimum flow stress in the end drop, and the gap is a result of shrinkage only.

The following analysis assumes that the lead will first slip downward until the axial shrinkage gap is completely transferred to the top of the lead. ("Top" in this context means the non-impact end.) Regardless of any friction that might exist, the radial shrinkage forces are assumed to be completely decayed due to creep in the lead, and no axial support is offered by the inner shell through friction.

At the lead solidification point of 620 °F, the lead fully fills the steel cavity without any gaps. As the cask cools to the minimum HAC temperature of -40 °F, the lead will shrink more than the cavity due to the greater thermal expansion coefficient of lead than steel, generating both axial and radial gaps. Both gaps are computed below and used in the shielding analysis in Section 5.3, *Shielding Model*.

Calculations going between 620 °F and -40 °F require two steps since the coefficients are referenced to 70 °F. Therefore, the temperature change between 620 °F and 70 °F is 550 °F, and between 70 °F and -40 °F is 110 °F. In the following calculations, the inner lead/steel interface is location 1, and the outer lead/steel interface is location 2. Thus,

D1S(T) = inner shell outer diameter at temperature T

D2S(T) = outer shell inner diameter at temperature T

D1L(T) = inner lead diameter at temperature T

D2L(T) = outer lead diameter at temperature T

LS(T) = length of steel cavity at temperature T

LL(T) = length of lead at temperature T

The thermal expansion or shrinkage of any dimension is equal to $\alpha\Delta T$, where α is the coefficient of thermal expansion, in/in/°F, and ΔT is the change in temperature. For example, if we denote the thermal expansion of steel between the temperatures of 70 °F and 620 °F as TES(620), then:

$$TES(620) = \left(\alpha_{s620}\Delta T_{620}\right) = 0.00545 \ in/in$$

where $\alpha_{s620} = 9.9(10^{-6})$ in/in/°F, and $\Delta T_{620} = 620 - 70 = 550$ °F.

Designation	α, in/in/°F, $\times 10^{-6}$ (Note 1)	ΔT, °F	Value, in/in	Thermal Expansion Description
TEL(620)	20.4	550	0.01122	Lead, between 620 and 70 °F
TEL(-40)	15.6	110	0.00172	Lead, between 70 and -40 °F
TES(620)	9.9	550	0.00545	Steel, between 620 and 70 °F
TES(-40)	8.2	110	0.00090	Steel, between 70 and -40 °F

Note 1: Thermal expansion coefficients taken from Table 2.2-1 for steel, and Table 2.2-4 for lead.

The inner shell outer diameter at the fabrication temperature of 70 °F is D1S(70) = 41 inches, the outer shell inner diameter is D2S(70) = 54 inches, and the length of the steel cavity, LS(70) = 54.5 inches. The dimensions of lead and steel at 620 °F are:

$$D1L(620) = D1S(620) = D1S(70)\left(1 + TES(620)\right) = 41.223 \ in$$

$$D2L(620) = D2S(620) = D2S(70)\left(1 + TES(620)\right) = 54.294 \ in$$

$$LL(620) = LS(620) = LS(70)\left(1 + TES(620)\right) = 54.797 \ in$$

The dimensions of the lead at 70 °F are:

$$D1L(70) = D1L(620)\left(1 - TEL(620)\right) = 40.760 \ in$$

$$D2L(70) = D2L(620)\left(1 - TEL(620)\right) = 53.685 \ in$$

$$LL(70) = LL(620)\left(1 - TEL(620)\right) = 54.182 \ in$$

The dimensions of the lead and steel at -40 °F are:

$$D1L(-40) = D1L(70)(1 - TEL(-40)) = 40.690 \; in$$

$$D2L(-40) = D2L(70)(1 - TEL(-40)) = 53.593 \; in$$

$$D1S(-40) = D1S(70)(1 - TES(-40)) = 40.963 \; in$$

$$D2S(-40) = D2S(70)(1 - TES(-40)) = 53.951 \; in$$

$$LL(-40) = LL(70)(1 - TEL(-40)) = 54.089 \; in$$

$$LS(-40) = LS(70)(1 - TES(-40)) = 54.451 \; in$$

Note that the inner diameter of the free state lead (D1L(-40)) is smaller than the outer diameter of the inner shell (D1S(-40)). Since these diameters must be the same, there must also be an adjustment to the lead outer diameter. Assuming the cross-sectional area of the lead column in the free state is equal to the area as installed in the cask, then:

$$A_{\text{Free State}} = A_{\text{Installed State}}$$

$$\pi/4(D2L(-40)^2 - D1L(-40)^2) = \pi/4(D2LI(-40)^2 - D1S(-40)^2)$$

where D2LI(-40) is the outer diameter of the lead at -40 °F, as installed. From this equation, D2LI(-40) = 53.801 inches and the area of the lead (the right side of the above equation) is 955.5 in^2. The radial gap between the lead and the outer shell is then:

$$Gap_{RAD} = \frac{(D2S(-40) - D2LI(-40))}{2} = 0.075 \; in$$

The axial gap between the cavity and the lead is:

$$Gap_{AXIAL} = LS(-40) - LL(-40) = 0.36 \; in$$

Next, the amount of lead that potentially undergoes flow strain will be calculated. From Figure 1 of [28], at a strain of 0.03 in/in, a temperature of 100 °F, and a strain rate of 10^2 s^{-1}, the lead flow stress is 2,200 psi. A strain rate of 10^2 s^{-1} is justified on page 1 of the same reference. (Note: according to the Cask Designer's Guide [29], Section 2.7.1, a value of flow stress as high as 5,000 psi could be justified.) This value for the flow stress (2,200 psi) will be conservatively utilized even though the lead shrinkage volume and the impact loading correspond to the minimum temperature of -40 °F.

In the lead column, the impact compressive stress will vary linearly from zero at the top to a maximum value at the bottom. The maximum weight that can be supported with a stress in the lead of 2,200 psi is:

$$W = \frac{\sigma_{DYN} A}{g} = 21,021 \; lb$$

where A = the lead area of 955.5 in^2 and g = 100 for the end drop.

The weight of the side poured lead is found using Figure 2.7-1. The volume of the lead is calculated based on a right circular annulus, minus the volumes labeled as A, B, and C. The basic volume is:

$$V_{BASIC} = \frac{\pi}{4}\left(OD^2 - ID^2\right)L = 52,863 \ in^3$$

where the lead cavity OD = 54 inches, the lead cavity ID = 41 inches, and the overall length L = 54.5 inches. The cross sectional area of volume A is $0.5 \times 4.4 \times 5.3 = 11.66 \ in^2$. The location of the center of gravity of the cross section is located one-third of the 4.4-inch dimension from the outer diameter, or 1.5 inches as shown on Figure 2.7-1. The diameter of the circle representing the center of gravity is thus $d_{CG} = 54.0 - (2 \times 1.5) = 51.0$ inches. The volume of A is:

$$V_A = \pi d_{CG} A = 1,868 \ in^3$$

The volumes of B and C are:

$$V_B = \frac{\pi}{4}\left(B_o^2 - B_i^2\right)B_L = 485 \ in^3$$

$$V_C = \frac{\pi}{4}\left(C_o^2 - C_i^2\right)C_L = 333 \ in^3$$

where B_o, B_i, and B_L = 43.1, 41.0, and 3.5 inches, respectively, and C_o, C_i, and C_L = 54.0, 52.0, and 2.0 inches, respectively. The total volume of the side lead is:

$$V_T = V_{BASIC} - V_A - V_B - V_C = 50,177 \ in^3$$

Since the density of lead is 0.41 lb/in^3, the weight of the side lead is $0.41 \times 50,177 = 20,573$ lb. Thus, since the lead weighs less than the amount that can be supported without flow (i.e., without permanent deformation), no slump due to the worst case end drop will occur. This result is conservative because a) it uses a flow stress corresponding to 100 °F along with the maximum impact at cold conditions; b) it uses a flow stress which is less than one-half of the value suggested by the Cask Designer's Guide; and c) it uses a bounding impact load. The total gap is therefore equal to the maximum axial shrinkage value of 0.36 inches. Conservatively, an upper bound value is applied to this result and used in the shielding analysis given in Section 5.3, *Shielding Model*.

Buckling Evaluation. In the end drop orientation, the outer shell will carry most of the axial loads due to its much greater stiffness compared to the inner shell. The end drop buckling analysis may be conservatively performed by considering only the outer shell. The maximum cold HAC impact of 100g is conservatively applied along with the bounding hot temperature case of 150 °F.

The only applied stress is axial. The weight supported by the outer shell may be conservatively estimated based on the total loaded weight (67,000 lb), less the payload and dunnage (12,000 lb), the lower impact limiter (5,000 lb), the side lead shield (20,573 lb, see the lead slump evaluation above), and the lead in the lid (2,777 lb, derived below). The lead shielding in the lid is slightly lighter than the lead in the lower end structure, thus the remaining weight to be supported is conservatively larger. The lead in the lid consists of a disk volume 44.0 inches in diameter and 2.12 inches thick, plus a disk volume 34.13 inches in diameter and 3.88 inches thick. The weight of the lead in the lid is:

$$W = \frac{\pi}{4}\left(44.0^2 \times 2.12 + 34.13^2 \times 3.88\right)0.41 = 2,777 \ lb$$

The total weight supported by the outer shell is therefore:

$$W_{tot} = 67,000 - 12,000 - 5,000 - 20,573 - 2,777 = 26,650 \text{ lb}$$

This result conservatively includes the significant weight of the lid steel and upper end steel structures, which do not need to be supported by the outer shell. Since the impact is the same for both ends, and the supported weight is conservatively overestimated, the evaluation applies for either a top-down end drop or a bottom-down end drop. The cross sectional area of the outer shell is:

$$A_{OS} = \frac{\pi}{4}\left(57.5^2 - 54.0^2\right) = 306.5 \text{ } in^2$$

The axial stress under a 100g end drop impact is:

$$\sigma_\phi = \frac{W_{tot}}{A_{OS}}(100) = 8,695 \text{ } psi$$

Conservatively, 9,000 psi will be used for the buckling calculation. No other stresses are applied in the end drop. The possibility of buckling of the outer shell due to end drop impact is evaluated using [14]. Consistent with Regulatory Guide 7.6 [2], a factor of safety corresponding to ASME B&PV Code, Service Level D is employed. In this case, the applicable factor of safety is 1.34 for normal conditions, as specified in [14]. All interaction check values, including the maximum value of 0.4387, are less than unity, as required. Therefore, buckling of the cask shells in the HAC free drop will not occur. The detailed buckling analysis is presented in Appendix 2.12.6, *Cask Shell Buckling Evaluations*.

2.7.1.3 Side Drop

The HAC side orientation free drop is evaluated using the finite element model described in Appendix 2.12.4, *Stress Analysis Finite Element Models*, and an acceleration of 100g as discussed in Section 2.7.1.1, *Impact Forces and Deformations*.

From Section 2.12.4.4.8, *Case No. 8, HAC Side Drop*, the maximum linearized primary membrane stress intensity resulting from the side drop impact of 100g is 32,680 psi, located at the bottom of the outer shell as shown in Figure 2.12.4-43. From Table 2.1-1, the limit on primary membrane stress is the lesser of $2.4S_m$ and $0.7S_u$, which for Type 304 forged material is $0.7S_u = 47,705$ psi at 150 °F. Applying a DLF of 1.15 from Section 2.7.1.5, *Dynamic Load Factor*, the margin of safety is:

$$MS = \frac{47,705}{(1.15)32,680} - 1 = +0.27$$

The maximum linearized membrane plus bending stress intensity is 55,740 psi, located at the bottom outside edge of the outer shell as shown in Figure 2.12.4-43. The allowable membrane plus bending stress, from Table 2.1-1, is the lesser of $3.6S_m$ or S_u, which for Type 304 forged material is $S_u = 68,150$ psi at 150 °F. The margin of safety is:

$$MS = \frac{68,150}{(1.15)55,740} - 1 = +0.06$$

For stress specifically in the containment boundary, the maximum linearized membrane stress is 19,770 psi at the top end of the inner shell, as shown in Figure 2.12.4-44c. (The locations of the linearization paths are shown in Figure 2.12.4-47.) The HAC membrane stress allowable is 47,705 psi. Applying the DLF of 1.15, the margin of safety is:

$$MS = \frac{47,705}{1.15(19,770)} - 1 = +1.10$$

The maximum linearized membrane plus bending stress in the containment boundary is 38,650 psi at the upper end structure shelf, outer location, as shown in Figure 2.12.4-44b. The HAC membrane plus bending stress allowable is 68,150 psi. Applying the DLF of 1.15, the margin of safety is:

$$MS = \frac{68,150}{1.15(38,650)} - 1 = +0.53$$

As shown, all cask body margins of safety for the HAC side drop condition are positive.

2.7.1.4 Oblique Drop

The 380-B is a relatively short package, having an overall length of just over 118 inches and a diameter over the impact limiters of 100 inches. The length between the center of the side impact forces (i.e., between the centers of the cylindrical portion of the impact limiters) is approximately 53 inches. For this reason, slapdown does not occur in near-horizontal side impacts. As shown in Table 2.12.5-11, the calculated results for the HAC free drop in two near-horizontal orientations (10° and 20° to the horizontal), the secondary impact is slightly (for 10°) or significantly (for 20°) lower than the primary impact. Thus, the oblique slapdown free drop orientations are not of concern. In addition, the predicted C.G.-over-corner orientation impact is significantly lower (maximum of 68.3g in the cold condition) than the bounding impact values used for the end and side orientation stress calculations (100g). Thus, the oblique C.G.-over-corner free drop orientation is not of concern.

2.7.1.5 Dynamic Load Factor

The DLF used in the impact analyses is calculated using NUREG/CR–3966 [30] (this quantity is called the DAF in that document). In Section 2.2.3 of [30], an estimated impact pulse duration is developed assuming a constant impact acceleration:

$$t_1 = \frac{Mv_o}{F_{max}}$$

This equation, however, underestimates the duration of a varying pulse such as a sinusoidal pulse, which is the closest shape to an actual, measured pulse. For a sinusoidal pulse, from Newton's Second Law:

$$F = Ma = MA\sin\omega t$$

The area under the pulse is the total change in velocity. Since the impact velocity is v_o, and the package comes to a complete stop during impact, the change in velocity is simply v_o. This can be written:

$$v_o = A \int_0^{\pi/\omega} \sin \omega t \, dt = -\frac{A}{\omega} \cos \omega t \Big|_0^{\pi/\omega} = \frac{2A}{\omega}$$

From this,

$$\omega = \frac{2A}{v_o}$$

Since the pseudo–frequency of the pulse is a full sine wave (two pulse lengths), the pulse length is equal to:

$$t_1 = \frac{T_1}{2} = \frac{1/f}{2} = \frac{2\pi/\omega}{2} = \frac{\pi}{\omega}$$

Substituting from above,

$$t_1 = \frac{\pi v_o}{2A}$$

where v_o is the free drop impact speed and A is the maximum acceleration, in/s^2. For the NCT 1-ft free drop where the impact velocity is 96.3 in/s and the bounding impact is 35g, $t_1 = 0.011$s. For the HAC 30-ft free drop where the impact velocity is 527.5 in/s and the bounding impact is 100g, $t_1 = 0.021$s.

The first mode natural frequency of the closure lid can be bounded by considering the upper closure plate. This 1.5-in thick plate will have a lower frequency than the 2.5-in thick inner containment plate. The natural frequency is found using [26], Table 36, Case 10a:

$$f = \frac{K_n}{2\pi} \sqrt{\frac{Dg}{wr^4}} = 275 \ Hz$$

where $K_1 = 10.2$, $g = 386.4$ in/s^2, and the closure plate radius, $r = 45.50/2 = 22.75$ inches. The weight of the plate per unit area is $0.29t = 0.435$ lb/in^2, where the plate thickness is 1.5 inches. Parameter D is found from:

$$D = \frac{Et^3}{12(1-v^2)} = 8.650(10^6) in - lb$$

where $E = 27.8(10^6)$ psi for Type 304 steel at 150 °F, $v = 0.31$, and the thickness, $t = 1.5$ inches. The period of the lid is equal to $1/f$, or $T = 1/275 = 0.0036$ s. The amplification factor for a half sine wave is given in Figure 2-15 of [30]. The abscissa of the figure is the ratio t_1/T. The smallest value of the ratio occurs in the NCT impact, where $t_1 = 0.011$ s:

$$\frac{t_{1-NCT}}{T} = 3.06$$

At this value, the corresponding DLF is bounded by a value of 1.15. The ratio for HAC, where t_1 equals 0.021s, is larger, and since it would fall further to the right on the abscissa, would yield a lower DLF.

The use of the closure plate to compute the overall DLF is conservative, since the plate with greater mass (the inner containment plate) will have a correspondingly greater influence on the

overall dynamic behavior of the lid and thus the DLF. It will have a higher frequency because thicker, thus a smaller period T and a larger ratio and a lower DLF. The DLF = 1.15 will be conservatively used for both NCT and HAC.

2.7.2 Crush

Since the weight of the 380-B package exceeds 1,100 lb, the crush test specified in 10 CFR §71.73(c)(2) does not apply.

2.7.3 Puncture

The 380-B package is evaluated for puncture resistance under HAC as defined in 10 CFR §71.73(c)(3). The puncture event is defined as a free drop from a height of 40 inches onto a vertical, cylindrical mild steel bar, 6 inches in diameter, in an orientation and in a location for which maximum damage is expected. Puncture performance of the 380-B package is divided into two categories: puncture on the impact limiters, which was evaluated by half-scale certification test, and puncture of the package body, which is evaluated by analysis.

2.7.3.1 Puncture on the Impact Limiters

Appendix 2.12.2, *Certification Test Plan*, discusses the strategy used to evaluate the puncture performance of the impact limiters under the worst-case conditions, including the test objectives and success criteria. Section 2.12.2.4.1, *Test Sequence and Damage Accumulation*, identifies the four puncture tests that were performed on the half-scale certification test unit (CTU). The results of these tests is summarized below. With the exception of puncture test P3, each puncture test was performed on the damage from a prior HAC free drop test. Details are to be found in Appendix 2.12.3, *Certification Test Results*. The configuration of each test is shown schematically in Figure 2.12.3-12.

Test P1. This test directly followed free drop D1 (end orientation), and was designed to create potential worst-case damage in the vicinity of the closure lid vent port, to be considered during the thermal evaluation. The bar impacted the shell at an oblique angle through the C.G. of the CTU and perforated the impact limiter shell, as expected. A cross section of the cumulative damage of free drop D1 and puncture drop P1 is shown in Figure 2.12.3-19. As shown in this figure and in Figure 2.12.3-18 and Figure 2.12.3-20, the puncture bar left a relatively 'clean' hole without excessive ripping of the shell of the foam. As discussed in Section 3.5.4, *'Last-A-Foam' Response under HAC*, the foam, when exposed to fire conditions forms an insulating char, which blocks the puncture hole and protects the vent port from fire temperatures. A more bounding worst-case puncture damage is associated with puncture test P2, as discussed below.

Test P2. This test directly followed free drop D2 (C.G.-over-corner orientation), and was designed to create potential worst-case damage in the area of the closure lid elastomer containment seal, to be considered during the thermal evaluation. The bar impacted the shell of the impact limiter through the C.G. of the CTU on the free drop damage from test D2 and perforated the impact limiter shell, as expected. A cross section of the cumulative damage of free drop D2 and puncture drop P2 is shown in Figure 2.12.3-32. As shown in Figure 2.12.3-33, the puncture bar left a relatively 'clean' hole without excessive ripping of the shell or of the

foam. This puncture damage has been chosen for thermal analysis as discussed in Section 3.5.3.5, *Description of Thermal Model for HAC*.

Test P3. The certification testing of the half-scale CTU was performed with an eye toward the potential future certification of the 380-B to the requirements of TS-R-1 [31]. It is necessary to consider, per TS-R-1 §727, the order of free drop and puncture relative to the maximum damage in the subsequent fire test. With this in view, puncture test P3 was performed on an undamaged impact limiter. Tests P3 and D3 were designed to result in the worst case cumulative free drop and puncture damage (relative to the fire test) which could result from performing the puncture test before the free drop test. The CTU was dropped on the puncture bar at an angle of 75° to the horizontal, impacting the tapered part of the limiter shell. The puncture bar perforated the shell and left an approximately 10-inch long hole, approximately parallel to the CTU axis. The orientation and test result is shown in Figure 2.12.3-37 through Figure 2.12.3-40. Subsequent to this test, the CTU was configured for the side drop as shown in Figure 2.12.3-41. On one end was the impact limiter with the P3 damage (designated as IL #3), with the puncture hole located at the bottom in the position where the side drop impact would occur. On the other end was a completely undamaged impact limiter (designated as IL #4). After the side drop, a puncture test (P4) was performed on IL #4, see below. A cross section of the cumulative damage from test P3 and free drop D3 is shown in Figure 2.12.3-45. The lateral deformation resulting from the side impact was essentially the same for both impact limiters as discussed in Section 2.12.3.4.6, *Free Drop Test D3*. Thus, the worst case combined damage from a puncture-first, free drop-second test sequence is not bounding compared to the opposite sequence. Of note, since the test sequence used for the certification tests P3/D3 on IL #3 did not comply with the requirements of 10 CFR 71.73(c), these results are offered in support of a safety demonstration according to the TS-R-1 regulation only. Of further note, the certification tests D3/P4 on IL #4, even though it shared the same free drop test (D3), <u>did</u> comply with the requirements of 10 CFR 71.73(c), and was unaffected by the reversal of test sequence used on IL#3.

Test P4. This test directly followed free drop D3 (side orientation), and was designed to take advantage of any potential weakening of the corner joint between the cylindrical side shell and the flat annular shell of the limiter which might have occurred due to the side drop deformation. The bar impacted the shell of the impact limiter through the C.G. of the CTU on the free drop damage from test D3 on IL #4 and perforated the impact limiter shell, as expected. A cross section of the cumulative damage of free drop D3 and puncture drop P4 is shown in Figure 2.12.3-59. As shown in Figure 2.12.3-52, the puncture bar penetrated through the impact limiter side and perforated the top annular shell. Exposure at both ends of the damage could lead to a 'chimney' in the hypothetical fire event; however, the damage is located relatively far from the elastomer containment seal and this damage is not considered bounding for the fire thermal analysis. If the puncture location had been closer to the seal, it would not have broken through the upper annular shell. In that case, the damage would have been similar to test P2, which is considered bounding for the thermal analysis as noted above.

2.7.3.2 Puncture on the Cask Body

The puncture resistance of the outer surface of the cask body is evaluated using Nelms' Equation [32], which is used to determine the resistance to puncture of lead–backed stainless steel shells. For the NCT hot case temperature of 150 °F, the ultimate strength of the Type 304 outer shell is $S_u =$

73,000 psi from Table 2.2-1. The bounding weight of the 380-B package, including impact limiters, is W = 67,000 lb. The required thickness of the outer shell to resist puncture is:

$$t = \left(\frac{W}{S_u}\right)^{0.71} = 0.94 \; inches$$

The thickness of the outer shell is 1.75 inches. The margin of safety on the cask outer shell thickness is:

$$MS = \frac{1.75}{0.94} - 1 = +0.86$$

Therefore, puncture of the 380-B package is not of concern.

2.7.4 Thermal

The 380-B package is designed to withstand the HAC 30 minute fire specified in 10 CFR §71.73(c)(4). The thermal evaluation is presented in Section 3.4, *Thermal Evaluation for Hypothetical Accident Conditions*.

2.7.4.1 Summary of Pressures and Temperatures

As shown in Table 3.1-2, the maximum internal cask pressure as a result of the HAC fire event is bounded by a value of 100 psig.

From Table 3.1-1, as a result of the HAC fire event, the maximum temperature of any part of the cask, including closure bolts but not including the thermal shield, may be bounded by a temperature of 700 °F. Conservatively, as used in the calculations below, all stainless steel components will be assumed to be made from forged Type 304 material, which has a lower ultimate strength than plate material. From Table 2.2-2, S_u = 59,200 psi at 700 °F. The value of S_u for the closure bolts at 700 °F is equal to 128,400 psi, from Table 2.2-3.

2.7.4.2 Differential Thermal Expansion

The 380-B packaging does not include a lodgment, basket, or other internal structure. The 380-B payload consists of shielded devices that are located within the payload cavity by means of non-structural dunnage/blocking. Thus, differential thermal expansion is not of concern.

2.7.4.3 Stress Calculations

The finite element model described in Appendix 2.12.4, *Stress Analysis Finite Element Models,* is loaded with the maximum internal cask pressure of 100 psi, and gives the result discussed in Section 2.12.4.4.9, *Case No. 9, HAC Fire Event Pressure*, and shown in Figure 2.12.4-49. The maximum overall stress intensity which results from the model is 12,677 psi, located near a stress concentration caused by the bolt preload. Since this value is less than the lowest (primary membrane) stress allowable, it is not necessary to identify the individual stress components.

From Table 2.1-1, the limit on the primary membrane stress intensity is the lesser of $2.4S_m$ or $0.7S_u$, which for Type 304 forged material is $2.4S_m = 37{,}920$ psi at the bounding temperature of 700 °F. The margin of safety is:

$$MS = \frac{37{,}920}{12{,}677} - 1 = +1.99$$

Thus, cask stress due to the fire event pressure is not of concern.

From Section 4.4 of [11], the maximum non-prying tensile force per bolt, Fa_max, due to the pressure load is:

$$Fa\_\max = \frac{\pi D \lg^2 (Pli - Plo)}{4Nb} = 4{,}922 \; lb$$

where Dlg = 47.5 inches is the diameter of the containment seal, Nb = 36 is the quantity of closure bolts, Pli = 100 psig is the peak internal pressure, and Plo = 0 psig. This load is bounded by the bolt preload of 50,667 lb from Section 2.6.1.5, *Closure Bolts*. Thus, the average axial bolt stress is:

$$Sba = 1.2732 \frac{(50{,}667)}{Dbs^2} = 37{,}591 \; psi$$

where the bolt shank diameter, Dbs = 1.31 inches as discussed in Section 2.6.1.5. From Table 6.3 of [11], for HAC the allowable average tensile stress is the smaller of $0.7S_u$ or S_y at the peak bolt temperature. From Section 2.7.4.1, *Summary of Pressures and Temperatures*, the peak temperature of the closure lid is bounded by 700 °F. Although the closure bolts will be somewhat cooler than this value, the peak temperature will be conservatively used. From Table 2.1-1, the allowable stress is $0.7S_u = 89{,}880$ psi, where $S_u = 128{,}400$ psi from Section 2.7.4.1. The margin of safety is:

$$MS_{Sba} = \frac{89{,}880}{Sba} - 1 = +1.39$$

Thus the closure bolts are not of concern for the HAC fire event.

Per Regulatory Guide 7.6, paragraph C.7, the extreme range of stress must be considered. Of all the various allowable stresses corresponding to the different conditions evaluated (including fabrication stresses and normal conditions of transport), the largest allowable stress is equal to the material ultimate strength, S_u. It is therefore conservative to assume that S_u bounds all stresses actually developed in the structure. For Type 304 stainless steel, $S_u = 75{,}000$ psi at 70 °F. The maximum possible stress intensity range is twice this value, or 150,000 psi. Applying a factor of four to account for possible stress concentrations at structural discontinuities gives a total elastic stress range of 600,000 psi. The alternating component is one-half of this value, or 300,000 psi. To account for temperature effects, this value of alternating stress is factored by the ratio of modulus of elasticity. This ratio is formed between the modulus of elasticity at room temperature (at which the test data applies directly) and the modulus of elasticity at the maximum temperature, conservatively bounded by a temperature of 700 °F for any structural part of the package. The adjusted stress is:

$$S_{alt} = 300,000 \frac{E_{70°F}}{E_{700°F}} = 342,339 \ psi$$

where $E_{70°F} = 28.3(10^6)$ psi and $E_{700°F} = 24.8(10^6)$ psi. Per Table I-9.2 of the ASME B&PV Code [13], the allowable value for S_{alt} at 10 cycles is 870,000 psi. The margin of safety is:

$$MS = \frac{870,000}{342,339} - 1 = +1.54$$

Considering the significant conservatism used in the underlying assumptions (e.g., use of allowable stress rather than smaller actual stresses, assuming worst case stresses are fully reversing, use of the maximum factor of stress concentration), it is apparent that the actual margin of safety is larger than 1.54. Thus, the requirement of paragraph C.7 of Regulatory Guide 7.6 is met.

2.7.5 Immersion – Fissile

An immersion test for fissile material packages is required by 10 CFR §71.73(c)(5). Since the 380-B does not transport fissile materials, this requirement does not apply.

2.7.6 Immersion – All Packages

An immersion test for all packages is required by 10 CFR §71.73(c)(6), in which a separate, undamaged specimen must be subjected an equivalent pressure of 21.7 psig. As shown in Section 2.6.4, *Increased External Pressure*, the 380-B package was evaluated for a bounding pressure load case which included a minimum of 21.7 psig external pressure on the inner shell. The possibility of buckling of the inner shell was evaluated using ASME B&PV Code Case N-284-4 [14]. As noted in Section 2.6.4, all interaction check values, including the maximum value of 0.4500, was less than unity, as required. This evaluation is conservative for the following reasons:

- The evaluation included the lead shrinkage pressure, which is not required for HAC

- The factor of safety was set at a value of 2.00 for NCT, whereas, per [14], a factor of 1.34 may be used for HAC

Thus, the immersion load case of 10 CFR §71.73(c)(6) is not of concern.

2.7.7 Deep Water Immersion Test (for Type B Packages Containing More than 10^5 A_2)

For Type B packages containing an activity of more than 10^5 A_2, 10 CFR §71.61 requires that an undamaged containment system withstand an external pressure of $p_o = 290$ psig for a period of not less than one hour without collapse, buckling, or inleakage of water. As shown in Table 1.2-1, the payload represents a maximum activity of less than 10^5 A_2. Therefore, this requirement does not apply to the 380-B package.

2.7.8   Summary of Damage

From the analyses presented, it is shown that the HAC sequence does not result in significant damage to the 380-B package, and that all stress criteria established for HAC in Section 2.1.2, *Design Criteria*, are satisfied. The margins of safety resulting from the analyses performed in this section are shown in Table 2.7-2. The 380-B cask body and internal components were evaluated primarily by analysis, and the impact limiters and attachments were evaluated by test. The test results confirmed that the impact acceleration of 100g used in the analyses was bounding for all free drop orientations. The tests are summarized below.

The analysis of the cask body and internal components under free drop impact includes the cask body structure, the closure lid, and the closure bolts. Bounding orientations of end and side drop are evaluated. An evaluation of oblique drop orientations demonstrates that the end and side drop orientations govern over the C.G.-over-corner and slapdown orientations. The cask body is analyzed using finite element analysis, in which the cask is loaded by self-weight and contents weight, and supported by the impact limiters. It is shown that the lead shielding does not reach its flow strength under maximum impact conditions, and thus lead slump does not occur nor does the lead apply lateral loading to the cask shells. The minimum margin of safety from the finite element analysis, which applies to the entire cask structure and which corresponds to the side drop impact case, is +0.06. The minimum margin of safety for the containment boundary components is +0.39. All of the manual evaluations result in larger margins of safety, as shown in Table 2.7-2. The end drop buckling analysis of the package outer shell, performed using ASME B&PV Code Case N-284-4, results in a maximum check value of 0.4387, which is well below the limit of unity, as required by the Code Case. An evaluation of lead axial thermal contraction is performed, and results in a value of 0.36 inches. This value is considered in the shielding evaluation documented in Chapter 5.0, *Shielding Evaluation*. An analysis of the puncture test on the cask body was performed using Nelms' equation, and resulted in a margin of safety of +0.86. The maximum internal pressure and temperature generated in the HAC fire event are applied to the results of the cask body finite element model. The immersion analysis of the inner shell, performed using ASME B&PV Code Case N-284-4, results in a maximum check value of 0.4500, which is well below the limit of unity, as required. Therefore, since all margins of safety are positive, the criteria of Section 2.1.2, *Design Criteria*, are satisfied for the 380-B package.

The impact limiter design was tested using half-scale certification test units of the production design, and a dummy cask body. The impact limiters successfully performed their role in limiting the impact acceleration to a value lower than the bounding value of 100g used for stress analysis. In addition, the test showed that the calculated maximum strains in the energy-absorbing polyurethane foam were conservative. A total of three HAC free drops and four puncture drops were performed on the CTUs. The tests included one combination of free drop and puncture damage in which the puncture test occurred prior to the free drop test, in order to support a safety demonstration according to the requirements of TS-R-1. Due to the weight of the package, all of the puncture tests perforated the impact limiter steel shells, but no gross disintegration of the impact limiters occurred, and their ability to provide thermal protection of the thermally sensitive elastomer seals was not compromised. An unexpected failure of a weld seam occurred, but the performance of the reinforced weld in subsequent tests demonstrated that the problem has been successfully addressed. The impact limiter attachments successfully

retained the impact limiters on the cask. Therefore the impact limiters satisfy their design criteria established in Section 2.1.2.2, *Other Structures*.

Table 2.7-1 – HAC Free Drop Impact and Deformation: Comparison Between Certification Test and Analytical Prediction

Free Drop Orientation and Condition	Test Result[1]		Prediction[2]	
	Impact, g	Deformation, in	Impact, g	Deformation, in / % strain
End (cold)	78	5.4	92.8	5.5 / 22.1
C.G.-over-corner (warm)	49	11.9	46.0	15.8 / 79.8
Side (warm)	60	7.1	55.6	12.1 / 57.3

1. Test results extracted from Table 2.12.5-9.
2. Predictions extracted from Table 2.12.5-11. Strain is equal to the deformation divided by the initial distance of foam along the crush direction.

Table 2.7-2 – Minimum Margins of Safety from HAC Evaluations

Component	Loading Condition	Minimum Margin of Safety
Free Drop		
Cask body (FEA) (Bounding)	End drop, bottom down, membrane stress	+2.43
	End drop, bottom down, membrane + bending	+0.31
	End drop, top down, membrane stress	+1.82
	End drop, top down, membrane + bending stress	+0.42
	Side drop, membrane stress	+0.27
	Side drop, membrane + bending stress	+0.06
Cask body (FEA) (Containment Boundary)	End drop, bottom down, membrane stress	+3.80
	End drop, bottom down, membrane + bending	+0.39
	End drop, top down, membrane stress	+3.84
	End drop, top down, membrane + bending stress	+0.47
	Side drop, membrane stress	+1.10
	Side drop, membrane + bending stress	+0.53
Closure bolts	End drop, top down	+0.59
Cask outer shell	End drop, buckling (Code Case N-284-4)	0.4387*
Puncture		
Cask outer shell	Nelms' Equation	+0.86
Thermal		
Containment boundary	Internal pressure, fire conditions	+1.99
Closure bolts	Internal pressure, fire conditions	+1.39
Cask	Range of stress	+1.54
Immersion		
Cask inner shell	Immersion pressure (Code Case N-284-4)	0.4500*

*Maximum check value must be less than unity, see Appendix 2.12.6, *Cask Shell Buckling Evaluations*.

Security-Related Information
Figure Withheld Under 10 CFR 2.390.

Figure 2.7-1 – Side Lead Shield Cavity Dimensions

2.8 Accident Conditions for Air Transport of Plutonium

This section does not apply, since plutonium is not transported in the 380-B package.

2.9   Accident Conditions for Fissile Material Packages for Air Transport

This section does not apply, since fissile material is not transported in the 380-B package.

2.10 Special Form

This section does not apply, since special form is not claimed for the 380-B package.

2.11 Fuel Rods

This section does not apply, since fuel rods are not transported in the 380-B package.

2.12 Appendices

2.12.1 References

1. Title 10, Code of Federal Regulations, Part 71 (10 CFR 71), *Packaging and Transportation of Radioactive Material*, 01–01–11 Edition.

2. U. S. Nuclear Regulatory Commission, Regulatory Guide 7.6, *Design Criteria for the Structural Analysis of Shipping Cask Containment Vessels*, Revision 1, March 1978.

3. U. S. Nuclear Regulatory Commission, Regulatory Guide 7.8, *Load Combinations for the Structural Analysis of Shipping Casks for Radioactive Material*, Revision 1, March 1989.

4. ANSI N14.5–2014, *American National Standard for Radioactive Materials – Leakage Tests on Packages for Shipment*, American National Standards Institute (ANSI), Inc.

5. U. S. Nuclear Regulatory Commission, Regulatory Guide 7.11, *Fracture Toughness Criteria of Base Material for Ferritic Steel Shipping Cask Containment Vessels with a Maximum Wall Thickness of 4 Inches (0.1 m)*, June 1991.

6. R. E. Monroe, H. H. Woo, and R. G. Sears, *Recommended Welding Criteria for Use in the Fabrication of Shipping Containers for Radioactive Materials*, NUREG/CR–3019, UCRL–53044, U.S. Nuclear Regulatory Commission, March 1985.

7. L. E. Fischer, W. Lai, *Fabrication Criteria for Shipping Containers*, NUREG/CR–3854, UCRL–53544, U.S. Nuclear Regulatory Commission, March 1985.

8. American Society of Mechanical Engineers (ASME) Boiler and Pressure Vessel Code, Section III, *Rules for Construction of Nuclear Facility Components*, Division 1 – Subsection NB, *Class 1 Components*, 2010 Edition with 2011 Addenda.

9. American Society of Mechanical Engineers (ASME) Boiler and Pressure Vessel Code, Section III, *Rules for Construction of Nuclear Facility Components*, Division 1 – Subsection NF, *Supports,* 2010 Edition with 2011 Addenda.

10. American Society of Mechanical Engineers (ASME) Boiler and Pressure Vessel Code, Section III, *Rules for Construction of Nuclear Facility Components*, Division 1 – Appendix F, *Rules for Evaluation of Service Loadings with Level D Service Limits,* 2010 Edition with 2011 Addenda.

11. G.C. Mok, L.E. Fischer, S.T. Hsu, *Stress Analysis of Closure Bolts for Shipping Casks*, NUREG/CR–6007, UCRL–ID–110637, U.S. Nuclear Regulatory Commission, January 1993.

12. W.R. Holman, R. T. Langland, *Recommendations for Protecting Against Failure by Brittle Fracture in Ferritic Steel Shipping Containers Up to Four Inch Thick*, NUREG/CR–1815, UCRL–53013, U.S. Nuclear Regulatory Commission, August 1981.

13. American Society of Mechanical Engineers (ASME) Boiler and Pressure Vessel Code, Section III, *Rules for Construction of Nuclear Facility Components*, Division 1, Appendix I, *Design Fatigue Curves*, 2010 Edition with 2011 Addenda.

14. American Society of Mechanical Engineers (ASME) Boiler and Pressure Vessel Code, Section III, *Rules for Construction of Nuclear Power Plant Components*, Division 1, Class MC, Code Case N–284–4, *Metal Containment Shell Buckling Design Methods*, 2010 Edition, Supplement 11.

15. American Society of Mechanical Engineers (ASME) Boiler and Pressure Vessel Code, Section IX, *Qualification Standard for Welding and Brazing Procedures, Welders, Brazers, and Welding and Brazing Operators*, 2010 Edition with 2011 Addenda.

16. American Society of Mechanical Engineers (ASME) Boiler and Pressure Vessel Code, Section III, *Rules for Construction of Nuclear Facility Components*, Division 1 – Subsection NE, *Class MC Components,* Article NE–4220, 2010 Edition with 2011 Addenda.

17. American Society of Mechanical Engineers (ASME) Boiler and Pressure Vessel Code, Section III, *Rules for Construction of Nuclear Facility Components*, Division 1 – Subsection NB, *Class 1 Components*, Article NB–2540, and Section V, *Nondestructive Examination*, Article 5, *Ultrasonic Examination Methods for Materials,* 2010 Edition with 2011 Addenda.

18. American Society of Mechanical Engineers (ASME) Boiler and Pressure Vessel Code, Section III, *Rules for Construction of Nuclear Facility Components*, Division 1 – Subsection NB, *Class 1 Components*, Article NB–2570, and Section V, *Nondestructive Examination*, Article 2, *Radiographic Examination,* 2010 Edition with 2011 Addenda.

19. ANSI/AWS D1.6/D1.6M:2007, *Structural Welding Code–Stainless Steel*, American Welding Society (AWS).

20. American Society of Mechanical Engineers (ASME) Boiler and Pressure Vessel Code, Section III, *Rules for Construction of Nuclear Facility Components*, Division 1 – Subsection NB, *Class 1 Components*, and Section V, *Nondestructive Examination*, Article 2, *Radiographic Examination*, 2010 Edition with 2011 Addenda.

21. American Society of Mechanical Engineers (ASME) Boiler and Pressure Vessel Code, Section III, *Rules for Construction of Nuclear Facility Components*, Division 1 – Subsection NB, *Class 1 Components*, and Section V, *Nondestructive Examination*, Article 4, *Ultrasonic Examination Methods for Materials*, 2010 Edition with 2011 Addenda.

22. American Society of Mechanical Engineers (ASME) Boiler and Pressure Vessel Code, Section III, *Rules for Construction of Nuclear Facility Components*, Division 1 – Subsection NB, *Class 1 Components*, and Section V, *Nondestructive Examination*, Article 6, *Liquid Penetrant Examination*, 2010 Edition with 2011 Addenda.

23. American Society of Mechanical Engineers (ASME) Boiler and Pressure Vessel Code, Section III, *Rules for Construction of Nuclear Facility Components*, Division 1 – Subsection NF, *Supports,* and Section V, *Nondestructive Examination*, Article 6, *Liquid Penetrant Examination*, 2010 Edition with 2011 Addenda.

24. American Society of Mechanical Engineers (ASME) Boiler and Pressure Vessel Code, Section III, *Rules for Construction of Nuclear Facility Components*, Division 1 – Subsection NF, *Supports,* and Section V, *Nondestructive Examination*, Article 4, *Ultrasonic Examination Methods for Materials*, 2010 Edition with 2011 Addenda.

25. American Society of Mechanical Engineers (ASME) Boiler and Pressure Vessel Code, Section III, *Rules for Construction of Nuclear Facility Components*, Division 1 – Subsection NB, *Class 1 Components*, Article NB–6220, 2010 Edition with 2011 Addenda.

26. Roark's Formulas for Stress and Strain, Sixth Edition, McGraw–Hill, New York, 1989.

27. ANSI N14.23, *Design Basis for Resistance to Shock and Vibration of Radioactive Material Packages Greater Than One Ton in Truck Transport (DRAFT)*, 1980, American National Standards Institute, Inc, New York.

28. U.S. Energy Research and Development Administration, *A Survey of Strain Rate Effects for Some Common Structural Materials Used in Radioactive Material Packaging and Transportation Systems*, Battelle Columbus Laboratories, August 1976.

29. L.B. Shappert, *Cask Designer's Guide,* ORNL-NSIC-68, February 1970.

30. T.A. Nelson and R. C. Chun, *Methods for Impact Analysis of Shipping Casks*, NUREG/CR–3966, UCID–20639, U.S. Nuclear Regulatory Commission, November 1987.

31. International Atomic Energy Agency, *Regulations for the Safe Transport of Radioactive Material*, TS-R-1, 2009 Edition.

32. A. Nelms, *Structural Analysis of Shipping Casks, Effect of Jacket Physical Properties and Curvature on Puncture Resistance*, ORNL–TM–1312, Vol. 3, Oak Ridge National Laboratory, 1968.

33. Bechtel Power Corporation, *Topical Report, Design of Structures for Missile Impact*, BC-TOP-9A, Revision 2, September 1974.

34. International Atomic Energy Agency, *Advisory Material for the IAEA Regulations for the Safe Transport of Radioactive Material*, TS-G-1.1, 2008 Edition.

35. Livermore Software Technology Corp. (LTSC), *LS-DYNA® Keyword User's Manual Volume I*, Version R7.0, February 2013, Livermore, CA.

36. Livermore Software Technology Corp. (LTSC), *LS-DYNA® Keyword User's Manual Volume II, Material Models*, Version R7.0, February 2013, Livermore, CA.

37. *Design Guide for use of Last-A-Foam® FR-3700 for Crash & Fire Protection of Radioactive Material Shipping Containers*, Issue 005, General Plastics Manufacturing Company, Tacoma, WA.

38. American Society of Mechanical Engineers (ASME) Boiler and Pressure Vessel Code, Section II, *Materials*, Part D, *Properties*, 2010 Edition with 2011 Addenda.

39. American Society of Mechanical Engineers (ASME) Boiler and Pressure Vessel Code, Section II, *Materials*, Part A, *Ferrous Material Specifications*, 2010 Edition with 2011 Addenda.

40. Docket 71-9355, *435-B Transport Package Safety Analysis Report*, Rev. 2, AREVA Federal Services LLC.

41. Avallone, E. A., and Baumeister, T, III., *Marks' Standard Handbook for Mechanical Engineers*, 10th Edition, 1996, McGraw-Hill, Inc.

42. Shigley, J.E., and Mischke, C.R., *Mechanical Engineering Design*, 5th Edition, 1989, McGraw-Hill, Inc.

43. ASTM B 16/B 16M-10, *Standard Specification for Free-Cutting Brass Rod, Bar and Shapes for Use in Screw Machines*, American Society for Testing and Materials (ASTM).

44. ASM Handbook® (Formerly Tenth Edition, Metals Handbook), Volume 2, *Properties and Selection: Nonferrous Alloys and Special-Purpose Materials*, ASM International, page 310.

2.12.2 Certification Test Plan

This appendix delineates the certification tests to be performed on the 380-B cask impact limiters. The justification for choosing the specific tests is presented and discussed. Since this material served for test planning purposes, the future tense is used. The results of the tests are provided in Appendix 2.12.3, *Certification Test Results*.

The 380-B package includes a conventional, austenitic stainless steel cask shielded by lead and closed by a bolted lid, thus testing of the cask body is not necessary. The licensing basis for the cask body is by analysis. Physical testing will focus only on the impact limiters and attachments. The licensing basis for the impact limiters will be a combination of half-scale physical test and analysis. Many years of experience have demonstrated that the free drop and puncture drop damage of steel-shell, polyurethane foam-filled impact limiters can be adequately modeled using scaled test specimens.

The test unit configuration will therefore consist of a half-scale dummy cask and half-scale impact limiters and attachments. Testing will consist of free drops and puncture drops. Test data will consist of measured accelerations and measurements of the damaged configuration.

2.12.2.1 Certification Strategy

The strategy of the certification test program is to demonstrate the adequacy of the 380-B package impact limiter design. The requirements of both 10 CFR 71 [1] and TS-R-1 [31] will be considered to ensure that the most restrictive requirements of both are met. The NRC regulations state that the free drop impact takes place before the puncture test, while the tests described in §727 of [31] must be completed in a sequence such that any damage suffered is the worst-case for the following thermal testing.

The impact limiters were designed using computer software to predict the impact (maximum at cold temperature) and the crush deformation (maximum at warm temperature) as discussed in Appendix 2.12.5, *Free Drop Impact Evaluation*. The certification tests will demonstrate the performance of the impact limiters in both the hypothetical accident condition (HAC) free drop and puncture drop events. Free drop impact acceleration and deformation results will be used to validate (i.e., benchmark) the computer simulations for use in non-tested orientations or conditions. Puncture drop deformation results will be used to demonstrate impact limiter structural integrity and in the HAC thermal analysis as discussed in Section 3.4, *Thermal Evaluation for Hypothetical Accident Conditions*.

Several orientations will be tested to ensure that the worst-case series of free and puncture drop events has been considered. The maximum combination of free and puncture drop deformation will be used in the thermal analysis. The thermal analysis will show that during the HAC fire event, the temperature of the elastomer O-ring seals does not exceed safe limits, and the lead does not melt.

Since a half-scale test unit will be used, a scaling of the various test parameters is necessary. All of the dimensions of the test unit will be one half of the full-scale design. Dimensional results from the half-scale test unit (e.g., crush distance) must be multiplied by a factor of two to obtain the full-scale equivalent result. Similarly, the measured accelerations must be divided by two to convert to full-scale. The half-scale test unit weight will be 1/8 the weight of the full-scale design.

2.12.2.2 Initial Test Conditions

2.12.2.2.1 Temperature

For free drop testing where maximum impact is desired, the foam behavior must correspond to the minimum temperature of the packaging. Of the two regulations considered [1][31], the bounding minimum temperature is -40 °F as found in [31]. At this temperature, the polyurethane foam will exhibit its maximum crush resistance and generate the maximum impact in the given orientation. To avoid the need to chill such a large package to a uniform temperature of -40 °F, equivalent foam strength may be used. The equivalent foam must exhibit essentially the same stress-strain curve as the production foam, at a somewhat higher temperature. In this way, the impact obtained will be essentially the same as the impact that would be obtained using the production foam at -40 °F. As shown in Figure 2.12.2-1, a nominal foam density of 17 lb/ft^3 at a temperature of 0 °F will provide essentially the same stress-strain curve as the production foam density of 16 lb/ft^3 at -40 °F. Other effects of this small, 1 lb/ft^3 upward adjustment in density on the test results will be negligible.

For free drop testing where maximum foam crush deformation is desired, the foam behavior must correspond to the NCT warm temperature of the packaging. From the package thermal analysis, the bulk average foam temperature under maximum heat conditions is bounded by a temperature of 130 °F (see Section 3.3, *Thermal Evaluation for Normal Conditions of Transport*). To avoid the need to heat the package to this temperature, equivalent foam strength may be used. The equivalent foam must exhibit essentially the same stress-strain curve as the production foam, at a somewhat lower temperature. In this way, the crush deformation obtained will be essentially the same as the deformation that would be obtained using the production foam at 130 °F. As shown in Figure 2.12.2-1, a foam density of 15 lb/ft^3 at a temperature of 100 °F will provide essentially the same stress-strain curve as the production foam density of 16 lb/ft^3 at 130 °F. Other effects of this small, 1 lb/ft^3 downward adjustment in density on the test results will be negligible.

2.12.2.2.2 Test Facilities and Instrumentation

The certification drop and puncture testing will be conducted using a drop pad having a mass of at least 10 times the weight of the certification test unit (CTU), or at least 83,750 lb. The top of the pad will be covered by an embedded steel plate of adequate thickness such that the drop pad will represent an essentially unyielding surface. The half-scale puncture bar will be a 3-in diameter bar of mild steel, mounted perpendicular to the drop pad, and having an edge radius not exceeding 1/8-inch. The bar will be reinforced by gussets at its base and fastened securely to the pad. The length of the bar will permit the bar to do maximum damage before the package becomes supported by the drop pad. More than one length of bar may be used. Puncture bars will not be reinforced beyond what is necessary to provide rigidity at the baseplate joint.

CTU temperature will be measured by means of thermocouples embedded in the foam. As a minimum, the region of foam expected to undergo crush deformation will be monitored.

The primary means of recording the results of the certification testing will be physical measurements and observations of the CTU before and after testing. In addition, each free drop impact will be recorded using active accelerometers. Since puncture drop impacts are not governing for impact, puncture drops do not need to be instrumented. As a minimum, conventional speed video cameras and still photography will record each event.

2.12.2.2.3   Certification Test Unit Configuration

The certification tests will be performed using a test unit consisting of a dummy cask assembled with impact limiters that are exact duplicates, in half-scale, of the production impact limiters. Any discrepancies will be described in Section 2.12.3.3, *Certification Test Unit Configuration*. The impact limiter attachments, including the welds of the mating attachments to the dummy cask, will be exact half-scale duplicates of the production attachments. The dummy cask will be made of steel and lead, and possess a weight of 1/8 of the weight of the full-scale cask (consistent with half-scale). The dummy cask's impact limiter interface dimensions and features, and its overall length, will be in half-scale.

The impact limiters will be constructed using the same materials and details as the full-scale limiters, using half-scale dimensions. Care will be taken to avoid excessive reinforcement of the welds. The polyurethane foam will possess the crush properties discussed in Section 2.12.2.2.1, *Temperature*. The impact limiters will receive a certificate of compliance with all fabrication drawing and specification requirements.

2.12.2.3 Identification of Worst-Case Test Orientations

Herein, the discussion of the worst-case test orientations utilizes the full scale 380-B package dimensions and weights.

2.12.2.3.1   Test Objectives

The objectives of the certification test program are:

1. To confirm maximum free drop impact accelerations obtained from computer calculations.
2. To confirm maximum free drop deformation obtained from computer calculations.
3. To validate (i.e., benchmark) the computer simulations for orientations and conditions not tested.
4. To demonstrate the general structural integrity of the impact limiter during impact.
5. To demonstrate the effectiveness of the impact limiter attachments in both free drop and puncture drop events.
6. To quantify the worst-case damage for the HAC fire event thermal analysis.

These objectives form naturally into two groups: free drop impact and puncture damage.

2.12.2.3.2   Free Drop Impacts

Due to the 380-B package axisymmetric design, the full spectrum of possible free drop orientations is limited to the following:

*   Vertical End Drop
*   Near Vertical End Drop
*   Center of Gravity (C.G.)-over-Corner
*   Slapdown
*   Side drop

Computer modeling is used to guide the selection of worst-case orientations. Preliminary runs of the type provided in Appendix 2.12.5, *Free Drop Impact Evaluation*, are used for this purpose.

(Only the final runs are presented in Appendix 2.12.5.) The drop orientations selected for testing are shown in Figure 2.12.2-2.

Vertical End Drop. Due to the tapered design of the impact limiter, a vertical end drop may not achieve the governing free drop impact acceleration or the governing crush damage. However, the vertical end drop orientation is of critical importance to the analysis of the cask body shells, the closure lid bolts, and lead slump. Thus, this drop test will be performed cold (as defined by Section 2.12.2.2.1, *Temperature*) to maximize the impact loading in the supporting analysis.

Near Vertical End Drop. In a near vertical end drop, the impact limiter will have a smaller initial contact area and larger available stroke and thus the free drop impact accelerations will be bounded by the vertical end drop. Additionally, due to the tapered impact limiter design, this orientation cannot apply any significant additional loading on the impact limiter attachments beyond that applied by the vertical end drop free drop orientation. Therefore, this orientation does not need to be performed.

C.G.-over-Corner. The C.G.-over-corner orientation achieves the smallest cross section and therefore should govern the free drop deformation. This drop test will be performed warm (as defined by Section 2.12.2.2.1, *Temperature*) to maximize the free drop deformation.

Slapdown. The aspect ratio of the cask length to outer diameter of the impact limiters is 0.68. With this shorter type package, the secondary impact will not be greater than the primary impact in a slapdown free drop orientation. This orientation is therefore not limiting for either the free drop impact accelerations or free drop deformation. Therefore, this orientation does not need to be performed.

Side Drop. The side drop has the most limited available stroke of any orientation and thus the drop performance could be affected by a puncture prior to the drop. This could create the maximum amount of deformation expected near the lid elastomeric seal area for the following thermal testing. Therefore, this orientation will be performed warm (as defined by Section 2.12.2.2.1, *Temperature*) to determine the maximum amount of deformation expected near the lid elastomeric seal area.

2.12.2.3.3   Puncture Drops

According to [33], the minimum full scale thickness to prevent the puncture bar from penetrating the steel skin of the impact limiters is:

$$t = \frac{E^{\frac{2}{3}}}{672 * D} = 0.91 \; inches$$

where E is potential energy, ft-lb, of the 380-B before a 40-inch puncture drop, and D = 6 inches in diameter. Therefore, the 0.25 inch thick stainless steel shell is expected to perforate in most orientations. To satisfy 10 CFR 71, consideration will be given to puncture tests occurring after each free drop orientation. In addition, to satisfy TS-R-1, consideration will be given to the effect of puncture testing prior to each free drop, relative to the effect on the subsequent fire event. Puncture orientations are shown in Figure 2.12.2-3.

All punctures will be performed at the prevailing bulk foam temperature of the related free drop since the metal is expected to puncture and the foam has little puncture resistance at any temperature. The temperature of the foam should be recorded prior to each puncture drop.

End Plate Puncture. The cask vent ports, located in the cask lid, are sealed using an elastomeric O-ring seal that may be damaged in the HAC fire event. Therefore, damage of the impact limiters in the vent port region could allow excessive temperatures in the vent port seals. An attack from a puncture bar with the center of gravity of the cask more or less above the vent ports, contacting the damage from an end drop, will cause the worst-case damage to the impact limiter around the vent port. An attack in the thinner center portion of the impact limiter is not of concern due to the thickness of the lid being more than the required thickness to prevent penetration. Also, an attack in the thinner center portion of the impact limiter through the C.G. cannot be in the region around the vent port, and thus is not of concern.

Due to the large size of the impact limiter area relative to the 6-inch diameter of the puncture bar, this puncture test would have a negligible influence on the free drop if it were performed prior to the free drop. Thus, this puncture will be performed after the vertical end drop. This test order satisfies both the test order requirement of 10 CFR 71 as well as the worst-case test order requirement of TS-R-1.

C.G.-over-Corner Puncture. The cask lid is closed using two elastomeric O-ring face seals that may be damaged in the HAC fire event. The worst-case damage to the impact limiter in the cask lid area would be a puncture towards the side of the lid of the cask in the C.G.-over-corner drop damage. The bar should be oriented so that the potential penetration depth is not hindered by the resistance of the cask end structure. This puncture test would have a negligible influence on the free drop if performed before the drop for the same reason as stated above. Thus, this puncture will be performed after the C.G.-over-corner free drop. This test order satisfies both the test order requirement of 10 CFR 71 as well as the worst-case test order requirement of TS-R-1.

Oblique Side Puncture. The 90-degree outside radial joint of the impact limiter is comprised of a relatively stiff structural angle, as compared to the rest of the impact limiter skin materials. This joint may be weakened by a free side drop. Thus, the bar shall be positioned on the side drop damage, such that the C.G. of the cask is essentially over the bar, and so it obliquely strikes the side shell near the reinforcement. This would examine the possibility that significant foam exposure could occur in the weakened joint region from the cask rolling off of the bar, if the impact limiter becomes impaled on it. This puncture will be performed after the side free drop, which satisfies the test order requirement of 10 CFR 71.

Consideration of the effects of a puncture prior to the free drop yields the possibility that puncture damage to the side drop crush region could increase free drop deformation, which could lead to hard contact and high impact, or loss of thermal protection of the elastomer seals. An essentially axial puncture orientation is expected to create the most damage to the side crush area. Since the bar axis would not be toward the C.G., further damage could occur as the package tips off of the bar. The puncture should be aligned with the side free drop. This puncture will be performed prior to the side free drop, satisfying the test order requirements of TS-R-1.

In the analytical fire thermal analysis, the cumulative damage from the puncture and subsequent side free drop should be considered as potentially aligned with a melt-out plug for possible formation of a chimney.

2.12.2.3.4   NCT Free Drop

For the 380-B package, which will have a licensed weight of 67,000 lb, the required normal conditions of transport (NCT) free drop height is 1 foot [1]. This represents only 3.3% of the energy

of the HAC free drop height of 30 feet. Thus, the effect of the NCT free drop on the maximum impact, crush deformation, and attachment integrity is negligible. Therefore, the NCT free drop does not need to be included in the certification test program.

2.12.2.4 Summary of Certification Tests

Based on the discussions in Section 2.12.2.3, *Identification of Worst-Case Test Orientations*, the planned certification tests for the 380-B package are summarized below and in Table 2.12.2-1. Free drops are depicted in Figure 2.12.2-2 and puncture drops in Figure 2.12.2-3.

The order of free drops and punctures is provided as a guide. The tests may in fact be performed in any order, except that the order of the puncture drops must be performed relative to the free drops as stated in Table 2.12.2-1. All free drops will be instrumented with active accelerometers. Instrumentation of the puncture drops is not anticipated. If stated to be cold or warm, the bulk average temperature of the foam must be per the discussion given in Section 2.12.2.2.1, *Temperature*. Interference of damage is expected to be negligible.

The test sequence envisions several separate half-scale impact limiter test articles attached to the same dummy cask. Impact limiter 1 will be constructed using the 17 lb/ft³ foam, while the rest, impact limiters 2, 3, and 4, will be constructed using the 15 lb/ft³ foam density. The weight difference between impact limiters 1 and 2 will be negligible to the package total weight and will not noticeably affect the location of the package C.G.

Optionally, a steel plate, having the weight and C.G. location of an impact limiter, may be used in place of an upper impact limiter in free drop orientations where only the lower impact limiter provides the package impact mitigation (i.e. vertical end drop and C.G.-over-corner). Any expected impact on the steel plate location due to a final tip over should be negligible for such drop orientations.

The test series consists of three, 30-foot free drops, and four, 40-inch puncture drops. The order of the certification tests are described in the section below and Table 2.12.2-1. Note that since all test articles are identical, each end of the test package qualifies as the package "top", as necessary. No tests need to be performed on the package "bottom".

2.12.2.4.1 Test Sequence and Damage Accumulation

For the following test sequence, the certification test unit (CTU) number corresponds to the impact limiter number(s) required for the test.

Test D1. CTU-1, Limiter No. 1 will be tested in the end drop orientation at cold temperature. The purpose of this test is to quantify the maximum end drop impact acceleration, and to prepare a surface for the subsequent puncture (test P1).

Test P1. CTU-1, Limiter No. 1 will be dropped on the puncture bar through the package C.G., near the edge of the end drop damage from test D1. The axis of the bar should pass within approximately one bar radius of the vent port location when the cask axis is approximately 58° from the horizontal. This orientation of the cask allows the center of the puncture bar, package C.G. and vent port location to align while still striking the damage from test D1. Any azimuth location may be used.

The purpose of this test is to create the worst-case damage around the vent port for the thermal analysis. To determine if this is the worst-case for the thermal analysis, the puncture damage may be imposed on the warm end drop analytical deformations.

Test D2. CTU-2, Limiter No. 2 will be tested in the C.G.-over-corner orientation (50 degrees off horizontal). The temperature will be warm as specified by Section 2.12.2.2.1, *Temperature*. The purpose of this test is to quantify the maximum crush strain in the C.G.-over-corner orientation, and to prepare a surface for the subsequent puncture test (test P2). Azimuth shall be between the impact limiter attachment bolts since this will not have a measurable effect on the free drop response and will ensure maximum damage for the subsequent puncture drop.

Test P2. CTU-2, Limiter No. 2 will be dropped on the puncture bar through the package C.G., on the damage from test D2. The bar should clear both the corner reinforced regions of the impact limiter skin while the cask axis is approximately 40 degrees off horizontal to maximize the perforation into the remaining impact limiter foam near the side of the cask lid. Due to the D2 damage being between the impact limiter attachments, the worst-case foam damage will occur near to the lid elastomeric seal area. The purpose of this test is to create the worst-case damage around the cask lid elastomer seals for the thermal analysis.

Test P3. CTU-3, Limiter No. 3 will be dropped onto essentially the center of the tapered region of the impact limiter while the package is oriented at 75 degrees from horizontal. This orientation evaluates the possibility that significant damage could occur from a puncture prior to free drop. The azimuth location shall be between the impact limiter attachment bolts since this will not have a measurable effect on the free drop response and will ensure maximum damage for the subsequent puncture drop. The puncture bar should be sufficiently long to allow full damage to occur in impact limiter No. 3 before the package gains support from the ground.

Test D3. CTU-3.4, Limiter Nos. 3 and 4 will be tested in the horizontal side drop orientation at warm temperature. The package shall be oriented such that P3 puncture damage is positioned directly below the cask since Test P3 could degrade the energy absorption capability of impact limiter No. 3 by some amount. The purpose of this test is to quantify the maximum deformation of the impact limiters, both damaged (I.L. No. 3) and undamaged (I.L. No. 4). This test will prepare a surface for subsequent puncture testing done on impact limiter No. 4.

Test P4. CTU-4, Limiter No. 4 will be dropped onto the puncture bar through the package C.G. with an impact point on the side drop impact damage from test D3. Due to the possible weakening of the impact limiter 90 degree radial joint after test D3, the package shall be dropped on the puncture bar through the package C.G., near the edge drop damage from test D3. The package shall be oriented at an approximate angle of 25 degrees off horizontal as shown in Figure 2.12.2-3. The exact impact point and package azimuth may be chosen by the AFS Test Engineer in light of the damage which occurs in D3.

2.12.2.4.2   Measurements

Measurements of the certification test results will be made in explicit support of the test objectives identified in Section 2.12.2.3, *Identification of Worst-Case Test Orientations*, and will consist of configuration (dimensional) measurements of the damage, and acceleration measurements of the free drops. Temperature measurements will be made on an ongoing basis to fully characterize the bulk average temperature of the foam.

Measurements of the free drop deformation damage will take springback of the limiter into account, and by use of crush gages or other techniques, attempt to obtain the maximum crush at the moment of impact. Puncture measurements should be made from the prevailing damage surface and record the depth and diameter, or other relevant information, of the puncture test damage. A conventional speed video and still photographic record of each drop and puncture will be made.

Accelerometers will be redundant, and placed at the CTU center of gravity and/or as directed by the AFS Test Engineer. The data will be filtered to obtain the rigid body impact, using the guidance of a fast Fourier transform (FFT), or equivalent, of the time history data. A filtering frequency of between approximately 300 and 600 Hz is anticipated (150 to 300 Hz, full-scale) according the guidance in paragraph 701.9 of [34].

2.12.2.5 Acceptance Criteria

The following are the acceptance criteria for certification testing of the 380-B package:

1. The impact limiter shells must retain their general integrity for all impacts and deformations. Ripped welds or other tears or fissures are acceptable as long as they are limited in extent and compatible with the HAC fire thermal analysis. Full puncture perforation of the impact limiter shells is expected.

2. The impact limiter attachments must retain the limiters on the cask. A limited degree of distortion or dislodging of the limiters is acceptable, but must be compatible with the HAC fire thermal analysis.

3. The impact limiters must maintain package deceleration to acceptable levels. The safety analyses will utilize the results of the certification test or of the impact analysis, whichever is greater, as inputs.

4. The maximum damage to the limiter from the single worst-case free drop and puncture test sequence must fall within the bounding assumptions used in the HAC fire thermal analysis.

Table 2.12.2-1 - Summary of Certification Tests

No.	Test Description[1]	Impact Limiter (I.L.)	Temperature[2]	Purpose of Test & Expected Damage
D1	End Drop	#1	Cold	Maximum end impact
P1	End Drop Puncture	#1	Not controlled	Maximum damage in vent port region for thermal analysis
D2	C.G. over corner drop	#2	Warm	Obtain maximum stroke damage
P2	C. G. over corner puncture	#2	Not controlled	Maximum damage in cask lid elastomer seal region for thermal analysis
P3	Oblique on Taper	#3	Not controlled	Maximum limiter degradation **prior to drop D3** for TS-R-1 requirements
D3	Side Drop	#3 and #4	Warm	Quantifies possible maximum accumulation of free drop and puncture damage (I.L. #3) – minimum foam available for following puncture damage (I.L. # 4)
P4	On test D3 damage	#4	Not controlled	Quantifies possible maximum puncture damage that could affect a free drop orientation

Notes:

1. All free drops (Dx) are from 30 feet, and all punctures (Px) are from 40 inches.

2. See Section 2.12.2.2.1, *Temperature*.
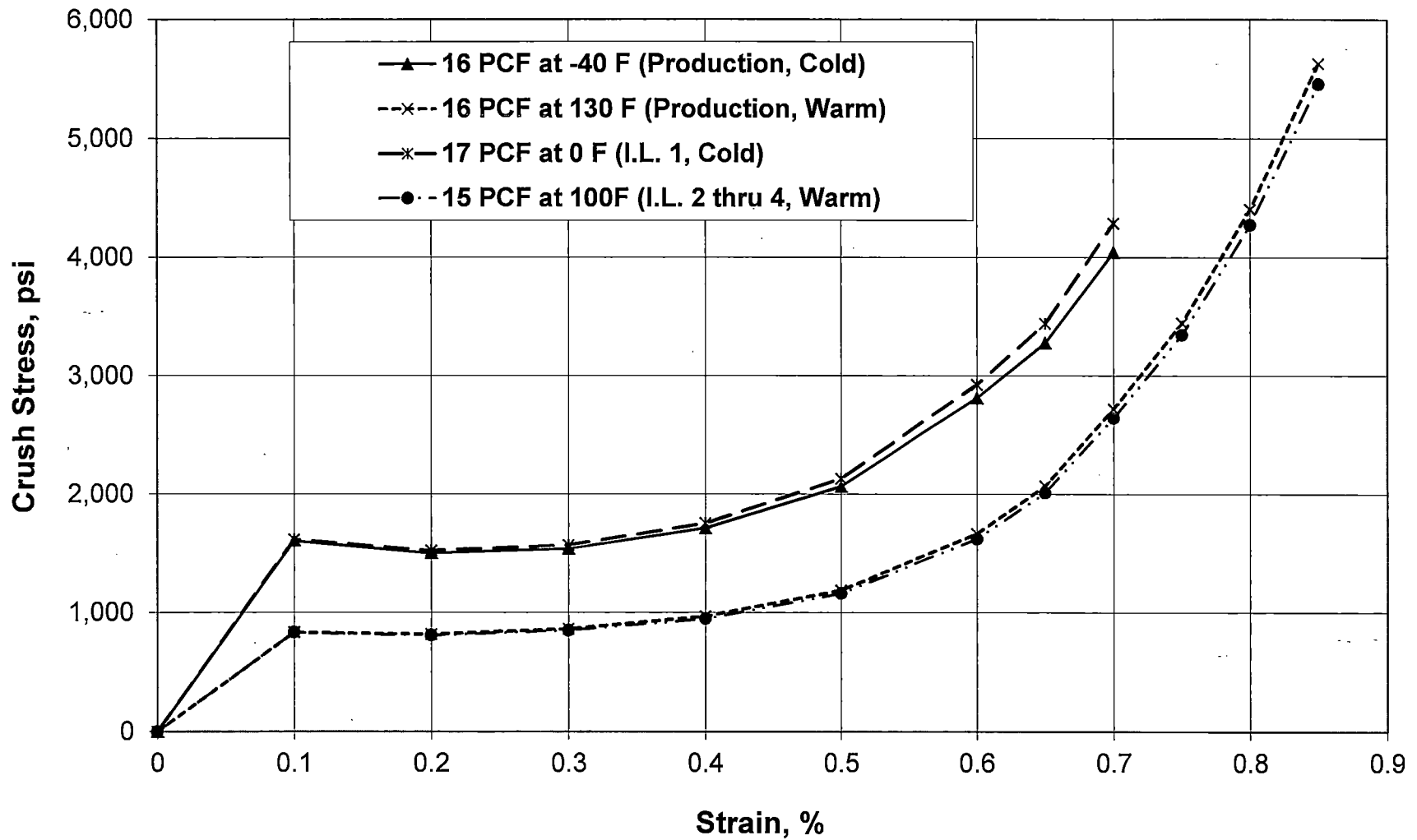
Figure 2.12.2-1 – 380-B Nominal Foam Crush Strength Curves for Production and Test Units
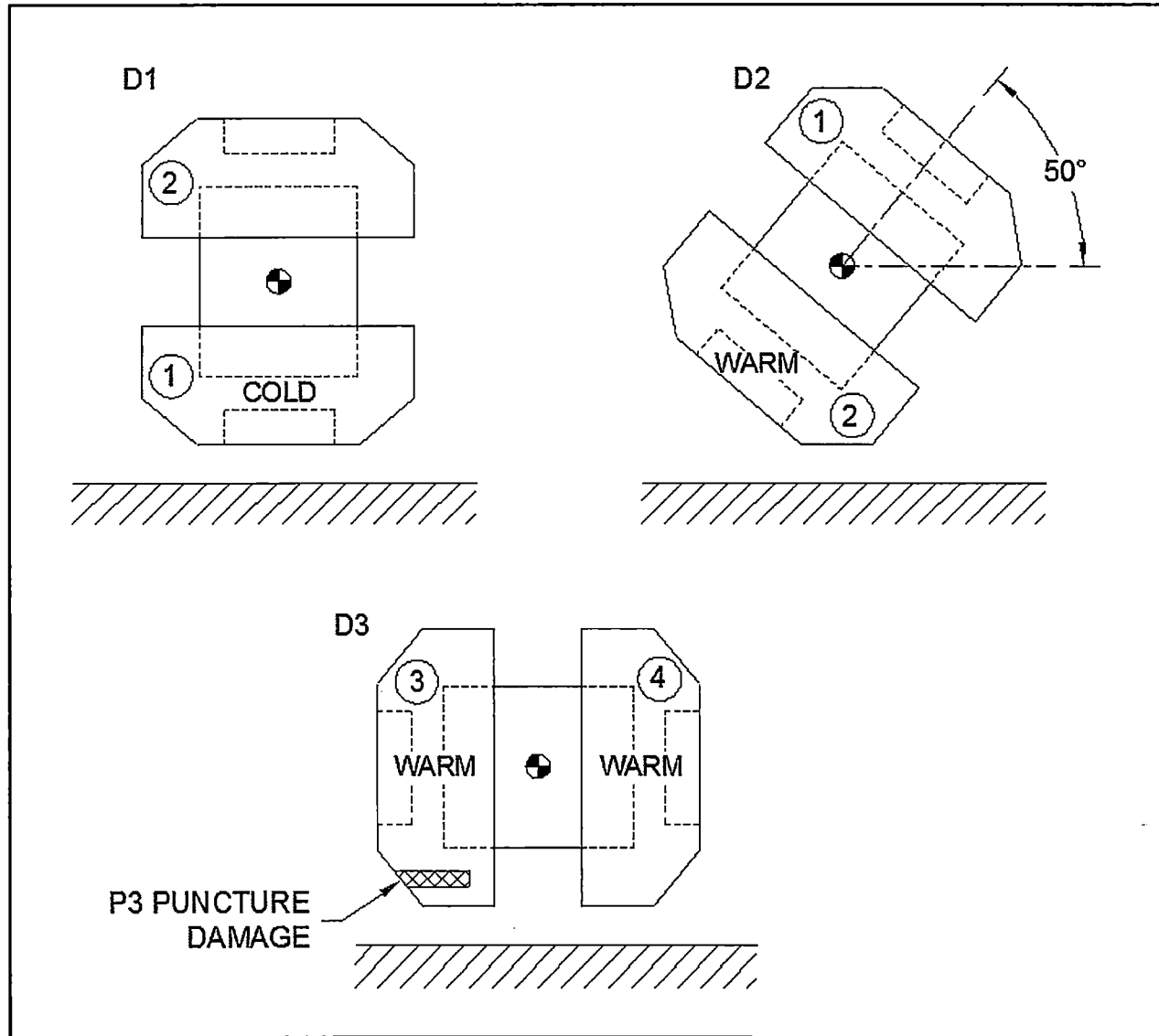
Figure 2.12.2-2 – 380-B Package Free Drop Orientations
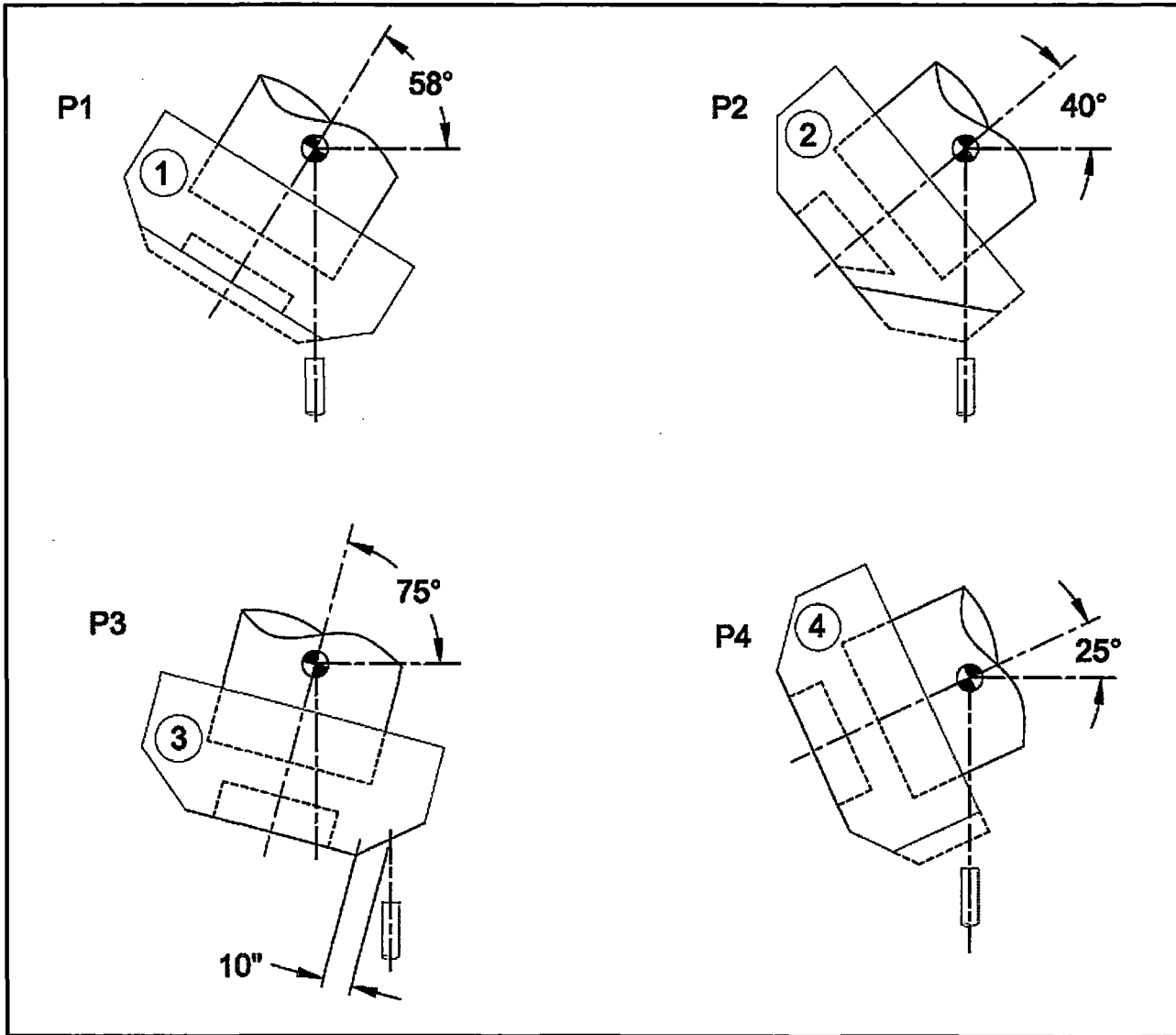
Figure 2.12.2-3 – 380-B Package Puncture Drop Orientations

2.12.3 Certification Test Results

This appendix presents the results of certification testing on the 380-B package that addresses the performance requirements of 10 CFR 71 [1] and TS-R-1 [31]. This material summarizes the results collected during performance of the tests outlined in Section 2.12.2, *Certification Test Plan*.

2.12.3.1 Introduction

Demonstration of compliance of the 380-B package design with the requirements of 10 CFR §71.73 and TS-R-1 §727 is primarily achieved using analysis. Certification testing is used to demonstrate the performance of the polyurethane foam-filled impact limiters and attachments. The tests reported in this appendix were performed using half-scale test impact limiters, attachments, and a dummy cask that had 1/8 of the weight of the full-scale cask (consistent with half-scale), as shown in Figure 2.12.3-1 and Figure 2.12.3-2. Both the impact limiters and the attachments (including the limiter attachment components and the cask attachment components) were half-scale duplicates of the full-scale design materials and construction. The impact limiter test specimens were in full compliance with the drawings in Section 1.3.3, *Packaging General Arrangement Drawings*, except for the scale factor of 1/2, and with the exceptions discussed below in Section 2.12.3.3, *Certification Test Unit Configuration*.

The objectives of these tests were to demonstrate the general structural integrity of the impact limiters and attachments in free drop and puncture events, to confirm the maximum impact magnitudes, and to verify that the maximum damage to the impact limiters is bounded by the assumptions used in the thermal and criticality analyses. Further discussion of the tests, including a justification of the tests chosen, is provided in Appendix 2.12.2, *Certification Test Plan*. A comparison of the test results to the impact limiter calculations is given in Section 2.12.5.6.1, *Benchmark Results*.

2.12.3.2 Test Facilities and Instrumentation

2.12.3.2.1 Test Facilities

Testing was performed at Lampson International LLC in Pasco, Washington, beginning August 14, 2014. The drop pad weighed approximately 110,000 lb, including a 2-inch thick, embedded steel plate impact surface. The pad therefore represented an essentially unyielding surface for the certification test units (CTUs), which weighed between approximately 8,266 lb and 8,303 lb.

The half-scale puncture bars were made of carbon steel, 3 inches in diameter, with an edge radius between 0.10 and 0.12 inches. The average puncture bar yield strength was 52 ksi and the average tensile strength was 74 ksi. The bar lengths were 24 inches for P1, P2, and P4, and 32 inches for P3. The puncture bars were mounted perpendicularly to the impact surface, and welded to the drop pad for puncture testing. A quantity of four (4) stiffeners, each 8 inches by 8 inches by 1/2-inch thick, on a 22-inch square by 3/4-inch thick baseplate were used for each puncture bar assembly.

2.12.3.2.2 Temperature

The temperature of the polyurethane foam in the impact limiter was controlled for free drops D1, D2, and D3. The D1 free drop was performed with the impact limiter polyurethane foam in the cold condition. A refrigerated container was present onsite to chill the CTU prior to testing. The D2 and D3 free drops were performed with the impact limiter foam at warm temperature. An insulated enclosure with warm ambient air, provided by household resistance heaters, was onsite to warm the foam. All puncture tests used prevailing temperature. The foam temperatures were measured by means of thermocouples (TC) inserted in 1/4-inch drilled holes in the impact limiters. The specific locations and depths into the foam of the thermocouples for each impact limiter are as shown in Figure 2.12.3-5 through Figure 2.12.3-10.

2.12.3.2.3 Accelerometers

Accelerometers were used to record the impact of each free drop. Accelerations of the puncture drops were not recorded. For the end drop and center of gravity (C.G.)-over-corner drop orientations, the measurement axis of the accelerometers was parallel with the CTU axis. For the horizontal side drop orientation, the measurement axis was transverse to the CTU axis. The mounting locations for the accelerometers were centered on the dummy cask body, which is the approximate CTU C.G. location, with four locations equally spaced about the dummy cask axis, see Section 2.12.3.7, *Filtered Accelerometer Time Histories*.

The raw data was conditioned and low-pass filtered at a cutoff frequency of 500 Hz. Per the guidance given in TS-G-1.1, *Advisory Material for the IAEA Regulations for the Safe Transport of Radioactive Material*, [34] an appropriate cutoff frequency range is found from:

$$f_c = [100 \text{ to } 200] \times \left(\frac{100}{m}\right)^{\frac{1}{3}} = 300 \text{ to } 600 \text{ Hz}$$

Where m is the mass of the package in metric tonnes (8,400 lb equals 3.81 metric tonnes). From this, a reasonable cutoff frequency of 500 Hz was chosen.

2.12.3.3 Certification Test Unit Configuration

The certification testing was performed using half-scale impact limiters, impact limiter attachment bolts, and a dummy cask. The impact limiters, impact limiter attachment bolts, cask lugs, and cask lug welds to the dummy cask are all half-scale representations of the production design. The dummy cask is a half-scale representation of the production cask outer dimensional envelope and weight.

Tests involving damage to only one impact limiter (i.e., all except the side drop) utilized the ballast plate on the non-impact end to facilitate simpler and safer drop orientation rigging, see Figure 2.12.3-3 and Figure 2.12.3-4 for the test unit configuration with the ballast plate. The ballast plate models the weight of the impact limiter on the non-impacted end of the CTU and also closely models the rotational moment of inertia of the whole CTU about a transverse axis. The assembled CTU weights were between 8,266 lb and 8,303 lb as shown in Table 2.12.3-1. The specific configuration of the CTU for a given test is as noted in Table 2.12.3-1 and includes which impact limiter(s) is present (i.e., CTU-1 represents the dummy cask assembled with impact limiter-1 and the ballast plate, and CTU-3.4 represents the dummy cask assembled with impact limiters-3 and 4).

Any differences between the CTU packaging design and the production design is discussed and justified below.

1. The impact limiter foam for the production design is nominally 16 lb/ft^3. For the purpose of testing at hot and cold temperatures, as described and justified in Section 2.12.2.2.1, *Temperature*, one of the CTU impact limiters (-1) had 17 lb/ft^3 foam for testing at cold temperature, and three (-2, -3, and -4) had 15 lb/ft^3 foam for testing at warm temperature.

2. The CTU impact limiters each had four 1/4-inch drilled holes for thermocouple probes as described in Section 2.12.3.2.2, *Temperature*. These holes did not have a significant effect on the crush behavior of the impact limiters in any drop or puncture event.

3. Two of the CTU impact limiters, serial numbers A2-01 and A1-01, corresponding to impact limiter-1 and -2, did not have the reinforcing ring located over the full penetration weld in Zone A3, sheet 4, of drawing 1916-02-03-SAR. The reinforcing ring was not present on the D1 or D2 free drops. The reinforcing ring would have no effect on the end drop (D1) since the weld didn't fail and there was essentially no deformation at the weld site. The effectiveness of the reinforcement for the C.G.-over-corner drop (D2) is discussed in Section 2.7.1.1, *Impact Forces and Deformations*. Two of the CTU impact limiters, serial numbers A1-02 and A1-03, corresponding to impact limiter-3 and -4 respectively, did include the reinforcing ring over the full penetration weld located in Zone A3, sheet 4, of drawing 1916-02-03-SAR. The half-scale reinforcing ring has a 35.0-inch ID and 37.0-inch OD. The half-scale reinforcing ring is the same thickness and material as the base material (0.120-inch, ASTM A240, Type 304) and is welded all around the ID and OD with full thickness fillet welds. The reinforcing ring was added during the test program as result of a nonconforming weld that split during the D2 free drop. The complete joint penetration weld on impact limiter-2 was found to have very little fusion and was not in conformance with the design. The decision was made to reinforce the remaining two impact limiters for the D3 free drop and include the reinforcement in the full-scale production design. Additional information on the test results from free drop D2 can found in Section 2.12.3.4.3, *Free Drop Test D2*.

4. The dummy cask was modified / repaired on both ends over a 3.00-inch axial length by a 0.12-inch reduction to its outer diameter. The reduction length is 1/3 of the 9.0-inch dummy cask to impact limiter engagement; therefore the overall interface of the impact limiter with the dummy cask is not affected. A thirty degree chamfer, not exceeding 1/4-inch in the radial direction, was also added to both ends of the dummy cask. These modifications were made to facilitate installation of the impact limiters as part of a two-pronged approach to remedy assembly difficulties with the dummy cask. The impact limiters had minor welding warpage on the inner diameter, near the bottom of the cask cavity, at the threaded attachment lug bosses. The welding warpage also caused misalignment of the impact limiter attachment bolts and was subsequently repaired by hydraulic jacking. Neither of these repairs affects or influences the recorded acceleration data or test performance of the impact limiters and attachments.

2.12.3.4 Free Drop and Puncture Drop Test Results

The certification test program consists of three, HAC 30-ft free drops, and four, 40-inch puncture drops. The certification tests were performed according to the sequence in the test procedure.

There were three test series 1, 2, and 3. Test series 1 and 2 included a 30-ft free drop test followed by a 40-inch puncture drop test. Test series 3 included a 40-inch puncture drop test, followed by a 30-ft free drop test, followed by another 40-inch puncture drop test. A summary table of the tests is given in Table 2.12.3-2. The tests are depicted in Figure 2.12.3-11 and Figure 2.12.3-12.

Low pass filtered accelerometer results given in the following sections are shown in Section 2.12.3.7, *Filtered Accelerometer Time Histories*. The acceleration peak values are resolved to a value that is perpendicular to the ground, as necessary. Due to the necessity of mounting some accelerometers with their mounting threads facing upwards and others with the threads facing downwards, both positive and negative signals were recorded. However, all results shown in the following sections are given as positive.

For free drop test D1 that was a vertical bottom-down drop, the accelerometers were mounted with their measurement axes parallel to the impact direction. Therefore, the accelerometer readings require no adjustment.

For test D2, which was the C.G.-over-corner free drop, the accelerometers were mounted with their measurement axes parallel to the cask axis. The accelerometer reading is divided by the cosine of 40°, which corresponds to the recorded angle between the cask axis and vertical, to obtain the impact perpendicular to the ground.

For test D3 that was a side drop, the accelerometers were mounted with their measurement axes transverse to the cask axis. Therefore, the accelerometer readings require no adjustment to be perpendicular to the ground.

All puncture drop tests were performed from a height of 40 inches above the top of the puncture bar. The bars remained securely attached to the drop pad during each test. A new puncture bar was used for each test. All the puncture bars, except P3, became damaged from contact with the CTUs at their top rounded edge. The bars for test P2 and P4 were also slightly bent, and the bar for test P3 was significantly bent.

The impact limiter attachment bolts were not touched between the free drop test and the associated (subsequent) puncture drop test. Likewise, the impact limiter bolts were not touched on impact limiter-3 between the P3 puncture drop test and the subsequent D3 free drop test.

For each test, the temperature of the polyurethane foam was recorded. The cold temperature target for the bulk of the polyurethane foam was 0 °F, and the warm temperature target was 100 °F. The temperature of the foam for puncture drops was accepted at the prevailing temperature and recorded at the time of the test.

The following sections also present and discuss test measurements and observations made subsequent to the tests.

2.12.3.4.1 Free Drop Test D1

Test D1 was performed on CTU-1, impact limiter-1 (S/N A2-01), and consisted of a 30-ft HAC free drop test in the bottom-down orientation, with the axis vertical. The free drop test orientation is shown in Figure 2.12.3-13. The polyurethane foam temperature readings for test D1 were -19.0 °F, -19.7 °F, -12.7 °F, and -9.7 °F. The average foam temperature was -15.3 °F, which was below the maximum test temperature of 0 °F. The accelerometer results are shown below.

Accelerations for Free Drop Test D1, Low Pass Filter Cutoff at 500 Hz					
Accelerometer No.	1	2	3	4	**Average**
Max Acceleration	156g	152g	153g	159g	**155g**
Full-Scale Equivalent Acceleration (Half-Scale Value / 2)					**78g**

During the drop event the CTU impacted the drop pad and subsequently rebounded vertically approximately 2-ft into the air, then hit the drop pad vertically a second time, and bounced up unevenly causing it to tipover on to its side.

The 30-ft end drop resulted in minimal damage to impact limiter-1. The tapered end of the impact limiter had some buckling of the outer shell near the impact surface. The tapered end diameter of the impact limiter had a pre-test diameter of 29.5 inches, which grew to 35 inches as evident by scratches from contact with the drop pad. This is an increase of 5.5 inches on the diameter. The overall impact limiter crush in the axial direction based on the average before and after measurements is (23-13/16 + 23-3/4) / 2 – (22-1/8 + 22) / 2 = 1.72 inches. The half-scale deformation must be factored by two for relating to full-scale, which is then 11.0 inches for the tapered end diameter growth and 3.44 inches for the impact limiter axial crush. This amount of crush does not account for any potential springback that may have occurred. The end drop impact limiter damage is shown in Figure 2.12.3-14 and Figure 2.12.3-15.

2.12.3.4.2 Puncture Drop Test P1

Test P1 was performed on CTU-1, impact limiter-1 (S/N A2-01), and consisted of a 40-inch HAC puncture drop test. The test orientation was with impact limiter-1 down and the CTU axis at 56° from horizontal, which was within the allowed range of 58° ± 3°. The CTU azimuth was located such that the target was between impact limiter attachment bolts. The initial contact point with the puncture bar was approximately at the crushed outer edge of the impact limiter with the puncture bar essentially aligned with the CTU C.G. The puncture drop test orientation is shown in Figure 2.12.3-16. The polyurethane foam temperature readings for test P1 were 54.5 °F, and 1 °F. The large temperature difference is explained by one thermocouple being a short probe and the other a long probe, see Figure 2.12.3-5, which demonstrates the ambient heat flowing into the core of the impact limiter and the large heat capacity of the lead filled dummy cask. The average foam temperature was 27.8 °F. There was no temperature requirement for the puncture drop test other than the prevailing foam temperature needed to be recorded.

During the puncture drop event the CTU landed on target hitting the puncture bar, which penetrated the impact limiter as expected, causing the CTU to ultimately come to rest on the puncture bar as shown in Figure 2.12.3-17. The puncture bar sheared a 3-inch diameter half circle through the outer shell on the leading edge of the impact, and then tore an inverted "V" on the back end of the puncture as shown in Figure 2.12.3-18 and Figure 2.12.3-20. The overall impact limiter shell puncture damage is 3 inches wide by 6-3/8 inches tall. The penetration of the puncture bar into the foam measured 3 inches in diameter by 11 inches deep, as shown in Figure 2.12.3-19. The sheared/torn metal of the outer shell was removed from the bottom of the puncture hole and the remaining foam was drilled through, approximately aligned with the axis of the puncture hole, to measure 2 inches from the surface of the remaining foam to contact with the inner plate of the impact limiter. The puncture bar appeared to have made contact with the

inner plate of the impact limiter on the leading edge of the puncture bar. The puncture bar was damaged on the leading rounded edge during the test. The damage includes a flat spot 1-1/2 inches wide by 3/8 inch long. Therefore, some of the 2 inches between the surface of the foam and inner plate must be springback (i.e., air gap).

The impact limiter attachment bolts were removed and all had residual tightness. All of the bolts also appeared to be in good condition with no deformation as shown in Figure 2.12.3-21. The bolts did exhibit significant flaking and chipping of their electroless nickel plating, which is not attributed to testing but rather to poor plating quality. The poor plating quality did not degrade the structural performance of the bolts during drop testing.

All of the cask lugs and welds were structurally sound and showed no damage except for the occasional small dent attributed to falling shackles from the rigging above during the test.

2.12.3.4.3   Free Drop Test D2

Test D2 was performed on CTU-2, impact limiter-2 (S/N A1-01), and consisted of a 30-ft HAC free drop test. The test orientation was with impact limiter-2 down and the CTU axis at 48° from horizontal, which was within the C.G.-over-corner orientation allowed range of 50° ± 3°. The CTU azimuth was between impact limiter attachment bolts. The free drop test orientation is shown in Figure 2.12.3-22. The polyurethane foam temperature readings for test D2 were 98.5 °F, 98.7 °F, 99.7 °F, and 103.1 °F. The average foam temperature was 100.0 °F, which was equal to the minimum test temperature of 100 °F. The data from accelerometer-1 was lost or not recorded due to a cable cut during the test. Data from accelerometers-3 and -4 were partially lost, also due to their cables being cut during the test, however the maximum impacts were saved. The plots in Section 2.12.3.7, *Filtered Accelerometer Time Histories* show how much data was recorded. The accelerometer results are shown below.

Accelerations for Free Drop Test D2, Low Pass Filter Cutoff at 500 Hz					
Accelerometer No.	1	2	3	4	**Average**
Max Acceleration	-	67g	81g	78g	**75g**
⊥ to drop pad (Half-Scale Value / cos40)	-	87g	106g	102g	**98g**
Full-Scale Equivalent Acceleration (Half-Scale Value / 2)					**49g**

During the C.G.-over-corner free drop event the CTU impacted the drop pad and subsequently rebounded vertically approximately 1-ft into the air and simultaneously rotated forward, and then hit the concrete edge of the drop pad (with the ballast plate) and rolled onto the ballast plate into the gravel adjacent to the drop pad as shown in Figure 2.12.3-23.

The 30-ft C.G.-over-corner free drop resulted in significant damage to the impact limiter, as expected, since the test orientation and warm temperature were chosen to maximize deformation. The deformed impact patch on the impact limiter resulting from contact with the drop pad was an oval 22-1/2 inches tall by 34 inches wide as shown in Figure 2.12.3-24. The maximum crush depth perpendicular to the impact patch towards the CTU C.G., based on the before and after measurements, is (10-9/16 − 4-1/8) x cos(40) = 4.93 inches. The half-scale deformation must be factored by two for relating to full-scale, which is then 9.86 inches for the impact limiter crush. This

amount of crush does not account for any potential springback that may have occurred. The impact patch height and width is 45 inches by 68 inches in full-scale.

The most significant damage result from the C.G.-over-corner free drop is the split open complete joint penetration (CJP) weld on the flat surface of the impact limiter facing the top of the CTU as shown in Figure 2.12.3-25. Visual inspection of the split weld showed significant lack of fusion (or penetration) in the weld and was estimated to be less than 50% of the thickness of the base material. The split of the all-around weld encompassed 45% of the perimeter approximately centered on the drop azimuth. The weld was definitely not CJP and could not develop the full membrane strength of the impact limiter shell. The nonconforming weld issue found on this impact limiter lead to serious concern that the two remaining untested impact limiters also had nonconforming welds in the same joint. This joint would also be tested in their respective side drop, D3. Therefore, a reinforcing ring was added over the top of the assumed nonconforming weld of both side drop test impact limiters. The reinforcing ring has a 35.0-inch ID and 37.0-inch OD. The ring is the same thickness and material as the base material (0.120-inch, ASTM A240, Type 304) and is welded all around the ID and OD with full thickness fillet welds. See Figure 2.12.3-35 and Figure 2.12.3-36. This reinforcement will carry-over to the production design.

Despite the damage associated with the nonconforming weld, the decision was made to proceed with the planned cumulative puncture drop test on impact limiter-2. Collecting the puncture damage data on the C.G.-over-corner deformations was considered too valuable to not perform the test.

2.12.3.4.4 Puncture Drop Test P2

Test P2 was performed on CTU-2, impact limiter-2 (S/N A1-01), and consisted of a 40-inch HAC puncture drop test. The test orientation was with impact limiter-2 down and the CTU axis at 40° from horizontal, which was within the allowed range of 40° ± 3°. The CTU azimuth was located such that the target was between impact limiter attachment bolts. The initial contact point with the puncture bar was on the damaged surface from free drop test D2 and aligned with the CTU C.G. The puncture drop test orientation is shown in Figure 2.12.3-26. The polyurethane foam temperature readings for test P2 were 100.7 °F, and 104.1 °F. The average foam temperature was 102.4 °F. There was no temperature requirement for the puncture drop test other than the prevailing foam temperature needed to be recorded.

During the C.G.-over-corner puncture drop event the CTU landed on target hitting the puncture bar, which penetrated the impact limiter as expected. The CTU stopped when the puncture bar hit the inner plate of the impact limiter. The CTU then rotated forward, pivoting on the puncture bar embedded in the impact limiter, causing the top of the CTU to contact the drop pad as shown in Figure 2.12.3-27. The puncture bar sheared a 3-inch diameter half circle through the outer shell on the leading edge of the impact, and then tore an elongated continuation of the half circle on the back end of the puncture as shown in Figure 2.12.3-33. The overall impact limiter shell puncture damage is 3 inches wide by 7-1/2 inches tall. The penetration of the puncture bar into the foam measured 3 inches in diameter by 11 inches deep on the leading edge and 6 inches deep at the trailing edge. Damage to impact limiter-2 can also be seen in Figure 2.12.3-28 through Figure 2.12.3-33.

The puncture bar was damaged on the leading rounded edge during the test. The damage includes a flat spot 1-3/4 inches wide by 3/4 inch long. The puncture bar also bent approximately 1/2-inch measured at the top.

The impact limiter attachment bolts were removed and all had residual tightness. All of the bolts also appeared to be in good condition with no deformation as shown in Figure 2.12.3-34. The bolts did exhibit more flaking and chipping of their electroless nickel plating, which is not attributed to testing but rather to poor plating quality. The poor plating quality did not degrade the structural performance of the bolts during drop testing.

All of the cask lugs and welds were structurally sound and showed no damage except for the occasional small dent attributed to falling shackles from the rigging above during the test.

2.12.3.4.5   Puncture Drop Test P3

Test P3 was performed on CTU-3, impact limiter-3 (S/N A1-02), and consisted of a 40-inch HAC puncture drop test. This test was designed for possible future licensing to the rules of the IAEA, as described in the Section 2.12.2.3.3, *Puncture Drops*. The test orientation was with impact limiter-3 down and the CTU axis at 77° from horizontal, which was within the allowed range of 75° ± 3°. The CTU azimuth was located such that the target was between impact limiter attachment bolts and at the orientation planned for the upcoming D3 free drop test. The initial contact point with the puncture bar was on the undamaged tapered surface, approximately 5 inches outside the small tapered end outer diameter, as shown in Figure 2.12.3-12. The puncture drop test orientation is shown in Figure 2.12.3-37. The polyurethane foam temperature readings for test P3 were 81.0 °F, and 79.5 °F. The average foam temperature was 80.3 °F. There was no temperature requirement for the puncture drop test other than the prevailing foam temperature needed to be recorded.

The CTU landed on target hitting the puncture bar, which penetrated the impact limiter as expected. The CTU seamlessly transitioned from displacement in drop direction to rotating backward, pivoting on and significantly bending the embedded puncture bar, until the opposite side of the impact limiter contacted the drop pad, as shown in Figure 2.12.3-38 and Figure 2.12.3-39. The puncture bar sheared a 3-inch diameter half circle through the outer shell on the leading edge of the impact, and then tore an inverted "V" on the back end of the puncture as shown in Figure 2.12.3-40. The overall impact limiter shell puncture damage is 3 inches wide by 6 inches tall to the foam and 8 inches tall to the shell. The penetration of the puncture bar into the foam measured 3 inches wide by 10 inches deep. The hole in the foam at the 10-inch depth was 5 inches tall.

The puncture bar was not damaged on the leading rounded edge during the test. However, the puncture bar was significantly bent about its length above the weldment stiffeners. Note, this puncture bar was 8 inches longer than the other puncture bars to ensure there was sufficient length in this orientation to impart all the drop energy to the bar before contacting the drop pad.

After the P3 oblique on taper puncture drop, the ballast plate was removed and impact limiter-4 (S/N A1-03) was installed. The CTU with both impact limiters (CTU-3.4) was then thermally conditioned prior to the subsequent 30-ft side drop.

2.12.3.4.6   Free Drop Test D3

Test D3 was performed on CTU-3.4, impact limiter-3 (S/N A1-02) and impact limiter-4 (S/N A1-03), and consisted of a 30-ft HAC free drop test in the side drop orientation, with the axis horizontal. The free drop test orientation is shown in Figure 2.12.3-41. The polyurethane foam temperature readings for impact limiter-3 for test D3 were 102.2 °F, 104.0 °F, 104.5 °F, and 101.1 °F. The polyurethane foam temperature readings for impact limiter-4 for test D3 were

103.5 °F, 102.8 °F, 105.0 °F, and 107.4 °F. The average foam temperatures were 103.0 °F, and 104.7 °F respectively, for impact limiters-3 and -4, which was above the minimum test temperature of 100 °F. The accelerometer results are shown in the table below.

Accelerations for Free Drop Test D3, Low Pass Filter Cutoff at 500 Hz					
Accelerometer No.	1	2	3	4	**Average**
Max Acceleration	118g	119g	117g	122g	**119g**
Full-Scale Equivalent Acceleration (Half-Scale Value / 2)					**60g**

During the side drop event the CTU impacted the drop pad and subsequently rebounded vertically approximately 1-1/2 to 2-ft into the air, then hit the drop pad horizontally a second time, did an approximately 30° counterclockwise spin about the drop axis, and finally came to a rest in the horizontal orientation, after a little minor rocking on the deformed surfaces of the impact limiters, as shown in Figure 2.12.3-42.

The 30-ft side drop resulted in moderate damage to impact limiters-3 and -4. The OD of the impact limiters had some buckling of the outer shell near the impact surface. The deformed impact patch on impact limiter-3 resulting from contact with the drop pad was an oval 16-7/8 inches tall by 29 inches wide. The deformed impact patch on impact limiter-4 resulting from contact with the drop pad was an oval 16-1/2 inches tall by 30 inches wide as shown in Figure 2.12.3-44. The overall impact limiter-3 crush based on the average before and after measurements is (8-1/16 + 7-13/16) / 2 – (5-1/2 + 5-9/16) / 2 = 2.41 inches. The overall impact limiter-4 crush based on the average before and after measurements is (8-1/4 + 8) / 2 – (5-7/16 + 5-7/16) / 2 = 2.69 inches. The half-scale deformation must be factored by two for relating to full-scale, which for impact limiter-3 is 4.82 inches and for impact limiter-4 is 5.38 inches. This amount of crush does not account for any springback that occurred. The springback, or distance the impact limiter non-permanently displaced during the impact, was estimated to be 1-inch. The springback was estimated by measuring the difference parallel to the drop between the center of the impact patch and the perimeter of the impact patch. To account for springback and determine the maximum crush, 2 inches is added to the full-scale crush, bringing the maximum to 6.82 inches for impact limiter-3 and 7.38 inches for impact limiter-4. The impact patch measurements are taken where there are obvious signs of contact with the drop pad. The impact patch heights and widths are 33-3/4 inches by 58 inches and 33 inches by 60 inches in full-scale. The side drop impact limiter damage is also shown in Figure 2.12.3-48 and Figure 2.12.3-49.

Impact limiter-3 had a 4-inch tear in the OD weld seam on both sides of the impact patch. The tear width was small, 1/16 to 1/8-inch wide, with very little direct foam exposure. The more visible tear is shown in Figure 2.12.3-46. Note that impact limiter-3 also had puncture test damage prior to the D3 free drop that is included in Figure 2.12.3-43 through Figure 2.12.3-45. In Figure 2.12.3-43, a small amount of foam can be seen on the drop pad coming from the P3 puncture damage. The prior puncture test damage did not appear to be detrimental to the crush performance of the impact limiter, as it had slightly less crush than impact limter-4.

Prior to moving on with puncture drop test P4, impact limiter-3 was removed to install the ballast plate. Bolt-2 was located adjacent to the impact site on impact limiter-3 and was found to have no residual tightness, however all the other bolts did have residual tightness. The impact damage is

centered on bolts 1 and 12. All the impact limiter-3 bolts also appeared to be in good condition, except for the aforementioned plating issue, with no deformation as shown in Figure 2.12.3-47.

The reinforcing ring added to the assumed non-conforming CJP weld on both side drop impact limiters performed well. Both impact limiters experienced significant buckling of the shell in that region and the seam did not split. The results compared to the D2 free drop are significantly better.

2.12.3.5 Puncture Drop Test P4

Test P4 was performed on CTU-4, impact limiter-4 (S/N A1-03), and consisted of a 40-inch HAC puncture drop test. The test orientation was with impact limiter-4 down and the CTU axis at 23° from horizontal, which was within the allowed range of 25° ± 3°. The CTU azimuth was located such that the target was between impact limiter attachment bolts. The initial contact point with the puncture bar was on the surface damaged by the D3 free drop test, and aligned with the CTU C.G. The puncture drop test orientation is shown in Figure 2.12.3-50. The polyurethane foam temperature readings for test P4 were 99.9 °F, and 96.5 °F. The average foam temperature was 98.2 °F. There was no temperature requirement for the puncture drop test other than the prevailing foam temperature needed to be recorded.

During the puncture drop event on the D3 free drop damage the CTU landed on target hitting the puncture bar, which penetrated the impact limiter as expected, causing the CTU to ultimately come to rest on the puncture bar as shown in Figure 2.12.3-51 through Figure 2.12.3-53. The puncture bar sheared a 3-inch diameter half circle through the outer shell on the leading edge of the impact, and then continued to tear on the back end of the puncture as shown in Figure 2.12.3-54 through Figure 2.12.3-59. The overall impact limiter shell puncture damage is 3 inches wide by 3-3/4 inches tall. The penetration of the puncture bar into the foam measured 3 inches in diameter by 7 inches deep. The puncture bar went through the impact limiter and pushed the sheared/torn impact limiter outer shell to the dummy cask body. Impact limiter foam can be seen adhered to the dummy cask surface from the pressure in Figure 2.12.3-60.

The puncture bar was damaged on the leading rounded edge during the test. The damage includes a flat spot 1-1/2 inches wide by 1/2-inch long. The bar was also slightly bent.

The impact limiter attachment bolts were removed and all had residual tightness except bolt-1, which was directly adjacent to the puncture damage. Bolt-1 also appeared to have a slight bend along the shank, but none of the threads were damaged. All of the other bolts appeared to be in good condition, except for the plating, with no deformation as shown in Figure 2.12.3-61.

All of the cask lugs and welds were structurally sound and showed no damage except for the occasional small dent attributed to falling shackles from the rigging above during the test.

2.12.3.6 Summary of Test Results

Certification testing for the 380-B was performed on half-scale impact limiters and attachments (including the limiter attachment components and the cask attachment components) using one dummy cask and four impact limiters. A total of three 30-ft HAC free drops, and four puncture drops were performed on the test units. Free drop accelerations were recorded for use in finite element model benchmarking and other structural analyses. The deformations of the impact limiters that could have an effect on performance in the HAC fire event were recorded. There were no significant deformations or substantial degradation to the impact limiter attachment components and the cask attachment components performance.

Table 2.12.3-1 – Certification Test Unit Weight, lb

Component	CTU-1	CTU-2	CTU-3	CTU-3.4	CTU-4
	(lb)	(lb)	(lb)	(lb)	(lb)
Dummy Cask[7]	7,080	7,080	7,080	7,080	7,080
Top Impact Limiter[7]	NA	NA	NA	590[4]	590[4]
Bottom Impact Limiter[7]	618[1]	600[2]	600[3]	600[3]	NA
Ballast Plate[5,8]	572.5	572.5	572.5	NA	572.5
Impact Limiter Bolts[6]	9.5 (12 Qty.)	9.5 (12 Qty.)	9.5 (12 Qty.)	19 (24 Qty.)	9.5 (12 Qty.)
Hoist Rings[7]	14 (2 Qty.)	14 (2 Qty.)	14 (2 Qty.)	14 (2 Qty.)	14 (2 Qty.)
Total	8,280/8,294[9]	8,276	8,276	8,303	8,266
Drop Test Number	D1/P1[9]	D2 & P2	P3	D3	P4
Average Total[10]	8,282				

Notes:

1. Impact Limiter-1, Serial Number: A2-01, Foam Density 17 lb/ft^3.
2. Impact Limiter-2, Serial Number: A1-01, Foam Density 15 lb/ft^3.
3. Impact Limiter-3, Serial Number: A1-02, Foam Density 15 lb/ft^3.
4. Impact Limiter-4, Serial Number: A1-03, Foam Density 15 lb/ft^3.
5. Ballast plate weight includes swivel hoist ring, and six attachment bolts with washers.
6. Impact limiter bolts and washers calculated to weigh 19 lb for 24 Qty.
7. Dummy cask, hoist rings, and individual impact limiter weights are referenced from the supplier final data package.
8. Ballast plate assembly weight is calculated using the referenced component weights and the assembled weight of CTU-1 measured on-the-hook prior to placement in the refrigeration container.
9. CTU-1 was 8,280 lb for free drop test D1 that did not need the two cask body hoist rings to accommodate the rigging orientation. The two hoist rings were added for puncture test P1.
10. The average considers the CTU weight for all seven drop tests.

Table 2.12.3-2 – Summary of Certification Tests

No.	Test Description	Test Limiter	CTU	Temperature
D1	End Drop	1	1	Cold
P1	End Drop Puncture	1	1	Not controlled
D2	CG-over-corner drop	2	2	Warm
P2	CG-over-corner puncture	2	2	Not controlled
P3	Oblique on Taper	3	3	Not controlled
D3	Side Drop	3 and 4	3.4	Warm
P4	On test D3 damage	4	4	Not controlled

Notes:

1. All free drops (Dx) are from 30 feet, and all punctures (Px) are from 40 inches.

Four (4) swivel hoist rings for test rigging.
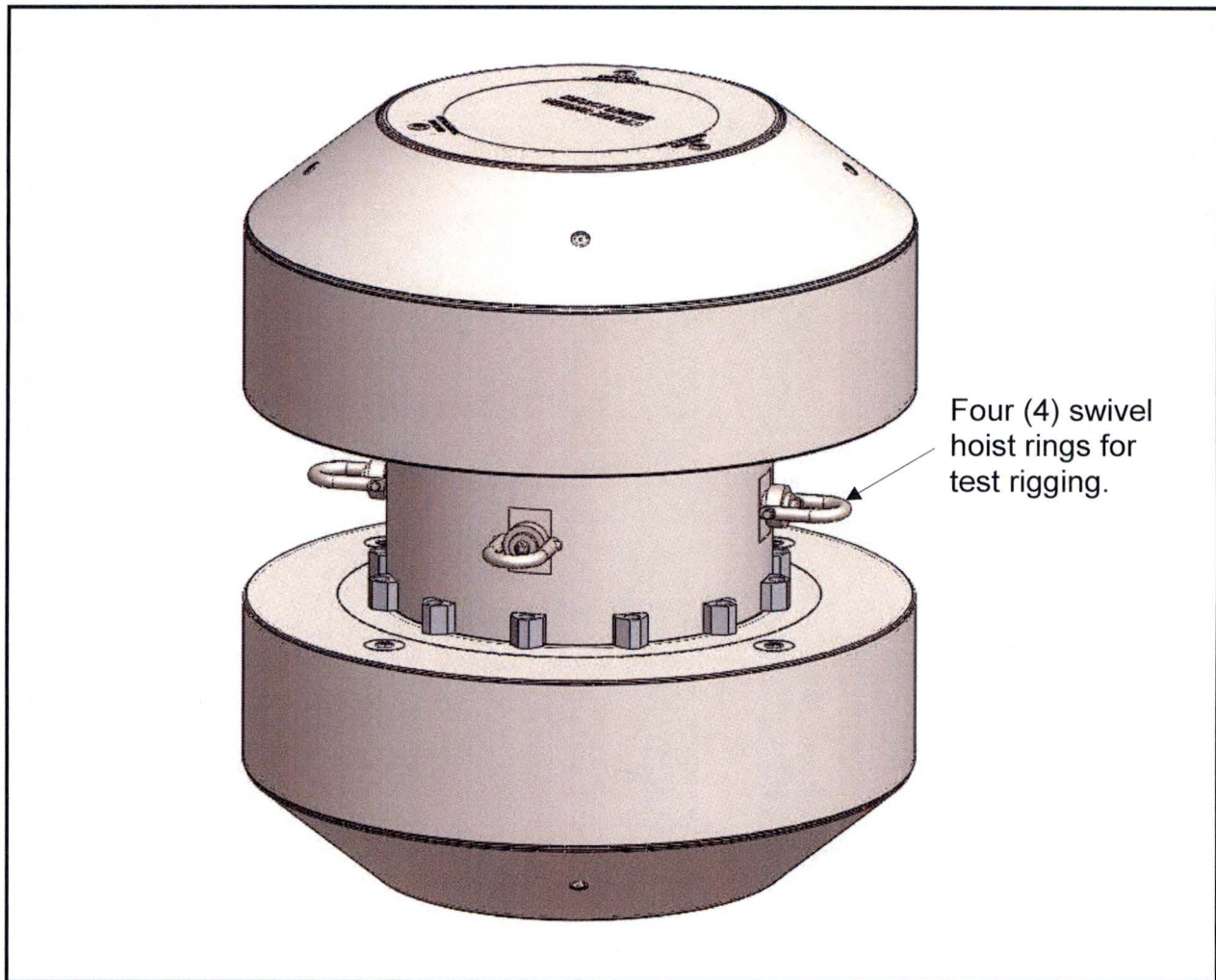
Figure 2.12.3-1 – 380-B Half-Scale Test Unit

Dummy Cask

Production Impact
Limiter and Attachments
in Half-Scale
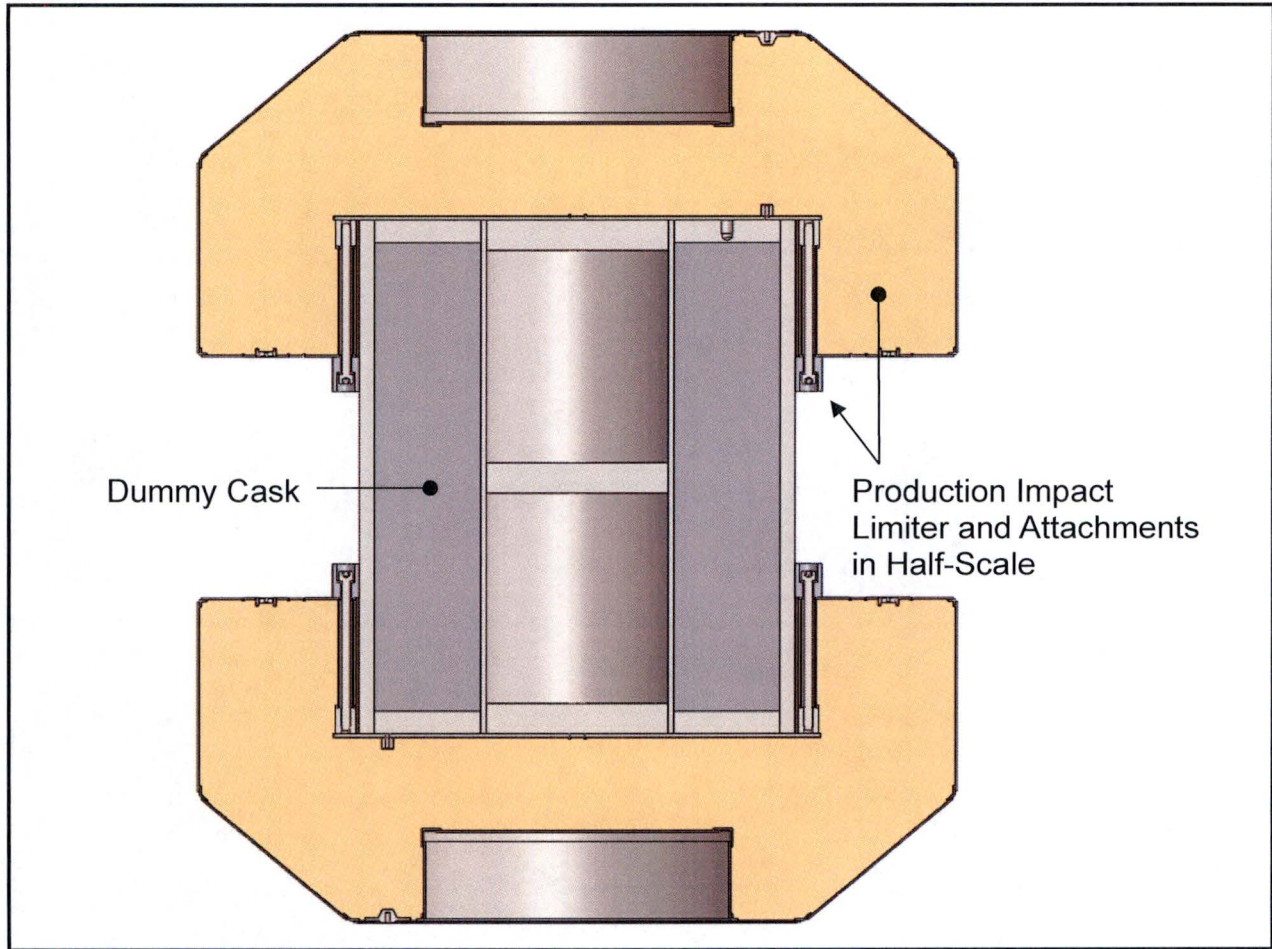
Figure 2.12.3-2 – 380-B Half-Scale Test Unit Cross-Section
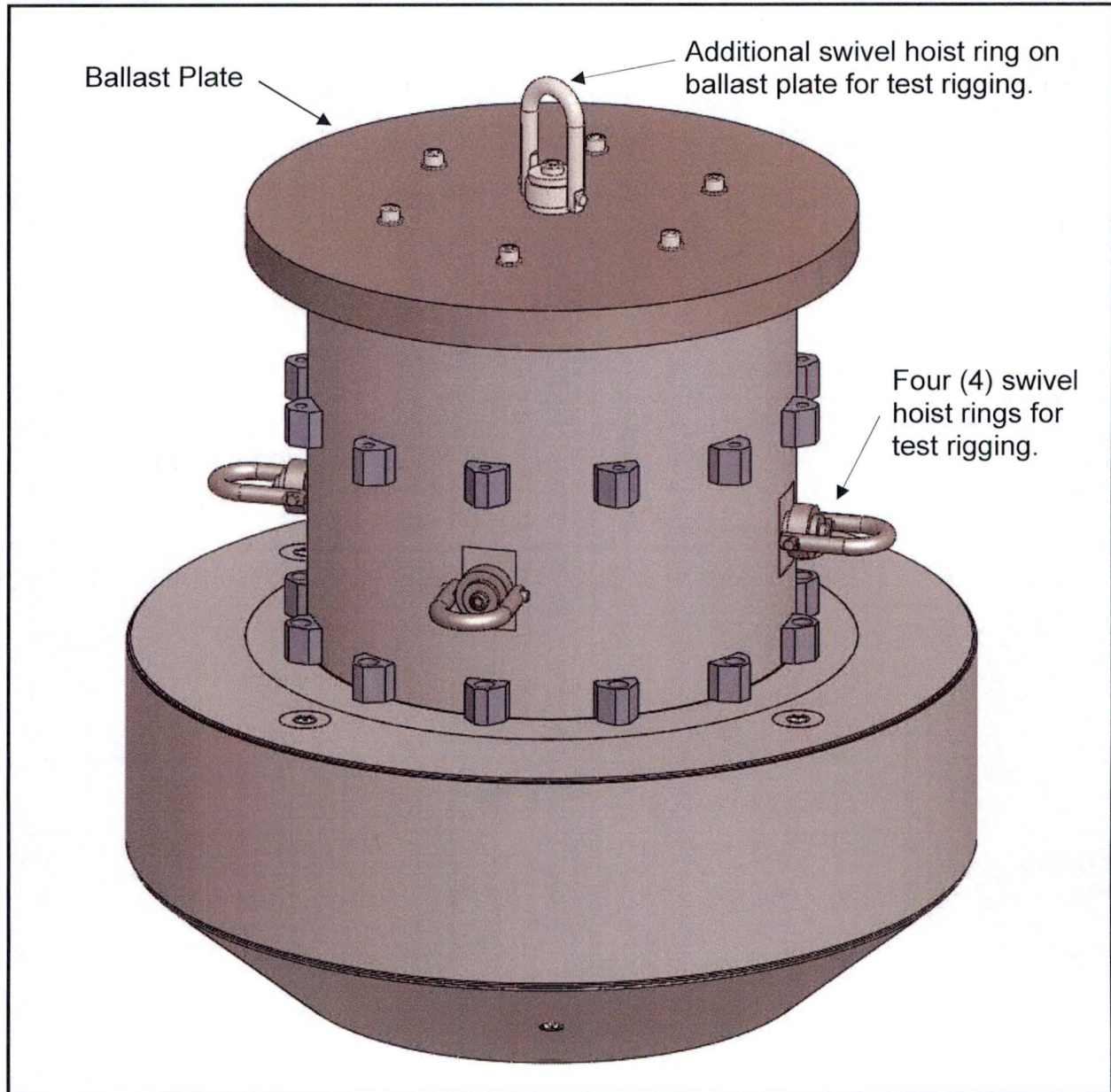
Figure 2.12.3-3 – 380-B Half-Scale Test Unit with Ballast Plate

Ballast Plate

Dummy Cask

Production
Impact Limiter
and Attachments
in Half-Scale
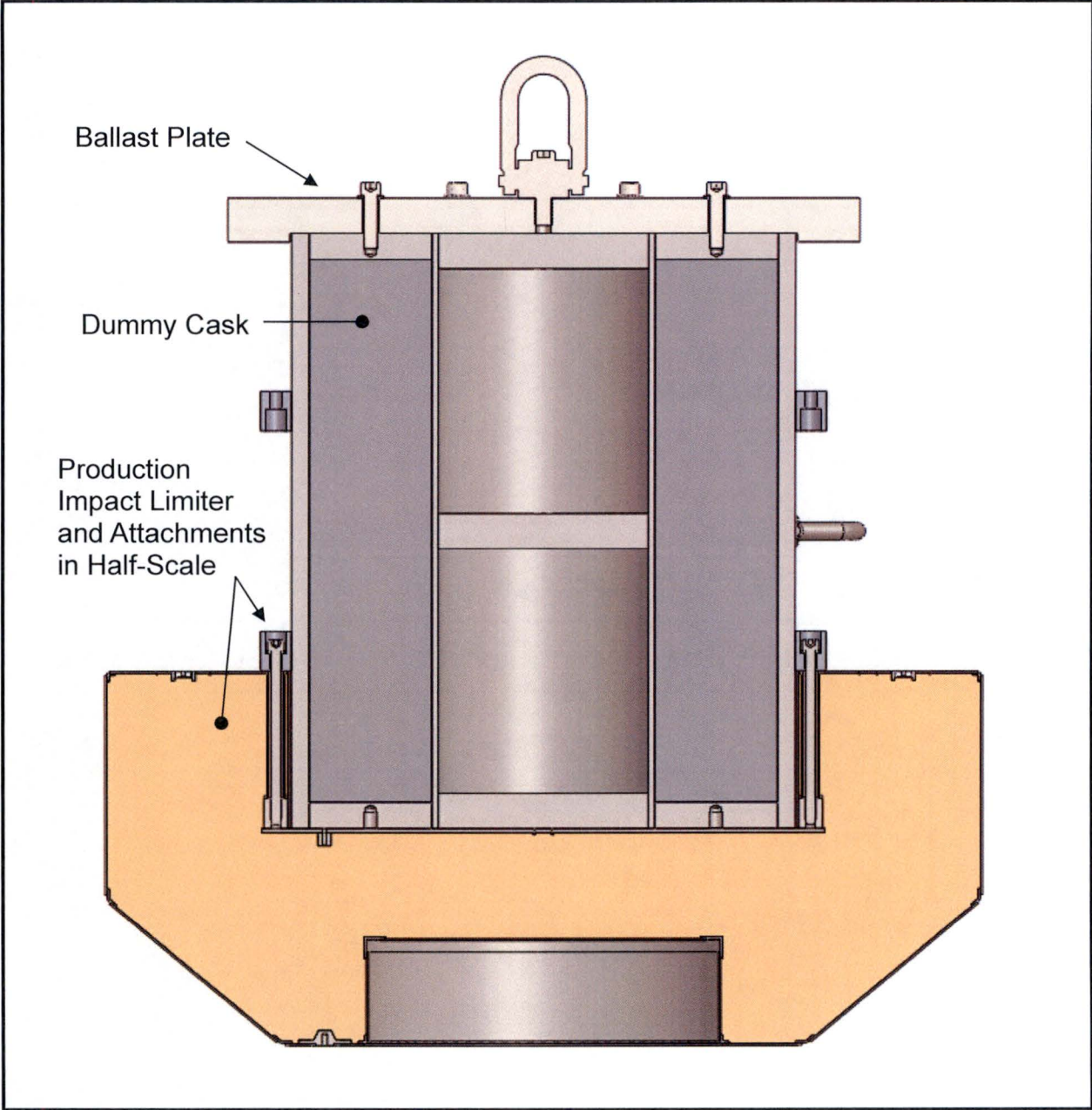
Figure 2.12.3-4 – 380-B Half-Scale Test Unit with Ballast Plate Cross-Section
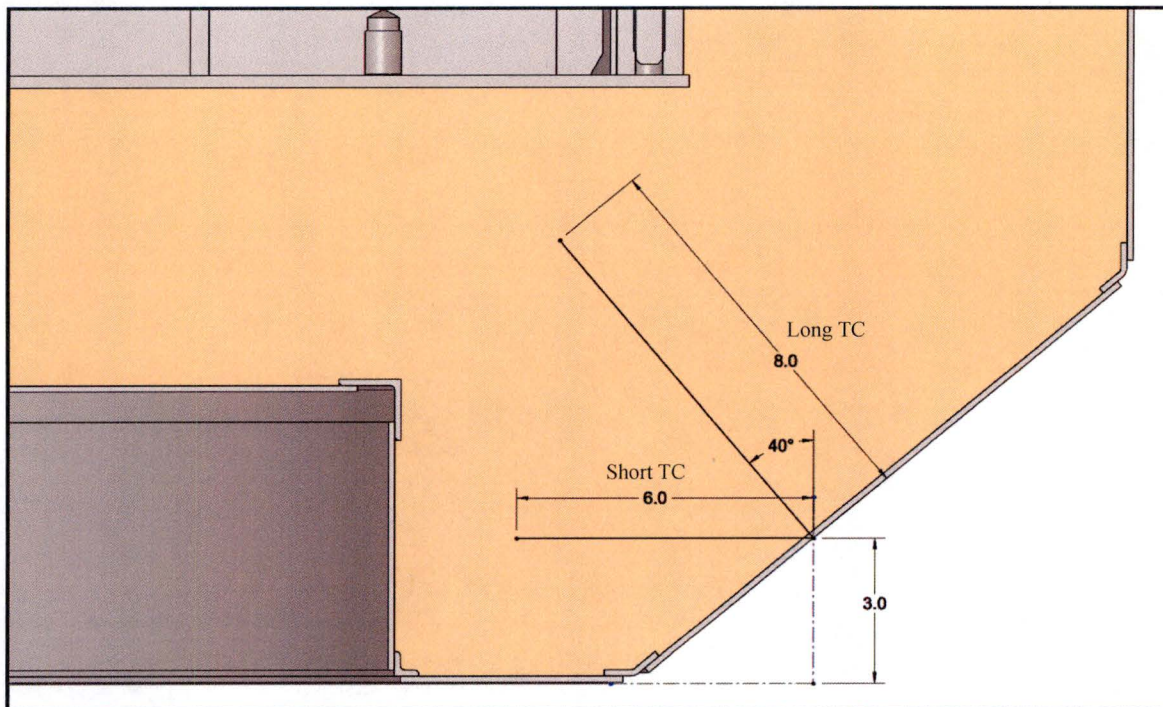
Figure 2.12.3-5 – Depth View, Impact Limiter A2-01, Cold D1 Free Drop
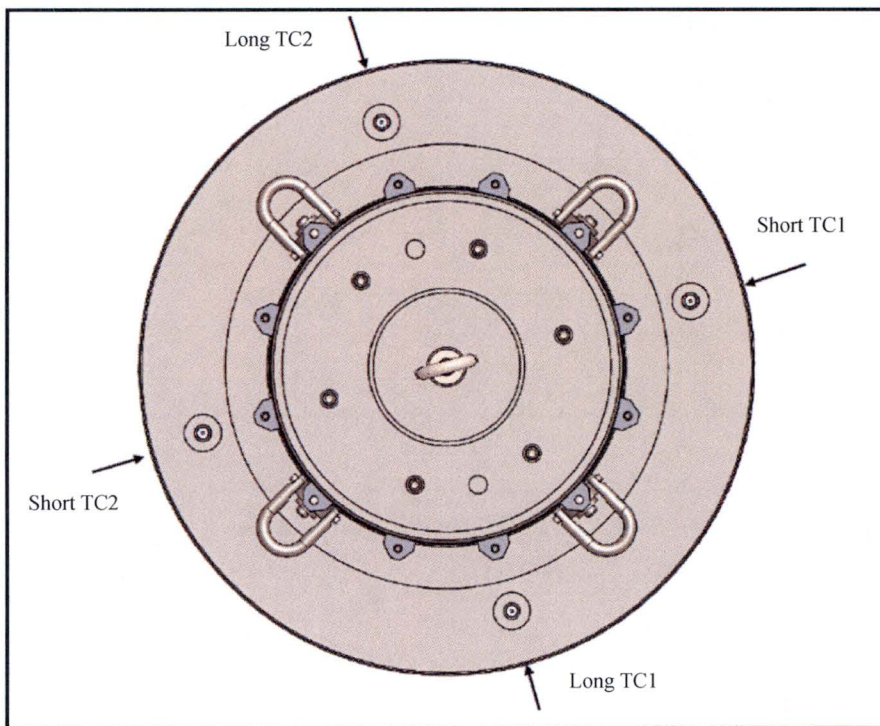
Figure 2.12.3-6 – Plan View, Impact Limiter A2-01, Cold D1 Free Drop
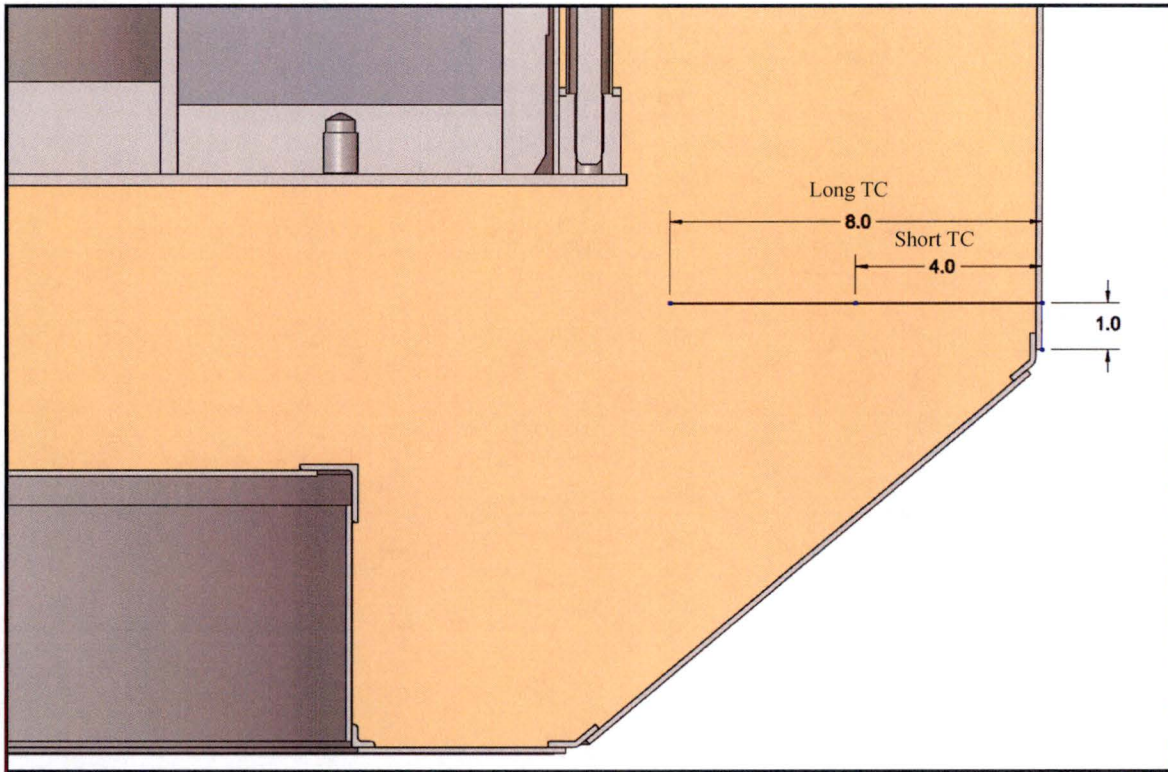
Figure 2.12.3-7 – Depth View, Impact Limiter A1-01, Warm D2 Free Drop
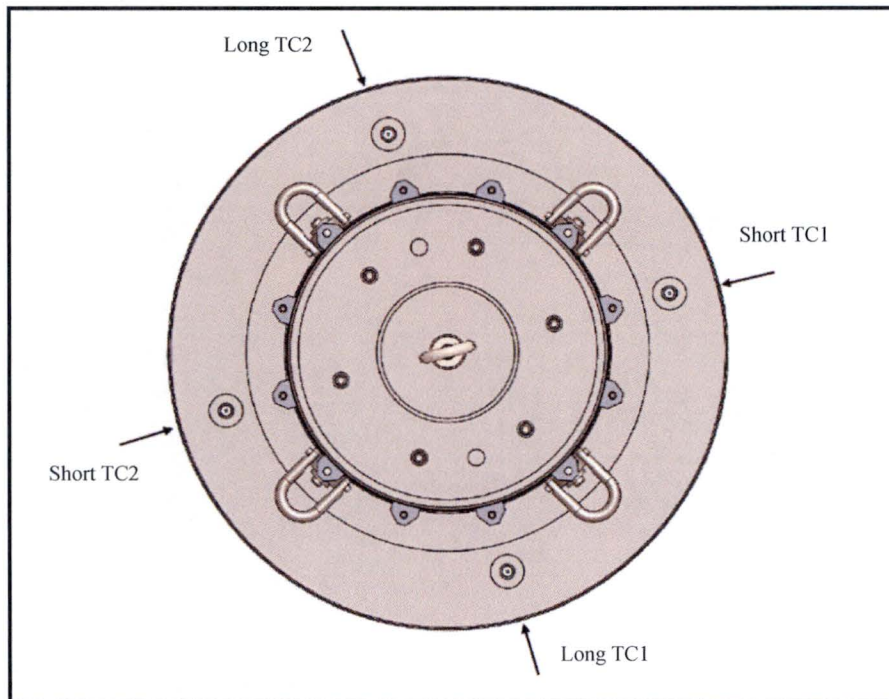
Figure 2.12.3-8 – Plan View, Impact Limiter A1-01, Warm D2 Free Drop
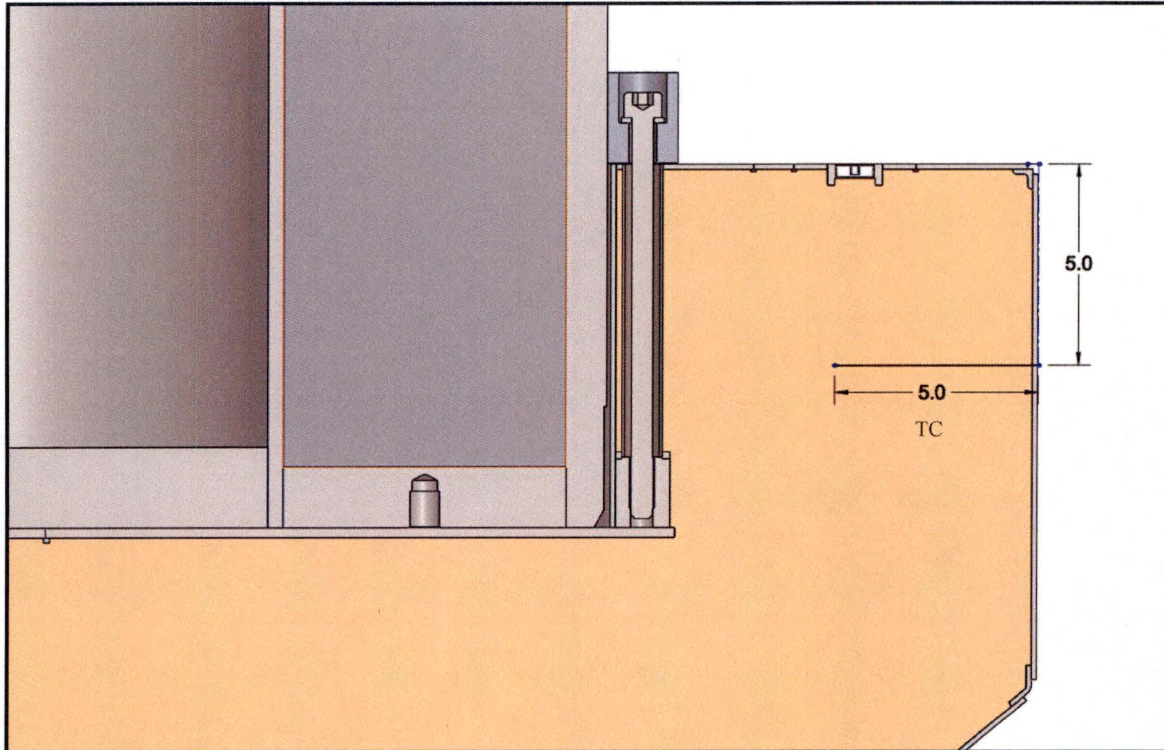
Figure 2.12.3-9 – Depth View, Impact Limiters A1-02 and A1-03, Warm D3 Free Drop
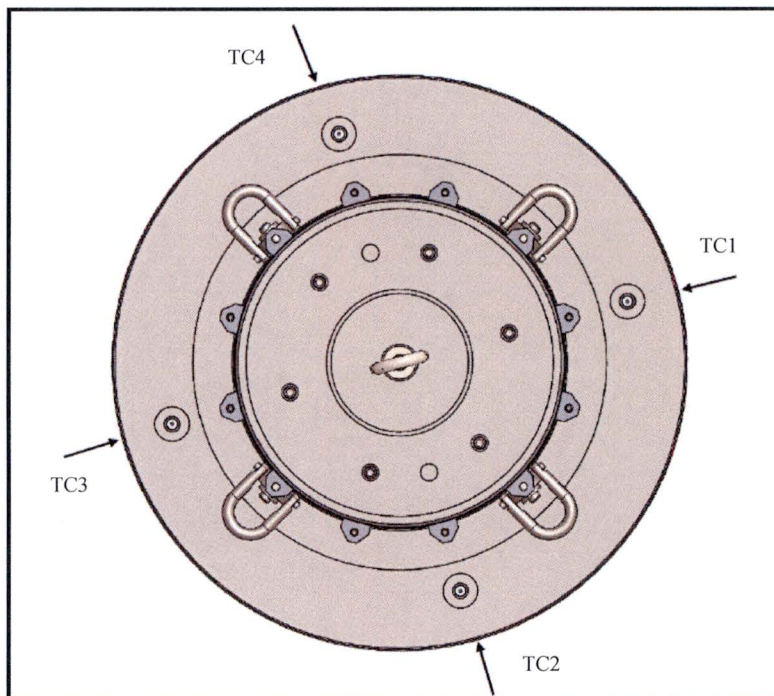
Figure 2.12.3-10 – Plan View, Impact Limiters A1-02 and A1-03, Warm D3 Free Drop
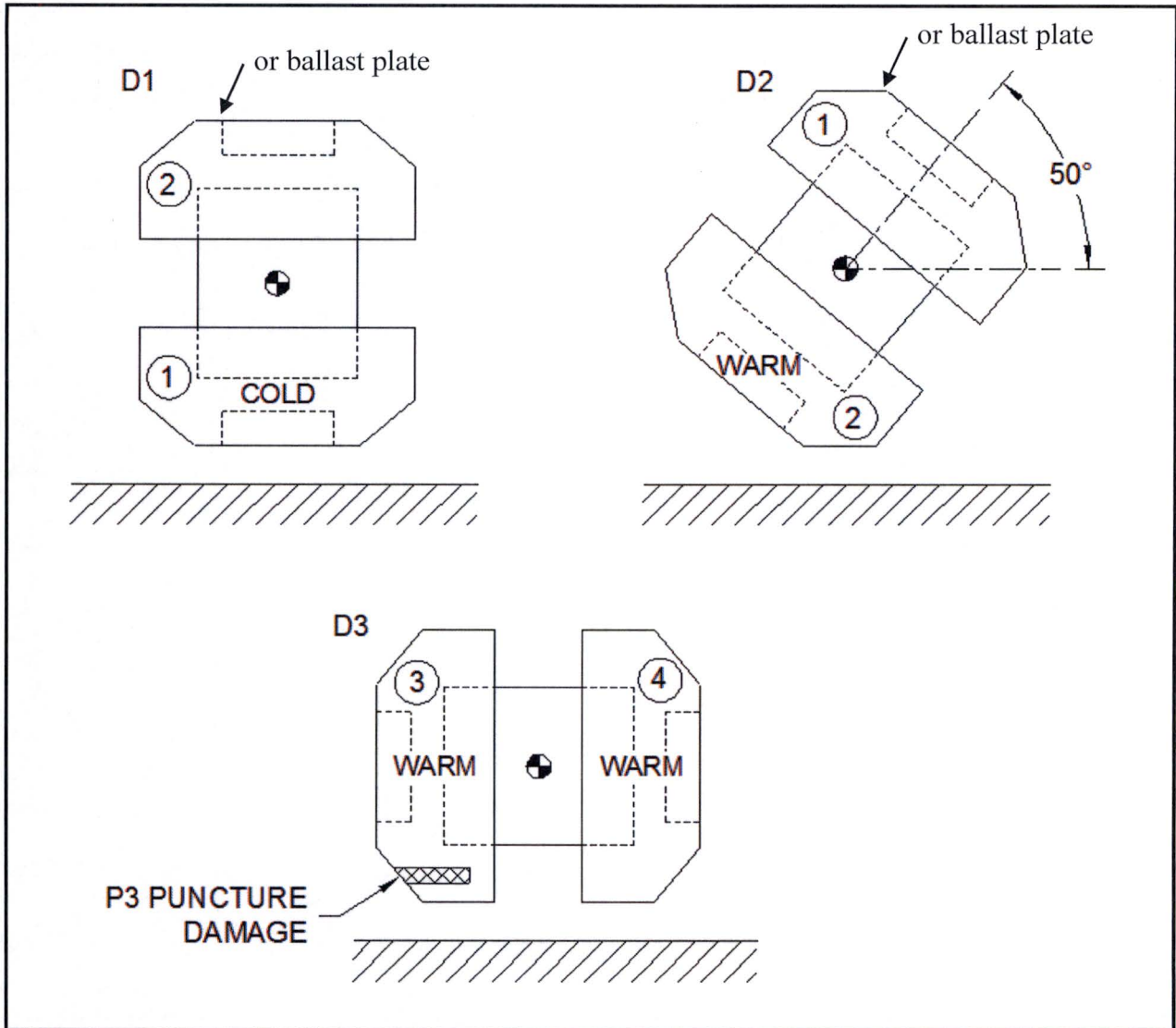
Figure 2.12.3-11 – Free Drop Summary Sheet
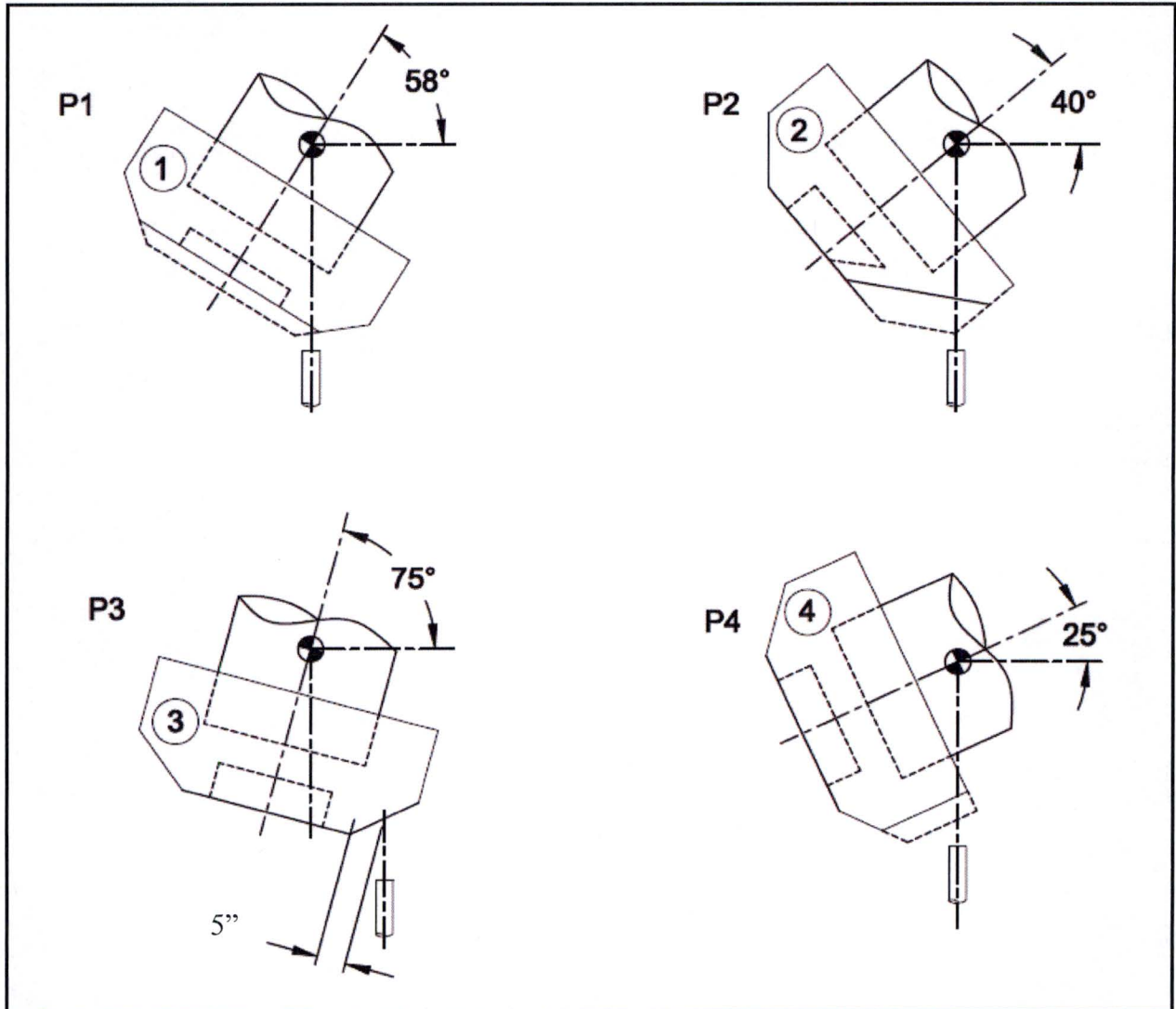
Figure 2.12.3-12 – Puncture Drop Summary Sheet

Figure 2.12.3-13 – CTU-1 Free Drop Test D1 Orientation

Figure 2.12.3-14 – CTU-1 D1 Damage to Bottom Surface
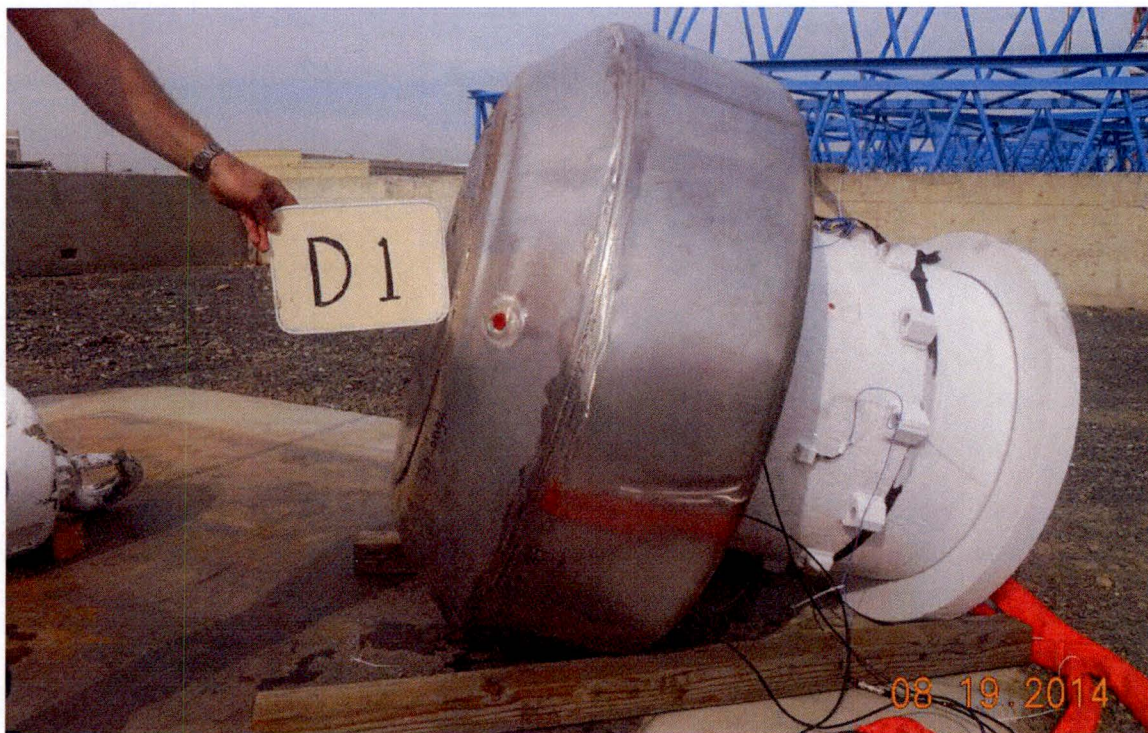
Figure 2.12.3-15 – CTU-1 D1 Damage Side View
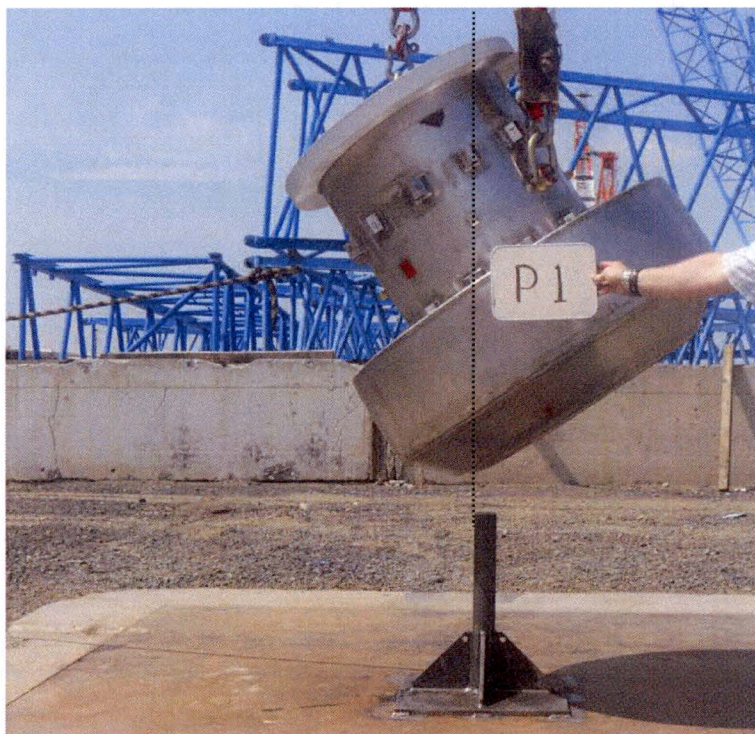
Figure 2.12.3-16 – CTU-1 Puncture Drop Test P1 Orientation

Figure 2.12.3-17 – CTU-1 Condition after P1 Puncture Drop Test

Figure 2.12.3-18 – Impact Limiter-1 Damage after P1 Puncture Drop Test

P1 Direction
through CG

2"

11"

3"

Reference Puncture Bar 3" OD x 24" L
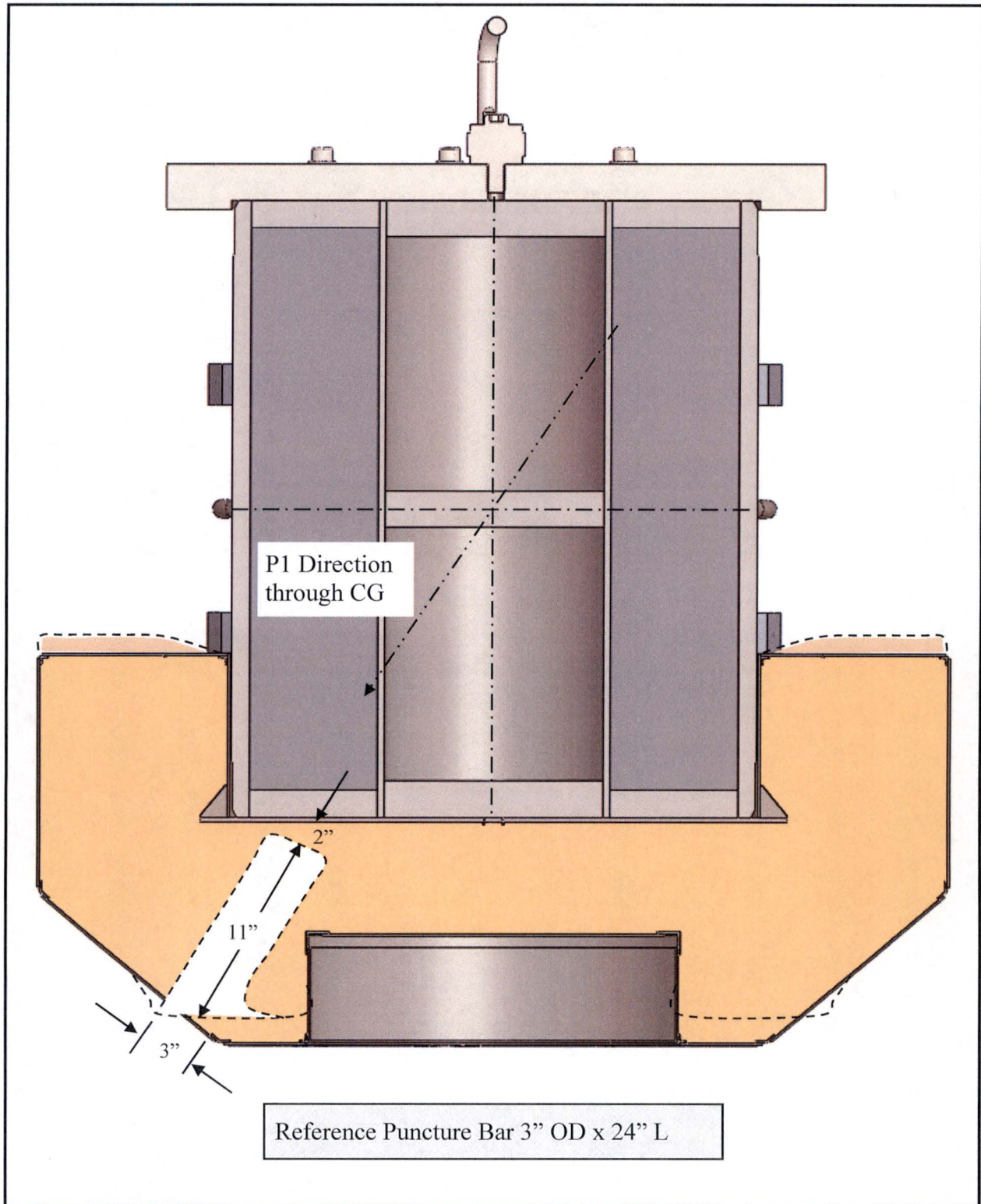
Figure 2.12.3-19 – D1 & P1 Post-Test Section View Impact Limiter-1

Figure 2.12.3-20 – Impact Limiter-1 Damage after P1 Puncture Drop Test
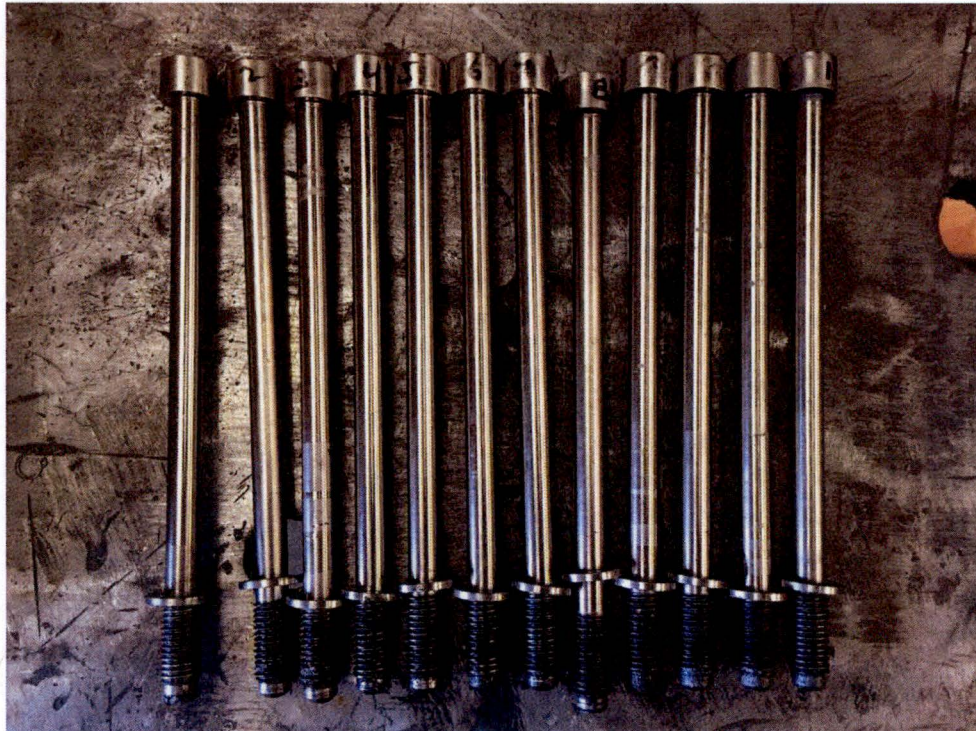
Figure 2.12.3-21 – Impact Limiter-1 Bolts after D1 and P1
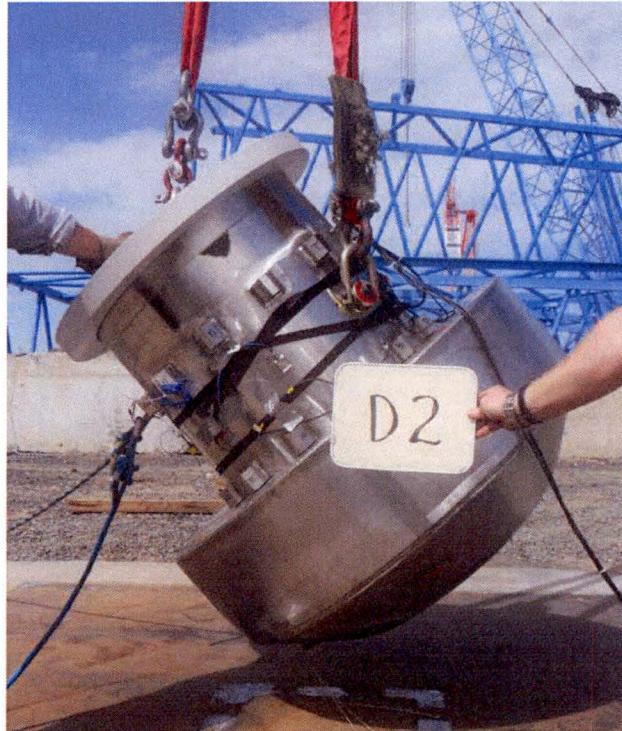
Figure 2.12.3-22 – CTU-2 Free Drop Test D2 Orientation
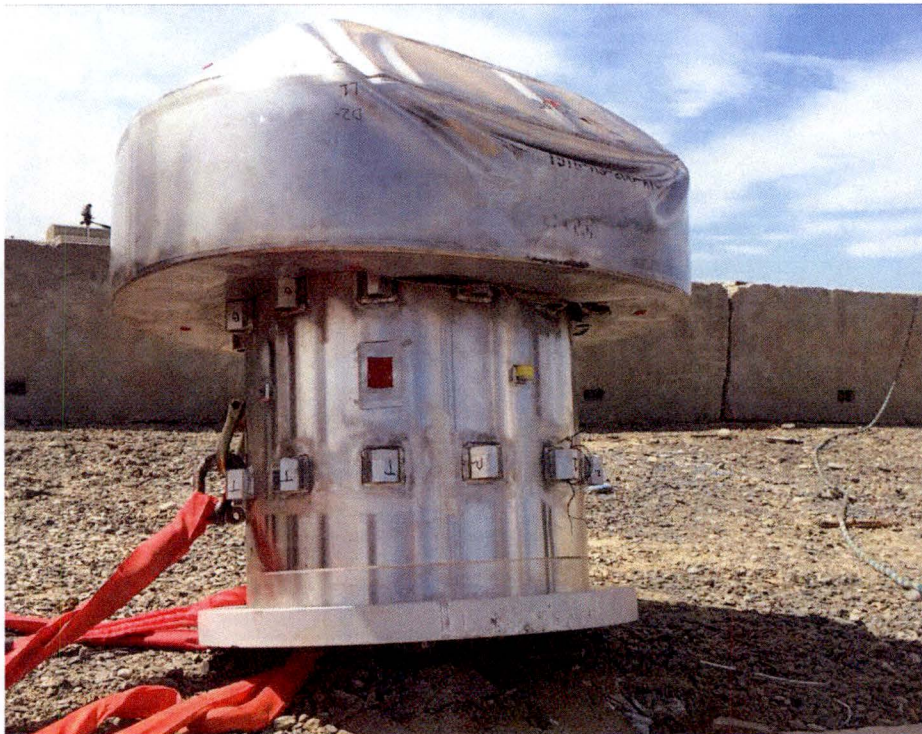
Figure 2.12.3-23 – CTU-2 Condition after D2 Free Drop Test

Figure 2.12.3-24 – CTU-2 Damage after D2 Free Drop Test

Figure 2.12.3-25 – CTU-2 Damage after D2 Free Drop Test
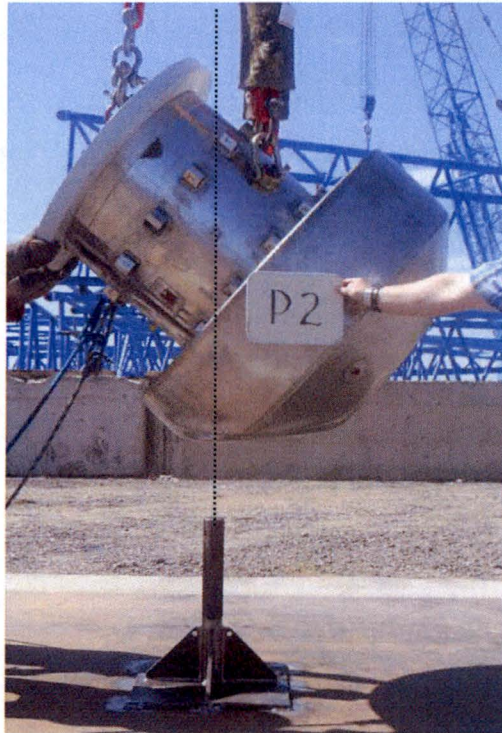
Figure 2.12.3-26 – CTU-2 Puncture Drop Test P2 Orientation

Figure 2.12.3-27 – CTU-2 Condition after P2 Puncture Drop Test

Figure 2.12.3-28 – CTU-2 Condition after P2 Puncture Drop Test

Figure 2.12.3-29 – CTU-2 Damage after P2 Puncture Drop Test

Figure 2.12.3-30 – Impact Limiter-2 Weld Failure after D2 and P2 Tests
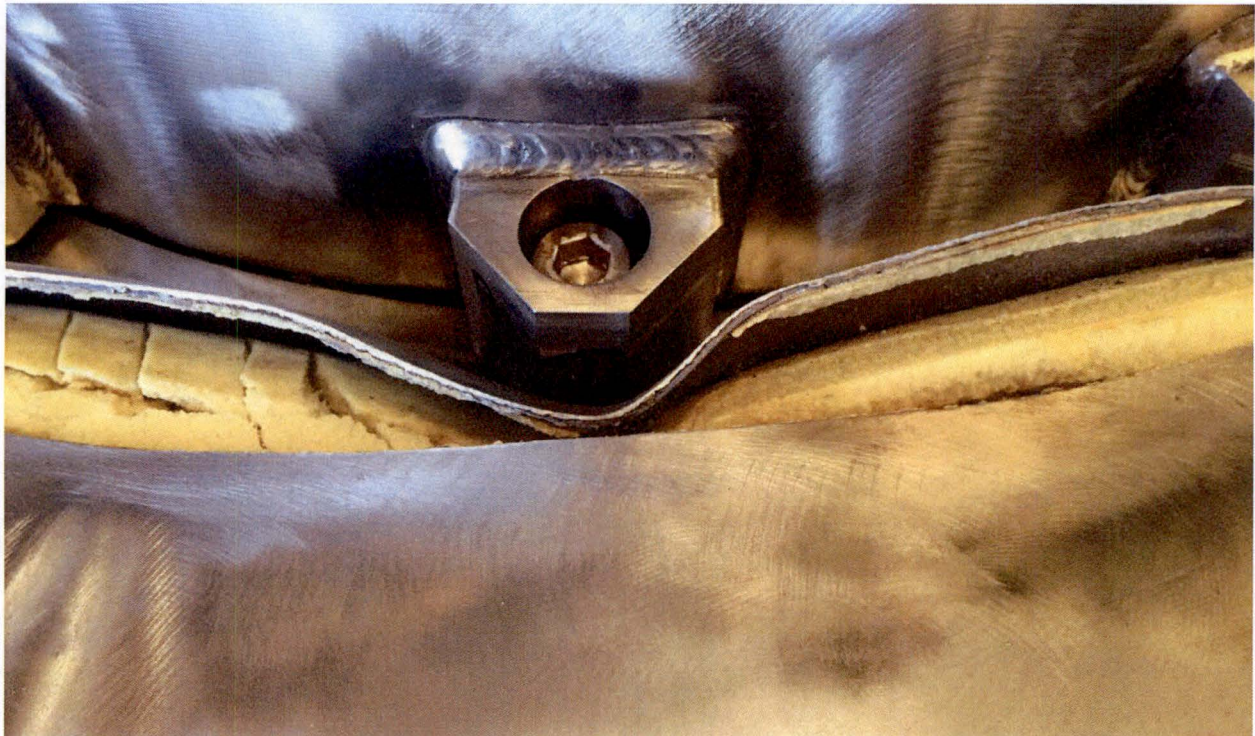
Figure 2.12.3-31 – Impact Limiter-2 Weld Failure after D2 and P2 Tests
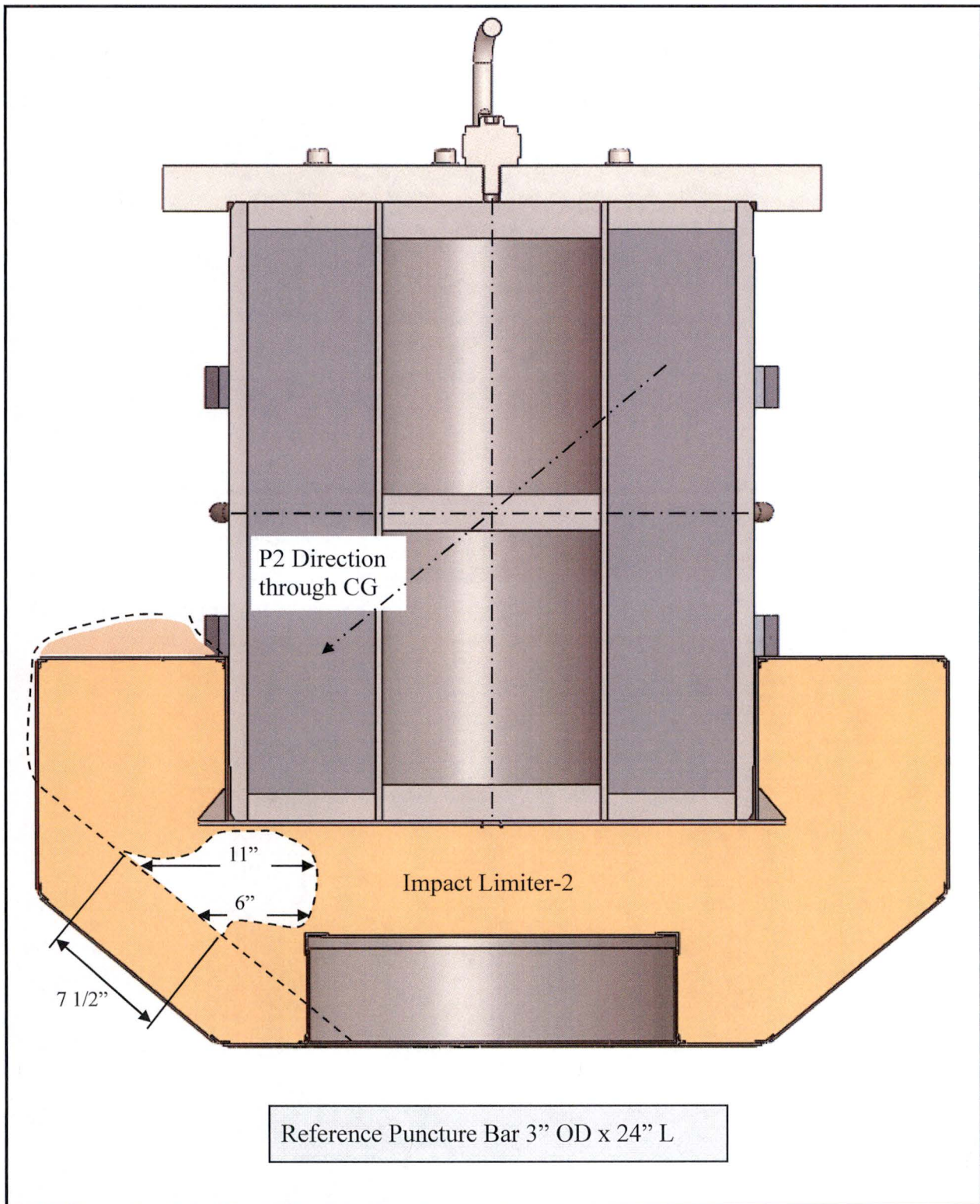
Figure 2.12.3-32 – D2 & P2 Post-Test Section View Impact Limiter-2

Figure 2.12.3-33 – Impact Limiter-2 Damage after P2 Puncture Drop Test

Figure 2.12.3-34 – Impact Limiter-2 Bolts after D2 and P2

Figure 2.12.3-35 – Impact Limiter-3 with Reinforcing Ring
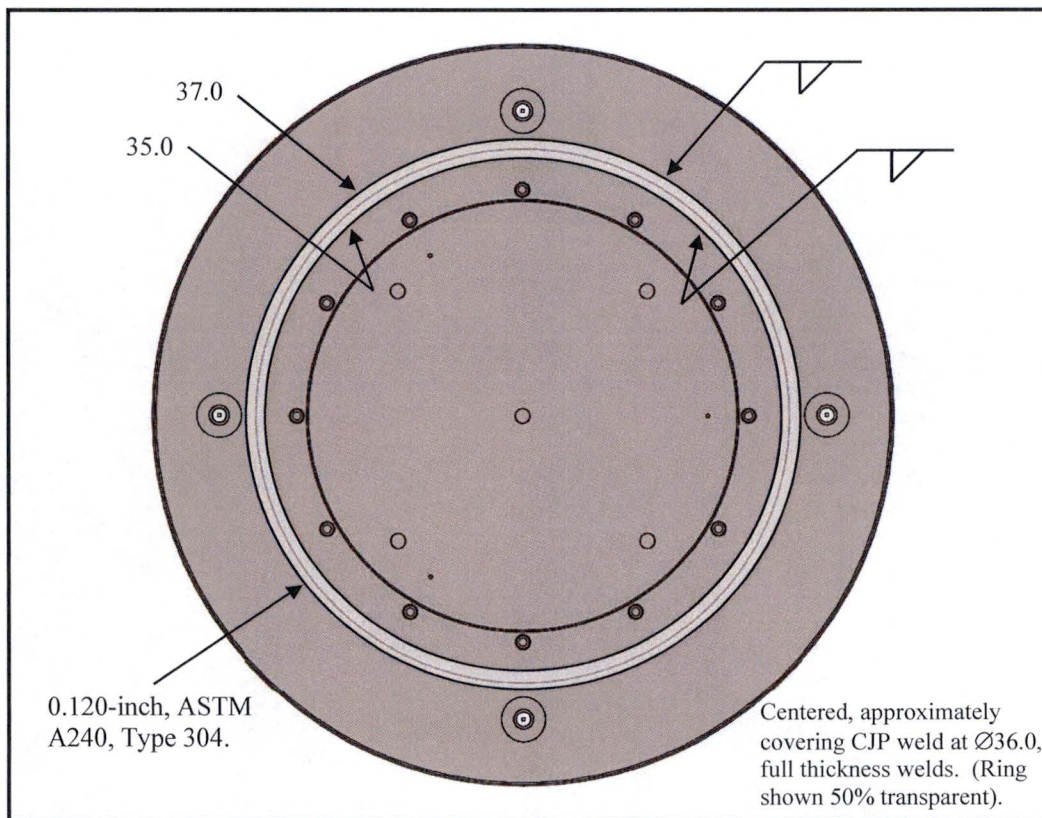
Figure 2.12.3-36 – Impact Limiter Added Reinforcing Ring

Figure 2.12.3-37 – CTU-3 Puncture Drop Test P3 Orientation

Figure 2.12.3-38 – CTU-3 Condition after P3 Puncture Drop Test

Figure 2.12.3-39 – CTU-3 Condition after P3 Puncture Drop Test

Figure 2.12.3-40 – Impact Limiter-3 Damage after P3 Puncture Drop Test
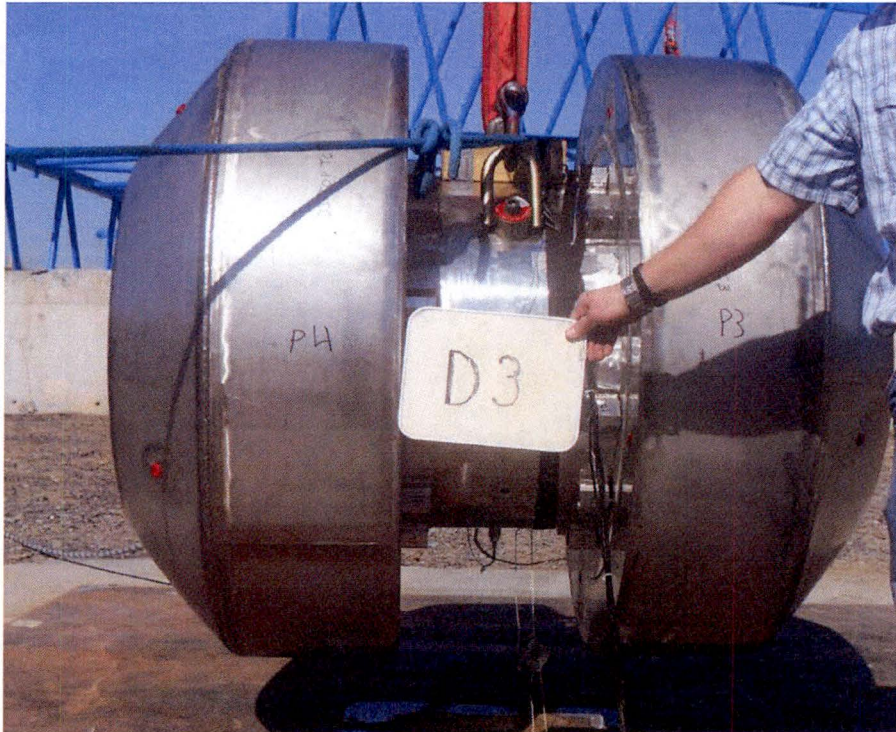
Figure 2.12.3-41 – CTU-3.4 Free Drop Test D3 Orientation
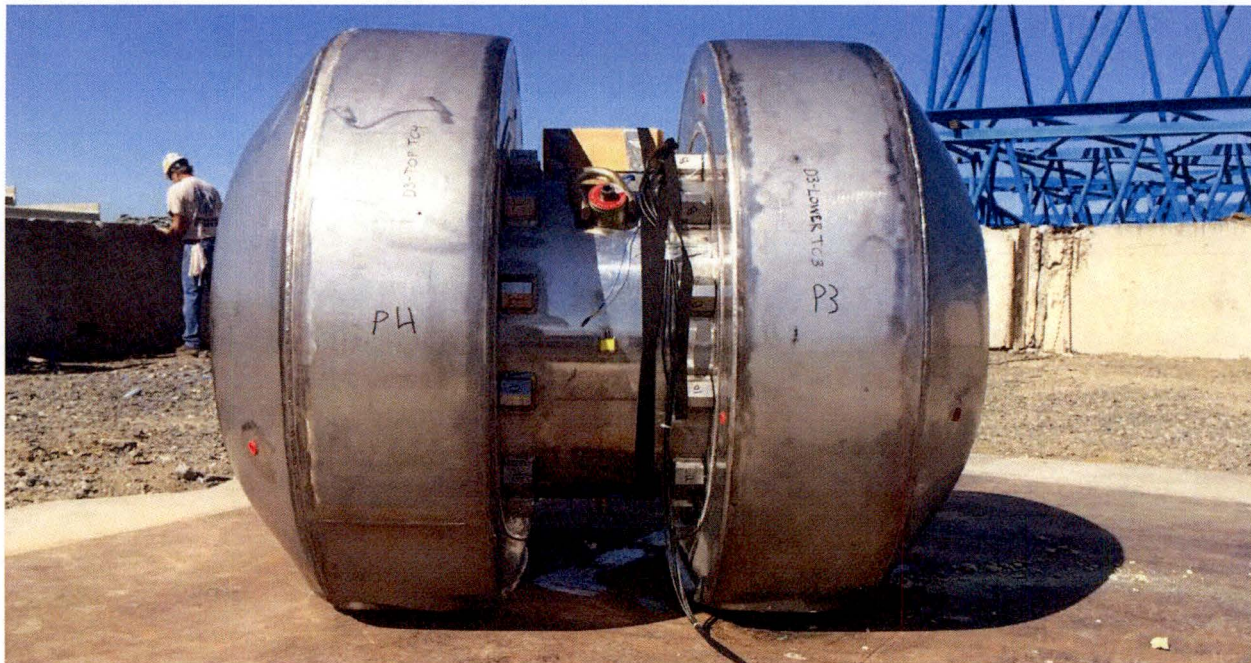
Figure 2.12.3-42 – CTU-3.4 Condition after D3 Free Drop Test

Figure 2.12.3-43 – Impact Limiter-3 after P3 and D3 Free Drop Test

Figure 2.12.3-44 – CTU-3.4 Condition after D3 Free Drop Test

P3 Direction through CG

5"

10"

6"

Impact Limiter-3

Reference Puncture Bar 3" OD x 32" L
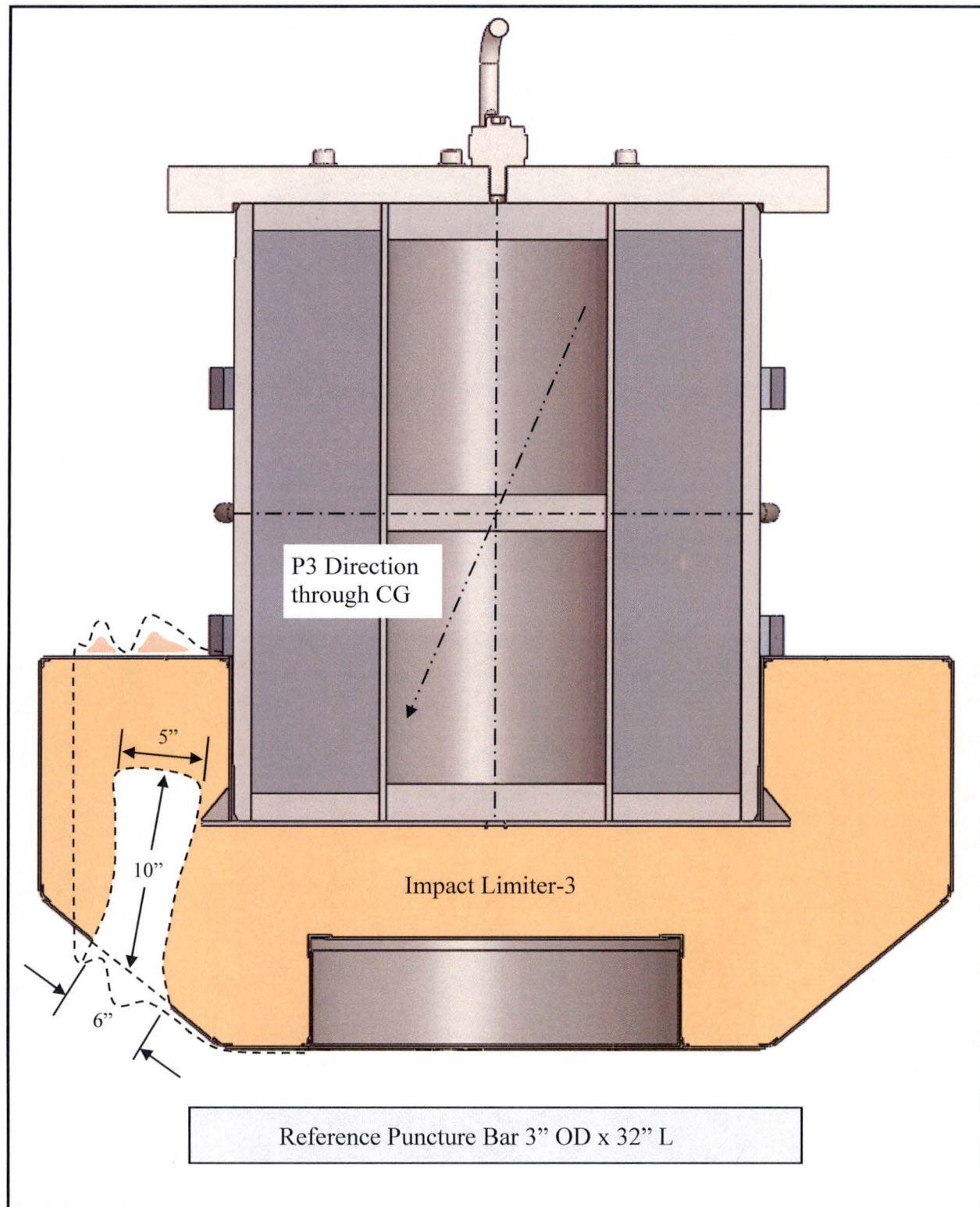
Figure 2.12.3-45 – P3 & D3 Post-Test Section View Impact Limiter-3

Figure 2.12.3-46 – Impact Limiter-3 Damage after P3 and D3 Tests

Figure 2.12.3-47 – Impact Limiter-3 Bolts after P3 and D3 Tests
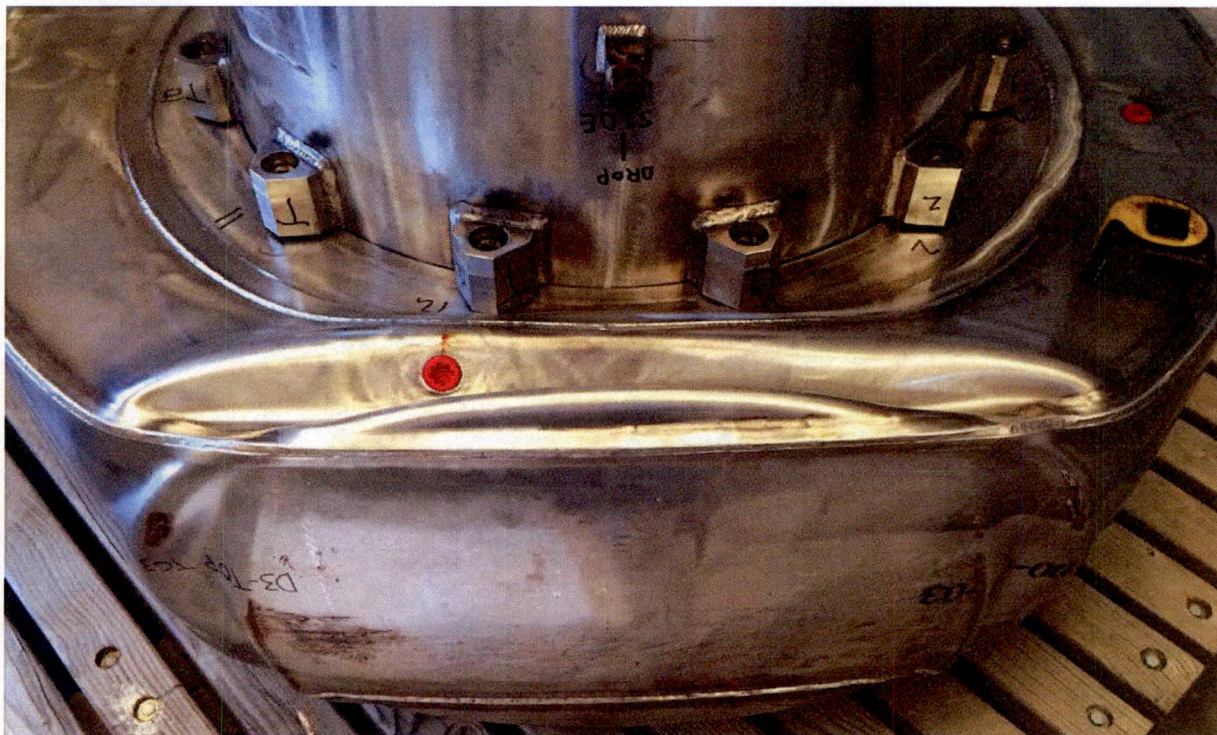
Figure 2.12.3-48 – Impact Limiter-4 Damage after D3 Free Drop Test

Figure 2.12.3-49 – Impact Limiter-4 Damage after D3 Free Drop Test
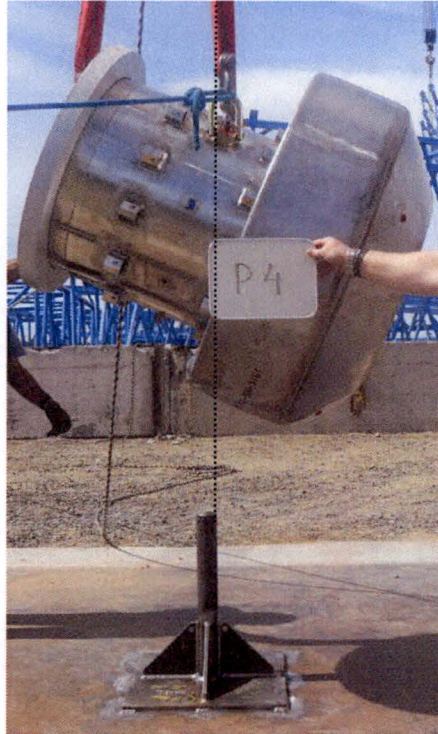
Figure 2.12.3-50 – CTU-4 Puncture Drop Test P4 Orientation

Figure 2.12.3-51 – CTU-4 Condition after P4 Puncture Drop Test
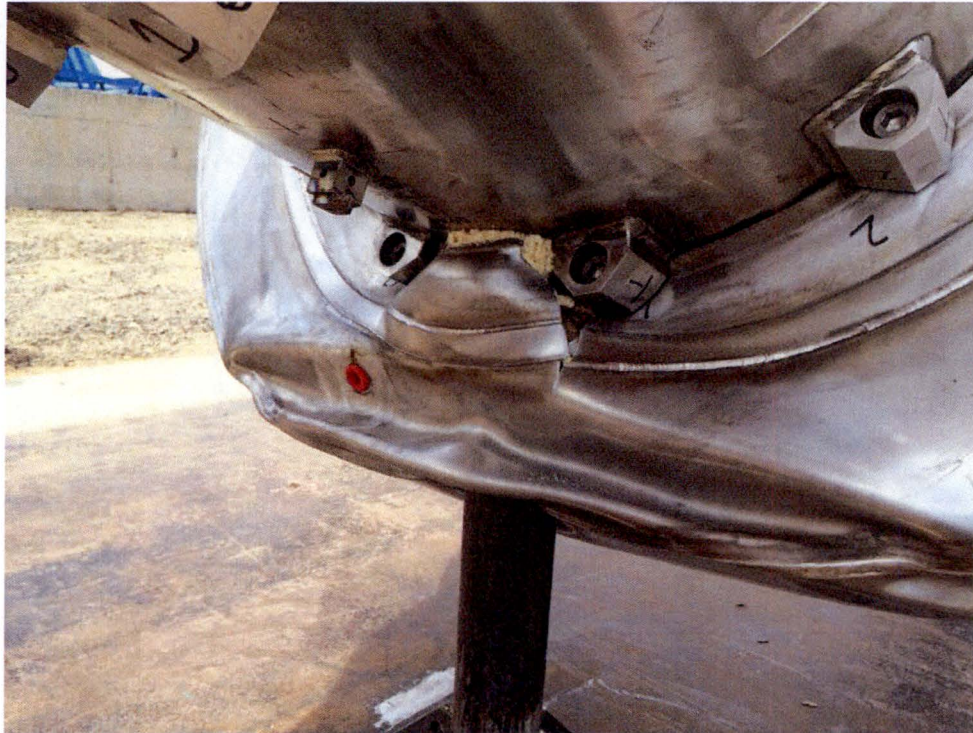
Figure 2.12.3-52 – CTU-4 Condition after P4 Puncture Drop Test

Figure 2.12.3-53 – CTU-4 Condition after P4 Puncture Drop Test

Figure 2.12.3-54 – Impact Limiter-4 Damage after D3 and P4 Tests
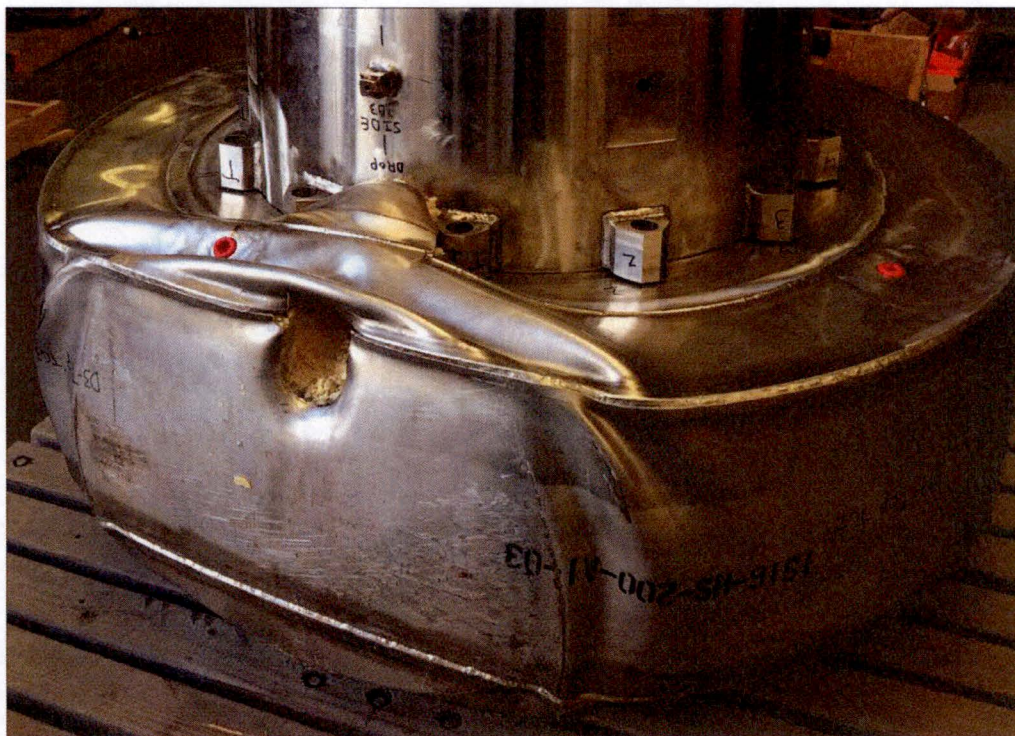
Figure 2.12.3-55 – Impact Limiter-4 Damage after D3 and P4 Tests

Figure 2.12.3-56 – Impact Limiter-4 Entry Damage after P4 Puncture Drop Test

Figure 2.12.3-57 – Impact Limiter-4 Exit Damage after P4 Puncture Drop Test

Figure 2.12.3-58 – Impact Limiter-4 Exit Damage without Cask

3 3/4"

7

P4 Direction
through CG

Impact Limiter-4

Reference Puncture Bar 3" OD x 24" L
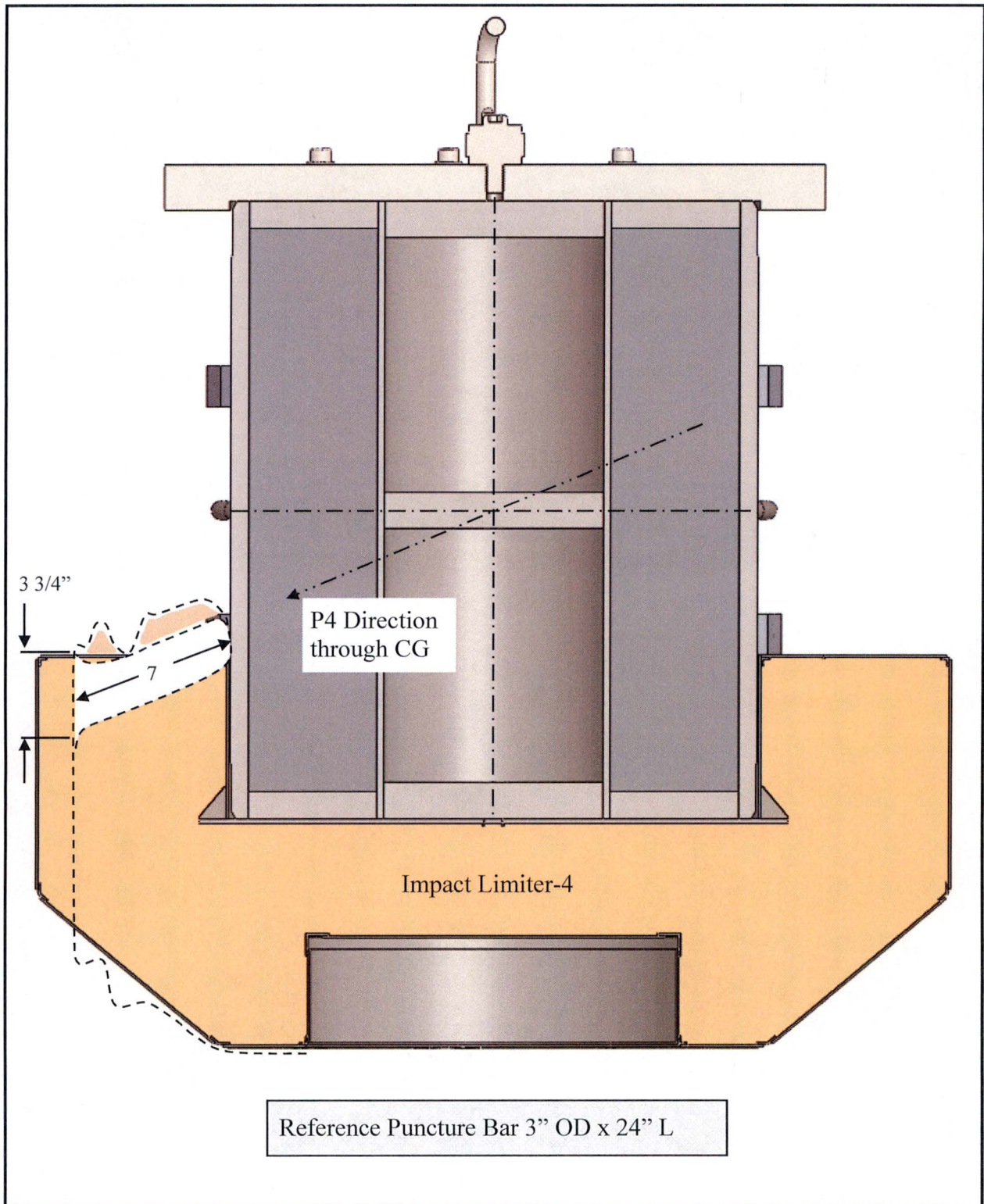
Figure 2.12.3-59 – D3 & P4 Post-Test Section View Impact Limiter-4
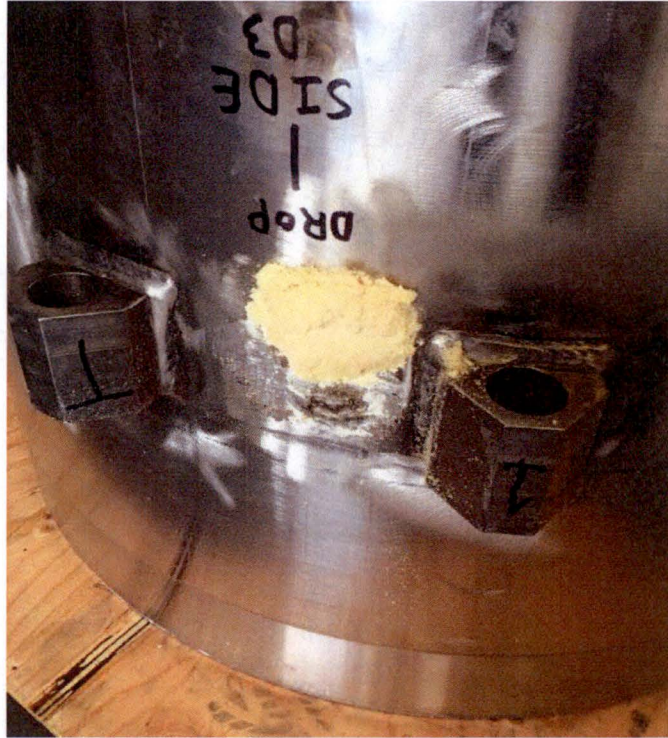
Figure 2.12.3-60 – Cask with adhered foam after P4 Puncture Drop Test

Figure 2.12.3-61 – Impact Limiter-4 Bolts after D3 and P4 Tests

2.12.3.7 Filtered Accelerometer Time Histories

Accelerometer time history plots are provided below. Information identifying each plot is given below the figure as: drop test number; channel no.; and filter cutoff frequency (500 Hz in all cases).

Accelerometers were located midway between swivel hoist rings (4 total @ 0°, 90°, 180°, 270° positions)

Drop1 - Channel 1: LP 500Hz

Drop1 - Channel 2: LP 500Hz

Drop1 - Channel 3: LP 500Hz

Drop1 - Channel 4: LP 500Hz

Drop2 - Channel 2: LP 500Hz

In test D2, three of the four signal cables were severed during the drop. As a result, channel 1 data was completely lost, while channel 2 was completely intact. Channels 3 and 4 lost signal after the primary impulse was recorded, and peak accelerations were recovered for these cases.

Drop2 - Channel 3: LP 500Hz

Drop2 - Channel 4: LP 500Hz

Drop3 - Channel 1: LP 500Hz

Note that the pulse sign is negative because the transducer orientation was reversed for this drop.

Drop3 - Channel 2: LP 500Hz

Drop3 - Channel 3: LP 500Hz

Drop3 - Channel 4: LP 500Hz

Test ID	Peak Acceleration, g			
	ACC1	ACC2	ACC3	ACC4
DROP1	156	152	153	159
DROP2	—	67	81	78
DROP3	118	119	117	122

NOTE: DROP2 measurements were obtained with accelerometers rotated 40° from vertical.

2.12.4 Stress Analysis Finite Element Models

This appendix describes the finite element analysis of the 380-B cask body and closure lid. The structural components considered are the lower end structure, the bottom outer plate, the inner shell, the outer shell, the upper end structure, and the closure lid (including the lid outer plate). Both NCT and HAC are considered. Loading types include internal pressure, thermal, free drop and HAC fire pressure.

2.12.4.1 Analysis Model Description

The finite element model of the 380-B cask body and closure lid is used to calculate stress under NCT and HAC in the structural members of the cask, which consist of the upper and lower end structures, the inner shell, the outer shell, the bottom outer plate and the closure lid (including the lid main structure and outer plate). The impact limiters, the impact limiter attachments, the thermal shield, the inner cover, the payload, the payload locating dunnage and the personnel barrier are not modeled structurally, but their mass is accounted for as discussed in Section 2.12.4.2.3, *Free Drop Impact Loads*. The lead shielding material in the lid, sides, and bottom of the cask body is also not explicitly modeled, and is further discussed in Section 2.12.4.2.3, *Free Drop Impact Loads*. The closure lid bolts are included in the model to determine the lid and cask interactions. The closure lid bolt stresses are analyzed in Section 2.6.1.5, *Closure Bolts*, and Section 2.7.1.2, *End Drop*. The model is built in ANSYS Revision 11.0 and 14.5.7 using half symmetry along a vertical plane through the cask center. The structural elements are SOLID185, 8-node bricks, the closure bolt elements are BEAM4, and the contact interface between the lid and the cask is modeled with contact elements CONTA173 and TARGE170. For load cases which do not include inertia forces, the model is constrained by the symmetry plane, fixed nodes at the edge of the cask outer bottom surface and a single fixed node at the bottom cask center and the top lid center. When inertia loads are applied, the model constraint is individually discussed in the following sections. The finite element mesh is shown in Figure 2.12.4-1.

2.12.4.2 Loading of the Model

2.12.4.2.1 Pressure Loads

A pressure of 25 psi, corresponding to the design pressure identified in Section 2.6.1.1, *Summary of Pressures and Temperatures*, is applied to the interior surface of the model in each case with a NCT hot ambient temperature initial condition. The pressure is applied to all element interior surfaces which fall within the location of the inner (containment) O-ring. For cases with a NCT cold ambient temperature initial condition, no pressure is applied to the interior surface of the model.

A pressure of 100 psi, corresponding to the HAC fire event identified in Section 2.7.4.1 *Summary of Pressures and Temperatures*, is applied in the HAC fire event pressure case. The pressure is applied to all element interior surfaces which fall within the location of the inner (containment) O-ring.

2.12.4.2.2 Thermal Loads

Thermal loading is a secondary stress and is therefore not considered for HAC load cases. NCT thermal loading is discussed below:

A detailed thermal analysis is performed in Chapter 3.0, *Thermal Evaluation*. As shown in Figure 3.3-2 and Figure 3.3-7 the temperature difference through the 380-B cask body and closure lid is less than 11 °F during NCT. Because this gradient is small, the secondary thermal stress developed in the 380-B cask body and closure lid would be insignificant for the NCT load cases, and therefore, no thermal stress evaluation is performed.

Another source of thermal loading is the lead gamma shield used in the annulus between the inner and outer shells. Due to different thermal expansion coefficients, the lead gamma shielding applies a radial pressure to the outer surface of the inner shell under NCT hot and cold conditions. As shown in Section 2.6.1.2.2, *Lead*, this pressure can be assigned an upper bound value of 225 psi under NCT hot conditions. For the Case No 2, Lead Shrinkage Pressure, this pressure is applied to the inner shell outer surface over the entire length of the side lead cavity. As shown in Section 2.6.2, *Cold*, the lead shrinkage pressure can be assigned an upper bound value of 376 psi under NCT cold conditions. For the NCT cold free drop cases, 3b, 5b, and 7b, this pressure is applied to the inner shell outer surface over the entire length of the side lead cavity. Additional treatment of lead in cases that include free drop impact loads is discussed below.

2.12.4.2.3   Free Drop Impact Loads

Stress is generated in the 380-B cask body and closure lid in a free drop impact through self-weight of the components and the applied inertial loads of components not modeled. The resulting forces are reacted over the interface areas of the impact limiter(s). A bounding impact deceleration field of 35 g is applied for the NCT cases as discussed in Section 2.6.7, *Free Drop*, and 100 g is applied for the HAC cases as discussed in Section 2.7.1.1, *Impact Forces and Deformations*. As shown in Section 2.7.1, *Free Drop*, the governing orientations for stress analysis are the end drop (top end down and bottom end down), and the side drop.

The weight of the 380-B package is 67,000 lb from Table 2.1-2. The weight of the payload (including payload locating dunnage) and the impact limiter (including the impact limiter attachments) not in contact with the ground (e.g., the one on top in an end drop) are accounted for by applying pressure to the region of contact. Conservatively the weight of the personnel barrier is added to the impact limiter weight. The applied load is equal to the weight of the component(s) multiplied by the appropriate impact g-load divided by the contact area. Half of each component weight is used for half symmetry, as appropriate, and the contact areas are calculated using the drawings in Appendix 1.3.3, *Packaging General Arrangement Drawings*. The density of stainless steel is 0.29 lb/in³. The weight of the thermal shield and inner cover is included in the cask body model by a slight adjustment of the material density.

The lead gamma shielding is not explicitly modeled and assumed to have no structural strength. As shown in Section 2.7.1.2, *End Drop*, the lead shielding does not reach its flow strength under maximum impact conditions, and thus lead slump does not occur nor does the lead apply lateral loading to the cask shells. Therefore, the weight of the lead is modeled as a pressure applied on the bearing surfaces below the lead body or, for the side drop case, as a density adjustment to the inner and outer shells. The density of the lead is 0.41 lb/in³. See the sections discussing each load case for additional detail.

Once all of the impact loads have been applied, the model is constrained at a minimum number of nodes for stability. The impact limiter support loads are then adjusted until near-perfect balance is achieved between the applied loads (i.e. inertia loads of the cask structure, lead, and

separate components) and the impact reaction. In each case, the total reaction force is essentially equal to the total decelerated weight (i.e., total weight of the 380-B package, less the weight of the limiter(s) contacting the ground) times 35 (NCT) or 100 (HAC). Greater detail on the application of the inertia loads, the lead pressure loads, and the displacement constraints is provided in the sections discussing each load case.

Each stress calculated from the quasi-static model is increased by the dynamic load factor (DLF), equal to 1.15, as calculated in Section 2.7.1.5, *Dynamic Load Factor*. The DLF was calculated for the lid outer plate and the DLF calculated for the stiffer main cask end structures would be lower.

2.12.4.3 Material Properties

Material properties for Case No. 1 through Case No. 8 are evaluated at the bounding NCT hot temperature of 150 °F. The modulus of elasticity is $E = 27.8 \times 10^6$ psi for the cask body and closure lid from Table 2.6-1. The modulus of elasticity for the closure bolts is $E = 28.05 \times 10^6$ psi from Table 2.6-1. Poisson's ratio is equal to 0.31 as identified in Section 2.2.1, *Material Properties and Specifications*. Allowable stresses are evaluated at the NCT hot temperature of 150 °F.

Material properties for Case No. 9 (HAC Fire Event Pressure) are evaluated at 700 °F, which bounds the maximum temperature of any part of the cask in a HAC fire event (see Section 2.7.4.1, *Summary of Pressures and Temperatures*. The modulus of elasticity is $E = 24.8 \times 10^6$ psi for the cask body and closure lid from Table 2.2-1 or Table 2.2-2. The modulus of elasticity for the closure bolts is $E = 24.9 \times 10^6$ psi from Table 2.2-3. Allowable stresses are evaluated at a temperature of 700 °F.

2.12.4.4 Load Cases and Allowable Stress

NCT load cases are identified which allow the evaluation of the model stresses using the allowable stresses defined in Table 2.1-1. The NCT allowable stress values are taken from Table 2.6-1 for a temperature of 150 °F. The primary membrane (P_m) allowable stress is S_m, which is equal to 20,000 psi. The primary membrane plus bending ($P_m + P_b$) stress allowable is $1.5S_m$, or 30,000 psi, and the primary plus bending plus secondary ($P_m + P_b + Q$) stress allowable is $3.0S_m$, or 60,000 psi.

For the HAC free drop load cases, allowable stress values depend on the value of S_u, which is smaller for the forged material used for the upper and lower end structures and the closure lid (see Table 2.2-2). At a temperature of 150 °F, the minimum value of $S_u = 68,150$ psi. The primary membrane (P_m) allowable stress is the lesser of $2.4S_m$ or $0.7S_u$, or a minimum of 47,705 psi. The primary membrane plus bending ($P_m + P_b$) stress allowable is the lesser of $3.6S_m$ or S_u, or a minimum of 68,150 psi.

For the HAC fire case, The HAC membrane stress allowable is the minimum of $2.4S_m$ or $0.7S_u$. From Table 2.2-2 at 700 °F, the HAC membrane stress allowable is $2.4S_m = 37,920$ psi.

In some cases the resulting stresses are relatively low, thus it is not necessary to separately identify the membrane stress. In these cases, the margin of safety may be conservatively determined by applying the maximum stress intensity to the primary membrane stress allowable.

For most cases, the stress resulting from the model is separated, using a linearization technique, into membrane and bending components for application of appropriate stress allowables.

The load cases and allowable stresses are listed in the following table. Note: the design pressure of 25 psi is present in Case No. 1 through Case No. 8. Case No. 9 uses an internal pressure of 100 psi for the fire event. Load Case no. 3b, 5b, and 7b do not have an applied internal pressure. These three load cases apply the NCT cold lead shrinkage pressure of 376 psi to the outer surface of the inner shell and no internal pressure is applied, consistent with Regulatory Guide 7.8 [3]. The NCT hot lead shrinkage pressure of 225 psi is not applied to the outer surface of the inner shell for Load Case no. 3, 5, and 7. The NCT hot lead shrinkage pressure is bounded by the NCT cold lead shrinkage pressure for evaluation with the NCT free drops. The NCT hot and cold lead shrinkage pressures are not included in any of the HAC load cases. The lead shrinkage pressure causes a self-limiting, strain-controlled, secondary stress for which there is no applicable HAC stress allowable per Table 2.1-1.

Case No.	Section No.	Description	Stress Evaluated
1	2.12.4.4.1	Design Pressure Only	Primary
2	2.12.4.4.2	Lead Shrinkage Pressure	Primary + Secondary
3	2.12.4.4.3	NCT Bottom-Down End Drop	Primary
4	2.12.4.4.4	HAC Bottom-Down End Drop	Primary
5	2.12.4.4.5	NCT Top-Down End Drop	Primary
6	2.12.4.4.6	HAC Top-Down End Drop	Primary
7	2.12.4.4.7	NCT Side Drop	Primary
8	2.12.4.4.8	HAC Side Drop	Primary
9	2.12.4.4.9	HAC Fire Event Pressure	Primary
3b	2.12.4.4.10	NCT Bottom-Down End Drop with Cold Lead Shrinkage Pressure	Primary + Secondary
5b	2.12.4.4.11	NCT Top-Down End Drop with Cold Lead Shrinkage Pressure	Primary + Secondary
7b	2.12.4.4.12	NCT Side Drop with Cold Lead Shrinkage Pressure	Primary + Secondary

2.12.4.4.1   Case No. 1, Design Pressure Only

In this case, the only applied load is the design pressure of 25 psig, applied to the interior of the cask body and closure lid at a radius less than or equal to that of the inner (containment) O-ring. The model is constrained by the symmetry plane, fixed nodes at the edge of the cask outer bottom surface and a single fixed node at the bottom cask center and the top lid center.

Results are shown in Figure 2.12.4-2. Due to the bolt preload and coarse mesh around the bolts, there is an artificial stress concentration from the bearing stress between the lid and the upper end structure at the edge of the bolt step in the cask lid main structure, see Figure 2.12.4-3 and Figure 2.12.4-4. The lid to cask body bearing stress was evaluated below and found to be

acceptable. Therefore, the elements adjacent to the stress concentration were unselected as shown in Figure 2.12.4-5 to remove this artifact of the model. The entire model with elements unselected is shown Figure 2.12.4-6. The peak stress intensity is 14,333 psi at the edge of the removed elements. This high stress is still a result of the stress concentration but will be used as the peak model stress. This is conservative because, as shown in Figure 2.12.4-6, the maximum stress intensity in the inner shell and the upper and lower end structures is less than 1,600 psi. Conservatively using the NCT membrane stress allowable of 20,000 psi, the margin of safety is:

$$MS = \frac{20,000}{14,333} - 1 = +0.40$$

Closure Lid to Cask Body Bearing

The closure lid and cask body must be evaluated for maximum average bearing stress. The contact area is based on the top of the upper end structure out to the closure bolt circle (due to the step located there) with the closure bolts half holes removed. The total area can be calculated as:

$$A_c = \frac{\pi}{4}(52^2 - (38.25 + 2 \times 0.25)^2) - (1/2) \times 36 \frac{\pi}{4} 1.56^2 = 910.0 \, in^2$$

where the bolt circle diameter (where the lid step starts) is 52 inches, the inner diameter of the upper end structure is 38.25 inches, the inner diameter edge chamfer is 0.25 inches, and there are 36 bolt holes (cut in half by the lid step) each with a 1.56 inch diameter.

The maximum contact force occurs in the HAC top down end drop when the lid is loaded by the weight of the cask body, lower lead shielding, annular lead shielding and lower impact limiter. The payload, payload locating dunnage and upper impact limiter do not contribute to bearing at the cask to lid interface. The maximum force is:

$$F_c = Wg = (67,000 - 10,000 - 2,000 - 5,000) \times 100 = 5,000,000 \, lb$$

Component weights are taken from Table 2.1-2. The HAC acceleration is 100 g, from Section 2.7.1.1, *Impact Forces and Deformations*. The maximum average stress at the contact is:

$$\sigma_c = \frac{F_c}{A_c} = \frac{5,000,000 \, lb}{910.0 \, in^2} = 5,495 \, psi$$

From Table 2.6-1, the average bearing stress allowable (i.e., the material yield stress) is 27,500 psi. Applying the DLF of 1.15, the margin of safety is:

$$MS = \frac{27,500}{1.15(5,495)} - 1 = +3.35$$

Thus, even though the finite element model generates high contact (compressive) stresses at the edge of the bolt circle step due to the abrupt geometric discontinuity and course mesh, there is no risk of deformation of the lid at the lid/body interface due to the worst-case impact loading. Removal (by deselection) of some of these high-stress elements thus allows a clearer examination of the state of stress in the rest of the cask structure.

2.12.4.4.2   Case No. 2, Lead Shrinkage Pressure

Case No. 2 starts with the 25 psig pressure of Case No. 1 and adds the NCT hot lead shrinkage pressure to the outside surface of the inner shell, all along the lead cavity. The lead shrinkage load is calculated in Section 2.6.1.2.2, *Lead*. The model is constrained by the symmetry plane, fixed nodes at the edge of the cask outer bottom surface and a single fixed node at the bottom cask center and the top lid center.

Results are shown in Figure 2.12.4-7. The same elements, as discussed in Case No. 1, were unselected to remove the artificial stress concentration due to bolt preload stress. The peak stress intensity is 14,139 psi at the edge of the removed elements. This high stress is still a result of the stress concentration but will be used as the peak model stress. This is conservative because, as shown in Figure 2.12.4-7, the maximum stress intensity in the inner shell and upper and lower end structures is less than 11,000 psi. Since the result includes secondary stress, the allowable is 60,000 psi. The margin of safety is:

$$MS = \frac{60,000}{14,139} - 1 = +3.24$$

2.12.4.4.3   Case No. 3, NCT Bottom-Down End Drop

In this case, the applied loads are the design pressure from Case No. 1 and the 35 g free drop impact loading. The free drop loads are described in Section 2.12.4.2.3, *Free Drop Impact Loads*. The cask body orientation is vertical, with the bottom end down. The weight of the annular lead applies a pressure based on depth applied on the bearing surfaces below the lead body. The weight of the lower lead is modeled as two separate pressure loads based on the inner and outer lead columns above the upper surface of the lower closure plate. The weight of the upper lead shielding is modeled as two constant vertical distributed pressure loads and a linearly increasing pressure load based on the weight of the inner, outer and chamfered lead columns above the lower inside surface (lead cavity bottom) of the cask lid main structure. The bottom-down end drop loading is shown in Figure 2.12.4-8. The model is constrained by the symmetry plane, fixed nodes at the edge of the cask outer bottom surface and a single fixed node at the bottom cask center and the top lid center.

Results are shown in Figure 2.12.4-9 and Figure 2.12.4-10. The same elements, as discussed in Case No. 1, were unselected to remove the artificial stress concentration due to bolt preload stress. The maximum stress intensity in the cask body is located in four areas shown on the symmetry plane: the bottom outer plate center, bottom outer plate edge, cavity bottom plate center, cavity bottom plate edge. Each of these locations was evaluated to find the highest stress. The stress was linearized through each cross section to obtain the maximum primary membrane and membrane plus bending stress intensities. Locations evaluated and associated stresses are shown in the table below. Stress linearization plots are shown in Figure 2.12.4-11 through Figure 2.12.4-14.

| Path | Location | Maximum stress intensity (psi) | Linearized stress | | Figure |
			Membrane (psi)	Membrane + Bending (psi)	
1	bottom outer plate - center	14,890	4,359	15,420	2.12.4-11
2	bottom outer plate - edge	17,360	3,821	16,420	2.12.4-12
3	cavity bottom plate - center	14,910	2,383	15,510	2.12.4-13
4	cavity bottom plate - edge	15,860	3,165	15,260	2.12.4-14

From the table above, the maximum primary membrane stress is 4,359 psi at the center of the bottom outer plate. The NCT membrane stress allowable is 20,000 psi. Applying the DLF of 1.15, the margin of safety is:

$$MS = \frac{20,000}{1.15(4,359)} - 1 = +2.99$$

From the table above, the maximum membrane plus bending stress is 16,420 psi at the edge (1 inch in from edge) of the bottom outer plate. The NCT membrane plus bending stress allowable is 30,000 psi. Applying the DLF of 1.15, the margin of safety is:

$$MS = \frac{30,000}{1.15(16,420)} - 1 = +0.59$$

2.12.4.4.4 Case No. 4, HAC Bottom-Down End Drop

Case No. 4 is the same as Case No. 3, except with an HAC inertia field of 100 g.

Results are shown in Figure 2.12.4-15 and Figure 2.12.4-16. The same elements, as discussed in Case No. 1, were unselected to remove the artificial stress concentration due to bolt preload stress. The maximum stress intensity in the cask body is located in four areas shown on the symmetry plane: the bottom outer plate center, bottom outer plate edge, cavity bottom plate center, cavity bottom plate edge. Each of these locations was evaluated to find the highest stress. The stress was linearized through each cross section to obtain the maximum primary membrane and membrane plus bending stress intensities. Locations evaluated and associated stresses are shown in the table below. Stress linearization plots are shown in Figure 2.12.4-17 through Figure 2.12.4-20.

Path	Location	Maximum stress intensity (psi)	Linearized stress		Figure
			Membrane (psi)	Membrane + Bending (psi)	
1	bottom outer plate - center	40,600	12,110	42,050	2.12.4-17
2	bottom outer plate - edge	47,830	10,170	45,240	2.12.4-18
3	cavity bottom plate - center	41,040	6,321	42,680	2.12.4-19
4	cavity bottom plate - edge	43,590	8,638	41,910	2.12.4-20

From the table above, the maximum primary membrane stress is 12,110 psi at the center of the bottom outer plate. The HAC membrane stress allowable is 47,705 psi. Applying the DLF of 1.15, the margin of safety is:

$$MS = \frac{47,705}{1.15(12,110)} - 1 = +2.43$$

From the table above, the maximum membrane plus bending stress is 45,240 psi at the edge (1 inch in from edge) of the bottom outer plate. The HAC membrane plus bending stress allowable is 68,150 psi. Applying the DLF of 1.15, the margin of safety is:

$$MS = \frac{68,150}{1.15(45,240)} - 1 = +0.31$$

For stress specifically in the containment boundary, the maximum membrane stress is 8,638 psi at the edge of the inner cavity bottom plate. The HAC membrane stress allowable is 47,705 psi. Applying the DLF of 1.15, the margin of safety is:

$$MS = \frac{47,705}{1.15(8,638)} - 1 = +3.80$$

The maximum membrane plus bending stress in the containment boundary is 42,680 psi at the center of the cavity bottom plate. The HAC membrane plus bending stress allowable is 68,150 psi. Applying the DLF of 1.15, the margin of safety is:

$$MS = \frac{68,150}{1.15(42,680)} - 1 = +0.39$$

2.12.4.4.5   Case No. 5, NCT Top-Down End Drop

In this case, the applied loads are the design pressure from Case No. 1 and the 35 g free drop impact loading. The free drop loads are described in Section 2.12.4.2.3, *Free Drop Impact Loads*. The cask body orientation is vertical, with the top end down. The weight of the annular lead applies a pressure based on depth applied on the bearing surfaces below the lead body. The weight of the lower lead is modeled as two separate pressure loads based on the inner and outer lead columns above the upper surface of the lower end structure lead cavity. The weight of the

upper lead shielding is modeled as three constant vertical distributed pressure loads based on the weight of the inner, outer and chamfered lead columns applied to the cask lid outer plate. The top-down end drop loading is shown in Figure 2.12.4-21. The model is constrained by the symmetry plane, fixed nodes at the edge of the cask outer bottom surface and a single fixed node at the bottom cask center and the top lid center.

Results are shown in Figure 2.12.4-22 and Figure 2.12.4-23. The same elements, as discussed in Case No. 1, were unselected to remove the artificial stress concentration due to bolt preload stress. The maximum stress intensity in the cask body is still a resultant of bearing stress. The bearing stress was shown to be acceptable in Section 2.12.4.4.1, *Case No. 1, Design Pressure Only*, thus, other areas of the cask are evaluated for high stress. There is high stress intensity at the bottom outside edge of the lid inner plate rotated 45 degrees, and on the symmetry plane at the edge of the lid inner plate, the center of the lid inner plate, the center of the lid outer plate, and the lid outer plate edge. All five of these locations were evaluated to find the highest stress. At each location, the stress was linearized through the cross section to obtain the maximum primary membrane and membrane plus bending stress intensities. Locations evaluated and associated stresses are shown in the table below. Stress linearization plots are shown in Figure 2.12.4-24 to Figure 2.12.4-28.

Path	Location	Maximum stress intensity (psi)	Linearized stress		Figure
			Membrane (psi)	Membrane + Bending (psi)	
1	lid outer plate - center	15,660	5,873	16,170	2.12.4-24
2	lid outer plate - edge	15,880	4,804	15,120	2.12.4-25
3	lid inner plate – center	14,120	2,969	14,370	2.12.4-26
4	lid inner plate – outside edge	16,130	3,184	13,300	2.12.4-27
5	lid inner plate – outside edge at 45°	20,070	2,711	12,880	2.12.4-28

From the table above, the maximum primary membrane stress is 5,873 psi at the center of the lid outer plate. The NCT membrane stress allowable is 20,000 psi. Applying the DLF of 1.15, the margin of safety is:

$$MS = \frac{20,000}{1.15(5,873)} - 1 = +1.96$$

From the table above, the maximum membrane plus bending stress is 16,170 psi at the center of the lid outer plate. The NCT membrane plus bending stress allowable is 30,000 psi. Applying the DLF of 1.15, the margin of safety is:

$$MS = \frac{30,000}{1.15(16,170)} - 1 = +0.61$$

2.12.4.4.6   Case No. 6, HAC Top-Down End Drop

Case No. 6 is the same as Case No. 5, except with an HAC inertia field of 100 g.

Results are shown in Figure 2.12.4-29 and Figure 2.12.4-30. The same elements, as discussed in Case No. 1, were unselected to remove the artificial stress concentration due to bolt preload stress. The maximum stress intensity is at the outside edge of the lid inner plate rotated 45 degrees. There is also high stress intensity on the symmetry plane at the outside edge of the lid inner plate, the center of the lid inner plate, the center of the lid outer plate, and the lid outer plate edge. All five of these locations were evaluated to find the highest stress. At each location, the stress was linearized through the high stress cross sections to obtain the maximum primary membrane and membrane plus bending stress intensities. Locations evaluated and associated stresses are shown in the table below. Stress linearization plots are shown Figure 2.12.4-31 through Figure 2.12.4-35.

| Path | Location | Maximum stress intensity (psi) | Linearized stress | | Figure |
			Membrane (psi)	Membrane + Bending (psi)	
1	lid outer plate - center	40,350	14,690	41,690	2.12.4-31
2	lid outer plate - edge	42,830	11,270	40,800	2.12.4-32
3	lid inner plate – center	39,560	7,766	40,260	2.12.4-33
4	lid inner plate – outside edge	42,990	8,573	35,400	2.12.4-34
5	lid inner plate – outside edge at 45°	53,680	7,391	34,330	2.12.4-35

From the table above, the maximum primary membrane stress is 14,690 psi at the center of the lid outer plate. The HAC membrane stress allowable is 47,705 psi. Applying the DLF of 1.15, the margin of safety is:

$$MS = \frac{47,705}{1.15(14,690)} - 1 = +1.82$$

From the table above, the maximum membrane plus bending stress is 41,690 psi at the center of the lid outer plate. The HAC membrane plus bending stress allowable is 68,150 psi. Applying the DLF of 1.15, the margin of safety is:

$$MS = \frac{68,150}{1.15(41,690)} - 1 = +0.42$$

For stress specifically in the containment boundary, the maximum membrane stress is 8,573 psi at the bottom outside edge of the closure lid bottom plate. The HAC membrane stress allowable is 47,705 psi. Applying the DLF of 1.15, the margin of safety is:

$$MS = \frac{47,705}{1.15(8,573)} - 1 = +3.84$$

The maximum membrane plus bending stress in the containment boundary is 40,260 psi at the bottom center of the closure lid bottom plate. The HAC membrane plus bending stress allowable is 68,150 psi. Applying the DLF of 1.15, the margin of safety is:

$$MS = \frac{68,150}{1.15(40,260)} - 1 = +0.47$$

HAC Top-Down End Drop Lid Deflection

The mating surface of the lid features a step relief located at the bolt circle. This relief prevents any contact from occurring between the lid and the body outside of the bolt circle, thus preventing prying loads from being applied to the closure bolts. In the top-down configuration, the lid rotates about the step edge, reducing the 0.06-inch gap at the outer edge of the lid. The minimum gap maintained can be found by comparing the deflection of lid and flange nodes at the outside edge of the model. The minimum gap is 0.048 inches. Thus, no prying loads can occur.

2.12.4.4.7   Case No. 7, NCT Side Drop

In this case, the applied loads are the design pressure from Case No. 1 and the 35 g free drop impact loading. The free drop loads are described in Section 2.12.4.2.3, *Free Drop Impact Loads*. The cask body orientation is horizontal. The payload impact load, lower lead shielding pressure, upper lead shielding pressure and supporting impact limiter reactions are applied as pressures over an included angle of 150 degrees (75 degrees on the half symmetry model), which represents the circumferential extent of contact. These pressures are modeled using cosine distributions about the symmetry plane. The resulting load is maximum at the symmetry plane, reducing to zero at a point $\theta_{max} = 75$ degrees away from the symmetry plane, as shown in the illustration below.
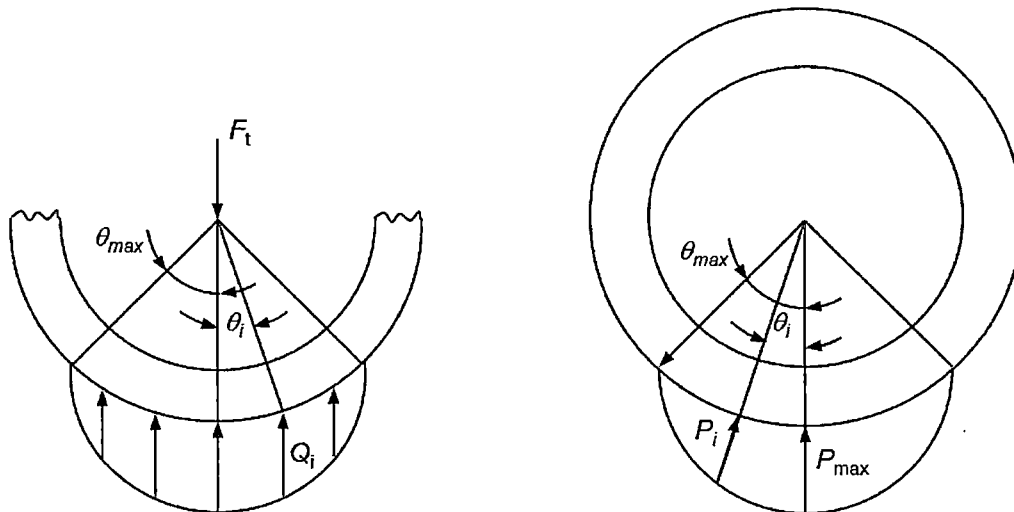
If the clearance between the contacting elements (such as the body end structures and the impact limiters) were zero then the angle could be taken as 180 degrees (90 degrees on the half symmetry model). The choice of 150 degrees (75 degrees on the half symmetry model) reflects the fact that some clearance exists between the contents, the top and bottom lead shields, and the impact limiters and their respective supporting surfaces. Because the contents, the lead, and the impact limiters each possess some compliance, a smaller angle is not justified.

The annular lead is applied as an increase in density of the cask shells. Half of the weight of the body lead (one quarter, in the half-symmetry model) is applied to the upper half of the inner shell (quarter shell, in the half symmetry model), and the other half of the weight of the body lead (quarter) is applied to the lower half (quarter) of the outer shell. The weight is applied as an increase in density above that of the density of the metal components alone. The annular lead load is carried by the body shells, therefore the weight of the lead can be readily distributed to the two shells as a change in mass. Lead has a very small load bearing capacity, and because the clearance to the outer shell is small, it is reasonable to assume that the lower half of the lead is carried by the outer shell.

The weight of the lower lead shielding is modeled as two pressure loads based on the weight of the upper and lower lead columns above the surface of the lower end structure lead cavity side. The weight of the upper lead shielding is modeled as two pressure loads based on the weight of the upper and lower lead columns above the surface of the cask lid main structure lead cavity side. The side drop loading is shown in Figure 2.12.4-36. The model is constrained by the symmetry plane, fixed nodes at the top and bottom of the cask and a single fixed node at the center of the cask.

Results are shown in Figure 2.12.4-37 and Figure 2.12.4-38. The same elements, as discussed in Case No. 1, were unselected to remove the artificial stress concentration due to bolt preload stress. The maximum stress intensity is shown on the symmetry plane at the bottom of the outer shell. There is also high stress intensity at the lower end structure annular lead cavity step. Both of these locations were evaluated to find the highest stress. The stress was linearized through the cross sections to obtain the maximum primary membrane and membrane plus bending stress intensities. Locations evaluated and associated stresses are shown in the table below. Stress linearization plots are shown in Figure 2.12.4-39 and Figure 2.12.4-40.

Path	Location	Maximum stress intensity (psi)	Linearized stress		Figure
			Membrane (psi)	Membrane + Bending (psi)	
1	outer shell	19,820	11,500	19,780	2.12.4-39
2	lower end structure - step	19,610	3,568	17,490	2.12.4-40

From the table above, the maximum primary membrane stress intensity is 11,500 psi in the outer shell. The NCT membrane stress allowable is 20,000 psi. Applying the DLF of 1.15, the margin of safety is:

$$MS = \frac{20,000}{1.15(11,500)} - 1 = +0.51$$

From the table above, the maximum membrane plus bending stress is 19,780 psi in the outer shell. The NCT membrane plus bending stress allowable is 30,000 psi. Applying the DLF of 1.15, the margin of safety is:

$$MS = \frac{30,000}{1.15(19,780)} - 1 = +0.32$$

2.12.4.4.8   Case No. 8, HAC Side Drop

Case No. 8 is the same as Case No. 7, except with an HAC inertia field of 100 g.

Results are shown in Figure 2.12.4-41 and Figure 2.12.4-42. The same elements, as discussed in Case No. 1, were unselected to remove the artificial stress concentration due to bolt preload stress. The maximum stress intensity is shown on the symmetry plane at the bottom of the outer shell. There is also high stress intensity at the lower end structure annular lead cavity step. The maximum stress in the containment boundary is located on the symmetry plane at the top of the annular lead cavity, shown in Figure 2.12.4-47. The stated locations were evaluated to find the highest stress. The stress was linearized through the cross sections to obtain the maximum primary membrane and membrane plus bending stress intensities. Locations evaluated and associated stresses are shown in the table below. Stress linearization plots are shown in Figure 2.12.4-43, Figure 2.12.4-44, Figure 2.12.4-44a, Figure 2.12.4-44b, and Figure 2.12.4-44c.

| Path | Location | Maximum stress intensity (psi) | Linearized stress | | Figure |
			Membrane (psi)	Membrane + Bending (psi)	
1	outer shell	55,850	32,680	55,740	2.12.4-43
2	lower end structure – step	54,690	9,701	49,100	2.12.4-44
3	upper end structure shelf – inner	44,540	8,472	37,560	2.12.4-44a
4	upper end structure shelf – outer	44,880	8,236	38,650	2.12.4-44b
5	top end of inner shell	29,170	19,770	26,730	2.12.4-44c

From the table above, the maximum primary membrane stress is 32,680 psi in the outer shell. The HAC membrane stress allowable is 47,705 psi. Applying the DLF of 1.15, the margin of safety is:

$$MS = \frac{47,705}{1.15(32,680)} - 1 = +0.27$$

From the table above, the maximum membrane plus bending stress is 55,740 psi in the outer shell. The HAC membrane plus bending stress allowable is 68,150 psi. Applying the DLF of 1.15, the margin of safety is:

$$MS = \frac{68,150}{1.15(55,740)} - 1 = +0.06$$

For stress specifically in the containment boundary, the maximum membrane stress is 19,770 psi at the top end of the inner shell. The HAC membrane stress allowable is 47,705 psi. Applying the DLF of 1.15, the margin of safety is:

$$MS = \frac{47,705}{1.15(19,770)} - 1 = +1.10$$

The maximum membrane plus bending stress in the containment boundary is 38,650 psi at the upper end structure shelf, outer location. The HAC membrane plus bending stress allowable is 68,150 psi. Applying the DLF of 1.15, the margin of safety is:

$$MS = \frac{68,150}{1.15(38,650)} - 1 = +0.53$$

2.12.4.4.9   Case No. 9, HAC Fire Event Pressure

The payload may be located within the inner container with wood dunnage. The wood dunnage is evaluated in Chapter 3, *Thermal Evaluation*, for the HAC fire event to establish a bounding pressure due to both the possible generation of pressure from the wood moisture content as well as the temperature increase of the air inside the cask. As shown in Table 3.1-2, the maximum internal cask pressure as a result of the HAC fire event is bounded by a value of 100 psi. The effect of this pressure on the closure bolts is evaluated in Section 2.7.4.3, *Stress Calculations*. The effect on the inner shell is evaluated here by rerunning Case No. 1 (Section 2.12.4.4.1, *Case No. 1, Design Pressure Only*) at 100 psi. As a result of the HAC fire event, the maximum temperature of any part of the cask may be bounded by a temperature of 700 °F as stated in Section 2.7.4.1, *Summary of Pressures and Temperatures*.

Results are shown in Figure 2.12.4-48 and Figure 2.12.4-49. The same elements, as discussed in Case No. 1, were unselected to remove the artificial stress concentration due to bolt preload stress. The peak stress intensity is 12,677 psi at the edge of the removed elements. This high stress is still a result of the stress concentration but will be used as the peak model stress. Conservatively the maximum stress intensity will be compared to the membrane stress allowable. The HAC membrane stress allowable is the minimum of $2.4S_m$ or $0.7S_u$. From Table 2.2-2 at 700 °F, the HAC membrane stress allowable is $2.4S_m = 37,920$ psi. The margin of safety is:

$$MS = \frac{37,920}{12,677} - 1 = +1.99$$

2.12.4.4.10   Case No. 3b, NCT Bottom-Down End Drop with Cold Lead Shrinkage Pressure

In this case, the applied loads are the same as Case No. 3, except the design pressure is removed and the lead shrinkage is modeled as a bounding pressure of 376 psi on the outside surface of the inner shell. The free drop loads are described in Section 2.12.4.2.3, *Free Drop Impact Loads*. The cask body orientation is vertical, with the bottom end down. The weight of the annular lead applies a pressure based on depth applied on the bearing surfaces below the lead body. The weight of the lower lead is modeled as two separate pressure loads based on the inner and outer lead columns above the upper surface of the lower closure plate. The weight of the upper lead shielding is modeled as two constant vertical distributed pressure loads and a linearly increasing

pressure load based on the weight of the inner, outer and chamfered lead columns above the lower inside surface (lead cavity bottom) of the cask lid main structure. The bottom-down end drop loading is shown in Figure 2.12.4-8. The model is constrained by the symmetry plane, fixed nodes at the edge of the cask outer bottom surface and a single fixed node at the bottom cask center and the top lid center.

Results are shown in Figure 2.12.4-50 and Figure 2.12.4-51. The same elements, as discussed in Case No. 1, were unselected to remove the artificial stress concentration due to bolt preload stress. The maximum stress intensity in the cask body is located in four areas shown on the symmetry plane: the bottom outer plate center, bottom outer plate edge, cavity bottom plate center, cavity bottom plate edge. Each of these locations was evaluated to find the highest stress. The stress was linearized through each cross section to obtain the maximum primary membrane and membrane plus bending stress intensities. Locations evaluated and associated stresses are shown in the table below. Stress linearization plots are shown in Figure 2.12.4-52 through Figure 2.12.4-55.

Path	Location	Maximum stress intensity (psi)	Linearized stress		Figure
			Membrane (psi)	Membrane + Bending (psi)	
1	bottom outer plate - center	15,070	4,531	15,600	2.12.4-52
2	bottom outer plate - edge	17,530	4,003	16,580	2.12.4-53
3	cavity bottom plate - center	15,270	2,905	15,860	2.12.4-54
4	cavity bottom plate - edge	15,540	3,453	14,570	2.12.4-55

From the table above, the maximum primary membrane stress is 4,531 psi at the center of the bottom outer plate. The NCT membrane stress allowable is 20,000 psi. Applying the DLF of 1.15, the margin of safety is:

$$MS = \frac{20,000}{1.15(4,531)} - 1 = +2.84$$

From the table above, the maximum membrane plus bending stress is 16,580 psi at the edge (1 inch in from edge) of the bottom outer plate. The NCT membrane plus bending stress allowable is 30,000 psi. Applying the DLF of 1.15, the margin of safety is:

$$MS = \frac{30,000}{1.15(16,580)} - 1 = +0.57$$

The NCT membrane plus bending plus secondary stress allowable is 60,000 psi. The lead shrinkage pressure applied to the outside surface of the inner shell creates a self-limiting, strain-controlled, fabrication stress that must meet the NCT membrane plus bending plus secondary stress allowable. The inner shell, where the lead shrinkage pressure is applied, is not an area of

high stress as shown in the stress plots. Therefore, no comparison to the NCT membrane plus bending plus secondary stress allowable is necessary.

2.12.4.4.11   Case No. 5b, NCT Top-Down End Drop with Cold Lead Shrinkage Pressure

In this case, the applied loads are the same as Case No. 5, except the design pressure is removed and the lead shrinkage is modeled as a bounding pressure of 376 psi on the outside surface of the inner shell. The free drop loads are described in Section 2.12.4.2.3, *Free Drop Impact Loads*. The cask body is orientation is vertical, with the top end down. The weight of the annular lead applies a pressure based on depth applied on the bearing surfaces below the lead body. The weight of the lower lead is modeled as two separate pressure loads based on the inner and outer lead columns above the upper surface of the lower end structure lead cavity. The weight of the upper lead shielding is modeled as three constant vertical distributed pressure loads based on the weight of the inner, outer and chamfered lead columns applied to the cask lid outer plate. The top-down end drop loading is shown in Figure 2.12.4-21. The model is constrained by the symmetry plane, fixed nodes at the edge of the cask outer bottom surface and a single fixed node at the bottom cask center and the top lid center.

Results are shown in Figure 2.12.4-56 and Figure 2.12.4-57. The same elements, as discussed in Case No. 1, were unselected to remove the artificial stress concentration due to bolt preload stress. The maximum stress intensity in the cask body is still a resultant of bearing stress. The bearing stress was shown to be acceptable in Section 2.12.4.4.1, *Case No. 1, Design Pressure Only*, thus, other areas of the cask are evaluated for high stress. There is high stress intensity at the bottom outside edge of the lid inner plate rotated 45 degrees, and on the symmetry plane at the edge of the lid inner plate, the center of the lid inner plate, the center of the lid outer plate, and the lid outer plate edge. All five of these locations were evaluated to find the highest stress. At each location, the stress was linearized through the cross section to obtain the maximum primary membrane and membrane plus bending stress intensities. Locations evaluated and associated stresses are shown in the table below. Stress linearization plots are shown in Figure 2.12.4-58 to Figure 2.12.4-62.

Path	Location	Maximum stress intensity (psi)	Linearized stress		Figure
			Membrane (psi)	Membrane + Bending (psi)	
1	lid outer plate - center	15,670	5,859	16,180	2.12.4-58
2	lid outer plate - edge	15,820	4,783	15,060	2.12.4-59
3	lid inner plate - center	13,220	2,802	13,450	2.12.4-60
4	lid inner plate - outside edge	15,320	3,000	12,640	2.12.4-61
5	lid inner plate - outside edge at 45°	19,060	2,554	12,230	2.12.4-62

From the table above, the maximum primary membrane stress is 5,859 psi at the center of the lid outer plate. The NCT membrane stress allowable is 20,000 psi. Applying the DLF of 1.15, the margin of safety is:

$$MS = \frac{20,000}{1.15(5,859)} - 1 = +1.97$$

From the table above, the maximum membrane plus bending stress is 16,180 psi at the center of the lid outer plate. The NCT membrane plus bending stress allowable is 30,000 psi. Applying the DLF of 1.15, the margin of safety is:

$$MS = \frac{30,000}{1.15(16,180)} - 1 = +0.61$$

The NCT membrane plus bending plus secondary stress allowable is 60,000 psi. The lead shrinkage pressure applied to the outside surface of the inner shell creates a self-limiting, strain-controlled, fabrication stress that must meet the NCT membrane plus bending plus secondary stress allowable. The inner shell, where the lead shrinkage pressure is applied, is not an area of high stress as shown in the stress plots. Therefore, no comparison to the NCT membrane plus bending plus secondary stress allowable is necessary.

2.12.4.4.12   Case No. 7b, NCT Side Drop with Cold Lead Shrinkage Pressure

In this case, the applied loads are the same as Load Case 7, except the design pressure is removed and the lead shrinkage is modeled as a bounding pressure of 376 psi on the outside surface of the inner shell. The free drop loads are described in Section 2.12.4.2.3, *Free Drop Impact Loads*. The cask body orientation is horizontal. The payload impact load, lower lead shielding pressure, upper lead shielding pressure and supporting impact limiter reactions are applied as pressures over an included angle of 150 degrees (75 degrees on the half symmetry model), which represents the circumferential extent of contact. The annular lead is applied as an increase in density of the cask shells. Half of the weight of the body lead (one quarter, in the half-symmetry model) is applied to the upper half of the inner shell (quarter shell, in the half symmetry model), and the other half of the weight of the body lead (quarter) is applied to the lower half (quarter) of the outer shell. The weight is applied as an increase in density above that of the density of the metal components alone. The weight of the lower lead shielding is modeled as two pressure loads based on the weight of the upper and lower lead columns above the surface of the lower end structure lead cavity side. The weight of the upper lead shielding is modeled as two pressure loads based on the weight of the upper and lower lead columns above the surface of the cask lid main structure lead cavity side. The side drop loading is shown in Figure 2.12.4-36. The model is constrained by the symmetry plane, fixed nodes at the top and bottom of the cask and a single fixed node at the center of the cask.

Results are shown in Figure 2.12.4-63 and Figure 2.12.4-64. The same elements, as discussed in Case No. 1, were unselected to remove the artificial stress concentration due to bolt preload stress. The maximum stress intensity is shown on the symmetry plane at the bottom of the outer shell. There is also high stress intensity at the lower end structure annular lead cavity step. Both of these locations were evaluated to find the highest stress. The stress was linearized through the cross sections to obtain the maximum primary membrane and membrane plus bending stress

intensities. Locations evaluated and associated stresses are shown in the table below. Stress linearization plots are shown in Figure 2.12.4-65 and Figure 2.12.4-66.

| Path | Location | Maximum stress intensity (psi) | Linearized stress | | Figure |
			Membrane (psi)	Membrane + Bending (psi)	
1	outer shell	20,000	11,550	19,960	2.12.4-65
2	lower end structure - step	19,420	3,749	17,250	2.12.4-66

From the table above, the maximum primary membrane stress intensity is 11,550 psi in the outer shell. The NCT membrane stress allowable is 20,000 psi. Applying the DLF of 1.15, the margin of safety is:

$$MS = \frac{20,000}{1.15(11,550)} - 1 = +0.51$$

From the table above, the maximum membrane plus bending stress is 19,960 psi in the outer shell. The NCT membrane plus bending stress allowable is 30,000 psi. Applying the DLF of 1.15, the margin of safety is:

$$MS = \frac{30,000}{1.15(19,960)} - 1 = +0.31$$

The NCT membrane plus bending plus secondary stress allowable is 60,000 psi. The lead shrinkage pressure applied to the outside surface of the inner shell creates a self-limiting, strain-controlled, fabrication stress that must meet the NCT membrane plus bending plus secondary stress allowable. The inner shell, where the lead shrinkage pressure is applied, is not an area of high stress as shown in the stress plots. Therefore, no comparison to the NCT membrane plus bending plus secondary stress allowable is necessary.

2.12.4.5 Containment Closure Evaluation

Inelastic deformation of the containment closure and sealing system is generally unacceptable. From Table 2.6-1, the yield stress for the ASTM Type 304 stainless steel forged end structures in the region of the containment seal at the bounding temperature of 150 °F is 27,500 psi. For the purpose of illustration of inelastic behavior on the stress plots, this value is divided by the DLF of 1.15 to give an effective yield point of 23,913 psi. A close-up of the HAC stress intensity in the larger region of the containment seal is shown in Figure 2.12.4-45, Figure 2.12.4-46, and Figure 2.12.4-47 for the HAC bottom-down, top-down, and side free drops, respectively. In each case, the location of the containment seal is indicated. For convenience in creating the color index shown on each plot, an effective yield stress of 23,750 psi is conservatively chosen, and all areas red in color have stress above this value.

Figure 2.12.4-45 for the HAC bottom-down free drop orientation shows no stress anywhere in the region above the effective yield point. In Figure 2.12.4-46, for the HAC top-down orientation, any stress above effective yield is limited to either parts of the lid which are far from the seal area, such as in the stepped area of the lid, or in pinpoint areas caused by a sharp

discontinuity of the mesh. In Figure 2.12.4-47, for the HAC side orientation, the yield region is limited to the thinner cross section of the body structure and to the outer shell, both of which are relatively distant from the containment seal. In all HAC cases, the inelastic deformation that does exist is not of a magnitude to affect the relative configuration of the sealing surfaces or of the compression of the containment seal. Stresses in NCT cases are well below allowable yield stress and are not a concern.

2.12.4.6 Summary

Table 2.12.4-1 summarizes the bounding margins of safety of the 380-B package finite element analysis, as established in the sections above. Table 2.12.4-2 summarizes the margins of safety for the containment boundary for the HAC load cases. Since all margins of safety are positive, the structural performance of the 380-B is not of concern.

Table 2.12.4-1 – Finite Element Analysis Results

Analysis Description	Reference Section	Margin of Safety
Case No. 1, Design Pressure Only	2.12.4.4.1	+ 0.40
Case No. 2, Lead Shrinkage Pressure	2.12.4.4.2	+ 3.24
Case No. 3, NCT Bottom-Down End Drop	2.12.4.4.3	+ 0.59*
Case No. 4, HAC Bottom-Down End Drop	2.12.4.4.4	+ 0.31*
Case No. 5, NCT Top-Down End Drop	2.12.4.4.5	+ 0.61*
Case No. 6, HAC Top-Down End Drop	2.12.4.4.6	+ 0.42*
Case No. 7, NCT Side Drop	2.12.4.4.7	+ 0.32*
Case No. 8, HAC Side Drop	2.12.4.4.8	+ 0.06*
Case No. 9, HAC Fire Event Pressure	2.12.4.4.9	+ 1.99
Case No. 3b, NCT Bottom-Down End Drop with Cold Lead Shrinkage Pressure	2.12.4.4.10	+ 0.57*
Case No. 5b, NCT Top-Down End Drop with Cold Lead Shrinkage Pressure	2.12.4.4.11	+ 0.61*
Case No. 7b, NCT Side Drop with Cold Lead Shrinkage Pressure	2.12.4.4.12	+ 0.31*

*Minimum value shown.

Table 2.12.4-2 – Finite Element Analysis Results, HAC, Containment Boundary

Analysis Description	Reference Section	Margin of Safety
Case No. 4, HAC Bottom-Down End Drop	2.12.4.4.4	+ 0.39*
Case No. 6, HAC Top-Down End Drop	2.12.4.4.6	+ 0.47*
Case No. 8, HAC Side Drop	2.12.4.4.8	+ 0.53*

*Minimum value shown.

ELEMENTS

TYPE NUM

ANSYS

OCT 31 2013
09:37:02

380B CASK, HACSIDE
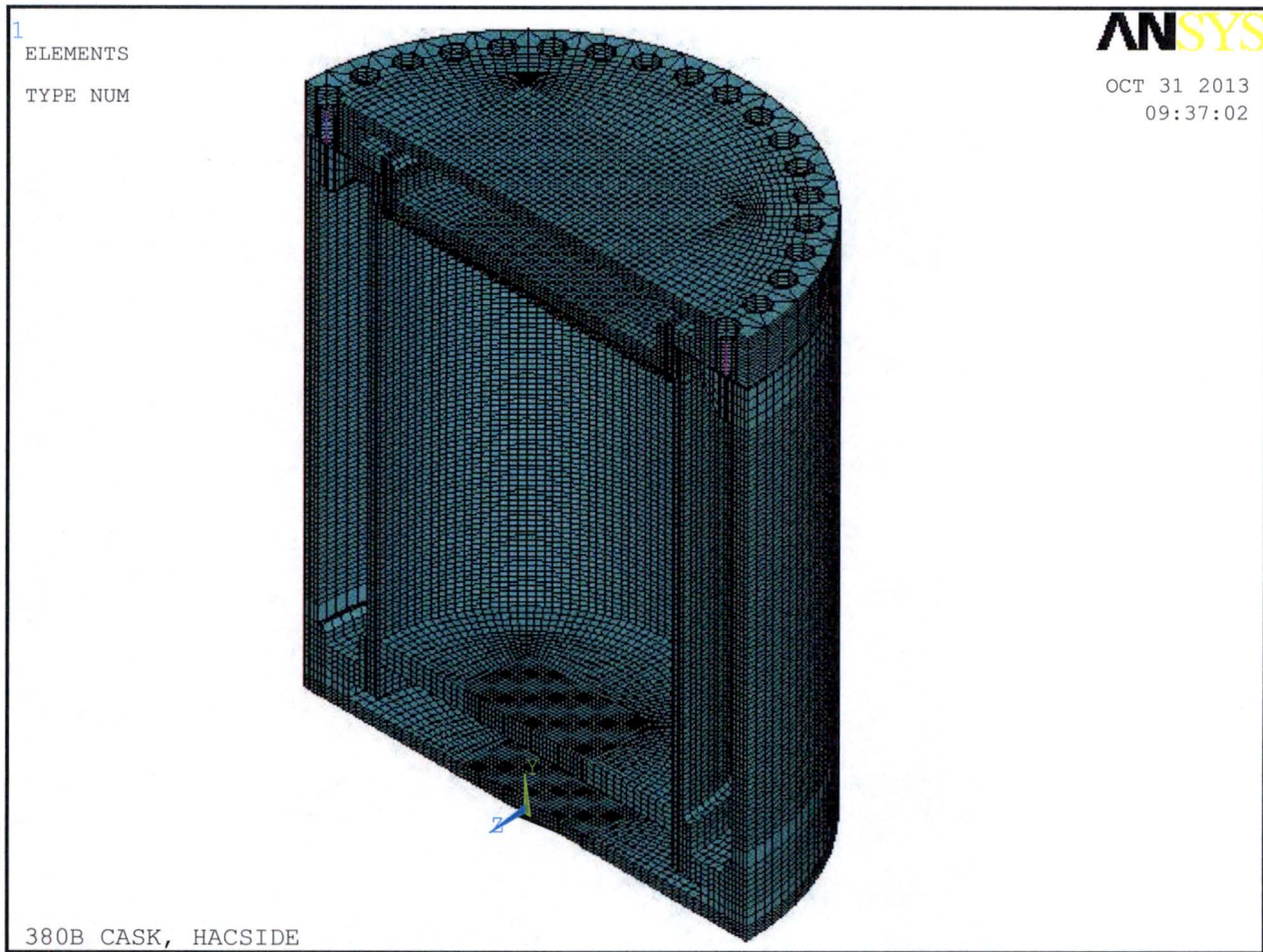
Figure 2.12.4-1 – Finite Element Mesh
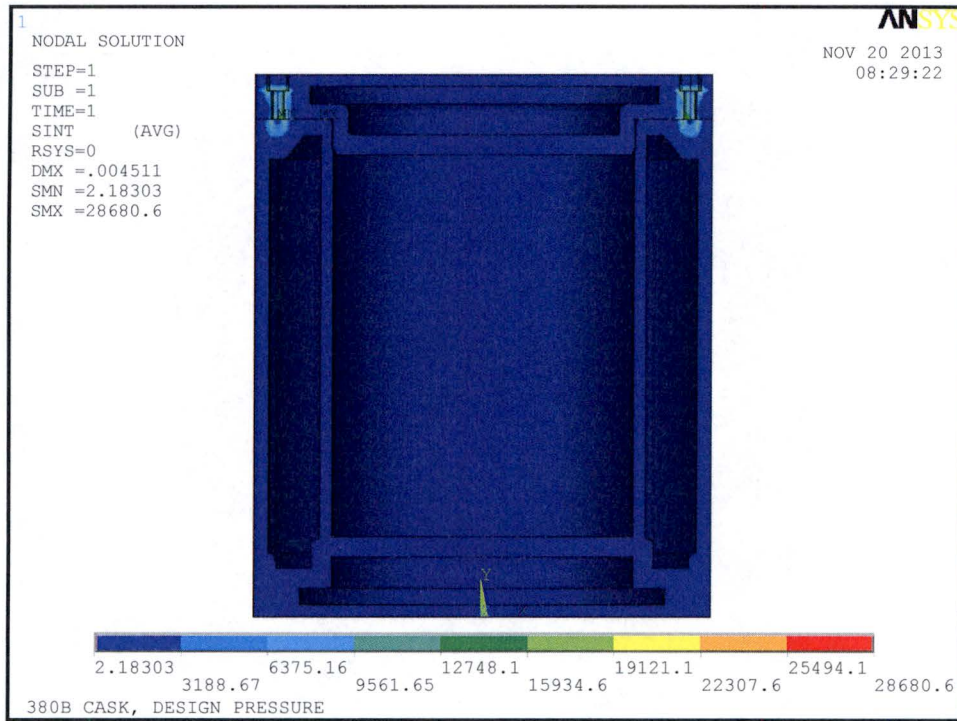
Figure 2.12.4-2 – Design Pressure Only with Bolt Stress Concentration
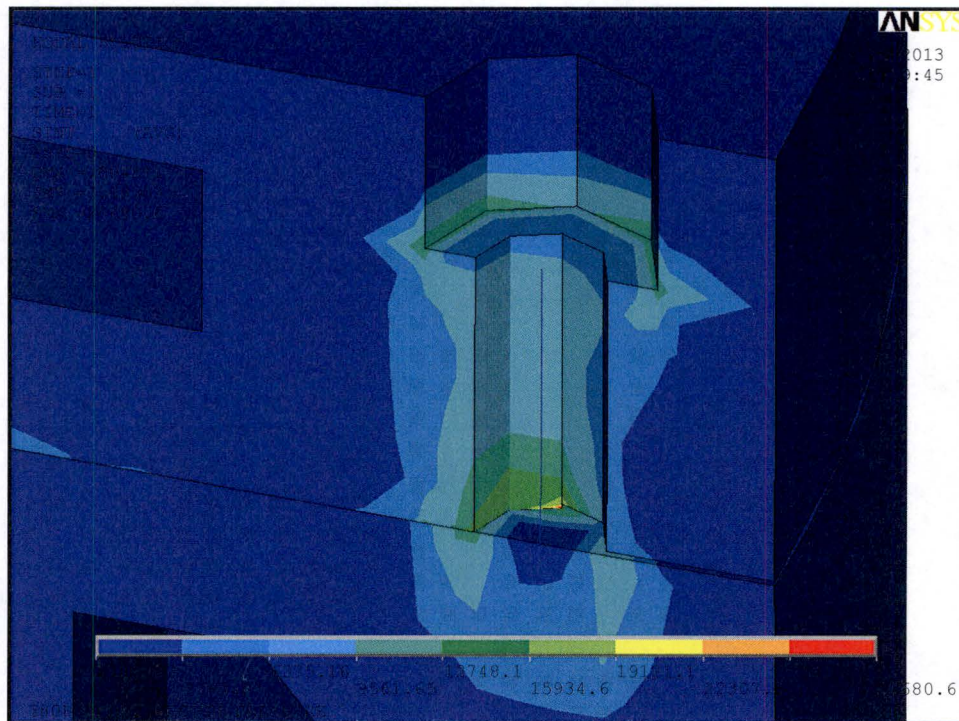
Figure 2.12.4-3 – Design Pressure Only Bolt Stress Concentration
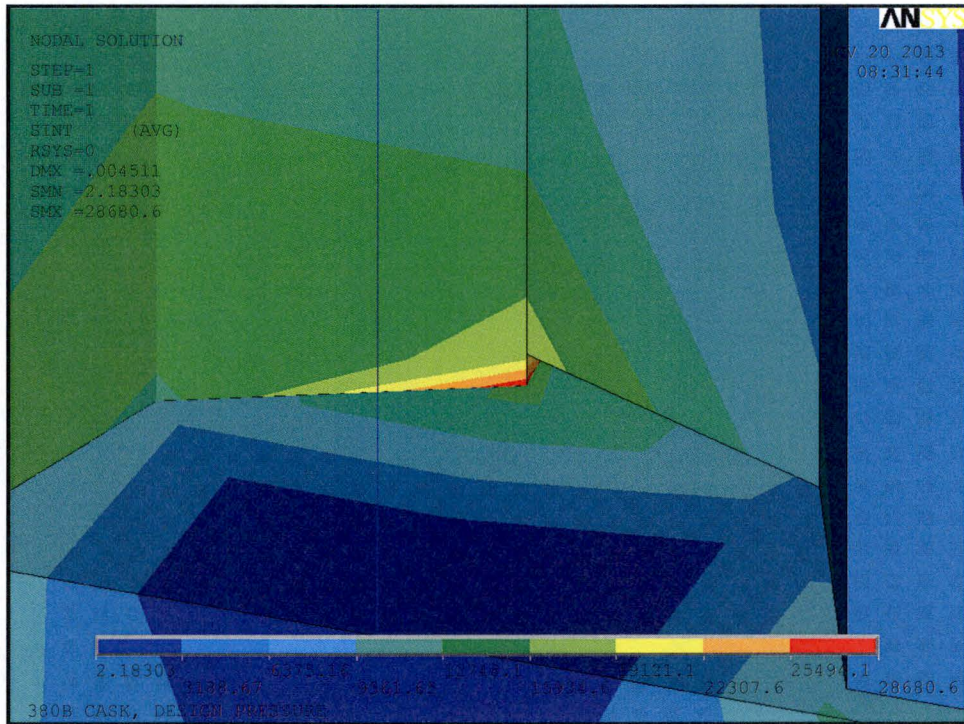
Figure 2.12.4-4 – Bolt Stress Concentration Close-Up
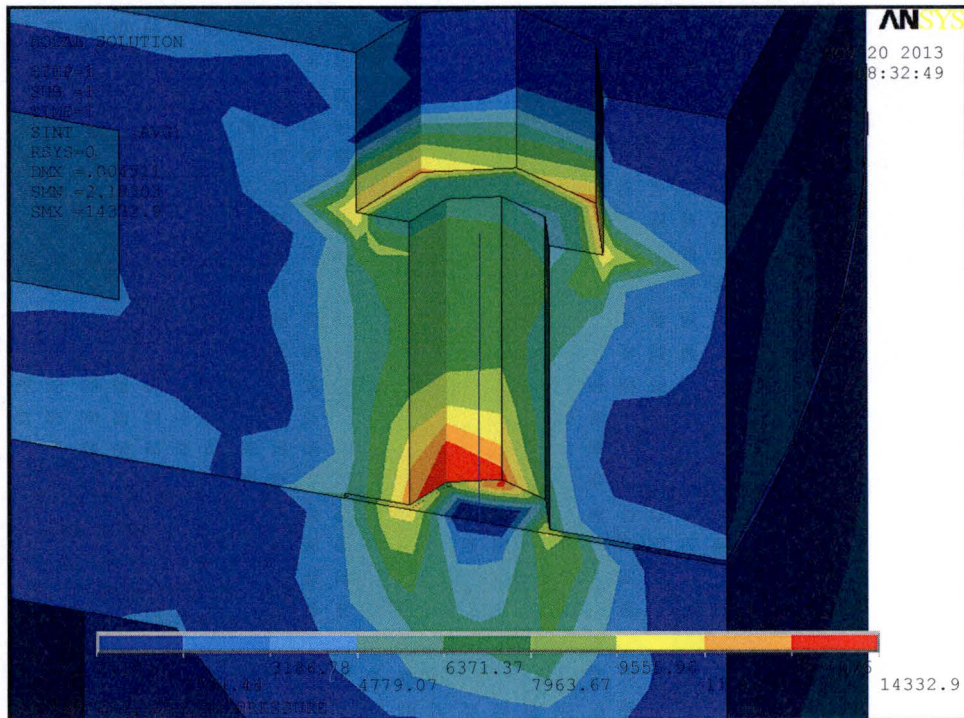
Figure 2.12.4-5 – Bolt Stress Concentration Elements Unselected
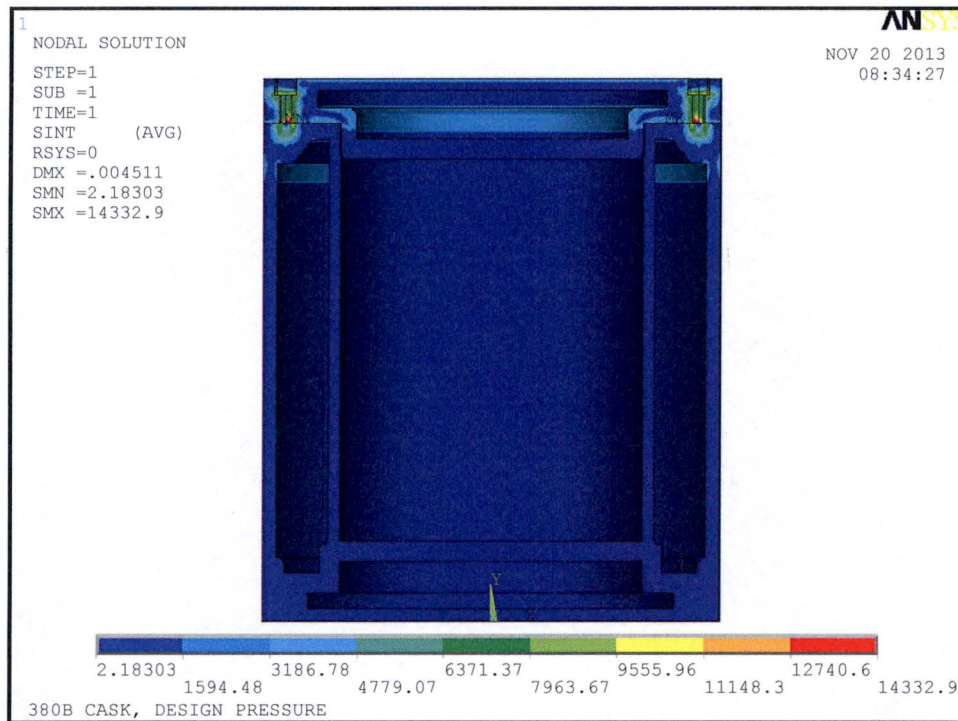
Figure 2.12.4-6 – Design Pressure Only
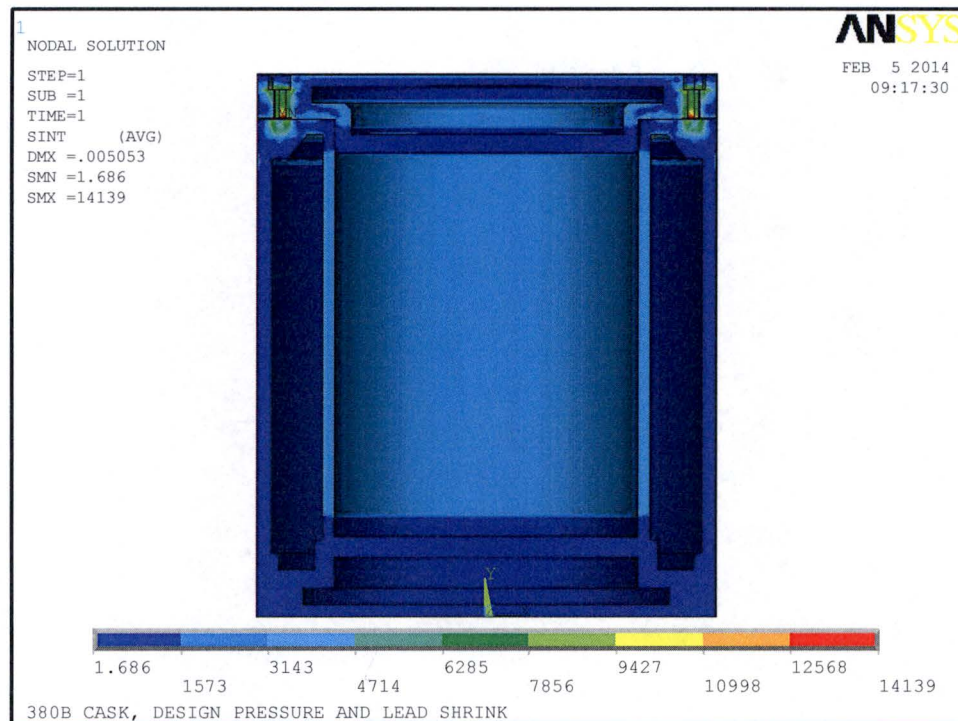
Figure 2.12.4-7 – Lead Shrinkage Pressure
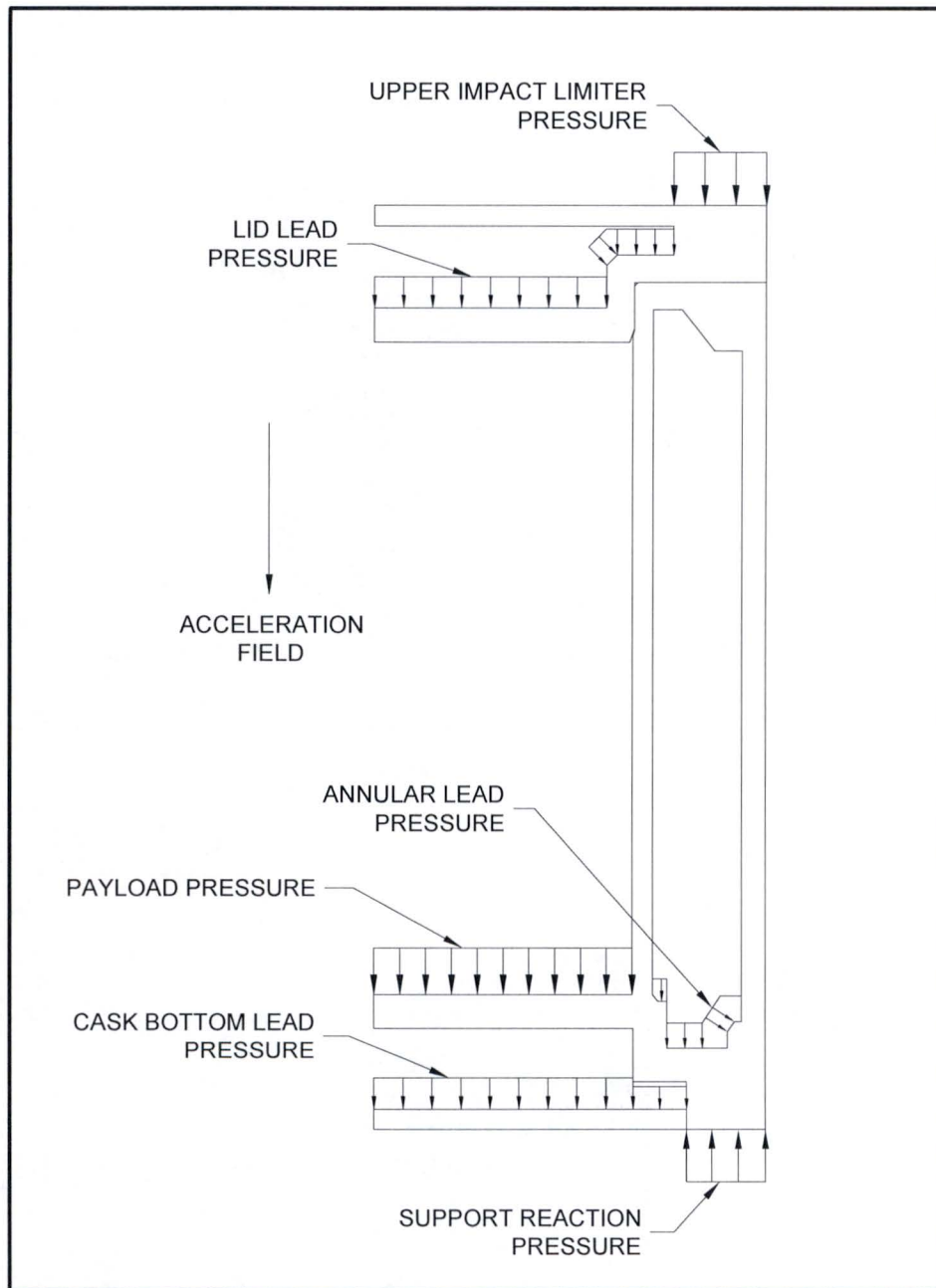
Figure 2.12.4-8 – Bottom-Down End Drop Loading
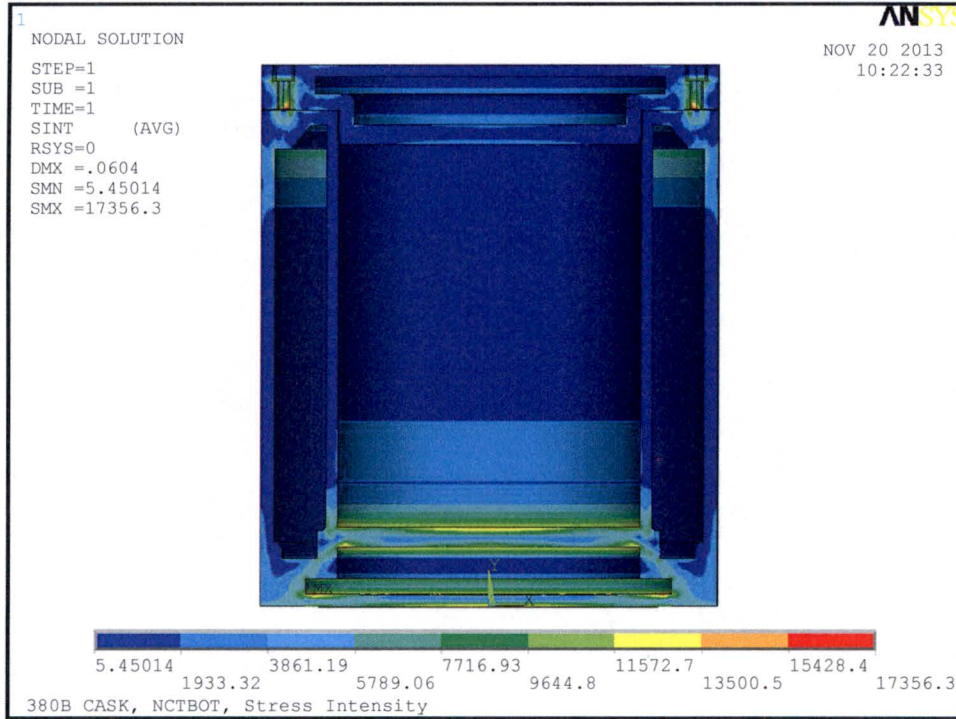
Figure 2.12.4-9 – NCT Bottom-Down End Drop
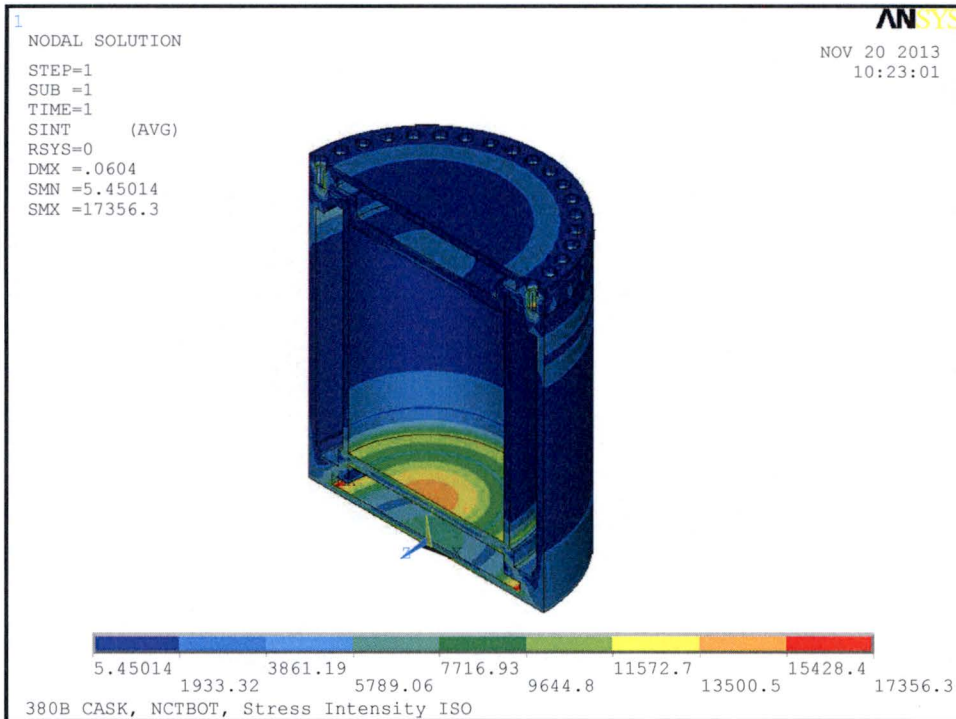
Figure 2.12.4-10 – NCT Bottom-Down End Drop Isometric
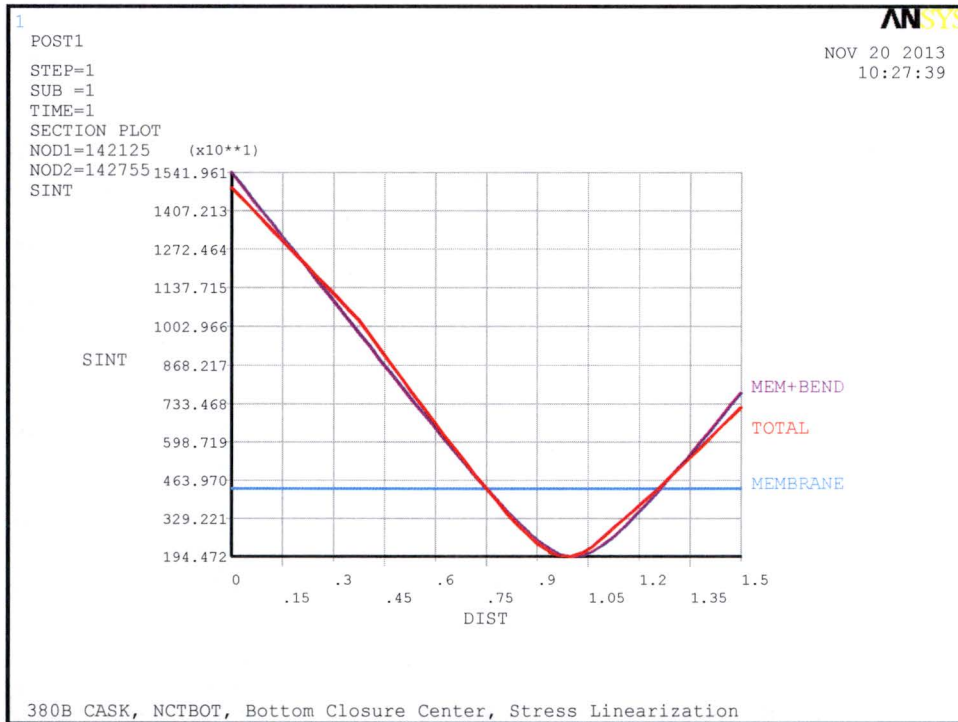
Figure 2.12.4-11 – NCT Bottom-Down Bottom Outer Plate Center
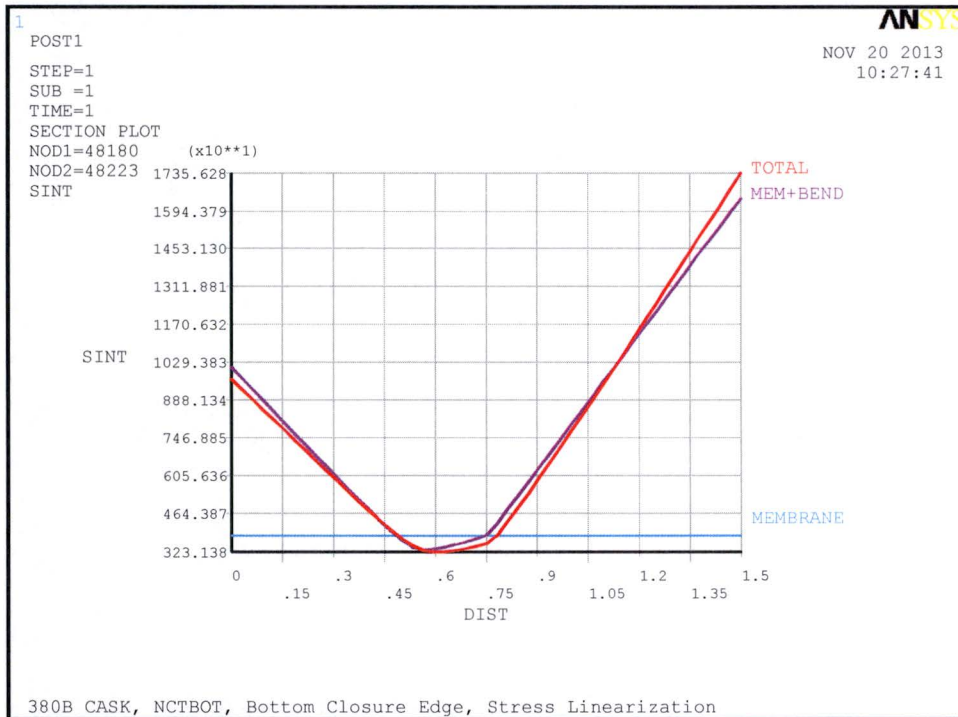
Figure 2.12.4-12 – NCT Bottom-Down Bottom Outer Plate Edge
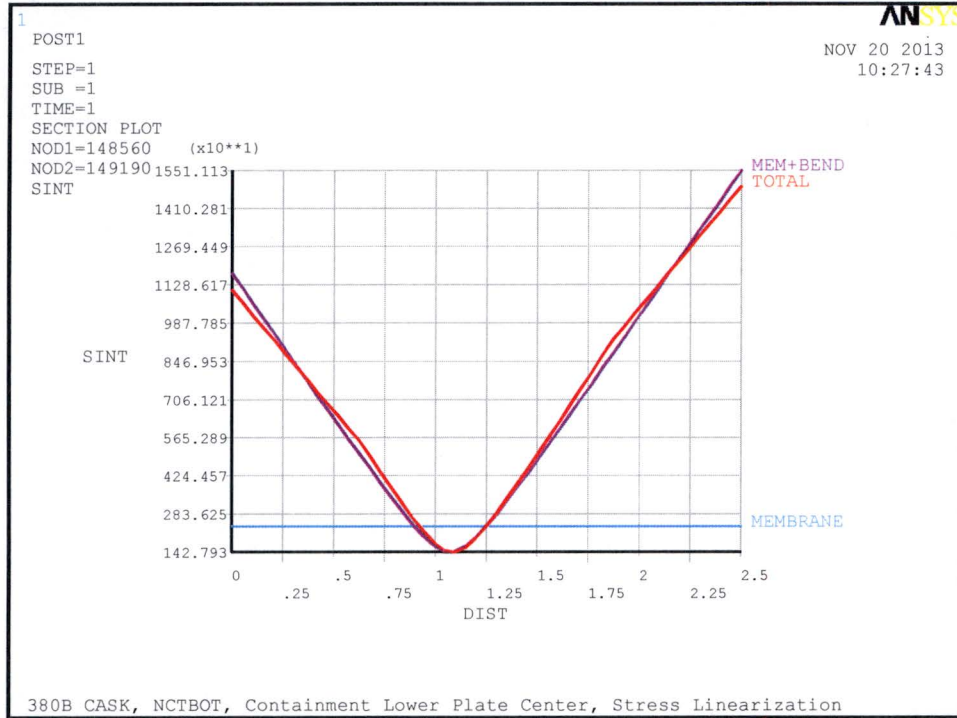
Figure 2.12.4-13 – NCT Bottom-Down Cavity Bottom Plate Center
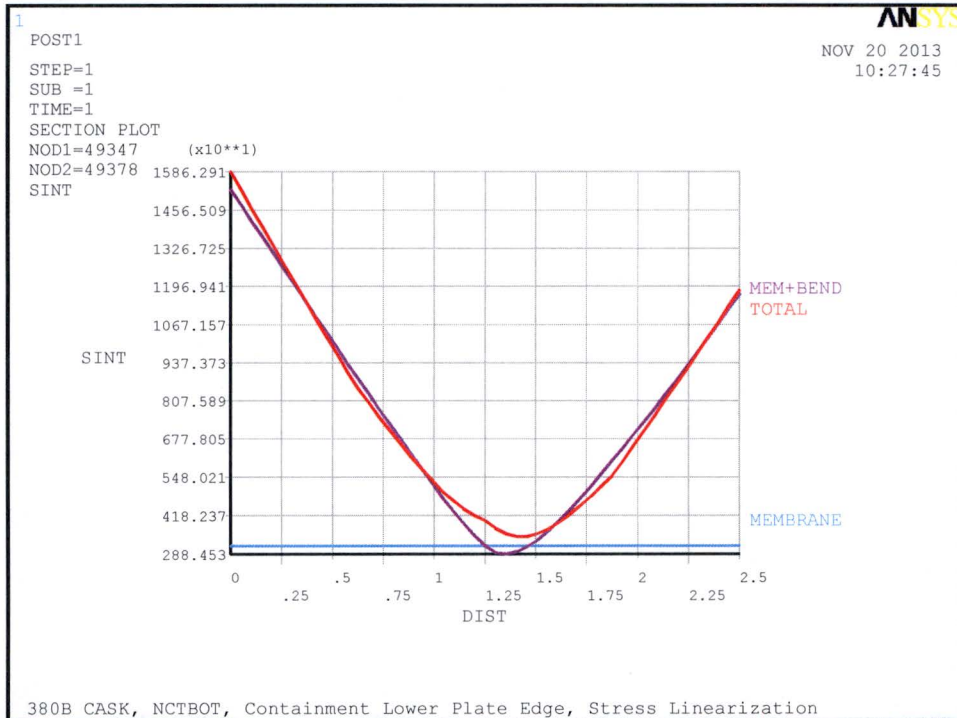
Figure 2.12.4-14 – NCT Bottom-Down Cavity Bottom Plate Edge
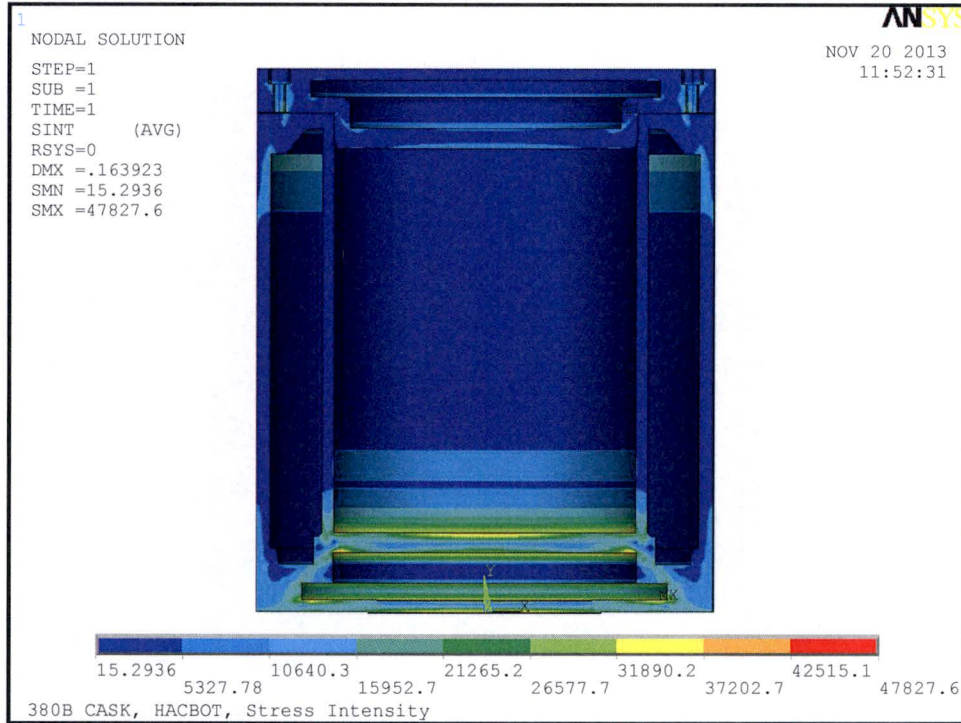
Figure 2.12.4-15 – HAC Bottom-Down End Drop
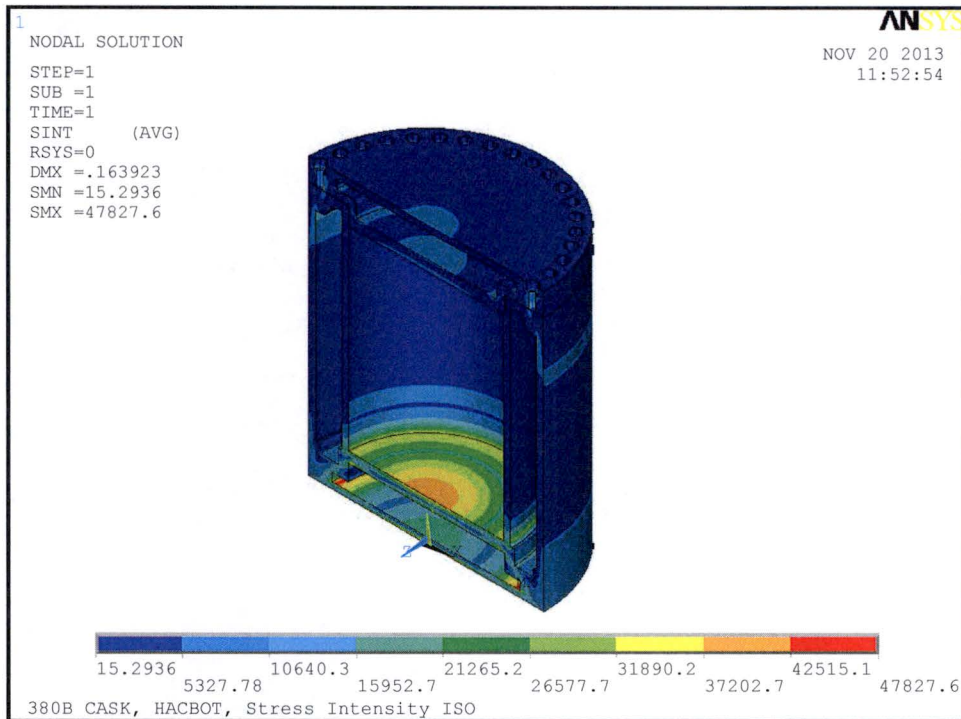
Figure 2.12.4-16 – HAC Bottom-Down End Drop Isometric
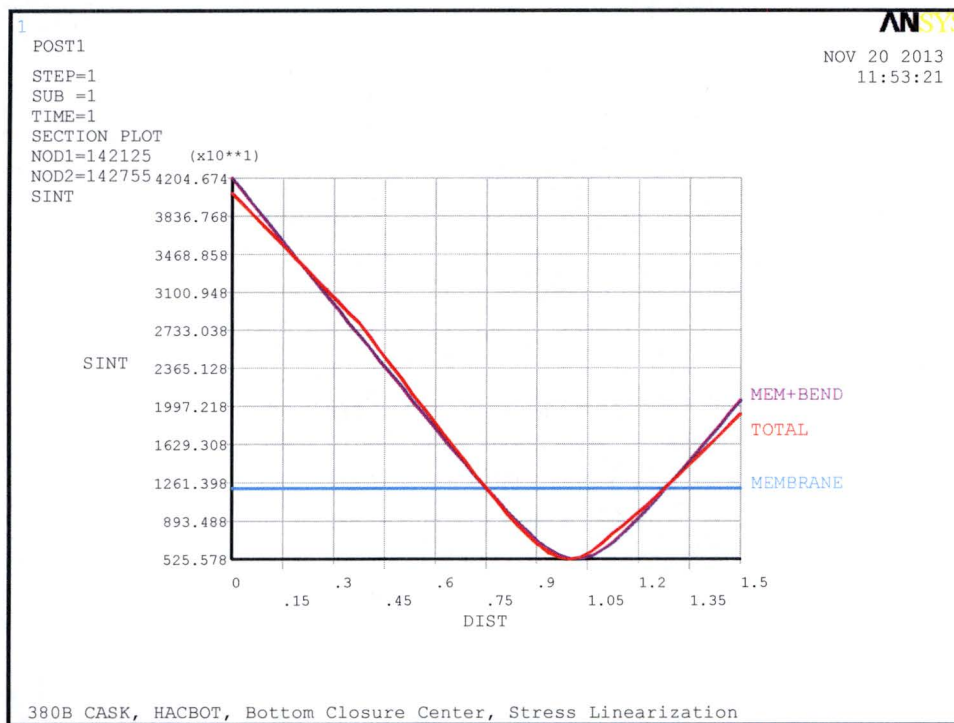
Figure 2.12.4-17 – HAC Bottom-Down Bottom Outer Plate Center
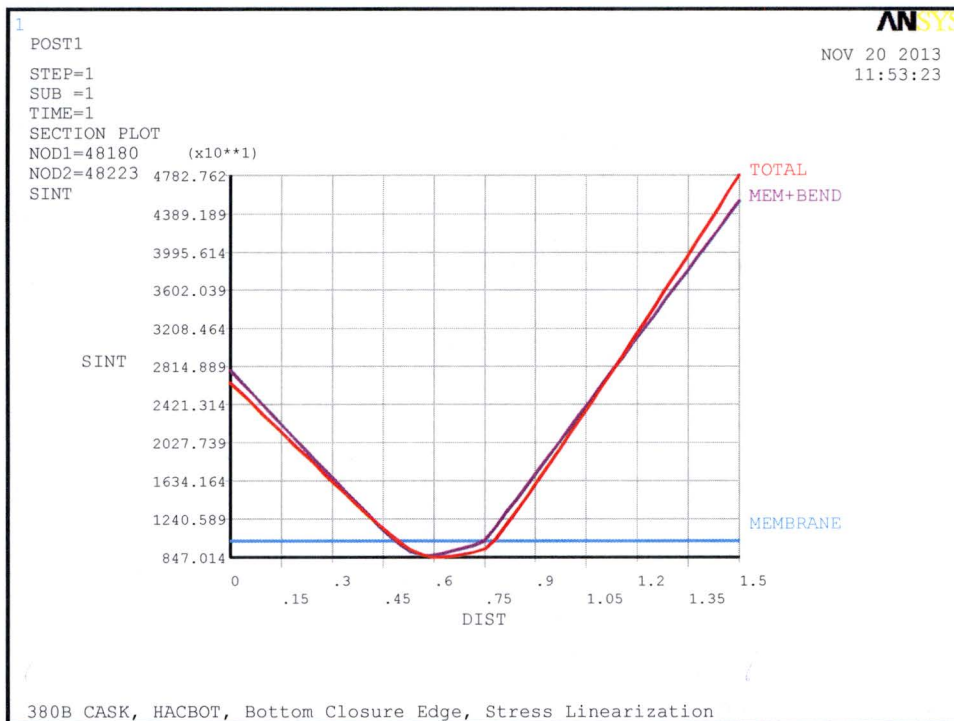
Figure 2.12.4-18 – HAC Bottom-Down Bottom Outer Plate Edge
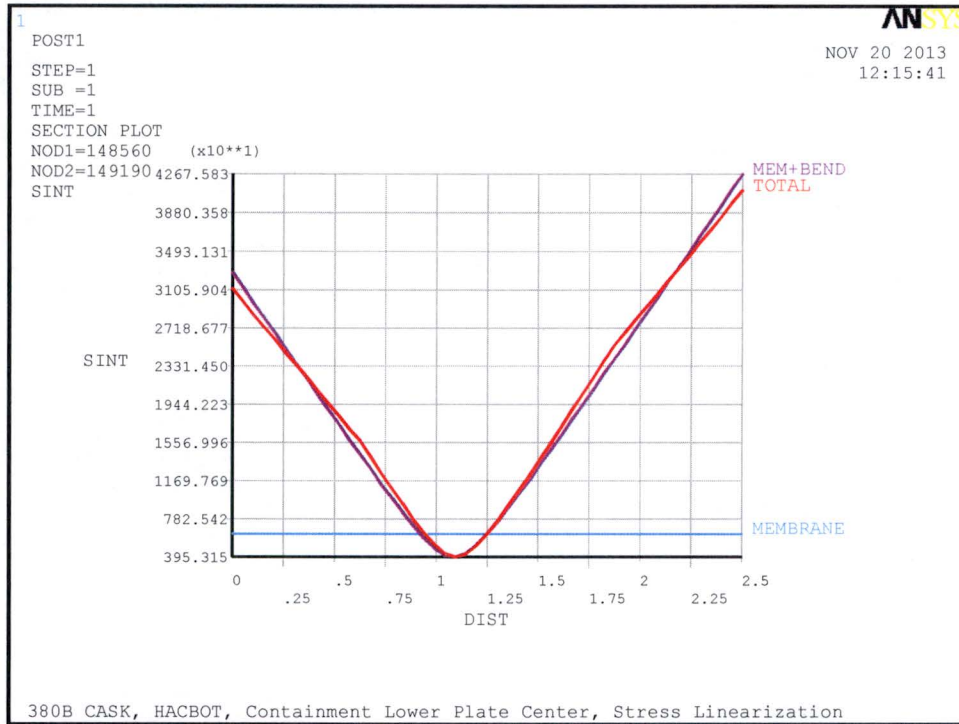
Figure 2.12.4-19 – HAC Bottom-Down Cavity Bottom Plate Center
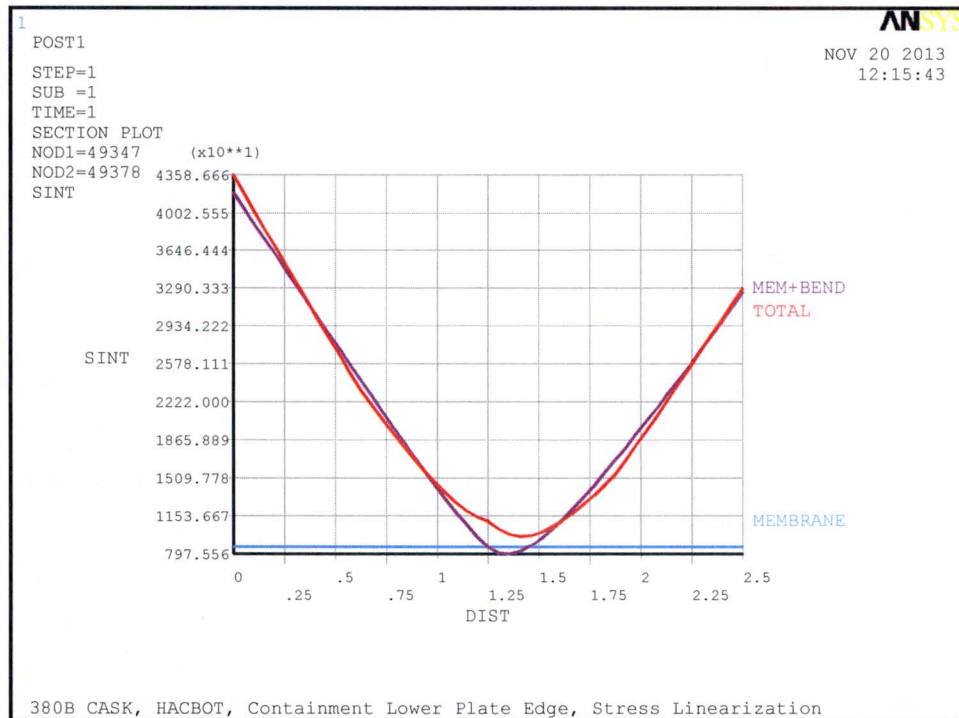
Figure 2.12.4-20 – HAC Bottom-Down Cavity Bottom Plate Edge
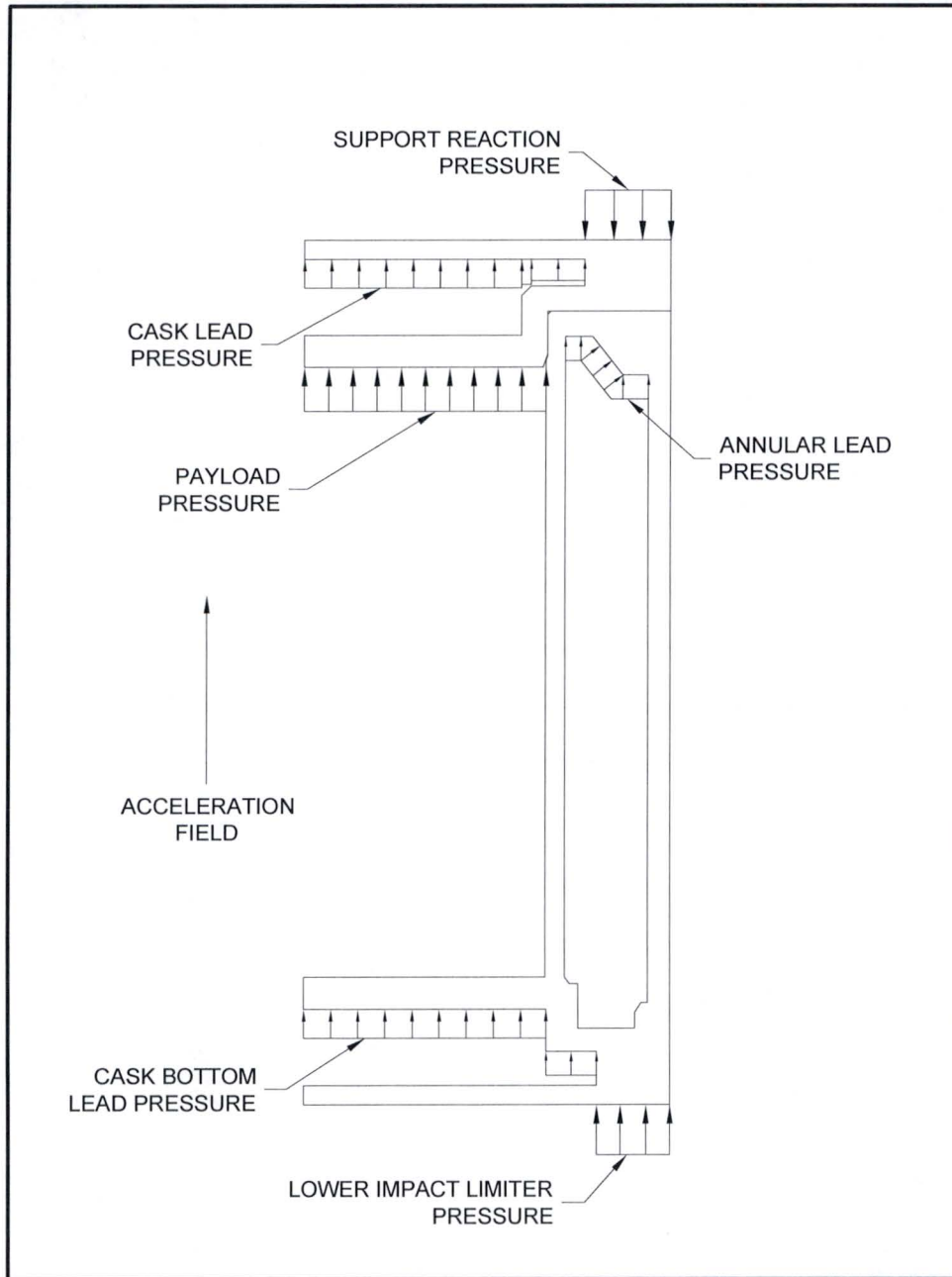
Figure 2.12.4-21 – Top-Down End Drop Loading
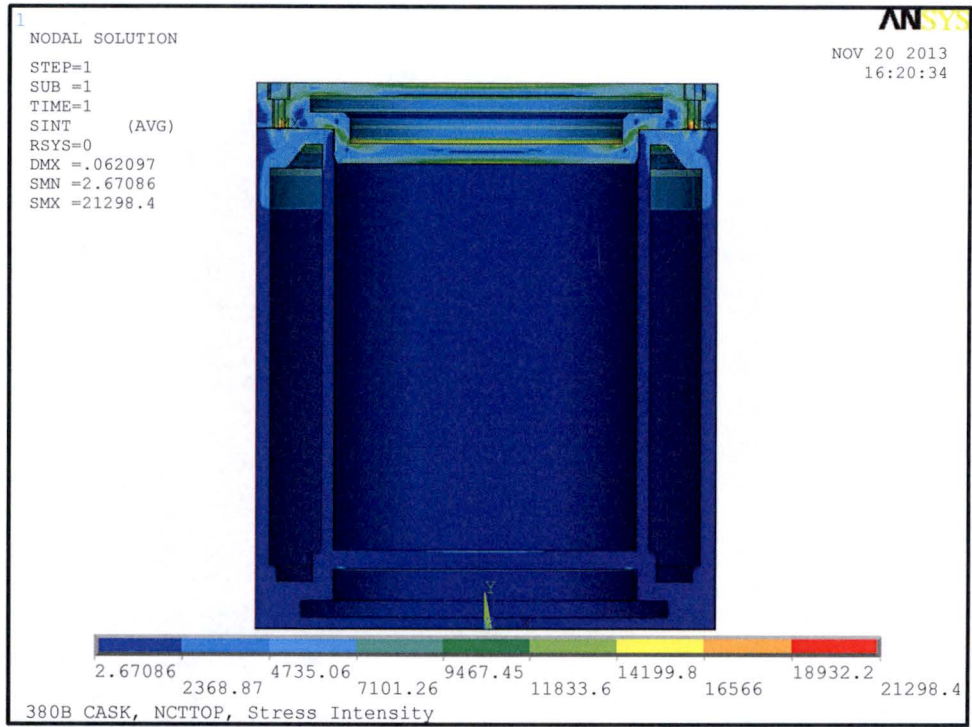
Figure 2.12.4-22 – NCT Top-Down End Drop
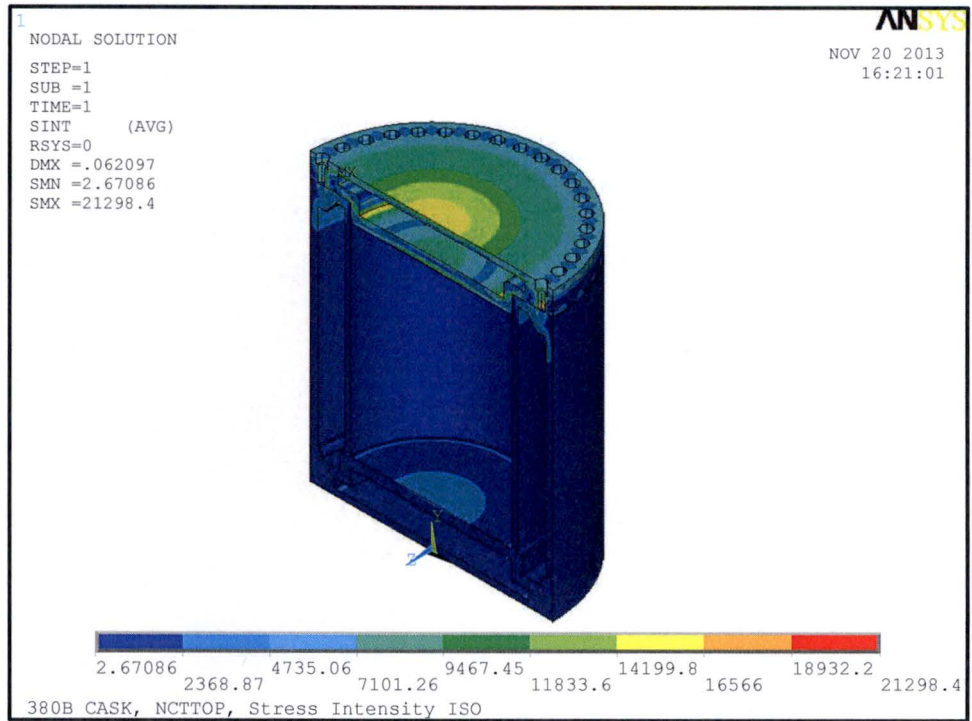
Figure 2.12.4-23 – NCT Top-Down End Drop Isometric
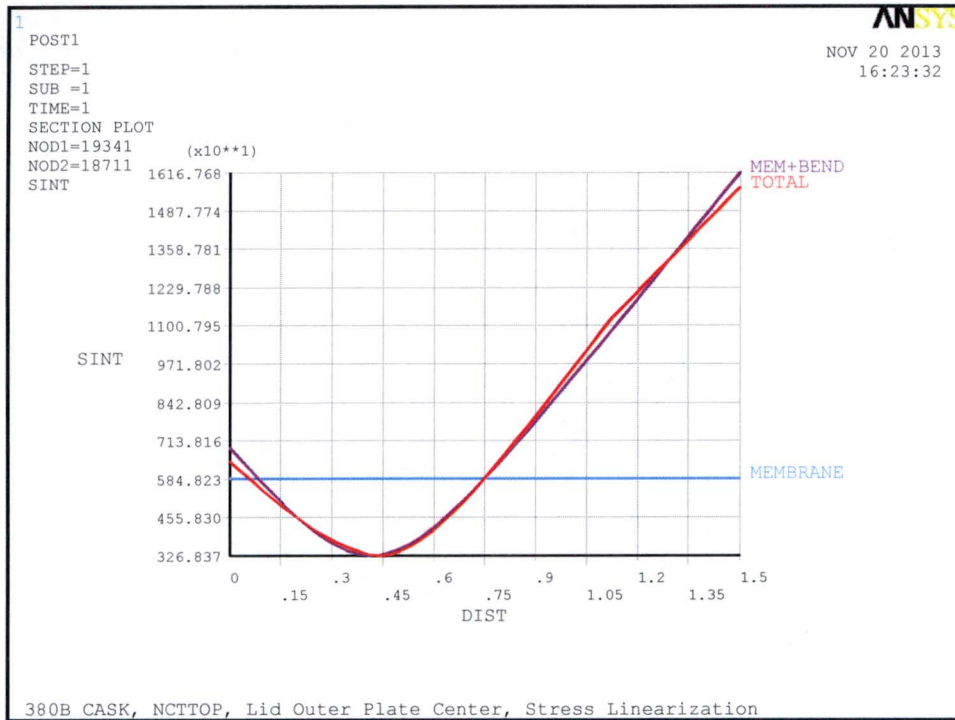
Figure 2.12.4-24 – NCT Top-Down Lid Outer Plate Center
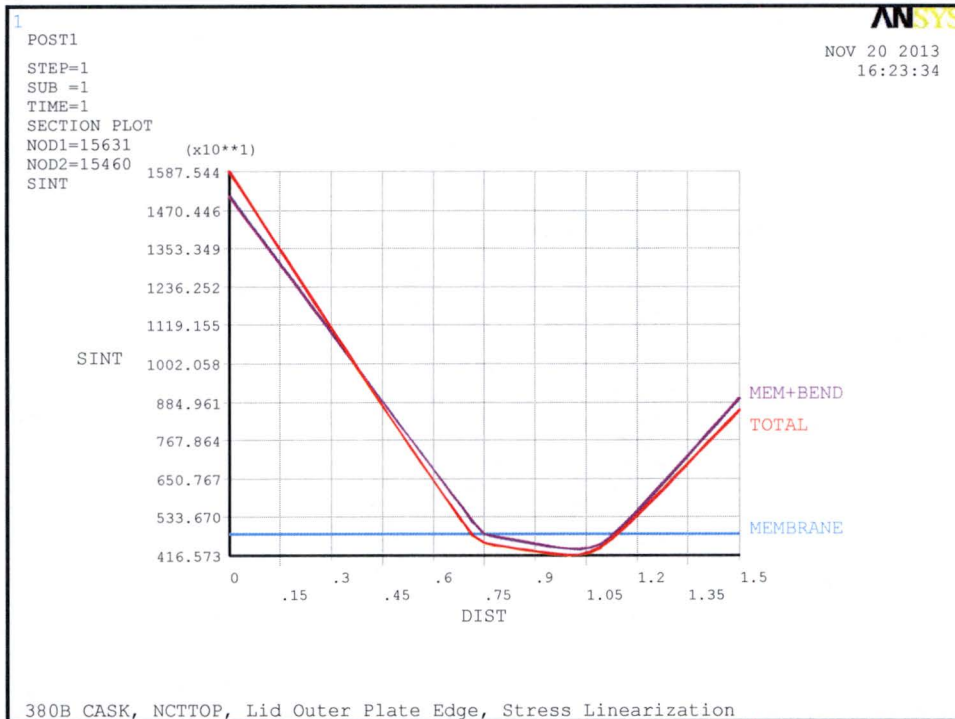
Figure 2.12.4-25 – NCT Top-Down Lid Outer Plate Edge
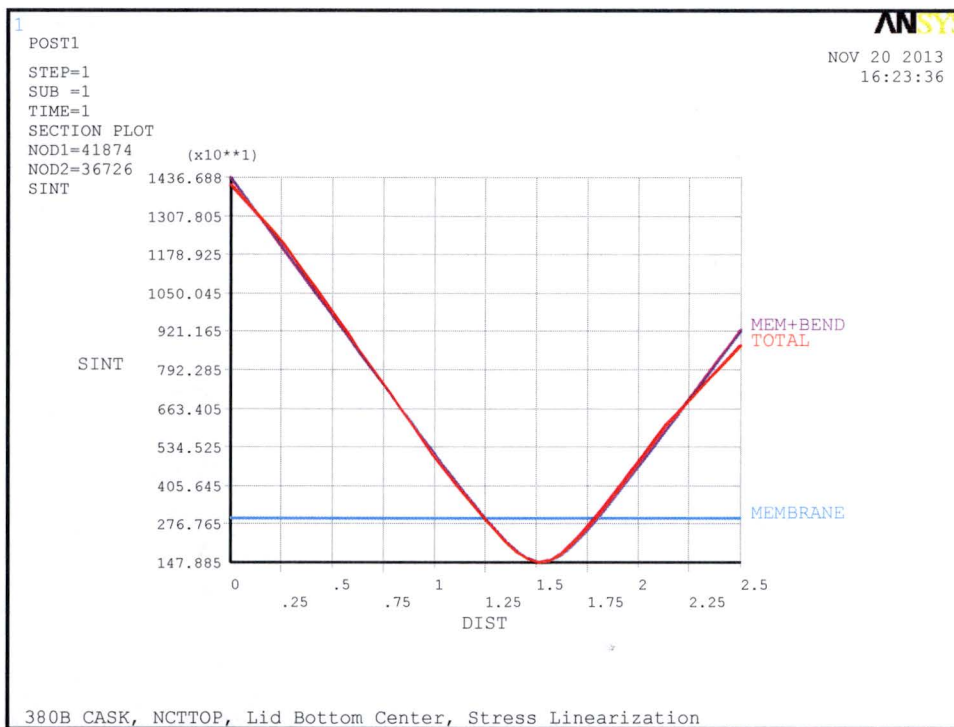
Figure 2.12.4-26 – NCT Top-Down Lid Inner Plate Center
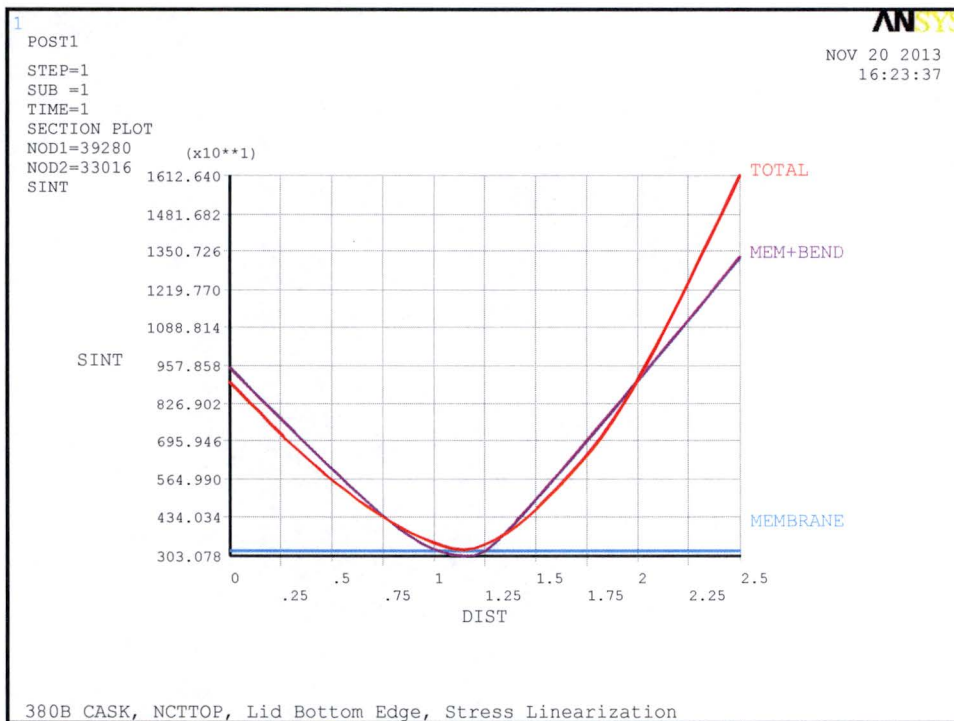
Figure 2.12.4-27 – NCT Top-Down Lid Inner Plate Edge
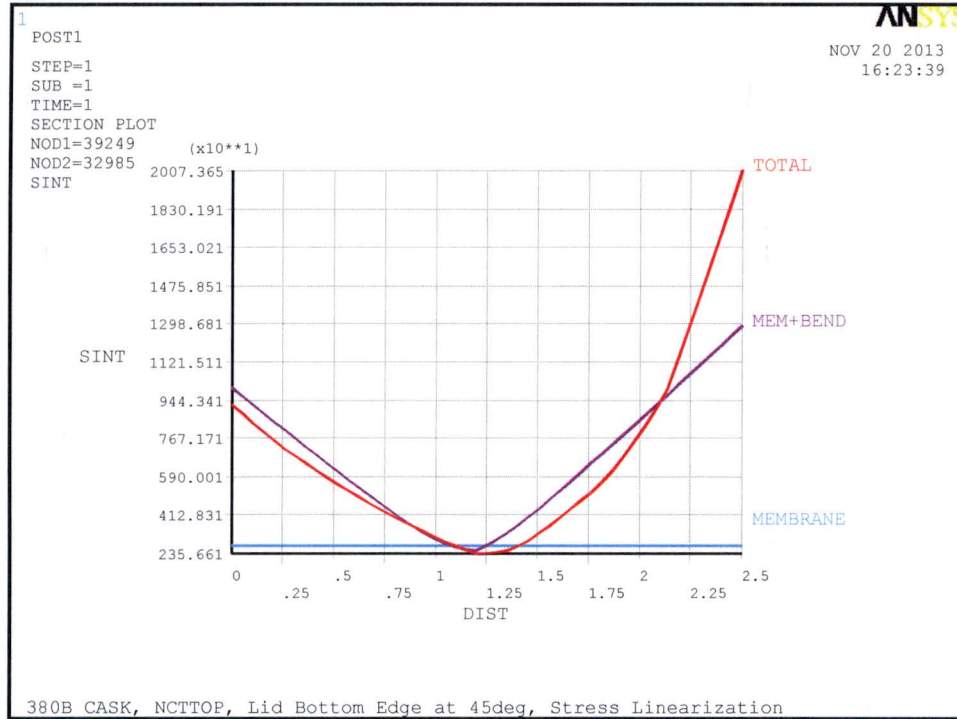
Figure 2.12.4-28 – NCT Top-Down Lid Inner Plate Edge at 45 Deg
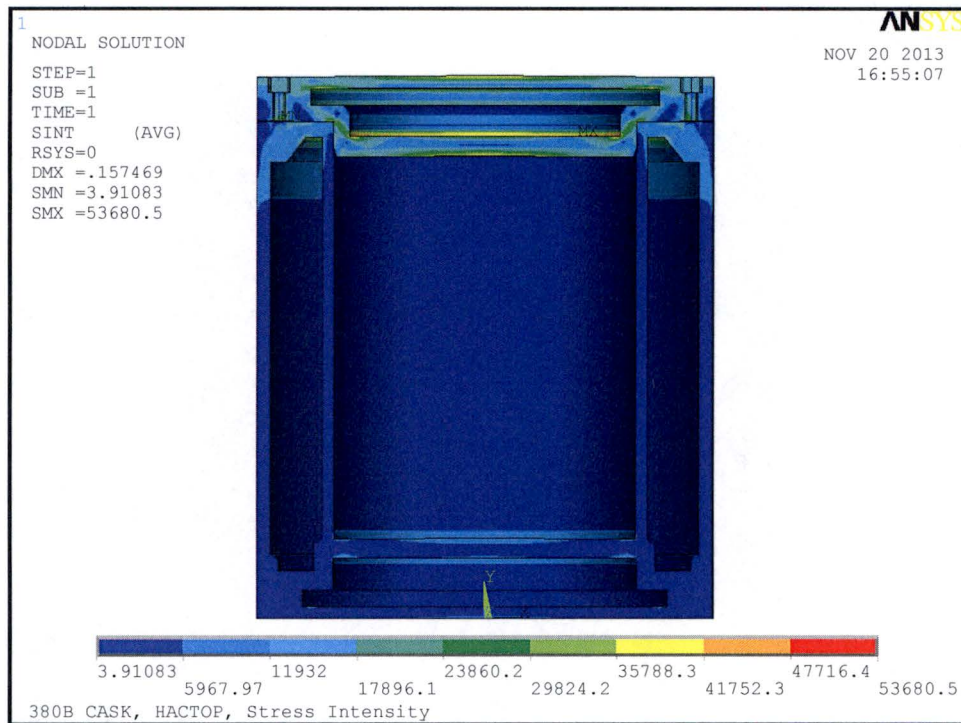
Figure 2.12.4-29 – HAC Top-Down End Drop
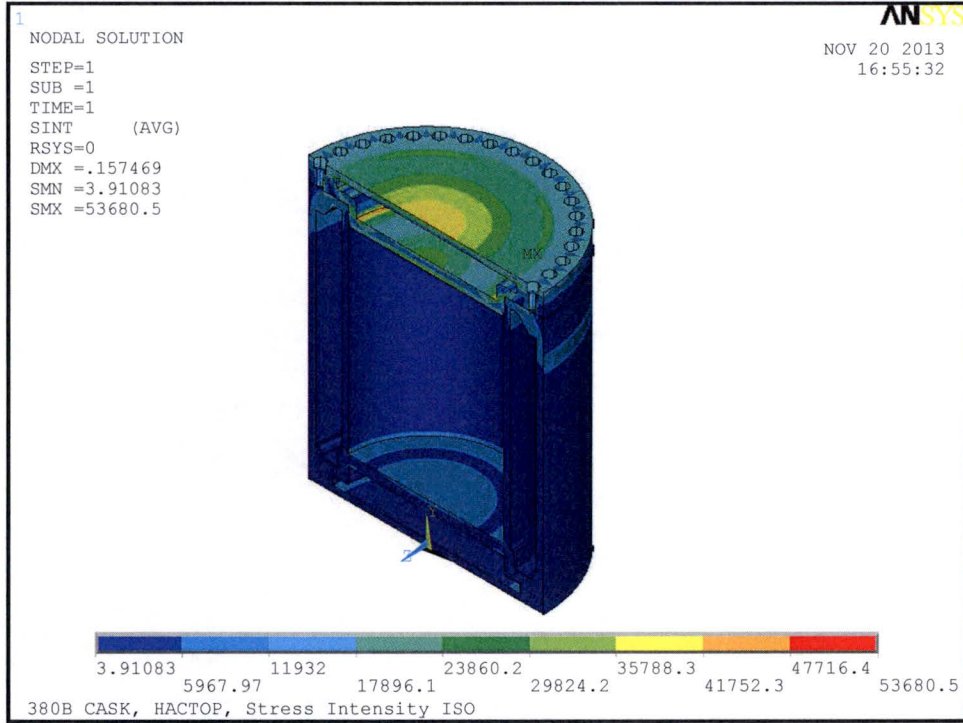
Figure 2.12.4-30 – HAC Top-Down End Drop Isometric
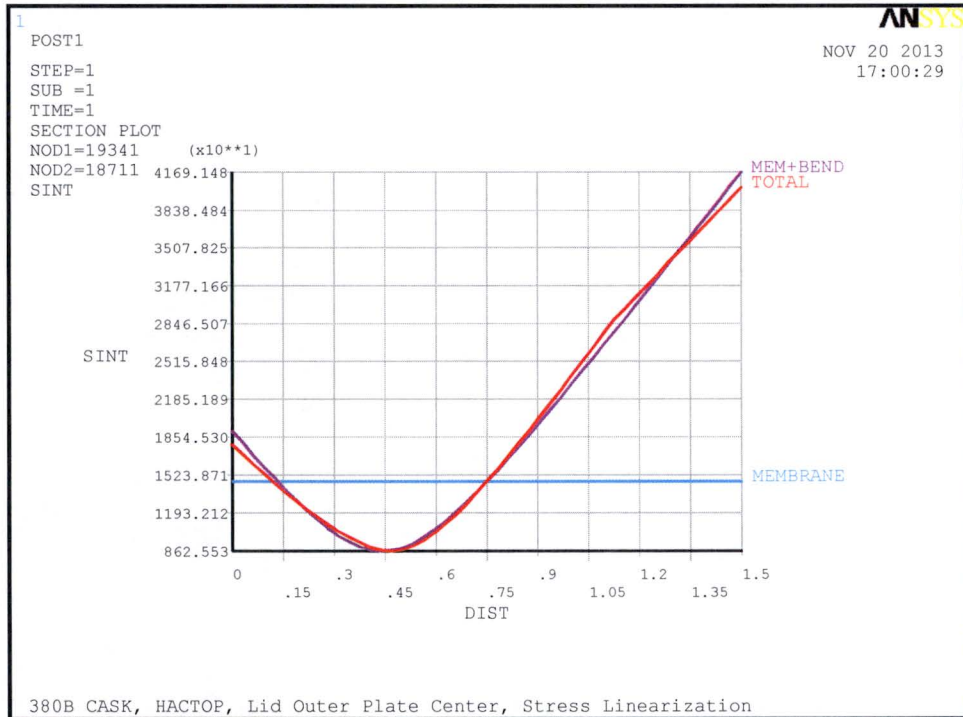
Figure 2.12.4-31 – HAC Top-Down Lid Outer Plate Center

Figure 2.12.4-32 – HAC Top-Down Lid Outer Plate Center
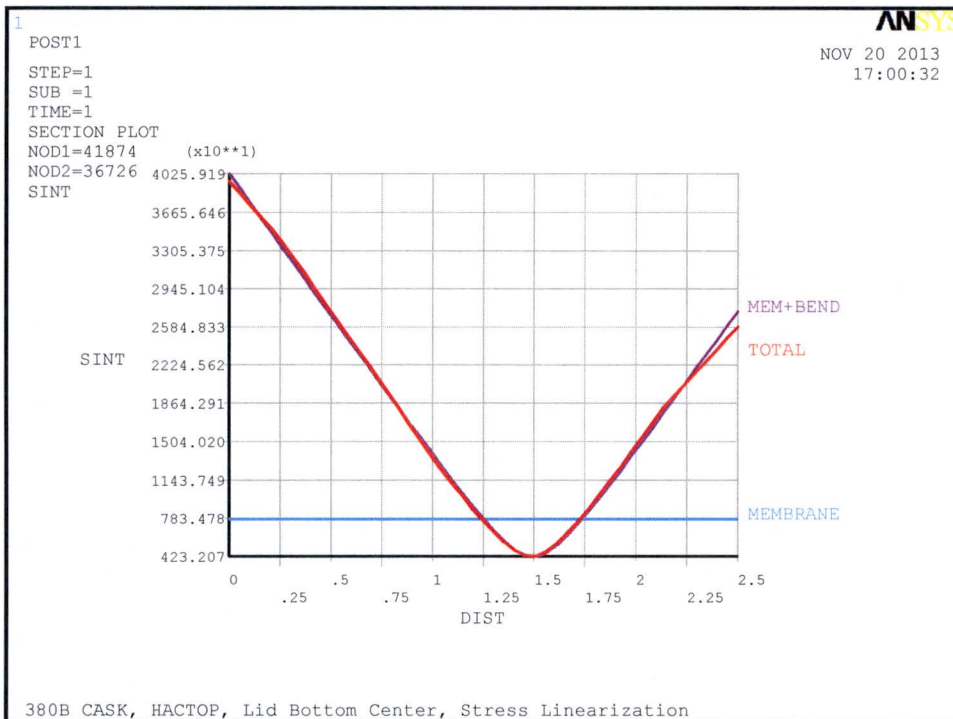
Figure 2.12.4-33 – HAC Top-Down Lid Bottom Center
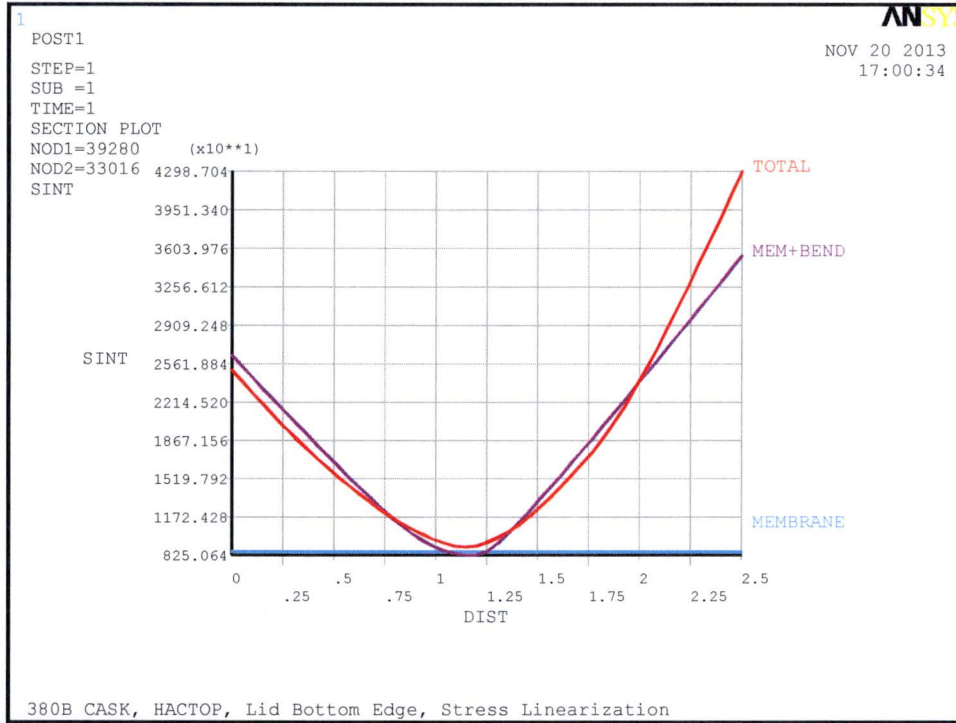
Figure 2.12.4-34 – HAC Top-Down Lid Bottom Edge
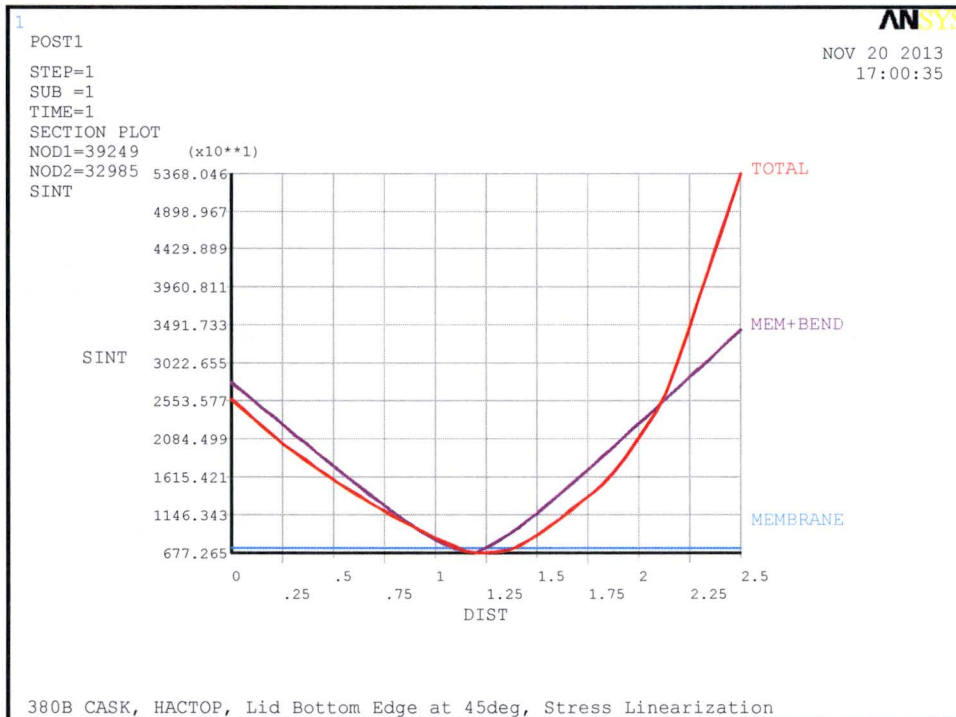
Figure 2.12.4-35 – HAC Top-Down Lid Bottom Edge at 45 Deg.
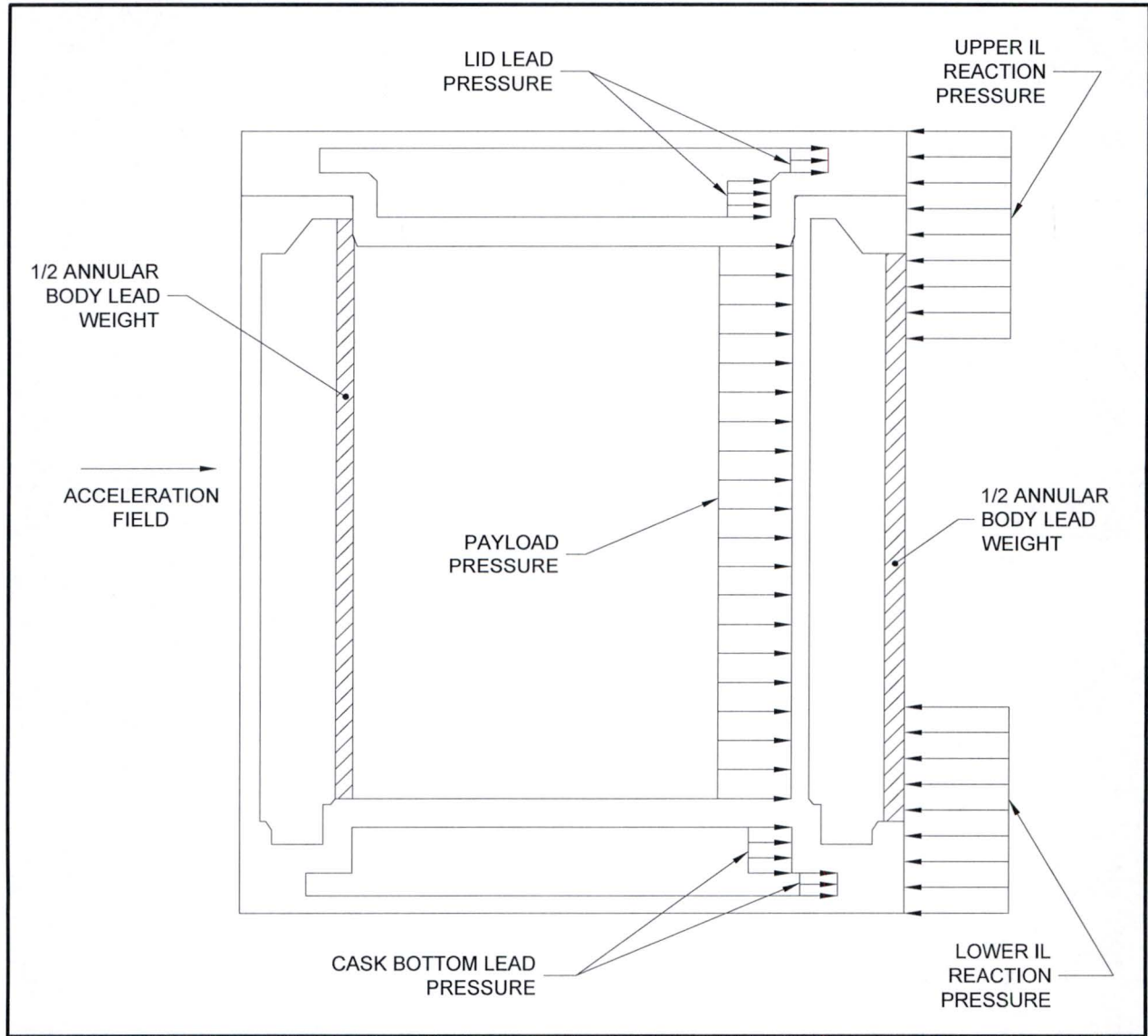
Figure 2.12.4-36 – Side Drop Loading
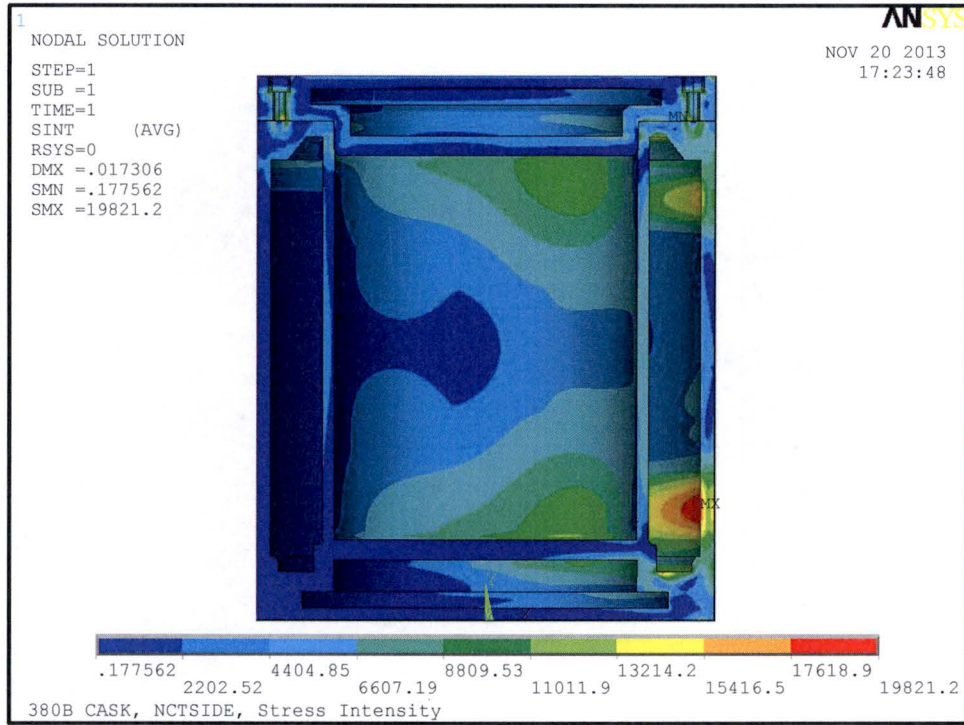
Figure 2.12.4-37 – NCT Side Drop
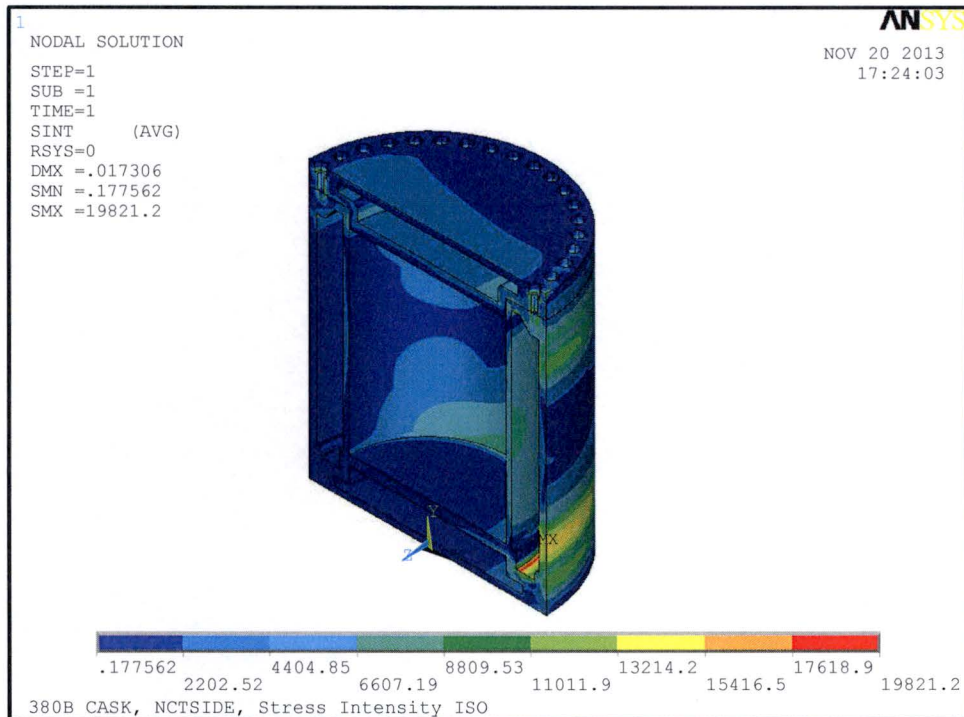
Figure 2.12.4-38 – NCT Side Drop Isometric
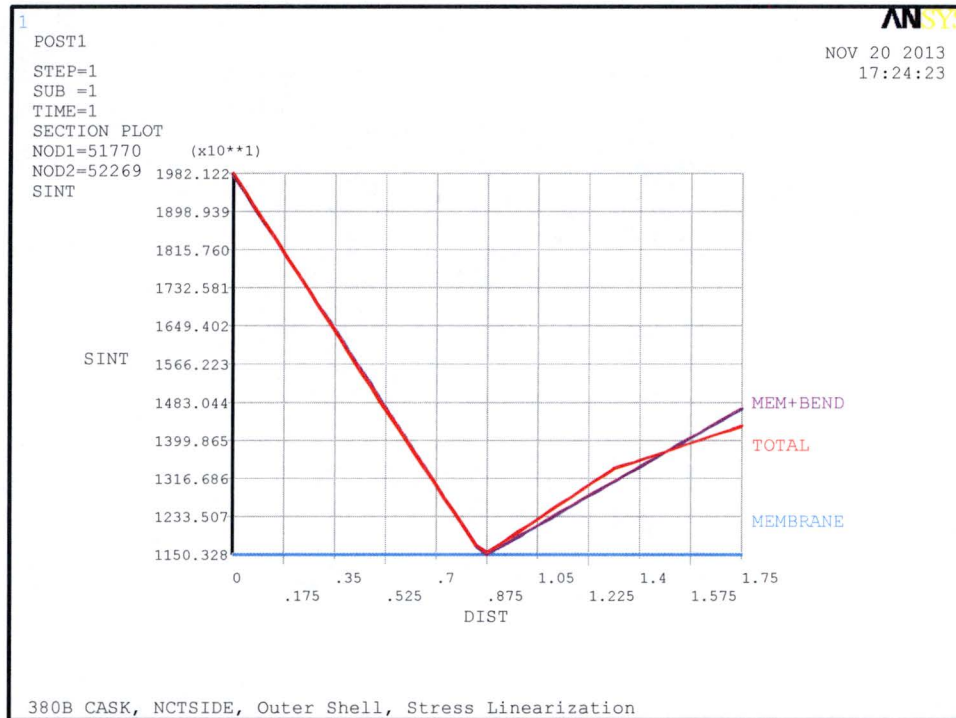
Figure 2.12.4-39 – NCT Side Drop Outer Shell
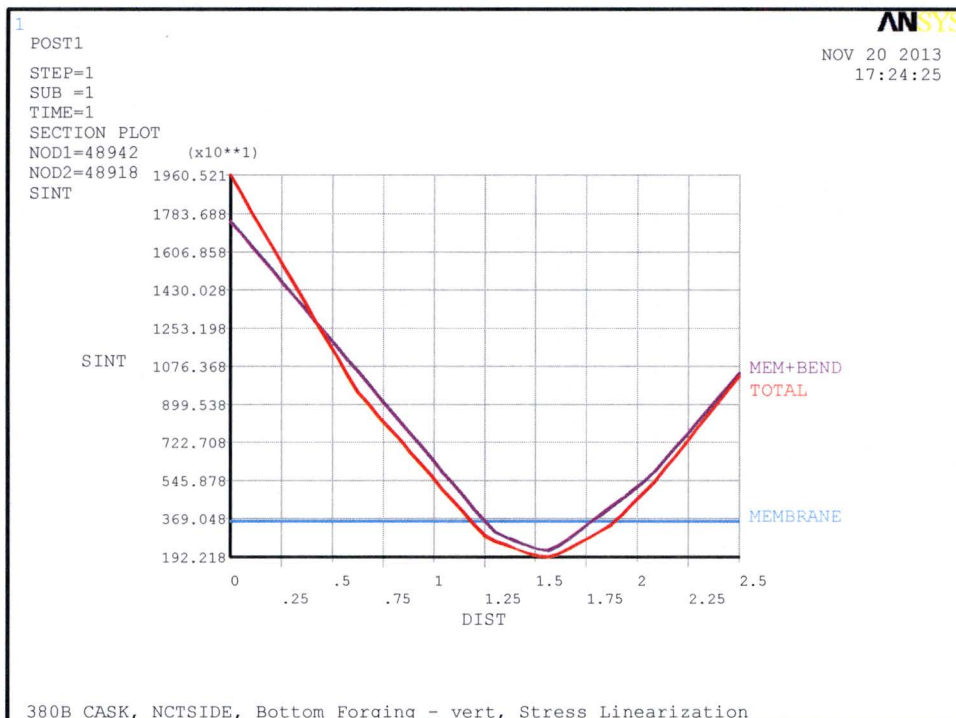
Figure 2.12.4-40 – NCT Side Drop Lower End Structure Step

(Within the figure, the term 'Bottom Forging' refers to the Lower End Structure.)
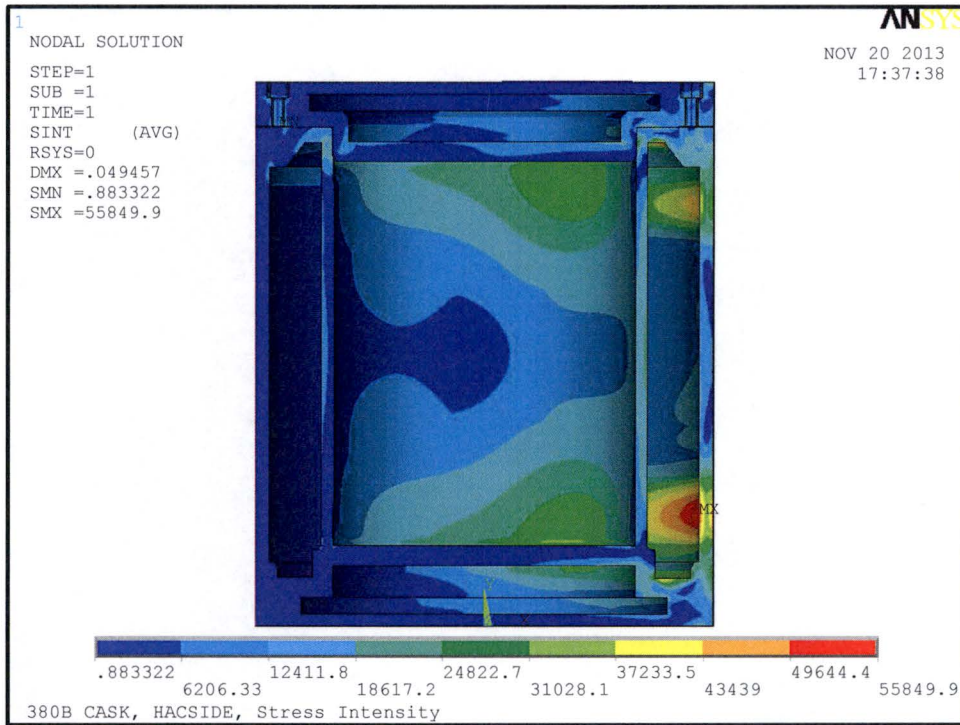
Figure 2.12.4-41 – HAC Side Drop
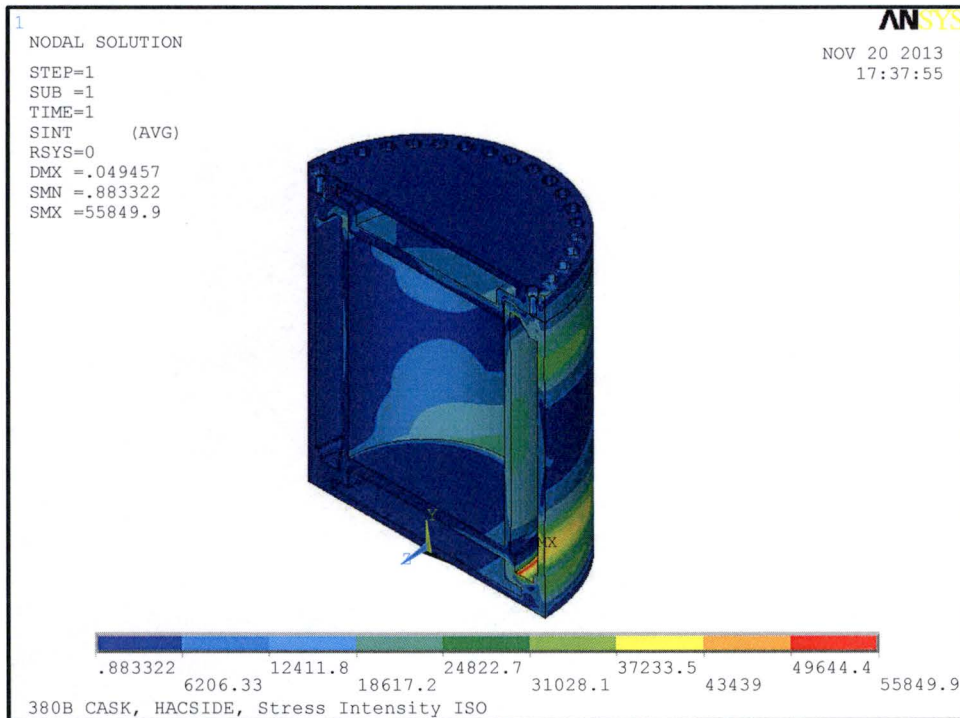
Figure 2.12.4-42 – HAC Side Drop Isometric
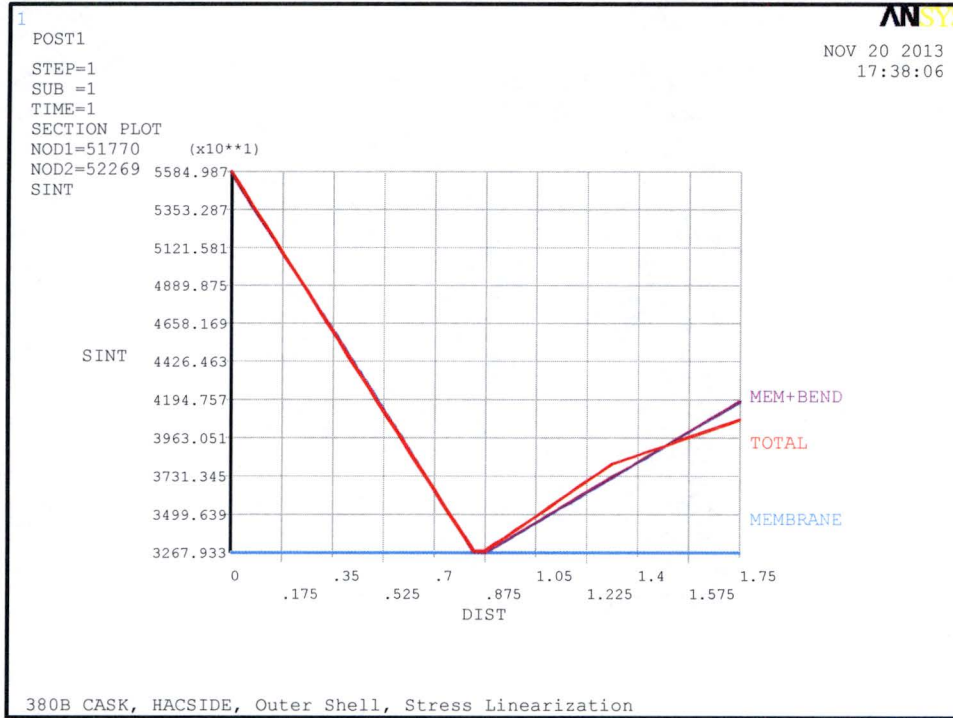
Figure 2.12.4-43 – HAC Side Drop Outer Shell
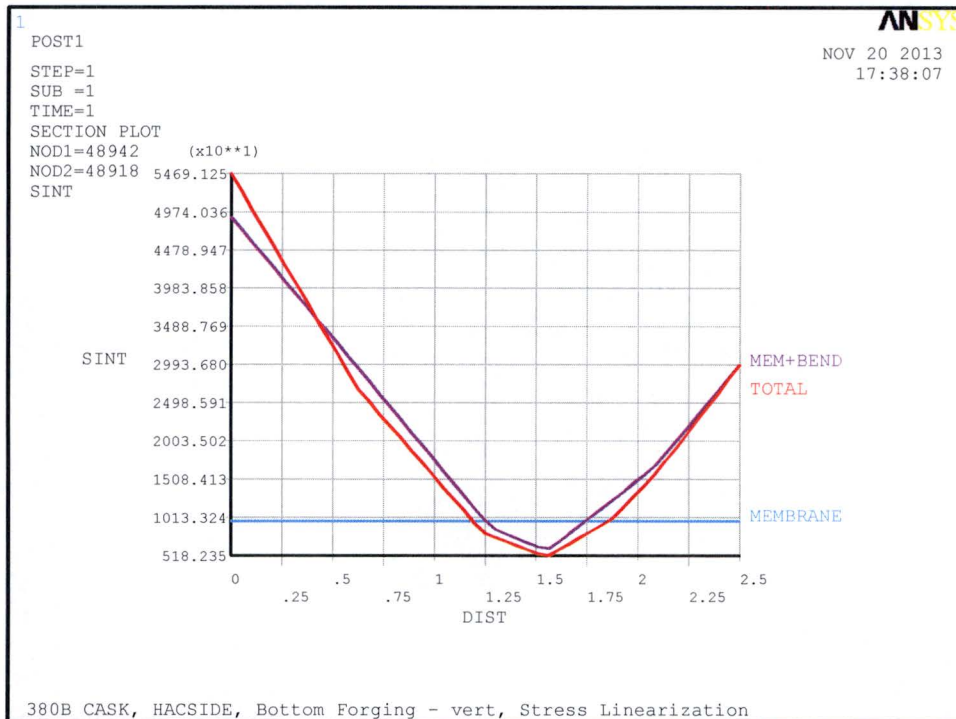
Figure 2.12.4-44 – HAC Side Drop Lower End Structure Step

(Within the figure, the term 'Bottom Forging' refers to the Lower End Structure.)
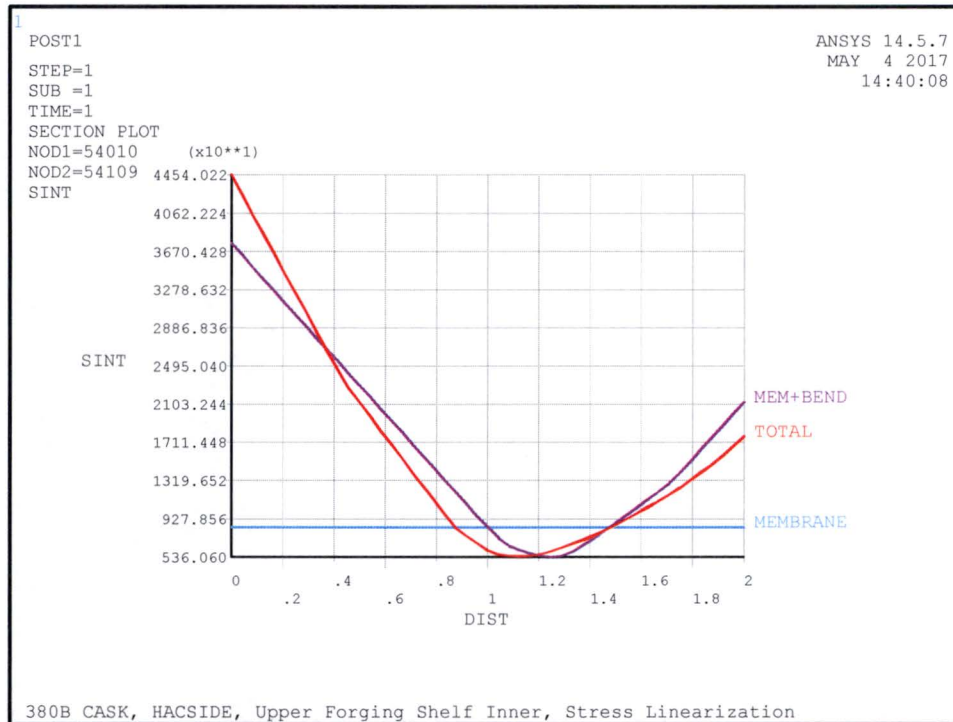
Figure 2.12.4-44a – HAC Side Drop Upper End Structure Shelf, Inner Location

(Within the figure, the term 'Upper Forging' refers to the Upper End Structure.)
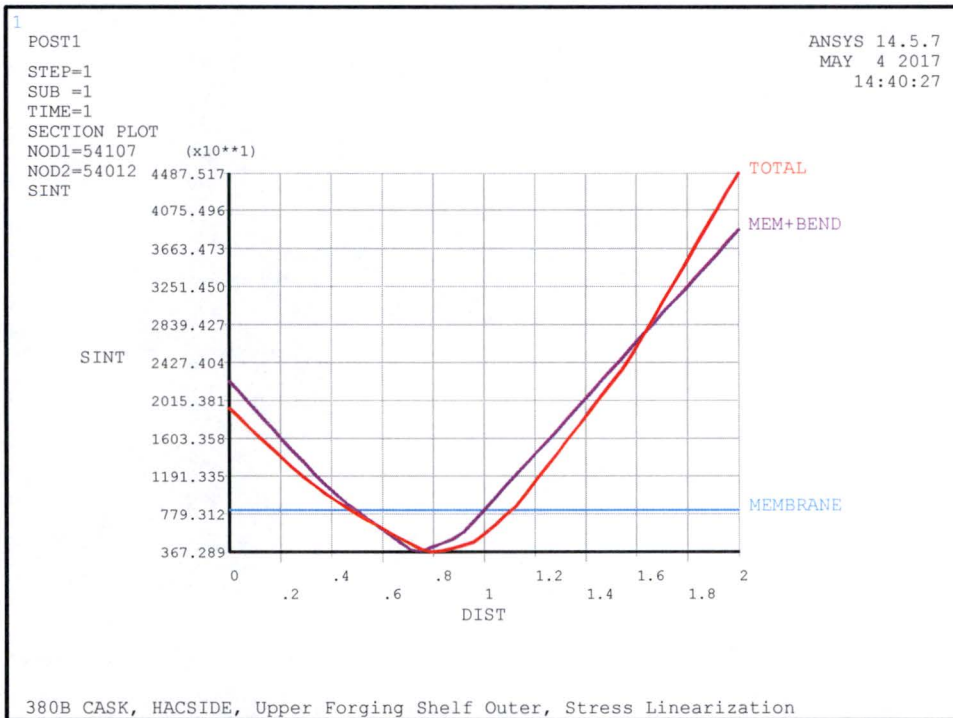
Figure 2.12.4-44b – HAC Side Drop Upper End Structure Shelf, Outer Location

(Within the figure, the term 'Upper Forging' refers to the Upper End Structure.)
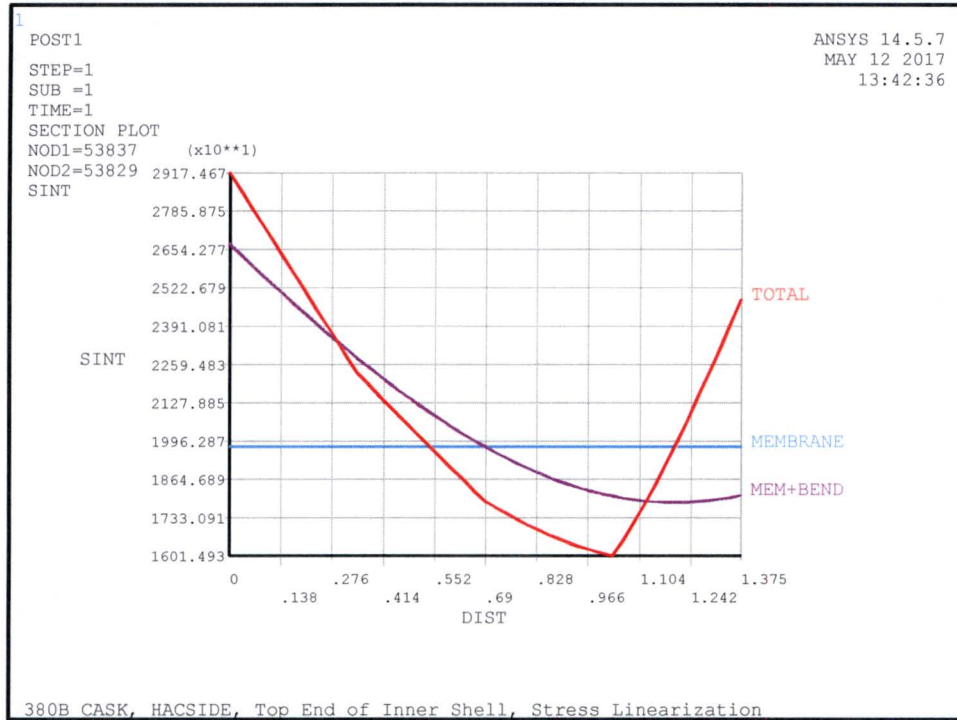
Figure 2.12.4-44c – HAC Side Drop, Top End of Inner Shell
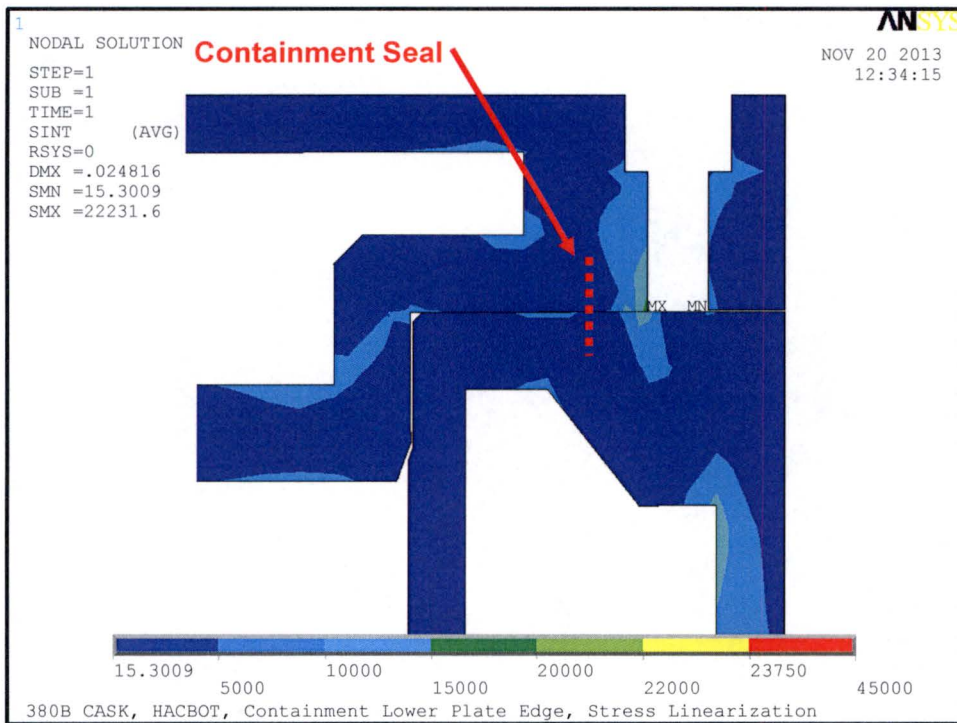
Figure 2.12.4-45 – HAC Bottom-Down Containment Seal
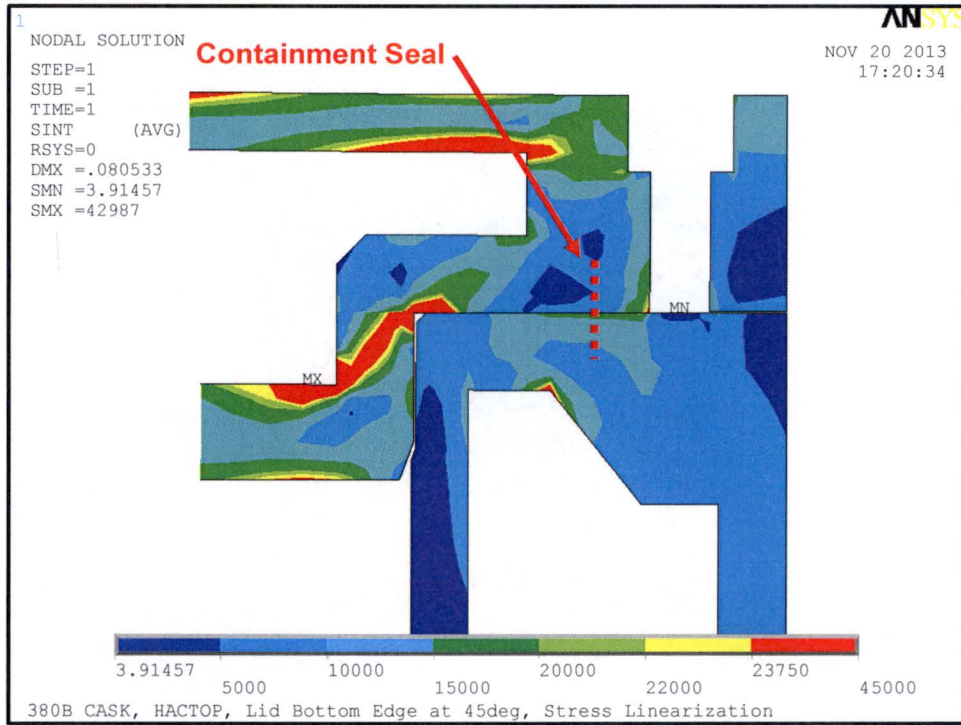
Figure 2.12.4-46 – HAC Top-Down Containment Seal
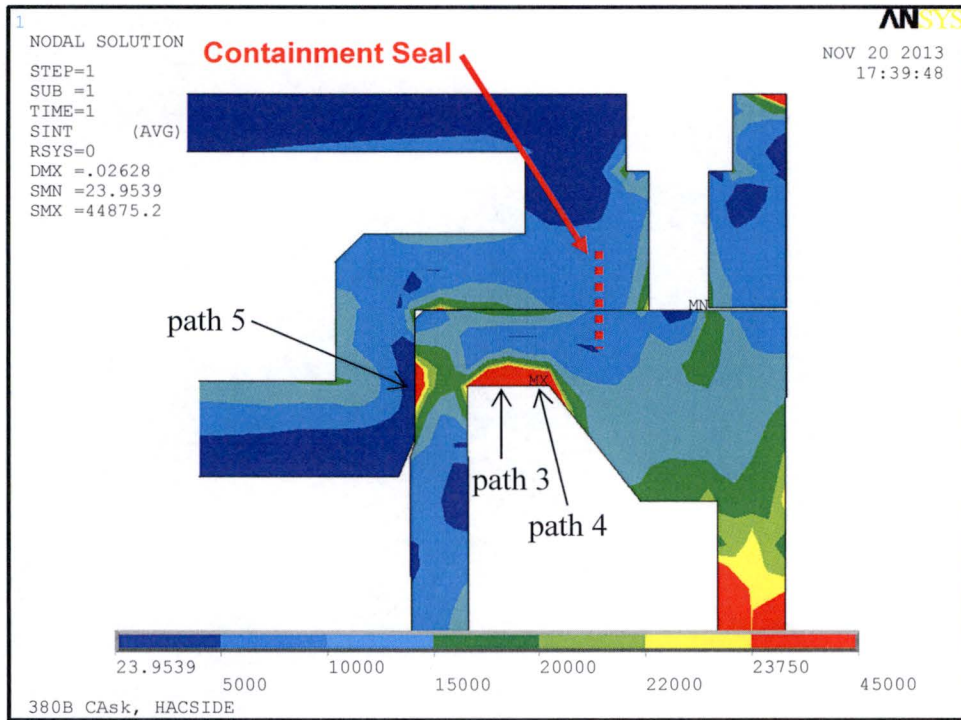
Figure 2.12.4-47 – HAC Side Drop Containment Seal

(Note: path 3 is vertical at the upper end structure shelf inner location, path 4 is vertical at the outer location, and path 5 is horizontal at the top end of the inner shell. See Section 2.12.4.4.8.)
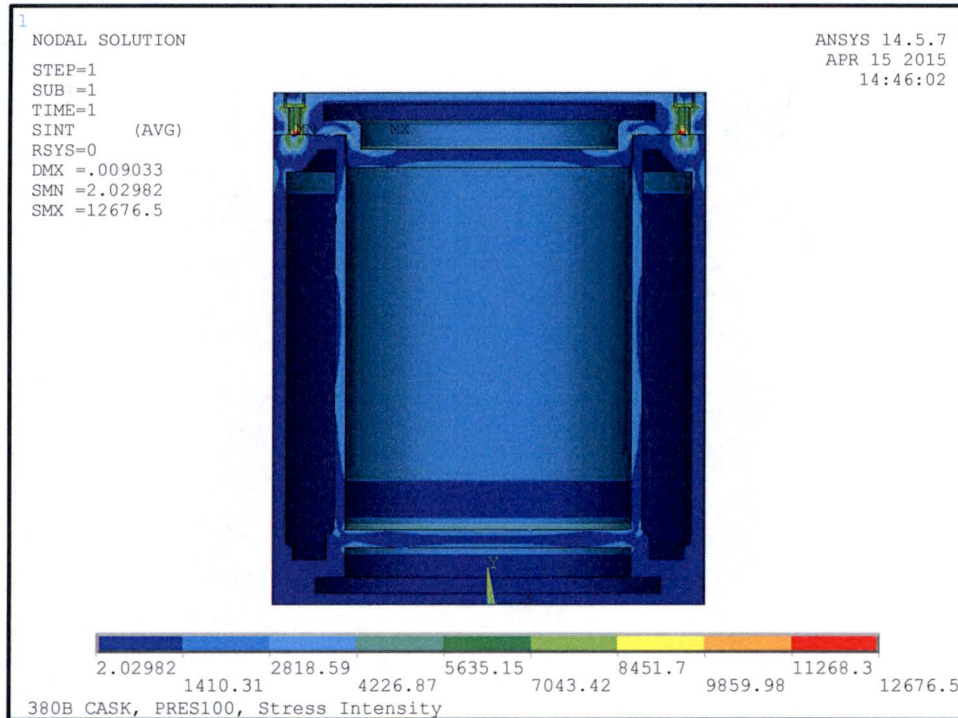
Figure 2.12.4-48 – HAC Fire Event Pressure
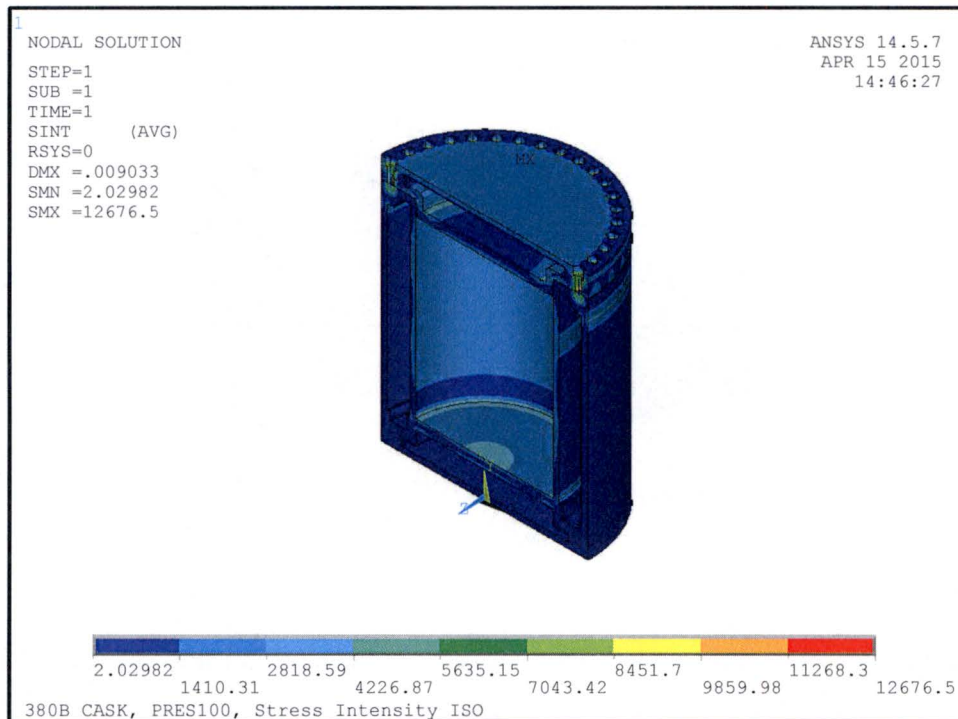
Figure 2.12.4-49 – HAC Fire Event Pressure Isometric
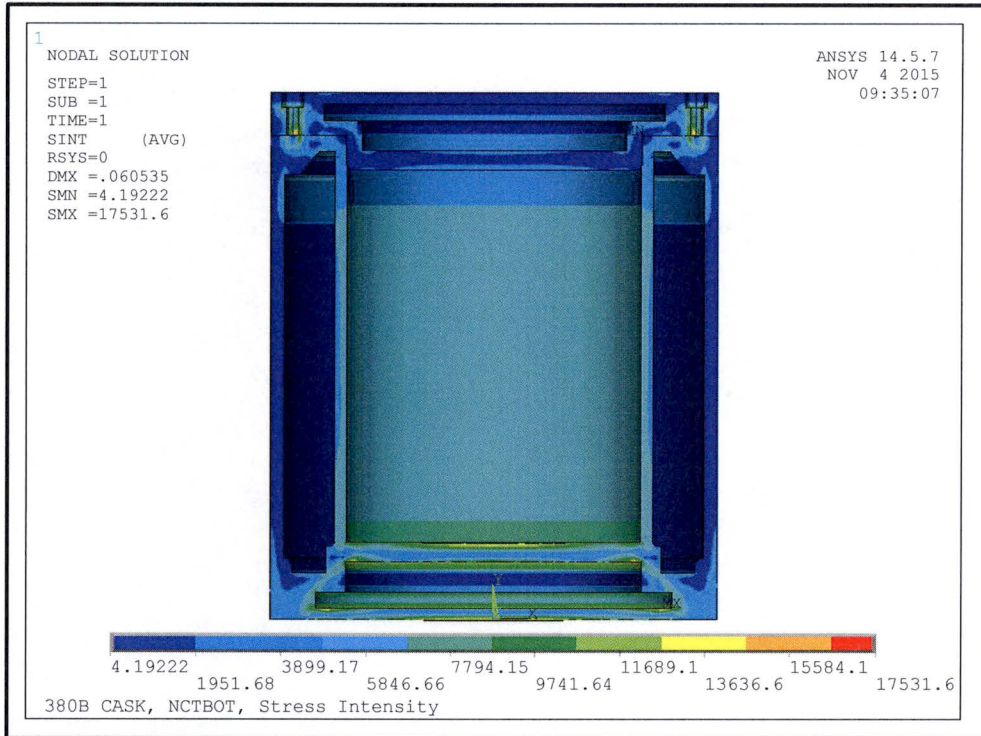
Figure 2.12.4-50 – NCT Bottom-Down End Drop with Cold Lead Shrinkage Pressure
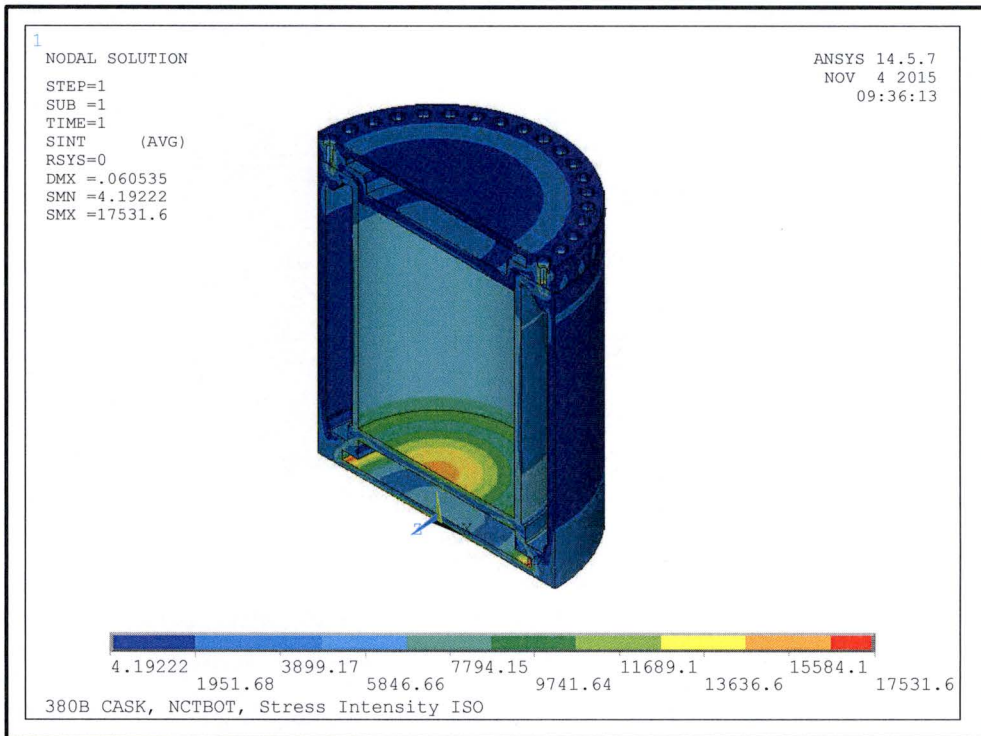
Figure 2.12.4-51 – NCT Bottom-Down End Drop Isometric with Cold Lead Shrinkage Pressure
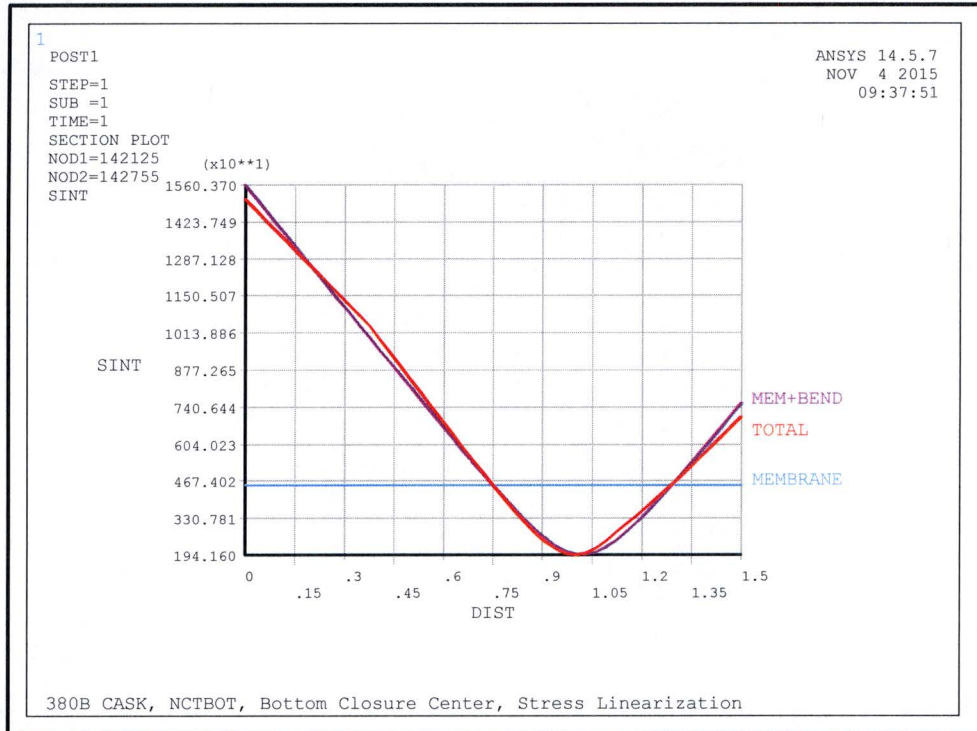
Figure 2.12.4-52 – NCT Bottom-Down Bottom Outer Plate Center with Cold Lead Shrinkage Pressure
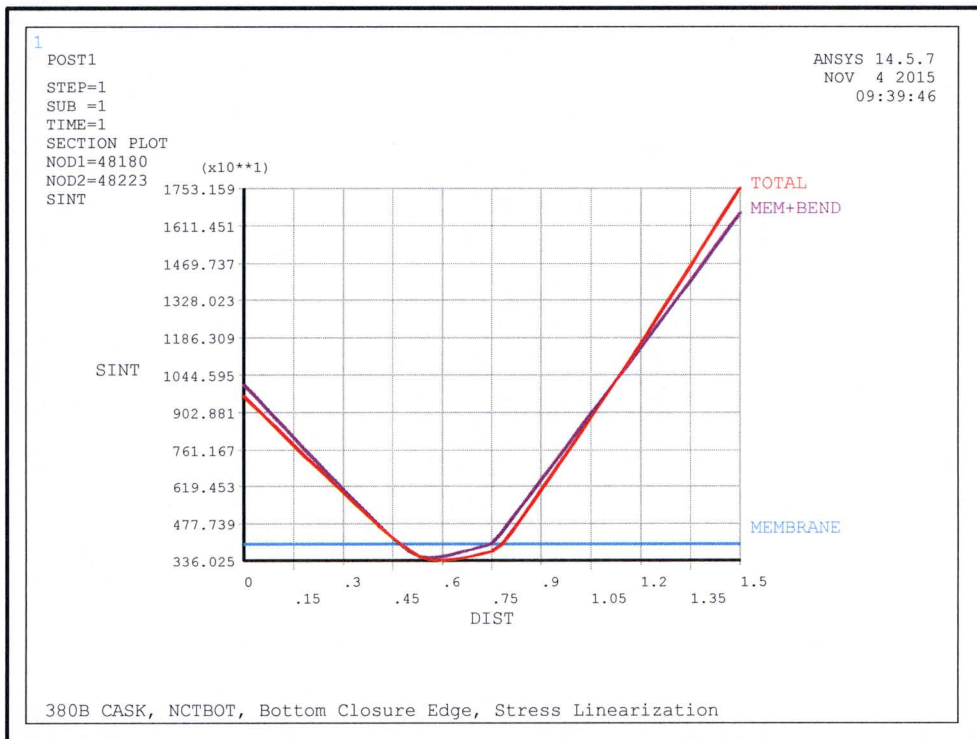
Figure 2.12.4-53 – NCT Bottom-Down Bottom Outer Plate Edge with Cold Lead Shrinkage Pressure
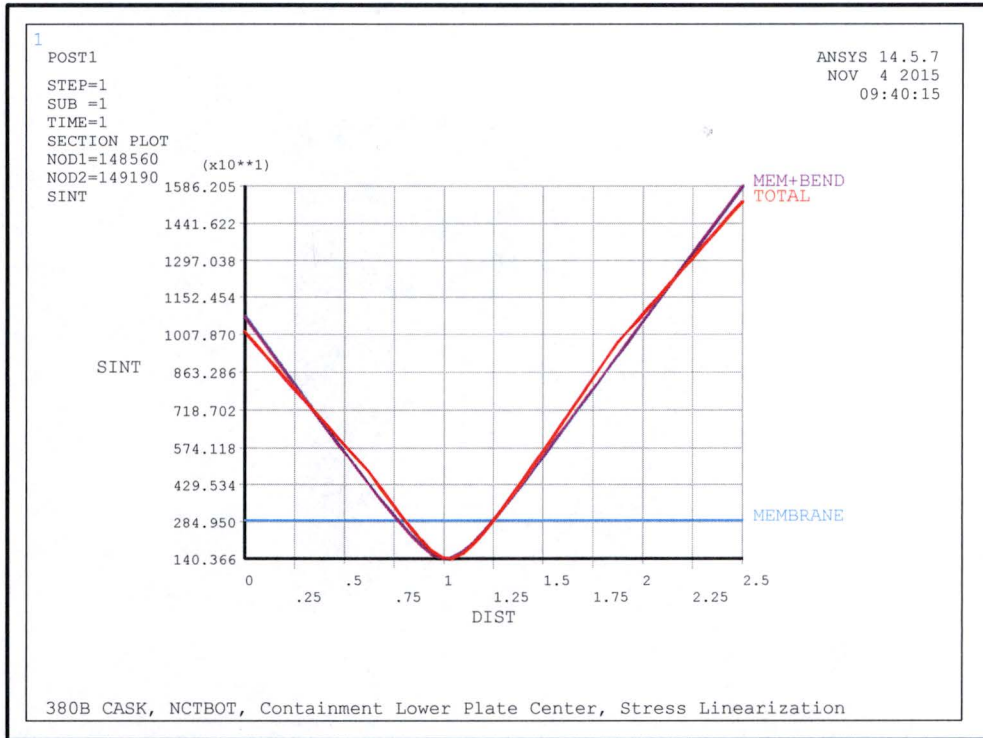
Figure 2.12.4-54 – NCT Bottom-Down Cavity Bottom Plate Center with Cold Lead Shrinkage Pressure
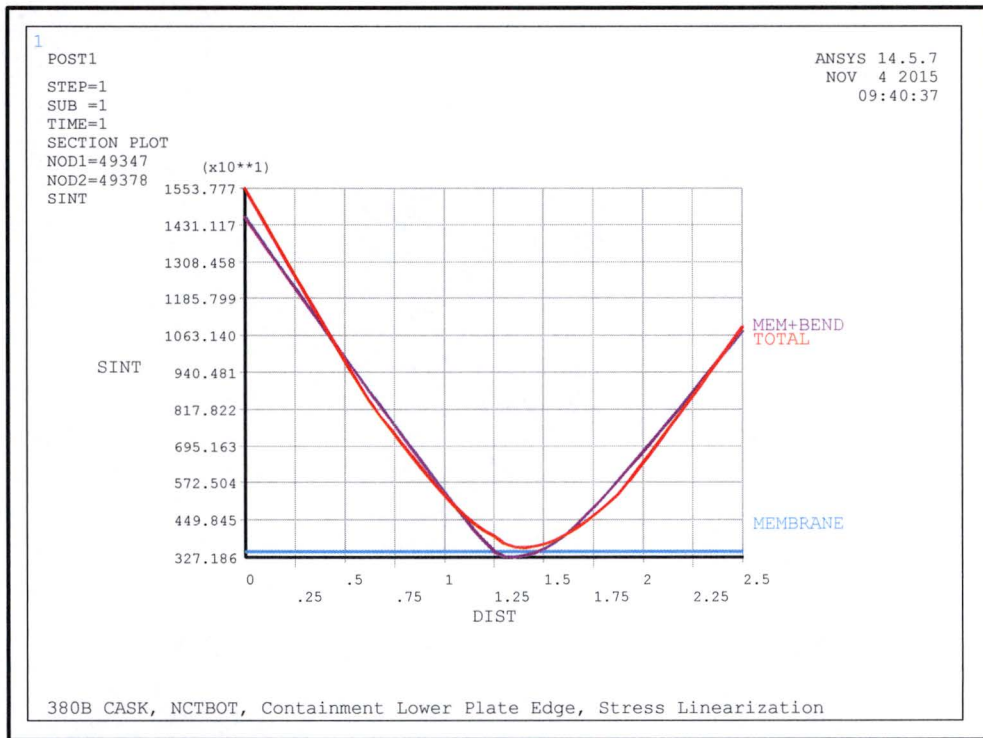
Figure 2.12.4-55 – NCT Bottom-Down Cavity Bottom Plate Edge with Cold Lead Shrinkage Pressure
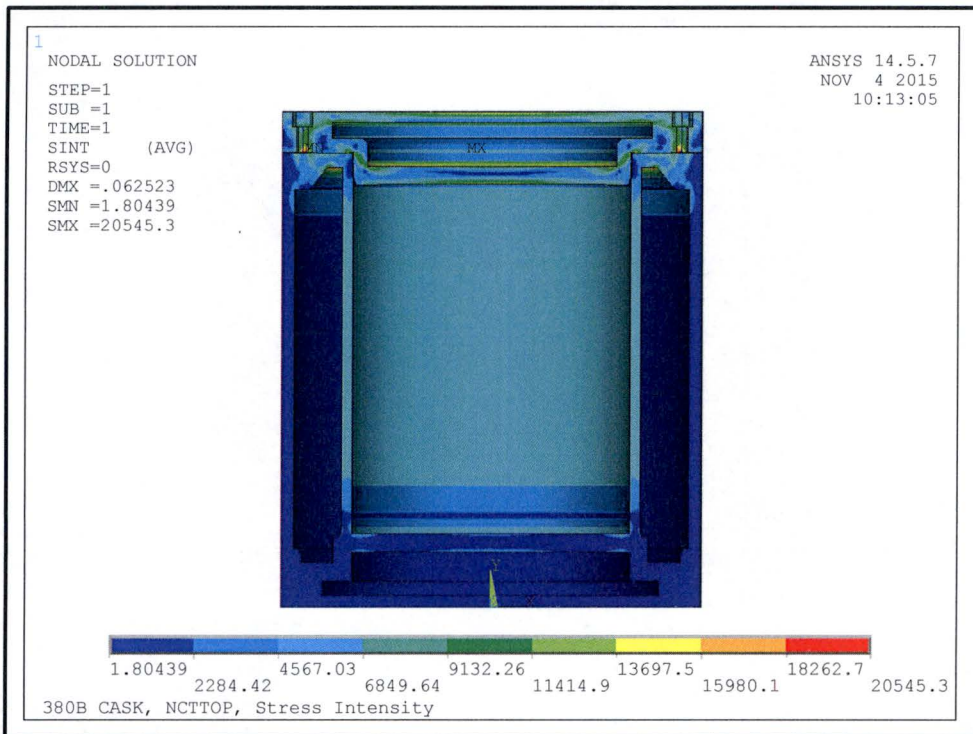
Figure 2.12.4-56 – NCT Top-Down End Drop with Cold Lead Shrinkage Pressure
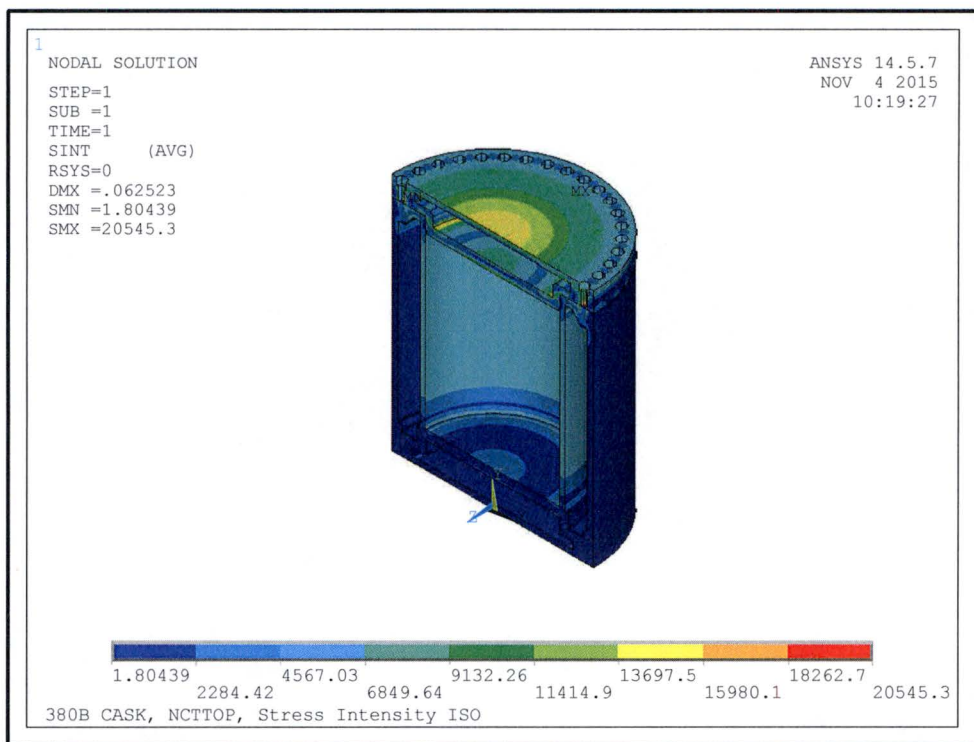
Figure 2.12.4-57 – NCT Top-Down End Drop Isometric with Cold Lead Shrinkage Pressure
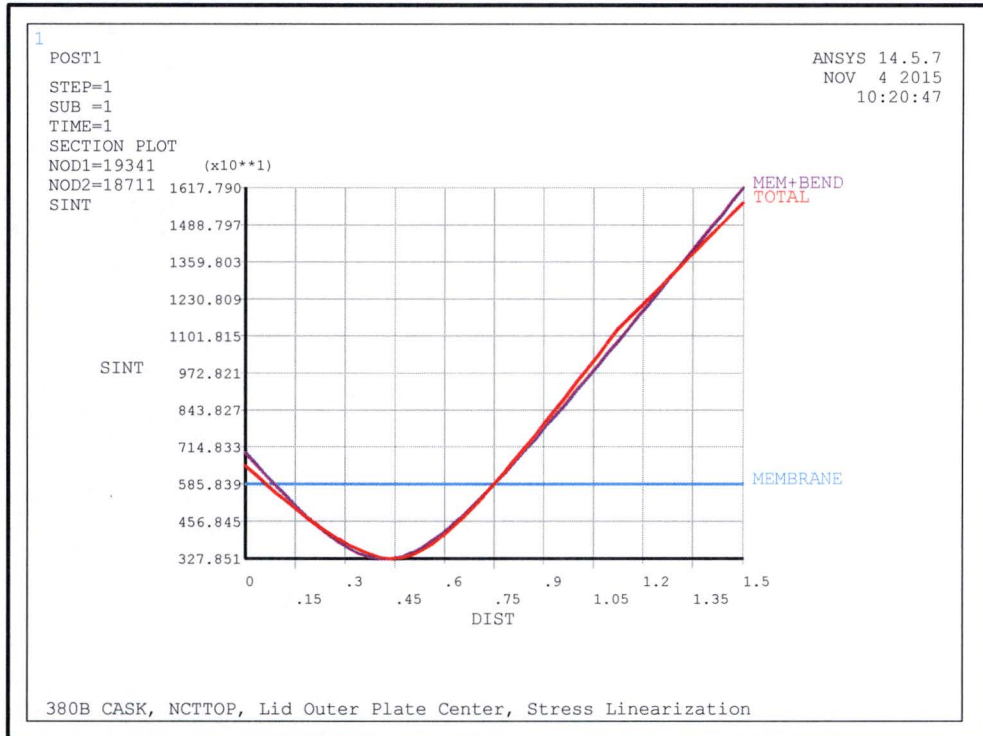
Figure 2.12.4-58 – NCT Top-Down Lid Outer Plate Center with Cold Lead Shrinkage Pressure
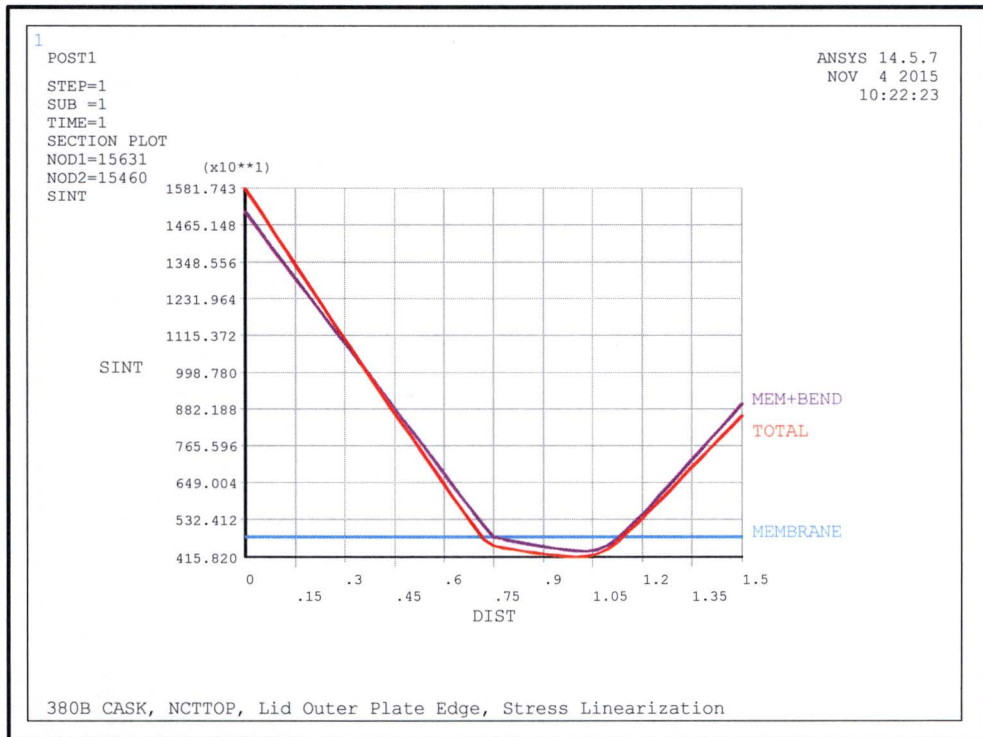
Figure 2.12.4-59 – NCT Top-Down Lid Outer Plate Edge with Cold Lead Shrinkage Pressure
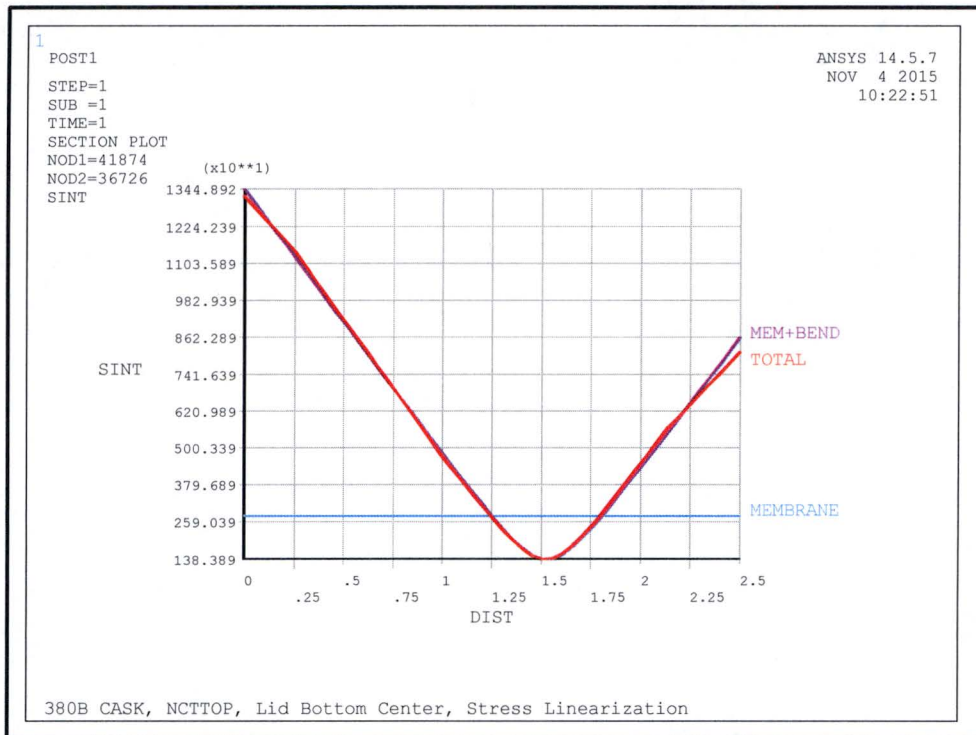
Figure 2.12.4-60 – NCT Top-Down Lid Inner Plate Center with Cold Lead Shrinkage Pressure
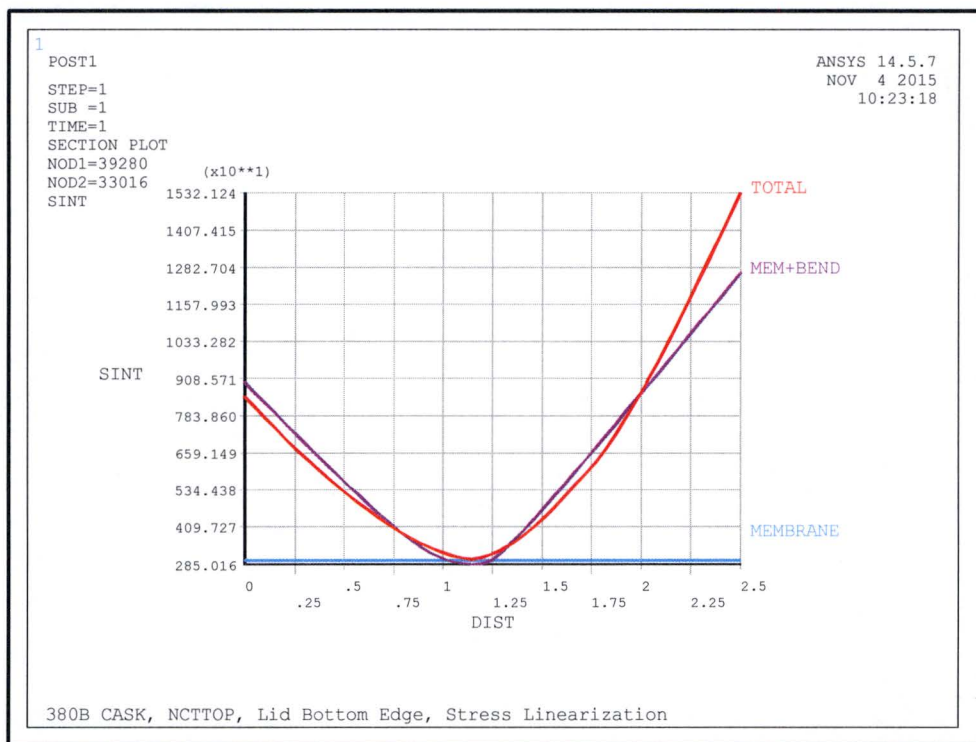
Figure 2.12.4-61 – NCT Top-Down Lid Inner Plate Edge with Cold Lead Shrinkage Pressure
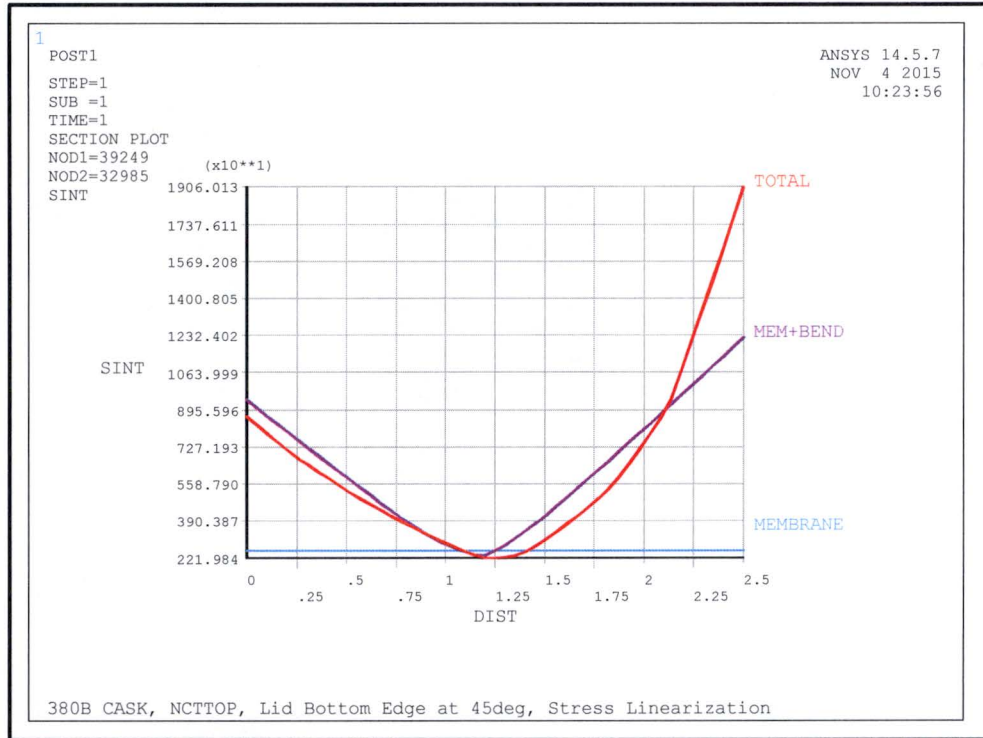
Figure 2.12.4-62 – NCT Top-Down Lid Inner Plate Edge at 45 Deg with Cold Lead Shrinkage Pressure
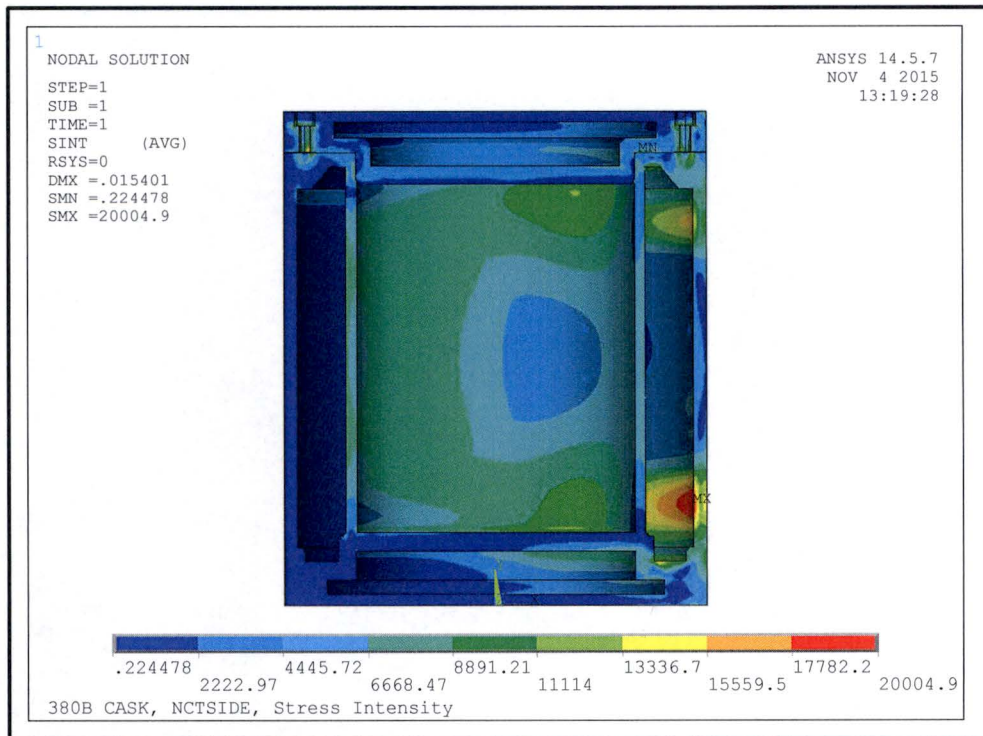
Figure 2.12.4-63 – NCT Side Drop with Cold Lead Shrinkage Pressure
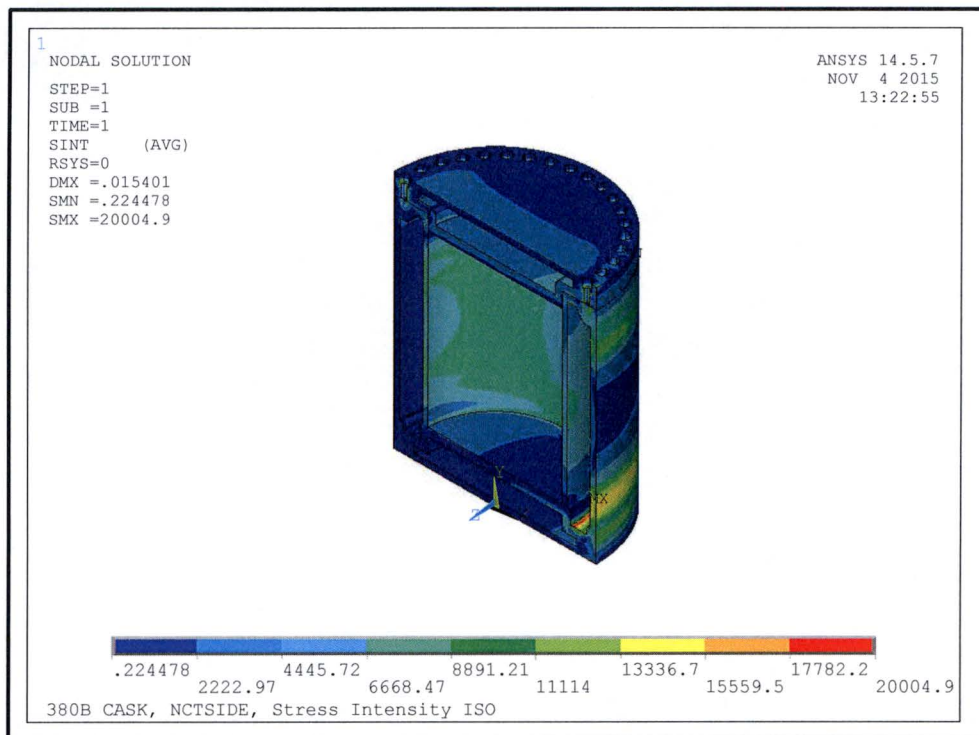
Figure 2.12.4-64 – NCT Side Drop Isometric with Cold Lead Shrinkage Pressure
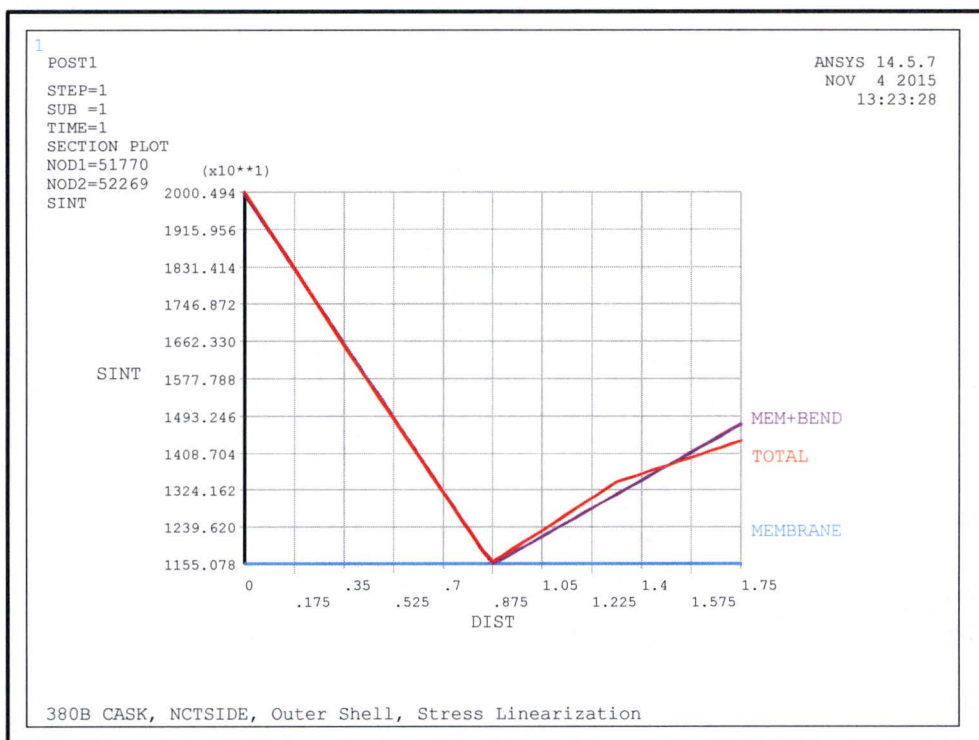
Figure 2.12.4-65 – NCT Side Drop Outer Shell with Cold Lead Shrinkage Pressure
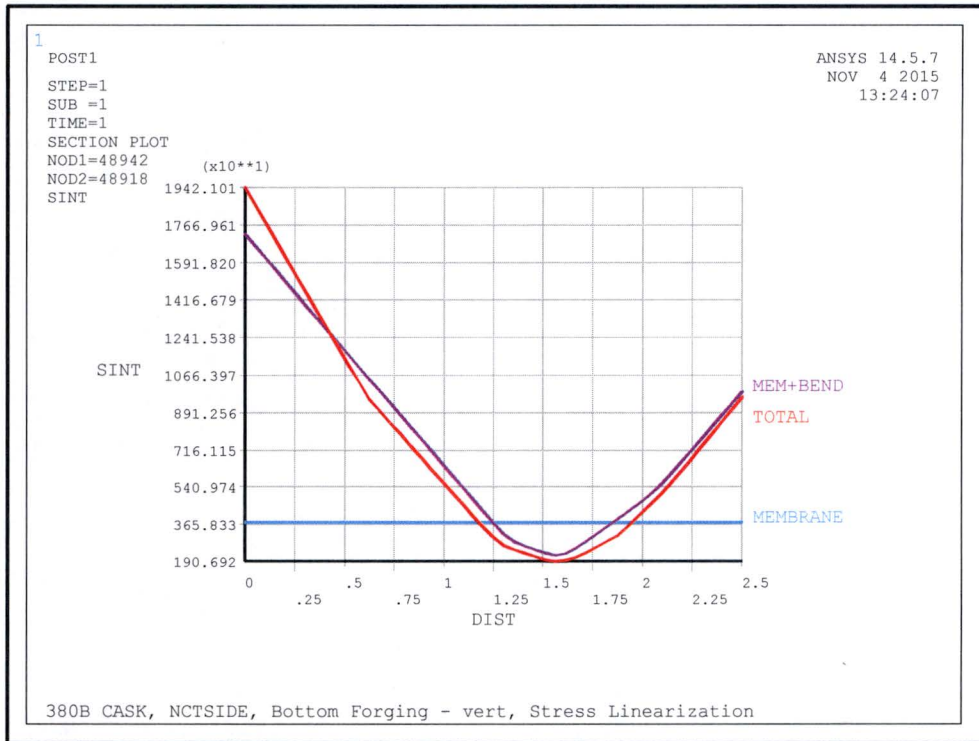
Figure 2.12.4-66 – NCT Side Drop Lower End Structure Step with Cold Lead Shrinkage Pressure

(Within the figure, the term 'Bottom Forging' refers to the Lower End Structure.)

This page left intentionally blank.

2.12.5 Free Drop Impact Evaluation

This appendix presents the analytical evaluation of the impact and crush performance of the 380-B package impact limiters. The impact magnitude and crush deformation of the limiters in several impact orientations, and at hot and cold bounding temperatures, is presented. The analysis is presented in detail, including the establishment of the crush properties of the polyurethane energy-absorbing foam and the impact response of the package using the LS-DYNA® computer program.

This appendix also includes a benchmark comparison between the analysis results and test results, which shows that the analysis results are bounding especially with respect to maximum deformations.

2.12.5.1 Introduction

The results presented by this appendix for the 380-B package impact limiter performance, specifically with respect to accelerations and impact limiter crush deformations from NCT and HAC free drops, is used as design input for other disciplines. The impact loads are used as input to the cask structural analysis, and the impact limiter crush deformations are used as input to the shielding and thermal analyses. The bounding free drop results, for orientations determined in Appendix 2.12.2, *Certification Test Plan,* are verified by half-scale testing reported in Appendix 2.12.3, *Certification Test Results.*

The licensing basis for the package is certification by analysis for all NCT and HAC conditions, with the exception of half-scale impact limiter testing that is used to verify the impact accelerations, crush deformations, and general structural integrity of the impact limiter and impact limiter attachments. Puncture damage to the impact limiter is certified in-whole by half-scale testing. No analysis is performed in this evaluation on the impact limiter puncture drop performance. The half-scale testing did include impact limiters and attachments produced in half-scale that were drop tested with a cask body representative in half-scale size and weight. The half-scale test unit was fitted with active accelerometers to record the free drop accelerations. The simulations must demonstrate the bounding certification test orientations were performed and the simulations should also provide bounding free drop accelerations and crush deformations.

2.12.5.2 Methodology

The NCT and HAC free drop impact limiter performance are evaluated using the finite element analysis (FEA) program LS-DYNA®, Version ls971 R7.0.0, 79055. The FEA program LS-DYNA® is commercially available software from the company Livermore Software Technology Corporation (LSTC). LS-DYNA® is highly nonlinear, transient dynamic finite element analysis code that uses explicit time integration. The program is extensively utilized for automotive crash simulations, which makes it very suitable to performing regulatory free drop simulations. LS-DYNA® is used with direction from the Keyword User's Manuals [35] and [36].

The impact limiters are modeled in full-scale and half-symmetry. The cask body, lid, and payload are not explicitly modeled. The cask is represented by a rigid hollow cylinder with closed ends and the payload is represented by a solid cylinder.

The package model is dropped on a completely rigid drop pad to analyze the energy absorbing capabilities of the polyurethane foam impact limiters. The package is initially positioned with its lowest point against the drop pad. The package is then given an appropriate initial velocity representing an initial height of 1 foot for NCT drops or 30 feet for HAC free drops. The package free drops are simulated at various impact orientations for both warm and cold temperature conditions. See Figure 2.12.5-1 for the FEA model.

There are no specific acceptance criteria for the impact limiter performance characteristics evaluated in this appendix, except that the simulations must demonstrate the bounding certification test orientations were performed, and that the maximum free drop impact accelerations and crush deformations are obtained. The impact limiter design is driven by the cask's ability to remain leak-tight and maintain adequate biological shielding, both of which are demonstrated by analysis in separate sections.

The FEA model is benchmarked with results from three HAC free drops performed during half-scale certification testing. The benchmark simulations use the FEA model with foam properties (i.e., density and temperature) and free drop orientations of the half-scale certification test program. The benchmark simulations and results are provided in Section 2.12.5.6.1, *Benchmark Results*.

2.12.5.3 Design Input

2.12.5.3.1 Conditions
The free drop test conditions are defined by 10 CFR 71 [1] and TS-R-1 [31], which include 1-foot NCT and 30-foot HAC free drops. The 380-B package has a maximum gross weight of 67,000 lb. from Section 2.1.3, *Weights and Centers of Gravity* and is therefore subject to the 1-foot NCT free drop. The free drops are performed on an essentially unyielding surface. The free drops must be tested at the worst case NCT temperature, which can be either warm or cold depending on the drop orientation. The minimum cold test temperature is -40 °F based on the steady-state requirement from paragraph 664 of TS-R-1 and the average foam warm NCT temperature is conservatively assumed to be 160 °F. The calculated NCT average impact limiter foam temperature from Section 3.3, *Thermal Evaluation for Normal Conditions of Transport* is 130 °F and the maximum foam temperature is 176 °F. The thermal analysis determines the warm NCT temperatures based on the payload wattage, initial conditions, and solar insolation as required by 10 CFR 71 and TS-R-1.

2.12.5.3.2 Geometry
The 380-B packaging is defined by the drawings in Appendix 1.3.3, *Packaging General Arrangement Drawings*. Key inputs for the free drop impact evaluation are summarized in Table 2.12.5-1. The finite element model is based on the packaging drawings including materials and full-scale dimensions. Therefore, the half-scale certification test results must be scaled for comparison with the simulation results. The CTU deformations must be scaled by 2 and the CTU accelerations must be scaled by 1/2.

2.12.5.3.3 Material Properties
The 380-B cask, cask impact limiter attachment lugs, and impact limiter shells are designed utilizing Type 304 stainless steel, predominately ASTM A240, A276, and A479. (ASTM A276, Type 304 is not used for any components of the cask body on drawing 1916-02-02-SAR.) At

70 °F, the minimum material yield strength is 30,000 psi and the minimum material ultimate strength is 75,000 psi from Table 2.2-1. The Modulus of Elasticity is 28.3×10^6 psi per Table 2.2-1, and Poisson's ratio is 0.31 from Section 2.2.1, *Material Properties and Specifications*.

The impact limiter attachment bolts are ASTM A564 Grade 630 Condition H1100 steel where, at 70 °F, the minimum material yield strength is 115,000 psi and the minimum material ultimate strength is 140,000 psi from Table 2.2-3. The Modulus of Elasticity is 28.5×10^6 psi per Table 2.2-3 for 17Cr-4Ni-4Cu steels, and Poisson's ratio is 0.31 from Section 2.2.1, *Material Properties and Specifications*.

The impact limiter shell is filled with General Plastics FR-3700 series polyurethane foam. The nominal foam density is 16 pounds per cubic foot (pcf). The polyurethane foam properties are developed from the General Plastics foam guide [37] and as described in Section 2.12.5.3.3.4, *Polyurethane Foam (*mat_crushable_foam)*.

The material models used in the simulations are described in the following sub-sections.

2.12.5.3.3.1 Type 304 Stainless Steel (*mat_plastic_kinematic)

The cask impact limiter attachment lugs, impact limiter shell, and internal impact limiter attachment lugs are modeled with a Type 304 stainless steel plastic kinematic material for all simulations. This is material model 3 for LS-DYNA® and material identification 1 in the input files. The following properties are from Section 2.2.1, *Material Properties and Specifications*, [38] and [39], and converted to true stress-strain as shown below.

- Stainless Steel A240 Type 304 at -20 °F to 100 °F

- $E = 28,300$ ksi, $Sy = 30.0$ ksi, $Su = 75.0$ ksi, elongation = 0.40 [39], density = 0.290 lb/in^3

- True Yield Stress: $Syt = Sy(1+(Sy/E+0.002)) = 30.1$ ksi

- True Ultimate Stress: $Sut = Su(1+eu) = 105.0$ ksi

  - Where eu = engineering ultimate strain (elongation)

- True Yield Strain: $eyt = \ln(1+ey) = 0.00306$

  - Where ey = engineering yield strain (Sy/E+0.002)

- True Ultimate Strain: $eut = \ln(1+eu) = 0.336$

- True Tangent Modulus: $Etant = (Sut-Syt)/(eut-eyt) = 225.0$ ksi

The material properties and strengths are for a temperature range of -20 °F to 100 °F. These values are used for both warm (160 °F) and cold (-40 °F) simulations, which is reasonable for the desired simulation data. The impact accelerations and crush deformations will not be significantly affected by the change in strength of the stainless steel impact limiter shell going outside the range of -20 °F to 100 °F to a range of -40 °F to 160 °F. The simulation results are predominantly driven by the crush strength of the polyurethane foam, which is adjusted for temperature in Section 2.12.5.3.3.4, *Polyurethane Foam (*mat_crushable_foam)*. For example, the yield strength of Type 304 stainless steel drops to 27.0 ksi at 160 °F, which is 10% less than 30.0 ksi at 100 °F. The 1/4-inch thick shell is thin compared to the 100-inch impact limiter outer diameter, and for example is assumed to provide 20% of the overall impact limiter strength. Therefore, a 10% change in material strength from temperature for the impact limiter shell would

result in a 2% change to the overall impact limiter strength, (0.20 x 0.10) x 100% = 2%. A 2% change to the crush strength of the impact limiter is negligible.

2.12.5.3.3.2 A564 Type 630 Condition H1100 (*mat_plastic_kinematic)

The impact limiter attachment bolt material is ASTM A564 Type 630 Condition H1100 stainless steel. The impact limiter bolt washer is ASTM A240, A276, or A479 Grade UNS S21800 stainless steel that has higher yield and ultimate strength than the cask impact limiter lugs. To simplify the model, the washers use the same material as the bolts. This is reasonable as the bolted joint stiffness is controlled by the relatively flexible impact limiter shells and lesser strength Type 304 stainless steel material components. The impact limiter bolts and washers use the plastic kinematic material model 3 for LS-DYNA®, which is labeled material identification 9 in the input files.

The impact limiter bolt and washer material properties and strength are conservatively taken at 200 °F for both warm and cold simulations. The impact limiter bolts are long and subjected to bending loads from deformation of the impact limiter. Therefore, the primary failure mode of concern is bending. The effective cumulative plastic strain of the impact limiter bolts is examined to determine their ability to maintain attachment of the impact limiter. The effective cumulative plastic strain will be conservative by utilizing the weaker warm temperature material properties.

The modulus of elasticity is 27.8×10^6 psi and Poisson's Ratio is input as 0.30. Poisson's Ratio from Section 2.2.1, *Material Properties and Specification* is 0.31, the difference is negligible and will not affect the desired effective cumulative plastic strain results. The elastic-plastic curve is represented by a bilinear curve with a yield strength of 106,300 psi and an ultimate strength of 140,000 psi at 14% elongation [39]. The tangent modulus for the slope of the plastic curve is determined below along with the true stress-strain properties.

- Precipitation Hardened Stainless Steel ASTM A564 Type 630 Condition H1100 at 200 °F

- $E = 27,800$ ksi, $Sy = 106.3$ ksi, $Su = 140.0$ ksi, elongation $= 0.14$, density $= 0.288$ lb/in^3

- True Yield Stress: $Syt = Sy(1+(Sy/E+0.002)) = 106.9$ ksi

- True Ultimate Stress: $Sut = Su(1+eu) = 159.6$ ksi

- True Yield Strain: $eyt = \ln(1+ey) = 0.00581$

- True Ultimate Strain: $eut = \ln(1+eu) = 0.131$

- True Tangent Modulus: $Etant = (Sut-Syt)/(eut-eyt) = 421.0$ ksi

2.12.5.3.3.3 Cask, Payload, and Drop Pad (*mat_rigid)

The cask, payload, and drop pad are modeled with the rigid material model 20 for LS-DYNA®. This material does not absorb energy and no stresses or strains are calculated for it. The density of each component is controlled to model the appropriate weight of the item. The elastic modulus and Poisson's ratio of steel are used, but only relevant to the contact algorithms. The cask material is labeled material identification 5 in the input files, the payload material is labeled material identification 6, and the drop pad material is labeled material identification 7. The cask, payload, and drop pad are constrained through their respective rigid material definition. The cask and payload are constrained in

the z-direction, and x and y-rotations. The drop pad is constrained in all directions and all rotations, which makes it a completely immovable target surface.

2.12.5.3.3.4 Polyurethane Foam (*mat_crushable_foam)

The 380-B impact limiters contain General Plastics FR-3700 series polyurethane foam that is modeled with a crushable foam material. This is material model 63 for LS-DYNA® and is labeled material identification 3 in the input files. The foam functions as an impact energy absorber around the cask base and lid. The design nominal foam density is 16 pcf. The minimum free drop test temperature requirement from TS-R-1 is -40 °F, the bulk average warm NCT temperature of the foam is 130 °F and the maximum foam temperature is 176 °F from Section 3.3, *Thermal Evaluation for Normal Conditions of Transport*. Foam crush strength curves are developed for -40 °F and 160 °F, which is conservatively greater than the NCT bulk average warm temperature. Using the near maximum warm NCT temperature of the foam conservatively bounds the maximum crush deformation for the warm simulations. The cooler foam inside the impact limiter that is heated less from the thermal NCT solar load will have greater crush strength and lessen the warm deformation.

The foam has specific crush strengths properties that are dependent on the foam density, temperature, orientation (parallel or perpendicular to foam rise), and dynamic factors. The foam design guide [37] has detailed descriptions and data for compensating the foam crush strength curve for these variables. The material property inputs required for performing the drop simulations are the foam crush strength curves compensated for the minimum temperature with maximum manufacturing tolerance (hardest foam) and maximum temperature with minimum manufacturing tolerance (softest foam). Separate foam crush strength curves are generated for this purpose. The final foam crush strength curves are presented in Table 2.12.5-5.

The foam crush strength curves are developed as follows:

1. In all cases, the foam crush strength curves are developed for each temperature and percent strain listed in the foam design guide using a spreadsheet. The crush strength curves are then extrapolated beyond 70% up to 85% in increments of 5% and interpolated to populate the crush strength curves for the desired temperatures of -40 °F and 160°F.

2. The nominal 15 pcf crush strength curves at 75 °F referenced from Table 2.12.4-2 of the 435-B SAR (Docket 71-9355) [40] are used as the basis for developing the 380-B foam crush strength curves.

3. The parallel and perpendicular crush strengths curves for 15 pcf foam at 75 °F are generated directly from the information in foam design guide. The basic equation for static crush strength is:

$$\sigma = Y\rho^S$$

Where σ is the crush strength in psi, ρ is the foam density in lb/ft^3, and Y and S are constants which depend on the strain level that is listed in the foam design guide.

4. The nominal 15 pcf data from the 435-B drop analysis described in step two is used with the foam design guide data for 15 pcf developed in step three to create a scale factor at each percent strain for both parallel and perpendicular crush strength curves. The scale factors are shown in Table 2.12.5-2.

5. The foam design guide is used to develop foam crush strength curves for 16 pcf at 75 °F that are subsequently scaled with the factor developed in step four, which are listed in Table 2.12.5-3. The scaled 16 pcf curves at 75 °F are then adjusted for temperature using the C_T values found in Tables 7 and 8 of the foam design guide.

$$\sigma_{Para}(\varepsilon) = C_T(\sigma_{Para\,75°F})$$

$$\sigma_{Perp}(\varepsilon) = C_T(\sigma_{Perp\,75°F})$$

6. A $\pm 10\%$ manufacturing tolerance is applied to the foam density of 16 pcf, which creates a density min/max of 14.4 pcf to 17.6 pcf. This min/max is then conservatively rounded to 14 pcf to 18 pcf.

7. The foam design guide is used to develop the foam crush strength curves for 18 pcf at 75 °F that are subsequently scaled with the factor developed in step four and are also shown in Table 2.12.5-3. The scaled 18 pcf curves at 75 °F are then adjusted for temperature using the foam design guide as shown in step five. The 18 pcf foam curves are calculated for the cold (-40 °F) free drop condition to determine maximum impact accelerations.

8. The foam design guide is used to develop the foam crush strengths curve for 14 pcf at 75 °F that are subsequently scaled with the factor developed in step four and are also shown in Table 2.12.5-3. The scaled 14 pcf curves at 75 °F are then adjusted for temperature using the foam design guide as shown in step five. The 14 pcf foam curves are calculated for the warm (160 °F) free drop conditions to determine maximum crush deformations.

9. For both 18 pcf and 14 pcf curves developed in steps seven and eight, the foam design guide method is used to apply the dynamic effects:

$$\sigma_{Dynamic} = Y_{int}\left(\sigma_{Static}\right)^S$$

Where Y_{int} and S are dynamic factors from Table 9 of the foam design guide, and σ_{Static} is the scaled and temperature adjusted static crush strength for 18 pcf and 14 pcf foam. The foam crush strength curves at 75 °F that are compensated for dynamic effects are shown in Table 2.12.5-4.

10. Lastly, the crush strength curves are adjusted for the particular drop orientations using the ellipse function shown below to combine the parallel and perpendicular crush strength curves, where the angle θ is measured from the horizontal i.e., 0° is horizontal side drop and 90° is vertical end drop. The dynamic crush strength curves used in the simulations at temperature and drop orientation are shown in Table 2.12.5-5.

$$\sigma = \frac{1}{\sqrt{\left(\dfrac{\sin\theta}{\sigma_{Para}}\right)^2 + \left(\dfrac{\cos\theta}{\sigma_{Perp}}\right)^2}}$$

2.12.5.4 Calculations

2.12.5.4.1   FEA Model Description

The 380-B FEA model is used to determine the impact loads, and impact limiter crush deformations for 10 CFR 71 NCT and HAC free drops. The NCT and HAC drop cases are from a height of 1 foot (for packaging over 33,100 lb) and 30 feet, respectively, as discussed in Section 2.12.5.3.1, *Conditions*. Impact loads are determined for the side drop, center-of-gravity (cg) over-corner drop, and end drop orientations. See Figure 2.12.5-2 through Figure 2.12.5-4 for the above described drop orientations. The cg-over-corner drop is inclined at an angle of 50 degrees from the horizontal plane, which assumes that the payload and dunnage weight are evenly distributed over the payload cavity. These three orientations are considered bounding for the 380-B package design. Orientations that include a primary impact followed by secondary slapdown impact are not bounding based on the small aspect ratio (length to diameter) of the packaging, which is nearly unity considering the overall packaging height and less than unity when not considering the conical section of the impact limiters. However, two slapdown simulations are performed to confirm that slapdown is not a concern for this package design. The slapdown angles simulated are 10° and 20° from horizontal. These FEA model orientations are shown in Figure 2.12.5-5 and Figure 2.12.5-6.

The 380-B FEA model consists of four components; the 380-B upper and lower impact limiters with attachments, a dummy cask, a dummy payload, and the impact surface, see Figure 2.12.5-1. A total of 57 parts are defined in LS-DYNA® for the half symmetric FEA model, which includes 825,324 nodes and 747,944 elements. The model consists of both solid and shell elements. The cask impact limiter lugs, impact limiter bolts and washers, and impact limiter lugs are modeled with solid type 2, fully integrated selectively reduced elements. The dummy cask body, dummy payload, and drop pad are modeled with solid type 1 constant stress elements, however they utilize the rigid material definition that does not calculate any stresses, only rigid body motions. The impact limiter shell is modeled with type 16 fully integrated shell elements with Lobatto integration and type 8 hourglass control. Activating the Lobatto integration style calculates the stresses of the outer integration points at the outer surface of the shell. The type 8 hourglass control is applicable for type 16 fully integrated shell elements, which activates full projection warping stiffness for accurate solutions. All shell elements have a shear correction factor of 5/6, as recommended by [35]. The impact limiter shell elements that are 1/2 inch and 1/4 inch thick have 5 integration points through their thickness. The shell elements for the impact limiter bolt recess tubes are 0.12 inch thick and have 3 integration points through their thickness. The impact limiter model does not include any of the joint backing angles. These components will have little effect on the package accelerations and deformations. The polyurethane foam in the impact limiters is modeled with the default, solid type 1 constant stress elements with type 5 Flanagan-Belytschko hourglass control, which is a stiffness form with exact volume integration for solid elements. A summary of the model parts and their characteristics is presented in Table 2.12.5-7.

The cask impact limiter lugs, impact limiter shells, and impact limiter lugs all use the plastic kinematic material for Type 304 stainless steel described in Section 2.12.5.3.3.1, *Type 304 Stainless Steel (*mat_plastic_kinematic)*. The impact limiter bolts and washers use the plastic kinematic material for 17-4PH described in Section 2.12.5.3.3.2, *A564 Type 630 Condition H1100 (*mat_plastic_kinematic)*. The dummy cask body, dummy payload, and drop pad use the

rigid material described in Section 2.12.5.3.3.3, *Cask, Payload, and Drop Pad (*mat_rigid)*. Lastly, the impact limiter polyurethane foam uses the crushable foam material described in Section 2.12.5.3.3.4, *Polyurethane Foam (*mat_crushable_foam)*. The end drop, side drop, and cg-over-corner drop each use the respective foam strength curve developed for their specific orientation. The two slapdown orientations use the foam strength curves for the side drop. The slapdown secondary impact theoretically occurs at the 0° side drop orientation, which makes use of the 0° orientation foam strength curve applicable. The primary impacts at 10° and 20° also both use the 0° orientation foam strength curve, which is reasonable based on the small strength difference between the 0° and 50° orientation strength curves in Table 2.12.5-5.

The model is half symmetrical with the symmetry plane cutting through four of the impact limiter bolts (two upper, and two lower). The nodes on the symmetry plane that do not have a rigid material definition (i.e., everything except the cask, payload, and drop pad) are constrained with the *boundary_spc_set command in the z-direction, and x and y-rotations. The cask, payload, and drop pad are constrained through their respective rigid material definition. The cask and payload are constrained in the z-direction, and x and y-rotations. The drop pad is constrained in all directions and all rotations, which makes it a completely immovable target surface.

The FEA model includes a wide array of structural interfaces and contacts. Structural interfaces are modeled with merged nodes, where permitted by the mesh generation, or by tied contact definitions. For instance, all the impact limiter shell joints have merged node interfaces, i.e., the mesh is continuous between the parts. The model does not include any of the impact limiter joint backing angles. This omission will have little effect on the package accelerations and overall deformations. The detailed behavior of the impact limiter joints is captured by half-scale certification testing. In other areas, like the cask impact limiter lugs to the cask outer wall, impact limiter bolt recess tubes, impact limiter lugs, and "threaded" impact limiter bolt areas are all connected with tied contact definitions. Tied contact definitions are used where the mesh between parts is not similar or continuous. The FEA model also has numerous contacts between parts. The most common contact definition used is automatic surface to surface with the optional card A set with soft equal to 2 for segment-based contact and the depth equal to 5 for checking surface and edge to edge penetrations. Typically the sbopt (segment-based contact options) is set to the default, 4 (sliding option), or 5 (sliding and warped segment checking) depending on the interface needs and associated cpu time cost. Options 4 and 5 typically require more cpu time, however they can be very useful in solving large deformation simulations. Other contact definitions and options are used where necessary to model the proper component interactions and prevent the simulations from experiencing error terminations.

Friction between the various parts is defined through the contact cards. The majority of contact interfaces have a coefficient of friction of zero. However, the contact interfaces with the impact limiter foam have a coefficient of friction of 0.40. The coefficient of friction of 0.40 is used for both static and sliding conditions. The value is used in part by matching results between the benchmark simulations and certification testing demonstrated in the 435-B drop analysis. The value of 0.40 is also considered reasonable in comparison with a survey of dry sliding friction values in Table 3.2.4 of [41], where hard steel on hard steel is 0.42, mild steel on mild steel is 0.57, nickel on mild steel is 0.64, aluminum on mild steel is 0.47, and nickel on nickel is 0.53. The coefficient of friction used between the package and drop pad is 0.10, which is also referenced from the 435-B SAR (Docket 71-9355) [40], Section 2.12.4.3.1.1, *Benchmark Model*. The

coefficient of friction of 0.10 is conservatively low, while still appearing to produce practical results. As noted in the 435-B SAR, Section 2.12.4.5.1, *Benchmark Results*, the coefficient of zero with the drop pad appeared to produce unrealistic results.

The impact limiter attachment bolts are preloaded with an axial force prior the free drop impact, to model the installation bolt torque. The preload is accomplished by creating an initial interference between the washers and the cask impact limiter lugs, see Figure 2.12.5-8, that is removed by using *contact_surface_to_surface_interference. The washer and lug initial interference is gradually removed by the *contact_surface_to_surface_interference developing the contact forces necessary to remove the initial penetrations. Therefore, the bolt is elongated and the joint is compressed to the extent necessary for offsetting the initial interference. The initial interference is determined by an iterative process as the axial bolt load is dependent on the joint stiffness. The preload for all simulations is approximately 20,000 lb for the full symmetry bolts, and 10,000 lb for the half symmetry bolts. The average preload for the upper and lower impact limiter bolts is shown in Figure 2.12.5-16 and Figure 2.12.5-17, respectively. The preload is determined by using $T = KFd$, equation 8-20 [42], where the nominal bolt torque T is 310 ft-lb from flag note 7 on drawing 1916-02-01-SAR, K is an assumed torque (nut) factor of 0.15, and d is the bolt thread diameter of 1.25 in. The bolts are to be lubricated with a nickel-based nuclear grade lubricant, which is why the torque factor is assumed to be 0.15.

The 380-B free drop simulations include gravity as a body acceleration load of 386.4 in/s². The simulations also include an initial free drop velocity of -96.3 in/s for 1-ft NCT and -527.5 in/s for 30-ft HAC. The initial velocities are determined by assuming the potential energy from the drop height is equal to the kinetic energy at the moment before impact with the drop pad. The resulting velocity is calculated by:

$$V = \sqrt{2gh}$$

Where g is the acceleration of gravity, 386.4 in/s², and h is the drop height in inches.

The 380-B FEA model weight in full symmetry is 66,277 lb, which is 1% less than the maximum package gross weight 67,000 lb. A summary of the model weight by component and part ID is shown in Table 2.12.5-6. The 380-B FEA model is shown in the various free drop orientations in Figure 2.12.5-2 through Figure 2.12.5-6, and a summary of the model parts and their characteristics is presented in Table 2.12.5-7. The model is shown with key dimensions measured from node-to-node or node-to-element surface in Figure 2.12.5-7 through Figure 2.12.5-10. Additional model views are included in Figure 2.12.5-11 through Figure 2.12.5-15. The colors associated with the various FEA model parts in the following figures have no meaning. The different colors are assigned by the program and only visually distinguish the different parts.

2.12.5.5 Acceptance Criteria

The objective of simulations documented in this appendix is to demonstrate that the bounding certification test orientations are performed, and that the maximum free drop impact accelerations and crush deformations are obtained. The impact limiter design is driven by the cask's ability to remain leak-tight and maintain adequate biological shielding, both of which are demonstrated by analysis in separate sections.

2.12.5.6 Results

This evaluation determines the free drop impact accelerations, and impact limiter crush deformations for several conditions using an FEA model to perform sixteen different simulations. The different simulations cover worst case free drop orientations, cold and warm temperatures, and 1-foot NCT and 30-foot HAC free drops. The simulations are post-processed for package accelerations, and impact limiter crush. The package acceleration is determined for input to the cask structural analysis, and the impact limiter crush is determined for input to the package shielding and thermal analyses.

Three additional simulations are performed to benchmark and validate the model results with results from half-scale certification testing, Appendix 2.12.3, *Certification Test Results*. Ultimately, the benchmarking operation is performed to ascertain the overall usefulness of the computational simulations and provide confidence that certain information extracted from the simulations can be used to demonstrate design robustness. The three benchmark simulations are all 30-foot HAC free drops including, the cold end drop (D1), warm cg-over-corner drop (D2), and warm side drop (D3).

In all cases, the time history acceleration data obtained from the numerical simulations contains high frequency structural vibration and numerically-induced noises that are filtered out to provide an accurate assessment of the loadings on the package. In post-processing these simulations, the time history acceleration data is processed with a low-pass Butterworth filter. The cutoff frequency is conservatively chosen to be 250 Hz based on the guidance given in Section 701.9 of TS-G-1.1 [34]. The cutoff frequency of 250 Hz also correlates with the equivalent cutoff frequency of 500 Hz used to filter the half-scale certification test accelerometer data discussed in Section 2.12.3.2.3, *Accelerometers*. The cutoff frequency range is determined below:

$$f_c = [100 \text{ Hz to } 200 \text{ Hz}] \times \left(\frac{100}{m}\right)^{\frac{1}{3}} = [100 \text{ Hz to } 200 \text{ Hz}] \times \left(\frac{100}{30.39}\right)^{\frac{1}{3}} = 149 \text{ Hz to } 297 \text{ Hz}$$

Where m is the mass of the package in metric tonnes. This recommendation from TS-G-1.1 applies to packages less than 100 metric tonnes with impact limiters.

The accelerations are plotted for the rigid body cask center-of-gravity in the end, side, and cg-over-corner free drops. The accelerations are plotted for the average of the cask impact limiter lugs at the upper and lower ends for the slapdown drops. The rigid body cask acceleration is taken from the rdbout ASCII file for part 50, and the upper and lower cask impact limiter lug accelerations are taken from the matsum ASCII file for parts 12 and 13. The acceleration plots are created as follows: plot the y-acceleration, select the scale tab, insert y-scale factor of 0.0025879917 (for the inverse of gravity, 386.4 in/sec^2) to display units in g and apply, check autofit, select filter tab, select filter bw, time sec, insert 250 Hz and apply, select minmax, and re-title axes.

The impact limiter crush is determined by taking node-to-node or node-to-element surface measurements for the geometry initial and final conditions. The difference between the initial and final states is the crush. Also, minimum foam measurements for the warm HAC simulations are determined.

2.12.5.6.1   Benchmark Results

The three benchmark simulations are the same as the subsequent sixteen design simulations except for the impact limiter foam strength. The benchmark simulations use foam strength data developed specifically to represent the conditions observed during the half-scale certification tests, which includes the as-tested foam temperatures from Appendix 2.12.3, *Certification Test Results* of -15.3 °F and 100 °F. The foam strength data for the benchmark simulations is developed using the same method as described in Section 2.12.5.3.3.4, *Polyurethane Foam (*mat_crushable_foam)* for the design simulations. The specific foam strength data used for the benchmark simulations is included in Table 2.12.5-8.

The benchmarking process involved performing numerous simulations and comparing the simulation results with the half-scale certification results. Various parameters of the model were adjusted to experimentally and iteratively narrow the simulation differences with the physical test data. The parameter changed through the course of benchmarking that had the most significant influence on narrowing the simulation differences with the physical test data is the 'damp' parameter in the foam material model (input file material id 3, *mat_crushable_foam). The 'damp' parameter is described by the LS-DYNA® manual [36] as follows: Rate sensitivity via damping coefficient (.05<recommended value<.50), with program default being .10. Preliminary simulations were performed with damp = .10 (the default value) and moved up to .50 during the benchmark process. All the benchmark simulations and subsequent design simulations herein use damp = .50.

The results compared for the benchmarking process are the impact accelerations, impact limiter crush, and impact patch length and width. The impact patch dimensions were measured on the half-scale certification test unit by locating signs, namely scuffs and abrasions, on the impact limiters that indicate contact with the drop pad. Similarly, impact patches on the simulation impact limiters are measured by observing what elements/nodes appear to contact the drop pad during the time history.

The half-scale certification test results are documented in Appendix 2.12.3, *Certification Test Results*. The benchmark accelerations conservatively approximate the test accelerations with the test accelerations being 0.8% to 6.8% less than the simulations. The benchmark deformations conservatively exceed the test deformations. The largest difference is with respect to the warm side drop (D3) maximum crush, where the test result is 31.6% less than the simulation. The benchmark measured 10.38 inches while the test only measured 7.10 inches. The benchmark simulations exceed the crush observed during testing and match or exceed the accelerations observed during testing. Therefore, the structural and thermal evaluations that use the acceleration and crush data as input are ultimately conservative. Table 2.12.5-9 provides a comparison between the results of the half-scale certification drop test and benchmark simulations. The results of the half-scale certification drop test are converted to full-scale equivalent for comparison with the benchmark simulations. All analyses are with respect to full-scale. Figure 2.12.5-18 through Figure 2.12.5-23 provide a general visual comparison between the half-scale certification test damage and the benchmark simulations. Comparison of the certification test and benchmark run acceleration time histories are provided in Figure 2.12.5-24 through Figure 2.12.5-26. The accelerometer data provided in Appendix 2.12.3 for the accelerometer number stated in the chart legend was converted to full scale by multiplying the time scale by two and the acceleration scale by 0.5. The C.G.-over-corner data was divided by cos(40) to obtain the acceleration perpendicular to the ground. As shown, the pulse shape and

duration of the benchmark and test data impact records compare well, and support the conclusion that the LS-DYNA® impact analyses of the 380-B are conservative.

2.12.5.6.2   NCT Free Drop Results

The 380-B package FEA simulations calculate a maximum NCT impact of approximately 33.8 g in the cold 1-ft end drop. The side drop and cg-over-corner drop are almost 50% less at 18.3 g and 15.4 g, respectively. The maximum NCT foam strain and deformation are estimated to be 14.6% and 2.9 inches in the warm 1-ft cg-over-corner drop case. The foam strain is calculated from the measured crush, for example: 2.9 inches of crush divided by the initial foam thickness of 19.8 inches shown in Figure 2.12.5-10 is equal to 14.6%. The NCT results are presented in Table 2.12.5-10, and Figure 2.12.5-27 through Figure 2.12.5-38.

2.12.5.6.3   HAC Free Drop Results

The 380-B package FEA simulations calculate a maximum HAC impact of approximately 92.8 g in the cold 30-ft HAC end drop case. The side drop is slightly less at 88.9 g and the cg-over-corner is less almost 30% at 68.3 g. The maximum foam strain and deformation are estimated to be 79.8% and 15.8 inches in the warm 30-ft HAC cg-over-corner drop case. The minimum foam distance after the 30-ft free drops is 3.9 inches, which occurs in the cg-over-corner orientation. The 10° and 20° slapdown simulation results confirm that slapdown is not a concern as expected for the geometry of the 380-B package, as neither of the slapdown simulations develops larger accelerations or foam strain, or lesser foam thicknesses than the side, cg-over-corner, and end drops. The HAC results are presented in Table 2.12.5-11, and Figure 2.12.5-39 through Figure 2.12.5-63.

The half-scale certification testing recorded no significant damage to the impact limiter bolts and no loss of attachment strength of the impact limiter to the cask, these results encompass all the HAC free drops and puncture drops performed during half-scale certification testing. Each impact limiter had a set of bolts that was used for one HAC free drop and one puncture drop. The test results demonstrate significant safety of the impact limiter attachment design.

2.12.5.7 Free Drop Impact Evaluation Summary

This document provides supporting drop simulation data for the certification testing performed on the 380-B package. The licensing basis for the package is certification by analysis for all NCT and HAC conditions, with the exception of half-scale impact limiter testing that is used to verify the impact accelerations, crush deformations, and impact limiter attachment performance. Puncture damage to the impact limiter is certified in-whole by half-scale testing. No analysis is performed on the impact limiter puncture drop performance. The free drop impact evaluation is used to confirm the worst-case orientations for testing, to determine the performance in orientations not tested, determine bounding impact loads for input to the cask structural analysis, and determine bounding impact limiter crush deformations for input to the shielding and thermal analyses.

The FEA simulations performed in this appendix include benchmark orientations that are compared directly to the certification test results. Free drop impact deformation and acceleration results are used to benchmark the finite element analysis model for use in non-tested orientations and conditions.

As discussed in Section 2.12.5.6.1, the simulation results compare well with the certification test results as shown in Table 2.12.5-9. The impact accelerations for all three certification test free drops were less than 7% less than the developed benchmark simulation results, and near 1% less for the D2 (warm cg-over-corner) and D3 (warm side drop) orientations. The impact patch sizes for all three certification test free drops were less than 8% less than the developed benchmark simulation results. The crush results for the D1 (cold end drop) and D2 (warm cg-over-corner) orientations were approximately 11% less than the developed benchmark simulation results, while the D3 (warm side drop) orientation was the largest outlier at nearly 32% less than the developed benchmark simulation result. The comparison of certification test free drop results with benchmark simulation results shows that the physical testing and model are in close agreement on the package impact acceleration response and conservative (i.e., model over predicts) on the package impact deformations. This demonstrates that the data collected from the simulations is reasonable, and useful.

The series of simulations performed for both NCT and HAC free drops demonstrates that the appropriate certification test orientations were performed. The cold end drop has the highest average packaging impact with accelerations of 33.8 g and 92.8 g for NCT and HAC, respectively. The warm cg-over-corner and side drop have the largest foam strain and/or impact limiter crush with corresponding minimum foam thickness. The warm cg-over-corner HAC free drop has 15.8 inches of crush at 79.8% foam strain and has a minimum 3.9 inches of foam. The slapdown simulation results confirm the package geometry is not conducive to primary impacts followed by rotation and more severe secondary impacts. All secondary impacts results are less than the associated primary impact results. The cold slapdown orientations do not have accelerations in excess of the end, side, or cg-over-corner free drops. The warm slapdown orientations do not have primary impact foam strain that exceeds the warm cg-over-corner foam strain, and the secondary impact foam strain does not exceed the warm side drop foam strain.

Therefore, all the certification tests are demonstrated by this appendix and the test plan, Appendix 2.12.2, *Certification Test Plan*, to be worst case, and appropriate for the license application. Additionally, the results herein for NCT and HAC free drops, shown in Table 2.12.5-10 and Table 2.12.5-11, are conservative and a safe for use in structural, thermal, and shielding evaluations.

Table 2.12.5-1 – Key Design Input Summary

DESIGN INPUT	Value	Unit
Impact Limiter Outside Diameter	100.0	in
Impact Limiter Overall Length	43.0	in
Impact Limiter Conical Diameter	60.0	in
Impact Limiter Conical Length	16.8	in
Impact Limiter End Thickness	25.0	in
Impact Limiter Hole Diameter	40.0	in
Impact Limiter Hole Length	12.0	in
Cask Outside Diameter	57.5 (excluding the thermal shield)	in
Cask Overall Length	68.13	in
Payload Weight (including dunnage)	12,000	lb
Impact Limiter Weight (each)	5,000	lb
Cask Weight	45,000	lb
Cask and Payload Weight	57,000	lb
Licensed Gross Package Weight	67,000	lb
Drop Height	1.0 (NCT) or 30.0 (HAC)	ft
Drop Angle from Horizontal	0.00 (side), 50.00 (cg-over), 90.00 (end)	deg

Notes:
1. Dimensions are referenced from Appendix 1.3.3, *Packaging General Arrangement Drawings*.
2. Weights are referenced from Table 2.1-2.

Table 2.12.5-2 – Foam Scale Factor

Strain	15 pcf GP Curve from 435-B [40], psi		15 pcf Foam Design Guide Method, psi		Scale Factor	
%	Parallel	Perpendicular	Parallel	Perpendicular	Parallel	Perpendicular
10	629	603	708	701	0.889	0.860
20	630	625	726	717	0.868	0.872
30	668	670	766	757	0.872	0.885
40	754	769	837	826	0.901	0.931
50	964	977	1,013	1,006	0.951	0.971
60	1,436	1,445	1,403	1,403	1.024	1.030
65	1,886	1,903	1,758	1,761	1.073	1.081
70	2,645	2,691	2,395	2,382	1.104	1.130
75	3,551	3,629	3,086	3,065	1.151	1.184
80	4,819	4,952	4,033	3,994	1.195	1.240
85	6,540	6,758	5,270	5,205	1.241	1.298

Table 2.12.5-3 – Foam Static Crush Strength

	Static Crush Strength, psi					
	18 pcf at 75 °F		16 pcf at 75 °F		14 pcf at 75 °F	
Strain	Foam Orientation		Foam Orientation		Foam Orientation	
%	Para	Perp	Para	Perp	Para	Perp
10	886	852	710	681	552	529
20	896	893	714	709	551	546
30	960	967	759	763	582	583
40	1,101	1,127	862	880	653	665
50	1,425	1,449	1,107	1,123	831	842
60	2,150	2,168	1,657	1,668	1,233	1,239
65	2,768	2,773	2,160	2,174	1,631	1,650
70	3,977	4,043	3,056	3,108	2,267	2,307
75	5,310	5,402	4,094	4,178	3,049	3,122
80	7,222	7,377	5,561	5,703	4,135	4,259
85	9,821	10,075	7,552	7,784	5,607	5,811

Table 2.12.5-4 – Foam Dynamic Crush Strength

	Dynamic Crush Strength, psi					
	18 pcf at 75 °F		16 pcf at 75 °F		14 pcf at 75 °F	
Strain	Foam Orientation		Foam Orientation		Foam Orientation	
%	Para	Perp	Para	Perp	Para	Perp
10	1,438	1,381	1,144	1,096	883	844
20	1,352	1,348	1,075	1,068	829	821
30	1,399	1,409	1,109	1,114	852	853
40	1,559	1,596	1,220	1,246	924	941
50	1,928	1,959	1,501	1,522	1,130	1,144
60	2,696	2,718	2,086	2,101	1,560	1,569
65	3,575	3,582	2,796	2,815	2,117	2,141
70	4,137	4,202	3,213	3,266	2,413	2,454
75	5,458	5,548	4,254	4,337	3,207	3,280
80	7,329	7,480	5,705	5,844	4,294	4,418
85	9,841	10,084	7,650	7,875	5,750	5,950

Table 2.12.5-5 – Foam Crush Strength at Temperature and Drop Angle

	Dynamic Crush Strength, psi					
	18 pcf at -40 °F			14 pcf at 160 °F		
Strain	Drop Orientation[1], Degrees			Drop Orientation[1], Degrees		
%	0	50	90	0	50	90
10	1,986	2,042	2,085	527	543	555
20	1,905	1,907	1,908	531	541	549
30	1,966	1,956	1,948	567	574	579
40	2,240	2,193	2,161	641	634	629
50	2,686	2,673	2,664	782	780	778
60	3,656	3,671	3,682	1,103	1,101	1,100
65	4,685	4,764	4,822	1,529	1,512	1,501
70	5,133	5,285	5,400	1,896	1,894	1,893
75	6,512	6,785	6,999	2,612	2,606	2,602
80	8,389	8,845	9,215	3,650	3,649	3,649
85	10,804	11,525	12,129	5,090	5,103	5,112
100[2]	52,500	52,500	52,500	52,500	52,500	52,500

Notes:
1. The drop orientation is with respect to the horizontal, where 0° is the side drop, and 90° is the end drop. The 0° side drop is perpendicular to foam rise and the 90° end drop is parallel to foam rise.
2. For all crush strength curves, the foam is assumed to lock-up hard at 100% strain and reach a crush strength equal to the flow stress of Type 304 stainless steel at 75 °F. The flow stress is the average of the material yield and ultimate strength: (30,000 psi + 75,000 psi) / 2 = 52,500 psi. This assumption increases simulation stability by decreasing negative volume errors, where the foam elements become so compressed and distorted that the mesh is no longer viable for the program to solve.

Table 2.12.5-6 – FEA Model Weight Summary

Component	Part IDs	Half Symmetry Model		Full Symmetry
	(see Table 2.12.5-7 for descriptions)	mass	weight	weight
		lb·s^2/in	lb	lb
Upper Impact Limiter	15-24, 131-137, 142	6.0854	2,351	4,703
Lower Impact Limiter	25-34, 121-127, 141	6.0855	2,351	4,703
Loaded Cask Body	39, 50, 12, 13	73.3873	28,357	56,714
Total Package	all except 40 (drop pad)	85.7627	33,139	66,277

Table 2.12.5-7 – FEA Model Part Descriptions

Part ID	Part Description	Material	Material ID	Section Type	Section Type ID	Element Type	Element Type ID	Thickness
12	cask upper impact limiter lugs	Type 304	1	solid	2	fully integrated S/R	2	na
13	cask lower impact limiter lugs	Type 304	1	solid	2	fully integrated S/R	2	na
15	uil foam	GP FR3716	3	solid	1	constant stress	1	na
16	uil conical end plate	Type 304	1	shell	3	fully integrated	16	0.25
17	uil conical plate	Type 304	1	shell	3	fully integrated	16	0.25
18	uil outer wall	Type 304	1	shell	3	fully integrated	16	0.25
19	uil end plate	Type 304	1	shell	3	fully integrated	16	0.25
20	uil inner wall	Type 304	1	shell	3	fully integrated	16	0.25
21	uil cask end plate	Type 304	1	shell	4	fully integrated	16	0.50
22	uil cut-out cylinder	Type 304	1	shell	3	fully integrated	16	0.25
23	uil cut-out end plate	Type 304	1	shell	3	fully integrated	16	0.25
24	uil lugs	Type 304	1	solid	2	fully integrated S/R	2	na
25	lil foam	GP FR3716	3	solid	1	constant stress	1	na
26	lil conical end plate	Type 304	1	shell	3	fully integrated	16	0.25
27	lil conical plate	Type 304	1	shell	3	fully integrated	16	0.25
28	lil outer wall	Type 304	1	shell	3	fully integrated	16	0.25
29	lil end plate	Type 304	1	shell	3	fully integrated	16	0.25
30	lil inner wall	Type 304	1	shell	3	fully integrated	16	0.25
31	lil cask end plate	Type 304	1	shell	4	fully integrated	16	0.50
32	lil cut-out cylinder	Type 304	1	shell	3	fully integrated	16	0.25
33	lil cut-out end plate	Type 304	1	shell	3	fully integrated	16	0.25

34	lil lugs	Type 304	1	solid	2	fully integrated S/R	2	na
35	uil washers	17-4PH	9	solid	2	fully integrated S/R	2	na
37	lil washers	17-4PH	9	solid	2	fully integrated S/R	2	na
39	dummy payload	rigid body	6	solid	1	constant stress	1	na
40	drop pad	rigid body	7	solid	1	constant stress	1	na
50	dummy cask	rigid body	5	solid	1	constant stress	1	na
101-107	uil attachment bolts	17-4PH	9	solid	2	fully integrated S/R	2	na
111-117	lil attachment bolts	17-4PH	9	solid	2	fully integrated S/R	2	na
121-127	lil tubes	Type 304	1	shell	5	fully integrated	16	0.12
131-137	uil tubes	Type 304	1	shell	5	fully integrated	16	0.12
141	lil stiffeners	Type 304	1	shell	3	fully integrated	16	0.25
142	uil stiffeners	Type 304	1	shell	3	fully integrated	16	0.25

Notes:
1. uil = Upper Impact Limiter
2. lil = Lower Impact Limter

Table 2.12.5-8 – Benchmark Foam Crush Strength at Temperature and Drop Angle

Strain	Dynamic Crush Strength, psi					
	17 pcf at -15.3 °F			15 pcf at 100 °F		
	Drop Orientation[1], Degrees			Drop Orientation[1], Degrees		
%	0	50	90 (D1)	0 (D3)	50 (D2)	90
10	1,649	1,696	1,732	807	839	864
20	1,585	1,589	1,592	799	813	824
30	1,637	1,631	1,627	843	852	859
40	1,861	1,820	1,793	957	946	938
50	2,223	2,213	2,205	1,155	1,161	1,166
60	3,024	3,037	3,047	1,609	1,624	1,635
65	3,906	3,966	4,009	2,173	2,190	2,202
70	4,292	4,423	4,522	2,571	2,654	2,718
75	5,476	5,708	5,891	3,450	3,586	3,691
80	7,083	7,473	7,793	4,698	4,936	5,128
85	9,163	9,782	10,308	6,398	6,794	7,123
100[2]	52,500	52,500	52,500	52,500	52,500	52,500

Notes:

1. The drop orientation is with respect to the horizontal, where 0° is the side drop, and 90° is the end drop. The 0° side drop is perpendicular to foam rise and the 90° end drop is parallel to foam rise.
2. For all crush strength curves, the foam is assumed to lock-up hard at 100% strain and reach a crush strength equal to the flow stress of Type 304 stainless steel at 75 °F. The flow stress is the average of the material yield and ultimate strength: (30,000 psi + 75,000 psi) / 2 = 52,500 psi. This assumption increases simulation stability by decreasing negative volume errors, where the foam elements become so compressed and distorted that the mesh is no longer viable for the program to solve.

Table 2.12.5-9 – Benchmark Results Comparison

Result	D1 (Cold End Drop)	D2 (Warm CG-Over-Corner Drop)	D3 (Warm Side Drop)
	17 pcf foam at -15.3 °F	15 pcf foam at 100 °F	15 pcf foam at 100 °F
Max Acceleration (Test)[1]	78 g	49 g	60 g
Max Acceleration (Benchmark)[1]	83.7 g	49.4 g	60.7 g
Percent Less[3]	-6.8%	-0.8%	-1.2%
Max Crush (Test)[2]	5.44 in	11.86 in	7.10 in
Max Crush (Benchmark)	6.01 in	13.53 in	10.38 in
Percent Less[3]	-9.48%	-12.34%	-31.60%
Impact Patch (Test)	70 in OD	45 in x 68 in	33 3/8 in x 59 in
Impact Patch (Benchmark)	71.1 in OD	43.9 in x 73.8 in	33.6 in x 63.2 in
Percent Less[3]	-1.5%	2.5% x -7.9%	-0.7% x -6.6%

Notes:
1. The test accelerations were low-pass filtered at 500 Hz and the benchmark accelerations are low-pass filtered at 250 Hz, to be equivalent for full-scale.
2. All test crush measurements include a 2-in full-scale addition to compensate for impact limiter springback. A 1-in springback was observed in the half-scale side drop test and measured by the non-flatness of the impact patch, see Section 2.12.3.4.6, *Free Drop Test D3*.
3. Percent less is defined as the percentage amount less of the test result from the simulation benchmark result, where a negative (-) connotes less than.
   Percent less = -(1-test/benchmark)×100

Table 2.12.5-10 – NCT Simulation Acceleration and Crush Results Summary

Bounding Foam[1]	Orientation	Acceleration	Strain	Crush
		g	%	in
18 pcf Foam at -40 °F	Side Drop	18.3	6.6	1.4
	CG-Over-Corner (50deg) Drop	15.4	9.1	1.8
	End Drop	33.8	2.4	0.6
14 pcf Foam at 160 °F	Side Drop	11.2	9.9	2.1
	CG-Over-Corner (50deg) Drop	8.8	14.6	2.9
	End Drop	18.9	4.4	1.1

Notes:
1. Bounding foam includes the coldest NCT temperature and a positive (+) 10% manufacturing tolerance applied to the nominal 16 pcf foam density that subsequent develops a conservatively stronger foam stress versus strain curve. Alternately, the converse bound foam includes a temperature in excess of the NCT bulk average foam temperature and a negative (-) 10% manufacturing tolerance applied to the nominal 16 pcf foam density that subsequently develops a conservatively weaker foam stress versus strain curve.

Table 2.12.5-11 – HAC Simulation Acceleration and Crush Results Summary

Bounding Foam[3]	Orientation	Acceleration	Strain	Crush	Minimum Foam[2]
		g	%	in	in
18 pcf Foam at -40 °F	Side Drop	88.9	33.6	7.1	NA
	CG-Over-Corner (50deg) Drop	68.3	47.4	9.4	
	End Drop	92.8	22.1	5.5	
	10° Slapdown Drop[1]	66.6 / 65.0	43.6 / 29.4	9.2 / 6.2	
	20° Slapdown Drop[1]	65.0 / 43.6	52.1 / 20.4	11.0 / 4.3	
14 pcf Foam at 160 °F	Side Drop	55.6	57.3	12.1	8.9
	CG-Over-Corner (50deg) Drop	46.0	79.8	15.8	3.9
	End Drop	49.0	42.6	10.6	14.1
	10° Slapdown Drop[1]	46.9 / 45.4	67.2 / 54.9	14.2 / 11.6	8.3 / 10.0
	20° Slapdown Drop[1]	44.3 / 30.5	76.7 / 42.3	16.2 / 9.0	7.4 / 12.6

Notes:
1. Slapdown results are listed in order of primary impact / secondary impact.
2. The minimum foam measurement is taken from the cask outer surface to the impact limiter foam outer surface, which excludes the thickness and any spring-back of the impact limiter outer shell.
3. Bounding foam includes the coldest NCT temperature and a positive (+) 10% manufacturing tolerance applied to the nominal 16 pcf foam density that subsequent develops a conservatively stronger foam stress versus strain curve. Alternately, the converse bound foam includes a temperature in excess of the NCT bulk average foam temperature and a negative (-) 10% manufacturing tolerance applied to the nominal 16 pcf foam density that subsequently develops a conservatively weaker foam stress versus strain curve.

380-B Cold HAC End Drop (30 FT)

Upper Impact Limiter

Dummy Payload

Dummy Cask

Cask Impact Limiter Lug

Lower Impact Limiter

Drop Pad

Symmetry Plane
(Z-axis normal)
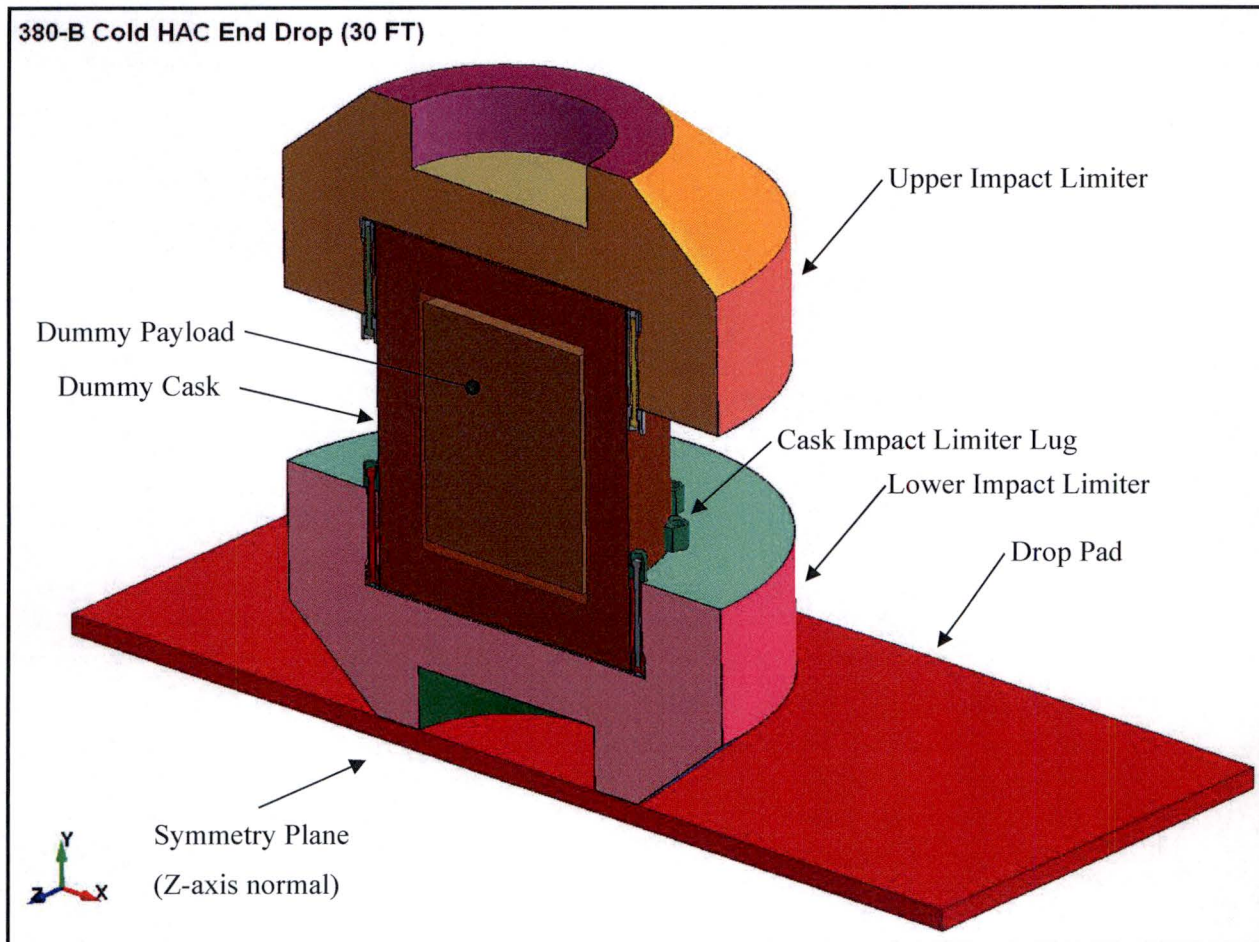
Figure 2.12.5-1 – 380-B FEA Model
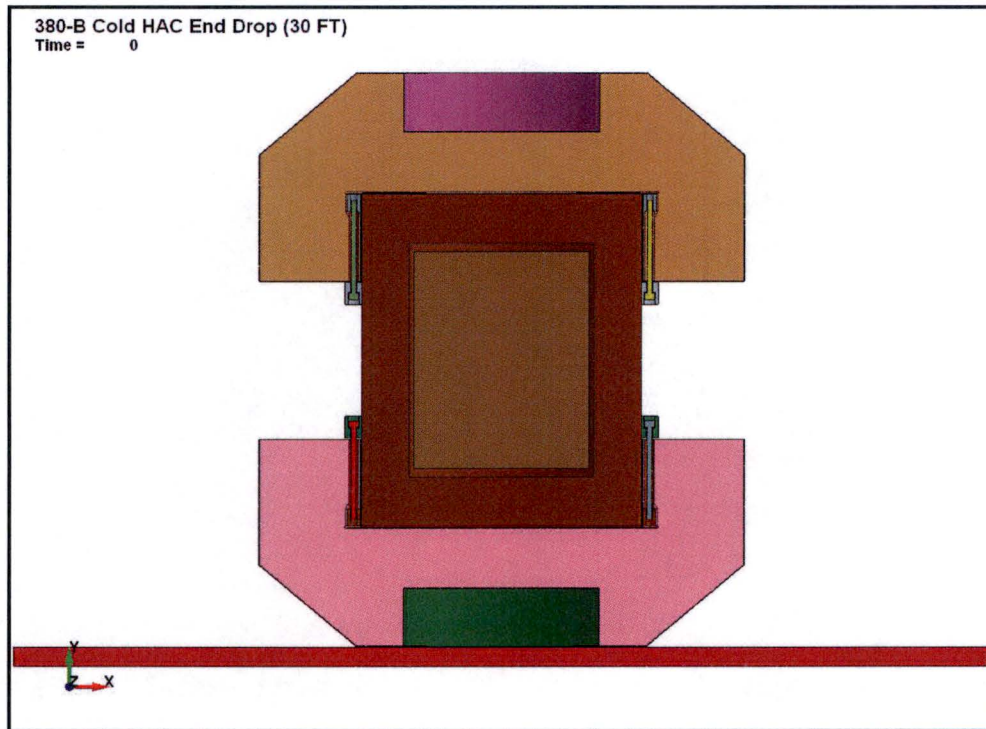
Figure 2.12.5-2 – End Drop Orientation
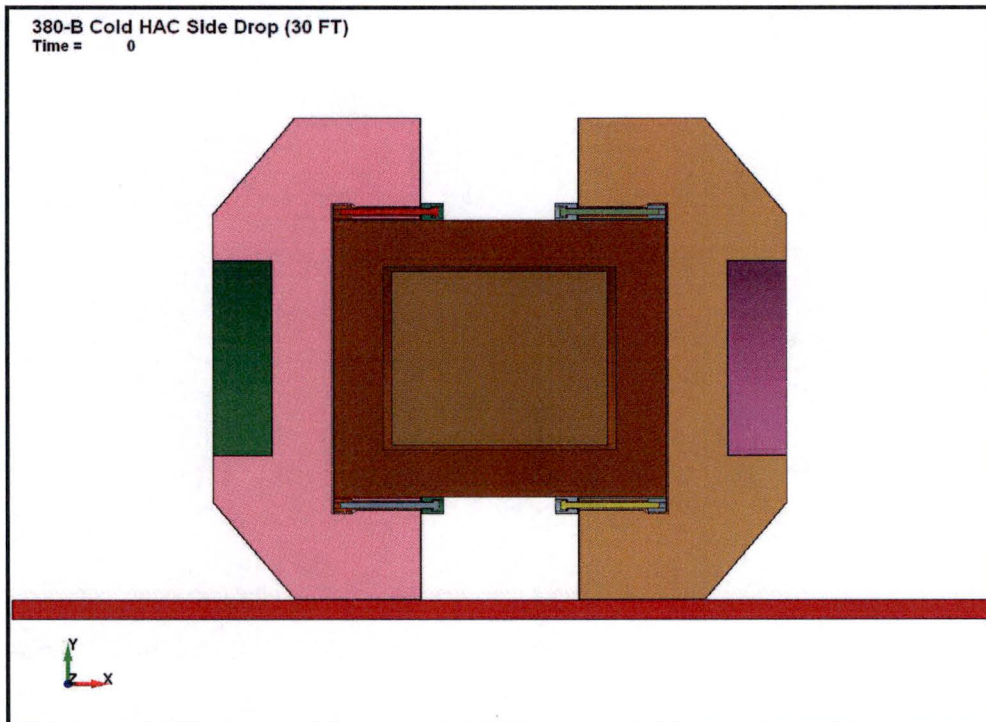
Figure 2.12.5-3 – Side Drop Orientation
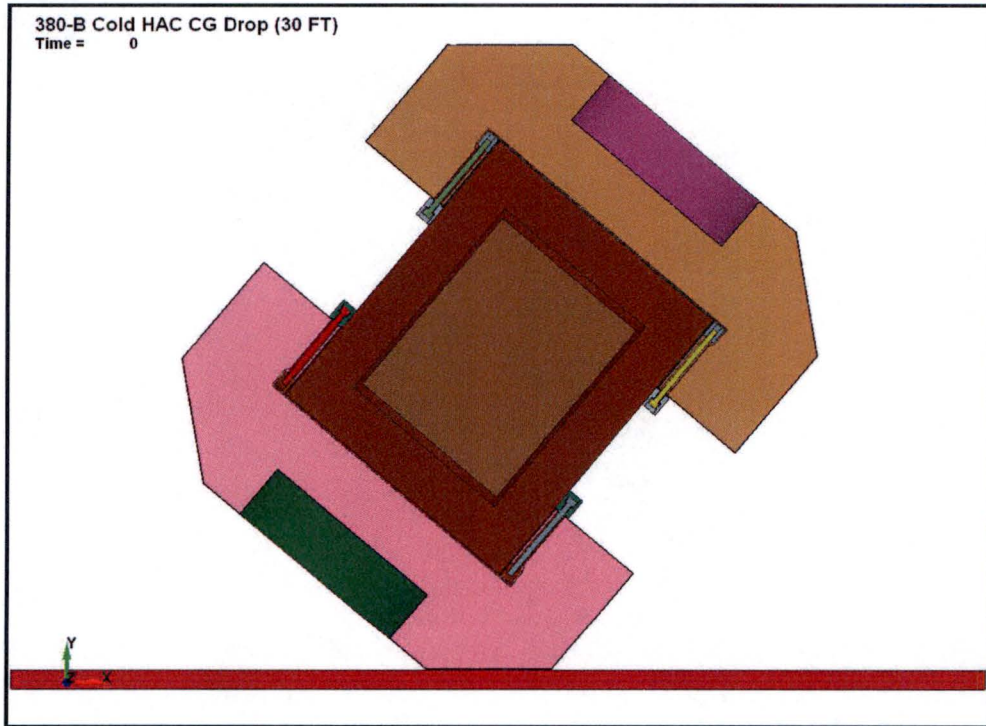
Figure 2.12.5-4 – Center of Gravity Over Corner Drop Orientation (50°)
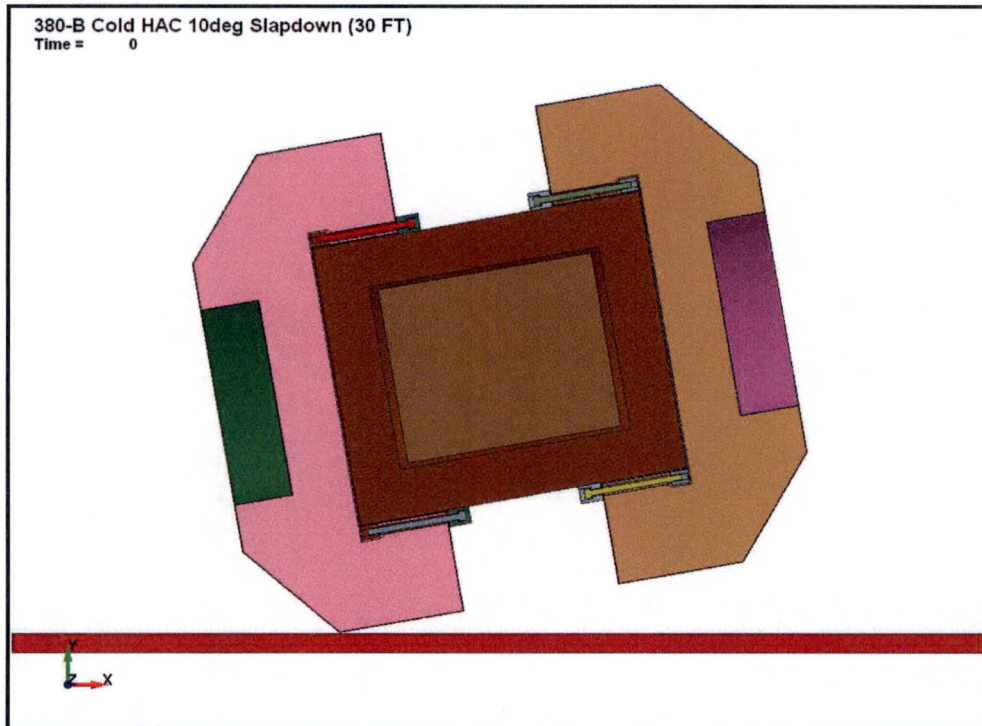
Figure 2.12.5-5 – 10° Slapdown Orientation
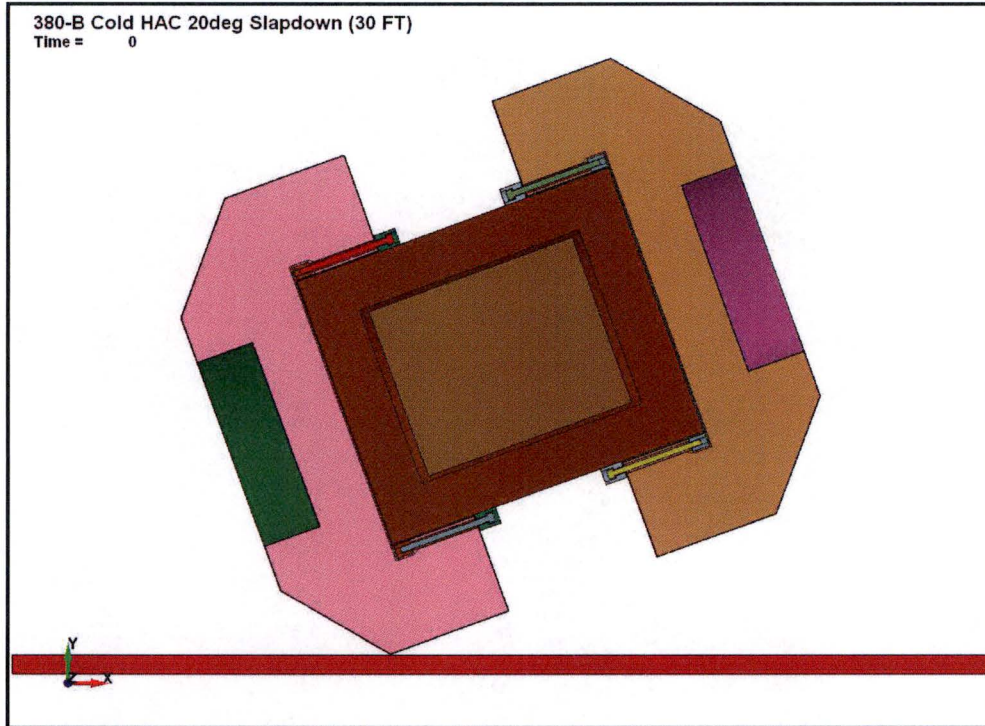
Figure 2.12.5-6 – 20° Slapdown Orientation

Security-Related Information
Figure Withheld Under 10 CFR 2.390.

Figure 2.12.5-7 – FEA Model Outer Dimensions

Security-Related Information
Figure Withheld Under 10 CFR 2.390.

Figure 2.12.5-8 – FEA Model Impact Limiter Cask Attachment Lug View

Security-Related Information
Figure Withheld Under 10 CFR 2.390.

Figure 2.12.5-9 – FEA Model Impact Limiter Attachment Bolt View

Security-Related Information
Figure Withheld Under 10 CFR 2.390.

Figure 2.12.5-10 – Initial Foam Measurements
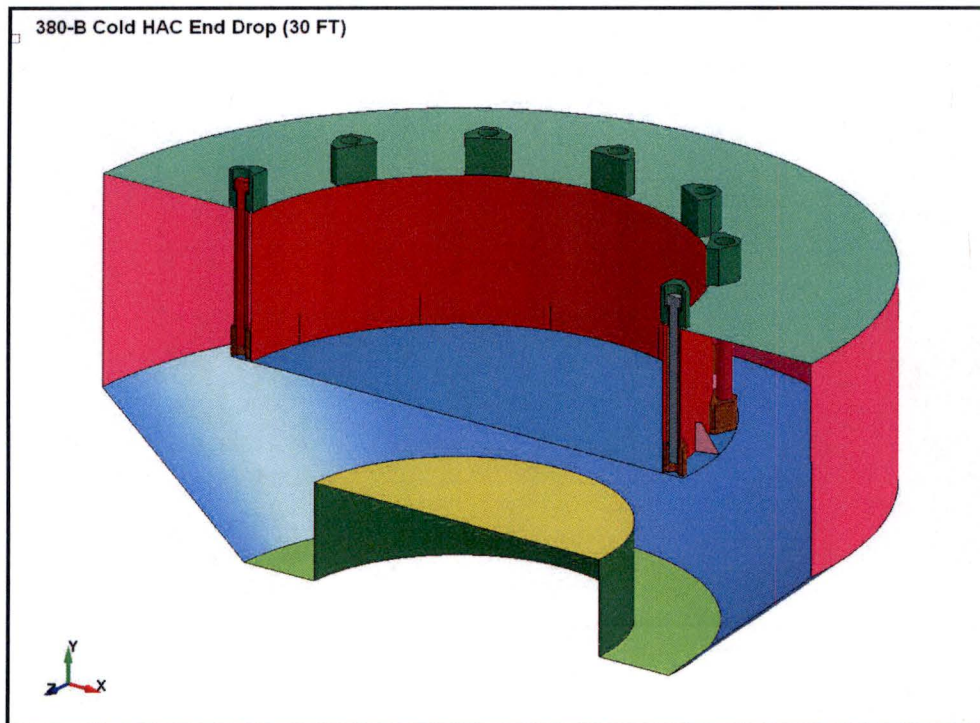
Figure 2.12.5-11 – FEA Model Impact Limiter Shell and Attachment Components
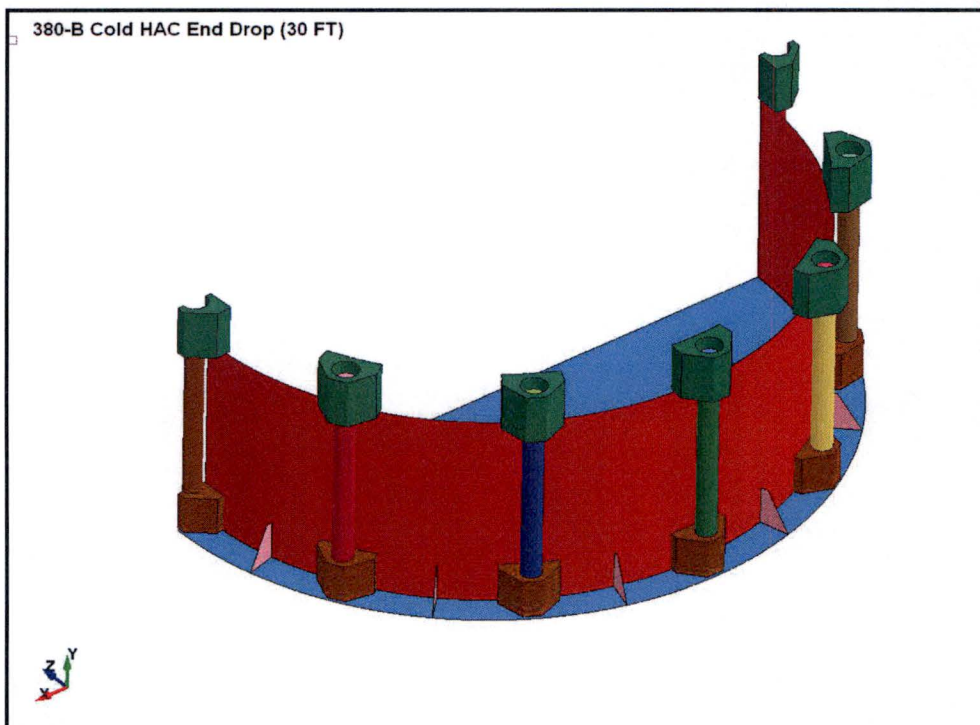
Figure 2.12.5-12 – FEA Model Impact Limiter Inner Shell and Attachment Components
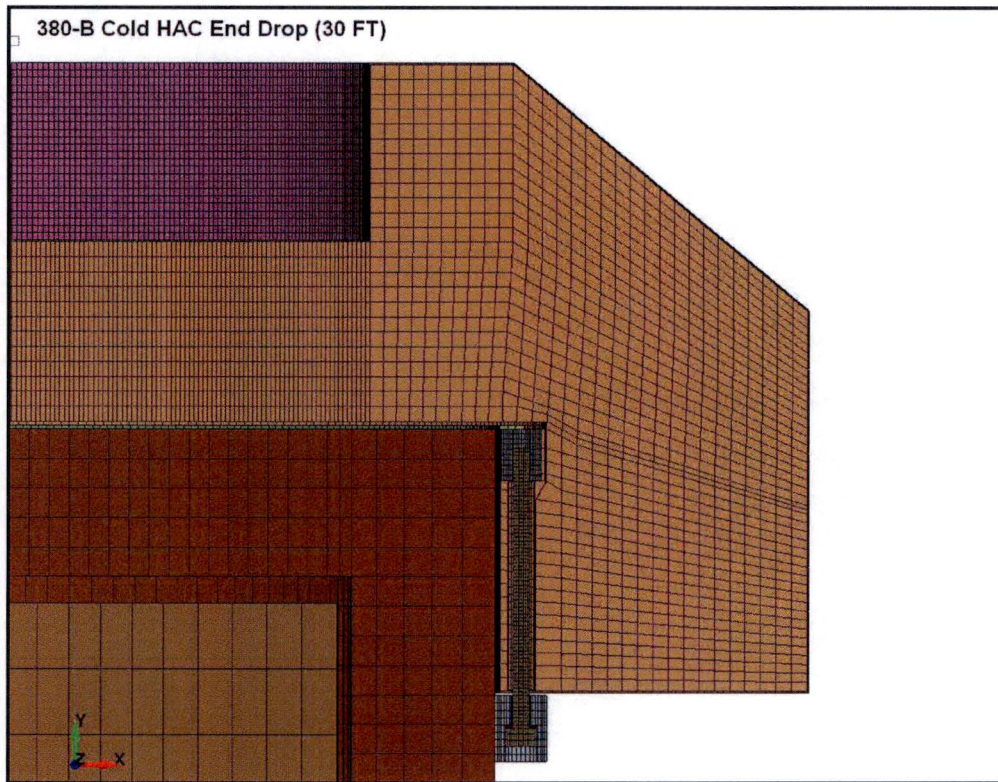
Figure 2.12.5-13 – FEA Model Upper Impact Limiter Mesh View
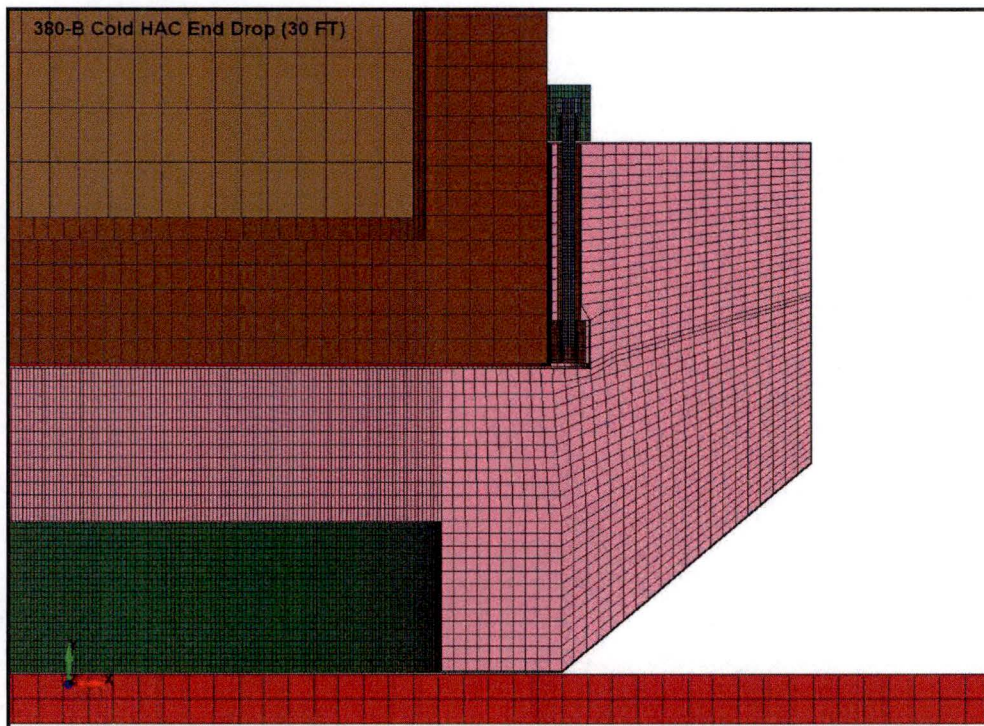
Figure 2.12.5-14 – FEA Model Lower Impact Limiter Mesh View
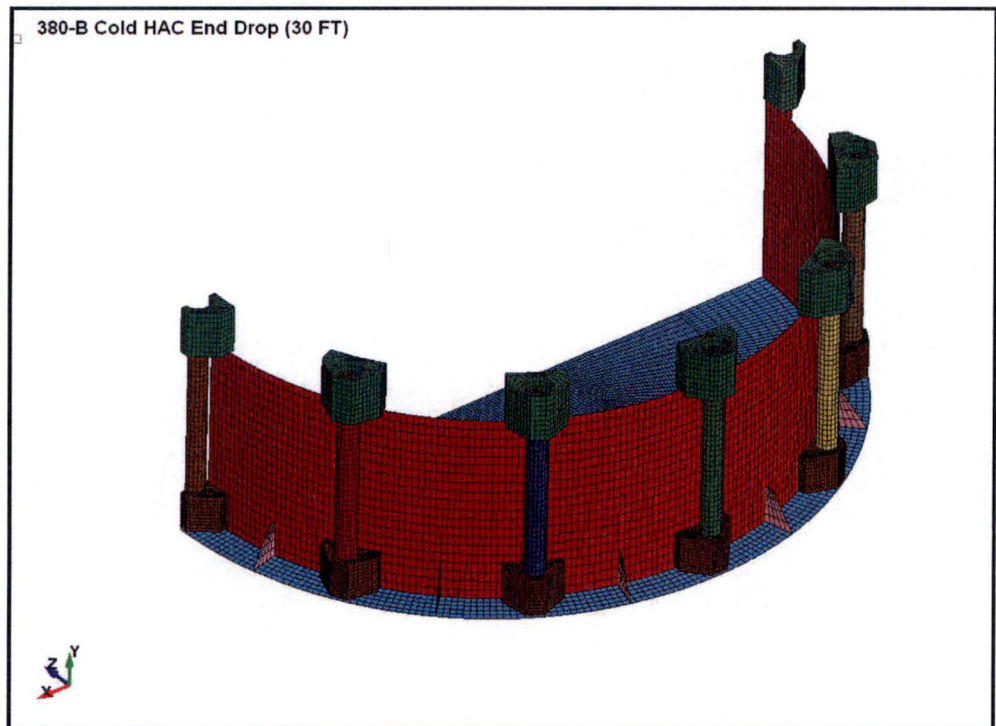
Figure 2.12.5-15 – FEA Model Impact Limiter Inner Shell and Attachment Components Mesh View
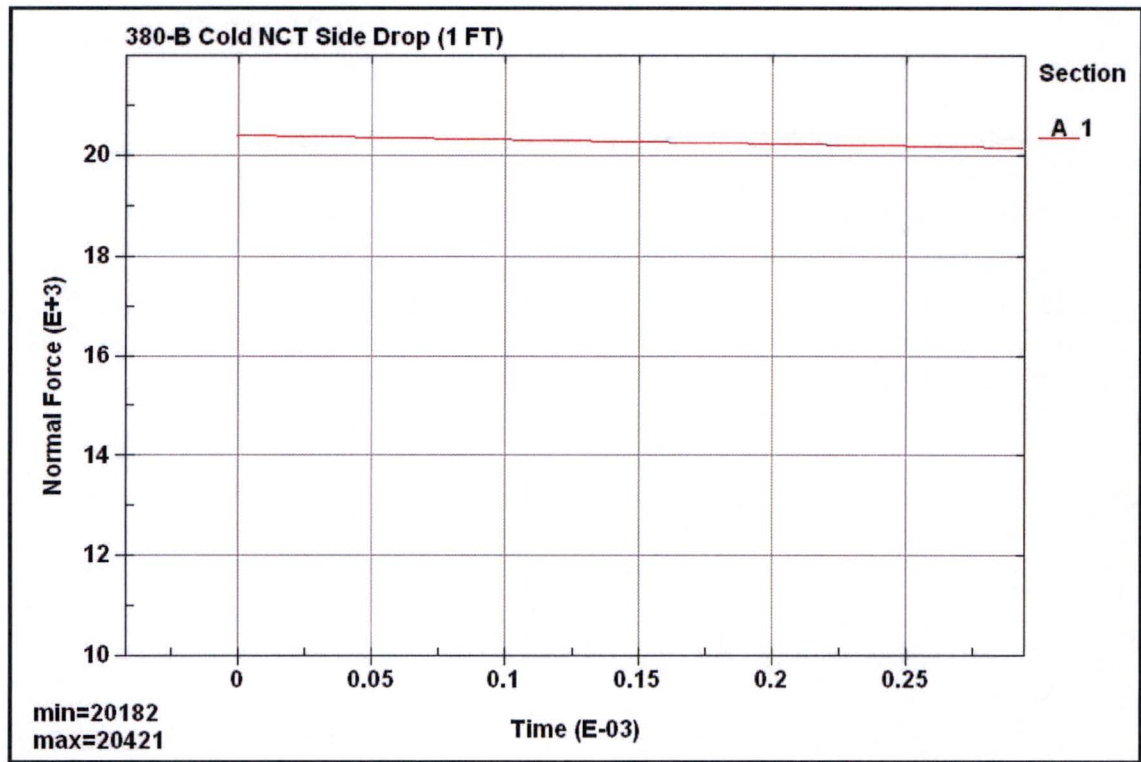
Figure 2.12.5-16 – Average Upper Impact Limiter Bolt Preload
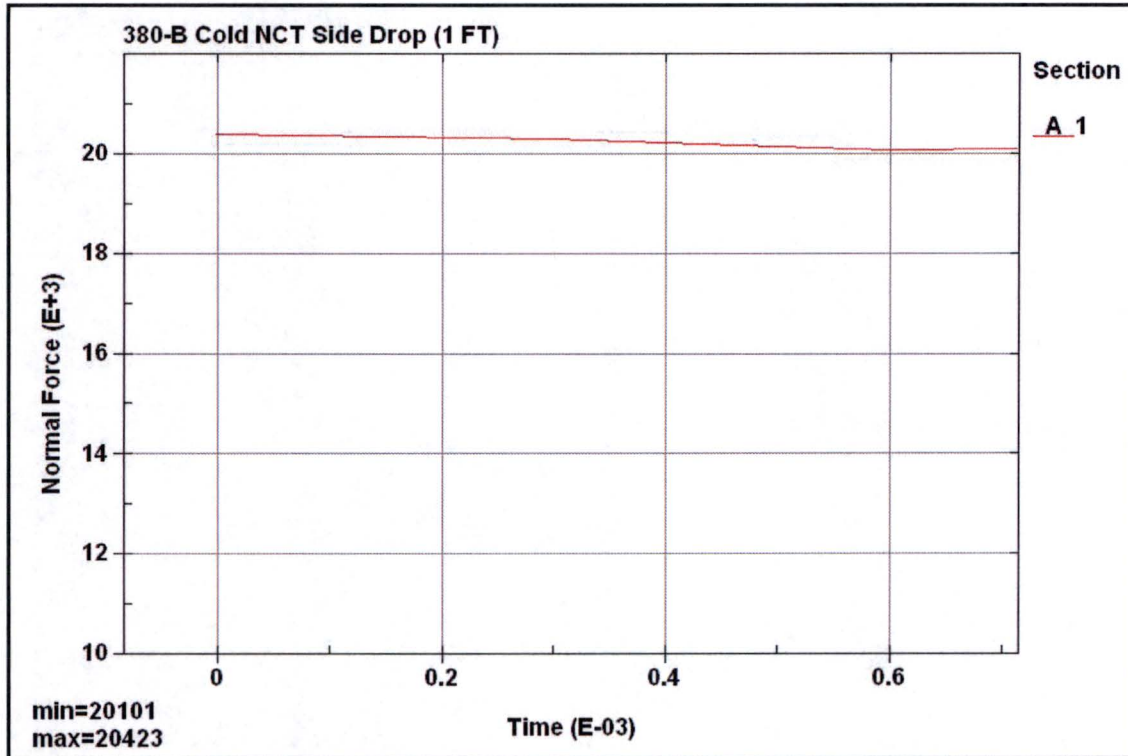
Figure 2.12.5-17 – Average Lower Impact Limiter Bolt Preload
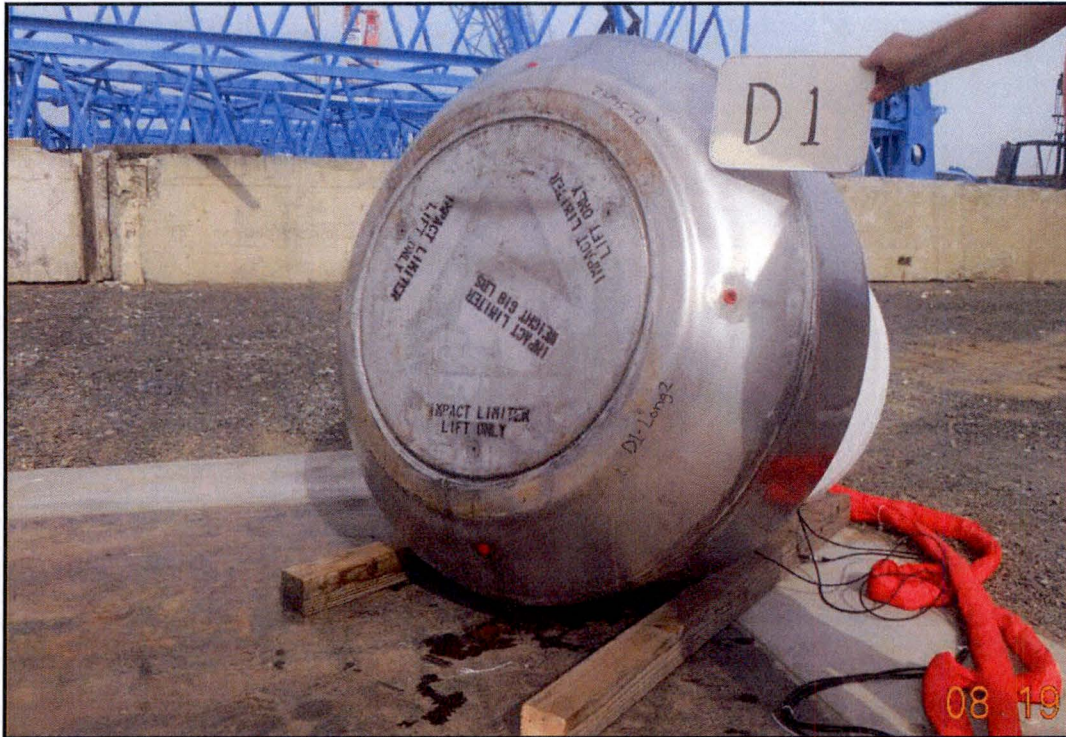
Figure 2.12.5-18 – CTU-1 D1 Damage to Bottom Surface
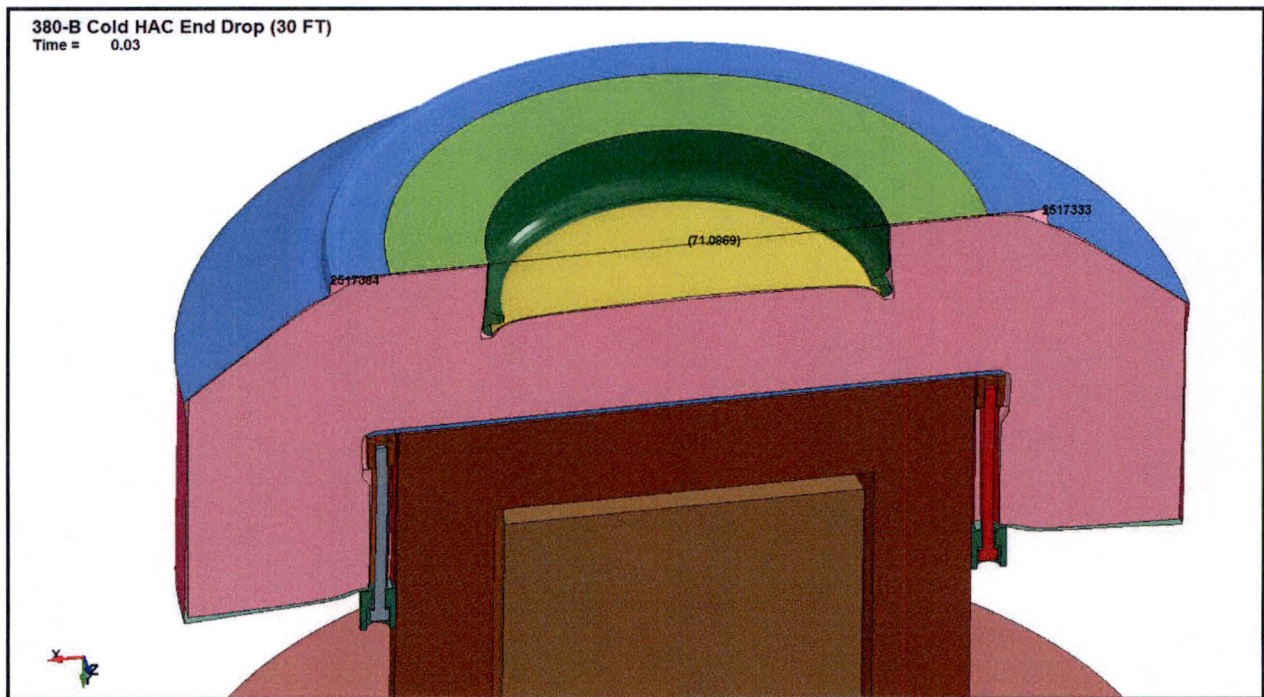
Figure 2.12.5-19 – Benchmark D1 Damage to Bottom Surface

Figure 2.12.5-20 – CTU-2 Damage after D2 Free Drop Test
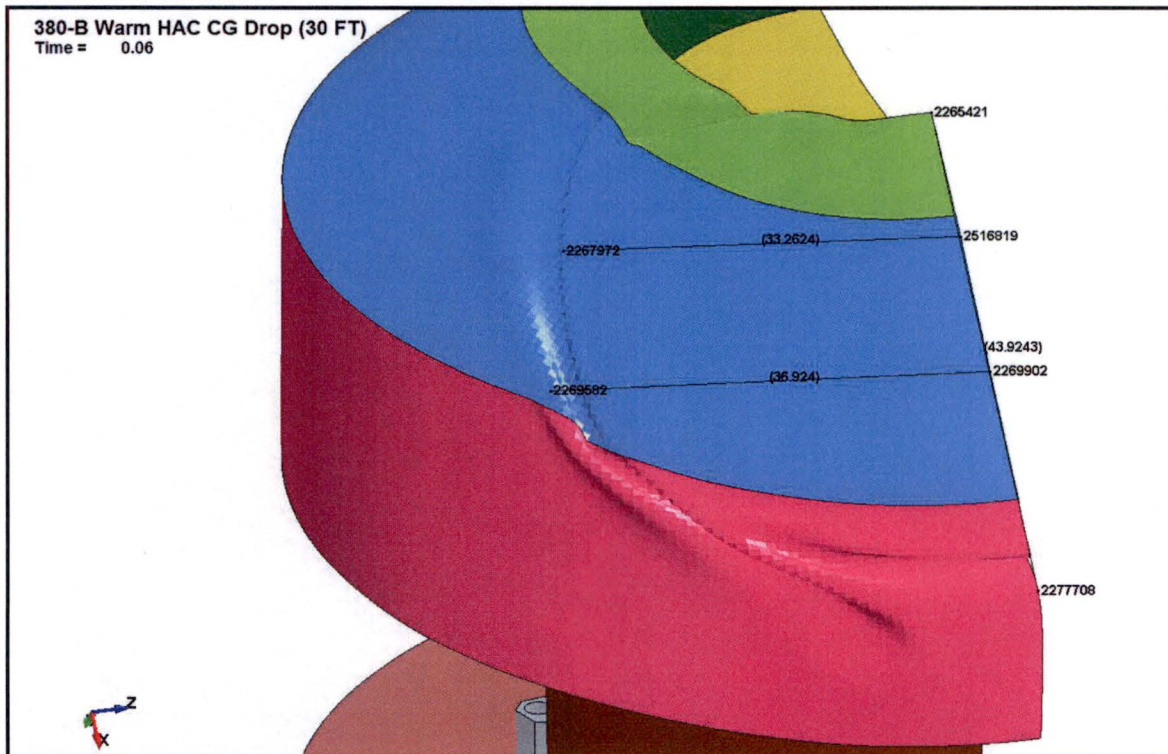
Figure 2.12.5-21 – Benchmark D2 Damage to Bottom Surface

Figure 2.12.5-22 – CTU-3.4 Condition after D3 Free Drop Test
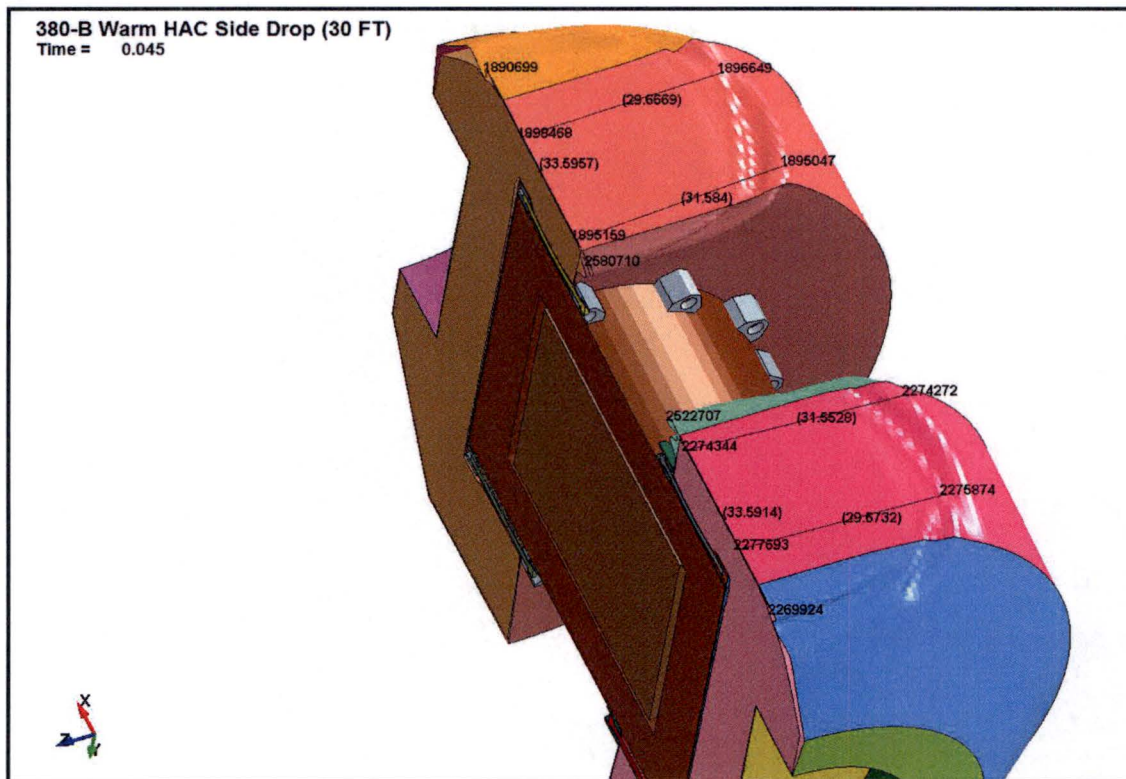
Figure 2.12.5-23 – Benchmark D3 Damage to Bottom Surface
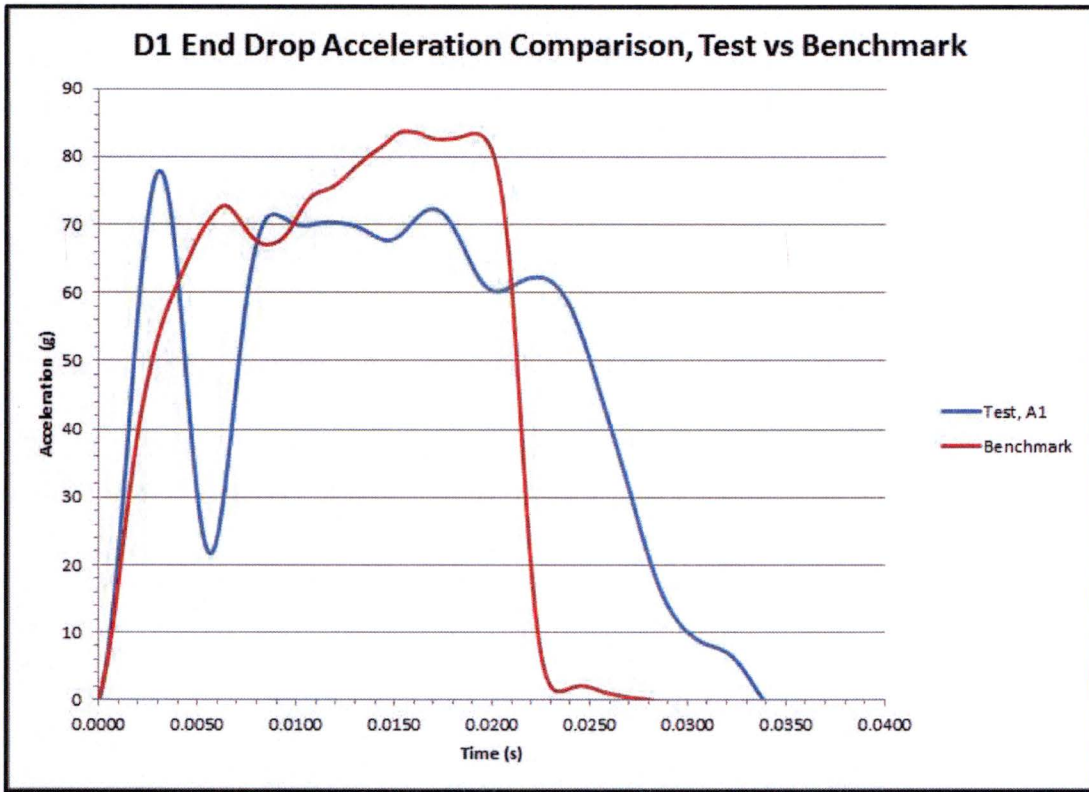
Figure 2.12.5-24 – Benchmark D1 End Drop Acceleration
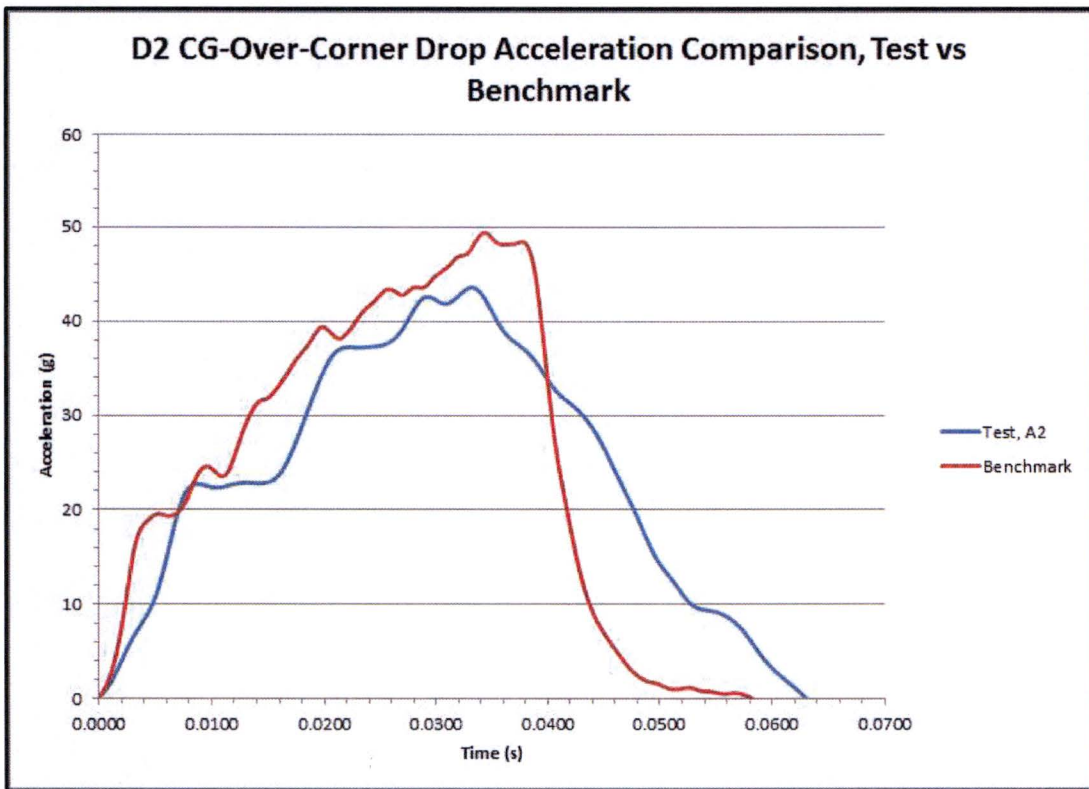
Figure 2.12.5-25 – Benchmark D2 CG-Over-Corner Drop Acceleration
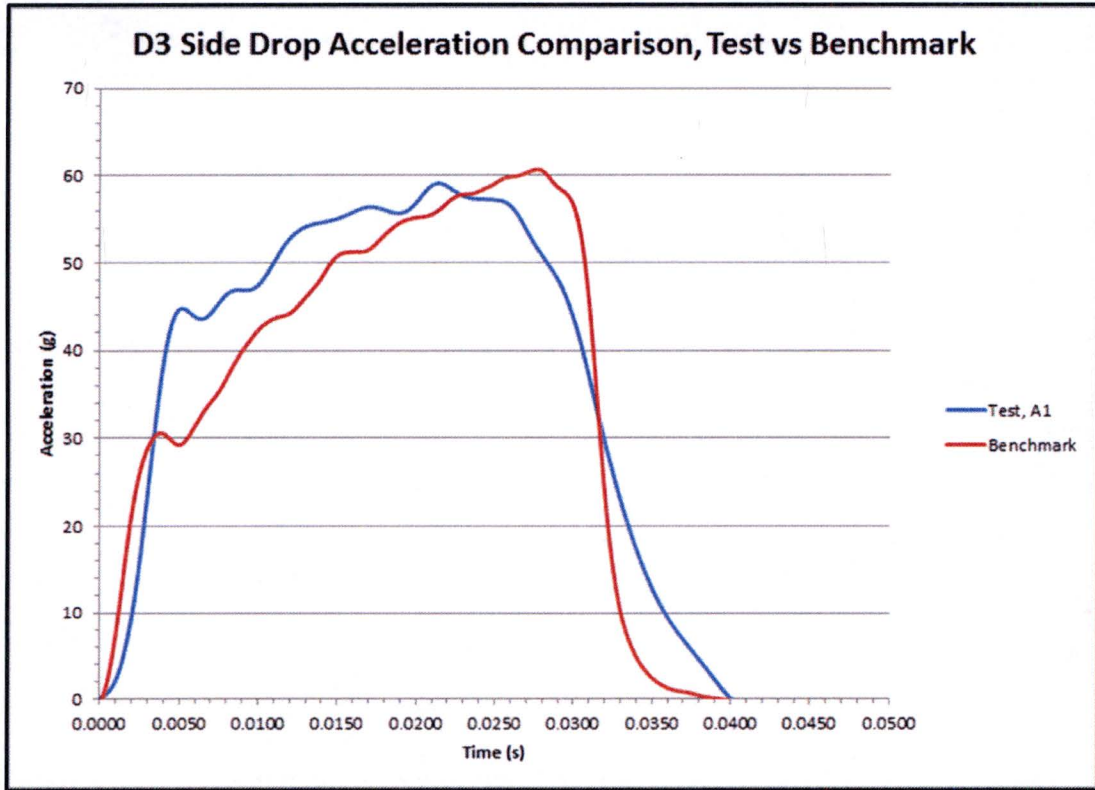
Figure 2.12.5-26 – Benchmark D3 Side Drop Acceleration
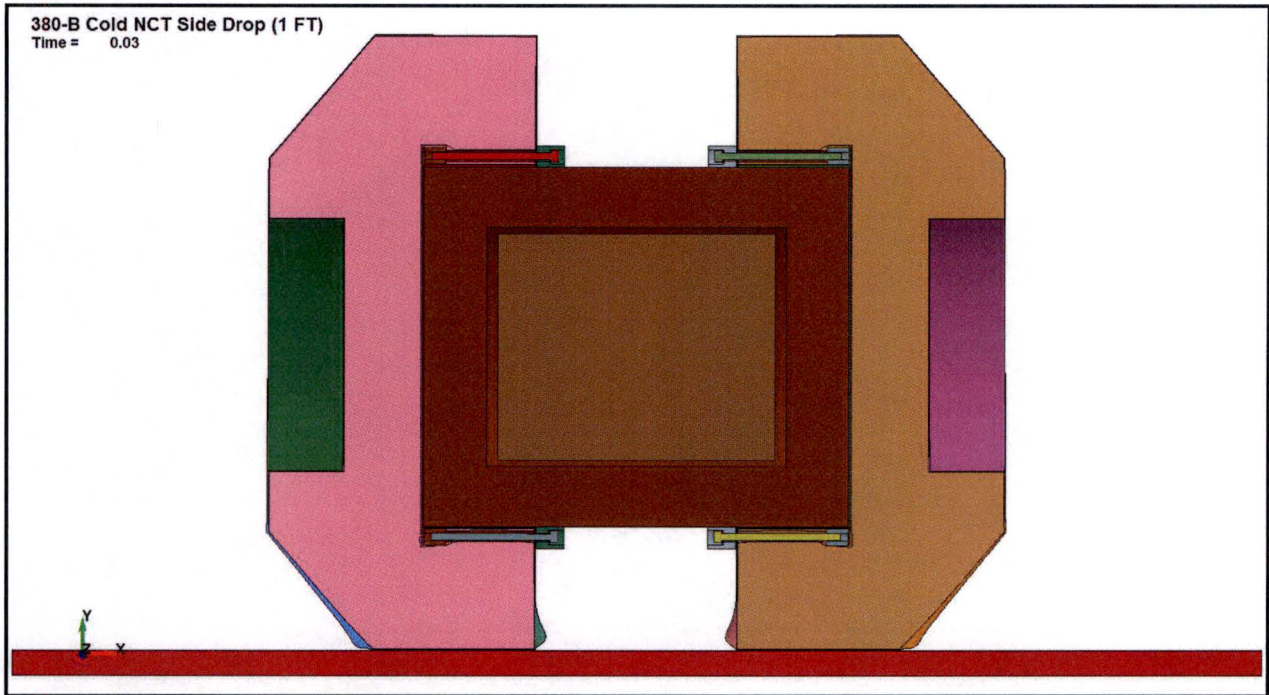
Figure 2.12.5-27 – Cold NCT Side Drop Deformation
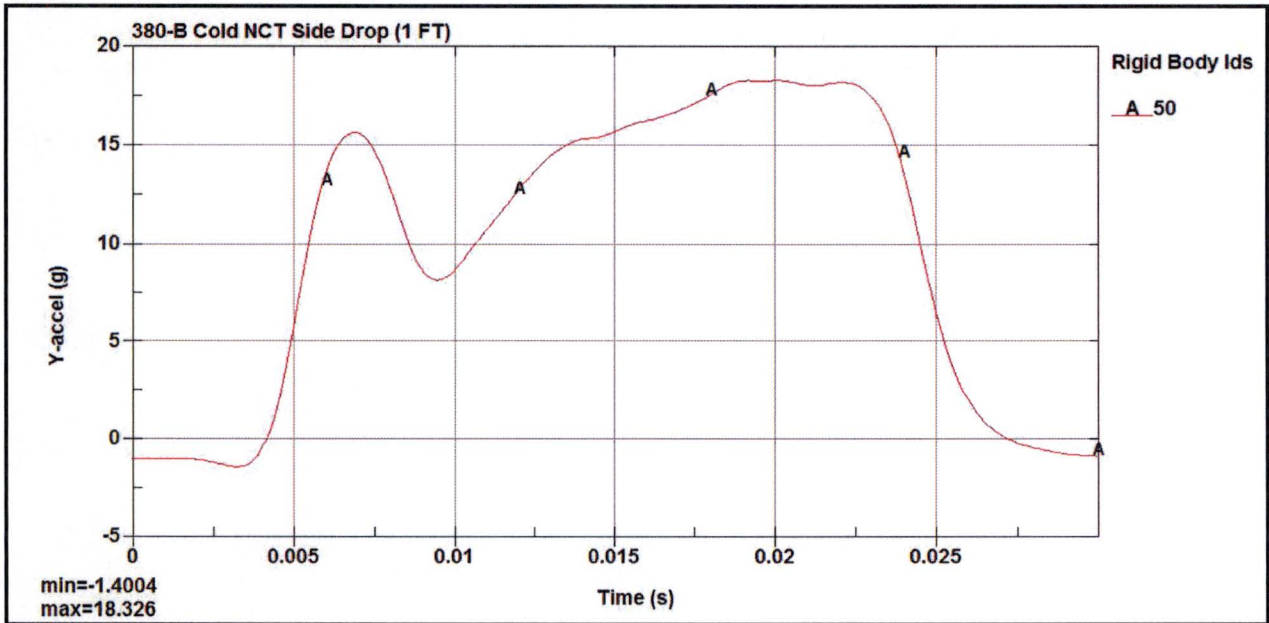
Figure 2.12.5-28 – Cold NCT Side Drop Acceleration
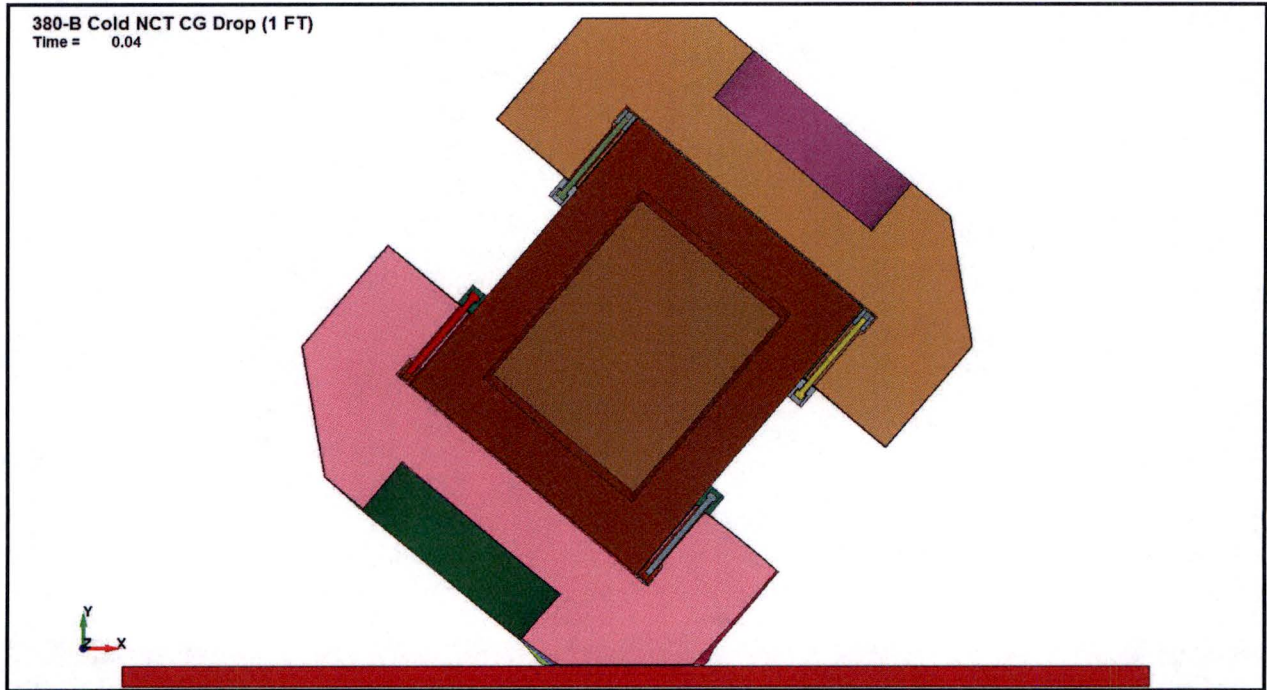
Figure 2.12.5-29 – Cold NCT CG-Over-Corner Drop Deformation
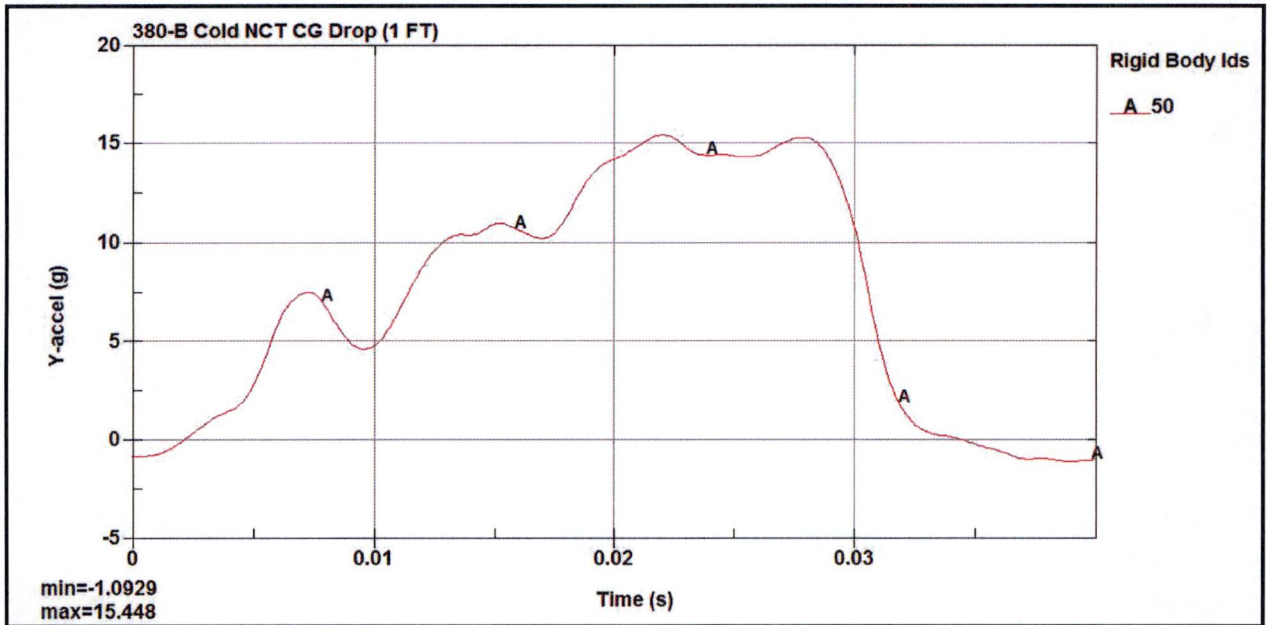
Figure 2.12.5-30 – Cold NCT CG-Over-Corner Drop Acceleration
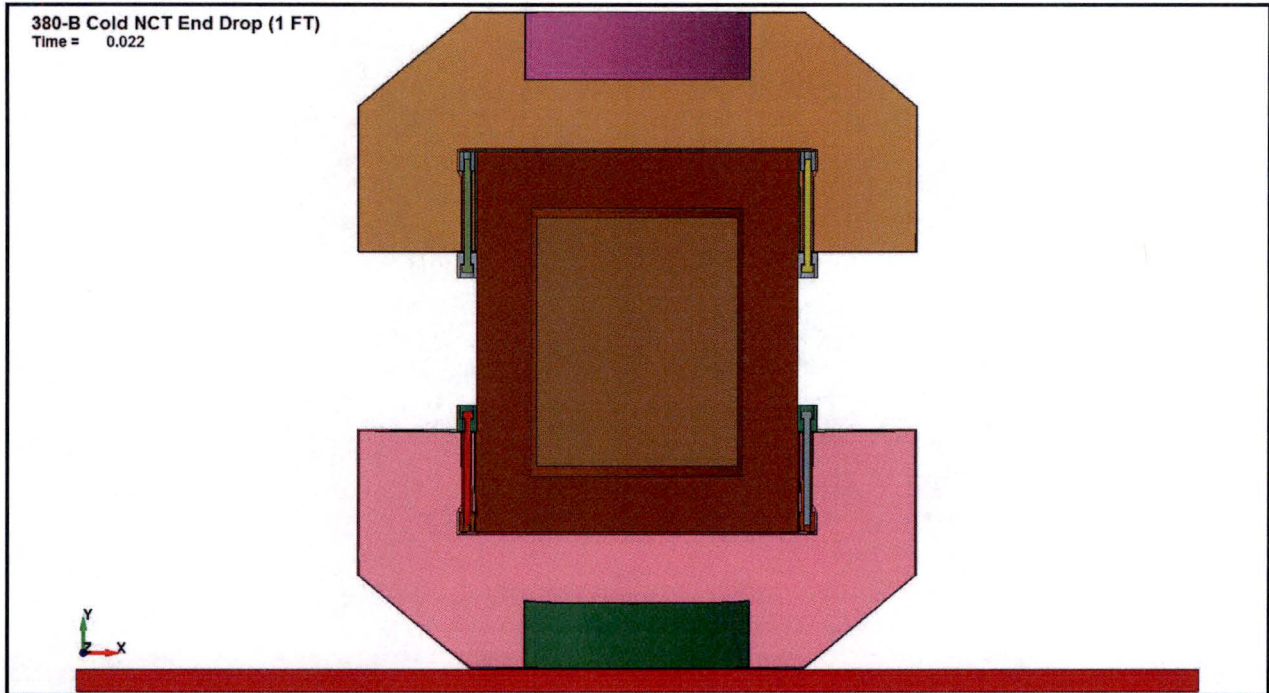
Figure 2.12.5-31 – Cold NCT End Drop Deformation
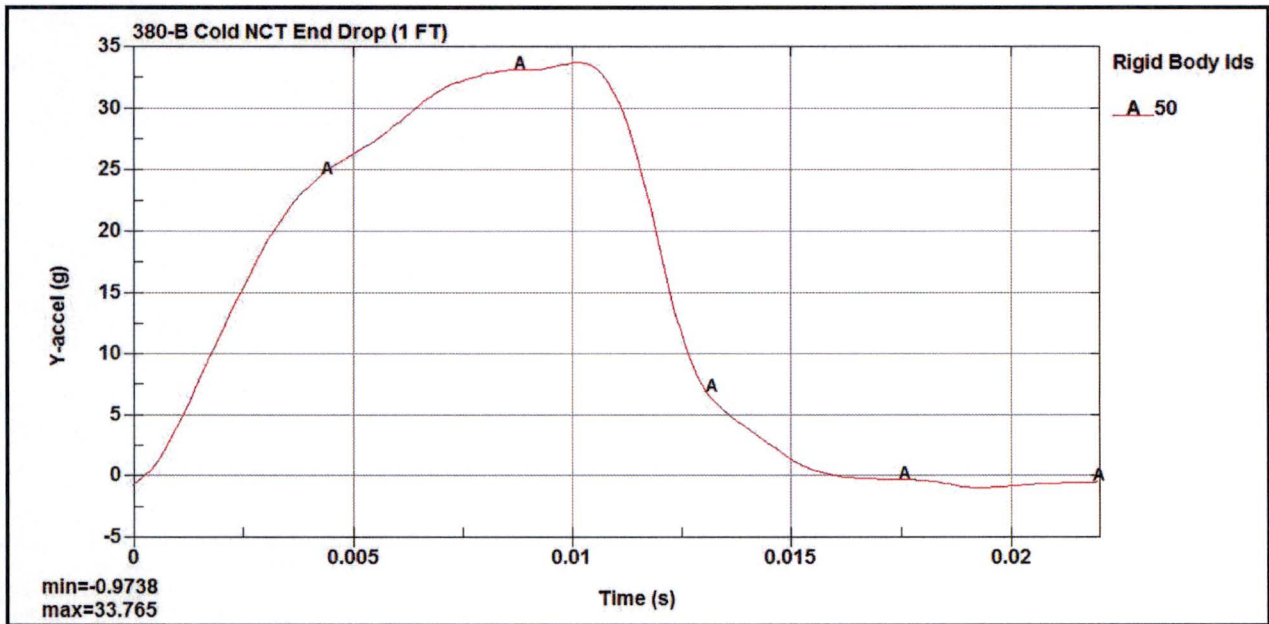
Figure 2.12.5-32 – Cold NCT End Drop Acceleration
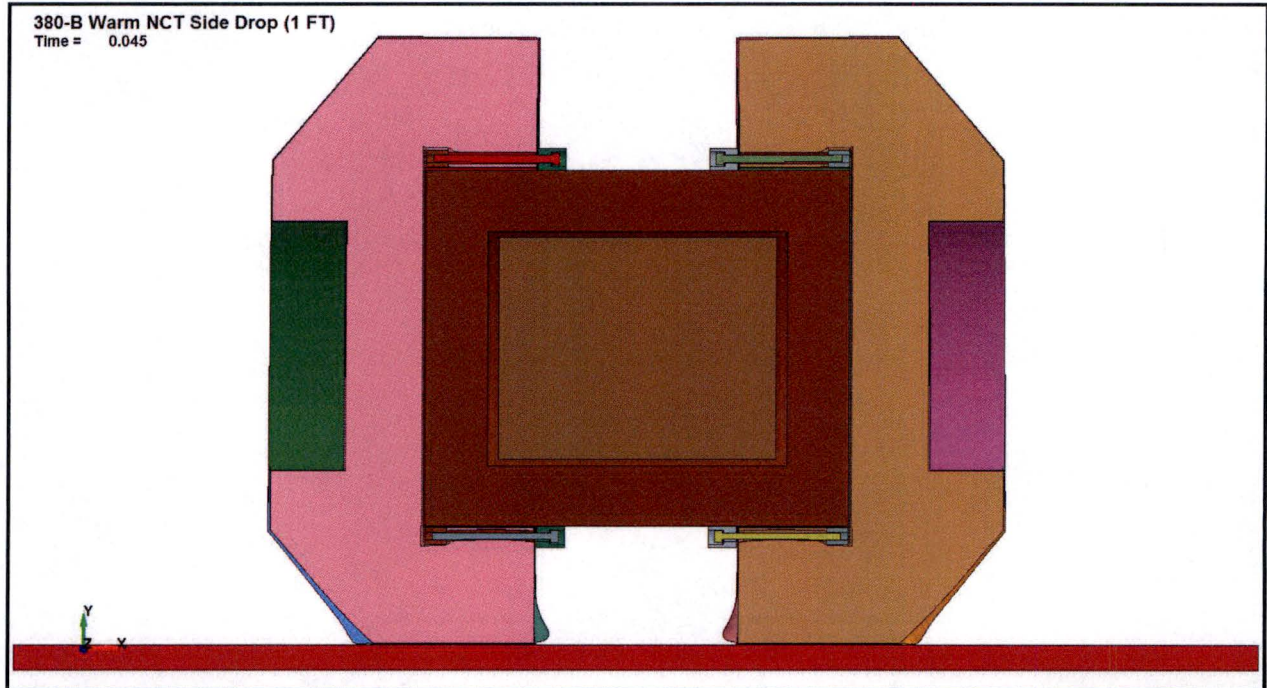
Figure 2.12.5-33 – Warm NCT Side Drop Deformation
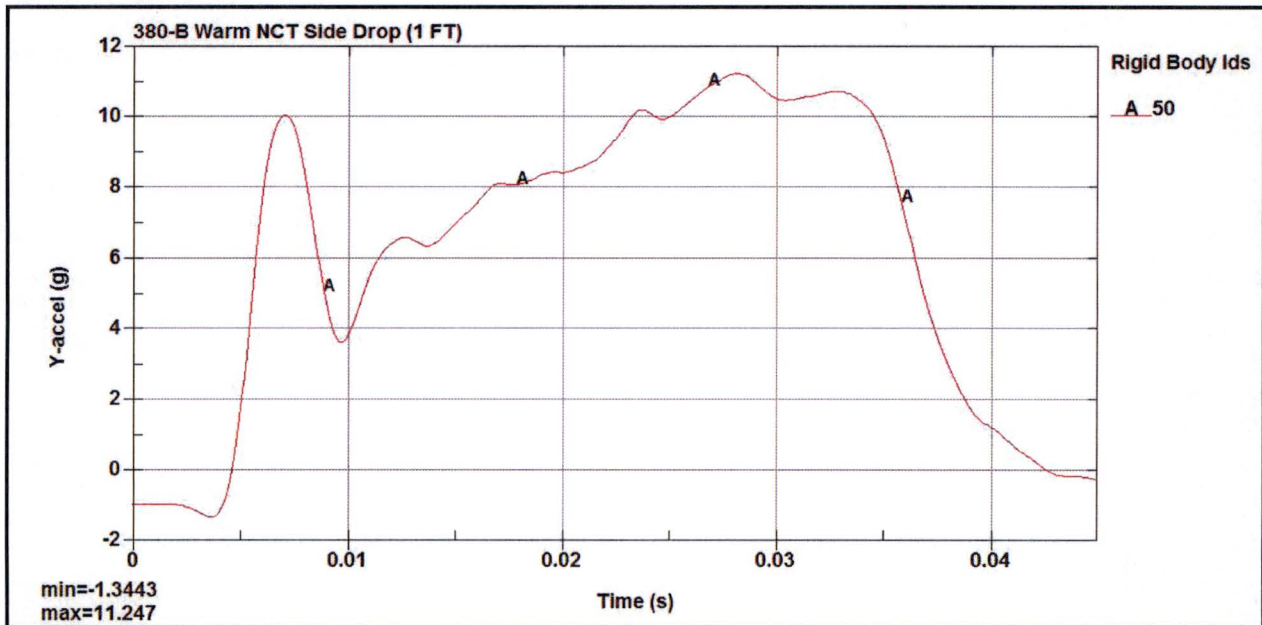
Figure 2.12.5-34 – Warm NCT Side Drop Acceleration
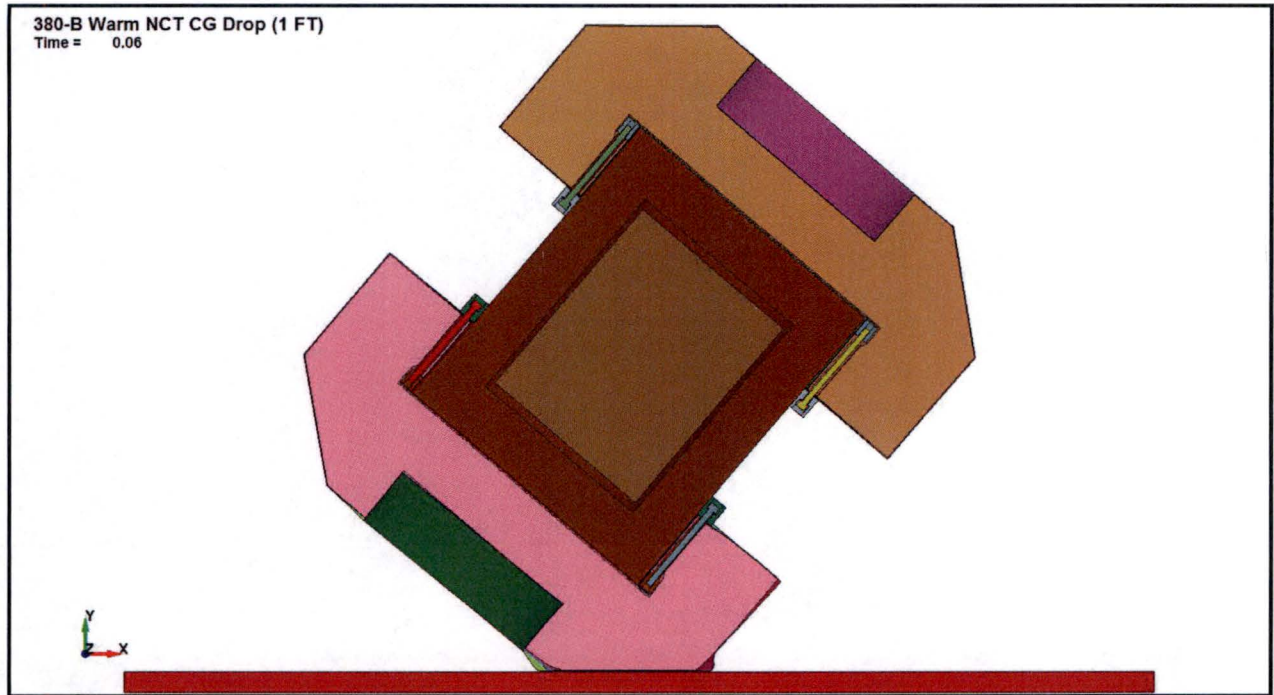
Figure 2.12.5-35 – Warm NCT CG-Over-Corner Drop Deformation
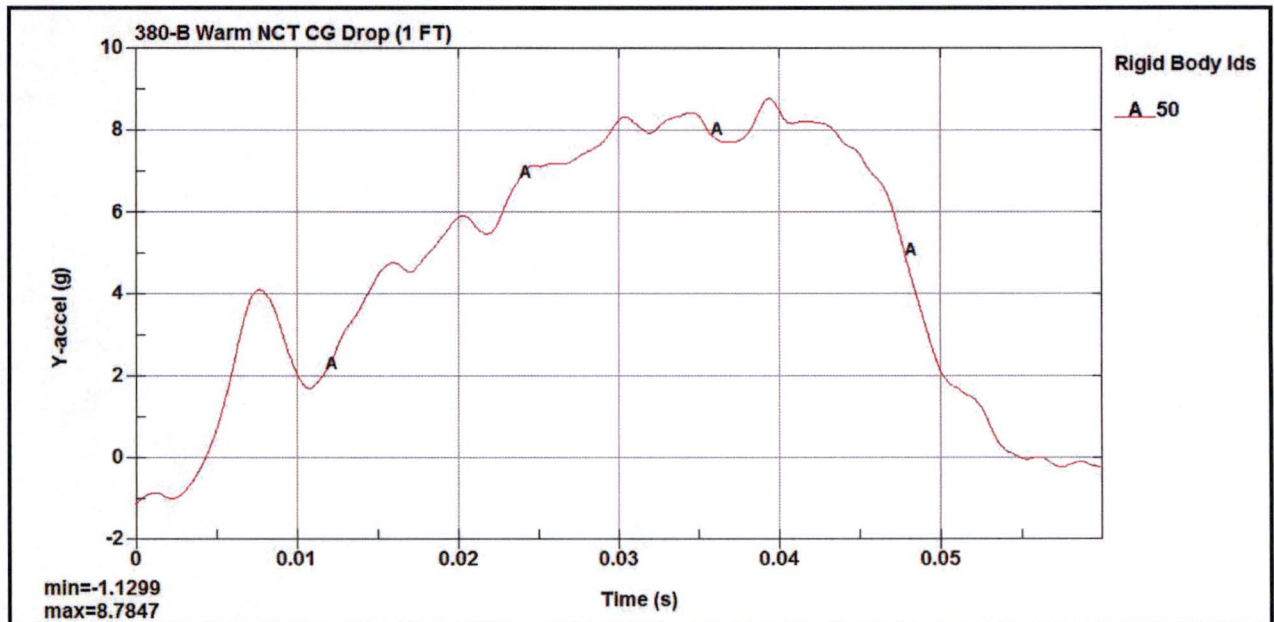
Figure 2.12.5-36 – Warm NCT CG-Over-Corner Drop Acceleration
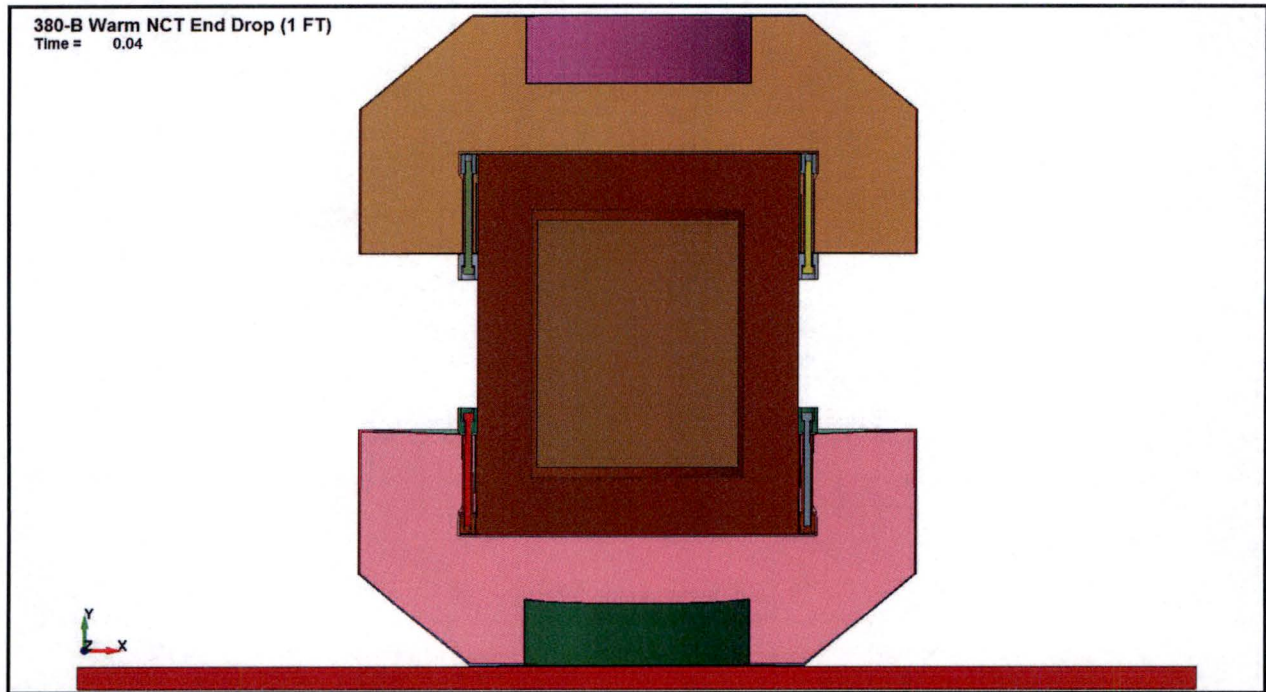
Figure 2.12.5-37 – Warm NCT End Drop Deformation
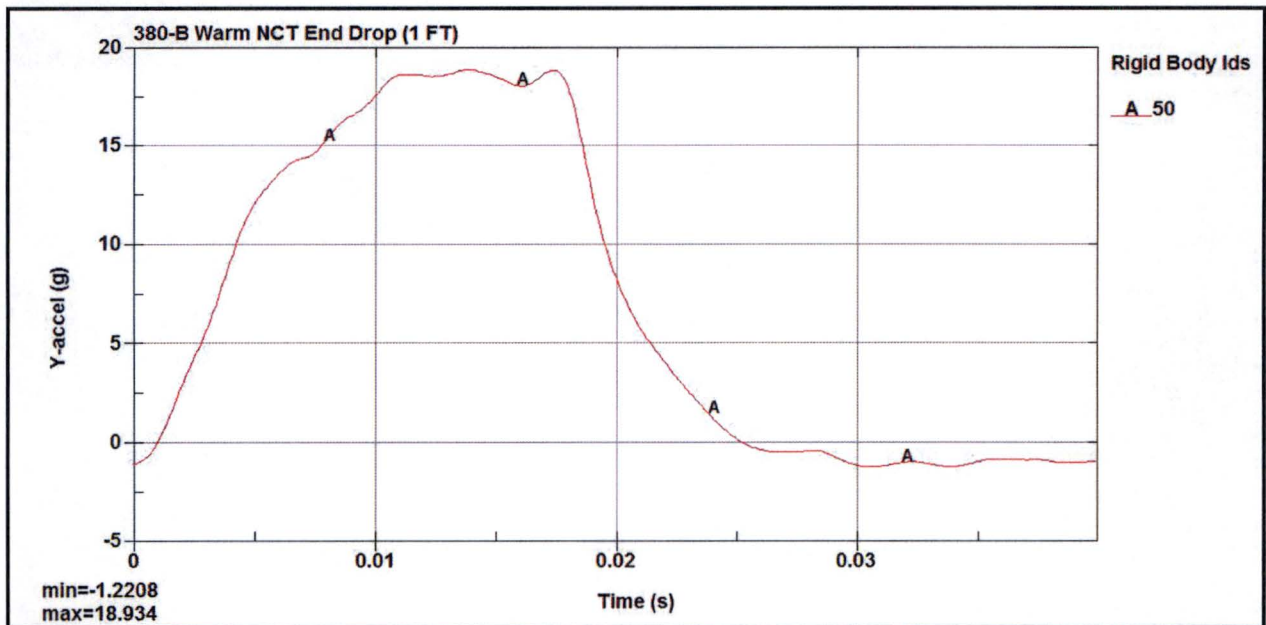
Figure 2.12.5-38 – Warm NCT End Drop Acceleration
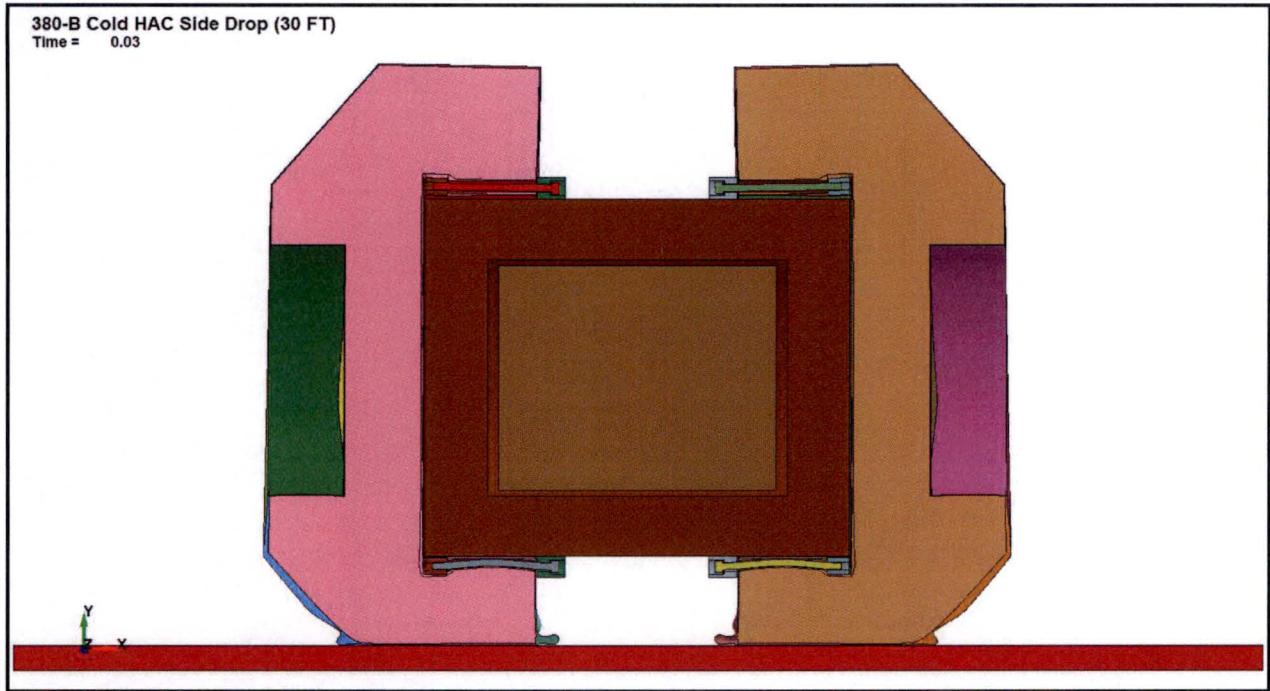
Figure 2.12.5-39 – Cold HAC Side Drop Deformation
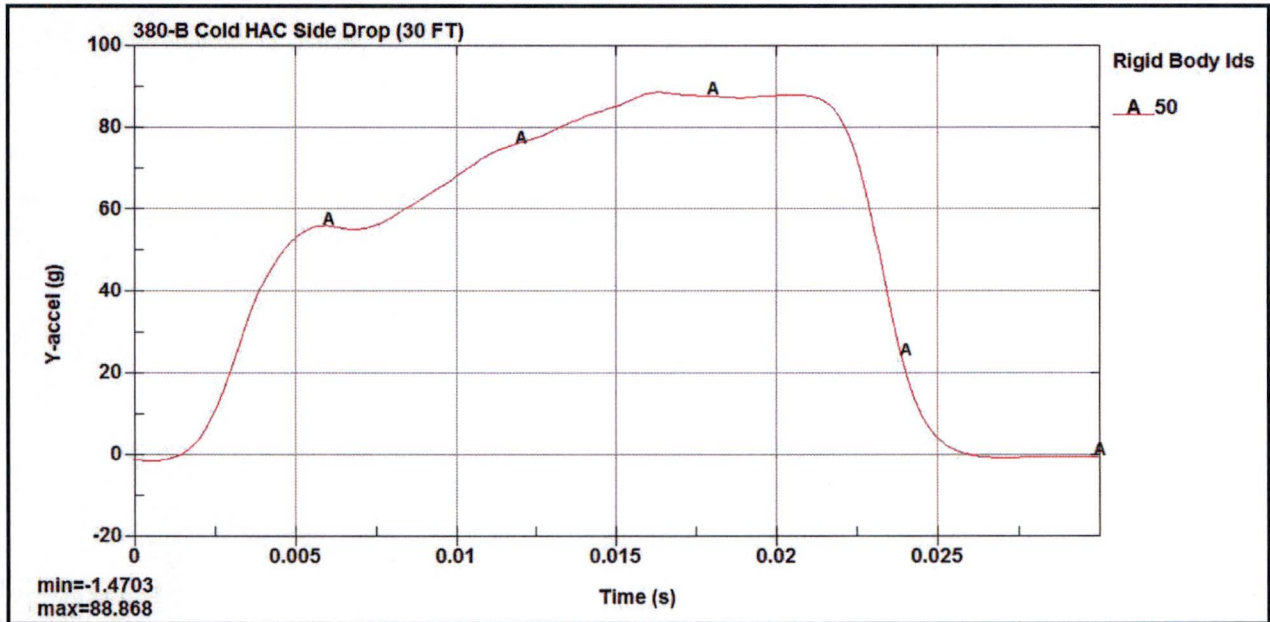
Figure 2.12.5-40 – Cold HAC Side Drop Acceleration
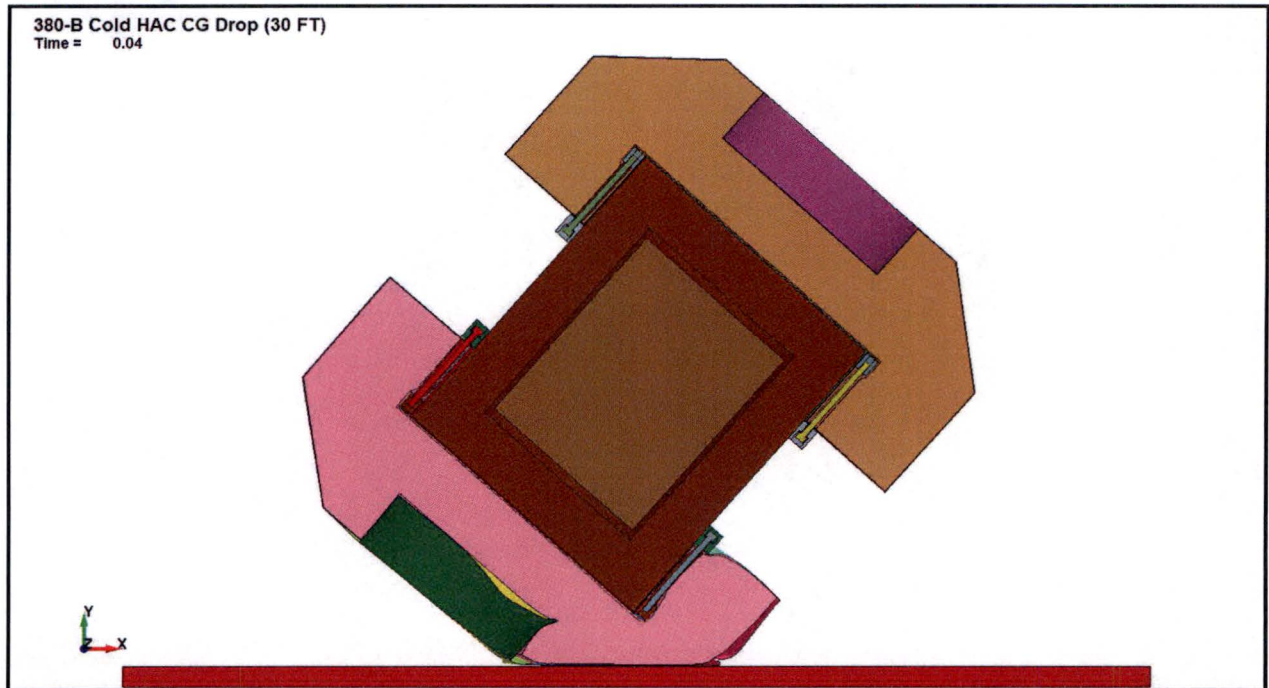
Figure 2.12.5-41 – Cold HAC CG-Over-Corner Drop Deformation
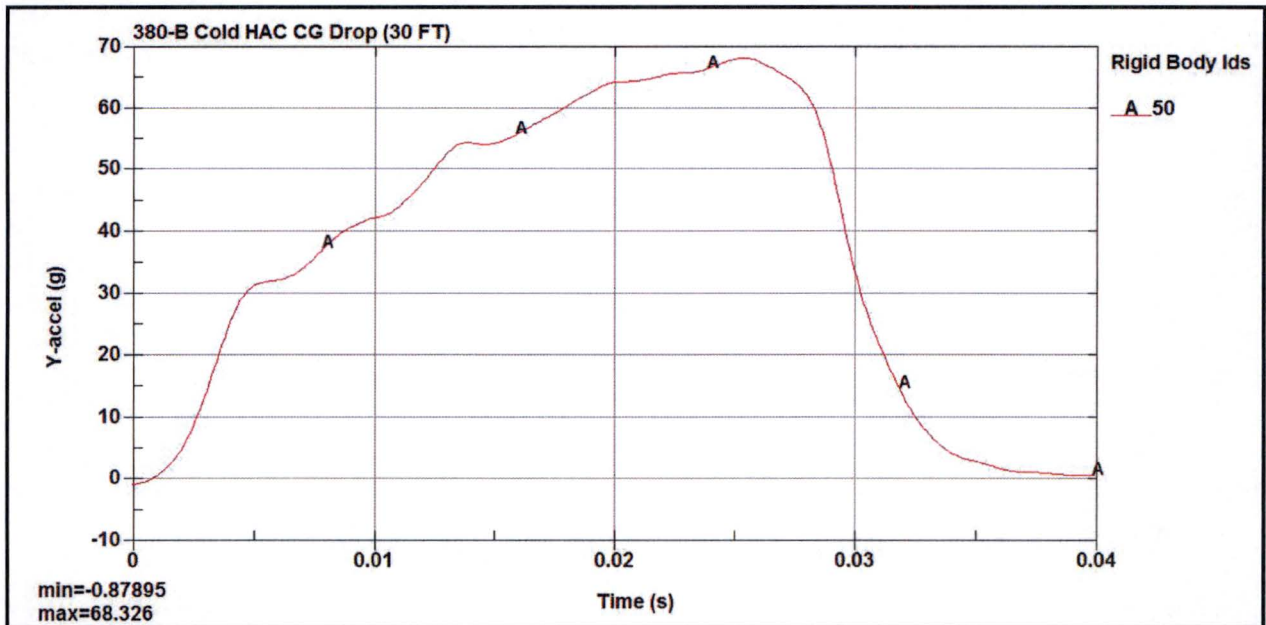
Figure 2.12.5-42 – Cold HAC CG-Over-Corner Drop Acceleration
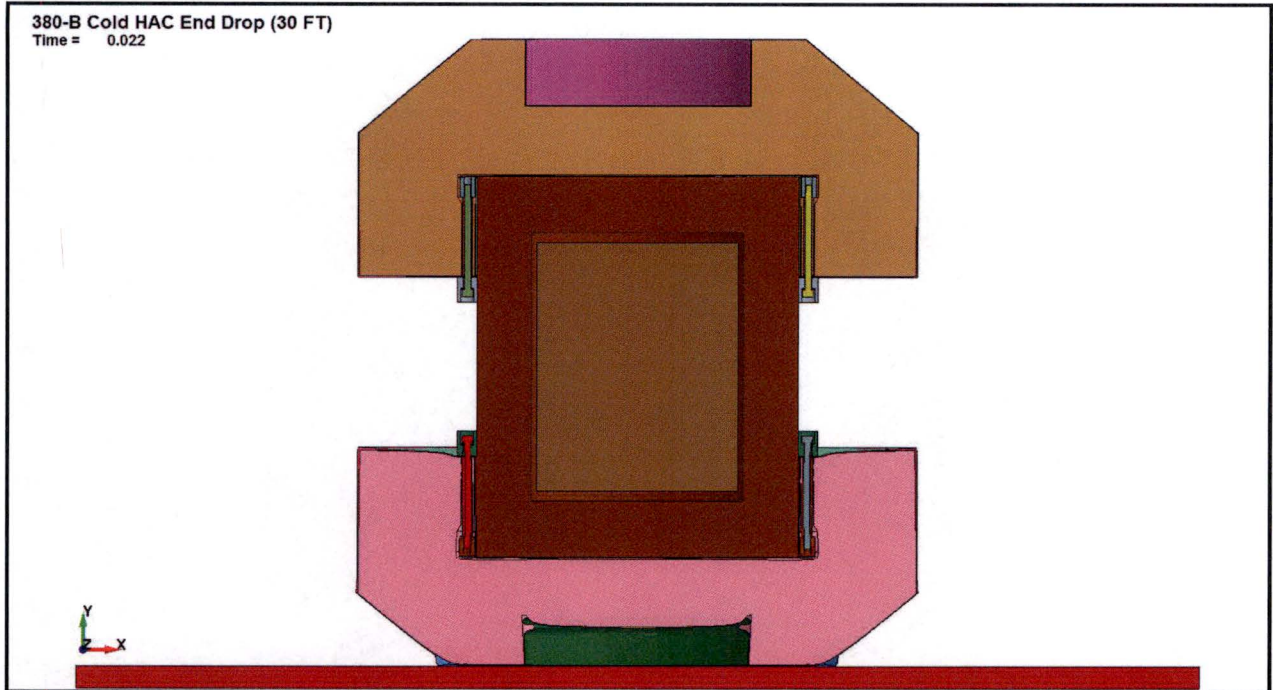
Figure 2.12.5-43 – Cold HAC End Drop Deformation
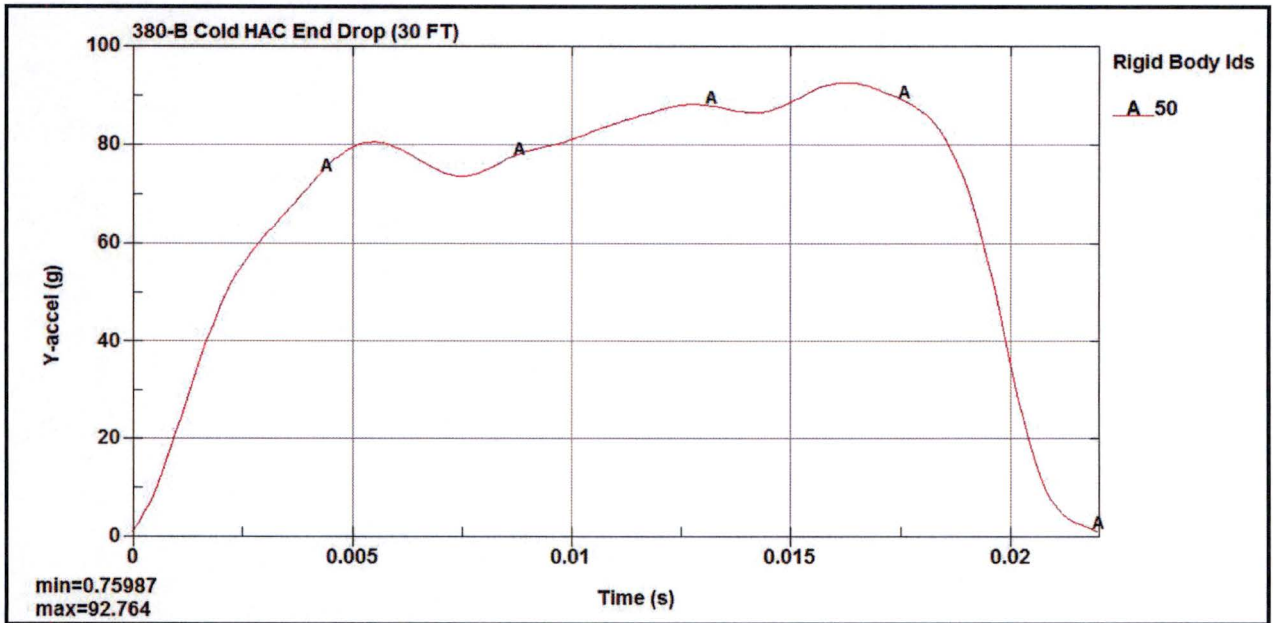
Figure 2.12.5-44 – Cold HAC End Drop Acceleration
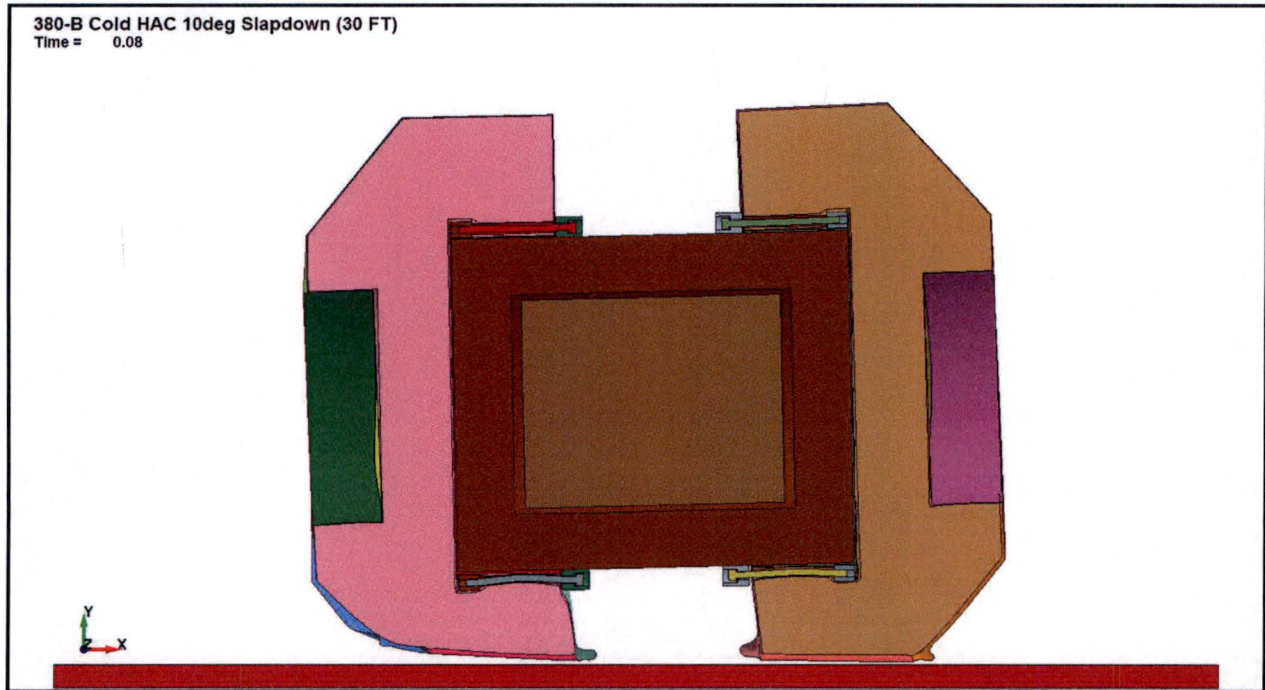
Figure 2.12.5-45 – Cold HAC 10° Slapdown Drop Deformation
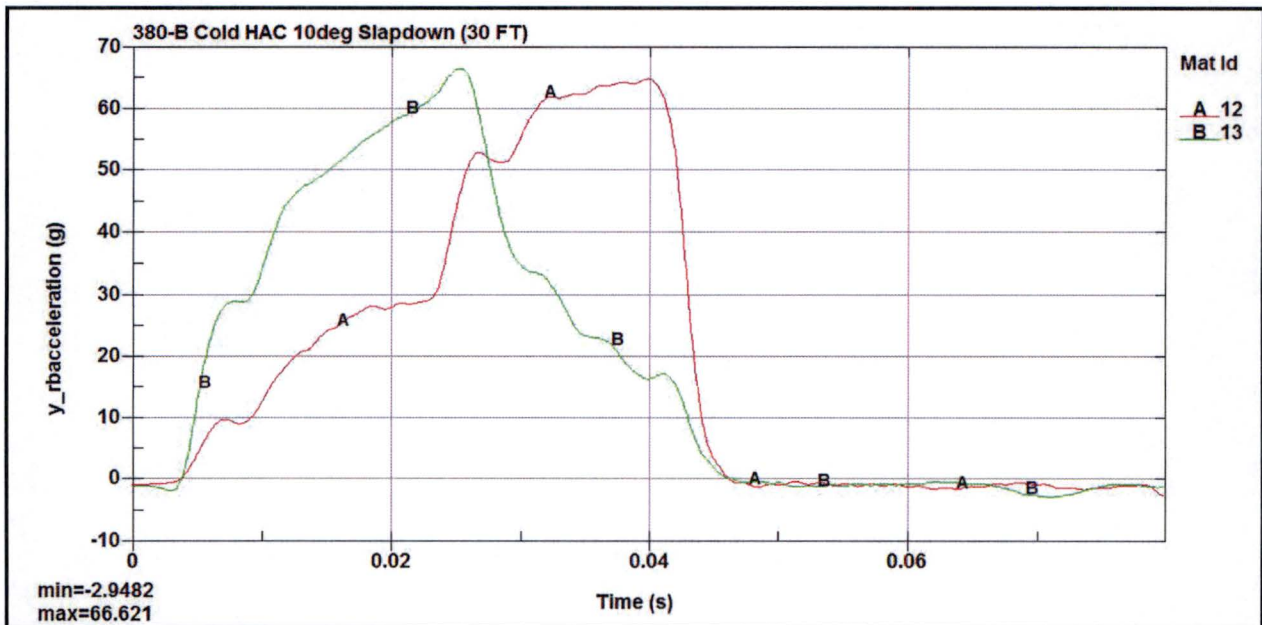
Figure 2.12.5-46 – Cold HAC 10° Slapdown Drop Acceleration
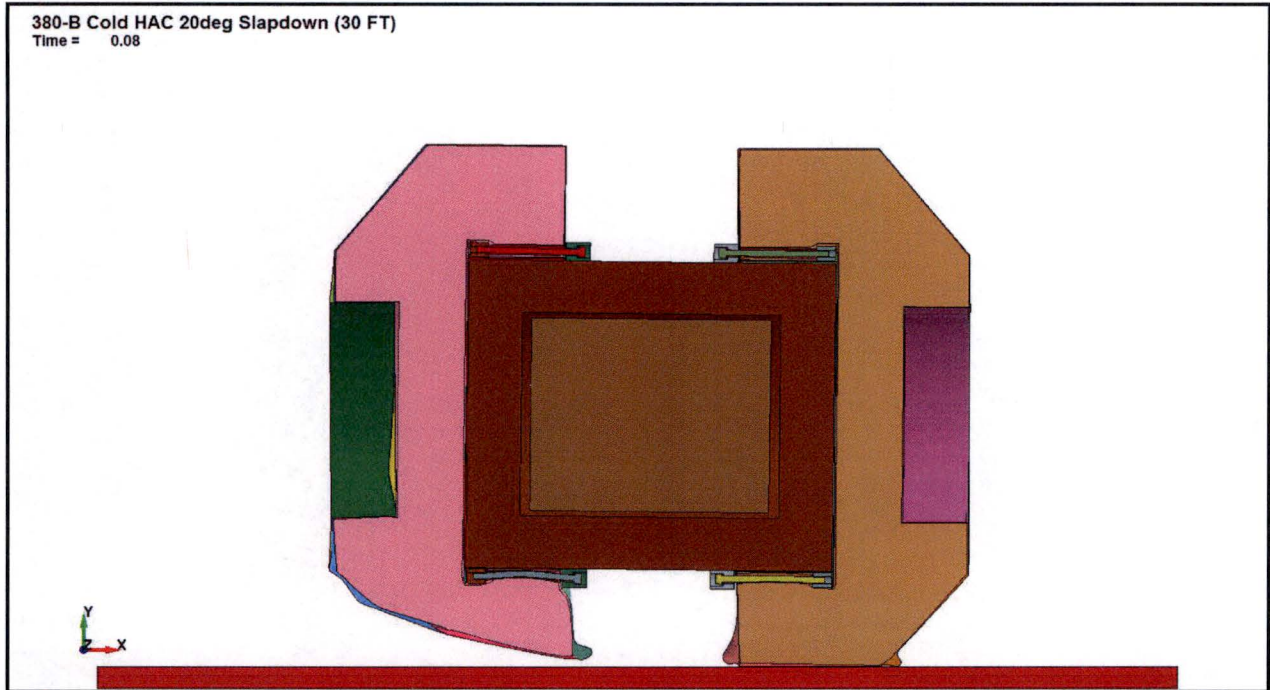
Figure 2.12.5-47 – Cold HAC 20° Slapdown Drop Deformation
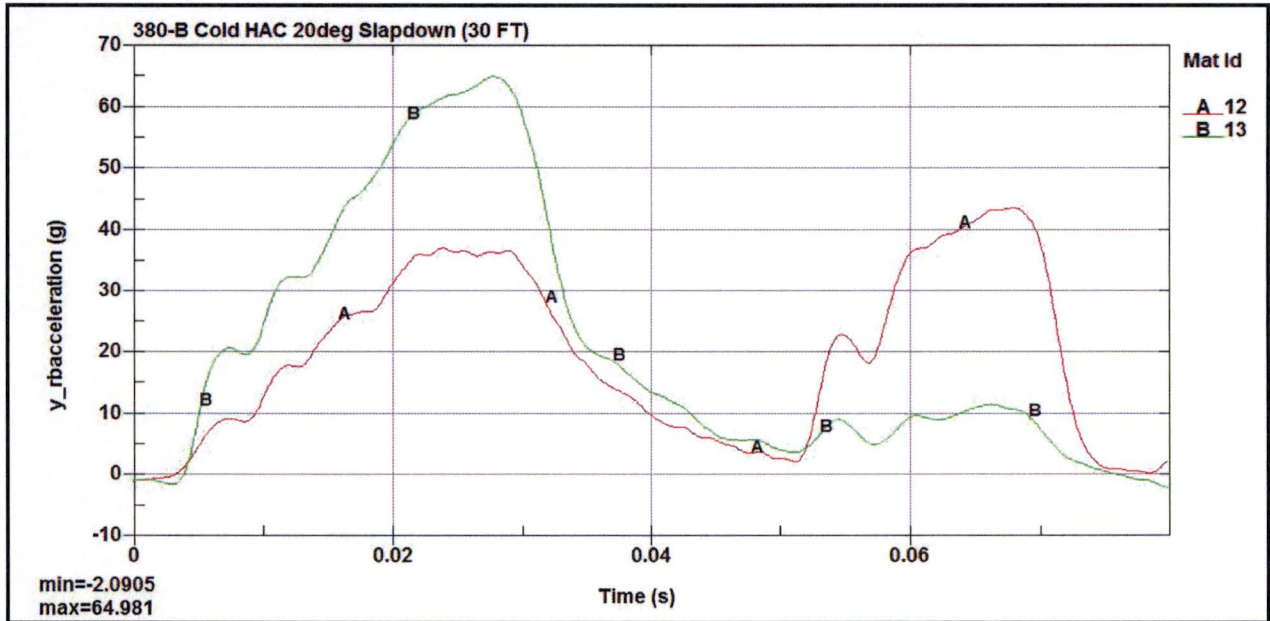
Figure 2.12.5-48 – Cold HAC 20° Slapdown Drop Acceleration
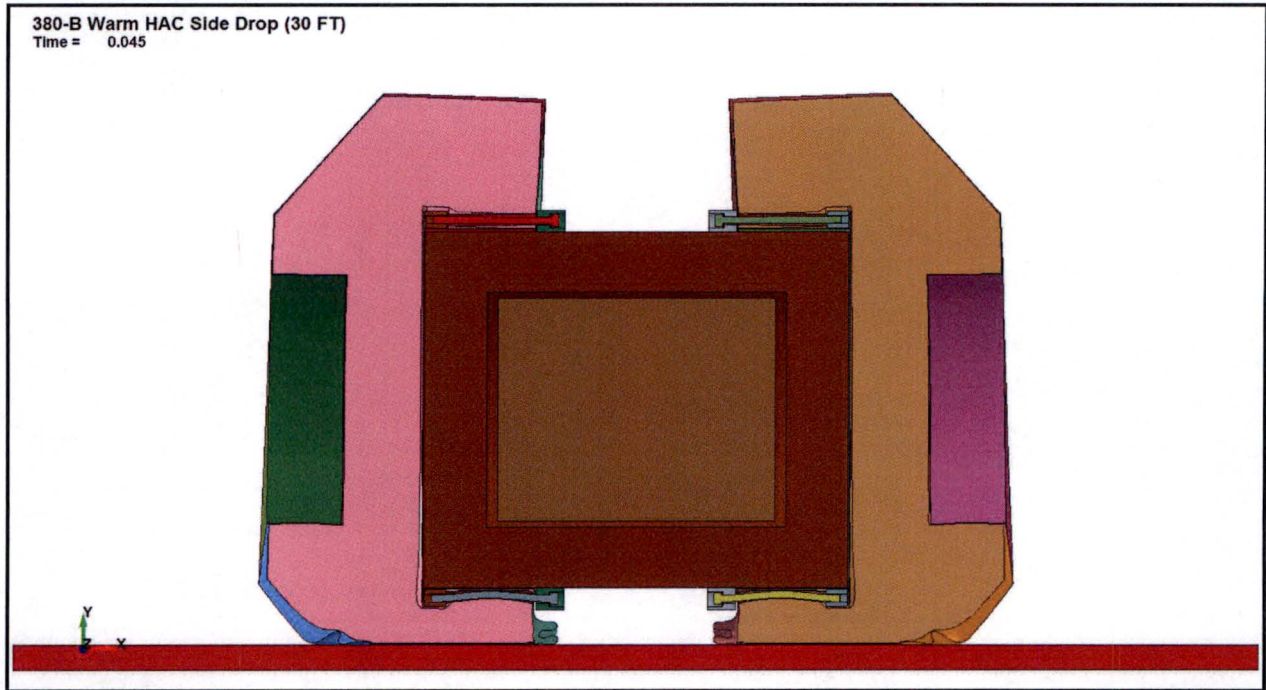
Figure 2.12.5-49 – Warm HAC Side Drop Deformation
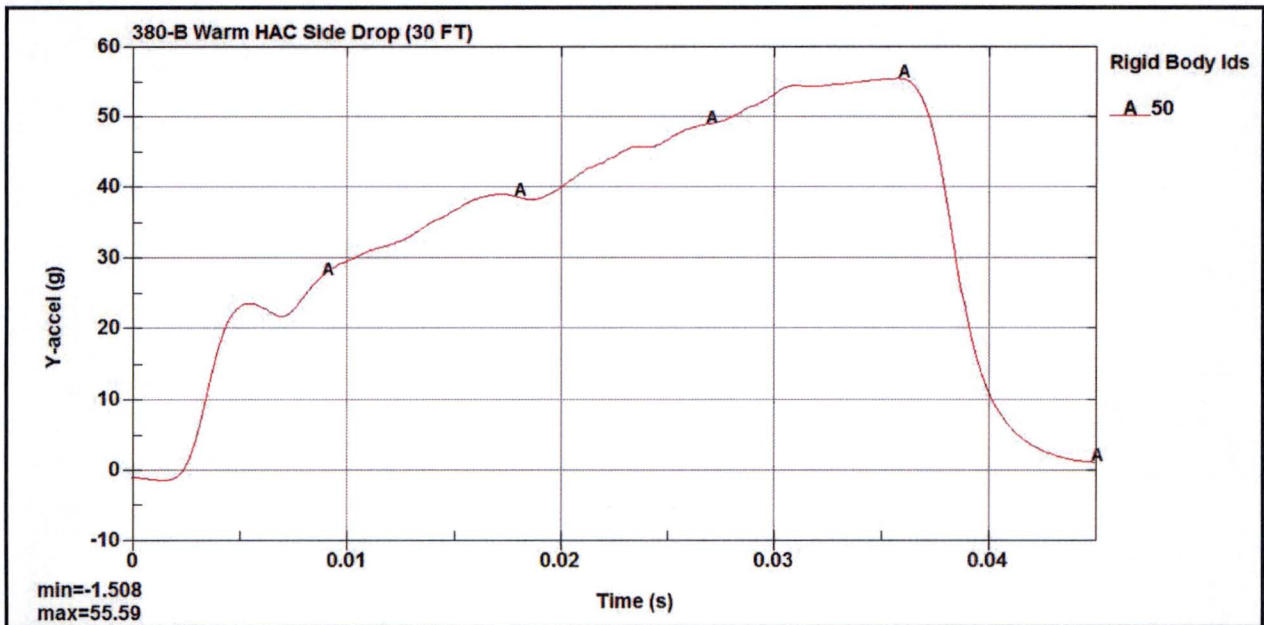
Figure 2.12.5-50 – Warm HAC Side Drop Acceleration
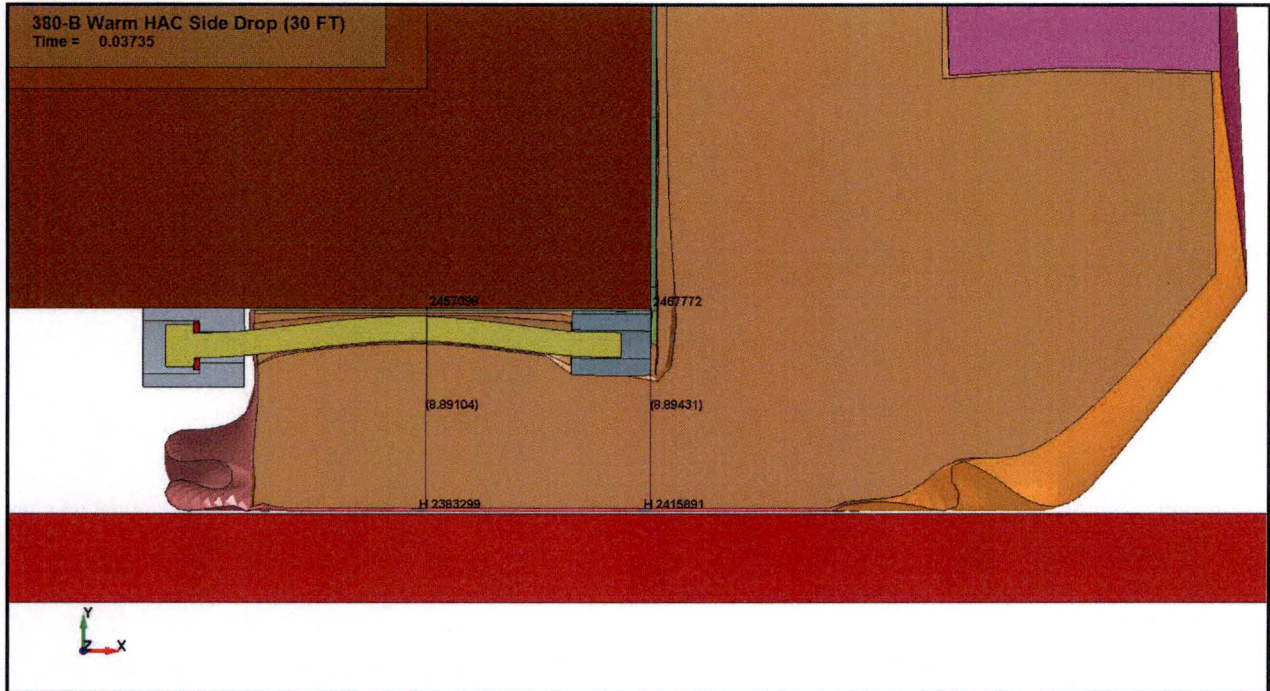
Figure 2.12.5-51 – Warm HAC Side Drop Minimum Foam
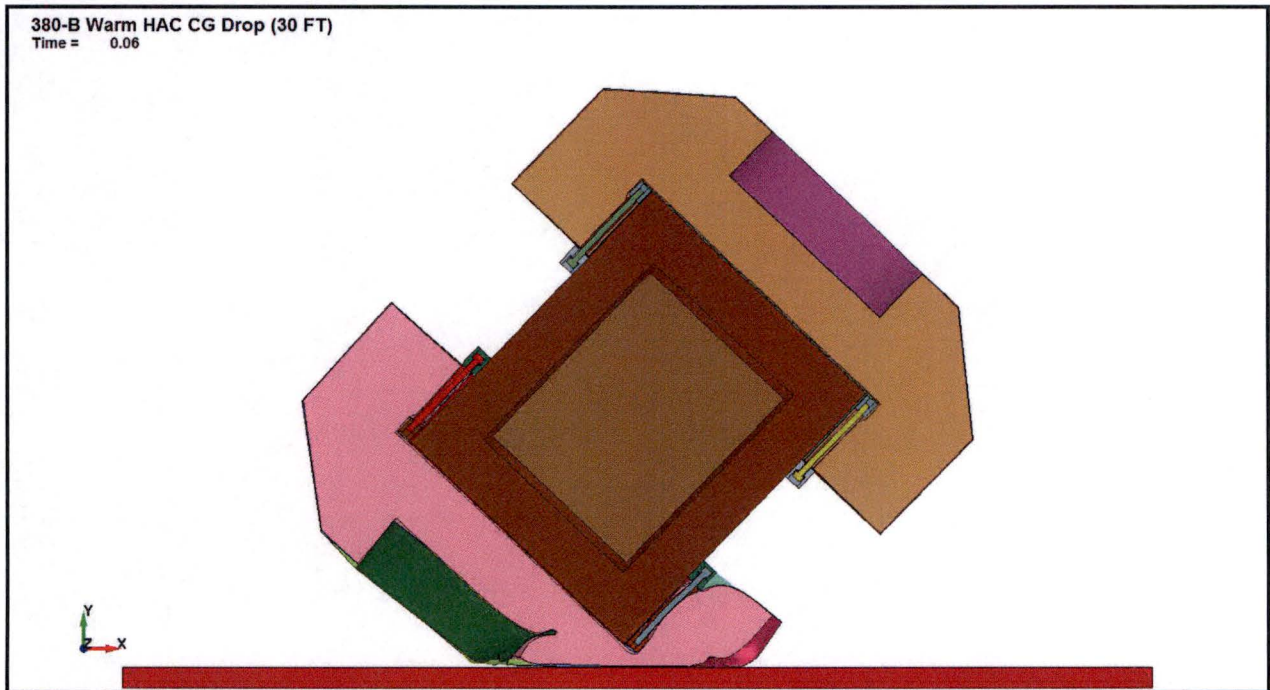
Figure 2.12.5-52 – Warm HAC CG-Over-Corner Drop Deformation
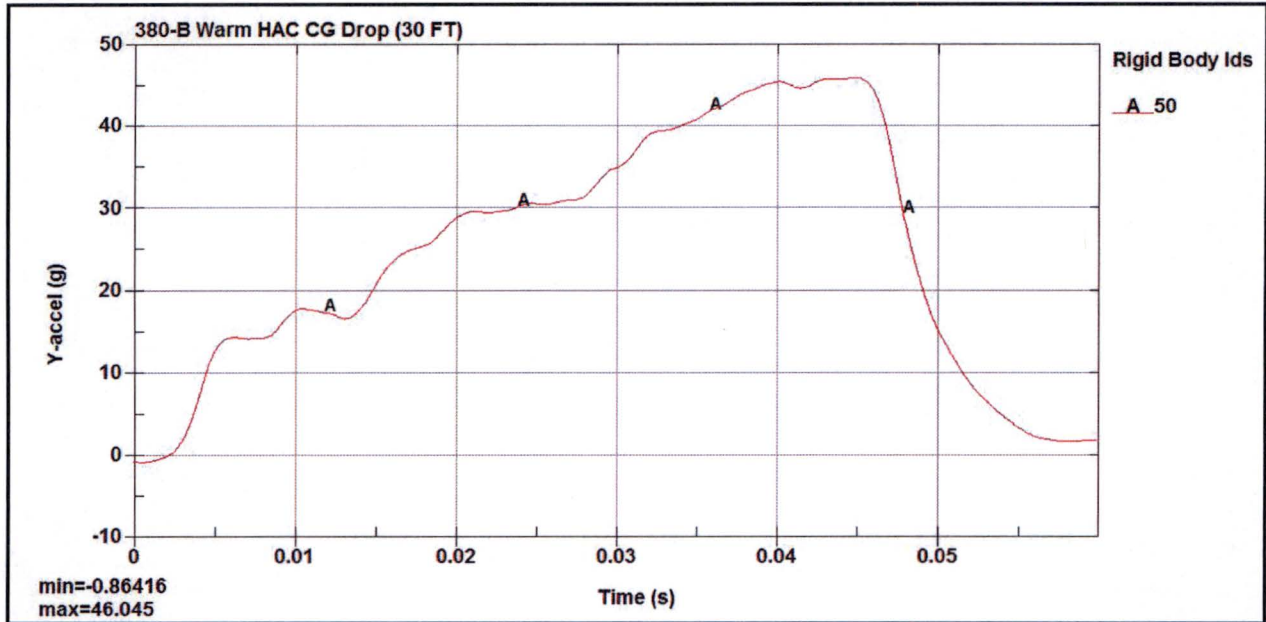
Figure 2.12.5-53 – Warm HAC CG-Over-Corner Drop Acceleration
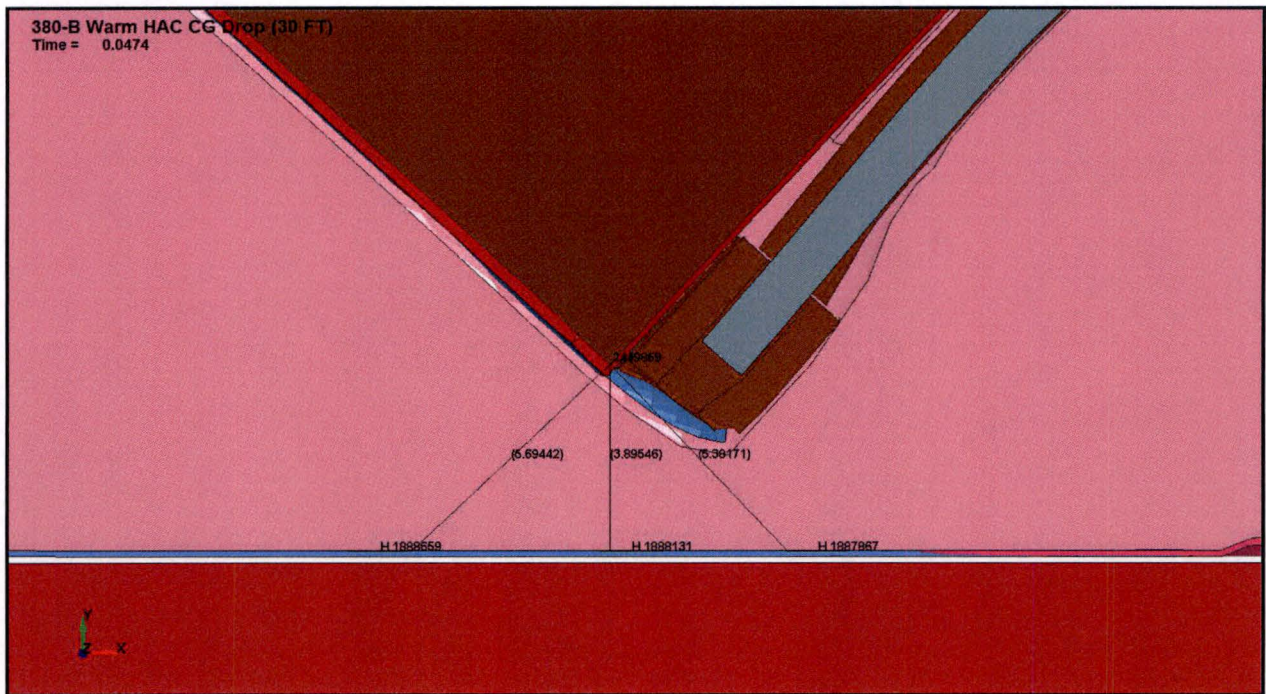
Figure 2.12.5-54 – Warm HAC CG-Over-Corner Drop Minimum Foam
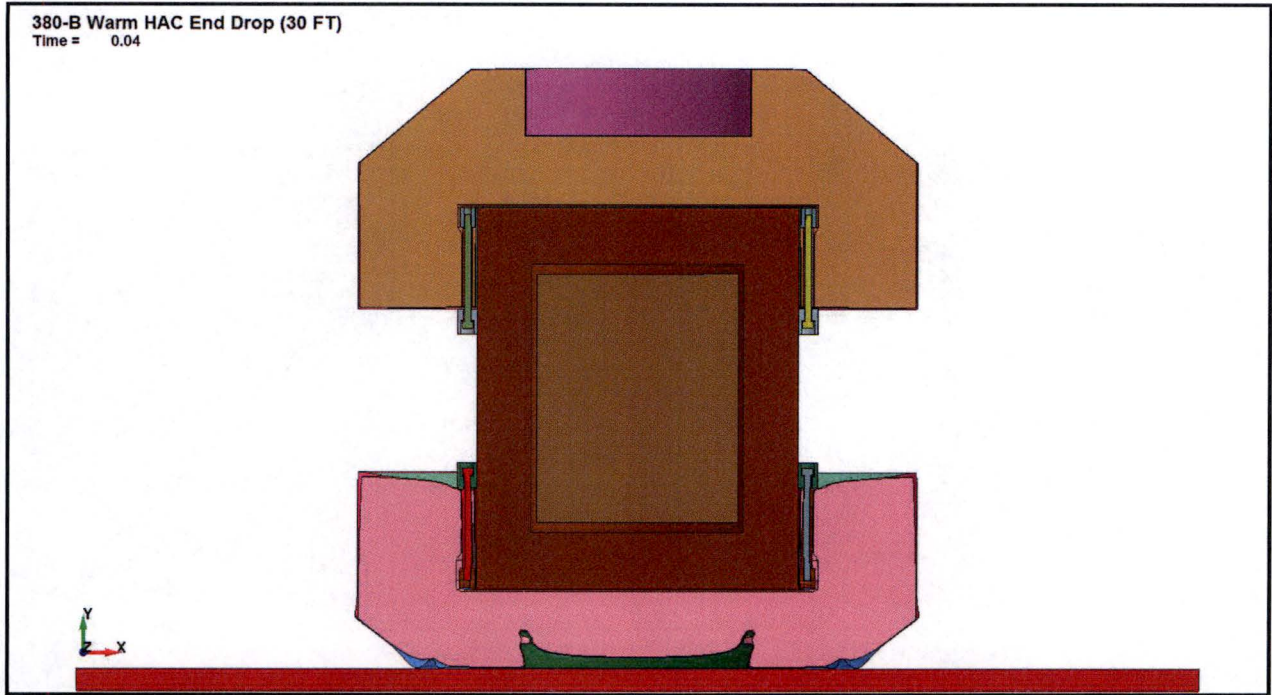
Figure 2.12.5-55 – Warm HAC End Drop Deformation
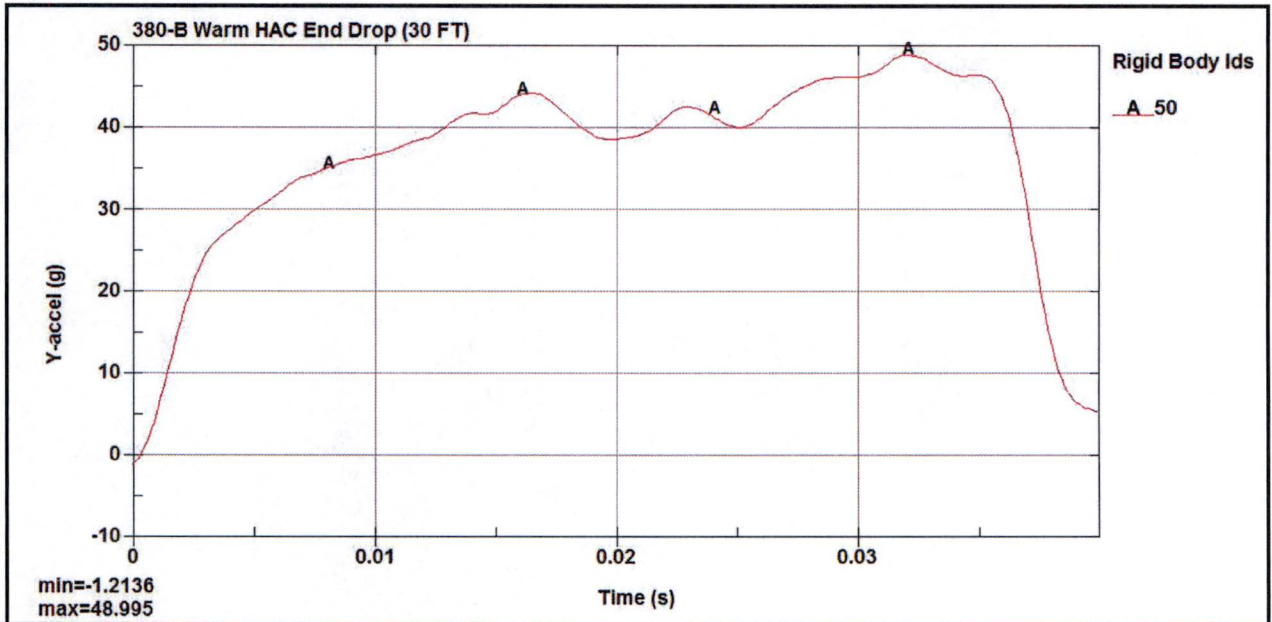
Figure 2.12.5-56 – Warm HAC End Drop Acceleration
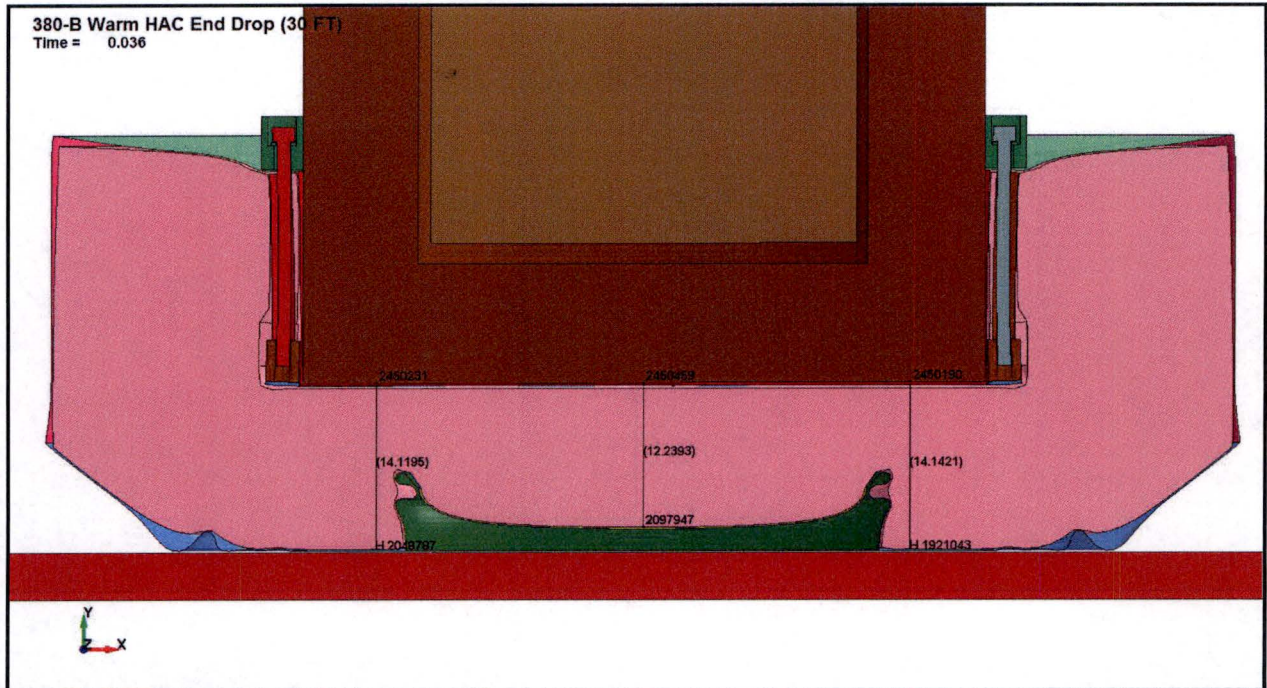
Figure 2.12.5-57 – Warm HAC End Drop Minimum Foam
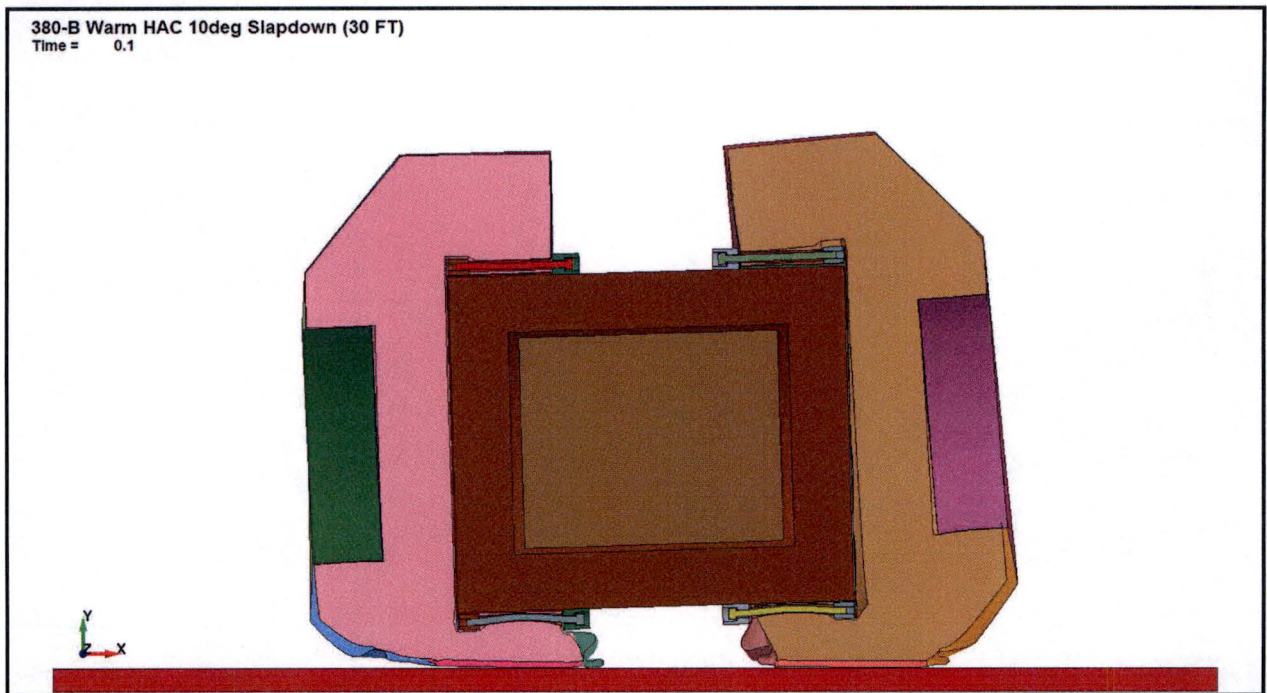
Figure 2.12.5-58 – Warm HAC 10° Slapdown Drop Deformation
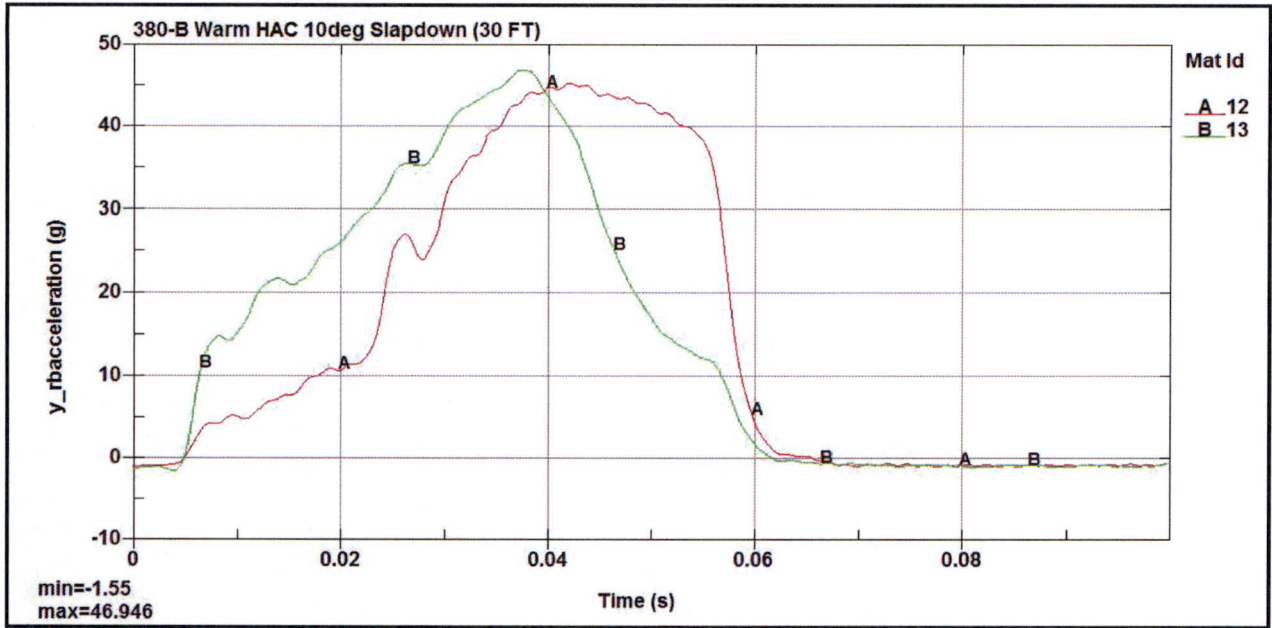
Figure 2.12.5-59 – Warm HAC 10° Slapdown Drop Acceleration
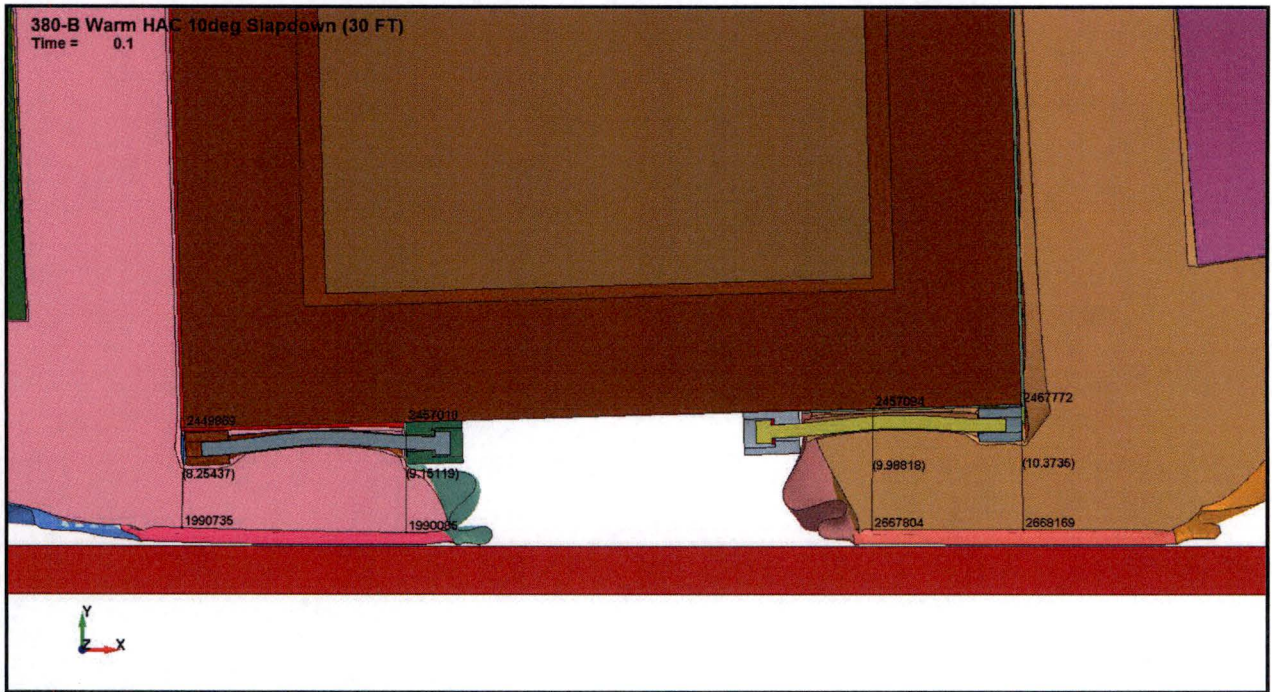
Figure 2.12.5-60 – Warm HAC 10° Slapdown Drop Minimum Foam
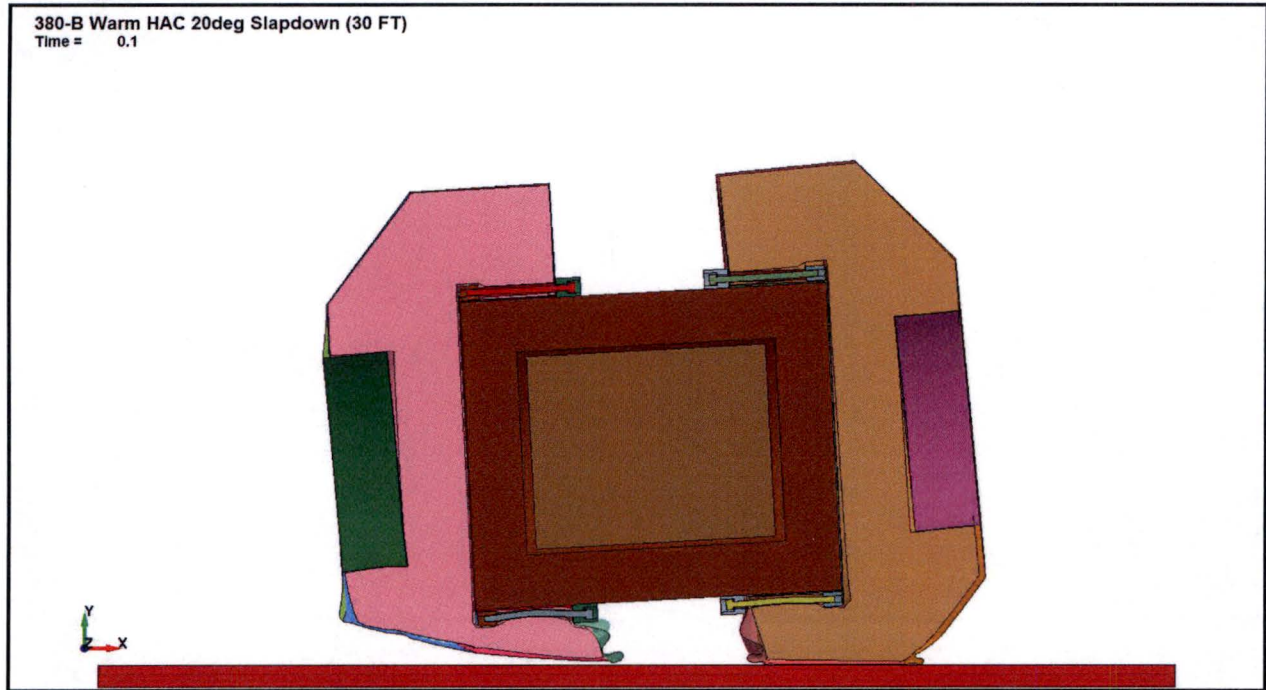
Figure 2.12.5-61 – Warm HAC 20° Slapdown Drop Deformation
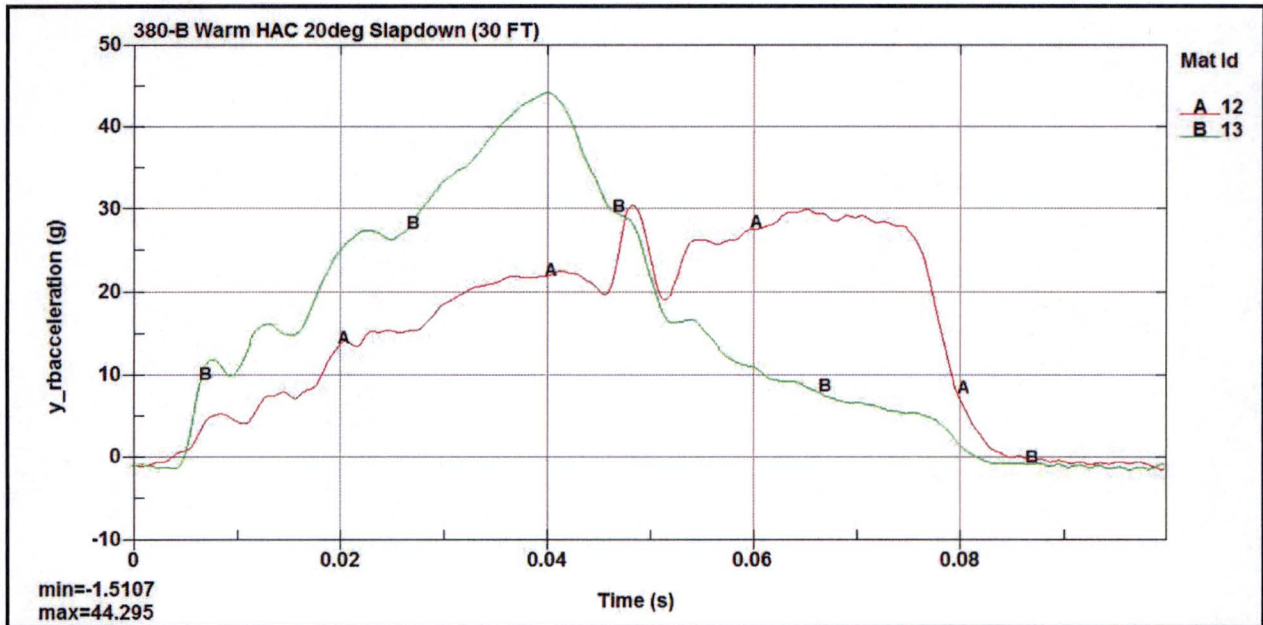
Figure 2.12.5-62 – Warm HAC 20° Slapdown Drop Acceleration
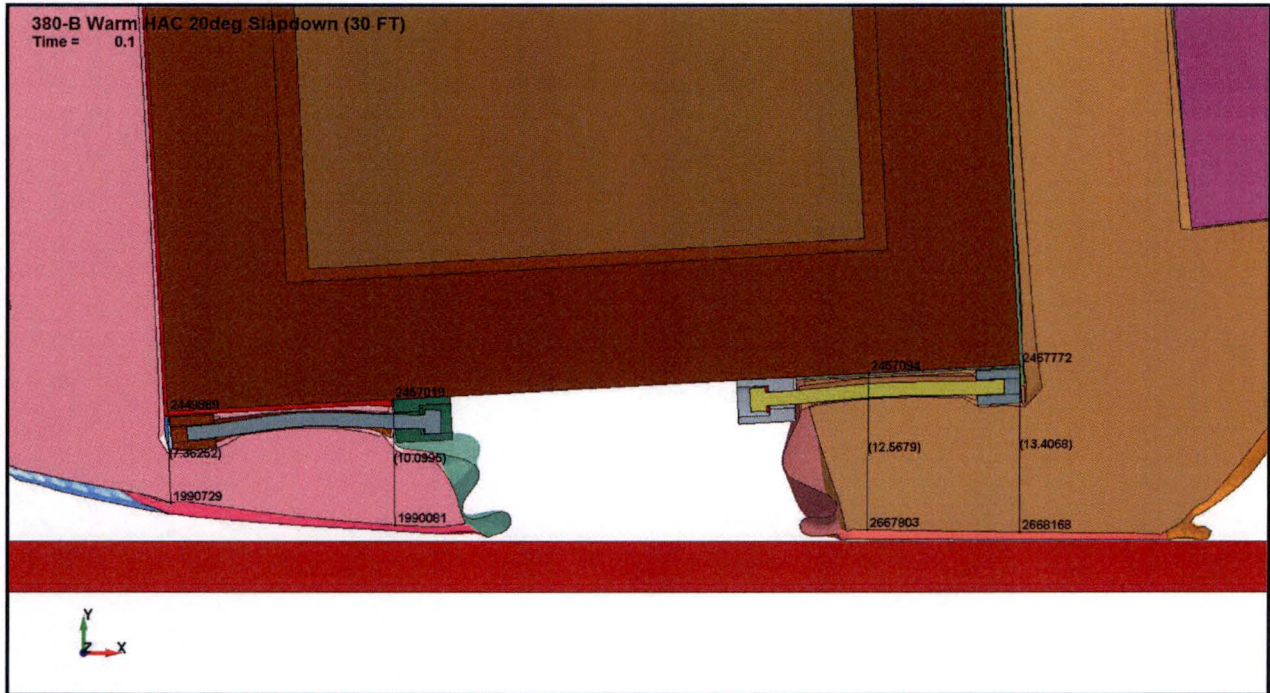
Figure 2.12.5-63 – Warm HAC 20° Slapdown Drop Minimum Foam

This page left intentionally blank.

2.12.6 Cask Shell Buckling Evaluations

This appendix provides details for the shell buckling evaluations discussed in Section 2.6.4, *Increased External Pressure*, and Section 2.7.1.2, *End Drop*. Buckling of the cask shells will be evaluated using ASME B&PV Code Case N-284-4 [14]. The method of buckling evaluation is as follows (paragraph numbers from Code Case N-284-4):

1) Determine the capacity reduction factors per -1511.
2) Determine the theoretical buckling values per -1712.1.1.
3) Determine the plasticity reduction factors per -1611.
4) Calculate the elastic buckling allowables per -1713.1.1.
5) Check elastic interactions per -1713.1.1.
6) Calculate the inelastic buckling allowables per -1713.2.1.
7) Check the inelastic interactions per -1713.2.1.

2.12.6.1 Input Parameters

The geometry, material, and stress inputs to the buckling calculations are given in Table 2.12.6-1.

2.12.6.2 Buckling Evaluation for Increased External Pressure

The following evaluation supports the discussion in Section 2.6.4, *Increased External Pressure*. As shown in Section 2.7.6, *Immersion – All Packages*, the buckling analysis performed for the NCT increased external pressure load case is extended to bound the HAC immersion load case. Thus, the single buckling evaluation shown here bounds both the NCT external pressure and HAC immersion load cases.

As discussed in Section 2.6.4, *Increased External Pressure*, the cask inner shell is subjected to a conservative combination of the lead shrinkage pressure and an external hydrostatic pressure of 21.7 psig. This loading conservatively takes no account of the stiffer outer shell. Consistent with Regulatory Guide 7.6 [2], a factor of safety corresponding to ASME Code, Service Level A is employed. In this case, the applicable factor of safety is 2.00 for normal conditions, as specified in [14]. This is conservative for the HAC immersion case for which [14] specifies a factor of safety of 1.34. As shown below, all interaction check values, including the maximum value of 0.4500, are less than unity, as required. Thus, the increased external pressure load case is not of concern for both the requirement of 10 CFR §71.71(c)(4) (i.e., increased external NCT pressure) and of 10 CFR §71.73(c)(6) (i.e., HAC immersion – all packages). The buckling equations will now be carried out.

-1511 Cylindrical Shells – Stiffened or Unstiffened

(a) Axial Compression

Use the larger of the values determined for $\alpha_{\phi L}$ from (1) and (2).

(1) Effect of R/t

Where R/t = 13.1667

R/t is less than 600, therefore use the smaller value of $\alpha_{\phi L}$ from the following:

$$\alpha_{\phi L} = 1.52 - 0.473 \log_{10}(R/t) = 0.9905$$

$$\alpha_{\phi L} = \frac{300\sigma_y}{E} - 0.033 = 0.2784$$

Therefore $\alpha_{\phi L} = 0.2784$, which is less than 0.9905.

(2) Effect of Length

Where $\quad M_\phi = \dfrac{L}{\sqrt{Rt}} = 9.2782$

M_ϕ is between 1.73 and 10, thus:

$$\alpha_{\phi L} = \frac{0.826}{M_\phi^{0.6}} = 0.2170$$

For axial compression the larger $\alpha_{\phi L}$ from (1) and (2) is used. Therefore $\alpha_{\phi L} = 0.2784$, which is larger than 0.2170.

(b) Hoop Compression

$\quad \alpha_{\theta L} = 0.8000$

(c) Shear

$\quad$ Where R/t = 13.1667, which is less than 250

$\quad \alpha_{\phi\theta L} = 0.8000$

-1712.1.1 Theoretical Local Buckling, Cylindrical Shells

(a) Axial Compression

$\quad$ Where $M_\phi = 9.2782$, which is greater than 1.73

$\quad C_\phi = 0.6050$

$\quad \sigma_{\phi e L} = C_\phi Et/R = 1{,}327{,}937 \; psi$

(b) External Pressure

(1) No End Pressure

$\quad$ M_ϕ is greater than 3.0 and less than 1.65 R/t = 21.7250, thus:

$$C_{\theta r} = \frac{0.92}{M_\phi - 1.17} = 0.1135$$

$\quad \sigma_{\theta e L} = \sigma_{reL} = C_{\theta r} Et/R = 249{,}125 \; psi$

(2) End Pressure Included

$$C_{\theta h} = \frac{0.92}{M_\phi - 0.636} = 0.1065$$

$$\sigma_{\theta eL} = \sigma_{heL} = C_{\theta h} Et / R = 233,761 \; psi$$

(c) Shear

M_ϕ is greater than 1.5 and less than 26, thus:

$$C_{\phi\theta} = \frac{4.82}{M_\phi^2}\left(1+0.0239 M_\phi^3\right)^{1/2} = 0.2510$$

$$\sigma_{\phi\theta eL} = C_{\phi\theta} Et / R = 550,929 \; psi$$

-1611 Plasticity Reduction Factors for Cylindrical Shells

(a) Axial Compression

$$\Delta = \frac{\alpha_{\phi L} \cdot \sigma_{\phi eL}}{\sigma_y} = 12.3233, \text{ therefore } \Delta > 6.25 \text{ and:}$$

$$\eta_\phi = \frac{1}{\Delta} = 0.0811$$

(b) Hoop Compression

$$\Delta = \frac{\alpha_{\theta L} \cdot \sigma_{\theta eL}}{\sigma_y} = 6.6433, \text{ (using } \sigma_{\theta eL} = 249,125\text{), therefore } \Delta \geq 4.2$$

$$\eta_\theta = \frac{1}{\Delta} = 0.1505$$

(c) Shear

$$\Delta = \frac{\alpha_{\phi\theta L} \cdot \sigma_{\phi\theta eL}}{\sigma_y} = 14.6914, \text{ therefore } \Delta \geq 1.7$$

$$\eta_{\phi\theta} = \frac{0.6}{\Delta} = 0.0408$$

-1713.1.1 Elastic Buckling for Cylindrical Shells

Using FS = 2 for NCT, allowable stresses are:

$$\sigma_{xa} = \frac{\alpha_{\phi L}\sigma_{\phi eL}}{FS} = 184,849 \; psi$$

$$\sigma_{ha} = \frac{\alpha_{\theta L}\sigma_{heL}}{FS} = 93,504 \; psi$$

$$\sigma_{ra} = \frac{\alpha_{\theta L}\sigma_{reL}}{FS} = 96,650 \; psi$$

$$\sigma_{\tau a} = \frac{\alpha_{\phi\theta L}\sigma_{\phi\theta eL}}{FS} = 220,372 \; psi$$

(a) Axial Compression Plus Hoop Compression

No interaction check required if $\sigma_\theta < \sigma_{ha}$. The hoop stress $\sigma_\theta = 5,398$ psi, which is less than σ_{ha}. Therefore, no interaction check is required.

(b) Axial Compression Plus Hoop Compression

No interaction check required if $\sigma_\phi < 0.5\sigma_{ha}(t_\theta/t_\phi)$. The axial stress $\sigma_\phi = 346$ psi, which is less than $0.5\sigma_{ha}$, and $t_\theta = t_\phi$. Therefore, no interaction check is required.

(c) Axial Compression Plus Shear

$$\frac{\sigma_\phi}{\sigma_{xa}} + \left(\frac{\sigma_{\phi\theta}}{\sigma_{\tau a}}\right)^2 = 0.0020 \leq 1.0$$

Since 0.0020 is much less than 1.0, the interaction check is acceptable.

(d) Hoop Compression Plus In-Plane Shear

$$\frac{\sigma_\theta}{\sigma_{ra}} + \left(\frac{\sigma_{\phi\theta}}{\sigma_{\tau a}}\right)^2 = 0.0560 \leq 1.0$$

Since 0.0560 is less than 1.0, the interaction check is acceptable.

(e) Axial Compression Plus Hoop Compression Plus In-Plane Shear

$$K_s = 1 - \left(\frac{\sigma_{\phi\theta}}{\sigma_{\tau a}}\right)^2 = 0.9999$$

Since K_s is essentially unity, the interaction checks for (a) and (b) above will not be significantly changed, and remain acceptable.

-1713.2.1 Inelastic Buckling for Cylindrical Shells

Allowable stresses:

$$\sigma_{xc} = \eta_\phi\sigma_{xa}, \quad \sigma_{rc} = \eta_\theta\sigma_{ra}, \quad \sigma_{\tau c} = \eta_{\phi\theta}\sigma_{\tau a}$$

$$\sigma_{xc} = 14,991 \; psi$$
$$\sigma_{rc} = 14,546 \; psi$$
$$\sigma_{\tau c} = 8,991 \; psi$$

(a) Axial Compression or Hoop Compression

$$\frac{\sigma_\phi}{\sigma_{xc}} = 0.0231 \leq 1.0, \quad \frac{\sigma_\theta}{\sigma_{rc}} = 0.3711 \leq 1.0$$

The axial compression and hoop compression are both less than allowable, and therefore are acceptable.

(b) Axial Compression Plus Shear

$$\frac{\sigma_\phi}{\sigma_{xc}} + \left(\frac{\sigma_{\phi\theta}}{\sigma_{xc}}\right)^2 = 0.1020 \le 1.0$$

Since 0.1020 is less than 1.0, the interaction check is acceptable.

(c) Hoop Compression Plus Shear

$$\frac{\sigma_\theta}{\sigma_{rc}} + \left(\frac{\sigma_{\phi\theta}}{\sigma_{xc}}\right)^2 = 0.4500 \le 1.0$$

Since 0.4500 is less than 1.0, the interaction check is acceptable.

2.12.6.3 Buckling Evaluation for End Drop Impact

The following evaluation supports the discussion in Section 2.7.1.2, *End Drop*. As shown in Section 2.6.7, *Free Drop*, the evaluation for the HAC free drop is bounding for the NCT free drop. Thus, only the HAC buckling evaluation is shown.

The cask shells are subject to buckling loads in the end drop orientation. Due to its much greater stiffness compared to the inner shell, the cask outer shell will carry most of the axial loading. Thus, the outer shell is conservatively assumed to carry the entire axial load without assistance from the inner shell. No other stresses are applied for the end drop buckling evaluation. An impact of 100g is applied. The geometry, material, and stress inputs to the buckling calculations are given in Table 2.12.6-1. As shown below, all interaction check values, including the maximum value of 0.4387, are less than unity, as required. Thus, the cask shells will not buckle under the conditions of 10 CFR §71.71(c)(7) (NCT free drop) nor the conditions of 10 CFR §71.73(c)(1) (HAC free drop). The buckling equations will now be carried out.

-1511 Cylindrical Shells – Stiffened or Unstiffened

(a) Axial Compression

Use the larger of the values determined for $\alpha_{\phi L}$ from (1) and (2).

(1) Effect of R/t

Where R/t = 15.9286

R/t is less than 600, therefore use the smaller value of $\alpha_{\phi L}$ from the following:

$$\alpha_{\phi L} = 1.52 - 0.473 \log_{10}(R/t) = 0.9514$$

$$\alpha_{\phi L} = \frac{300\sigma_y}{E} - 0.033 = 0.2638$$

Therefore $\alpha_{\phi L} = 0.2638$, which is less than 0.9514.

(2) Effect of Length

$$\textit{Where} \quad M_\phi = \frac{L}{\sqrt{Rt}} = 7.1589$$

M_ϕ is between 1.73 and 10, thus:

$$\alpha_{\phi L} = \frac{0.826}{M_\phi^{0.6}} = 0.2536$$

For axial compression the larger $\alpha_{\phi L}$ from (1) and (2) is used. Therefore $\alpha_{\phi L} = 0.2638$, which is larger than 0.2536.

(b) Hoop Compression

$\alpha_{\theta L} = 0.8000$

(c) Shear

Where R/t = 15.9286, which is less than 250

$\alpha_{\phi\theta L} = 0.8000$

-1712.1.1 Theoretical Local Buckling, Cylindrical Shells

(a) Axial Compression

Where M_ϕ = 7.1589, which is greater than 1.73

$C_\phi = 0.6050$

$\sigma_{\phi eL} = C_\phi Et / R = 1,055,901 \ psi$

(b) External Pressure

(1) No End Pressure

M_ϕ is greater than 3.0 and less than 1.65 R/t = 26.2822, thus:

$$C_{\theta r} = \frac{0.92}{M_\phi - 1.17} = 0.1536$$

$\sigma_{\theta eL} = \sigma_{reL} = 268,077 \ psi$

(2) End Pressure Included

M_ϕ is greater than 3.5 and less than 1.65 R/t = 26.2822, thus:

$$C_{\theta h} = \frac{0.92}{M_\phi - 0.636} = 0.1410$$

$\sigma_{\theta eL} = \sigma_{heL} = 246,086 \ psi$

(c) Shear

M_ϕ is greater than 1.5 and less than 26, thus:

$$C_{\phi\theta} = \frac{4.82}{M_\phi^2}\left(1 + 0.0239 M_\phi^3\right)^{1/2} = 0.2940$$

$\sigma_{\phi\theta eL} = 513,116 \ psi$

<u>-1611 Plasticity Reduction Factors for Cylindrical Shells</u>

(a) Axial Compression

$$\Delta = \frac{\alpha_{\phi L} \cdot \sigma_{\phi eL}}{\sigma_y} = 10.1290 \text{, therefore } \Delta > 6.25 \text{ and:}$$

$$\eta_\phi = \frac{1}{\Delta} = 0.0987$$

(b) Hoop Compression

$$\Delta = \frac{\alpha_{\theta L} \cdot \sigma_{\theta eL}}{\sigma_y} = 7.7986 \text{, (using } \sigma_{\theta eL} = 268,077 \text{), therefore } \Delta \geq 4.2$$

$$\eta_\theta = \frac{1}{\Delta} = 0.1282$$

(c) Shear

$$\Delta = \frac{\alpha_{\phi \theta L} \cdot \sigma_{\phi \theta eL}}{\sigma_y} = 14.9270 \text{, therefore } \Delta \geq 1.7$$

$$\eta_{\phi\theta} = \frac{0.6}{\Delta} = \frac{0.6}{14.9270} = 0.0402$$

<u>-1713.1.1 Elastic Buckling for Cylindrical Shells</u>

Using FS = 1.34 for HAC, allowable stresses are:

$$\sigma_{xa} = \frac{\alpha_{\phi L}\sigma_{\phi eL}}{FS} = 207,871 \; psi$$

$$\sigma_{ha} = \frac{\alpha_{\theta L}\sigma_{heL}}{FS} = 146,917 \; psi$$

$$\sigma_{ra} = \frac{\alpha_{\theta L}\sigma_{reL}}{FS} = 160,046 \; psi$$

$$\sigma_{\tau a} = \frac{\alpha_{\phi \theta L}\sigma_{\phi \theta eL}}{FS} = 306,338 \; psi$$

(a) Axial Compression Plus Hoop Compression

No interaction check required if $\sigma_\theta < \sigma_{ha}$. The hoop stress $\sigma_\theta = 0$, which is less than σ_{ha}. Therefore, no interaction check is required.

(b) Axial Compression Plus Hoop Compression

No interaction check required if $\sigma_\phi < 0.5\sigma_{ha}(t_\theta/t_\phi)$. The axial stress $\sigma_\phi = 9,000$ psi, which is less than $0.5\sigma_{ha}$, and $t_\theta = t_\phi$. Therefore, no interaction check is required.

(c) Axial Compression Plus Shear

$$\frac{\sigma_\phi}{\sigma_{xa}} + \left(\frac{\sigma_{\phi\theta}}{\sigma_{\tau a}}\right)^2 = 0.0433 \leq 1.0$$

Since 0.0433 is less than 1.0, the interaction check is acceptable.

(d) Hoop Compression Plus In-Plane Shear

$$\frac{\sigma_\theta}{\sigma_{ra}} + \left(\frac{\sigma_{\phi\theta}}{\sigma_{\tau a}}\right)^2 = 0.0000 \leq 1.0$$

Since 0.0000 is less than 1.0, the interaction check is acceptable.

(e) Axial Compression Plus Hoop Compression Plus In-Plane Shear

$$K_s = 1 - \left(\frac{\sigma_{\phi\theta}}{\sigma_{\tau a}}\right)^2 = 1.0000$$

Since K_s is equal to unity, the interaction checks for (a) and (b) above will be unchanged, and remain acceptable.

-1713.2.1 Inelastic Buckling for Cylindrical Shells

Allowable stresses:

$$\sigma_{xc} = \eta_\phi \sigma_{xa}, \quad \sigma_{rc} = \eta_\theta \sigma_{ra}, \quad \sigma_{\tau c} = \eta_{\phi\theta} \sigma_{\tau a}$$

$$\sigma_{xc} = 20{,}517 \; psi$$

$$\sigma_{rc} = 20{,}518 \; psi$$

$$\sigma_{\tau c} = 12{,}315 \; psi$$

(a) Axial Compression or Hoop Compression

$$\frac{\sigma_\phi}{\sigma_{xc}} = 0.4387 \leq 1.0, \quad \frac{\sigma_\theta}{\sigma_{rc}} = 0.0000 \leq 1.0$$

The axial compression and hoop compression are both less than allowable, and therefore are acceptable.

(b) Axial Compression Plus Shear

$$\frac{\sigma_\phi}{\sigma_{xc}} + \left(\frac{\sigma_{\phi\theta}}{\sigma_{\tau c}}\right)^2 = 0.4387 \leq 1.0$$

Since 0.4387 is less than 1.0, the interaction check is acceptable.

(c) Hoop Compression Plus Shear

$$\frac{\sigma_\theta}{\sigma_{rc}} + \left(\frac{\sigma_{\phi\theta}}{\sigma_{\tau c}}\right)^2 = 0.0000 \leq 1.0$$

Since 0.0000 is less than 1.0, the interaction check is acceptable.

Table 2.12.6-1 - Input Parameters

Input Parameter	NCT External Pressure (Inner Shell)	HAC End Drop (Outer Shell)
Outside dia, in. (OD)	41.0	57.5
Inside dia, in. (ID)	38.0	54.0
Mean radius, in. (R)	19.75	27.875
Shell thickness, in. (t)	1.5	1.75
Cylindrical length, in. (L)	50.5	50.0
Temperature, °F	-40	150
Material	Type 304	Type 304
Yield strength, psi (σ_y)	30,000	27,500
Elastic mod., psi (E)	$28.9(10^6)$	$27.8(10^6)$
Weight, lb	NA	21,100
Maximum impact, g	NA	100
Ext. radial pressure, psi	410	NA
Ext. axial pressure, psi	24.8	NA
Axial stress, (σ_ϕ), psi	346	9,000
Hoop stress (σ_θ), psi	5,398	0
Shear stress ($\sigma_{\phi\theta}$), psi	2,526	0
Factor of safety (FS)	2.00	1.34

This page left intentionally blank.

3.0 THERMAL EVALUATION

This chapter identifies and describes the principal thermal design aspects of the 380-B package. The 380-B package is used to transport radioactive sealed sources for recovery and management operations. This application seeks authorization of the 380-B package as a Type B(U)–96 shipping container in accordance with the provisions of Title 10, Part 71 of the Code of Federal Regulations [1]. The packaging also meets the requirements of TS-R-1 [2]. Further guidance for the evaluation is taken from NUREG-1609 [3] and Regulatory Guide 7.8 [4].

Specifically, all package components are shown to remain within their respective temperature limits under the normal conditions of transport (NCT). Further, per 10 CFR §71.43(g), the maximum temperature of the accessible package surfaces is demonstrated to be less than 185 °F for the maximum decay heat loading, an ambient temperature of 100 °F, and no insolation. Finally, the 380-B package is shown to retain sufficient thermal protection following the HAC free and puncture drop scenarios to maintain all package component temperatures within their respective short term limits during the regulatory fire event and subsequent package cool-down.

3.1 Description of Thermal Design

The 380-B packaging consists of three principal components: 1) a lead-shielded cask body, 2) a bolted closure lid, and 3) upper and lower impact limiters. The principal components comprising the package are discussed in Section 1.2.1, *Packaging*, and illustrated in Figure 1.2-1 through Figure 1.2-5. A glossary of terms is presented in Appendix 1.3.2, *Glossary of Terms and Acronyms*. Detailed drawings of the package design are presented in Appendix 1.3.3, *Packaging General Arrangement Drawings*.

For more detail and an illustration of the principal components, see Figures 1.1-1 and Figure 1.1-2 of Section 1.0, *General Information*.

3.1.1 Design Features

The 380-B packaging consists of three principal components: 1) a lead-shielded cask body, 2) a bolted closure lid, and 3) upper and lower impact limiters. The terminology "cask" refers to the lid and body assembly, "packaging" refers to the cask with the impact limiters attached, and the term "package" refers to the packaging loaded with contents. Information regarding package layout, component dimensions, materials of fabrication, etc. are taken from the assembly drawing and its associated lower tier drawings.

The packaging provides a payload cavity that is 38 inches in diameter and 45.75 inches high to the base of the inner cover. A personnel barrier fabricated of expanded metal or flattened expanded metal with a minimum 75% free area is used between the impact limiters during transport. The barrier is required for radiological and not thermal purposes as the cask surface temperature remains below the allowable limit for exclusive shipments.

The 380-B cask body is a right circular cylinder 62.5 inches long and 57.5 inches in diameter (not including the impact limiter attachment lugs and the thermal shield). It is composed of upper and lower end structures that connect circular inner and outer shells. The 1.5-inch thick inner shell, the 1.75-inch thick outer shell, and the end structures are fabricated Type 304 stainless steel. Lead located between the two circular shells and in the end closure structure provides radiological shielding for the enclosed payloads. The cask body design yields a large

thermal mass-to-surface area ratio capable of absorbing the high heat flux generated during the HAC fire event and limiting the temperature rise within the interior of the package.

The cask design incorporates a thermal shield over most, but not all, of the outer shell not covered by the impact limiters. The shield consists of an outer sheet of 12 gauge (0.105-inch thick) Type 304 stainless steel that is offset from the outer shell by three 0.105-inch diameter wires on approximately 4.5-inch centers and by 1-inch wide, 0.105-inch thick closure strips at the edges of the shield. The thermal shield provides significant shielding of the outer shell from the high heat fluxes associated with the HAC fire accident event.

The lead shielding is made from any grade of ASTM B29, lead, or optionally, lead meeting Federal Specification QQ-L-171E, Grade A or C. The 6.5-inch thick lead shield in the side of the cask body will be cast-in-place using a controlled lead pour procedure that minimizes residual gaps between the lead and the steel shells. For conservatism, the thermal design assumes a uniform gap exists between the outer radius of the side wall lead and the inner radius of the outer shell. Appendix 3.5.3, *Analytical Thermal Model,* describes how this gap is incorporated as a function of temperature for NCT. The potential presence of the gap is ignored for HAC so as to maximize the heat flow into the packaging. The thickness of the bottom and lid closures is 10 inches with a lead thickness of 6 inches and with inner and outer Type 304 stainless steel plate thicknesses of 2.5 and 1.5 inches, respectively. The lead shielding at the bottom and lid will be fabricated from lead sheet material that is packed firmly into place to yield the required thickness. If necessary, packed lead wool or scrap lead will be used to ensure voids are filled between the seams and along the edges.

The lid serves as a combination end closure and radiological shield plug. The lid is attached to the cask body using thirty-six, 1-1/2-inch diameter bolts made of ASTM A564, Type 630 Condition H1100 (i.e., 17-4 PH) steel. The closure lid includes two O-ring seals made from butyl rubber (Rainier Rubber R0405-70) that are retained in dovetail grooves.

Two impact limiters of identical designs are attached at the ends of the 380-B cask to provide thermal and impact protection to the package. Each limiter is 100 inches in diameter and 43 inches long overall, with a conical section 17 inches long at the outer end. The outer ends of the limiters also incorporate a recess measuring 40 inches in diameter and 12 inches deep. A nominal 0.2 inch radial gap exists between the outer circumference of the cask body and the inner circumference of the impact limiter. The recesses at the outer ends of the limiters are covered by sheet metal to prevent moisture accumulation within the recesses. The impact limiters are filled with rigid, poured in place, closed-cell polyurethane foam with a nominal 16 lb/ft^3 (pcf) density. As described in Appendix 3.5.4, *'Last-A-Foam' Response under HAC,* thermal decomposition of the foam during the HAC event absorbs a majority of the heat energy entering the impact limiters.

The foam is encased in a stainless steel shell for structural protection. The shell is ¼ inches thick everywhere, except for a ½ inch thick inner end plate at the interface with the end of the cask body. Plastic melt-out plugs are incorporated into the exterior shells of the limiters. The plugs are designed to soften and be expelled during the HAC fire event, thus relieving any pressure buildup in the limiters due to foam decomposition under elevated temperatures. The external surfaces of the impact limiter shell are 'as-received' stainless steel. Each impact limiter is attached to the cask body via a set of twelve (12) ASTM A564, Type 630 Condition H1100 bolts that connect lugs mounted on the cask to lugs embedded in the impact limiter.

The void spaces within the packaging are filled with air at 0 psig.

3.1.2 Content's Decay Heat

The 380-B package can transport a variety of radioactive sources, as well as irradiation devices (shielded devices) containing sources. All sources are sealed and encapsulated. The nuclides that will be transported in the 380-B are listed in Table 1.2-1. The maximum decay heat in the package is 205W.

A generic payload is considered for this safety evaluation. To address the potential variability in the payload configuration, it's heat dissipation characteristics, and the associated dunnage required to support the device within the package, two dramatically different scenarios are assumed for the disposition of the decay heat on the inner surface of the cask as depicted in Figure 1.2-6. The intent of these two heat disposition scenarios is to bound the expected heat transfer mechanisms that could arise for any combination of device payload and its associated support dunnage.

The first heat disposition scenario considered assumes an open type of support dunnage fabricated from metal or wood timbers. Under this scenario, the bulk of the heat dissipated from the device would be removed via convection and a lesser portion by radiation. Since the package is transported in a vertical orientation, the heated air that is convected away from the device will rise up under thermal buoyancy forces, strike the underside of the inner cover, turn outward towards the cask inner shell, and then turn downward to flow along the inner shell. The heat dissipated via convection would be transferred to the underside of the inner cover and on the cask inner shell down to a point that is equal height with the bottom of the device. The heat dissipated via radiation would be spread along the height of the inner shell with the majority concentrated on portion of the cask shell directly opposite of the device.

The effects of this first heat disposition scenario are bounded in the modeling by assuming 100% of the dissipated decay heat is deposited on the underside of the inner cover and the upper 14.4 inches of the inner shell (i.e. vertical length above a 18.6 inch long device centered in the package cavity derived in Section 3.5.3.1, *Description of 380-B Packaging Thermal Model for NCT*). The dissipated heat is assumed to be evenly distributed amongst these surfaces on an area basis. This concentration of heat bounds that which could be deposited near the cask closure seals under any payload configuration and positioning within the cask cavity.

The second heat disposition scenario considered assumes a fully enclosing type of support dunnage like that achieved by fabricating the dunnage out of rigid foam or sheets of plywood and timbers. This 'restrictive' type of dunnage is assumed to fully enclose the ends of the device and essentially prevent heat transfer from the ends of the device. Instead, only a portion of the side wall of the device equal to 9.3 inches in height is assumed to be active in dissipating heat from the device (this dimension is derived and justified Section 3.5.3.1, *Description of 380-B Packaging Thermal Model for NCT*). The resultant heat dissipation from the device is assumed to be concentrated on an equal height portion of the cask inner shell directly opposite of the device. The device is assumed to be centered vertically within the cask cavity. The effects of the second heat disposition scenario bounds that which would arise under any reasonable concentrated heating of the cask sidewall.

The package temperatures that will arise in practice for any actual payload and dunnage combination is fully expected to lie somewhere between the levels predicted by two heat

disposition scenarios described above. As seen from the NCT results presented below, the effect of not specifically modeling the payload on the predicted packaging temperatures is very limited due to the low total decay load within the package.

3.1.3 Summary Tables of Temperatures

Table 3.1-1 provides a summary of the package component temperatures with the shielded device payload under normal and accident conditions. The temperatures for normal conditions are based on an analytical model of the 380-B package with an ambient temperature of 100 °F and the 10 CFR §71.71(c)(1) prescribed insolation applied as a hourly average (i.e., *NCT Hot* condition). The temperatures for accident conditions are based on a transient simulation using an analytical model of a damaged 380-B package. The damage conditions represent the worst-case hypothetical pre-fire damage predicted from a combination of physical drop testing using half-scale CTUs and analytical structural evaluations.

The NCT results demonstrate that significant thermal margins exist for all package components. Further, the NCT evaluations demonstrate that the accessible surface temperatures will be below the maximum 185 °F permitted by 10 CFR §71.43(g) for exclusive use shipment when transported in a 100 °F environment with no insolation (i.e., *NCT Hot (no solar)* condition). The HAC results also demonstrate that the design of the 380-B package provides sufficient thermal protection to yield component temperatures that are significantly below the acceptable limits defined for each component. See Sections 3.2.3, *Component Specifications*, Section 3.3, *Thermal Evaluation for Normal Conditions of Transport*, and Section 3.4, *Thermal Evaluation for Hypothetical Accident Conditions*, for more discussion.

3.1.4 Summary Tables of Maximum Pressures

Table 3.1-2 presents a summary of the maximum pressures predicted under NCT and HAC. The 380-B package has a design maximum pressure of 25 psig (39.7 psia). Based on an assumed fill gas temperature of 70 °F and one atmosphere, the maximum pressure rise under NCT will be 7.0 psig, while the maximum pressure rise under HAC will be 66.2 psig. Based on the NCT pressure, the maximum normal operating pressure (MNOP) is set at a bounding level of 10 psig. The maximum HAC pressure is conservatively assumed to be 100 psig.

Table 3.1-1 – Maximum NCT and HAC Temperatures

Location / Component	NCT, °F[1]	HAC, °F	Allowable Temperature, °F[2]	
			Normal	**Accident**
Inner Shell	133	294[6]	800	800
Outer Shell	132 / 141[3]	628	800	800
Lower End Structure	131	230	800	800
Closure Lid	138[6]	643	800	800
Closure Bolts	133	570	800	800
Lead - Side	133	404	620	620
- Lower	131	221	620	620
- Lid	136	311	620	620
Thermal Shield	129 / 138[3]	1,251	2,500	2,500
Main Containment Seal	133	288	250	400
Vent Port Sealing Washer	133	392	250	400
Upper End Structure	134	364	800	800
Impact Limiter - Max. Foam	144 / 176[3]	N/A	300	N/A
- Avg. Foam	130	N/A	300	N/A
- Shell	146 / 180[3]	1,472	2,500	2,500
- Attachment Bolts	133	1,183	800	2,500
Personnel Barrier	111 / 120[3]	N/A	2,500	2,500
Max. Accessible Surface without Insolation	103	N/A	185	N/A
Cask Cavity Bulk Gas	232[4]	294[5]	N/A	N/A

Notes: [1] Based on steady-state evaluation with 24-hour average of regulatory insolation loading, except where noted.

[2] See Section 3.2.3, *Component Specifications*, for basis of listed temperature criterion.

[3] Based on steady-state evaluation with 12-hour average of regulatory insolation loading.

[4] The NCT bulk gas temperature is determined in Section 3.3.2, *Maximum Normal Operating Pressure*.

[5] The HAC bulk gas temperature is discussed in Section 3.4.3.1, *Maximum HAC Pressures*.

[6] Maximum payload cavity containment temperature.

Table 3.1-2 – Summary of Maximum Pressures

Condition	Cask Cavity Pressure
NCT	7.0 psi gauge
HAC	66.2 psi gauge

3.2 Material Properties and Component Specifications

This section presents the thermal properties and specifications of the materials that affect heat transfer within the 380-B packaging. Included are the properties for air which is assumed to fill all void spaces within the package and which will surround the package exterior. The thermal absorptivities and emissivities appropriate for the package surface conditions for each thermal condition are identified.

3.2.1 Material Properties

The 380-B packaging is fabricated primarily of Type 304 austenitic stainless steel (predominately ASTM A240 and A479), lead, and polyurethane foam. The closure and impact limiter attachment bolts are fabricated from ASTM A564, Type 630 Condition H1100 (i.e., 17-4 PH) steel. 17-4 PH steel has approximately 90% of the thermal conductivity of Type 304 stainless steel at temperatures up to 800 °F and essentially the same conductivity for temperatures above 1,100 °F. In contrast, the specific heats of the two materials are similar at temperature levels below 600 °F, but the specific heat for 17-4 PH steel is approximately 70% of Type 304 stainless steel at temperatures in excess of 1,000 °F. As justified in Appendix 3.5.3.1, *Description of 380-B Packaging Thermal Model for NCT*, the thermal model does not specifically model the closure bolts, but does capture the individual impact limiter attachment bolts.

Table 3.2-1 presents the thermal properties of Type 304 stainless steel, ASTM A564, Type 630 steel, ASTM B29 lead, and polyurethane foam. Properties for temperatures between the tabulated values are calculated via linear interpolation within the heat transfer code. The thermal properties for Type 304 stainless steel are taken from the ASME material properties database [14] for 18Cr-8Ni, material group J, and the density is taken from an on-line materials database [13]. The thermal properties for ASTM A564, Type 630 steel are taken from the ASME material properties database [14] for 17Cr-4Ni-4Cu, material group I, and the density is taken from an on-line materials database [13]. The values listed in Table 3.2-1 are for any grade of ASTM B29 [16]. QQ L 171E Grade A or C lead, which is 99.9% lead plus a small amount of other elements, may be substituted for ASTM B29 lead. The nominal density for lead is 708 lb_m/ft^3 [13].

The polyurethane foam used in the impact limiters is based on a proprietary formulation that provides predictable impact-absorption performance under dynamic loading, while also providing an intumescent char layer that insulates and protects the underlying materials when exposed to HAC fire conditions. The thermal properties under NCT conditions are obtained from the manufacturer's website [10]. Because the website provides data at only a few specific densities and since the thermal conductivity of the material is tied to its density, interpolation is used to arrive at the listed material properties. Further, the manufacturing process for the poured in place foam can yield densities that vary from the targeted value. As such, the calculation for 16 lb_m/ft^3 (pcf) foam used in the impact limiter addresses the properties associated with a ±15% tolerance on the targeted foam density (i.e., 13.6 and 18.4 pcf foam). Since the low tolerance foam yields a lower thermal conductivity, it is assumed for NCT operations, while the higher thermal conductivity of the high tolerance density foam is used for HAC evaluation to conservatively bound the heat flow into the package. The performance of polyurethane foam during HAC is addressed in Appendix 3.5.4, *'Last-A-Foam' Response under HAC*.

The thermal properties for air, as derived from curve fits provided in [21], are presented in Table 3.2-2. Because the gas thermal conductivity varies significantly with temperature, the computer model calculates the thermal conductivity between the package and the ambient as a function of the mean film temperature. The calculation also assumes air is the backfill gas.

3.2.2 Emissivity & Absorption Data

The emissivity of 'as-received' Type 304 stainless steel has been measured as 0.20 to 0.28 [17, 18], while the emissivity of weathered Type 304 stainless steel has been measured as being between 0.36 to 0.46 [20]. Since the design does not specify acceptable surface finishes, the safety evaluation uses a range of emissivity values to reflect the possible surface finishes the fabricator may apply. The chosen range of emissivity values are intended to yield conservatively high package temperatures under both NCT and HAC, thus, removing surface finish as a parameter of interest. A conservatively low emissivity of 0.20 is assumed for stainless steel surfaces during NCT. This includes the various surfaces that form the cask cavity, the exterior surface of the cask body, and the thermal shield. Exception to this general assumption is made for the impact limiter shells and the personnel barrier since these surfaces will be exposed to weathering, surface abrasion, etc. The emissivity of the exterior surfaces of the impact limiter shells and the personnel barrier are assumed to be 0.40, based on a weathered Type 304 stainless steel surface. The polyurethane foam has an assumed emissivity of approximately 0.925 [19] based on a combination of the material type and surface roughness. The exterior surfaces of the impact limiters, personnel barrier, and thermal shield have a solar absorptivity of 0.52 for Type 304 stainless steel [20].

The emissivity values assumed for the HAC evaluation are as follows:

- the emissivity of all exterior surfaces exposed to the fire conditions is raised to 0.8 to reflect the potential oxidation of the surface, and/or accumulation of soot,

- the solar absorptivity of all exterior surfaces is raised to 1.0 to reflect the potential oxidation of the surface, and/or accumulation of soot, and to yield "full insolation" post-fire per Section 3.5.5.2 of NUREG-1609 [3],

- the emissivity for the inside face of the thermal shield sheet is increased from 0.2 to 0.45 to account for potential oxidization during the course of the HAC event,

- the emissivity of the cask surfaces not directly exposed to the fire, but nominally covered by the impact limiters is raised to 0.4 and emissivity of the opposing surfaces on the impact limiter are raised to 0.5 to account for possible condensation on the surfaces by volatile organic compounds (VOCs) generated during the fire, and

- the emissivity of all other package surfaces are raised from 0.20 to 0.30 to conservatively bound the potential surface condition at fabrication.

The A564 Type 630 stainless steel is assumed to have the same emissivity value as the Type 304 stainless steel under similar conditions.

3.2.3 Component Specifications

The acceptance criterion for normal conditions is that the package components remain within their respective thermal limits and that the 380-B packaging maintains containment for the

payload. Only a few materials used in the 380-B packaging are considered temperature sensitive. These are the butyl rubber compound used for the containment boundary and vent/test port seals, the polyurethane foam used in the impact limiters, and the lead used for radiological shielding. The other materials either have temperature limits above the maximum expected temperatures or are not considered essential to the function of the package.

The butyl rubber compound used for the containment and vent/test port seals is fabricated from Rainier Rubber compound R0405-70 [7]. Butyl rubber has a long term temperature range of at least -40 °F to 250 °F [8]. O-ring seal testing [9] performed to document in detail the high temperature ability of the specific R0405-70 rubber compound, showed the leak tight criteria were met for tests of 430°F for one hour, 400 °F for 8 hours, 380 °F for 24 hours, and 350 °F for 144 hours. For conservatism, a long-term limit of 250 °F, a short-term limit of 400 °F for 8 hours, and a low temperature limit of -40 °F are assumed for this analysis.

Below 250 °F the variation in the thermal properties with temperature for the proprietary polyurethane foam are slight and reversible. While small variations in the foam properties will occur between 250 and 500 °F as water vapor and non-condensable gases are driven out of the foam, the observed changes are very slight. For conservatism, a long-term limit of 300 °F is assumed for the foam. Between 325 and 435 °F, a slight foam weight reduction of approximately 2% (see Appendix 3.5.4, *'Last-A-Foam' Response under HAC*) will occur as water vapor and/or the gas used as the blowing agent is lost. There is no short term temperature limit for the foam used in the impact limiter as its decomposition under exposure to high temperatures is part of its mechanism for providing thermal protection during the HAC fire event. A short term temperature limit of 400 °F is assumed for foam used as dunnage/blocking within the package cavity to limit foam outgassing to an insignificant level. This temperature limit is conservatively below 500 °F where significant weight loss due to thermal decomposition begins to occur for the material. A detailed description of the foam's behavior under elevated temperatures is presented in Appendix 3.5.4, *'Last-A-Foam' Response under HAC*.

The QQ-L-171E lead used for payload shielding serves no structural purpose but avoidance of lead melting is desirable because of possible shielding loss associated with the movement of the lead within the cavity. As such, the temperature limitation for either normal or accident conditions is the melting point for lead of approximately 620 °F [13].

Type 304 and A564 Type 630 stainless steel have melting point above 2,500 °F [13], but in compliance with ASME B&PV Code [15], the allowable temperature is limited to 800 °F for structural components (e.g., the material's structural properties are relied on for loads postulated to occur in the respective operating mode or accidental free drop condition). As such, the appropriate upper temperature limit under normal conditions is 800 °F for stainless steel components that form the containment boundary or are used in the payload support. The upper limit for all other stainless steel components is assumed to be 2,500 °F for both normal and accident conditions.

The maximum accessible outside surface temperature of the exclusive use package is 185 °F or less when exposed to environment of 100 °F air temperature and in the shade [1].

The minimum allowable service temperature for all package components is below -40 °F.

Table 3.2-1 – Thermal Properties of Packaging Materials (2 pages)

Material	Temperature (°F)	Thermal Conductivity (Btu/hr-ft-°F)	Specific Heat (Btu/lb$_m$-°F)	Density (lb$_m$/in^3)
Stainless Steel Type 304	-40[①]	8.2	0.112	0.289
	70	8.6	0.114	
	100	8.7	0.115	
	200	9.3	0.119	
	300	9.8	0.123	
	400	10.4	0.126	
	500	10.9	0.129	
	600	11.3	0.130	
	700	11.8	0.132	
	800	12.3	0.134	
	1000	13.1	0.135	
	1200	14.0	0.138	
	1400	14.9	0.141	
	1500	15.3	0.142	
ASTM A564, Type 630	-40[①]	9.6	0.107	0.282
	70	10.0	0.109	
	100	10.1	0.110	
	200	10.6	0.115	
	300	11.2	0.121	
	400	11.7	0.126	
	500	12.3	0.133	
	600	12.8	0.139	
	700	13.1	0.144	
	800	13.4	0.152	
	1000	13.9	0.179	
	1200	14.3	0.226	
	1400	14.9	0.165	
	1500	15.5	0.159	

Table 3.2-1 – Thermal Properties of Packaging Materials (2 pages)

Material	Temperature (°F)	Thermal Conductivity (Btu/hr-ft-°F)	Specific Heat (Btu/lb$_m$-°F)	Density (lb$_m$/in^3)
Lead ASTM B29 (any grade)	-58	21.7	0.030	0.410
	32	20.4	0.030	
	80.6	30.0	0.030	
	158	19.9	0.031	
	260.6	19.4	0.032	
	428	18.4	0.033	
	608	16.5	0.033	
	620.6	16.4	0.036	
Polyurethane Foam	-	0.02750[2]	0.353	0.01065[2]
	-	0.02234[3]	0.353	0.00787[3]

Notes:

[1] Property values for -40 °F extrapolated from those at higher temperatures.

[2] Based on FR3716 'Last-a-Foam' properties [10]. Values based on high tolerance foam density (i.e., 16 pcf + 15%).

[3] Based on FR3716 'Last-a-Foam' properties [10]. Values based on low tolerance foam density (i.e., 16 pcf - 15%).

Table 3.2-2 – Thermal Properties of Air

Temperature (°F)	Density (lb_m/in^3) [1]	Specific Heat $(Btu/lb_m\text{-}°F)$	Dynamic Viscosity $(lb_m /ft\text{-}hr)$	Thermal Conductivity $(Btu/hr\text{-}ft\text{-}°F)$	Prandtl Number [2]	Coef. Of Thermal Exp. $(°R^{-1})$ [3]
-40		0.240	0.03673	0.0121		
0		0.240	0.03953	0.0131		
50		0.240	0.04288	0.0143		
100		0.241	0.04607	0.0155		
200		0.242	0.05207	0.0178		
300		0.243	0.05764	0.0199		
400	Use Ideal Gas Law w/ Molecular wt = 28.966	0.245	0.06286	0.0220		
500		0.248	0.06778	0.0240	Compute as $Pr = c_p\mu / k$	Compute as $\beta = 1/(°F+459.67)$
600		0.251	0.07242	0.0259		
700		0.253	0.07680	0.0278		
800		0.256	0.08098	0.0297		
900		0.259	0.08500	0.0315		
1000		0.262	0.08887	0.0333		
1200		0.269	0.09620	0.0366		
1400		0.274	0.10306	0.0398		
1500		0.277	0.10633	0.0412		

Table Notes:

[1] Density computed from ideal gas law as $\rho = PM/RT$, where R= 1545.35 ft-lbf/lb-mole-R, T= temperature in °R, P= pressure in lbf/ft², and M= molecular weight of air. For example, at 100 °F and atmospheric pressure of 14.69lbf/in², ρ = (14.69*144 in²/ft²*28.966 lbm/lb-mole)/(1545.35*(100+459.67)) = 0.071 lbm/ft³.

[2] Prandtl number computed as $Pr = c_p\mu / k$, where c_p = specific heat, μ = dynamic viscosity, and k = thermal conductivity. For example, at 100 °F, Pr = 0.241*0.04607/0.0155 = 0.72.

[3] Coefficient of thermal expansion is computed as the inverse of the absolute temperature. For example, at 100 °F, β = 1/(100+459.67) = 0.00179.

3.3 Thermal Evaluation for Normal Conditions of Transport

This section presents the thermal and gas generation evaluation of the 380-B package under normal conditions of transport (NCT). The package and payload configurations are assumed to be as described in Section 3.1, *Description of Thermal Design*. The thermal model used in the evaluation is described in Appendix 3.5.3, *Analytical Thermal Model*, while the thermal properties assumed for the various components are presented in Section 3.2.1, *Material Properties*. These evaluations establish the thermal and gas safety basis required to assess compliance with the 10CFR71 safety criteria [1] for the NCT Hot, NCT Hot (no solar), and NCT Cold conditions. The safety basis for the NCT Hot ambient condition is evaluated using 12 and 24-hour averaged insolation loading. The evaluations also establish compliance with the IAEA TS-R-1 [2] safety criteria for normal conditions of transport. The package is assumed to be backfilled with air at atmospheric pressure at the time of loading.

3.3.1 Heat and Cold

The NCT thermal performance is determined using a 3-D thermal model of the 380-B package. The modeling uses approximately 26,000 nodes, 3,000 planar elements and 4,500 solid elements to represent and provide thermal resolution within the various packaging components that make up the simulated package segment. This modeling choice captures the full height of the packaging components and allows the incorporation of the varying insolation loads that will occur along the height of the package, while taking advantage of the assumed symmetry of the payload configuration and heat distribution within the package. The various packaging components are defined using a combination of planar and solid elements.

The thermal model is developed for use with the Thermal Desktop® [23] and SINDA/FLUINT [24] computer programs. Details of the thermal models, the analysis methodology, and mesh refinement studies are provided in Appendix 3.5.3, *Analytical Thermal Model*.

3.3.1.1 Maximum Temperatures

Table 3.3-1 presents the predicted 380-B package temperatures under the evaluated NCT scenario for the 'open' type dunnage configuration (see Section 3.1.2, *Content's Decay Heat*). Given the mass of the package, the maximum package component temperatures for all but the thermal shield, the personnel barrier, the peak foam temperature, outer shell, and the impact limiter shells are computed using the regulatory insolation loading averaged over 24 hours. The results demonstrate that large thermal margins exist for all packaging components with the minimum thermal margin of 117 °F (i.e., 250 - 133 °F) occurring for the cask closure seals. The relatively large ratio of surface area of the 380-B package to the relatively low 205 W heat loading allows the package to dissipate the maximum payload decay heat to the ambient conditions with only a small ΔT (~27 °F), as evidenced by the *NCT Hot (No Solar)* results for the closure lid under operations in an 100 °F ambient environment.

Evaluation of the package for an ambient air temperature of 100 °F without insolation loads demonstrates that the peak temperature for the accessible exterior surfaces of the packaging is below the maximum 185 °F permitted by 10 CFR §71.43(g) for exclusive use shipments. A peak accessible surface temperature of 103 °F is predicted.

Figure 3.3-1 and Figure 3.3-2 illustrate the predicted temperature distribution within the 380-B package under the NCT Hot condition and with the 'open' style dunnage support. The effect of concentrating the dissipated decay heat over the upper surface of the cask cavity under the 'open' style dunnage heat distribution scenario (see Section 3.1.2, *Content's Decay Heat*) is clearly visible in the figures. Despite this concentration, the combination of a relatively low decay heat loading and the thermal conductivity provided by the lead shielding yields a temperature gradient of only 7 °F in the inner shell between the cask lid and the cask lower end structure.

Figure 3.3-4 illustrates a comparative temperature distribution within the 380-B package for NCT Hot (No Solar) condition. As seen from a comparison between the figures and the results in Table 3.3-1, inclusion of insolation loads adds approximately 10 °F to the peak package component temperatures, approximately 20 °F to the peak thermal shield temperature, and approximately 50 °F to the peak impact limiter shell temperature.

Figure 3.3-3 repeats the temperature distributions from Figure 3.3-1 and Figure 3.3-2 for the cask body and lid, but without the lead shield material. The figure illustrates the less than 5 °F temperature differential expected in the radial direction through the cask body due to the combination of a low decay heat loading and the thermal spreading provided by the large thermal conductance of the lead shielding along the cask's long axis.

To assess the sensitivity of the predicted NCT temperatures to the assumed distribution of the decay heat over the interior surfaces of the cask cavity, the analysis for the *NCT Hot* condition was repeated for the 'restrictive' type dunnage configuration described in Section 3.1.2, *Content's Decay Heat*). As from the results presented in Table 3.3-2 and in Figure 3.3-6 and Figure 3.3-7, the peak lid and closure seal temperatures are 7 and 2 °F cooler, respectively, while the peak inner and outer shell and side lead temperatures are essentially unchanged. Concentrating the dissipated decay heat on a short vertical segment of the cask's inner shell results in a nearly uniform temperature distribution over the length of the cask cavity. Therefore, it is concluded that the exact configuration of payload device and its associated dunnage will have only a small impact on the peak temperatures reached within the packaging.

3.3.1.2 Minimum Temperatures

Table 3.3-1 and Figure 3.3-6 present the predicted package temperatures for the cold condition of transport (i.e., *NCT Cold*, see Appendix 3.5.3.4, *Design Basis Ambient Conditions*). The minimum package temperature will occur with a zero decay heat load and an ambient air temperature of -40 °F per 10 CFR §71.71(c)(2). Since a portion of the heat transfer is via radiation, the change in the temperature gradient between adjacent components of the packaging is larger for the cold ambient temperature versus the hot conditions. However, due to the relatively low decay heat loading, the differences are relatively small and not thermally significant.

The evaluation of this steady-state thermal condition requires no formal thermal calculation since all package components will eventually achieve the -40 °F temperature. As discussed in Section 3.2.3, *Component Specifications*, -40 °F is within the allowable operating temperature range for all package components.

3.3.2 Maximum Normal Operating Pressure

The maximum normal operating pressure (MNOP) is estimated based on no payload outgassing, but will arise from ideal gas expansion and outgassing from the payload dunnage. Since the payload isn't explicitly modeled, the bulk gas temperature is calculated assuming all 205 watts are transferred from the payload to the cask lid via natural convection only. This scenario is similar to the open dunnage case in Section 3.1.2, Content's Decay Heat. This method for predicting the bulk gas temperature is conservative since it neglects all radiative heat transfer between the payload and package cavity, and uses only 17% of the cavity surface area for convection. The bulk gas temperature (T_{gas}) is given by:

$$T_{gas} = q/h_c A + T_{cask}$$

where the total heat transfer (q) is 205 watts, the peak inner surface of the lid (T_{cask}) is 138°F from Table 3.3-1, and the surface area of the cask cavity (A) involved in convection is:

$$A = 0.25\pi(38 \text{ in.}/12)^2 = 7.88 \text{ ft}^2$$

where the cask cavity diameter is 38 inches. This area conservatively ignores the 14.4 inches involved in the convective heat transfer from Section 3.1.2, *Content's Decay Heat* in the first term of the heat equation above.

The natural convection coefficient (h_c) is calculated using the correlations for a horizontal flat plate that is cooler than the gas convecting to the plate's lower surface. The correlations are cited from Equations 3.12, 3.24, and 3.34 through 3.36 of [22], and are presented below:

$$h_c = Nu \times k/L_c$$

$$Nu = \left(Nu_l^{10} + Nu_t^{10}\right)^{0.1}$$

$$Nu_l = \frac{1.4}{\ln(1 + 1.677/C_l Ra^{0.25})}$$

$$Nu_t = 0.14 Ra^{1/3}$$

The characteristic length of the plates (L_C) is the surface area divided by the perimeter:

$$L_c = \frac{7.88 \text{ ft}^2}{\pi(38 \text{ in.}/12)} = 0.79 \text{ ft}$$

The equations above were iteratively solved for both the *NCT HOT* and *NCT Hot (No Solar)* scenarios:

	k (Btu/hr-ft²-°F)	Pr	Ra	h_C (Btu/hr-ft²-°F)	T_{cask} (°F)	T_{gas} (°F)
NCT HOT (12hr Solar)	0.0174	0.71	3.04E+07	0.97	138	232
NCT Hot (No Solar)	0.0172	0.71	3.19E+07	0.97	127	218

The air properties and dimensionless heat transfer numbers given above are calculated using the values given in Table 3.2-2 at the predicted film temperature. The laminar coefficient (C_L) for a Prandtl number of 0.71 is 0.515 per Table of 3.1 [22].

The peak pressure developed within the package cavity during NCT due to ideal gas expansion is estimated by assuming that the package cavity is filled with air at 70 °F and atmospheric

pressure following the loading procedure. Combining this temperature with the predicted bulk gas temperature under the *NCT Hot* condition, the ideal gas law yields:

$$\text{Pressure Rise from Ideal Gas Expansion} = 14.7\text{psia}\frac{(232°F + 460°F)}{70°F + 460°F} - 14.7 \text{ psia} = 4.4 \text{ psig}$$

No out-gassing will occur for dunnage fabricated of metallic or polyurethane foam components. However, dunnage fabricated of wood has the potential of contributing to the pressurization of the cask cavity due to long-term evaporation of the moisture content in the wood. The rate of cavity pressurization is a highly complex function of the total amount of wood used, the size of the wood components, the moisture content, and its drying rate at the environmental conditions in the cask cavity.

To avoid the complexity of an exact calculation, the safety evaluation uses a simple methodology to bound the maximum cask cavity pressure rise associated with moisture evaporation from wood dunnage. This methodology is based on the fact that the maximum partial pressure of the water within the cask cavity can't rise above the saturation pressure for water at the temperature of the inner shell. That conclusion is based on the knowledge that the inner cask shell will serve as a condensing surface whenever the partial pressure for water within the cavity rises above the saturation pressure associated with the temperature of the inner shell. Once reached, any subsequent moisture evaporation from the wood dunnage would be removed via condensation on the inner shell surface, thus limiting the maximum partial pressure for water regardless of the amount of moisture present in the dunnage

The saturation pressure of water at the peak payload cavity containment temperature (i.e., 138 °F from Table 3.3-1) is 2.6 psi [from Table 4.2.19, Reference 29]. As such, the maximum cavity gas pressure under NCT when wood dunnage is used will not rise above the sum of the partial pressure of water and the pressure rise due to ideal gas expansion, or 2.6 psi + 4.4 psig = 7.0 psig.

For conservatism, the MNOP within the package cavity is set at a bounding level of 10 psig. Table 3.3-3 summarizes the estimated cavity pressures for the evaluated transport conditions and dunnage material. As shown in Appendix 5.5.4, *Gas Generation due to Radiolysis*, pressure resulting from radiolysis of the dunnage from the package contents is not of concern.

Table 3.3-1 – NCT Temperatures for 380-B Package with Open Dunnage Support

Component	Temperature (°F)			
	NCT Hot[4] (No Solar)	NCT Hot[1][4]	NCT Cold[4]	Allowable[2]
Inner Shell	123	133	5	800
Outer Shell	122	132 / 141[3]	4	800
Lower End Structure	119	131	2	800
Closure Lid	127[5]	138[5]	9	800
Closure Bolt	123	133	5	800
Lead - Side	122	133	4	620
- Lower	119	131	1	620
- Lid	126	136	8	620
Thermal Shield	119	129 / 138[3]	0	2,500
Main Containment Seal	123	133	5	250
Vent Port Sealing Washer	123	133	5	250
Upper End Structure	123	134	5	800
Impact Limiter - Max. Foam	125	144 / 176[3]	7	300
- Avg. Foam	109	130	-10	300
- Shell	125	146 / 180[3]	8	2,500
- Attachment Bolts	122	133	4	800
Personnel Barrier	101	111 / 120[3]	-19	2,500
Max. Accessible Surface	103	-	-	185

Notes: [1] Based on steady-state evaluation with 24-hour average of regulatory insolation loading, except where noted.

[2] See Section 3.2.3, *Component Specifications*, for basis of listed temperature criterion

[3] Based on steady-state evaluation with 12-hour average of regulatory insolation loading.

[4] Results based on the maximum decay heat of 205W.

[5] Maximum payload cavity containment temperature.

Table 3.3-2 – NCT Temperatures for 380-B Package with Restrictive Dunnage Support

Component	Temperature (°F) NCT Hot[1][3]	Temperature (°F) Allowable[2]
Inner Shell	133	800
Outer Shell	131	800
Lower End Structure	131	800
Closure Lid	131	800
Closure Bolt	130	800
Lead - Side	132	620
- Lower	131	620
- Lid	131	620
Thermal Shield	129	2,500
Main Containment Seal	131	250
Vent Port Sealing Washer	130	250
Upper End Structure	131	800
Impact Limiter - Max. Foam	143	300
- Avg. Foam	129	300
- Shell	146	2,500
- Attachment Bolts	133	800
Personnel Barrier	111	2,500
Max. Accessible Surface	-	185

Notes: [1] Based on steady-state evaluation with 24-hour average of regulatory insolation loading, except where noted.

[2] See Section 3.2.3, *Component Specifications*, for basis of listed temperature criterion.

[3] Results based on the maximum decay heat of 205 W.

Table 3.3-3 – NCT Pressures for 380-B Packaging

Condition	Package Cavity Pressure	
	Wood Dunnage	**Metallic or Polyurethane Foam Dunnage**
NCT Hot (No Solar) [1]	6.7 psi gauge	4.1 psi gauge
NCT Hot	7.0 psi gauge	4.4 psi gauge
NCT Cold[2]	-1.8 psi gauge	-1.8 psi gauge

Notes: [1] Calculated using the ideal gas law with a bulk gas temperature of 218 °F, and the same 2.6 psig saturated water pressure as the *NCT HOT* case.

[2] Calculated using the ideal gas law with the 5 °F inner shell temperature from Table 3.3-1.
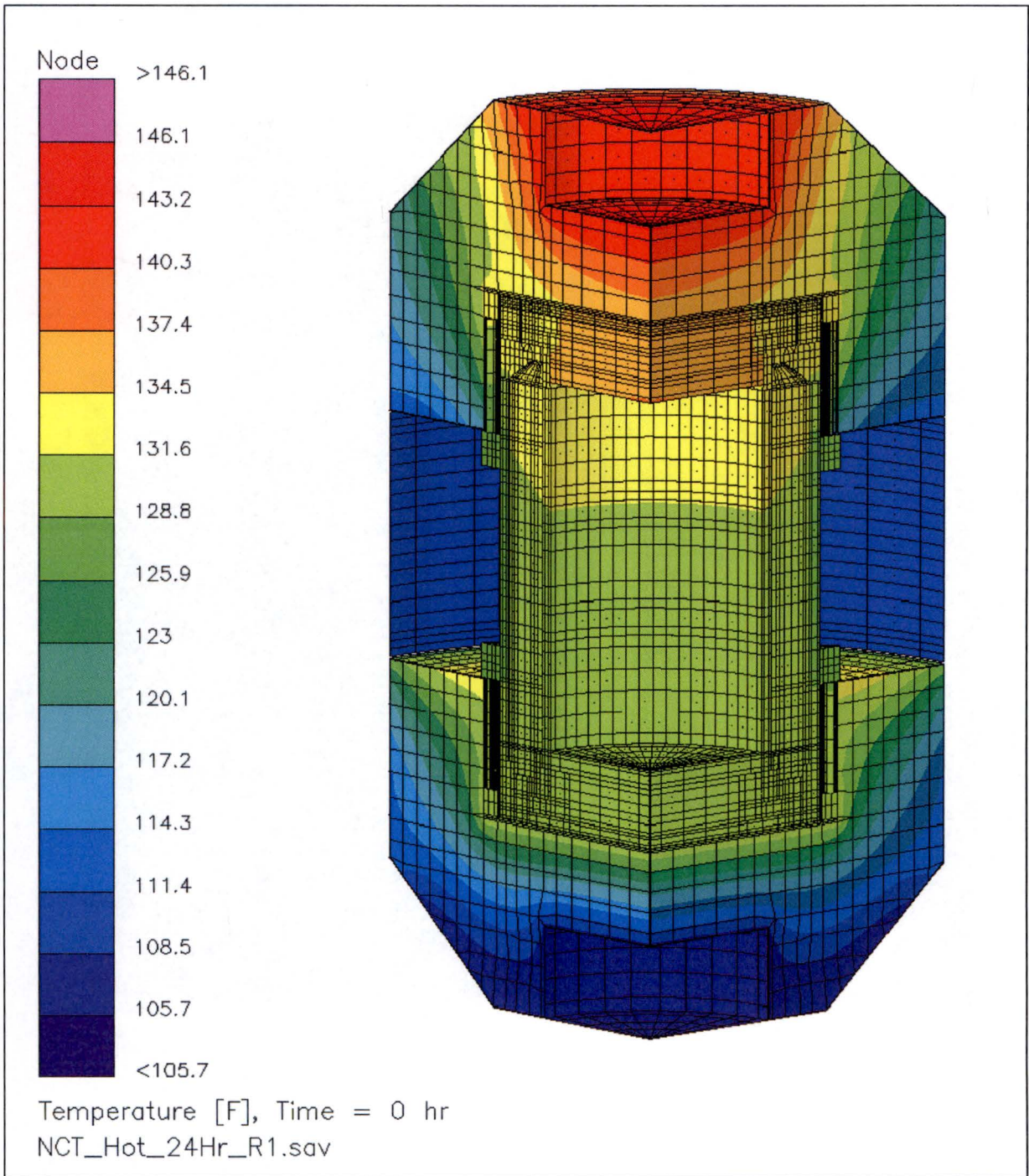
Note: Results shown for 24-hour average insolation loading

Figure 3.3-1 – NCT Hot Temperature Distribution for 380-B
Packaging with Open Dunnage Support
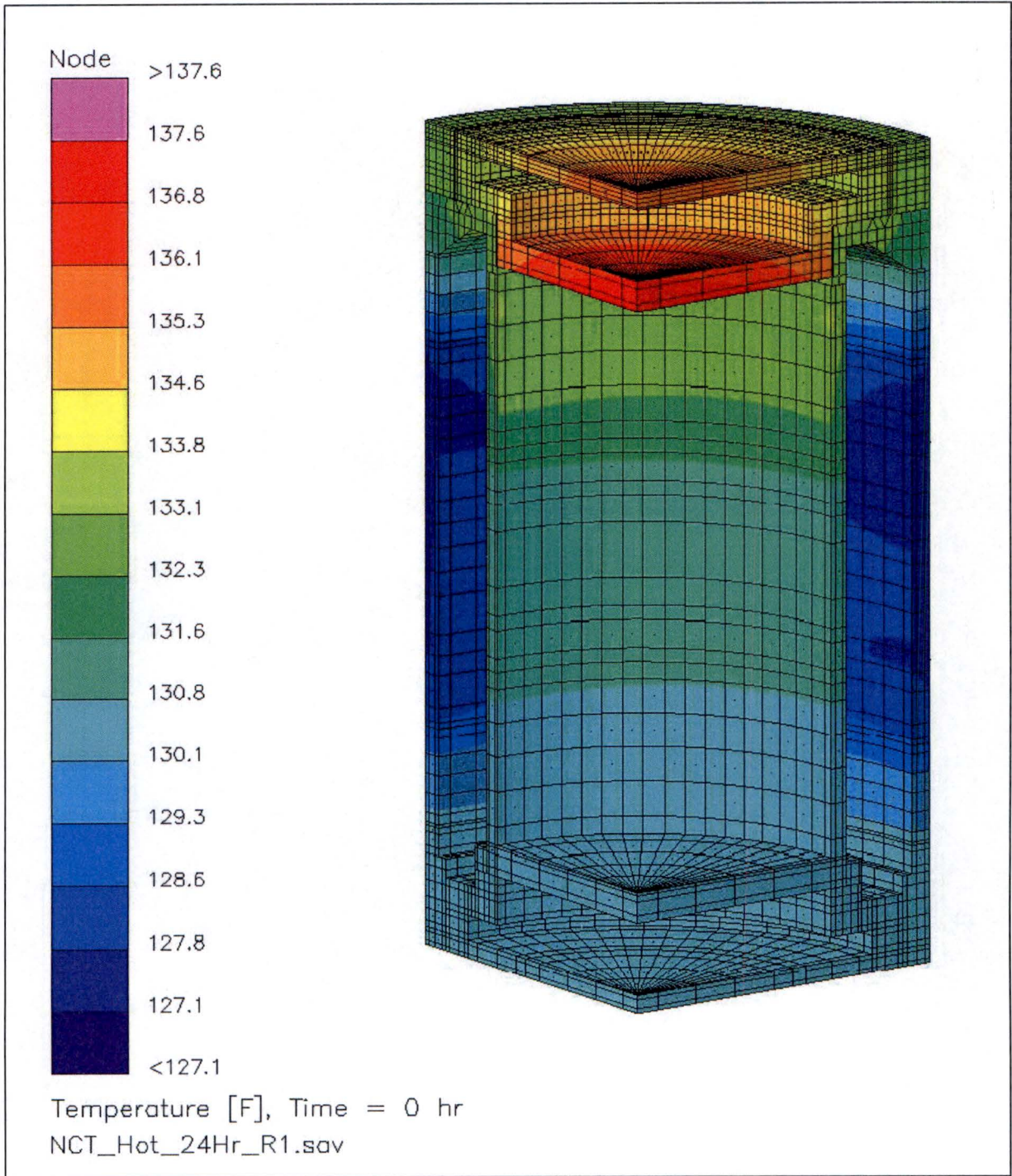
Note: Results shown for 24-hour average insolation loading

Figure 3.3-2 – NCT Hot Temperature Distribution for 380-B Shells
with Open Dunnage Support
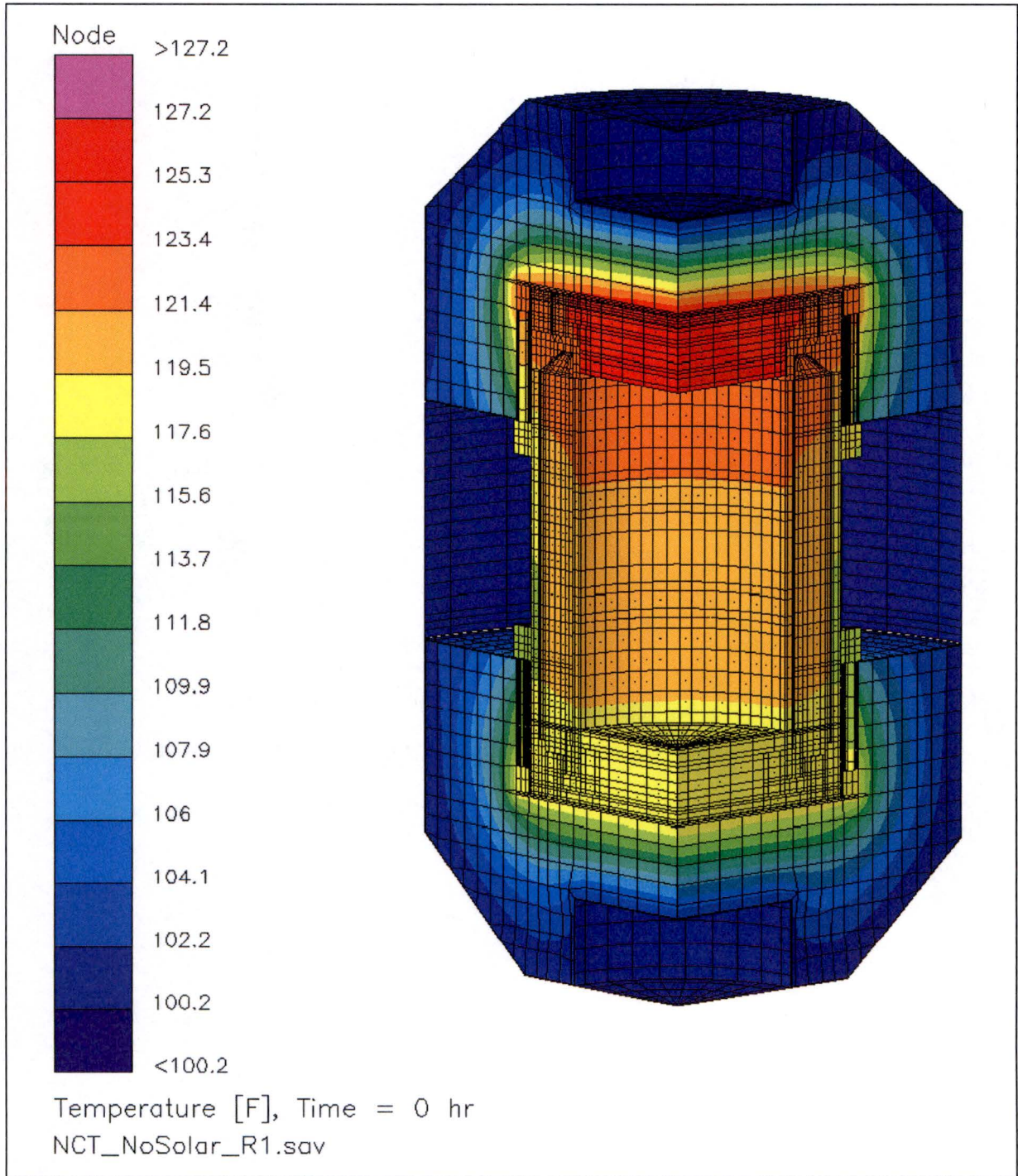
Figure 3.3-3 – NCT Hot (No Solar) Temperature Distribution for 380-B Packaging with Open Dunnage Support
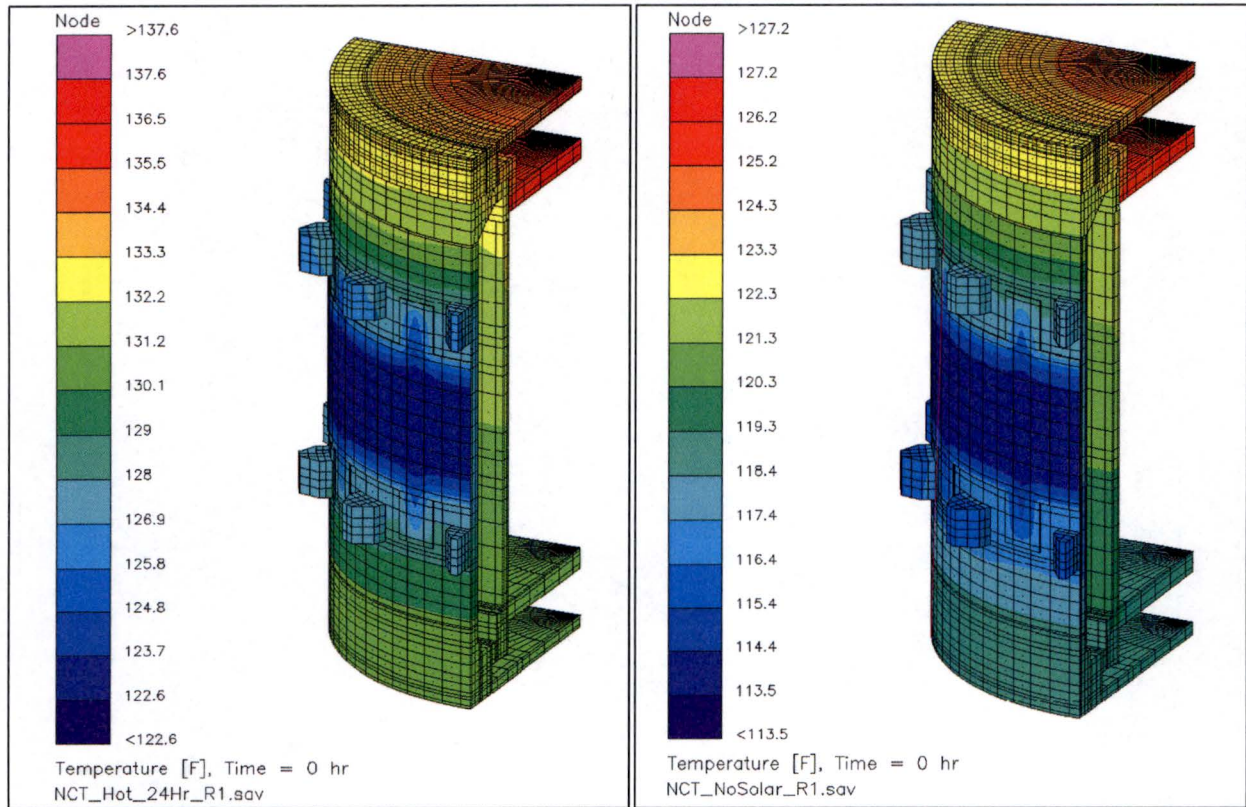
Note: Results shown for 24-hour average insolation loading   Note: Results shown for no insolation loading

Figure 3.3-4 – NCT Cask Shell Temperature Distribution with
Open Dunnage Support
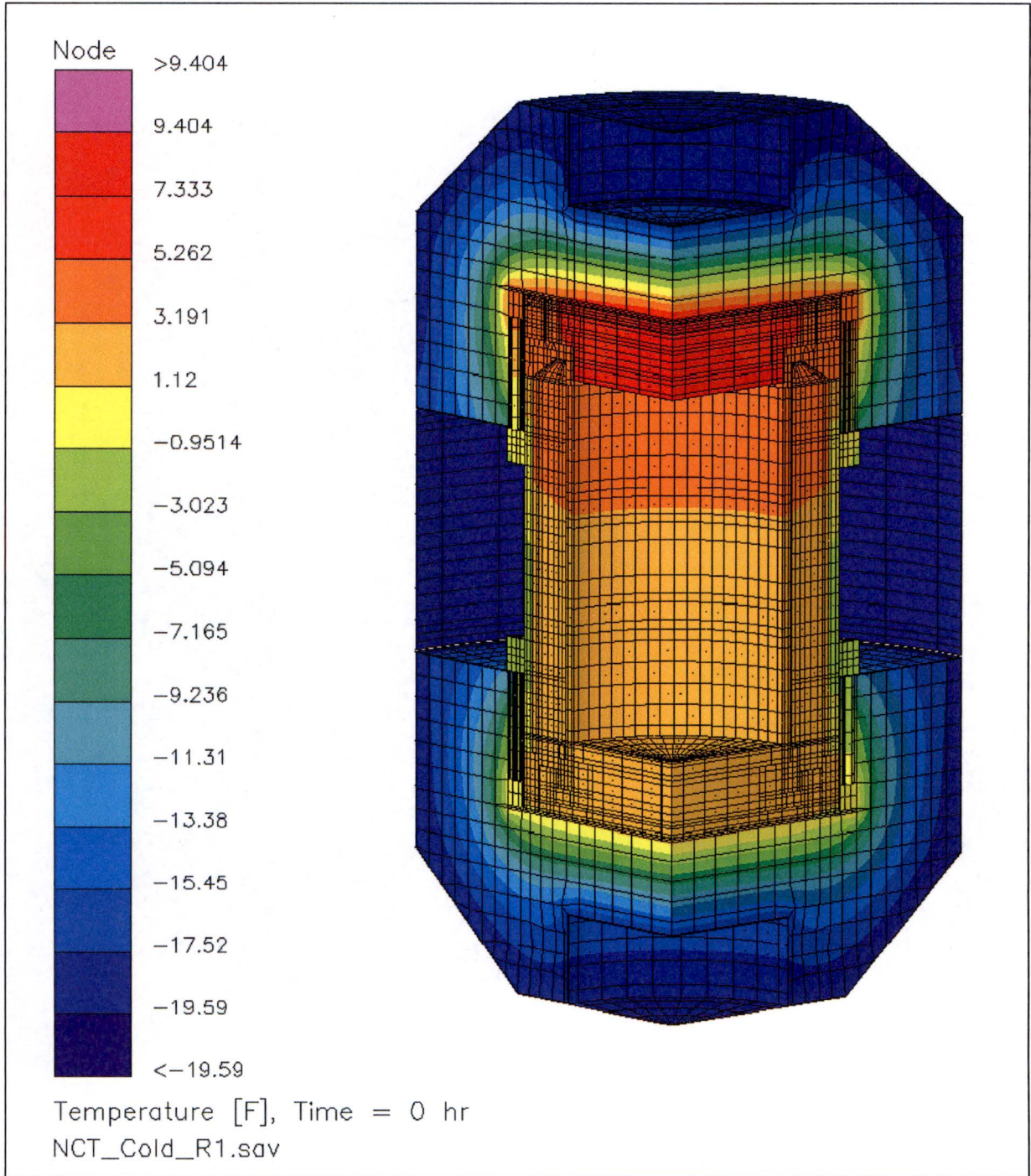
Figure 3.3-5 – NCT Cold Temperature Distribution for 380-B Packaging with Open Dunnage Support

Node

>146
146
143.2
140.3
137.4
134.5
131.6
128.7
125.9
123
120.1
117.2
114.3
111.4
108.6
105.7
<105.7

Temperature [F], Time = 0 hr
NCT_Hot_24Hr_EndCapDun_R1.sav
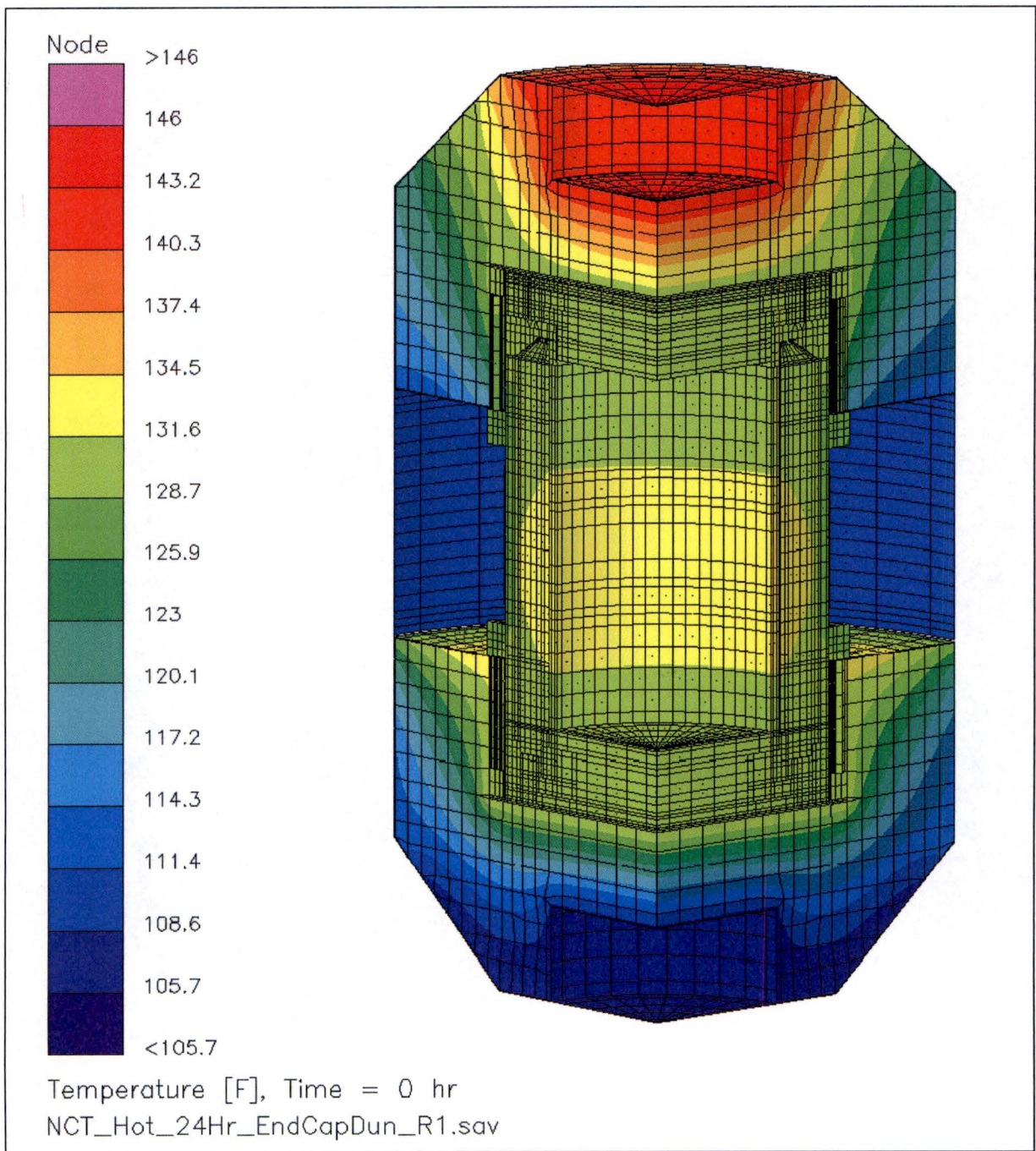
Note: Results shown for 24-hour average insolation loading

Figure 3.3-6 – NCT Hot Temperature Distribution for 380-B Packaging with Restrictive Dunnage Support

Node

	>133.3
	133.3
	132.8
	132.3
	131.9
	131.4
	130.9
	130.5
	130
	129.5
	129.1
	128.6
	128.2
	127.7
	127.2
	126.8
	<126.8

Temperature [F], Time = 0 hr
NCT_Hot_24Hr_EndCapDun_R1.sav
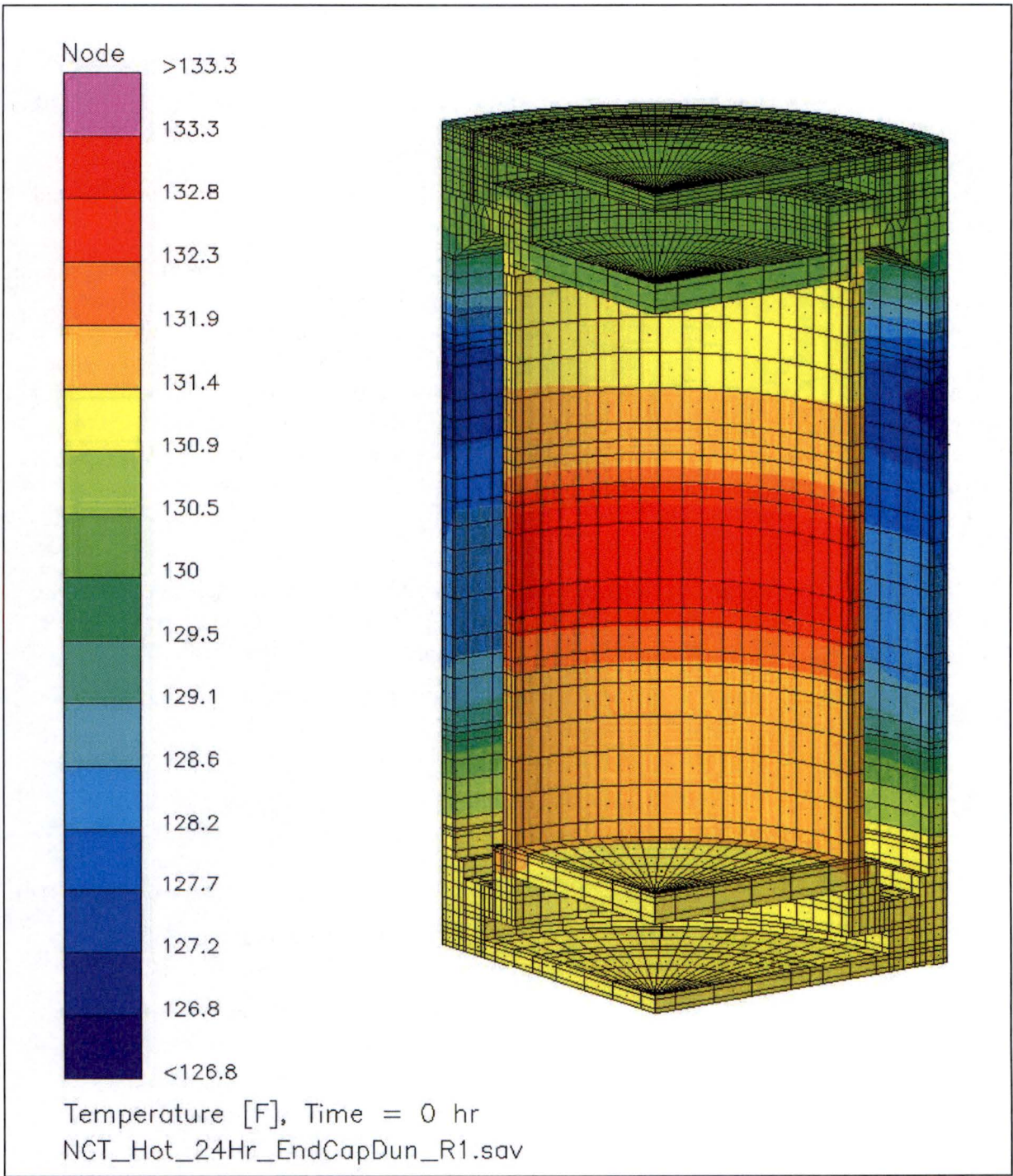
Note: Results shown for 24-hour average insolation loading

Figure 3.3-7 – NCT Hot Temperature Distribution for 380-B Cask Shells with Restrictive Dunnage Support

3.4 Thermal Evaluation for Hypothetical Accident Conditions

This section presents the thermal evaluation of the 380-B package under HAC specified in 10 CFR §71.73(c)(4) and IAEA TS-R-1. The evaluation is based on modified versions of the analytical NCT thermal models for the 380-B package. Appendix 3.5.3.5, *Description of Thermal Model for HAC*, presents a description of the modifications made to the NCT model to reflect HAC.

Physical testing using prototypic half-scale certification test units (CTUs) is used to establish the expected level of damage sustained by the 380-B packaging from the 10 CFR 71.73 prescribed free and puncture drops preceding the HAC fire event. The configuration and initial conditions of the test article, the test facilities and instrumentation used, and the test results are documented in Section 2.12.3, *Certification Test Results*. An overview of the test results, the rationale for selecting the worst-case damage scenario, and the details of the thermal modeling used to simulate the package conditions during the HAC fire event are provided in Appendix 3.5.3.5, *Description of Thermal Model for HAC*.

3.4.1 Initial Conditions

The initial conditions assumed for the package prior to the HAC event are described below in terms of the modifications made to the NCT thermal model to simulate the assumed package conditions prior to and during the HAC event. These thermal model modifications are:

- simulated the expected worst-case damage arising from the potential HAC free drops, determined in Appendix 3.5.3.5, *Description of Thermal Model for HAC*, and added the associated worst-case puncture drop damage,

- assume a horizontal package orientation following the regulatory drop event, add heat transfer to and from the base of the package to simulate a fully engulfing fire event, and ignore the potential for self-shading in determining the insolation loading,

- increased the emissivity of all external surfaces to 0.8 and the solar absorptivity to 1.0 to account for possible oxidation and/or soot accumulation on the surfaces,

- increased the emissivity of the interior surface of the thermal shield from 0.2 to 0.45 to account for potential oxidization during the course of the HAC event,

- the emissivity of the cask surfaces not directly exposed to the fire, but nominally covered by the impact limiters is raised to 0.4 and emissivity of the opposing surfaces on the impact limiter are raised to 0.5 to account for possible condensation on the surfaces by volatile organic compounds (VOCs) generated during the fire,

- increase the emissivity of all other package surfaces from 0.20 to 0.30 to conservatively bound the potential surface condition at fabrication,

- include credit for potential heat transfer between the thermal shield and the cask body via the wire wrap standoffs,

- assume that the personnel barrier and the sheet over the recess cavities on the impact limiters are torn off during the regulatory drop event that precedes the HAC fire,

- removed a minimum of 2.7 inches of foam from the exterior portions of the impact limiter foam block and added heat transfer via radiation within the impact limiter enclosures with an emissivity of 0.925 to account for the loss of polyurethane foam from thermal decomposition. While this foam volume would be gradually lost over the course of the 30-minute fire event, the modeling conservatively assumes this foam volume is lost instantaneously at the start of the fire event, and

- assumed an initial temperature distribution equivalent to the package at steady-state conditions with 'open' style payload dunnage decay heat distribution (see Section 3.1.2, *Content's Decay Heat*), a 100 °F ambient and 24-hour averaged regulatory insolation. The chosen decay heat distribution provides the maximum starting temperature for the cask closure seals, while the inclusion of the effects of insolation prior to the fire event exceeds the requirement of 10 CFR §71.73(b) and complies with the requirement of IAEA.

3.4.2 Fire Test Conditions

The fire test conditions analyzed to address the 10 CFR §71.73(c) requirements are as follows:

- The initial pre-fire ambient conditions are assumed to be 100 °F ambient with solar insolation,

- At time = 0, a fully engulfing fire environment consisting of a 1,475 °F ambient with an effective emissivity of 1.0 is used to simulate the average flame temperature of the hydrocarbon fuel/air fire event. The assumption of an average flame emissivity of 1.0 conservatively bounds the minimum 0.9 flame emissivity specified by 10 CFR §71.73(c)(4).

- The convection heat transfer coefficients between the package and the ambient during the 30-minute fire event are based on an average gas velocity of 10 m/sec [26]. Following the 30-minute fire event the convection coefficients are based on still air.

- The ambient condition of 100 °F with insolation is assumed following the 30-minute fire event. A solar absorptivity of 1.0 is assumed for "full insolation" post-fire per Section 3.5.5.2 of NUREG-1609 [3].

The transient analysis is continued for 11.5 hours after the end of the 30-minute fire event to ensure the modeling captures the peak package temperatures.

3.4.3 Maximum Temperatures and Pressure

Table 3.4-1 presents the predicted peak component temperature for the 380-B package under HAC as predicted for the end of the 30-minute fire and throughout the modeled 12 hour transient event. As seen from the table, the thermal mass of the cask body and the thermal protection afforded by the impact limiters and the thermal shield limits the temperature rise within the packaging components below the maximum short term limits for all packaging components. The

minimum thermal margin occurs for the vent port sealing washer which is predicted to peak at 392 °F approximately 2 minutes after the end of the fire. This peak temperature is 8 °F below the 400 °F short term temperature for butyl rubber. The next lowest thermal margin of 112 °F occurs for the main containment seal which is predicted to reach a maximum temperature of 288 °F versus an allowable short term temperature limit of 400 °F for butyl rubber. This is reached 27.5 minutes following the end of the 30-minute fire event. Although the vent port sealing washer is near 400°F, it is above 350 °F for only 20 minutes as illustrated in Figure 3.4-7. The margins on the seals are deemed acceptable since the butyl rubber seal material has been proven to meet the leak tight criteria after tests of 430°F for one hour, and 400 °F for 8 hours (as discussed in Section 3.2.3, *Component Specifications*).

The minimum thermal margin for the structural components of the cask occurs for the lid with a predicted peak temperature of 643 °F, yielding a thermal margin of 157 °F, based on a conservatively low allowable temperature limit of 800 °F. The second lowest structural component thermal margin occurs for the outer shell at the base of the impact limiter attachment lugs. The predicted peak temperature of 628°F yields a thermal margin of 172°F. The peak inner shell temperature of 294 °F occurs approximately 47 minutes after the end of the fire event.

Figure 3.4-1 presents the temperature distribution within the package at the end of the 30-minute fire event. The large thermal gradients noted along the outer edges of the remaining impact limiter foam demonstrates the significant thermal protection afforded by even a small thickness of remaining foam. The relatively large foam thicknesses incorporated in the impact limiters provides a large safety margin against material lost to thermal decomposition or drop deformation.

Figure 3.4-2 illustrates the temperature distribution within the cask body at the end of the 30-minute fire event, and Figure 3.4-3 illustrates the associated temperature distribution within the cask shells only (heat shield removed). A comparison of the two figures demonstrates the effectiveness of the thermal shield in limiting the peak temperature in the outer shell of the package.

The effect of the drop damage on the HAC peak temperatures can be seen in the Figure 3.4-4 surface temperature distribution. The primary asymmetry caused by the CG-over-corner drop and subsequent worst case puncture bar damage is an approximate 460°F increase in the local lid temperature seen in the left side of the figure over the average lid temperature. This local temperature rise results from the localized foam loss (see discussion in Appendix 3.5.3.5, *Description of Thermal Model for HAC*) associated with the modeled CG-over-corner drop and worst case puncture bar damage. The simulated direct contact between the limiter and the cask over a 120° arc centered about the centerline of the drop damage can be seen in the wider band of elevated cask surface temperature noted at the top of the cask shell versus that seen at the bottom of the cask shell. Likewise, the increased limiter-to-cask gap over the upper circumference of the package resulting from the drop damage is seen in the inward shift and lowering of the peak cask surface temperature along the right side of the figure.

Figure 3.4-5 presents the temperature distribution of the package closure lid at the end of the 30-minute fire event. It also depicts the locations of the vent port sealing washer relative to the modeled symmetry plane. As can be seen the peak temperature on the cask lid is in the region of the exposed impact limiter attachment lug which yields a bounding temperature for the vent port sealing washer.

Figure 3.4-6 illustrates the predicted temperature gradient within the impact limiter attachment bolts and lugs at the end of the 30-minute fire event.

Figure 3.4-7 presents the transient temperature profiles for selected cask components. As seen from the figure, all cask components reached their peak temperature point within one hour of termination of the 30-minute HAC fire.

3.4.3.1 Maximum HAC Pressures

The maximum HAC pressure is estimated based on no payload outgassing and the use of the peak inner shell temperature as means of estimating the bulk gas temperature. Given that the peak inner shell temperature will lead the bulk gas temperature under HAC conditions, this methodology is seen as sufficient for the purpose of this safety evaluation.

Assuming no thermal decomposition or outgassing from the packaging dunnage and/or the payload device, the peak cask cavity pressure under HAC conditions can be estimated based solely on ideal gas expansion. Under the HAC condition, the peak bulk average gas (i.e., inner shell) temperature is 294 °F. Based on an assumed backfill gas temperature of 70 °F, the predicted maximum pressure within the cask cavity is computed via:

$$\text{Pressure Rise From Ideal Gas Expansion} = 14.7\text{psia}\frac{(294^{\circ}\text{F} + 460 \ ^{\circ}\text{F})}{(70 \ ^{\circ}\text{F} + 460 \ ^{\circ}\text{F})} - 14.7 \text{ psia} = 6.2 \text{ psig}$$

Outgassing from dunnage fabricated of metallic components will not occur. The same is true for dunnage fabricated from polyurethane foam since the peak foam temperature will remain below the 325 °F temperature point where a slight weight loss and outgassing from polyurethane foam is noted as beginning (see Appendix 3.5.4, *'Last-A-Foam' Response under HAC*). In contrast, wood dunnage has the potential to contribute to the cask cavity pressurization due to the evaporation of the moisture content in the wood. As with the calculation for NCT, the rate of cavity pressurization is a highly complex function of the total amount of wood present, the size of the wood components, the moisture content, and the environmental conditions in the cask cavity. In reality, only a fraction of the total moisture will be released during the HAC transient since thicker pieces of wood require an extended exposure time to dry out.

To avoid the complexity of an exact calculation, the safety evaluation uses a simple methodology to bound the maximum cask cavity pressure rise associated with moisture evaporation. This methodology is based on the fact that the maximum partial pressure of the water within the cask cavity can't rise above the saturation pressure for water at the temperature of the inner shell. That conclusion is based on the knowledge that the inner cask shell serves as the heating source for the payload and dunnage during HAC and the saturation pressure associated with the temperature of the inner shell is the maximum partial pressure for water that can be reached regardless of the amount of moisture present in the dunnage.

The saturation pressure of water at the peak inner shell temperature (i.e., 294 °F) is 60 psia [from Table 4.2.19, Reference 29]. As such, the maximum cavity gas pressure under HAC when wood dunnage is used will not rise above the sum of the partial pressure of water and the pressure rise due to ideal gas expansion, or 60 psia + (6.2 psig + 14.7) - 14.7 = 66.2 psig.

For conservatism, a peak HAC pressure of 100 psig is assumed when wood dunnage is used and 15 psig when metallic or polyurethane foam dunnage is used.

3.4.3.2 Non-metallic Contents Materials Under HAC

Several non-metallic materials may be present in the 380-B cask and could be exposed to elevated temperatures in association with the HAC fire event. Polyurethane foam or wood may be utilized as blocking or dunnage. Lifting slings may optionally be left inside the cask for use in removal of the contents. Other materials may be present on the shielded device in a way that makes them difficult or impracticable to remove (such as paint). Since heat is flowing into the package during the HAC fire event, the highest temperature experienced by any materials within the cask will be the peak temperature of the cavity containment boundary. Per Table 3.4-1, the peak temperature is for the inner shell sidewall, at 294 °F. Thus, the peak temperature of any material inside the cask is bounded by the peak sidewall temperature. Table 3.4-2 lists each non-metallic material and its minimum thermal decomposition temperature based on published reference information. The minimum thermal decomposition temperature is typically based on the mass loss of a sample measured using thermogravimetric analysis (TGA). As shown, each non-metallic material has a significant margin of safety on its temperature limit, and gas generation or pressurization from the thermal decomposition of these materials in association with the HAC fire event will not occur. Of note, these materials are not important to safety, and consequently their function under NCT or HAC is not required. The potential evolution of water vapor from wood is conservatively evaluated in Section 3.3.2, *Maximum Normal Operating Pressure*, and Section 3.4.3.1, *Maximum HAC Pressures*.

3.4.4 Maximum Thermal Stresses

The maximum thermal stresses under the HAC condition are addressed in Section 2.7.4, *Thermal*.

Table 3.4-1 – Peak HAC Temperatures for 380-B Package

Component	Temperature (°F)			
	End of 30-Minute Fire	**Peak Transient**	**Allowable**[1]	**Thermal Margin**
Inner Shell	208	294[2][3]	800	506
Outer Shell	628	628	800	172
Lower End Structure	156	230	800	570
Closure Lid	643	643	800	157
Closure Bolt	570	570	800	230
Lead - Side	383	404[3]	620	216
- Lower	135	221	620	399
- Lid	301	311	620	309
Thermal Shield	1,251	1,251	2,500	1,249
Main Containment Seal	218	288[3]	400	112
Vent Port Sealing Washer	385	392[3]	400	8
Upper End Structure	354	364	800	436
Impact Limiter - Max. Foam	-	-	N/A	-
- Avg. Foam	-	-	N/A	-
- Shell	1,472	1,472	2,500	1,028
- Attachment Bolts	1,183	1,183	2,500	1,317
Personnel Barrier	-	-	N/A	-

Notes: [1] See Section 3.2.3, *Component Specifications*, for basis of listed temperature criterion.

[2] Maximum payload cavity containment temperature.

[3] Peak temperatures at time after end of fire: Vent Port Sealing Washer at 392 °F at 2 minutes, Main Containment Seal at 288 °F at 27 minutes, Side Lead 404 °F at 5 minutes, Inner Shell 294 °F at 47 minutes.

Table 3.4-2 – Non-metallic Contents Materials①

Material	Temperature limit and Data Source	Margin, °F
Polyurethane foam	Negligible degradation below 435 °F per Section 3.5.4, *'Last-a-Foam' Response under HAC Conditions*	141
Wood	Table 2 of [31] indicates a minimum temperature for 2.5% mass loss of 482 K (408 °F).	114
Rubber	Figure 19 of [32] shows weight loss is negligible below approximately 300 °C (572 °F).	278
Lifting Slings (Nylon)	578 K (581 °F) from pg. 204 of [33]	287
Lifting Slings (polyester)	Figure 1(a) of [34] shows negligible decomposition below approximately 350 °C (662 °F).	368
Lifting Slings (Kevlar©)	700 K (800 °F) from pg. 155 of [33]	506
Paint	Significant degradation does not occur below 200 °C to 300 °C (392 °F to 572 °F), from Figure 1 and Figure 2 of [35], Figure 1a from [36], and Figure 1 of [37].	98
Grease	Decomposition of the grease thickener begins at about 250 °C (482 °F), from Section 2.3 of [38].	188
Vacuum Grease②		90
Silicone Sealant	Degradation does not occur below 300 °C (572 °F), from Table 3 of [39] and Figure 5 of [40].	278
Graphite	800 °C (1,472 °F) from Table II of [32].	1,178
Epoxy Adhesive	Weight loss is less than 5% up to 318 °C (604 °F), per [41].	310
Acrylic or Acetal Plastic	Lower bound degradation (Acetal) does not occur below 210 °C (410 °F) [42].	116

Notes:

1. Maximum temperature of any material in this table is for the cask inner shell, equal to 294°F per Table 3.4-1, unless stated otherwise.

2. Maximum temperature of vacuum grease is for the vent port sealing washer, 392 °F per Table 3.4-1.
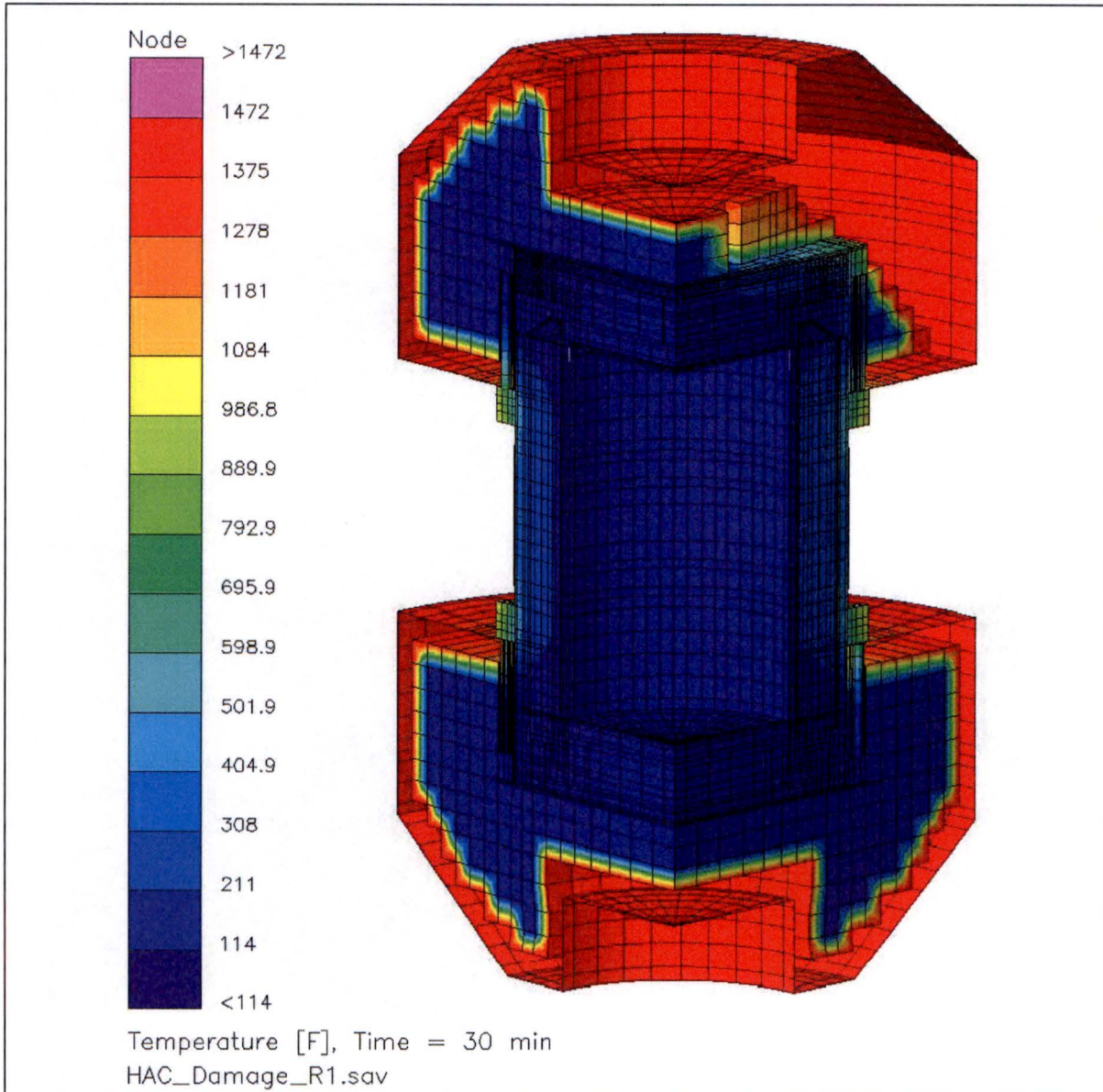
**Figure 3.4-1 – HAC Temperature Distribution at End of
30-Minute Fire**
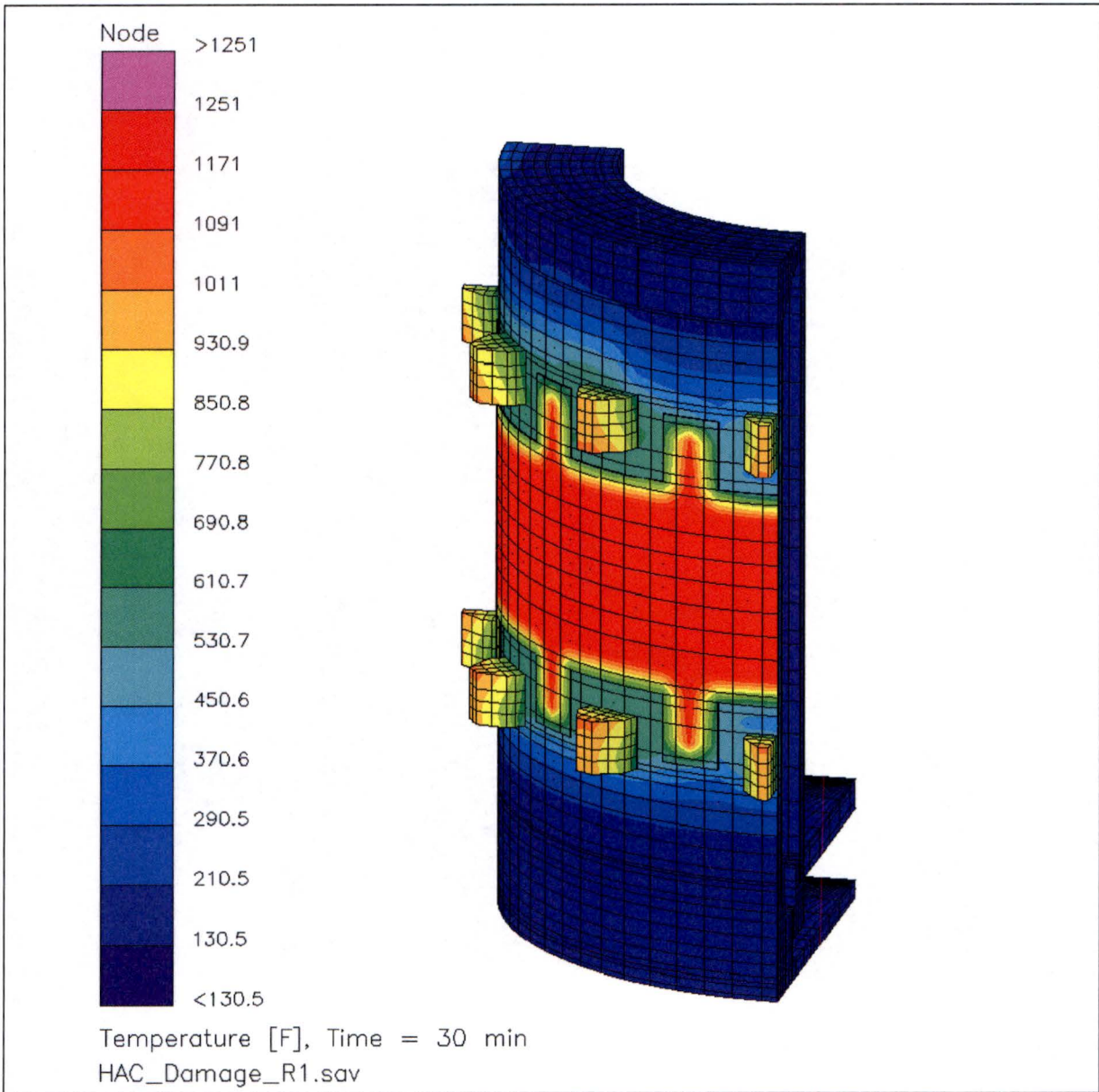
Figure 3.4-2 – Cask Body Temperature Distribution at End of 30-Minute Fire
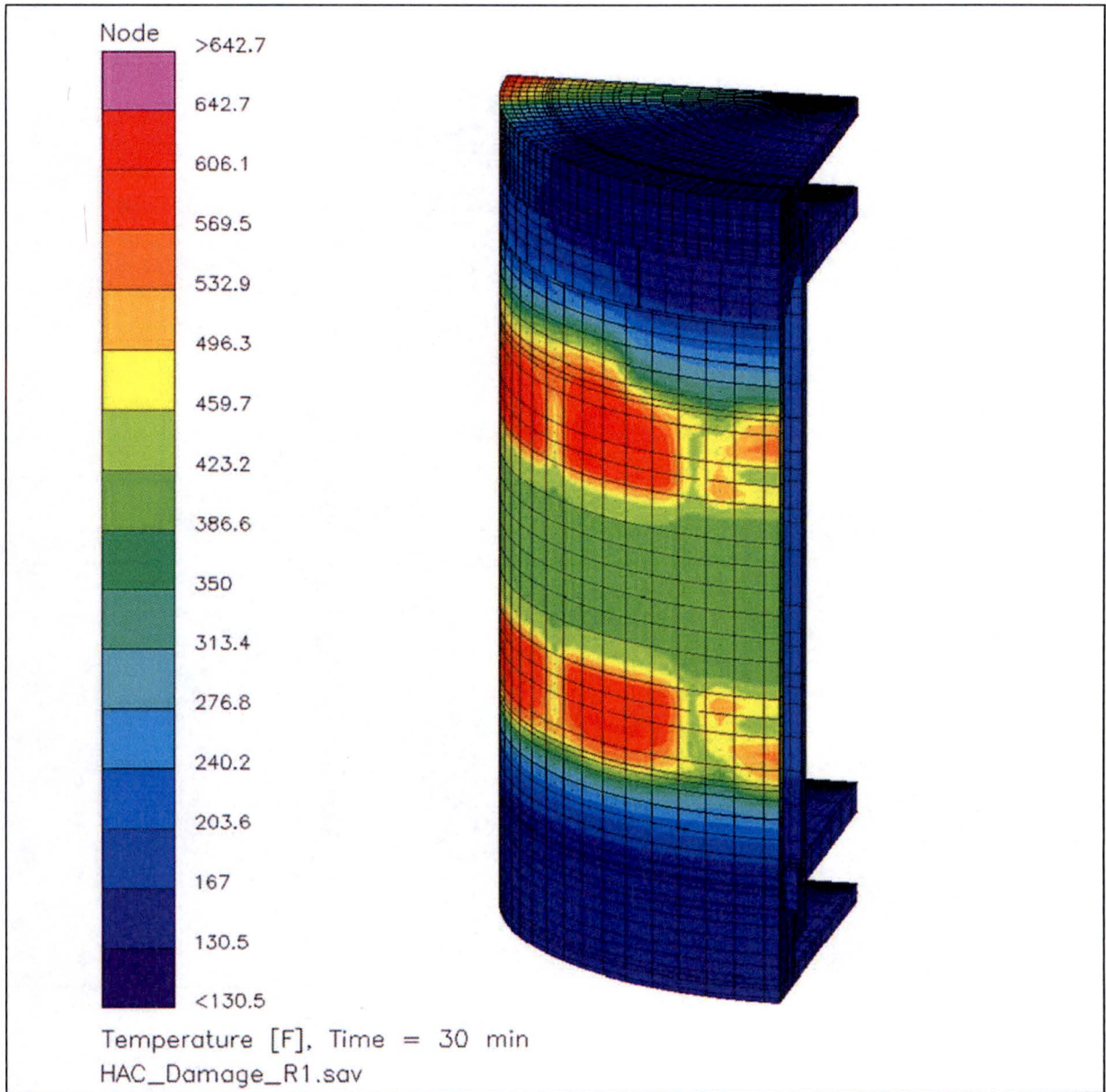
Figure 3.4-3 – Cask Shell Temperature Distribution at End of 30-Minute Fire

Node

>642.7
642.7
606.1
569.5
532.9
496.3
459.7
423.2
386.6
350
313.4
276.8
240.2
203.6
167
130.5
<130.5

Centerline of free
and puncture bar
drop damage

Beginning of
enlarged cask-
limiter gap

Cask Lug
Locations

Temperature [F], Time = 30 min
HAC_Damage_R1.sav
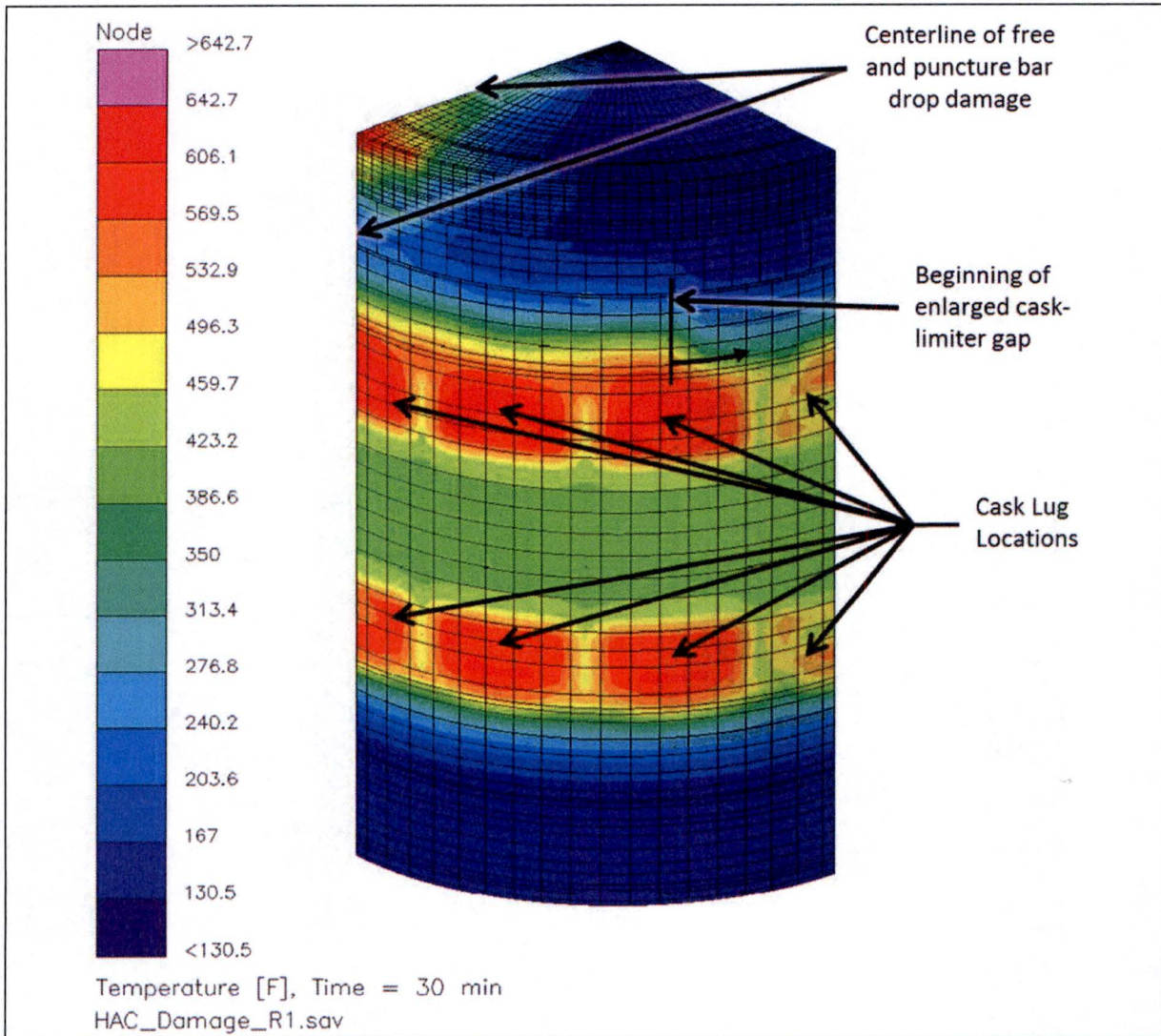
Figure 3.4-4 – Cask Surface Temperature Distribution at End
of 30-Minute Fire
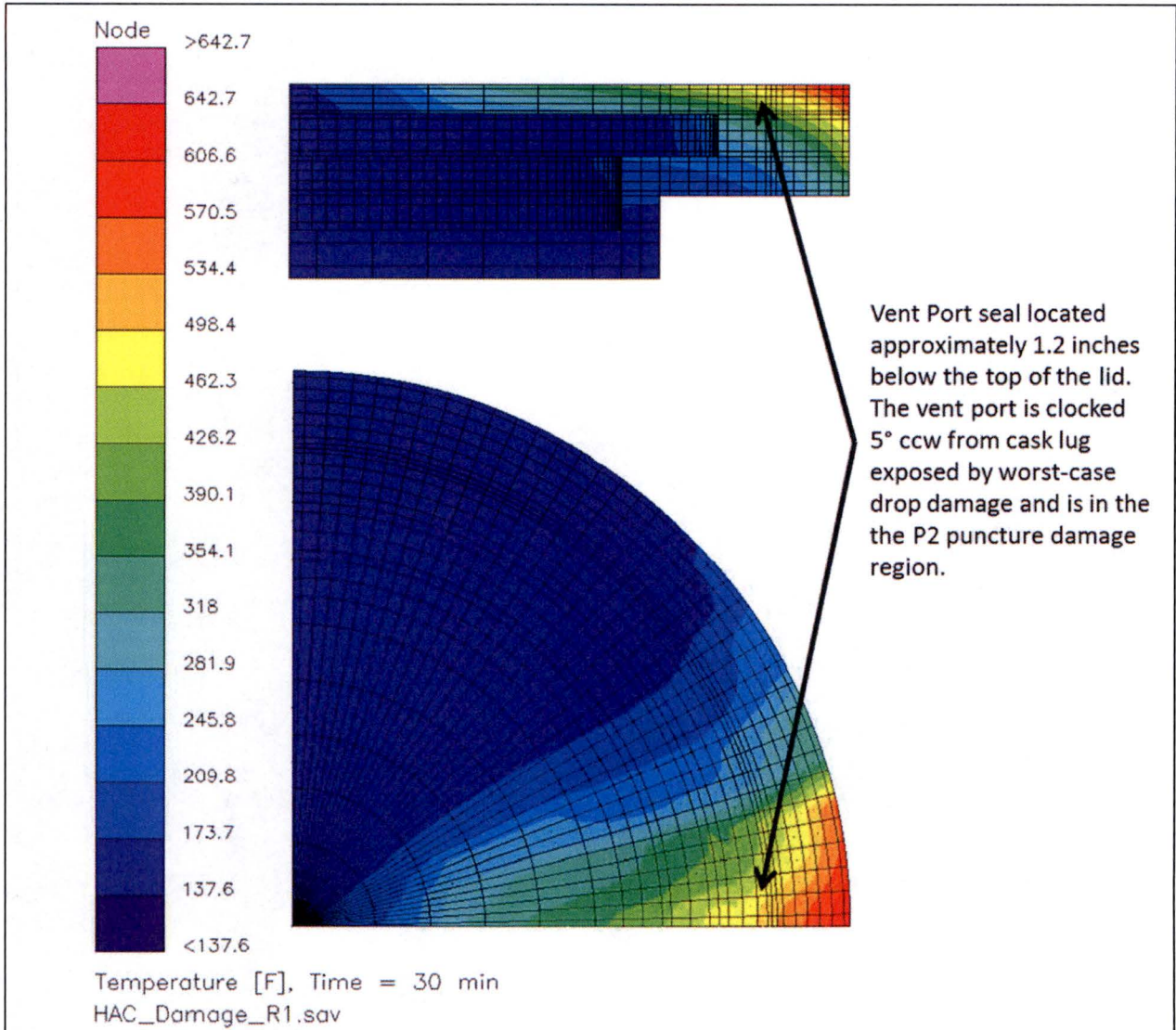
Figure 3.4-5 – Cask Closure Lid at End of 30-Minute Fire
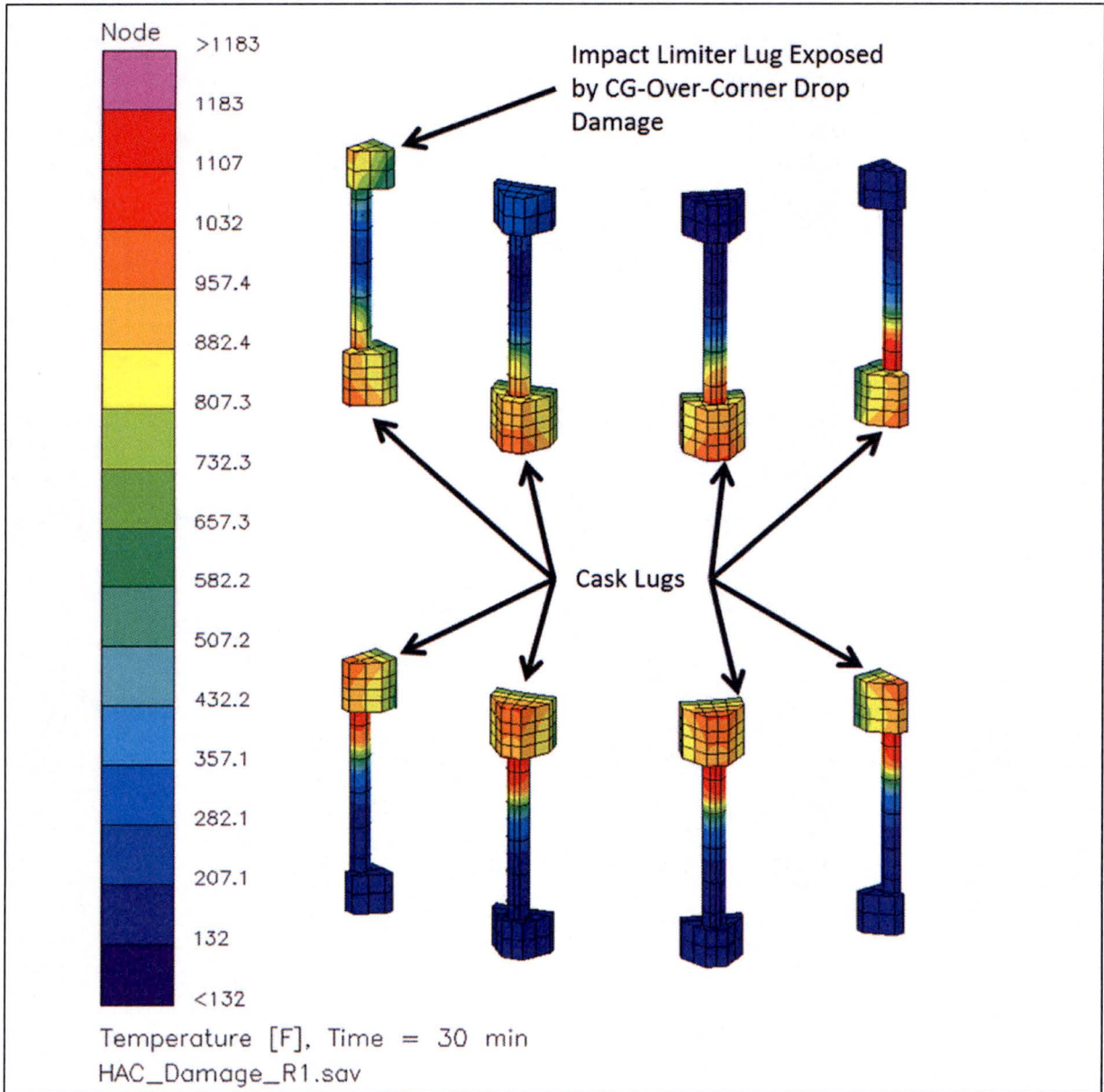
Figure 3.4-6 – Limiter Bolt/Lug Temperature Distribution at End of 30-Minute Fire
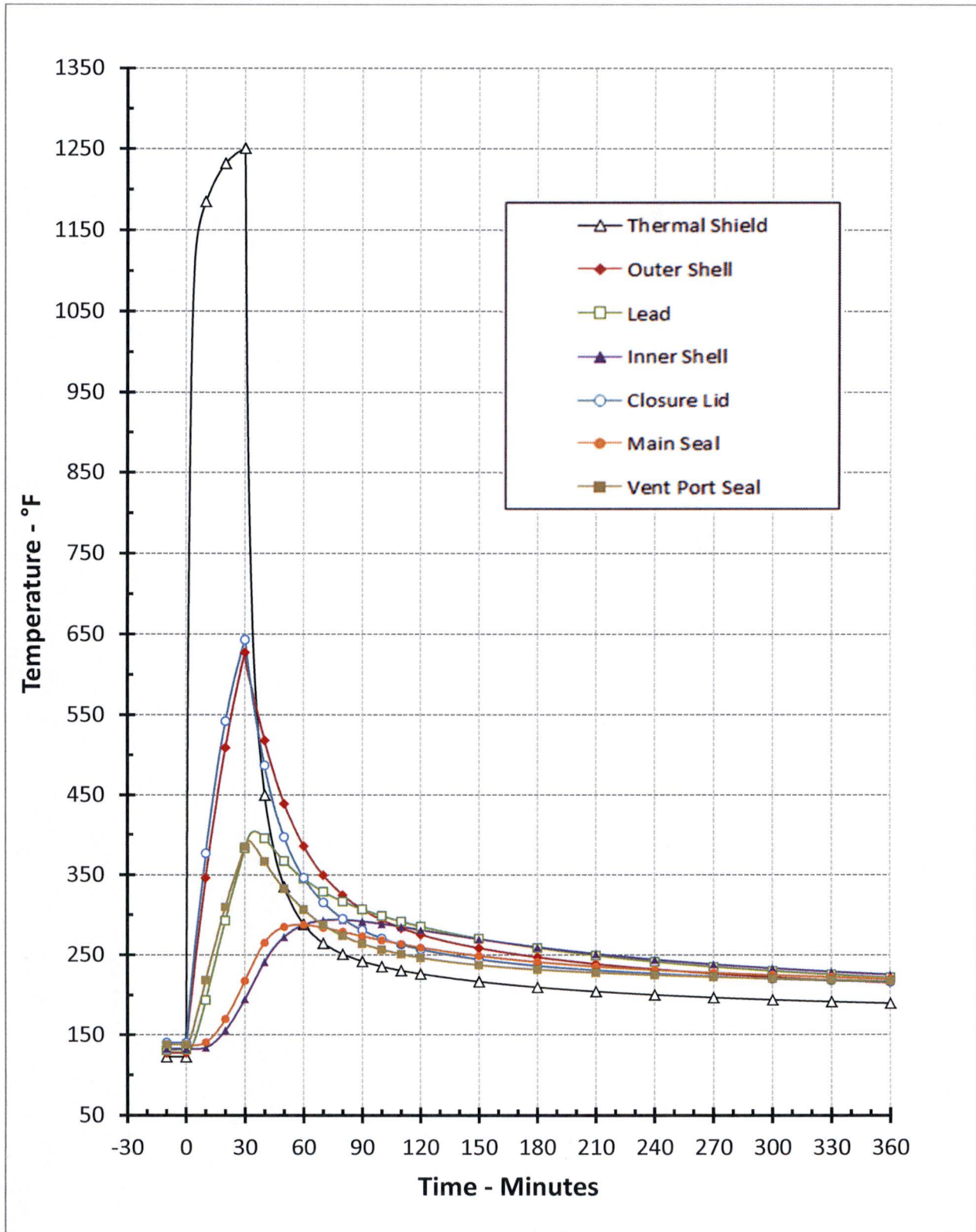
Figure 3.4-7 – Transient Temperature Profiles for HAC Fire
Event

3.5 Appendices

3.5.1   References

3.5.2   Computer Analysis Results

3.5.3   Analytical Thermal Model

3.5.4   'Last-A-Foam' Response under HAC

3.5.1 References

1. Title 10, Code of Federal Regulations, Part 71 (10 CFR 71), *Packaging and Transportation of Radioactive Material*, United States Nuclear Regulatory Commission (USNRC), 01–01–11 Edition.

2. International Atomic Energy Agency, *Regulations for the Safe Transport of Radioactive Material*, TS-R-1, 2009 Edition.

3. NUREG-1609, *Standard Review Plan for Transportation Packages for Radioactive Material*, Office of Nuclear Material Safety and Safeguards, U.S. Nuclear Regulatory Commission, Washington, DC 20555-0001, March 1999.

4. U. S. Nuclear Regulatory Commission, Regulatory Guide 7.8, *Load Combinations for the Structural Analysis of Shipping Casks for Radioactive Material*, Revision 1, March 1989.

5. Not Used.

6. Not Used.

7. Rainier Rubber Company, Seattle, WA, www.rainierrubber.com.

8. Parker O-Ring Material Offering Guide, ORD 5712, August 2002, *www.parkerorings.com*.

9. Westinghouse Hanford Company, *Radioisotope Thermoelectric Generator Transportation System Packaging O-ring Material Elevated Temperature Test Report*, WHC-SD-RTG-TRP-002, Rev 0.

10. Last-A-Foam™ On-line Data Sheet, *www.generalplastics.com*.

11. Williamson, C., and Iams, Z., *Thermal Assault and Polyurethane Foam - Evaluating Protective Mechanisms for Transport Containers*, General Plastics Manufacturing Company, Tacoma, WA, Waste Management '05 Symposium, Tucson, AZ, 2005.

12. Williamson, C., and Iams, Z., *Thermal Assault and Polyurethane Foam - Evaluating Protective Mechanisms*, General Plastics Manufacturing Company, Tacoma, WA, PATRAM International Symposium, Berlin, Germany, 2004.

13. Matweb, Online Material Data Sheets, *www.matweb.com*.

14. American Society of Mechanical Engineers (ASME) 2010 Boiler and Pressure Vessel (B&PV) Code with 2011a Addenda, Section II, Part D, *Properties (Customary) Materials*, July 2011.

15. American Society of Mechanical Engineers (ASME) Boiler & Pressure Vessel Code, Section III, *Rules for Construction of Nuclear Facility Components*, Division 1, Subsection NB, Class 1 Components, 2010 Edition.

16. Lead Industries Association, Inc., *Properties of Lead and Lead Alloys*, Booklet No. 5M-12-83, New York, NY.

17. Frank, R., and Plagemann, W., *Emissivity Testing of Metal Specimens*, Boeing Analytical Engineering coordination sheet No. 2-3623-2-RF-C86-349, August 21, 1986.

18. Banken, G., and Byeman, M., *Emissivity Testing of Type 304 Stainless Steel and 6061 Aluminum Specimens*, March 19, 2013.

19. Gubareff, G., Janssen, J., and Torborg, R., Thermal Radiation Properties Survey, 2nd Edition, Honeywell Research Center, 1960.

20. Azzazy, M., *Emissivity Measurements of 304 Stainless Steel*, Report #ATI-2000-09-601, prepared for Southern California Edison, by Azzazy Technologies, Inc., September 6, 2000.

21. Rohsenow, Hartnett, and Choi, Handbook of Heat Transfer, 3rd edition, McGraw-Hill Publishers, 1998.

22. Guyer, Eric, Handbook of Applied Thermal Design, McGraw-Hill, Inc., 1989.

23. Thermal Desktop®, Version 5.8, Cullimore & Ring Technologies, Inc., Littleton, CO, 2015.

24. SINDA/FLUINT, Systems Improved Numerical Differencing Analyzer and Fluid Integrator, Version 5.8, Cullimore & Ring Technologies, Inc., Littleton, CO, 2015.

25. AFS Calculation SD-THERMALDESKTOP-5.8-CALC-3018413, Rev. 0, *Thermal Desktop® and SINDA/FLUINT Version 5.8 Software Dedication Report*.

26. Schneider, M.E and Kent, L.A., *Measurements Of Gas Velocities And Temperatures In A Large Open Pool Fire, Heat and Mass Transfer in Fire*, HTD Vol. 73, 1987, ASME, New York, NY.

27. Mohamad, A., *Natural Convection in Open Cavities and Slots*, Numerical Heat Transfer, Part A, Vol 27, pp. 705-716, 1995.

28. Chan, Y., and Tien, C., *A Numerical Study of Two-Dimensional Laminar Heat Convection in Shallow Open Cavities*, International Journal of Heat and Mass Transfer, Vol 28, pp. 603-612, 1985.

29. Avallone, E., and Baumeister III, T., Mark's Standard Handbook for Mechanical Engineers, 10th Ed, McGraw-Hill.

30. Internal Atomic Energy Agency, *Advisory Material for the IAEA Regulations for the Safe Transport of Radioactive Material*, TS-G-1.1 (Rev. 1).

31. Morten Gunnar Gronli, Gabor Varhegyi, and Colomba Di Blasi, *Thermogravimetric Analysis and Devolatilization Kinetics of Wood*, Industrial & Engineering Chemistry Research, 2002, 41 (17), 4201-4208.

32. Sircar, Anil K., *Analysis of Elastomer Vulcanizate Composition by TG-DTG Techniques*, Center for Basic and Applied Polymer Research, University of Dayton, 1991.

33. Polymer Data Handbook, Oxford University Press, 1999.

34. K.S. Muralidhara and S. Sreenivasan, *Thermal Degradation Kinetic Data of Polyester, Cotton and Polyester-Cotton Blended Textile Material*, World Applied Sciences Journal, 11 (2): 2010.

35. Debora Pugia, Liliana Manfredi, Analia Vazquez, and Jose Kenny, *Thermal degradation and fire resistance of epoxy-amine-phenolic blends*, Polymer Degradation and Stability 73, (2001).

36. Shahla Ataei, Rosiyah Yahya, and Seng Neon Gan, *Study of Thermal Decomposition Kinetics of Palm Oleic Acid-Based Alkyds and Effect of Oil Length on Thermal Stability*, Journal of Polymers and the Environment, June 2012.

37. Kelly Roberts, Matthew J. Almond, and John W. Bond, *Using Paint to Investigate fires: An ATR-IR Study of the Degradation of Paint Samples Upon Heating*, Journal of Forensic Sciences, March 2013, Vol. 58, No. 2.

38. Fumihiko Yokoyama, *Optimization of Grease Properties to Prolong the Life of Lubricating Greases*, Journal of Physical Science and Application, 4 (4) (2014).

39. Jelena D. Jovanovic, Milutin N. Govedarica, Petar R. Dvornic, & Ivanka G. Popovic, *The thermogravimetric analysis of some polysiloxanes*, Polymer Degradation and Stability 61 (1998), 87 – 93.

40. G. Camino, S.M. Lomakin, and M. Lazzari, *Polydimethylsiloxane thermal degradation Part 1. Kinetic aspects*, Polymer 42 (2001), 2395 – 2402.

41. 3M Scotch-Weld™ Epoxy Adhesive DP100 Plus Clear Technical Datasheet, September 2016.

42. DuPont Material Safety Data Sheet, *"DELRIN" Acetal Resin/PTFE Blends All In Synonym List DEL012*, Revised 20-APR-2007.

3.5.2 Computer Analysis Results

Due to the size and number of the output files associated with each analyzed condition, results from the computer analysis are provided on a DVD.

3.5.3 Analytical Thermal Model

This section presents details of the thermal modeling used to simulate the 380-B packaging. The analytical model is developed for use with the Thermal Desktop® [23] and SINDA/FLUINT [24] computer programs. These programs work together to provide the functions needed to build, exercise, and post-process a thermal model. The codes have been validated for generating safety basis calculations for nuclear related projects [25] and have been used for numerous other safety evaluations.

The Thermal Desktop® computer program provides graphical input and output display functions, as well as computing the thermal mass, conduction, and radiation exchange conductors for the defined geometry and thermal/optical properties. Thermal Desktop® is designed to run as an application module within the AutoCAD™ design software. As such, all of the CAD tools available for generating geometry within AutoCAD™ can be used for generating a thermal model. In addition, the use of the AutoCAD™ layers tool presents a convenient means of segregating the thermal model into its various elements.

The SINDA/FLUINT computer program is a general purpose code that handles problems defined in finite difference (i.e., lumped parameter) and/or finite element terms and can be used to compute the steady-state and transient behavior of the modeled system. Although the code can be used to solve any physical problem governed by diffusion-type equations, specialized functions used to address the physics of heat transfer and fluid flow make the code primarily a thermal code.

Together, the Thermal Desktop® and SINDA/FLUINT codes provide the capability to simulate steady-state and transient temperatures using temperature dependent material properties and heat transfer via conduction, convection, and radiation. Complex algorithms may be programmed into the solution process for the purposes of computing heat transfer coefficients as a function of the local geometry, gas thermal properties as a function of species content, temperature, and pressure.

3.5.3.1 Description of 380-B Packaging Thermal Model for NCT

The temperature distribution within the 380-B packaging is computed using a quarter-symmetry model of the package. The modeling uses approximately 26,000 nodes, 3,000 planar elements and 4,500 solid elements to represent and provide thermal resolution within the various packaging components that make up the simulated package segment. This modeling choice captures the full height of the packaging components and allows the incorporation of the varying insolation loads that will occur along the height of the package, while taking advantage of the assumed symmetry of the payload configuration and heat distribution within the package. The various packaging components are defined using a combination of planar and solid elements. Program features within the Thermal Desktop® computer program automatically compute the various areas, lengths, thermal conductors, and view factors involved in determining the individual elements that make up the thermal model of the complete assembly.

Figure 3.5-1 and Figure 3.5-2 illustrate the 380-B packaging thermal model used for the NCT evaluations. As seen, the solid and plate type elements accurately capture the geometry of the various modeled components of the 380-B packaging, including the top and bottom end structures, the lid closure, and the shape of the lead cavity in cask sidewall. Also captured, but not easily seen due to the scale of the figure, is the thermal shield, including the effects of the wire wrap standoffs and the welded joints at the ends of the shield. The maximum spatial resolution provided by the thermal modeling for the package sidewall components is approximately 1.5 inches or less in the radial direction, 2.5 inches or less in the axial direction, and every 5° in the circumferential direction. Greater spatial resolution (i.e., smaller radial and axial distances) is provided near the cask ends and at the surfaces of the components where larger thermal gradients are expected. Lower radial resolution is used for the interior portions of the cask closures since the thermal gradient is expected to be relatively low.

For modeling simplicity, the thermal model does not specifically capture the bolt material and geometry for the closure bolts. These bolts are fabricated from ASTM A564, Type 630 Condition H1100 (i.e., 17-4 PH) steel which has approximately 90% of the thermal conductivity of Type 304 stainless steel at temperatures up to 800 °F and essentially the same conductivity for temperatures above 1,100 °F. In contrast, the specific heats of the two materials are similar at temperature levels below 600 °F, but the specific heat for 17-4 PH steel is approximately 70% of Type 304 stainless steel at temperatures in excess of 1,000 °F. Based on this information, ignoring the closure bolt material in the thermal model is expected to yield slightly conservative cask lid temperatures for NCT and to have essentially no impact on cask lid temperatures under HAC given the fact that the maximum lid temperature does not exceed 650 °F. Given the large thermal margin for the lid seals, this modeling simplicity is acceptable for evaluating the thermal safety of the design.

While the controlled lead pour procedure to be used to fill the lead cavity between the inner and outer shells of the cask body is expected to yield essentially no interface gap between the lead and the steel shells, the NCT modeling conservatively assumes a radial gap from lead shrinkage of 0.08 inch at -40 °F, and an axial gap at the top of the lead column of 0.50 inch at -40 °F. Since the size of the gap is a function of temperature, the NCT modeling uses a slightly non-linear relationship to compute the size of the local gap as a function of the lead and outer shell temperatures. The non-linear relationship is developed from the geometry of the cask shells and the differential thermal expansion coefficients for Type 304 stainless steel and lead. The gap size goes to zero at the melting point for lead. Heat transfer is computed as a combination of conduction across a variable size air gap and radiation. To maximize heat transfer into the package for HAC, the presence of the gap is ignored and direct contact is assumed.

The thermal model does capture the geometry and bolt material for the individual ASTM A564, Type 630 impact limiter attachment bolts (see Figure 3.5-2). Included in the limiter attachment modeling are the individual bolt lugs and the bolt tubes through the limiter foam. Since the manufacturing process for the poured-in-place polyurethane foam used to fill the impact limiter can yield densities that vary from the targeted value of 16 lb_m/ft^3 (pcf) and since the foam's conductivity is a function of its density, the thermal modeling conservatively assumes a low tolerance foam density (i.e., 16 pcf less 15% ≈ 13.6 pcf) for NCT evaluations and a high tolerance foam density (i.e., 16 pcf plus 15% ≈ 18.4 pcf) for HAC evaluations.

The package payload is not specifically modeled since a wide variety of payload configurations and payload support dunnage will occur and a predicted payload temperature is not required for

the safety evaluation. Instead, the payload is simply represented by a maximum decay heat loading of 205 W (see Section 3.1.2, *Content's Decay Heat*) that manifests itself as a smeared heat flux over selected portions of the payload cavity.

According to Section 7.1.4, *Qualifying the Payload for Transport*, the payload device heat output is limited to a maximum of 0.1 W/lb per device. Therefore, the smallest device that dissipates the maximum of 205 W is required to weigh at least 2,050 lb. If this device were a cylinder of solid lead with the length equal to the diameter (i.e. aspect ratio of 1) it would have a radius of approximately 9.3 inches and a length of 18.6 inches. The surface area of this lead cylinder bounds all the devices in the 380-B package dissipating 205 Watts for the following reasons: 1) the surface-area-to-volume ratio is lowest for a cylinder at an aspect ratio of one, 2) a real device will be less dense due to the presence of metal components, and 3) a real device will be less dense due to the internal cavity required to house the source.

An explicit modeling of the dunnage is not possible since it will be fabricated on-site from locally available materials and to no specific design to fit the specific payload to be transported. Therefore, NCT modeling is based on two dramatically different heat distribution scenarios. The intent of these two heat disposition scenarios, described in Section 3.1.2, *Content's Decay Heat*, is to bound the expected heat transfer mechanisms that could arise for any combination of device payload and its associated support dunnage. The first scenario assumes the dunnage is "open" and the payload decay heat is deposited toward the lid of the cask. This heat load is applied in the thermal model as a surface heat flux to the inner cover and the top 14.4 inches of the cask inner shell (i.e. he distance between the top of the 18.6 inch long device and the underside of the inner cover). The second scenario assumes the dunnage restricts the heat transfer to 50% of the side axial height of the device as required by Section 7.1.2, *Loading of Contents*. As established above, the smallest side axial height for a device dissipating 205 W is 18.6 inches. This heat load is applied in the thermal model as a surface heat flux to the inner shell over an area that is 9.3 inches tall and centered on the cask cavity. This heat load is applied in the thermal model as a surface heat flux to the inner shell over an area that is 9.3 inches tall and centered on the cask cavity.

The thermal shield is modeled as a surface element since its relative thinness will yield essentially zero ΔT across its thickness. Heat transfer between the shield and the underlying outer shell surface is modeled as a combination of radiation and conduction across a 0.105-inch thick air gap and conduction through a 0.105-inch diameter stainless steel wire wrap on 4.5-inch centers. For conservatism, the conduction through the wire wrap is ignored for NCT. The thermal modeling captures the extension of the thermal shield between the impact limiter attachment lugs and the seal welds that provide closure at the ends of the thermal shield.

As described in Appendix 3.5.3.6, *Convection Coefficient Calculation*, the value of convective heat transfer from the surfaces of the 380-B package is based on semi-empirical relationships for natural convection from isolated surfaces. Since the surfaces of the impact limiters intersect the exterior surfaces of the cask body, the cask body surfaces are not isolated surfaces. Instead, the presence of the inside ends of the limiters were examined for their potential to impede the natural convection airflow over the exposed vertically oriented surfaces of the cask body. When viewed in two dimensions, the impact limiter and cask resembles a horizontal cavity with an aspect ratio (i.e., height over width) of approximately 1.5. Under NCT conditions, the temperature levels on the thermal shield result in a Rayleigh number in the range of 3×10^8 to 4.8×10^8. The heat transfer from horizontal, open-ended cavities has been the subject of numerous studies [27, 28]

which show that, for this combination of aspect ratio and Rayleigh number, the heat transfer from the vertical channel surface is essentially equal in magnitude to the natural convection off an isolated vertical surface. Based on this result, the modeling assumes the semi empirical relationships for natural convection from isolated surfaces can be used without modification.

Although the minimum 75% open area ratio for the personnel barrier is not expected to impact the convective heat flow across it, the computed convection heat transfer coefficient for surfaces enclosed by the barrier is reduced by 15% as a conservatism. The heat transfer from the personnel barrier itself is computed assuming a 25% solid area factor. During the HAC fire event the package orientation is assumed to be lying horizontal with the personnel barrier missing. Without the shading of the personnel barrier the full regulatory solar insolation is applied to the exposed surfaces of the package.

3.5.3.2 Insolation Loads

The insolation loading on the 380-B package is based on the total 10CFR71.71(c)(1) specified insolation values over a 12 and 24-hour periods. The relative size of the impact limiters and the vertical orientation of the package during transportation have a significant effect on the level of package self shading. The amount of insolation incident on the package surfaces is further reduced by the presence of the personnel barrier which will block 25% of the insolation that would otherwise be received by the package surfaces enclosed by it. For the purpose of this safety evaluation, the portion of the cask body exterior surfaces at or above the attachment lugs for the upper limiter are assumed to receive only 4.5% of the regulatory insolation (i.e., 6% due to impact limiter shading times 75% for personnel barrier blockage). Similarly, the exterior surfaces between the attachment lugs are assumed to receive 26% of the regulatory level (i.e., 35% due to impact limiter shading times 75% for personnel barrier blockage), and the exterior surfaces at or below the attachment lugs for the lower limiter are assumed to receive 35% of the regulatory level (i.e., 46% due to impact limiter shading times 75% for personnel barrier blockage). 100% of the regulatory solar is assumed for all exterior surfaces of the impact limiters except for the following:

1) the upward facing, end surface of the lower impact limiter. A value of 56% is assumed to account for self-shading by the upper impact limiter and the personnel barrier (i.e., 75% times 75%),

2) the downward facing end surface of the upper impact limiter, the conical and base surfaces of the lower impact limiter. Zero insolation is assumed for the downward facing surface of the upper limiter and the base of the lower limiter, while 25% is assumed on the conical surface of the lower impact limiter,

3) the personnel barrier is modeled using a curved, closed (continuous) surface. Solar insolation on the personnel barrier is 25% of the regulatory amount to account for the openness of the expanded metal surface, since 75% of the solar loading passes through the barrier and is applied to the cask surface.

The estimated effect of package self shading on insolation loading is based on a conservative estimate of the solar shading lines for the various surfaces for the design summer day that serves as the basis for the regulatory solar loading values. These shading lines are then combined with a sinusoidal distribution of regulatory insolation loading over a 12 hour period to determine the amount of incident insolation that occurs before the sun rises above the determined shading line.

For example, the portion of the cask exterior between the cask lugs will be fully shaded when the sun rises more than 50° above the horizon. This will occur approximately during a period 3.3 hours after sunrise and 3.3 hours before sunset. The amount of insolation occurring on a vertical surface during this 6.6 hour time period is 259 Btu/ft² versus the total regulatory insolation loading of 738 Btu/ft², or 35% of the regulatory value. Figure 3.5-3 provides a visual summary of the insolation adjustments assumed by this modeling approach. The additional blockage due to the personnel barrier is accounted for separately, depending on whether or not the barrier is assumed to be present.

3.5.3.3 Bulk Average Gas Temperature

Given that the various potential payloads are not explicitly modeled, the bulk average gas temperature within the package cavity had to be estimated based on the use of the peak inner shell temperature and a bounding estimate of outgassing from the dunnage. No payload outgassing is assumed. Given that the peak inner shell temperature will lead the bulk gas temperature under HAC, this methodology is seen as sufficient for the purpose of this safety evaluation.

Assuming no thermal decomposition or outgassing from the packaging dunnage and/or the payload device, the peak cask cavity pressure under HAC can be estimated based solely on ideal gas expansion.

Outgassing from dunnage fabricated of metallic components will not occur. The same is true for dunnage fabricated from polyurethane foam since the peak foam temperature noted from the analysis remains below the 325 °F temperature point where a slight weight loss and outgassing from polyurethane foam is noted as beginning (see Appendix 3.5.4, 'Last-A-Foam' Response under HAC). In contrast, wood dunnage has the potential to contribute to the cask cavity pressurization due to the evaporation of the moisture content in the wood. As with the calculation for NCT, the rate of cavity pressurization is a highly complex function of the total amount of wood present, the size of the wood components, the moisture content, and the environmental conditions in the cask cavity. In reality, only a fraction of the total moisture will be released during the HAC transient since thicker pieces of wood require an extended exposure time to dry out.

To avoid the complexity of an exact calculation, the safety evaluation uses a simple methodology to bound the maximum cask cavity pressure rise associated with moisture evaporation. This methodology is based on the fact that the maximum partial pressure of the water within the cask cavity can't rise above the saturation pressure for water at the temperature of the inner shell. That conclusion is based on the knowledge that the inner cask shell serves as the heating source for the payload and dunnage during HAC and the saturation pressure associated with the temperature of the inner shell is the maximum partial pressure for water that can be reached regardless of the amount of moisture present in the dunnage.

3.5.3.4 Design Basis Ambient Conditions

The 380-B package is evaluated in accordance with 10CFR71 [1], IAEA TS-R-1 [2], and Regulatory Guide 7.8 [4] for the applicable NCT and HAC thermal loads. The evaluated load conditions are defined as follows:

- *NCT Hot:* An ambient temperature of 100 °F is used to evaluate the peak packaging temperatures for maximum decay heat and the 10 CFR §71.71(c)(1) prescribed insolation averaged over 12 and 24-hour periods.

- *NCT Hot (no solar):* This case is the same as NCT Hot, but without insolation, and serves as the basis for evaluation of the maximum temperature at the accessible surfaces of the package in accordance with 10 CFR §71.43(g) for exclusive use packages (i.e., ≤ 185 °F).

- *NCT Cold:* This case serves as an additional basis for evaluation of the maximum temperature gradients within the package. In accordance with 10 CFR §71.71, an ambient temperature of -20 °F and no insolation heating is assumed for this condition.

- *HAC Hot:* Thermal conditions prior to the event are taken from the NCT Hot condition (including isolation), followed by a thirty-minute transient with an ambient temperature of 1,475 °F with maximum decay heat, and then back to a steady-state ambient temperature of 100 °F with maximum decay heat and insolation per 10 CFR §71.71(c)(1).

3.5.3.5 Description of Thermal Model for HAC

The thermal model for HAC is a modified version of the analytical NCT thermal model described above. The use of the quarter symmetry NCT model provides a conservative basis for simulating the asymmetric damage expected for HAC. The principal differences between the NCT and HAC thermal models are changes to the assumed initial package conditions, the surface emissivity properties assumed to reflect oxidization and soot accumulation on surfaces exposed to the elevated fire temperatures, the thermal properties of the ambient environment during the 30-minute fire event, and the loss of foam mass in the impact limiters due to thermal decomposition under elevated temperatures.

The initial conditions assumed for the package prior to the HAC event are summarize below in terms of the modifications made to the NCT thermal model to simulate the assumed package conditions prior to and during the HAC event. These thermal model modifications are:

- assume a horizontal package orientation following the regulatory drop event, add heat transfer to and from the base of the package to simulate a fully engulfing fire event, and ignore the potential for self-shading in determining the insolation loading,

- increased the emissivity of all external surfaces to 0.8 for possible oxidation and/or soot accumulation on the surfaces,

- increased the solar absorptivity of all external surfaces to 1.0 to account "full insolation" per Section 3.5.5.2 of NUREG-1609 [3],

- increased the emissivity of the interior surface of the thermal shield from 0.2 to 0.45 to account for potential oxidization during the course of the HAC event,

- the emissivity of the cask surfaces not directly exposed to the fire, but nominally covered by the impact limiters is raised to 0.4 and emissivity of the opposing surfaces on the impact limiter are raised to 0.5 to account for possible condensation on the surfaces by volatile organic compounds (VOCs) generated during the fire,

- increase the emissivity of all other package surfaces from 0.20 to 0.30 to conservatively bound the potential surface condition at fabrication,

- include credit for potential heat transfer between the thermal shield and the cask body via the wire wrap standoffs,

- conservatively assume that the personnel barrier and the sheet over the recess cavities on the impact limiters are torn off during the regulatory drop event that precedes the HAC fire,

- removed a minimum of 2.7 inches of foam from the exterior portions of the impact limiter foam block and added heat transfer via radiation within the impact limiter enclosures with an emissivity of 0.925 to account for the loss of polyurethane foam from thermal decomposition. While this foam volume would be gradually lost over the course of the 30-minute fire event, the modeling conservatively assumes this foam volume is lost instantaneously at the start of the fire event,

- simulated the worst-case drop damage to the package (see below), and

- assumed an initial temperature distribution equivalent to the package at steady-state conditions with a 100 °F ambient and 24-hour averaged regulatory insolation. This assumption exceeds the requirement of 10 CFR §71.73(b) and complies with the requirement of IAEA.

Prior to the initiation of the HAC fire event the package is assumed to have experienced a regulatory drop event. Five drop orientations (i.e., end, side, CG-over-corner, 10° slap down, and 20° slap down) are considered for this evaluation using a numerical simulation (see Appendix 2.12.5, *Free Drop Impact Evaluation*). As expected, the results for warm conditions and with the low tolerance foam density provide the worst case package deformations. Figure 3.5-4 illustrates the predicted centerline crush depths (blue lines) that are expected to occur for the various drop orientations. These results were confirmed as being conservative by a series of certification half-scale drop tests, Appendix 2.12.3, *Certification Test Results*, as demonstrated by Table 3.5-1. Table 3.5-1 summarizes the foam crush depths as predicted by FEA analysis for the bounding foam condition of 14 pcf and 160 °F versus half scale drop tests for a foam condition of 15 pcf and 100 °F. Included in this summary is the FEA analytically predicted crush at the benchmark half scale drop test foam conditions.

The crush depths assumed for the thermal modeling are based on earlier predicted crush depths and are depicted in Figure 3.5-4 as red lines. As seen, the thermal modeling crush depths are slightly more conservative than the current analytical predicted crush depths (i.e. the blue lines).

In addition to the foam deformed as a result of drop crush, foam will be lost during the 30-minute fire event as the foam undergoes thermal decomposition (see Appendix 3.5.4, *'Last-A-Foam' Response under HAC*). Based on a low tolerance foam density of 13.6 pcf (i.e., 16 pcf x85%), the maximum expected foam loss (recession depth) due to thermal decomposition is 2.7 inches. If the 380-B impact limiter were manufactured at the highest acceptable density (i.e. 18.4 pcf) there would be less foam loss, which would result in more thermal protection to the cask body, and thus lower cask component temperatures at the end of the fire. In addition, the payload decay heat of 205W is insignificant relative to the heat load of the fire. This assertion is justified by the rapid decrease in peak temperatures of the cask components near the impact limiters at the end of the fire, as observed in Figure 3.4-7. Therefore, explicit modeling the lower bound of foam regression is not required to establish the thermal performance of the 380-B package during the post-fire cooldown.

The certification half-scale test program consisted of free drop and puncture testing of the impact limiters using a dummy cask. The certification test unit (CTU) configuration consisted of half-scale impact limiters and attachments, and a half-scale dummy cask. Tests involving only one impact limiter (i.e., all except the side drop) utilized a ballast plate on the non-impact end to facilitate simpler and safer drop orientation rigging for the test unit configuration with the ballast plate. The test program utilized one half-scale dummy cask and four half-scale impact limiters. Three of the impact limiters contained 15 lb/ft^3 polyurethane foam to evaluate the structural response of the package under warm initial conditions; and one impact limiter contained 17 lb/ft^3 polyurethane foam to evaluate cold initial conditions.

Based on the depicted crush lines in Figure 3.5-4 and the expected foam recession depth of 2.7 inches, the CG-over-corner drop orientation is seen as presenting the worst-case orientation since it results in a minimum foam depth of 4 inches (2.3 inches to the impact limiter attachment lug as illustrated in Figure 3.5-8) while all other drop orientations leave minimum foam depths significantly greater than 2.7 inches. As established in Appendix 3.5.4, *'Last-A-Foam' Response under HAC*, any amount of virgin foam in excess of approximately 3.2 inches (i.e., 2.7 + 0.5 inches) prior to the fire will be sufficient to prevent any significant temperature rise on the backside of the foam after the 30 minute fire event. Less foam regression will occur for the foam that has been crushed due to the associated increase in the local foam density. For example, at the centerline of the CG-over-corner drop damage, the effective foam density will be in excess of 44 pcf with an associated foam recession depth of only 0.3 inches. In that context, 2.3 inches of compacted foam will provide a substantial level of thermal protection.

While polyurethane foam will gradually decompose over the course of the 30-minute fire event, developing a thermal model to capture this transient thermal decomposition process would be a highly complex undertaking. Past experience has shown that such complex modeling is unnecessary to establish the safety basis for designs with the thickness and density of foam used for the 380-B impact limiters. Therefore, for simplicity and conservatism, the thermal modeling for HAC assumes a minimum of 2.7 inches of foam is lost instantaneously prior to the start of the fire event for all portions of the impact limiter not affected by drop damage. Lower amounts of foam are assumed to thermally decompose instantaneously in the area affected by the drop damage crush. This modeling methodology yields conservatively high component temperatures versus those achieved with a gradual foam loss.

Figure 3.5-5 illustrates the foam boundaries assumed by the thermal model at the start of the fire event for the upper and lower impact limiters. The 'missing' foam is due to the assumed CG-over-corner drop damage and subsequent foam decomposition during the fire event. For modeling purposes, the centerline of the drop damage is placed at one of the model's symmetry planes. As such, the thermal model assumes an equal level of damage exists on the opposite side of the symmetry plane.

Since the closure seals are the most temperature sensitive package component, the modeling conservatively assumes the drop damage occurs on the upper impact limiter. Figure 3.5-6 presents a detailed view of Figure 3.5-5 plus the foam loss due to the assumed P2 puncture bar damage (see discussion below). To maximize the potential compound damage, the centerline of the puncture bar damage is assumed to be aligned with the CG-over-corner drop damage. Again the thermal model assumes an equal level of puncture bar damage exists on the opposite side of the symmetry plane when determining the peak component temperatures.

As seen from the figure and accounting for the presence of a symmetry plane in the model, the total compound damage results in the entire side surface of one impact limiter attachment lug, a 20° subtended angle of the 0.5 inch thick end plate, and the first 3 inches of the impact limiter bolt tubes and inner shell surface are conservatively assumed to be void of any thermal protection by the polyurethane foam at the start of the 30-minute fire event. Further conservatism arises from the modeling assumption that the foam surfaces within the cavity formed by the puncture bar damage will not form a intumescent char that swells and at least partially fills the cavity. Instead it is assumed that the cavity dimensions remain constant throughout the fire event, thus maximizing the radiative and convective heat transfer with the fire environment.

Figure 3.5-7 and Figure 3.5-8 illustrate the analytically predicted foam deformation from the CG-over-corner drop orientation analysis, Appendix 2.12.5, *Free Drop Impact Evaluation*. Beyond the minimum foam depths, the analysis predicts the impact limiter deformation will effectively encapsulate 5 of the 12 cask lugs, drive the impact limiter shell into direct contact with the cask body over an approximate 120° angle, and widen the cask-to-impact limiter gap over the top half of the cask circumference from its pre-drop width of 0.188 inches to 0.65 inches. For conservatism, the potential encapsulation of the cask lugs by the impact limiter body is ignored for this safety evaluation. The HAC modeling does incorporate the hard contact between the limiter and cask body and the variation in cask-to-impact limiter gap noted from the drop analysis.

Modeling of the worst-case puncture bar damage is not addressed by the numerical simulation in Appendix 2.12.5, *Free Drop Impact Evaluation*. Instead, the potential damage resulting from puncture bar drops were determined by a series of certification half-scale drop tests, see Appendix 2.12.3, *Certification Test Results*. The puncture bar drop tests P1 to P4 address the worst cases among the creditable drop orientations.

Puncture Drop Test P1

The first puncture bar drop test, Test P1, was performed with the CTU axis at 56° from horizontal, and at an azimuth on the CTU that placed the target strike being between the impact limiter attachment bolts. The initial contact point with the puncture bar was approximately at the crushed outer edge of the impact limiter with the puncture bar aligned with the CTU cg. The puncture bar struck on target and penetrated the impact limiter causing the CTU to ultimately come to rest on the puncture bar. The half scale puncture bar sheared a 3-inch diameter half circle through the outer shell on the leading edge of the impact, and then tore an inverted "V" on the back end of the puncture as shown in Figure 3.5-9. The overall impact limiter shell puncture damage is 3 inches wide by 6-3/8 inches tall. The penetration of the puncture bar into the foam measured 3 inches in diameter by 11 inches deep, as shown in Figure 3.5-9. The sheared/torn metal of the outer shell was removed from the bottom of the puncture hole and the remaining foam was drilled through, approximately aligned with the axis of the puncture hole. A remaining depth of 2 inches (i.e. 4 inches full scale) was measured from the surface of the remaining foam to contact with the inner plate of the impact limiter. The puncture bar appeared to have made contact with the inner plate of the impact limiter on the leading edge of the puncture bar. The puncture bar was damaged on the leading rounded edge during the test. The half scale damage includes a flat spot on the puncture bar that measured 1-1/2 inches wide by 3/8 inch long.

Therefore, it can be assumed that some of the 2 inches measured between the surface of the foam and the inner plate must be due to springback (i.e., air gap).

Since the certification drop tests were conducted with a half-scale test article, all of the measured dimensions from the tests need to be doubled for full scale. As such, the P1 puncture bar drop is estimated to create a hole 6 inches in diameter by 22 inches in depth with a tear in the impact limiter skin that measures 6 inches by 12-3/4 inches tall. The cask lugs and welds were structurally sound and showed no damage except for the occasional small dent attributed to falling shackles from the rigging above during the test.

Puncture Drop Test P2

The second puncture bar drop test, Test P2, was performed with the CTU axis at 40° from horizontal. The CTU azimuth was located such that the target was between impact limiter attachment bolts. The initial contact point with the puncture bar was on the damaged surface from free drop test D2 and aligned with the CTU cg.

The P2 cg-over-corner puncture bar penetrated the outer skin and hit the inner plate of the impact limiter. The CTU then rotated forward, pivoting on the puncture bar embedded in the impact limiter, causing the top of the CTU to contact the drop pad (see Figure 2.12.3-27) while the impact limiter remained impaled on the puncture bar. The half-scale puncture bar sheared a 3-inch diameter half circle through the outer shell and then tore an elongated continuation of the half circle on the back end of the puncture, as shown in Figure 3.5-10. The resulting impact limiter shell damage measured 3 inches wide by 7-1/2 inches tall. The puncture bar penetration into the foam measured 3 inches in diameter by 11 inches deep on the leading edge and 6 inches deep at the trailing edge. Damage to the impact can also be seen in Figure 2.12.3-28 through Figure 2.12.3-33 of Appendix 2.12.3, *Certification Test Results*.

Following the D2 drop test, a weld failure was noted at the upper surface of the impact limiter at the inside radius, see Figure 3.5-11. Since this weld failure is attributed to a nonconforming weld joint and given that a 0.250 inch thick reinforcement ring with a 70 inch ID and 74 inch OD has been added to the design, this potential damage will be deemed as non-credible for the production impact limiters. The validity of this non-credible assumption was demonstrated by the subsequent D3, P3, and P4 drop test results which incorporated this design modification in half-scale and showed no weld failure. The remaining impact limiter welds and cask lugs were structurally sound and showed no damage except for the occasional small dent attributed to falling shackles from the rigging above during the test.

Scaling the measured dimensions from the tests to full scale yields a hole measuring 6 inches wide by 15 inches tall at the outer skin. A void cavity measuring 22 inches deep on the leading edge, 12 inches deep at the trailing edge, and 6 inches wide was created.

Puncture Drop Test P3

Test P3 consisted of a 40-inch HAC puncture drop test designed for possible future licensing to the rules of the IAEA. The test orientation was with impact limiter down and the CTU axis at 77° from horizontal. The CTU azimuth was located such that the target impact point was between impact limiter attachment bolts and at the orientation planned for the upcoming D3 free drop test. The initial contact point with the puncture bar was on the undamaged tapered surface, approximately 5 inches outside the small tapered end outer diameter, as shown in Figure 3.5-12.

The CTU landed on target hitting the puncture bar, which penetrated the impact limiter as expected. The CTU seamlessly transitioned from displacement in drop direction to rotating backward, pivoting on and significantly bending the embedded puncture bar, until the opposite side of the impact limiter contacted the drop pad, as shown in Figure 2.12.3-38 and Figure 2.12.3-39 of Appendix 2.12.3, *Certification Test Results*. The puncture bar sheared a 3-inch diameter half circle through the outer shell on the leading edge of the impact, and then tore an inverted "V" on the back end of the puncture. The overall impact limiter shell puncture damage is 3 inches wide by 6 inches tall to the foam and 8 inches tall to the shell. The penetration of the puncture bar into the foam measured 3 inches wide by 10 inches deep. The hole in the foam at the 10-inch depth was 5 inches tall.

The P3 test was conducted with an undamaged impact limiter. To create the worst case scenario for the P3 puncture damage, the damage noted above was superimposed on the bounding cg-over-corner 30-ft drop event. Figure 3.5-13 illustrates the resulting compound damage. (Of note, test sequence P3/D3 is not offered as demonstration of the requirements of 10 CFR 71.)

Puncture Drop Test P4

Test P4 simulated the final credible worst-case puncture drop scenario. The test orientation was with impact limiter down and the CTU axis at 23° from horizontal. The CTU azimuth was located such that the target was between impact limiter attachment bolts. The initial contact point with the puncture bar was on the surface damaged by the D3 side free drop test, and aligned with the CTU cg. The puncture drop test orientation is shown in Figure 2.12.3-50 of Appendix 2.12.3, *Certification Test Results*.

The CTU landed on target hitting the puncture bar, which penetrated the impact limiter, causing the CTU to ultimately come to rest on the puncture bar (see Figure 2.12.3-51 through Figure 2.12.3-53). The puncture bar sheared a 3-inch diameter half circle through the outer shell on the leading edge of the impact, and then continued to tear on the back end of the puncture. The overall impact limiter shell puncture damage is 3 inches wide by 3-3/4 inches tall. The penetration of the puncture bar into the foam measured 3 inches in diameter by 7 inches deep. The puncture bar went through the impact limiter and pushed the sheared/torn impact limiter outer shell to the dummy cask body (see Figure 3.5-14).

All of the cask lugs and welds were structurally sound and showed no damage except for the occasional small dent attributed to falling shackles from the rigging above during the test.

Bounding Puncture Bar Damage Scenario

While an attack in the center of the cask would result in a localized hot spot on the outer shell, the damage would be located too far from the thermally sensitive closure O-ring seals to be of concern. Similarly, an attack adjacent to the impact limiter that lands on the cask lugs or the portion of the outer shell not covered by the thermal shield would not cause any thermally significant damage. While a strike on the thermal shield between the cask lugs could raise the local shell temperatures, the higher temperatures that already exist because of the exposed cask lugs and shell surface area beyond the thermal shield means the added temperature gain would be minimal.

Of the four puncture bar attacks considered in the half-scale drop test of Appendix 2.12.3, *Certification Test Results*, the P1 damage is found to be thermally bounded by the P2 damage,

while the P4 damage is bounded by the P3 damage. While the P3 puncture bar damage would also potentially uncover a slice of the lid and upper end structure side surfaces to direct exposure to the ambient environment, its thermal effect is bounded by the P2 puncture bar damage given that the depth and relatively narrow cylindrical shape of the P3 cavity will significantly lower the heat transfer via radiation versus that seen for the P2 cavity.

The cg-over-corner remains the bounding 30-ft drop event. The thermal model assumption of 16.7 inches of crush bounds the structural estimate of 15.8 inches crush. As such, the bounding HAC evaluation addresses the cg-over-corner impact limiter damage with the P2 puncture bar damage added on.

The HAC analysis already assumes that the personnel barrier is torn away as a result of the drop event, so puncture bar damage to the personnel barrier is already encompassed by the assumed initial cask conditions.

3.5.3.6 Convection Coefficient Calculation

The 380-B package thermal model calls subroutines within SINDA/FLUINT to calculate convection heat transfer coefficients for natural (free) convection on the exterior package surfaces under both the regulatory NCT and the HAC post-fire conditions. During the NCT evaluations the convection coefficient values calculated for the free convection on the exterior package range from 0.95 Btu/hr-ft²-°F to 0.06 Btu/hr-ft²-°F. Immediately after the 30 minute HAC fire event the calculated free convection coefficients range from 1.45 to 1.20 Btu/hr-ft²-°F. These values gradually decrease as the package exterior surfaces cool; 720 minutes into the HAC fire event the calculated free convection coefficients range from 1.03 to 0.61 Btu/hr-ft²-°F.

The SINDA/FLUINT free convection subroutines use the semi-empirical relationships published in [22] to iteratively calculate the convection heat transfer coefficients (see Section 7.11.4.8 of [24]). The correlations utilized are described further herein.

The convective heat transfer coefficient, h_c, has a form of:

$$h_c = Nu \frac{k}{L}$$

where k is the thermal conductivity of the gas at the mean film temperature and L is the characteristic length of the vertical or horizontal surface. The convection coefficient is correlated via semi-empirical relationships against the local Rayleigh number and the characteristic length. The Rayleigh number is defined as:

where
$$Ra_L = \frac{\rho^2 g_c \beta L^3 \Delta T}{\mu^2} \times Pr$$

g_c = gravitational acceleration, 32.174 ft/s² β = coefficient of thermal expansion, °R⁻¹

ΔT = temperature difference, °F ρ = density of air at the film temperature, lb_m/ft³

μ = dynamic viscosity, lb_m/ft-s   Pr = Prandtl number = $(c_p \mu) / k$

L = characteristic length   , ft k = thermal conductivity at film temp., Btu/ft-hr-°F

c_p = specific heat, Btu/ lb_m -°F Ra_L = Rayleigh #, based on length 'L'

Note that k, c_p, and μ are each a function of air temperature as taken from Table 3.2-2. Values for ρ are computed using the ideal gas law, β for an ideal gas is simply the inverse of the

absolute temperature of the gas, and Pr is computed using the values for k, c_p, and μ. Unit conversion factors are used as required to reconcile the units for the various properties used.

The natural convection from a discrete vertical surface is computed using Equations 3-19, 3-21 to 3-25 of reference [22], which is applicable over the range $1 < $ Rayleigh number (Ra) $ < 10^{12}$:

$$Nu^T = \overline{C}_L Ra^{1/4}$$

$$\overline{C}_L = \frac{0.671}{\left(1 + (0.492/Pr)^{9/16}\right)^{4/9}}$$

$$Nu_L = \frac{2.8}{\ln(1 + 2.8/Nu^T)}$$

$$Nu_t = C_t^V Ra^{1/3}$$

$$C_t^V = \frac{0.13\,Pr^{0.22}}{\left(1 + 0.61\,Pr^{0.81}\right)^{0.42}}$$

$$Nu = \frac{h_c L}{k} = \left[(Nu_L)^6 + (Nu_t)^6\right]^{1/6}$$

The natural convection from a vertical cylindrical surface is computed by applying a correction factor to the laminar Nusselt number (Nu_L) determined using the same methodology and Nu_t for a vertical plate (see above). The characteristic dimension, L, is the height of the vertical cylinder and D is the cylinder's diameter. The correction factor as defined by Equations 3-39 to 3-41 of reference [22] is:

$$Nu_{L\text{-Cylinder}} = \frac{\delta}{\ln(1 + \delta)} Nu_{L\text{-Plate}}$$

$$\delta = \frac{1.8 \times L/D}{Nu_{Plate}^T}$$

$$Nu_{\text{Vert. Cylinder}} = \frac{h_c L}{k} = \left[(Nu_{L\text{-Cylinder}})^6 + (Nu_{t\text{-Plate}})^6\right]^{1/6}$$

Natural convection from horizontal surfaces is computed from Equations 3-34 to 3-38 of reference [22], where the characteristic dimension (L) is equal to the plate surface area divided by the plate perimeter. For a heated surface facing upwards or a cooled surface facing downwards and Ra > 1:

$$Nu = \frac{h_c L}{k} = \left[(Nu_L)^{10} + (Nu_t)^{10}\right]^{1/10}$$

$$Nu_L = \frac{1.4}{\ln\left(1 + 1.4/\left(0.835 \times \overline{C}_L Ra^{1/4}\right)\right)}$$

$$\overline{C}_L = \frac{0.671}{\left(1 + (0.492/Pr)^{9/16}\right)^{4/9}}$$

$$Nu_t = 0.14 \times Ra^{1/3}$$

For a heated surface facing downwards or a cooled surface facing upwards and $10^5 < Ra < 10^{10}$, the correlation is as follows:

$$Nu = Nu_L = \frac{0.527}{\left(1 + (1.9/Pr)^{9/10}\right)^{2/9}} Ra^{1/5}$$

Calculation of the convection coefficient from a horizontal cylindrical surface is computed using Equation 3-43, reference [22], where the characteristic length, D, is the outer diameter of the cylinder. This equation, applicable for $10^{-5} < Ra < 10^{12}$, is as follows:

$$Nu = \frac{h_c D}{k} = \left\{ 0.60 + \frac{0.387 Ra_D^{1/6}}{\left[1 + (0.559/Pr)^{9/16}\right]^{8/27}} \right\}^2$$

A constant convection heat transfer coefficient of 2.64 Btu/hr-ft²-°F (15 W/m²-°C) is used between the entire package exterior surface and the ambient during the 30-minute fire event. This constant value is based on an average gas velocity of 10 m/sec [26] over the bottom half of the package and the Colburn relation for forced convection of:

$$Nu = 0.036 \times Pr^{1/3} \times Re^{0.8}$$

Given the turbulent nature of the 30-minute fire event, a characteristic length of 0.25 feet is conservatively used for all surfaces to define the probable limited distance for boundary growth. The resulting convection coefficient of 15 W/m²-°C exceeds the 10 W/m²-°C suggested for large packages by IAEA advisory material [30].

3.5.3.7 Package Closure Lid Mesh Refinement

A mesh refinement study was conducted for the 380-B package closure lid for the HAC fire case. The package closure lid is the only massive object in the 380-B thermal model that has both significant thermal gradients due to the drop damage and low allowable component temperatures (i.e. the vent port seal and main component seal allowable of 400°F). The closure lid is created from 14 finite difference objects. The sub-division of these objects was increased incrementally (i.e. increasing the number of nodes per object) and re-run for a transient of 60 minutes. Incremental refinement was continued until the peak predicted temperatures of the seals and the peak temperature of the lid were stable. The results are summarized in Table 3.5-2.

The effect of the mesh refinement in the lid was to allow the heat to spread father in the circumferential direction, causing a generally lower component temperature compared to the base case (Rev. 0). It should also be noted that the increased mesh resolution in the closure lid resulted in a stable heat flux into the lid, as demonstrated by the stable average lid temperature shown in the last column of the table. Thermal model results are thus based on the coarsest mesh that demonstrated adequate refinement to capture the vent port peak temperature (i.e. a closure lid mesh of approximately 8,000 nodes).

The mesh density of the rest of the thermal model, other than the closure lid, was not refined. Refinement of the rest of the model would not yield an appreciable difference to the overall heat flux to the lid because:

- The heat flux flowing through the impact limiter to the package closure lid is primarily perpendicular to the plane of the impact limiter shell.

- The foam and upper end structure have a very low thermal gradient near the lid.

In addition, there are no thermally sensitive materials in the balance of the model. Thus, refinement of the rest of the model was unnecessary.

Table 3.5-1 – HAC Drop Test Foam Crush Summary

Orientation	FEA Analysis[1]		Drop Test Results[4]	
	Crush (in)	Minimum Foam (in)[3]	Crush (in)	Minimum Foam (in)[6]
Side Drop	12.1	8.9	7.10 10.38 Benchmark[5]	14.0
Cg-Over-Corner (50 deg) Drop	15.8	3.9	11.86 13.53 Benchmark[5]	7.9
End Drop	10.6	14.1	NA	NA
10° Slapdown Drop[2]	14.2 / 11.6	8.3 / 10.0	NA	NA
20° Slapdown Drop[2]	16.2 / 9.0	7.4 / 12.6	NA	NA

Notes: [1] FEA analysis assumes 14 pcf foam at 160°F.

[2] Slapdown results are shown in order of primary impact / secondary impact.

[3] The minimum foam measurement is taken from the cask outer surface to the impact limiter foam outer surface, which excludes the thickness and any spring-back of the impact limiter outer shell.

[4] The drop test results are scaled to full scale equivalent dimensions. Drop test conducted with 15 pcf foam at 100°F.

[5] Benchmark results represent FEA analysis at drop test conditions of 15 pcf foam at 100°F.

[6] The minimum foam measurement is taken from the cask outer surface to the impact limiter foam outer surface.

Table 3.5-2 – HAC Lid Mesh Refinement Results

File Name	Lid Node Count	Peak Temperature (°F)				Average Lid Temperature[1] (°F)
		Lid	Vent Port Sealing Washer	Main Containment Seal	Closure Bolt	
HAC_Damage_Phs5.sav	955	650	NR[2]	301	NR[2]	177
HAC_R0_Refine0.sav	2,747	601	368	276	519	179
HAC_R0_Refine1.sav	5,076	629	384	283	555	178
HAC_R0_Refine2.sav	8,186	634	386	283	553	177
HAC_R0_Refine3.sav	10,295	636	387	281	553	175
HAC_R0_Refine4.sav	14,907	639	384	284	552	172

Note: [1] The average temperature of the closure lid at the end of the 30-minute fire event.

[2] Not Reported; the original mesh (Rev. 0) did not have enough refinement to adequately capture the vent port sealing washer or closure bolt maximum temperature.
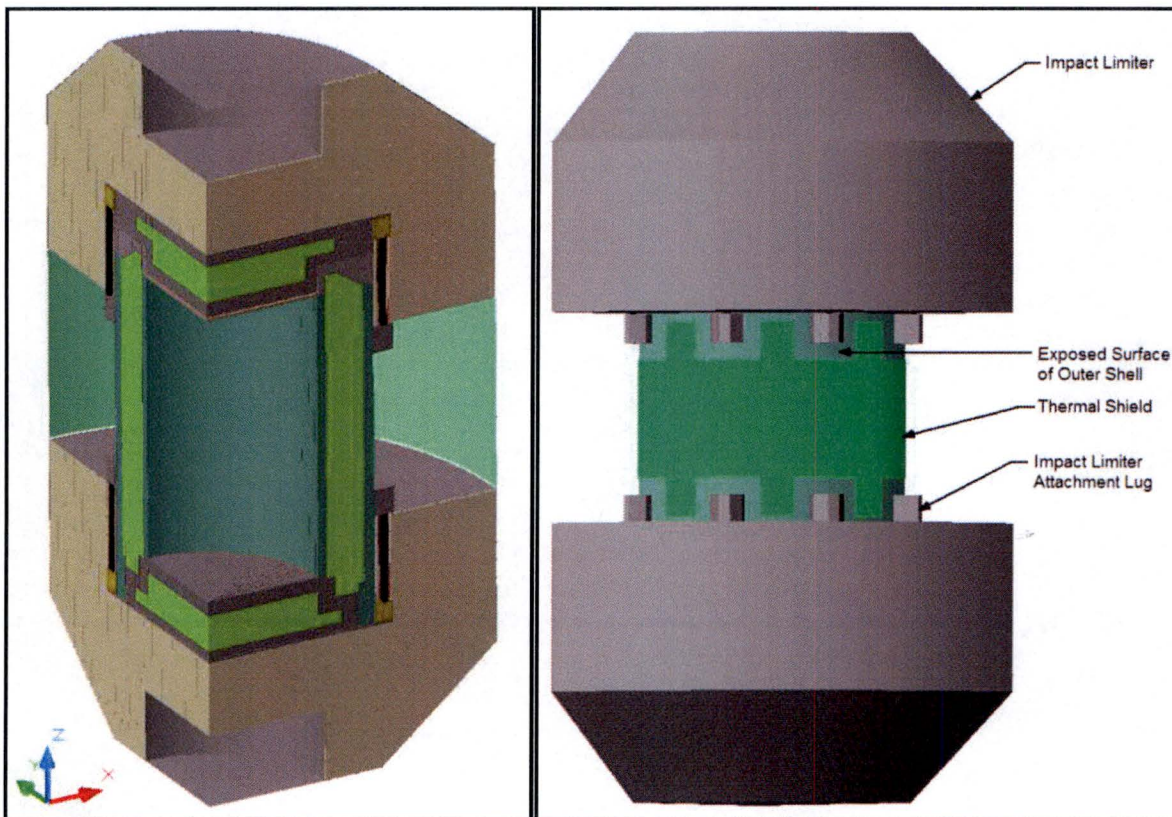
Note: Personnel barrier not shown in figure on right for clarity

Figure 3.5-1 – 380-B Packaging Model for NCT
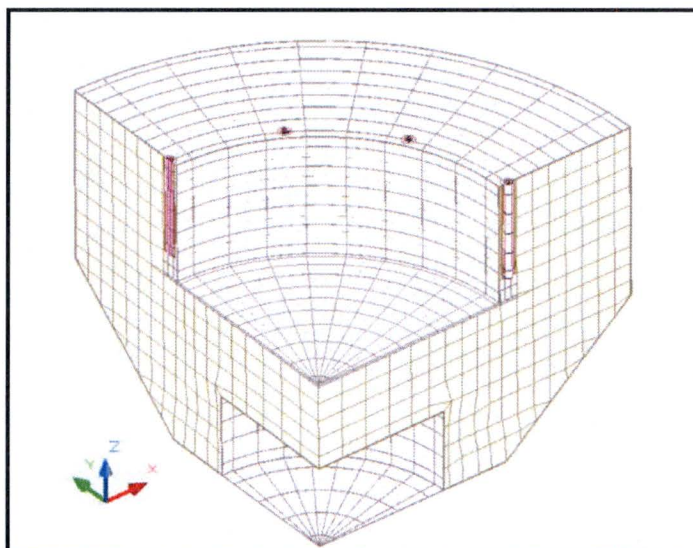
Figure 3.5-2 – 380-B Impact Limiter Model for NCT
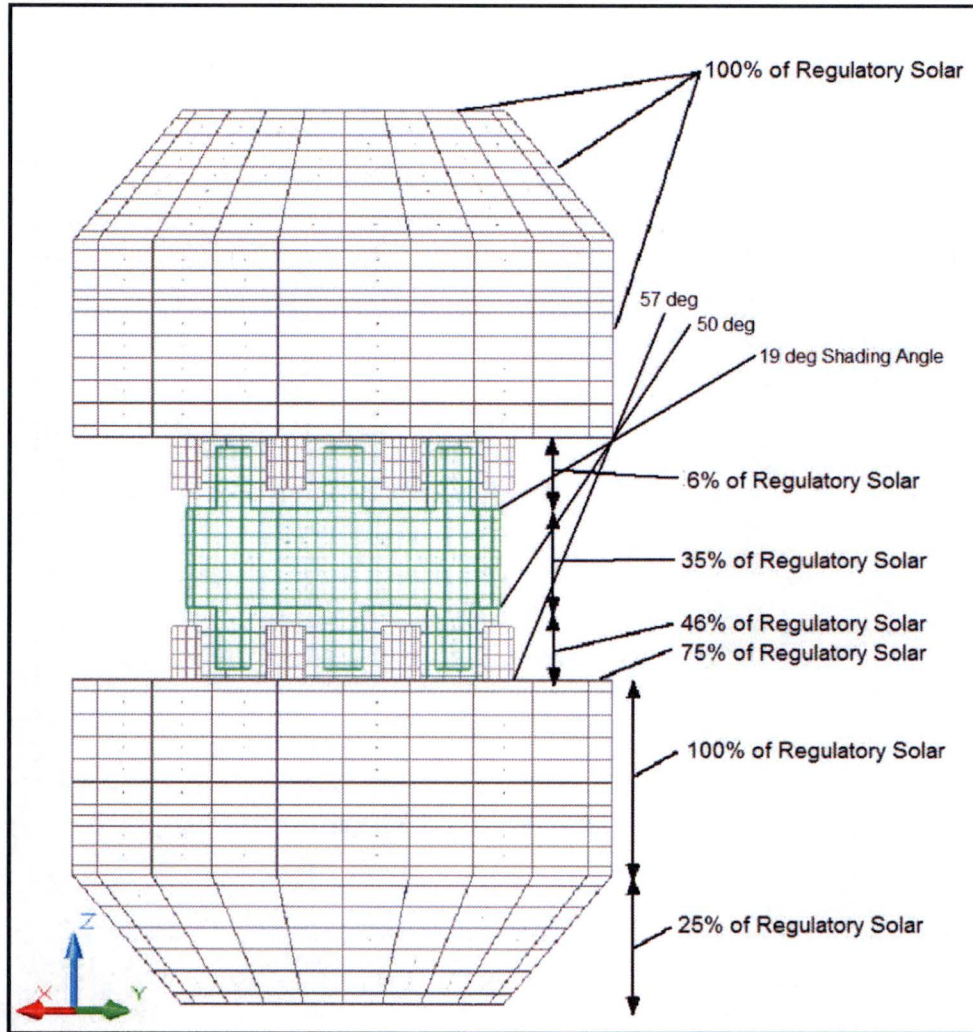
Note: The depicted adjustment factors don't account for presence of personnel barrier.

Figure 3.5-3 – Insolation Adjustment for Package Self-Shading
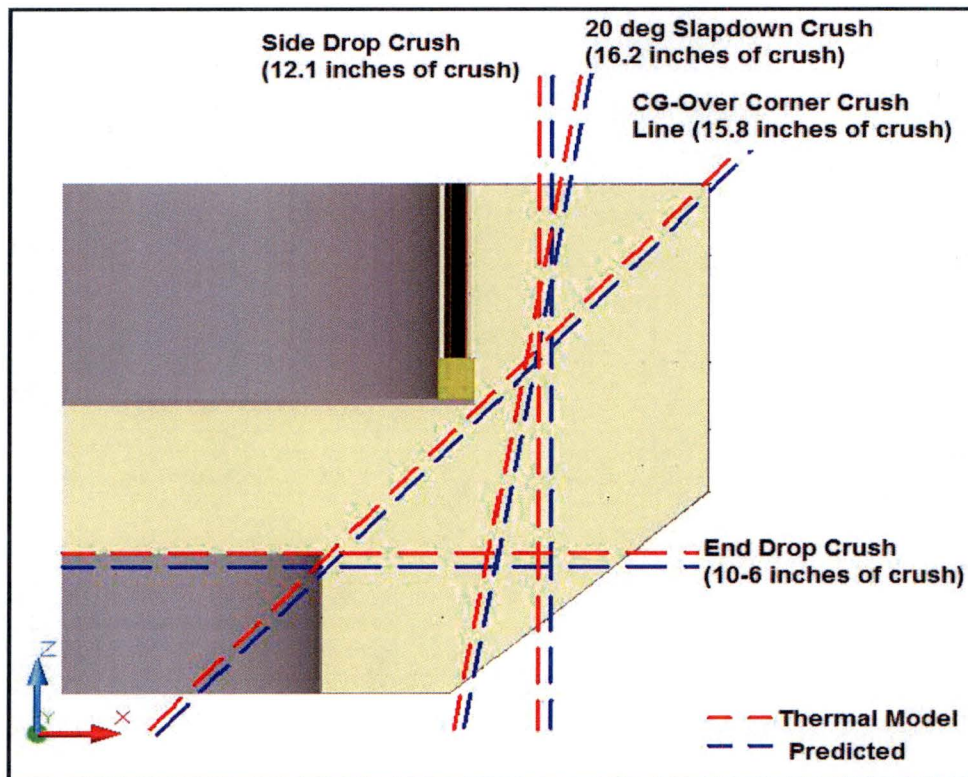
Figure 3.5-4 – Predicted HAC Drop Crush on Impact Limiters
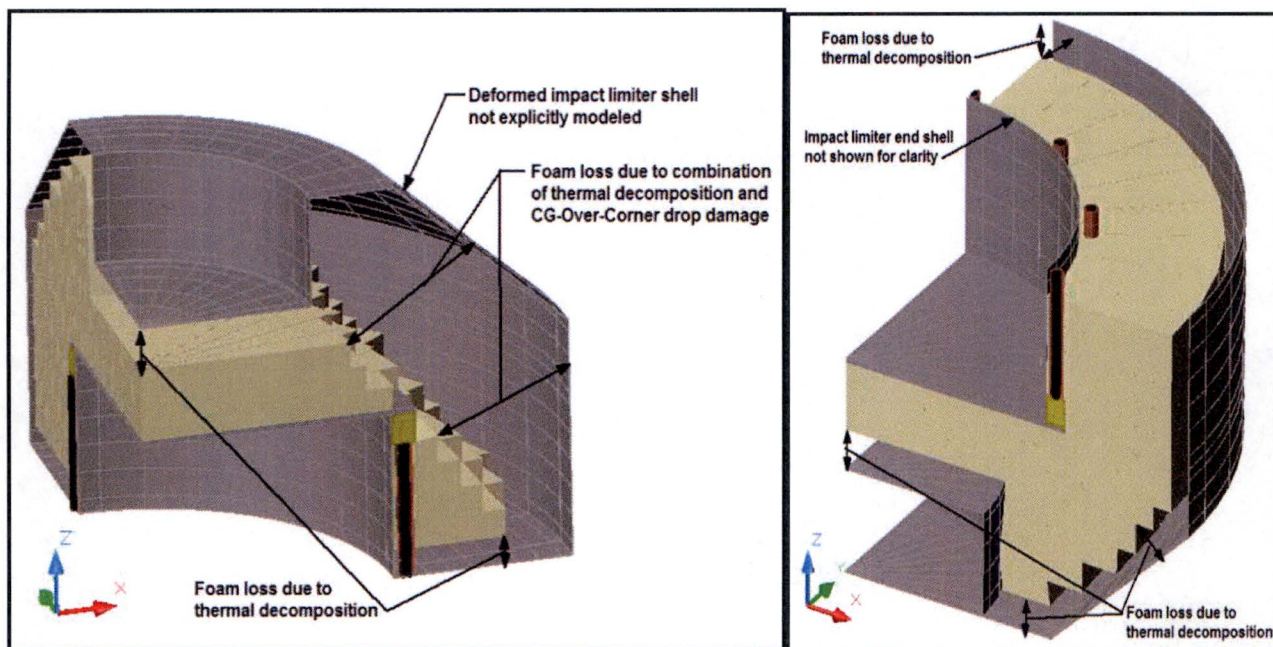
Note: CG-Over-Corner Damage to Top Limiter   Note: Undamaged Bottom Limiter

Figure 3.5-5 – Impact Limiter Model for HAC Drop and Fire Damage
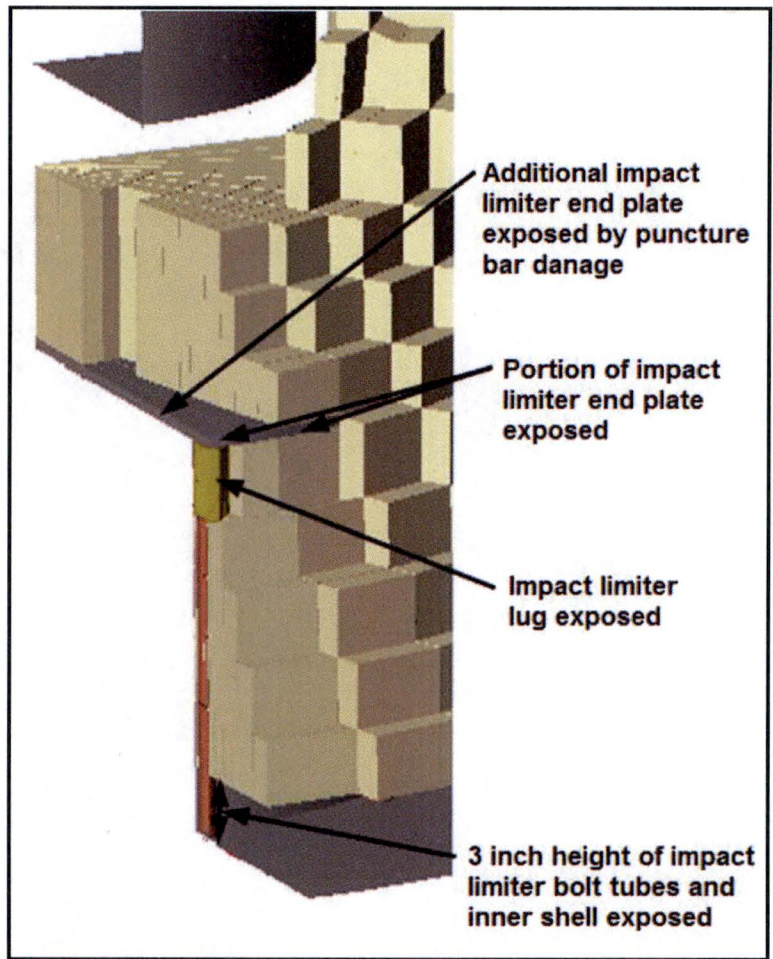
Figure 3.5-6 – Impact Limiter Surfaces Exposed Due to CG-Over-Corner Drop Crush, Fire, and Puncture Bar Damage
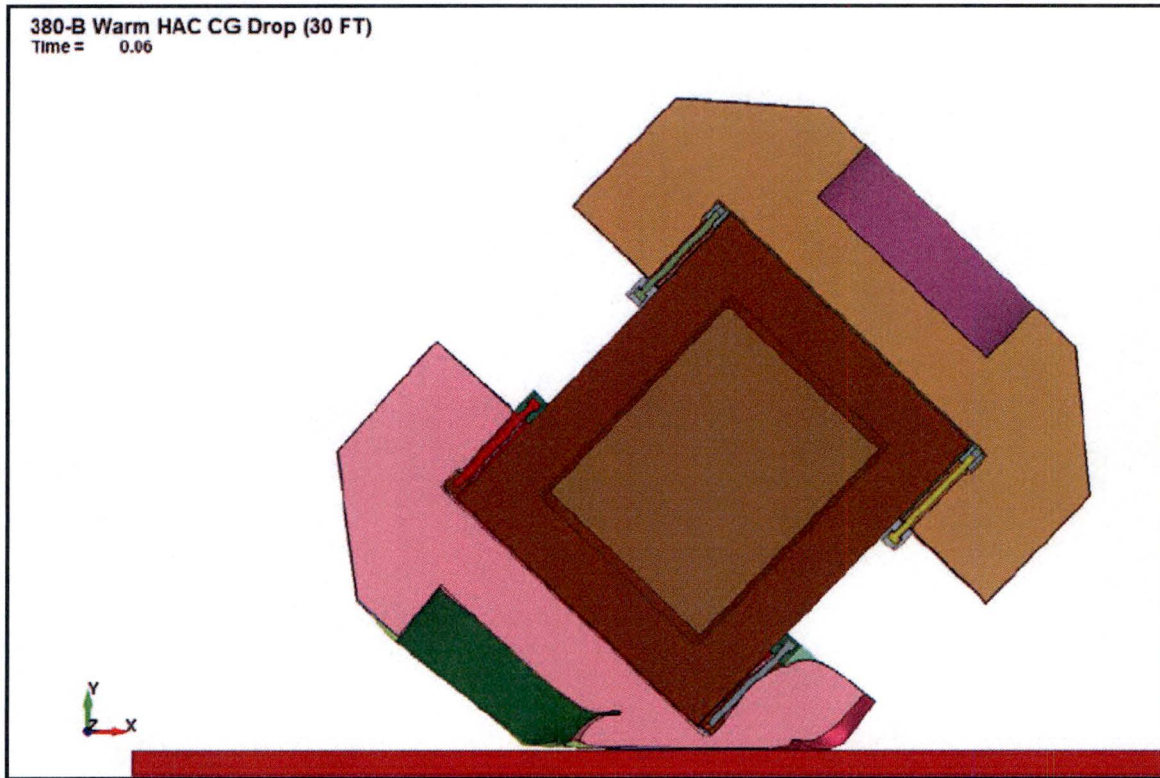
Figure 3.5-7 – Predicted HAC CG-Over-Corner Drop Crush
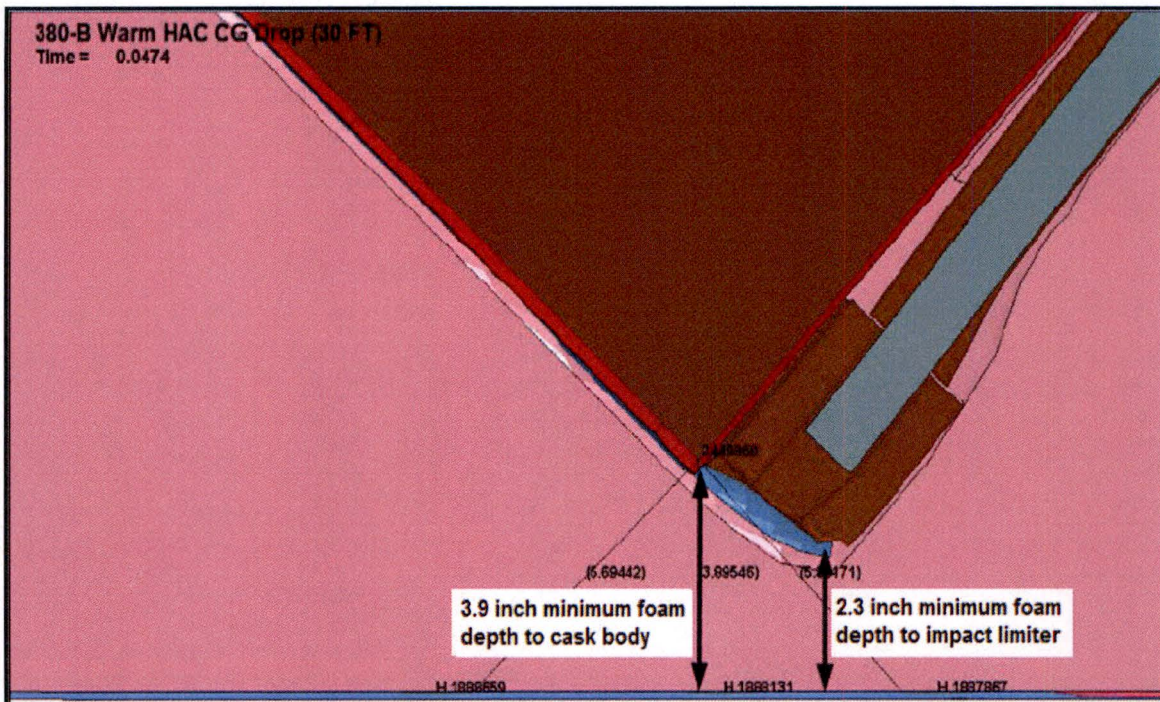
Figure 3.5-8 – Predicted HAC CG-Over-Corner Minimum Foam Depth
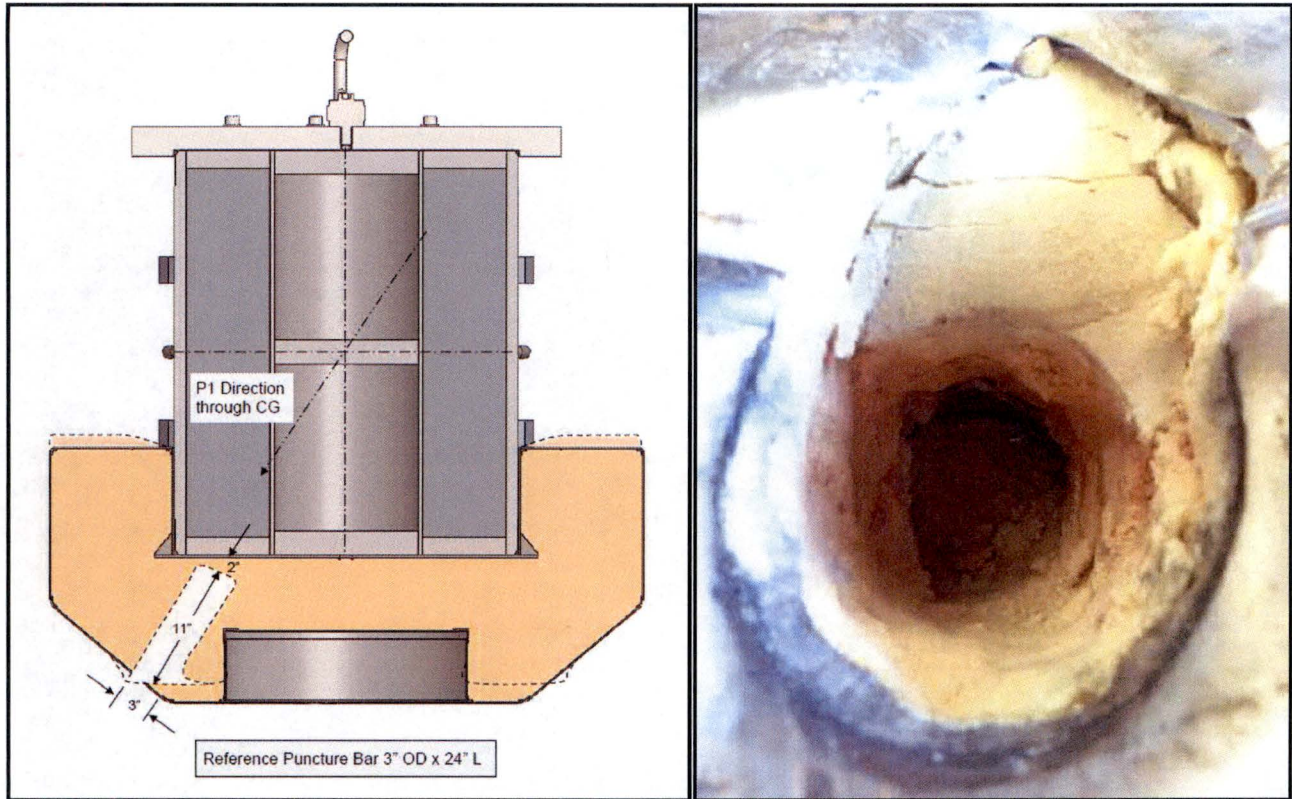
Note: Dimensions are from half-scale test and need to be doubled for full scale cask

Figure 3.5-9 – Impact Limiter Damage After P1 Drop Test
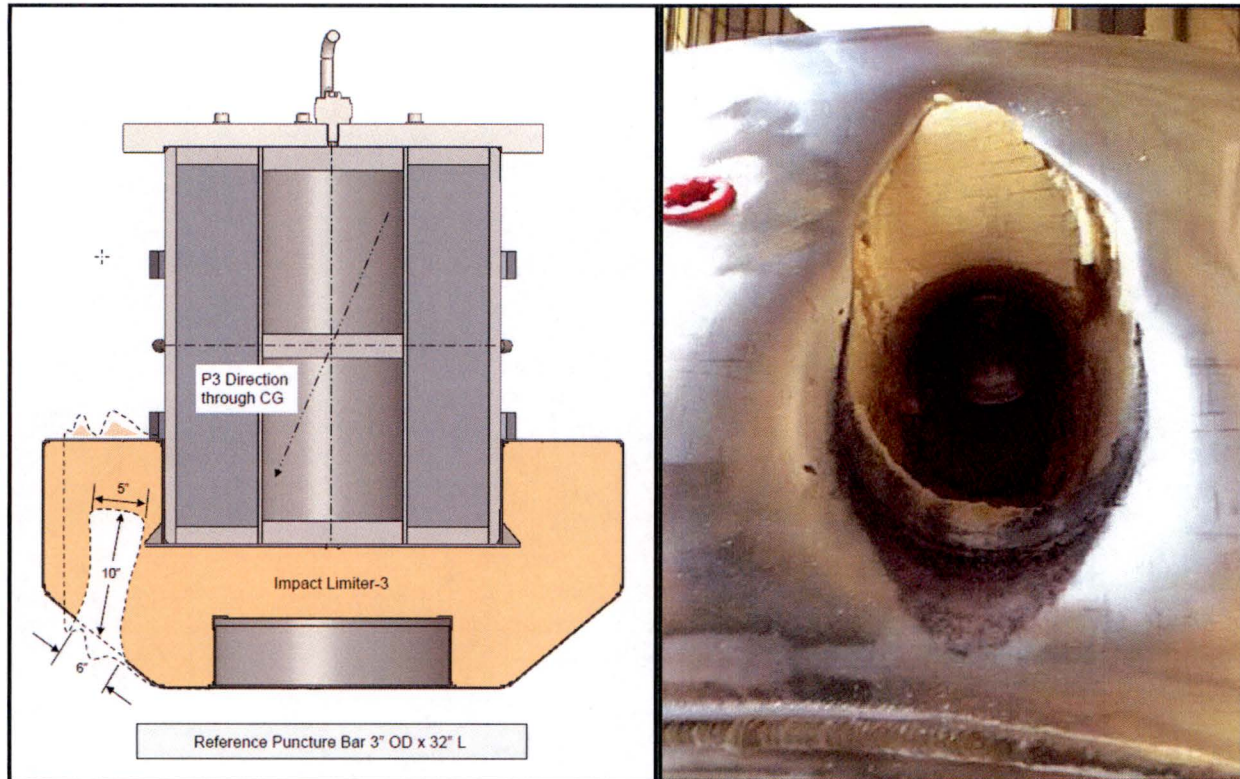
Note: Dimensions are from half-scale test and need to be doubled for full scale cask

Figure 3.5-10 – Impact Limiter Damage After P2 Drop Test

Note: Dimensions are from half-scale test and need to be doubled for full scale cask

Figure 3.5-11 – Impact Limiter Weld Failure After P2 Drop Test

Note: Dimensions are from half-scale test and need to be doubled for full scale cask

Figure 3.5-12 – Impact Limiter Damage After P3 Drop Test
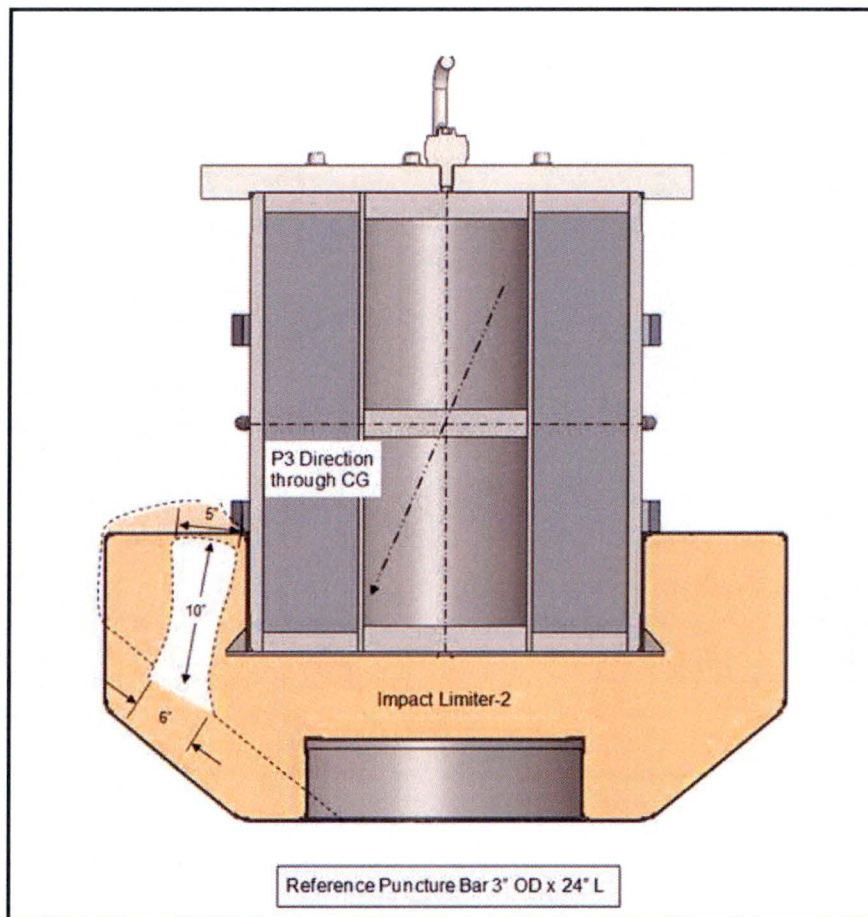
Note: Dimensions are from half-scale test and need to be doubled for full scale cask

Figure 3.5-13 – P3 Drop Damage Superimposed on CG-Over-Corner Impact Limiter Drop Damage
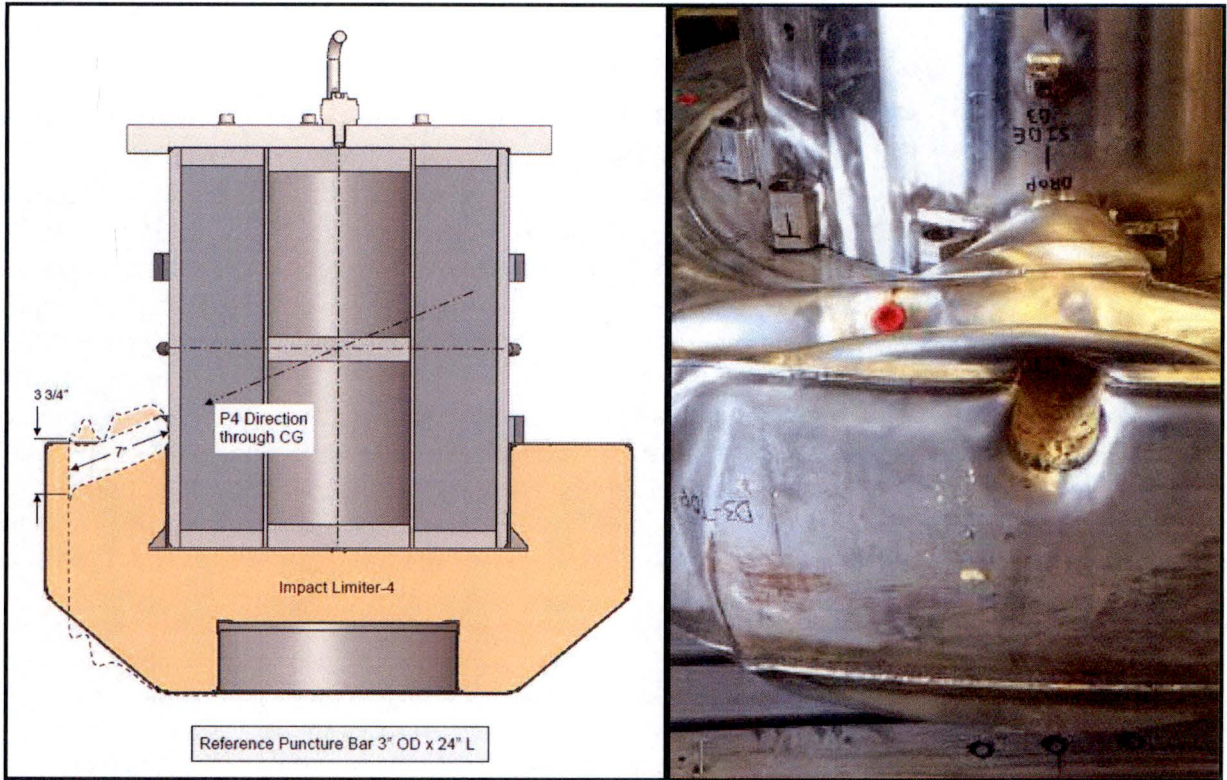
Note: Dimensions are from half-scale test and need to be doubled for full scale cask

Figure 3.5-14 – Impact Limiter Damage After P4 Drop Test

3.5.4 'Last-A-Foam' Response under HAC

The General Plastics LAST-A-FOAM® FR-3700 rigid polyurethane foam [10] used in the impact limiters has been used for numerous transportation packages. The FR-3700 formulation is specially designed to allow predictable impact-absorption performance under dynamic loading, while also providing a significant level of thermal protection under the HAC conditions. Upon exposure to fire temperatures, this proprietary foam decomposes into an intumescent char that swells and tends to fill voids or gaps created by free drop or puncture bar damage. This thermal decomposition absorbs a significant amount of the heat transferred into the foam, which is then expelled from the impact limiters as a high temperature gas. Because the char has no appreciable structural capacity and will not develop unless there is space available, the char will not generate stresses within the adjacent package components. Without available space the pyrolysis gases developed as a result of the charring process will move excess char mass out through the vent ports and prevent its buildup. Only as the charring process continues and space becomes available will the char be retained, filling the available space and plugging holes at the surface of the impact limiters. The thermal decomposition process does not alter or cause a chemical reaction within the adjacent materials.

The mechanisms behind the observed variations in the thermal properties and behavior of the FR-3700 foam at elevated temperatures are varied and complex. A series of fire tests conducted by General Plastics Manufacturing Co. conducted on 5-gallon cans filled with FR-3700 foam at densities from 6.7 to 25.8 lb/ft³ helped define the expected performance of the foam under fire accident conditions as documented in references [11] and [12]. Under the referenced fire tests, one end of the test article was subjected to an open diesel fueled burner flame at temperatures of 980 to 1,200 °C (1,800 to 2,200 °F) for more than 30 minutes. A thermal shield prevented direct exposure to the burner flame on any surface of the test article other than the hot face. Each test article was instrumented with thermocouples located at various depths in the foam. In addition, samples of the foam were subjected to thermogravimetric analysis (TGA) to determine the thermal decomposition vs. temperature. The exposure temperatures for the TGA tests varied from 70 to 1,500 °F, and were conducted in both air and nitrogen atmospheres. The result for the nitrogen environment (see Figure 3.5-15) is more representative of the low oxygen environment existing within the impact limiter shells encasing the foam. These test results indicate that the following steps occur in the thermal breakdown of the foam under the level of elevated temperatures reached during the HAC fire event:

- Below 250 °F, the variation in foam thermal properties with temperature is slight and reversible. As such, fixed values for specific heat and thermal conductivity are appropriate.

- Between 250 and 500 °F, small variations in foam thermal properties occur. The observed changes are so slight that the same thermal properties used for temperatures below 250 °F may also be used to characterize the thermal performance of the foam (i.e., thermal conductivity, specific heat, and density) between 250 and 500 °F.

- Between 325 and 435 °F, a slight foam weight reduction of approximately 2% (see Figure B-1) will occur as water vapor and/or the gas used as the blowing agent is lost.

- Irreversible thermal decomposition of the foam begins as the temperature rises above 500 °F and increases non-linearly with temperature. Based on the TGA testing (see Figure

3.5-15), approximately 2/3's of this decomposition occurs over a narrow temperature range centered about 670 °F.

- The decomposition is accompanied by vigorous out-gassing from the foam and an indeterminate amount of internal heat generation. The internal heat generation arises from the gases generated by the decomposition process that are combustible under piloted conditions. However, since the decomposition process is endothermic, the foam will not support combustion indefinitely. Further, the out-gassing process removes a significant amount of heat from the package via mass transport.

- The weight loss due to out-gassing not only has direct effect on the heat flux into the remaining virgin foam, but changes the composition of the resulting foam char since the foam constituents are lost at different rates. This change in composition affects both the specific heat and the thermal conductivity of the foam char layer.

- As temperature continues to rise, the developing char layer begins to take on the characteristics of a gas-filled cellular structure where radiative interchange from one cell surface to another becomes the dominant portion of the overall heat transfer mechanism. This change in heat transfer mechanisms causes the apparent heat conductivity to take on a highly non-linear relationship with temperature.

- Finally, at temperatures above 1,250 °F, the thermal breakdown of the foam is essentially completed and only about 5 to 10% of the original mass is left. In the absence of direct exposure to a flame or erosion by the channeling of the outgas products through the foam, the char layer will be the same or slightly thicker than the original foam depth. This char layer will continue to provide radiative shielding to the underlying foam material.

Since the thermal decomposition of the foam is an endothermic process, the foam is self-extinguishing and will not support a flame once the external flame source is removed. However, the gases generated by the decomposition process are combustible and will burn under piloted conditions. A portion of these generated gases can remain trapped within the charred layer of the foam after the cessation of the HAC fire event and continue to support further combustion, although at a much reduced level, until a sufficient time has passed for their depletion from the cell structure. This extended time period is typically from 15 to 45 minutes.

The sharp transition in the state of the foam noted in Figure 3.5-15 at or about 670 °F can be used to correlate the observed depth of the foam char following a burn test with the occurrence of this temperature level within the foam. The experimental correlation between the foam recession depth and the foam density published by General Plastics [12] is expressed by the relation:

$$y = -0.94581 - 11.64 \times \log_{10}(x)$$

where, y = the recession depth, cm

x = foam density (g/cm^3)

Based on this correlation, the recession depth expected for the nominal 16 pcf density foam used in the packaging is estimated to be 2.3 inches. The loss of foam could increase to a depth of approximately 2.7 inches for foam fabricated at the low end of the density tolerance (i.e., 13.6 pcf). As such, any amount of virgin foam in excess of approximately 3.2 inches (i.e., 2.7 inches + 0.5 inches) prior to the fire will be sufficient to prevent any significant temperature rise on the backside of the foam after a 30 minute fire event.

It should be noted that these results assume that the foam is enclosed within a steel shell with no significant opposing surface openings in the vertical direction. Note, the vent ports incorporated into the impact limiter shell are not considered to be significant surface openings. The presence of the steel enclosure shields the foam from the heat flux of a HAC fire event and contain the foam char that is generated.
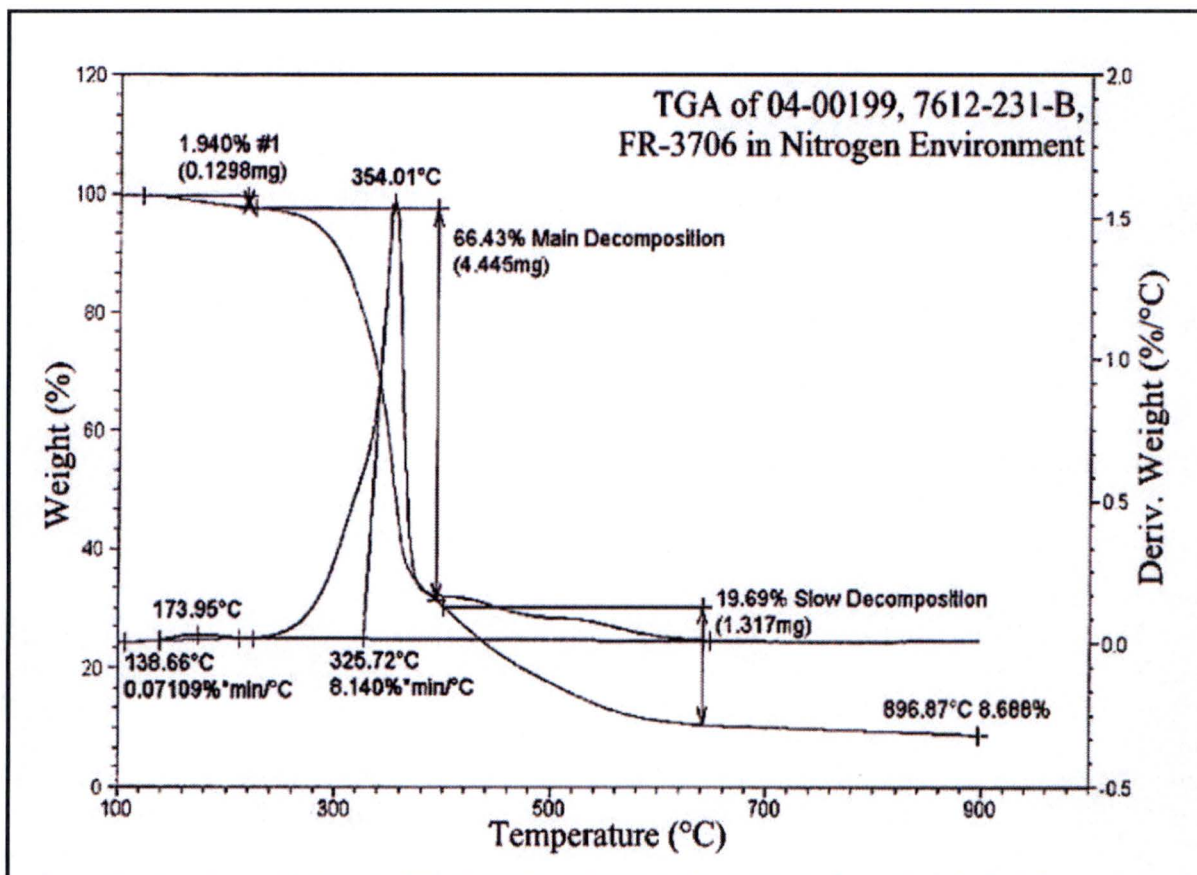
Figure 3.5-15 – TGA Analysis of Foam Decomposition in Nitrogen Environment

4.0 CONTAINMENT

4.1 Description of the Containment System

4.1.1 Containment Boundary

The 380-B package provides a single level of leaktight containment, defined as a leakage rate of less than 1×10^{-7} reference cubic centimeters per second (ref–cm^3/s), air, per ANSI N14.5 [1]. The containment boundary of the 380-B package consists of the following elements, depicted in Figure 4.1-1:

- The lower end structure
- The inner shell
- The upper end structure (including lead pour hole plug and welds)
- The containment O–ring seal (the inner elastomer seal in the closure lid)
- The closure lid main structure
- The vent port in the closure lid including elastomer sealing washer and brass port plug
- The vent port drill access hole plug and weld

Unless noted, all elements are made of ASTM Type 304 stainless steel in various product forms. A full description of the packaging is given in Section 1.2.1, *Packaging*.

4.1.2 Containment Penetrations

The vent port is the only containment penetration. The vent port is located in the closure lid flange, and communicates with the payload cavity through an inclined passage. Part of the passage consists of a groove located on the cask body upper end structure surface. The upper end of the inclined passage (i.e., the drill access hole) in the lid is closed with a plug welded in place. The vent port is designed and tested to ensure leaktight sealing integrity, i.e., a leakage rate not exceeding 1×10^{-7} ref–cm^3/s, per ANSI N14.5.

4.1.3 Seals

The elastomeric portion of the containment boundary is comprised of a nominally 3/8–inch diameter, O–ring face seal located in the inner groove in the closure lid, and a seal washer sealing element (an O–ring integrated with a stainless steel washer) for the vent port. The seals are made using a butyl elastomer compound suitable for continuous use between the temperatures of at least -40 ºF and 250 ºF [2], and capable of much higher temperatures during the HAC fire case transient. Further discussion of the thermal performance capabilities of the butyl rubber seals is provided in Chapter 3, *Thermal Evaluation*.

Two O–ring seals are provided in the closure lid: the inner seal is containment, and the outer forms an annular space for leakage rate testing of the containment seal. The leakage rate tests

used for various purposes are summarized in Section 4.4, *Leakage Rate Tests for Type B Packages*, and described in detail in Chapter 8, *Acceptance Tests and Maintenance Program*.

The O–ring containment seal is retained in the closure lid using a dovetail groove having a depth of 0.284 ± 0.003 inches, or $0.281 - 0.287$ inches. The O–ring has a cross sectional diameter of 0.375 ± 0.007 inches, or $0.368 - 0.382$ inches. The minimum compression corresponds to the maximum groove depth and the minimum O–ring cross–sectional diameter:

$$C_{Min} = 100 \times \left(1 - \frac{G_{Max}}{D_{Min}}\right) = 22\%$$

where $G_{Max} = 0.287$ inches and $D_{Min} = 0.368$ inches. The maximum compression corresponds to the minimum groove depth and the maximum O–ring cross–sectional diameter:

$$C_{Max} = 100 \times \left(1 - \frac{G_{Min}}{D_{Max}}\right) = 26\%$$

where $G_{Min} = 0.281$ inches and $D_{Max} = 0.382$ inches. According to Design Table 4-4 of the Parker O–ring Handbook [7], the nominal recommended compression is 16%. The limit for maximum compression is when the O–ring cross-section, adjusted for maximum temperature, fills the cross sectional area of the dovetail groove. This condition occurs for the 380-B package closure O–ring at a compression of 31.7%. The compression range of 22% to 26% will therefore provide satisfactory performance of the O–ring during all NCT and HAC.

4.1.4 Welds

All structural welds used in the containment boundary are full penetration and volumetrically inspected to ensure structural and containment integrity. The weld joining the inner shell to the upper end structure is ultrasonically inspected in accordance with the ASME B&PV Code, Subsection NB, Article NB–5000, and Section V, Article 4 [4]. The weld joining the inner shell and the lower end structure is radiograph inspected in accordance with the ASME B&PV Code, Subsection NB, Article NB–5000, and Section V, Article 2 [3]. All containment boundary welds are inspected by liquid penetrant inspection on the final pass in accordance with the ASME B&PV Code, Subsection NB, Article NB–5000, and Section V, Article 6 [5]. All containment boundary welds are confirmed to be leaktight as discussed in Section 8.1.4, *Fabrication Leakage Rate Tests*.

4.1.5 Closure

The closure lid completes the containment boundary, and is attached to the cask body using 36, 1-1/2-6 UNC socket head cap screws tightened to $850 - 950$ ft-lb. As shown in Chapter 2, *Structural Evaluation*, the closure lid cannot become detached by any internal pressure, NCT, or HAC events. The closure lid, including the vent port, is completely covered by the upper impact limiter, which is attached to the cask using twelve, 1-1/4-7 UNC socket head cap screws tightened to $280 - 340$ ft-lb. Thus, the containment opening cannot be inadvertently opened.
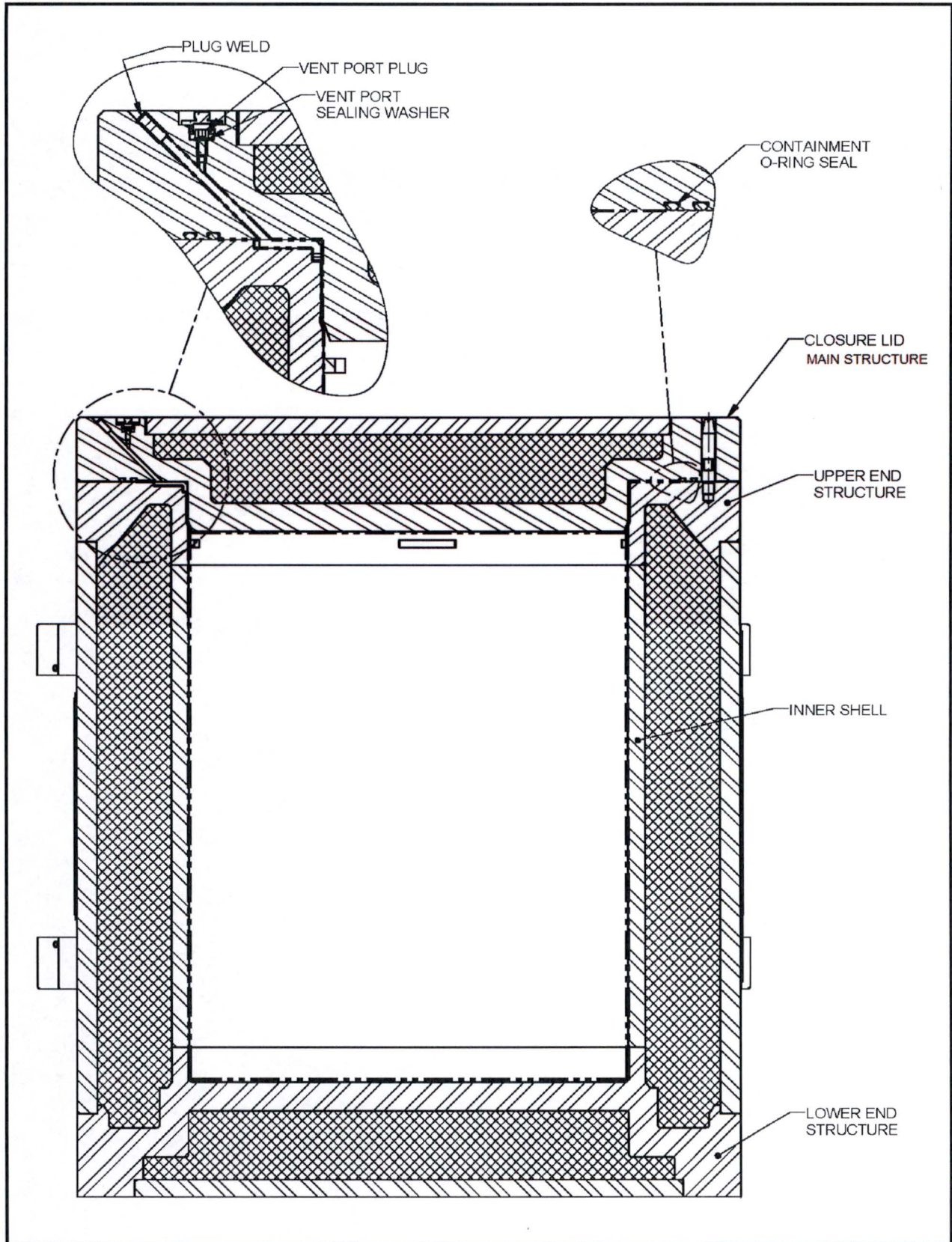
Figure 4.1-1 – 380-B Package Containment Boundary

4.2 Containment Under Normal Conditions of Transport

The results of the NCT structural and thermal evaluations presented in Sections 2.6, *Normal Conditions of Transport*, and 3.3, *Thermal Evaluation for Normal Conditions of Transport*, respectively, demonstrate that there is no release of radioactive materials per the "leaktight" definition of ANSI N14.5 under any of the NCT tests described in 10 CFR §71.71 [6].

4.3 Containment Under Hypothetical Accident Conditions

The results of the HAC structural and thermal evaluations performed in Sections 2.7, *Hypothetical Accident Conditions*, and 3.4, *Thermal Evaluation for Hypothetical Accident Conditions*, respectively, demonstrate that there is no release of radioactive materials per the "leaktight" definition of ANSI N14.5 under any of the hypothetical accident condition tests described in 10 CFR §71.73.

4.4 Leakage Rate Tests for Type B Packages

4.4.1 Fabrication Leakage Rate Tests

During fabrication, the containment boundary is leakage rate tested as described in Section 8.1.4, *Fabrication Leakage Rate Tests*. The fabrication leakage rate tests are consistent with the guidelines of Section 7.3 of ANSI N14.5. This leakage rate test verifies the containment integrity of the 380-B packaging to a leakage rate not to exceed 1×10^{-7} ref–cm^3/s, air.

4.4.2 Maintenance/Periodic Leakage Rate Tests

Annually, or at the time of damaged containment seal replacement or sealing surface repair, the containment O–ring seal and the vent port sealing washer are leakage rate tested as described in Section 8.2.2, *Maintenance/Periodic Leakage Rate Tests*. The maintenance/periodic leakage rate tests are consistent with the guidelines of Section 7.4 of ANSI N14.5. This test verifies the sealing integrity of the containment seals to a leakage rate not to exceed 1×10^{-7} ref–cm^3/s, air.

4.4.3 Preshipment Leakage Rate Tests

Prior to shipment of the loaded 380-B package, the containment O–ring seal and the vent port sealing washer are leakage rate tested per Section 7.4, *Preshipment Leakage Rate Test*. The preshipment leakage rate tests are consistent with the guidelines of Section 7.6 of ANSI N14.5. This test verifies the sealing integrity of the containment seals to a leakage rate sensitivity of 1×10^{-3} ref–cm^3/s, air.

As an option, the maintenance/periodic leakage rate tests, described in Section 8.2.2, *Maintenance/Periodic Leakage Rate Tests*, may be performed at the time of shipment instead of the tests described in Section 7.4, *Preshipment Leakage Rate Test*.

4.5 Appendix

4.5.1 References

1. ANSI N14.5–2014, *American National Standard for Radioactive Materials – Leakage Tests on Packages for Shipment*, American National Standards Institute (ANSI), Inc.

2. Parker O-Ring Material Offering Guide, ORD 5712, August 2002.

3. American Society of Mechanical Engineers (ASME) Boiler and Pressure Vessel Code, Section III, *Rules for Construction of Nuclear Facility Components*, Division 1 – Subsection NB, *Class 1 Components*, and Section V, *Nondestructive Examination*, Article 2, *Radiographic Examination*, 2010 Edition, 2011 Addenda.

4. American Society of Mechanical Engineers (ASME) Boiler and Pressure Vessel Code, Section III, *Rules for Construction of Nuclear Facility Components*, Division 1 – Subsection NB, *Class 1 Components*, and Section V, *Nondestructive Examination*, Article 4, *Ultrasonic Examination Methods for Welds*, 2010 Edition, 2011 Addenda.

5. American Society of Mechanical Engineers (ASME) Boiler and Pressure Vessel Code, Section III, *Rules for Construction of Nuclear Facility Components*, Division 1 – Subsection NB, *Class 1 Components*, and Section V, *Nondestructive Examination*, Article 6, *Liquid Penetrant Examination*, 2010 Edition, 2011 Addenda.

6. Title 10, Code of Federal Regulations, Part 71 (10 CFR 71), *Packaging and Transportation of Radioactive Material*, 01–01–11 Edition.

7. Parker O–ring Handbook, ORD–5700, Parker-Hannifin Corporation, Cleveland, OH, © 2007.

This page left intentionally blank.

5.0 SHIELDING EVALUATION

The 380-B package is used to transport radioactive sources in shielded devices. The shielding analysis for a variety of source isotopes is presented in this chapter. It is demonstrated that the 10 CFR 71 dose rate requirements are met for transportation of radioactive material in an exclusive use conveyance.

5.1 Description of Shielding Design

5.1.1 Design Features

The 380-B is a thick-walled cask that provides significant shielding against gamma radiation. The dimensions are based on the drawings provided in Appendix 1.3.3, *Packaging General Arrangement Drawings*. The cavity has an inner diameter of 38 inches and height of 48-1/8 inches. Radially, the cask features inner and outer shells of steel with a lead-filled annulus. The inner and outer steel shells have nominal thicknesses of 1.5 inches and 1.75 inches, respectively, with a nominal lead thickness of 6.5 inches. The lid and bottom ends offer identical bulk shielding, with an inner 2.5-inch steel plate, 6.0-inch lead shield, and an outer 1.5-inch steel plate. The cask does not provide hydrogenous neutron shielding.

5.1.2 Summary of Maximum Radiation Levels

The 380-B is transported vertically in an open vehicle under exclusive use. Therefore, normal condition of transport (NCT) dose rates are limited to 200 mrem/hr on the external (accessible) surfaces of the package (i.e., outer surfaces of impact limiters and outer surface of the personnel barrier), 200 mrem/hr on the projected surfaces of the vehicle, 10 mrem/hr at a distance of 2 m from the projected side surfaces of the vehicle, and 2 mrem/hr in any occupied location (vehicle driver). A personnel barrier is in place between the impact limiters, which remains attached during NCT events (see Section 2.6.7, *Free Drop*). Per Table 5.2 of NUREG-1609 [5], the dose rate on the non-accessible surfaces of the package beneath the personnel barrier is limited to 1,000 mrem/hr. Because only one package is shipped on the vehicle and the outer diameter of the impact limiters (100 inches) is nearly as wide as the vehicle (102 inches), the dose rates on the accessible surfaces of the package bound the dose rates on the surface of the vehicle, and the dose rates on the projected side surfaces of the vehicle are not explicitly computed.

Dose rate computations are documented in Section 5.4, *Shielding Evaluation*. The activity limits for the isotopes are selected so that computed dose rates are 95% of the regulatory limits; i.e., the maximum dose rate on the inaccessible package surface beneath the personnel barrier is 950 mrem/hr, the maximum dose rate on accessible package surface/personnel barrier is 190 mrem/hr, and the maximum dose rate 2 m from the vehicle side is 9.5 mrem/hr.

The limiting dose rate location is the inaccessible package surface beneath the personnel barrier. At this location a dose rate of 950 mrem/hr is achieved. On the accessible package surface, the maximum dose rate is 138.5 mrem/hr, which is below the limit of 200 mrem/hr by a large margin. At 2 m from the side surface of the vehicle, the maximum dose rate is 7.9 mrem/hr, which is below the limit of 10 mrem/hr. It is demonstrated that the dose rate in any occupied location is less than 1.6 mrem/hr.

For hypothetical accident conditions (HAC), the dose rate is limited to 1,000 mrem/hr at a distance of 1 m from the surface of the package. Dose rates are computed 1 m from the surface of the cask body. No credit is taken for the foam inside the impact limiters or potential distance provided by the impact limiter shells, although credit is taken for the steel of the impact limiter shells because the impact limiters remain attached in an accident. For HAC analysis, the maximum dose rate is demonstrated to be 215.1 mrem/hr when using a Co-60 source and occurs at the top of the package due to streaming through the clearance gap in the lid and the reduced lead thickness in this region.

5.2   Source Specification

Source terms are determined for a number of isotopes, which are summarized in Table . These isotopes may be alpha, beta, gamma, and/or neutron emitters, although from a shielding standpoint, only the corresponding gamma and neutron emissions contribute to the dose rate. The actinides may also be mixed with an (α,n) target material, such as beryllium. The decay heat of the 380-B package is limited to 205 watts. Therefore, each nuclide is also limited to 205 watts.

5.2.1   Gamma Source

Co-60

The decay of Co-60 is sufficiently simple to be treated explicitly. Each decay of Co-60 results in two gammas, with energies of 1.173 and 1.332 MeV [1]. The gamma source for 1 Ci of Co-60 is provided in Table . Because Co-60 creates high-energy gammas, the contribution from bremsstrahlung radiation may be neglected because the contribution due to this radiation is much less than the primary source.

Cs-137

The decay of Cs-137 is sufficiently simple to be treated explicitly. The decay of Cs-137 emits a 0.662 MeV gamma with an 85% probability [1]. The gamma source for 1 Ci of Cs-137 is provided in Table . Because Cs-137 creates a high-energy gamma, the contribution from bremsstrahlung radiation may be neglected because the contribution due to this radiation is much less than the primary source.

Sr-90

Sr-90 decays to Y-90, which is a minor gamma emitter. Sr-90 reaches equilibrium with Y-90 after approximately 20 days. To conservatively compute the source term, 1 Ci of both Sr-90 and Y-90 are input to SCALE6.0/ORIGEN-S [3] and is provided in Table . Note that Sr-90/Y-90 emits negligible gamma radiation. However, in ORIGEN-S, a UO_2 target is assumed for calculation of the bremsstrahlung radiation source. Therefore, almost the entire gamma source reported in Table is from bremsstrahlung radiation.

Ir-192

Ir-192 is a gamma emitter. There is an error in the SCALE6.0/ORIGEN-S data libraries for Ir-192 and SCALE6.0/ORIGEN-S cannot be used to determine the gamma source for this isotope. Therefore, for this isotope only, SCALE44/ORIGEN-S [4] is used to compute the gamma source term. The gamma source is provided in Table for 1 Ci.

Ra-226

Ra-226 is an alpha/gamma emitter. The gamma source input files are developed using SCALE6.0/ORIGEN-S. The Ra-226 gamma source for a decay time from 0.1 to 10 years is provided in Table for 1 Ci. The gamma sources for the energy groups that are primary contributors to the dose rate (0.6 to 2.5 MeV) peak at approximately 0.3 years of decay. The gamma source for the lower energy groups continue to increase slowly after 0.3 years, but these energy groups do not contribute to the dose rate. Therefore, the source at a decay time of 0.3

years is used in the shielding calculations. The contribution from bremsstrahlung radiation with a UO_2 target is conservatively included.

The alpha radiation will lead to a neutron source when mixed with an (α,n) target material, such as beryllium. The neutron source is discussed in Section 5.2.2, *Neutron Source*.

Decay Heat

The decay heat per Ci is also computed for each isotope using ORIGEN-S and is provided in Table . The decay heat includes daughter products. The Cs-137 conservatively includes 1 Ci of Ba-137m, and the Sr-90 conservatively includes 1 Ci of Y-90. For Ra-226, the decay heat increases slowly with time and peaks after approximately 80 years of decay, and the reported decay heat for Ra-226 is the peak value. The package is limited to 205 watts total heat generation. For most isotopes, the activity limit is governed by heat load rather than dose rate. The total activity to reach 205 watts is also listed in Table .

5.2.2 Neutron Source

A neutron source is generated by Ra-226 via (α,n) reactions. Target materials that result in an (α,n) source include oxygen, beryllium, and chlorine. The ORIGEN-S module of the SCALE6 code package is used to calculate the neutron sources. Quantities are input in grams rather than curies because the target materials are not radioactive.

Ra-226 sources exist either as a radium/beryllium mixture, or as radium with trace amounts of oxygen, carbon, sulfur, bromine, or chlorine (hydrous or anhydrous). Because the trace elements contain (α,n) target materials, it is conservatively assumed that the trace elements are present as compounds $RaSO_4$, $RaBr_2$ (hydrous), $RaCl_2$ (hydrous), $RaCl_2$ (anhydrous), or $RaCO_3$. The masses of the target elements are computed based on the chemical formulas provided. For $RaCl_2$ (hydrous), the H_2O mass is arbitrarily selected as five times the $RaCl_2$ mass, although adding water simply decreases the neutron source magnitude. For the Ra/Be mixture, an infinitely dilute mixture is conservatively assumed (infinite dilution is defined as a beryllium mass 1,000 times greater than the Ra-226 mass). Bromine is not an (α,n) target material, so $RaBr_2$ does not generate neutrons. Hydrous $RaBr_2$ would produce neutrons from O-17 and O-18, although it is bounded by $RaCl_2$ (hydrous).

The results for 1 Ci are summarized in Table . The maximum neutron source typically occurs after approximately 80 years of decay due to the slow in-growth of the alpha emitting daughter product Po-210. The sources provided in Table represent the maximum value of the source for each target. RaBe is by far the largest neutron source. Beryllium generates more neutrons than any other target material, and the infinite dilution assumption also increases the beryllium neutron source. Of the non-Be target compounds, $RaCl_2$ (anhydrous) has the largest neutron source. Therefore, $RaCl_2$ (anhydrous) is used to bound all non-Be targets, and RaBe is treated separately.

Table 5.2-1 – Allowable Source Nuclides

Nuclide	Form of Contents	Chemical Form
Co-60	Cobalt metal rods or wafers encapsulated in stainless steel or MP-35 capsules	Cobalt metal alloy
Cs-137	Powder, pellets, ceramic matrix as sealed sources	CsCl or CsO_2
Sr-90	Sr-90/Y-90 in a ceramic matrix for smaller sources, strontium titanate hot isostatic pressed pellets for larger sources, cladding typically Hastelloy metal, although other cladding materials are acceptable.	Strontium metal
Ir-192	Iridium metal rods encapsulated in stainless steel	Ir metal or pellets (wafers)
Ra-226	Radium salts in thin-walled Pt metal tubes or plaques, and Ra-226/Be mixtures	$RaBr_2$ hydrous $RaCl_2$ hydrous $RaCl_2$ anhydrous $RaSO_4$ $RaCO_3$

Table 5.2-2 – Gamma Source, 1 Ci Co-60

Line Energy (MeV)	Gamma Source (γ/s)
1.173	3.7E+10
1.332	3.7E+10

Table 5.2-3 – Gamma Source, 1 Ci Cs-137

Line Energy (MeV)	Gamma Source (γ/s)
0.662	3.145E+10

Table 5.2-4 – Gamma Source, 1 Ci Sr-90

E_{upper} (MeV)	Gamma Source (γ/s)
5.00E-02	1.603E+10
1.00E-01	5.603E+09
2.00E-01	3.909E+09
3.00E-01	1.282E+09
4.00E-01	9.361E+08
6.00E-01	6.294E+08
8.00E-01	2.853E+08
1.00E+00	1.218E+08
1.33E+00	7.182E+07
1.66E+00	1.359E+07
2.00E+00	2.438E+06
2.50E+00	1.252E+05
Total	2.888E+10

Table 5.2-5 – Gamma Source, 1 Ci Ir-192

E_{upper} (MeV)	Gamma Source (γ/s)
5.00E-02	1.994E+09
1.00E-01	3.602E+09
2.00E-01	3.023E+08
3.00E-01	1.271E+10
4.00E-01	3.736E+10
6.00E-01	2.055E+10
8.00E-01	3.031E+09
1.00E+00	1.095E+08
1.33E+00	1.926E+07
1.66E+00	4.233E+05
Total	7.969E+10

Table 5.2-6 – Gamma Source (γ/s), 1 Ci Ra-226

E_{upper} (MeV)	0.1 y	0.3 y	0.5 y	0.7 y	1.0 y	3.0 y	5.0 y	10.0 y
5.00E-02	1.430E+10	1.439E+10	1.446E+10	1.453E+10	1.463E+10	1.529E+10	1.591E+10	1.729E+10
1.00E-01	1.356E+10	1.359E+10	1.360E+10	1.360E+10	1.362E+10	1.371E+10	1.379E+10	1.396E+10
2.00E-01	4.267E+09	4.277E+09	4.283E+09	4.289E+09	4.298E+09	4.354E+09	4.407E+09	4.524E+09
3.00E-01	1.229E+10	1.231E+10	1.231E+10	1.231E+10	1.231E+10	1.232E+10	1.232E+10	1.233E+10
4.00E-01	1.483E+10	1.485E+10	1.485E+10	1.484E+10	1.484E+10	1.484E+10	1.484E+10	1.482E+10
6.00E-01	1.353E+09	1.355E+09	1.356E+09	1.356E+09	1.356E+09	1.359E+09	1.362E+09	1.367E+09
8.00E-01	1.874E+10	1.877E+10	1.876E+10	1.876E+10	1.876E+10	1.874E+10	1.873E+10	1.869E+10
1.00E+00	2.222E+09	2.224E+09	2.224E+09	2.224E+09	2.224E+09	2.222E+09	2.220E+09	2.216E+09
1.33E+00	9.685E+09	9.695E+09	9.695E+09	9.695E+09	9.690E+09	9.685E+09	9.675E+09	9.655E+09
1.66E+00	4.921E+09	4.927E+09	4.926E+09	4.926E+09	4.925E+09	4.921E+09	4.917E+09	4.906E+09
2.00E+00	8.210E+09	8.220E+09	8.220E+09	8.220E+09	8.220E+09	8.210E+09	8.205E+09	8.185E+09
2.50E+00	3.136E+09	3.140E+09	3.140E+09	3.140E+09	3.139E+09	3.137E+09	3.134E+09	3.127E+09
3.00E+00	4.949E+07	4.955E+07	4.955E+07	4.954E+07	4.954E+07	4.949E+07	4.945E+07	4.934E+07
4.00E+00	1.183E+07	1.185E+07	1.185E+07	1.185E+07	1.185E+07	1.184E+07	1.183E+07	1.180E+07
5.00E+00	6.715E+00	6.720E+00	6.725E+00	6.735E+00	6.745E+00	6.835E+00	6.920E+00	7.140E+00
6.50E+00	1.935E+00	1.937E+00	1.938E+00	1.940E+00	1.943E+00	1.969E+00	1.994E+00	2.057E+00
8.00E+00	2.461E-01	2.464E-01	2.465E-01	2.468E-01	2.472E-01	2.504E-01	2.536E-01	2.616E-01
1.00E+01	3.284E-02	3.288E-02	3.290E-02	3.293E-02	3.299E-02	3.342E-02	3.385E-02	3.491E-02
Total	1.076E+11	1.078E+11	1.081E+11	1.089E+11	1.096E+11	1.099E+11	1.102E+11	1.106E+11

Table 5.2-7 – Decay Heat

Nuclide	Decay Heat (watt/Ci)	Activity to Reach 205 watts (Ci)
Co-60	1.542E-02	13,294
Cs-137	5.040E-03	40,675
Sr-90	6.698E-03	30,606
Ir-192	6.150E-03	33,333
Ra-226	1.862E-01	1,101

Table 5.2-8 – Ra-226 Neutron Sources, 1 Ci Ra-226

		Neutron Sources (n/s)			
E_{upper} (MeV)	RaSO$_4$	RaCl$_2$ (anhydrous)	RaCl$_2$ (hydrous)	RaCO$_3$	RaBe
1.30E-06	3.472E-08	3.257E-14	6.100E-08	3.175E-08	0.000E+00
1.86E-06	9.000E-07	1.036E-13	1.588E-06	8.225E-07	0.000E+00
3.06E-06	1.950E-06	7.675E-06	3.949E-06	1.783E-06	0.000E+00
1.07E-05	1.572E-05	1.382E-04	3.679E-05	1.437E-05	0.000E+00
2.90E-05	1.084E-04	7.870E-04	2.421E-04	1.733E-04	0.000E+00
1.01E-04	5.060E-04	5.105E-03	1.240E-03	8.955E-04	0.000E+00
5.83E-04	7.035E-03	7.840E-02	1.781E-02	1.769E-02	0.000E+00
3.04E-03	1.002E-01	9.615E-01	2.425E-01	2.224E-01	8.880E-01
1.50E-02	1.203E+00	1.105E+01	2.879E+00	2.493E+00	5.050E+01
1.11E-01	2.682E+01	3.539E+02	7.155E+01	4.894E+01	2.298E+03
4.08E-01	1.350E+02	2.790E+03	4.257E+02	2.379E+02	3.575E+04
9.07E-01	2.678E+02	9.885E+03	1.150E+03	3.911E+02	3.517E+05
1.42E+00	4.126E+02	1.022E+04	1.400E+03	4.372E+02	4.756E+05
1.83E+00	5.300E+02	5.605E+03	1.295E+03	4.921E+02	2.880E+05
3.01E+00	2.590E+03	2.169E+03	4.676E+03	2.376E+03	1.635E+06
6.38E+00	1.729E+03	0.000E+00	3.050E+03	3.139E+03	7.585E+06
2.00E+01	2.902E-01	0.000E+00	5.155E-01	3.968E+02	5.225E+06
Total	5.695E+03	3.104E+04	1.207E+04	7.520E+03	1.560E+07

5.3 Shielding Model

5.3.1 Configuration of Source and Shielding

All sources are transported inside of devices that offer substantial shielding, and these devices are secured within the 380-B using dunnage. However, because the details of the device designs may not be known, and because the structural performance of the devices in an accident or during transport may not be known, no shielding credit is taken for the devices. Therefore, it is assumed that the source may become dislodged from the device under NCT or HAC and is "loose" inside the cask cavity. In the MCNP models, the source is modeled at the location that results in maximum dose rates. Locations for the source considered include bottom corner, upper corner, and side of the cask cavity.

All sources are sealed and encapsulated. Therefore, the source itself remains intact during NCT and HAC. For all isotopes other than Co-60, the source is conservatively modeled as a point. For sources modeled as a point, no credit is taken for the source encapsulation materials or for self-shielding provided by the source material. Because the Co-60 activity is limited by dose rate, limited self-shielding credit is taken for this isotope. Separate MCNP models are developed for the following sources: Co-60, Cs-137, Sr-90, Ir-192, Ra-226 (gamma), Ra-226 with a chlorine target (neutron), and Ra-226 with a beryllium target (neutron).

The Co-60 source is modeled as a solid cylinder of cobalt metal. From Table A-1 of 10 CFR 71, Co-60 has a specific activity of 1,100 Ci/g. Therefore, a 7,500 Ci source has a minimum mass of $7500/1100 = 6.8$ g. Cobalt has a density of 8.9 g/cm^3. Therefore, the smallest theoretical volume of a 7,500 Ci Co-60 source is $6.8/8.9 = 0.76$ cm^3. If it is assumed this source is a cylinder with a height equal to the diameter, height = diameter = 0.98 cm. This representation is conservative because no self-shielding credit is taken for inert materials in the cobalt matrix or encapsulation materials.

Packaging drawings may be found in Appendix 1.3.3, *Packaging General Arrangement Drawings*. Key dimensions used to develop the MCNP models are provided in Table . Nominal dimensions are used to develop the models, although a reduction in lead thickness due to shrinkage is explicitly addressed. Use of nominal dimensions is reasonable due to the multiple penalizing assumptions used in the analysis (i.e., the assumption that the source escapes the device and migrates to the worst possible location). The corresponding MCNP models are depicted in Figure through Figure .

It is shown in Section 2.7.1.2, *End Drop*, that a 0.075-in radial gap may exist between the lead and the outer shell due to lead shrinkage. This gap is modeled as 0.08-in in both the NCT and HAC models. Again from Section 2.7.1.2, an axial gap between the lead and steel of 0.36-in may also exist due to lead shrinkage. This gap represents the sum of the axial gaps that may exist on each end. In the NCT and HAC models, this axial gap is modeled as 0.4-in at both ends because the axial gap could be at either end.

In the NCT models, the impact limiters are modeled with a reduced height and diameter to simulate NCT free drop damage. This conservatively increases the package surface dose rates by reducing the distance to the source. Also, reducing the size of the impact limiters artificially reduces the mass of foam material. The NCT crush is maximized using low-density foam at 160 °F (see Table 2.12.5-10). The calculated crush depths are 2.1-in (side), 1.1-in (end), and 2.9-

in (center-of-gravity (CG) over corner). In the MCNP models, crush dimensions are modeled to bound the calculated crush values. The 2.9-in CG over corner crush is applied by moving the angled impact limiter surface inward 3.6-in perpendicular to the nominal surface location. The 2.1-in side crush is modeled by reducing the impact limiter diameter by $3.0*2 = 6.0$-in, and the 1.1-in end crush is modeled by reducing the impact limiter length by 2.1-in.

For HAC, the crush is more significant (see Table 2.12.5-11) and the foam may be partially consumed by fire. Therefore, in the HAC models, all foam is replaced by a void. Because the impact limiters remain attached, the steel shells of the impact limiters are included in the HAC models. However, the distance to the dose rate location is measured 1 m from the surface of the cask body; no credit is taken for distance that may be provided by the impact limiter steel shells.

The cask features a personnel barrier that is approximately the same diameter as the impact limiter diameter. Therefore, for NCT calculations the accessible package surface dose rate applies at the impact limiter radius. The lid-end impact limiter is capped with a non-removable rain cover, and this rain cover forms the outer top boundary of the package. The bottom-end impact limiter is capped in a similar manner as the lid-end impact limiter.

A stainless steel inner cover is present at the top of the package cavity. The component is offset 0.25-in from the bottom of the lid, but in the MCNP NCT models the component is conservatively modeled flush with the lid to reduce the distance from the source to the dose rate locations. In the HAC models, the inner cover is not modeled because it could be damaged.

All package features relevant to the shielding analysis are modeled explicitly, including the gap between the lid and cask wall, which is a streaming path. All steel/lead interfaces are modeled explicitly, as the steel provides a streaming path for gamma radiation.

A number of items are not modeled, either because it is conservative to not model the item, or because the item has a negligible effect on dose rates. The steel covers on the impact limiter recesses are conservatively not modeled. The personnel barrier is conservatively not modeled. The 12 ga (0.1054-inch) thermal shield is conservatively not modeled. The vent port groove is at a 45° angle at the inner wall of the cask and does not provide a streaming path. Therefore, the vent port groove is not modeled. The test port does not provide a streaming path and is not modeled. Likewise, bolt holes do not provide a streaming path and are not modeled.

5.3.2   Material Properties

Materials used in the MCNP models are stainless steel, lead, polyurethane foam, and cobalt metal. The stainless steel 304 (SS304) composition and density are provided in Table and are obtained from [3]. This SS304 specification is a generic specification for use in shielding applications. Lead is modeled as pure with a density of 11.35 g/cm^3. Polyurethane foam has a nominal density of 16.0 pounds per cubic foot (pcf), although a density of 14.0 pcf (0.224 g/cm^3) is conservatively modeled. The foam composition used in the models is provided in Table . The Co-60 source is modeled as a small cylinder of solid cobalt metal, density 8.9 g/cm^3.

Table 5.3-1 – Key Model Dimensions

Parameter	Drawing Dimension (in)	As-Modeled Dimension (in)
Cavity length, bottom of lid to bottom of cask	48.12 [=52.5-4.38]	Same
Cavity diameter	38.0	Same
Inner side steel thickness	1.5	Same
Lead side thickness	6.5 [=(57.50-38.0)/2-1.5-1.75]	6.42, includes 0.08-in reduction
Outer side steel thickness	1.75	Same
Lid inner steel plate thickness	2.5	Same
Lid lead thickness (total centerline)	6.0 [=8.5-2.5]	Same
Lid outer steel plate thickness	1.5	Same
Lid lead OD #1	34.1	Same
Lid lead OD #2	44.0	Same
Radial gap, lid to cavity	0.06 [=(38.25-38.13)/2]	Same
Bottom inner steel plate thickness	2.5 [=62.5-52.5-7.5]	Same
Bottom lead thickness (total centerline)	6.0 [=7.5-1.5]	Same
Bottom outer steel plate thickness	1.5	Same
Bottom lead OD #1	38.1	Same
Bottom lead OD #2	46.0	Same
Inner cover outer diameter	37.8	Same
Inner cover upper plate thickness	0.50	Same
Inner cover lower ring ID	33.8	Same
Inner cover lower ring height	1.5	Same
Impact limiter diameter	100.0	94.0, includes 3.0-in radial crush
Impact limiter overall height	43.1	41.0, includes 2.1-in axial crush
Impact limiter engagement	18.0	Same
Impact limiter shell thickness (horizontal shells in contact with the cask body)	0.5	Same
Impact limiter shell thickness (remaining shells)	0.25	Same

Table 5.3-2 – SS304 Composition

Component	Wt.%
C	0.08
Si	1.0
P	0.045
Cr	19.0
Mn	2.0
Fe	68.375
Ni	9.5
Density = 7.94 g/cm^3	

Table 5.3-3 – Foam Composition

Component	Wt.%
C	60
O	24
N	12
H	4
Density = 0.224 g/cm^3	
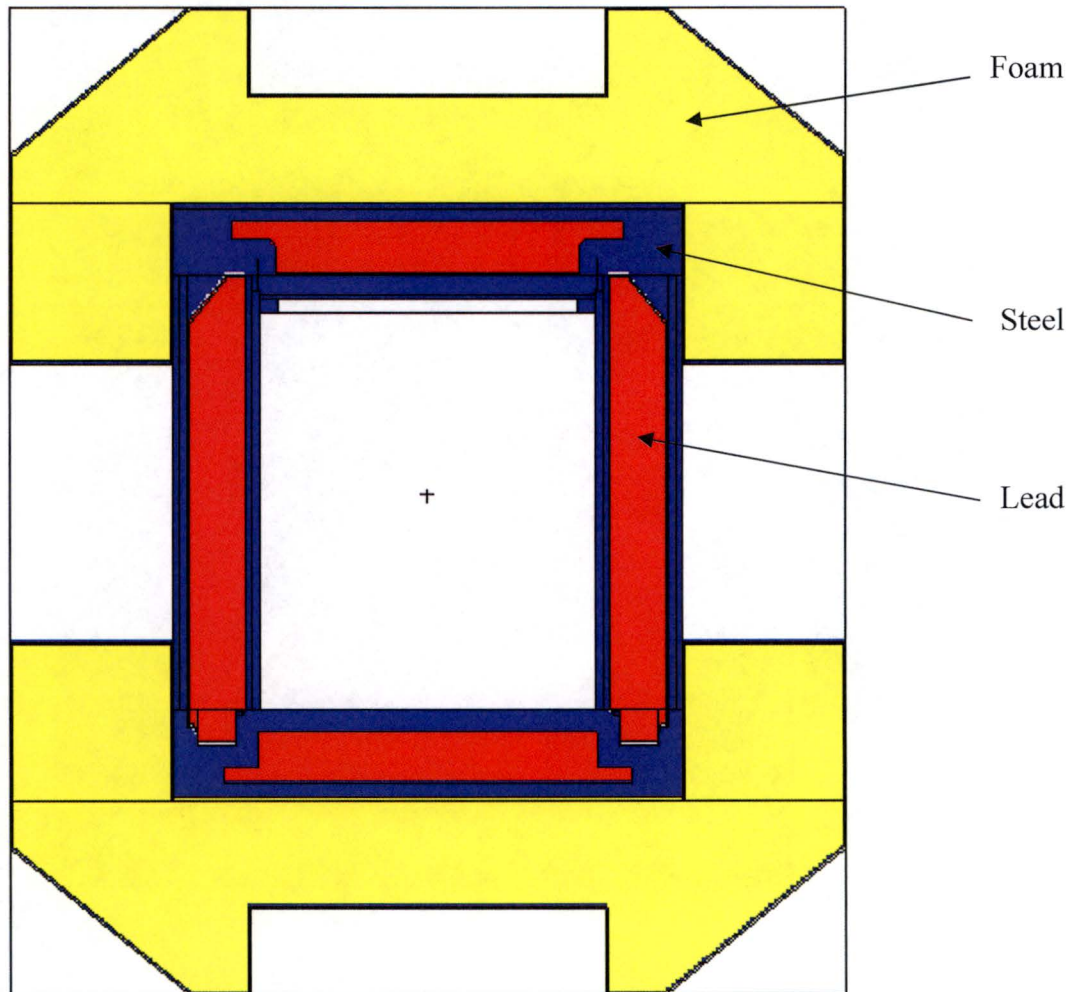
Figure 5.3-1 – NCT MCNP Model

Lid/body gap

Axial lead shrinkage 0.4-in

Inner cover

Radial lead shrinkage
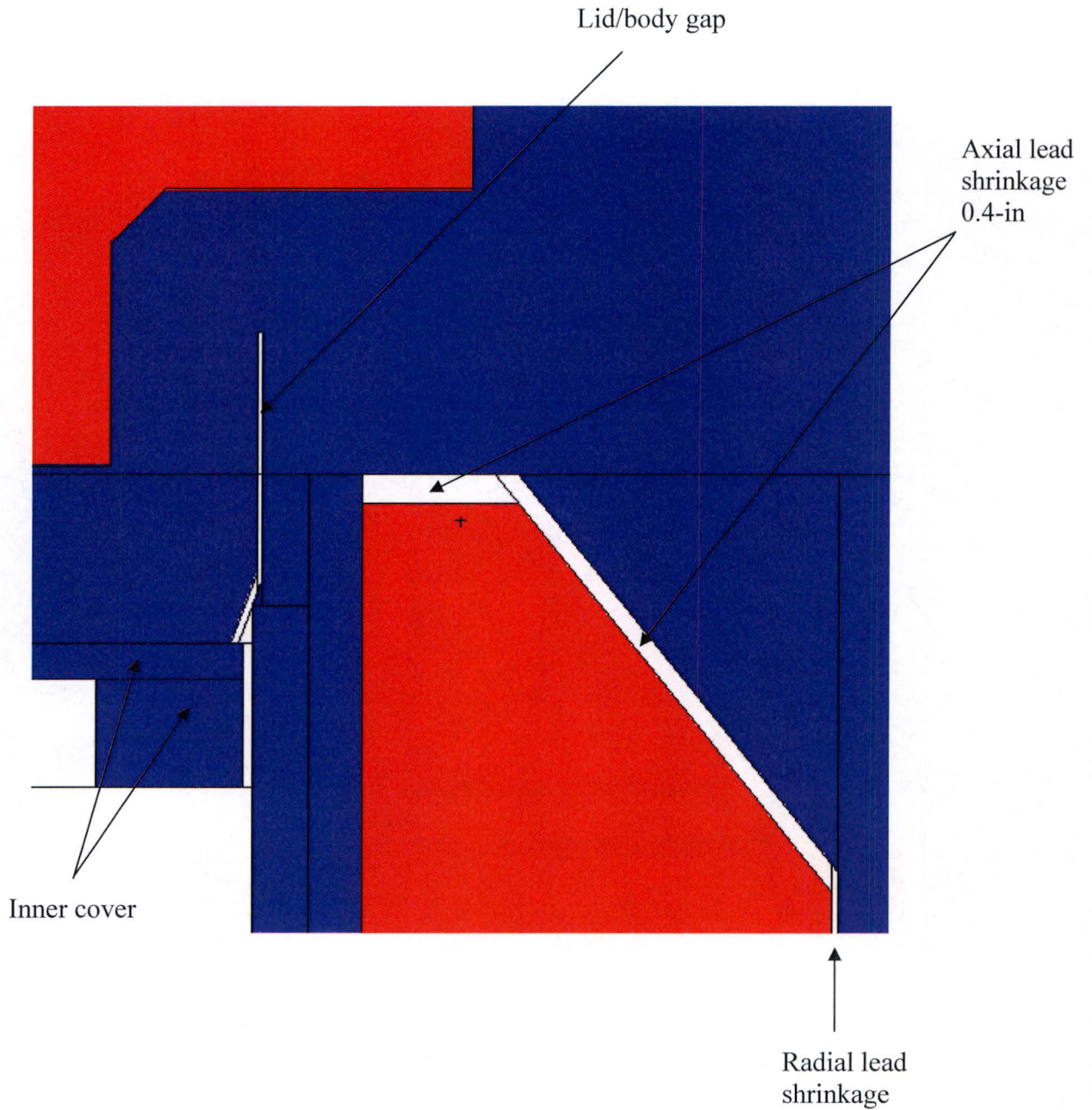
Figure 5.3-2 – NCT MCNP Model, Top Corner Close-Up
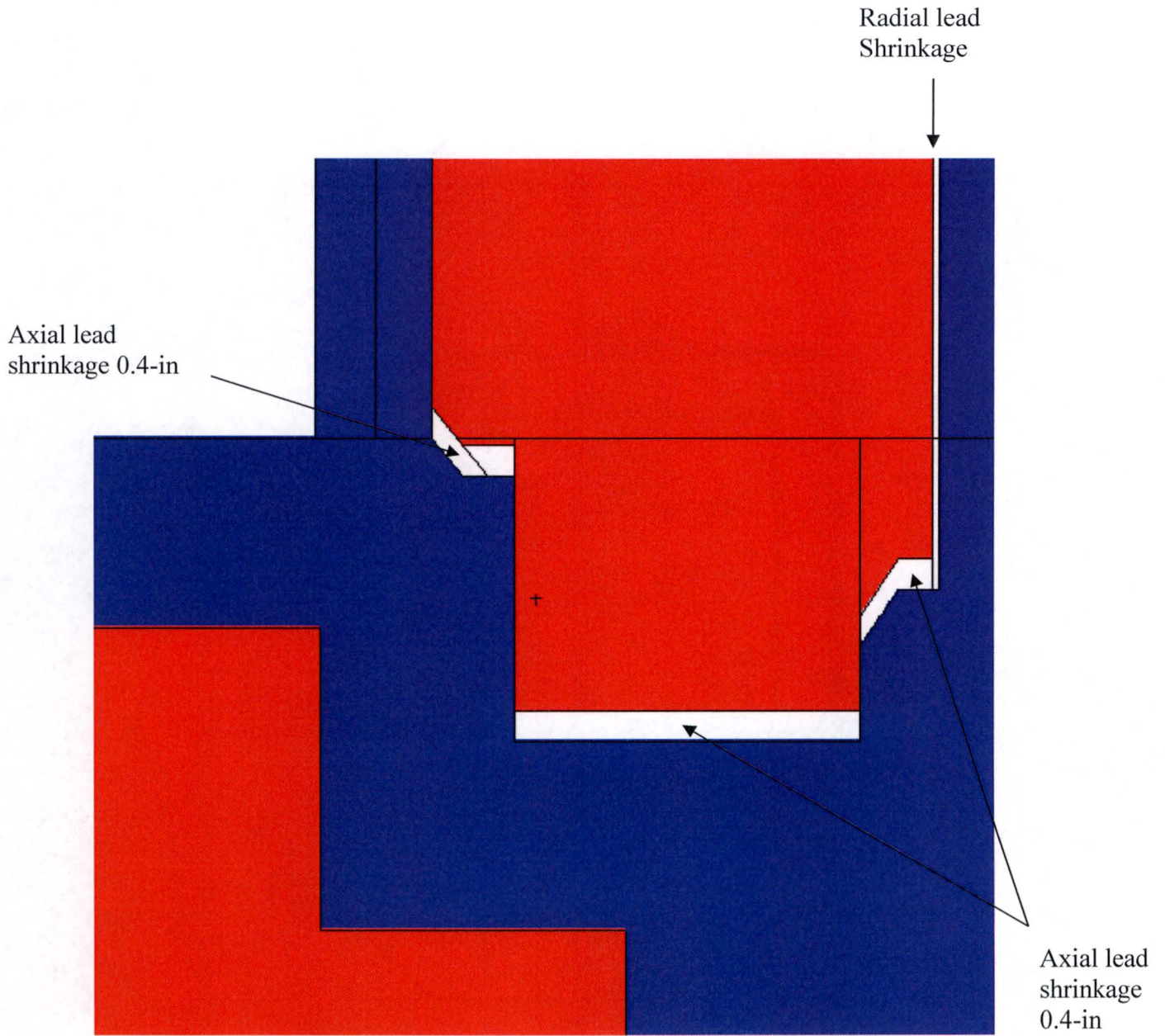
Figure 5.3-3 – NCT MCNP Model, Bottom Corner Close-Up

Foam modeled as void

Inner cover deleted

Axial lead shrinkage 0.4-in (both ends)
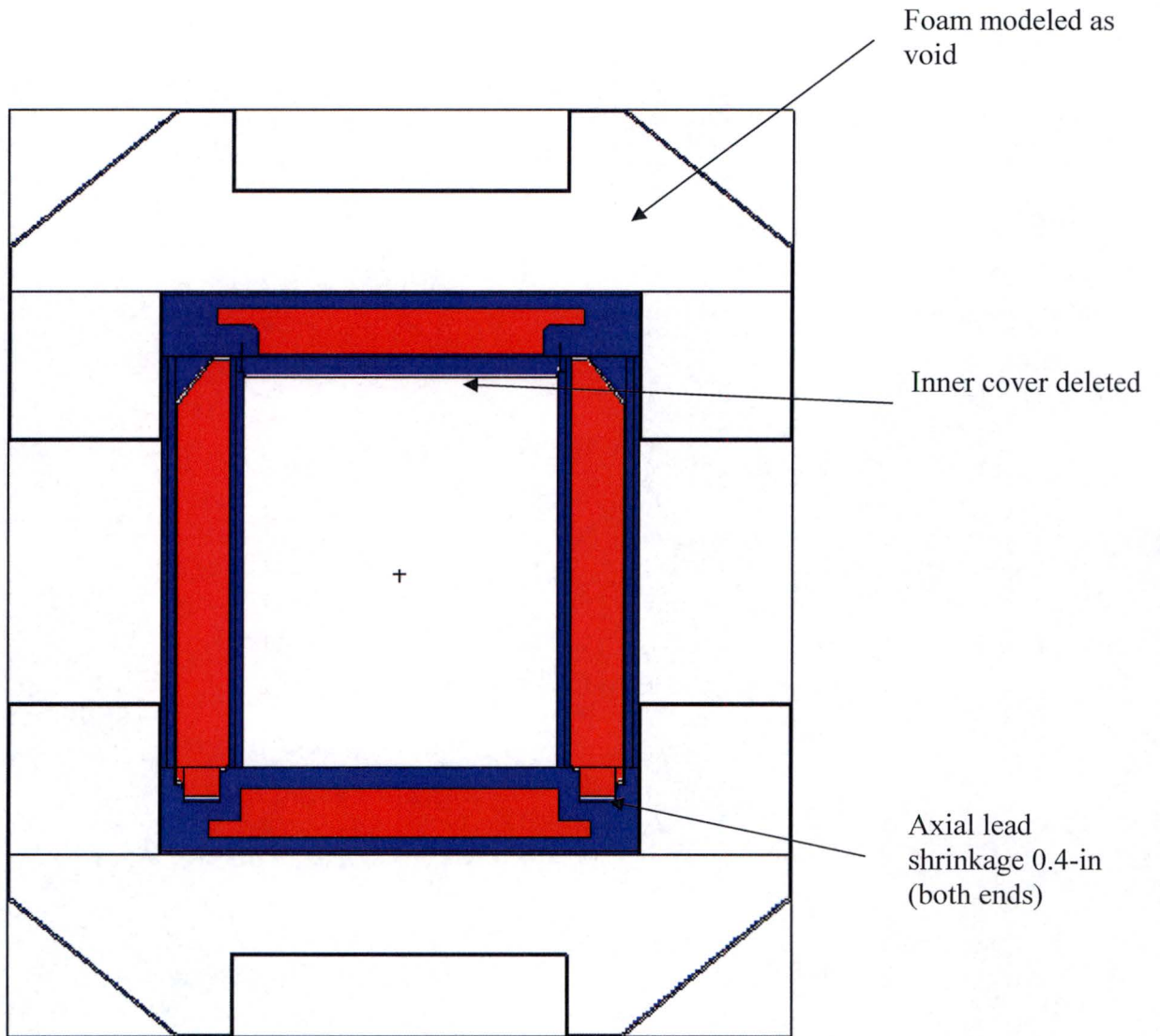
Figure 5.3-4 – HAC MCNP Model

5.4 Shielding Evaluation

5.4.1 Methods

MCNP5 v1.51 is used for the shielding analysis [2]. MCNP5 is a standard, well-accepted shielding program utilized to compute dose rates for shielding evaluations. Dose rates are calculated by tallying the neutron and gamma fluxes over volumes or surfaces of interest and converting these fluxes to dose rates.

A three-dimensional model is developed that captures all of the relevant design parameters of the 380-B package and contents, see the model description in Section 5.3.1, *Configuration of Source and Shielding*. Separate models are developed for NCT and HAC configurations.

Models are developed for each of the source types: Co-60, Cs-137, Sr-90, Ir-192, Ra-226 (gamma), Ra-226 with a chlorine target (neutron), and Ra-226 with a beryllium target (neutron). The source terms are defined in Section 5.2, *Source Specification*, for a 1 Ci source strength. Dose rates are computed for a 1 Ci source and are scaled by the source strength that results in dose rates 95% of the regulatory dose-rate limits, as discussed in Section 5.1.2, *Summary of Maximum Radiation Levels*.

Because the source is modeled as a point source (or over a small volume for Co-60), dose rates vary significantly due to the location of the source. The source will maximize the dose rates when located at the inner wall of the cask because this location minimizes the distance to the side of the package. Also, the corners feature reduced lead thickness, axial gaps due to lead shinkage, and a radial lid clearance gap, which greatly increases the gamma dose rate. Three general locations are investigated for the point source:

1. Bottom of the package at the cask inner diameter (bottom corner).
2. Mid-height of the package cavity at the cask inner diameter.
3. Top of the package at the cask inner diameter. The NCT models include the inner cover near the lid, and the source is constrained by this feature. In the HAC models the inner cover is not modeled, and the source is located at the bottom of the lid next to the cask inner diameter (top corner).

To accelerate model convergence in the gamma models, the importances of the cells are increased radially from the point source. When the gamma point source is near the corners of the lid or bottom, the splitting is performed by filling the cells with "splitting universes" that are simply concentric spheres with increasing importances. This method results in high importance cells in contact with the cask cavity, which will cause poor convergence if a source particle immediately enters a cell of high importance. To circumvent this problem, the cask cavity is filled with lead so that gammas that enter the cavity are attenuated, as shown in Figure . Filling the internal cavity with lead has a negligible effect on the calculated dose rates because the dose points of interest are in the opposite direction of the internal cavity lead. The cavity is not filled with lead in the gamma models when the source is at the cavity mid-height because concentric cylinders are used for splitting in these models rather than spheres. Likewise, the cavity is not filled with lead in the neutron models because the importances are low and filling the cavity with lead would not aid convergence.

Dose rates are primarily calculated using radial mesh tallies. Because the source is always located at the inner diameter of the cavity, the mesh tallies are focused on a segment 10° wide that is centered on the source. NCT mesh tallies are located at the inaccessible package side, package side at the impact limiter radius, at the top impact limiter flat surface, on the bottom impact limiter flat surface, and 2 m from the side of the trailer. The trailer is assumed to be a standard trailer; i.e., 8 ft, 6-in wide, or 102-in wide. Therefore, the dose rate on the side of the trailer is bounded by the dose rate on the side of the package, and the dose rates on the surfaces of the trailer are not explicitly computed.

Because a personnel barrier is used at the side of the package, the accessible package surface is defined as the surface of the impact limiters/personnel barrier, and dose rates are reported at the surface of the personnel barrier (although the personnel barrier itself is not modeled). The inaccessible package surface is defined as the package surface beneath the personnel barrier.

The mesh tally results are processed using Excel spreadsheets. The spreadsheets are constructed to select the maximum dose rate for each tally. The maximum dose rates for 1 Ci are then multiplied by the maximum desired source strength to determine the final dose rate.

The conical surfaces of the impact limiters form a portion of the outer boundary of the package and dose rates on the conical surfaces cannot be computed with mesh tallies. These dose rates are computed with standard surface tallies.

The dose rates for Co-60, Cs-137, Sr-90 and Ir-192 are solely due to gamma radiation. However, Ra-226 has both a gamma and neutron component, and each is explicitly computed. Because the 380-B does not have a hydrogenous neutron shield, secondary gamma radiation due to neutron capture is not computed because it is negligible (i.e., within the uncertainties of the Monte Carlo method).

HAC calculations are performed only for the two dose-rate-limited sources, Co-60 and Ra-226 (with beryllium). In the HAC calculations, mesh tallies are used to compute the dose rates 1 m from the cask body. The source is modeled in the bottom corner, side, and top corner.

5.4.2   Input and Output Data

Sample ORIGEN-S and MCNP input files are provided in Appendix 5.5.2, *Sample Input Files*.

The Monte Carlo uncertainty associated with the limiting dose rate location is less than 5% for Co-60 and Ra-226. Because the 380-B is designed to shield a strong Co-60 source, it is overdesigned for the lower-energy Cs-137, Sr-90, and Ir-192 sources. Therefore, proper model convergence for these isotopes is more difficult because the dose rates are very low. The Monte Carlo uncertainty associated with the limiting dose rates for Cs-137 and Sr-90 is ~10%, and for Ir-192 the uncertainty is as high as ~40%. However, the computed dose rates for Cs-137, Sr-90, and Ir-192 are essentially zero because these isotopes are limited by heat load, and further refinement of the method is not needed.

5.4.3   Flux-to-Dose Rate Conversion

ANSI/ANS-6.1.1-1977 flux-to-dose rate conversion factors are used in this analysis. These are obtained from the MCNP User's Manual [2], Tables H.1 and H.2, although these values have been converted to provide results in mrem/hr rather than rem/hr. These conversion factors are provided in Table .

5.4.4 External Radiation Levels

5.4.4.1 NCT Analysis

The package is transported vertically in an open trailer. Only one package may be transported per shipment and it is assumed to be centered on the trailer. Therefore, the applicable NCT dose rate limits for exclusive use transportation as defined by 10 CFR 71.47 are 1,000 mrem/hr on the inaccessible package surfaces beneath the personnel barrier, 200 mrem/hr on the accessible surfaces of the package, 200 mrem/hr on the surface of the trailer, and 10 mrem/hr at a distance of 2 m from the surface of the trailer.

The dose rate is also limited to 2 mrem/hr in any occupied location, although this dose rate limit does not apply to private carriers if exposed personnel wear radiation dosimetry devices. The dose rate in an occupied location is not computed explicitly in MCNP because it may be demonstrated with a hand calculation that this dose rate limit is met.

The occupied location (i.e., the driver of the vehicle) is estimated to be at least 25 feet from the centerline of the cask. $X_1 = 0$ cm is the cask centerline, $X_2 = 48.16$ cm is the location of the source at the inner diameter of the cask, $X_3 = 329.54$ cm is 2 m from the vehicle side, and $X_4 = 762$ cm is the occupied location. Therefore, the distance from the source to the 2 m dose rate location is $R_1 = X_3 - X_2 = 281.38$ cm, and the distance from the source to the occupied location is $R_2 = X_4 - X_2 = 713.84$ cm.

It is demonstrated with MCNP calculations that the dose rate 2 m from the side of the vehicle is <10 mrem/hr. All of the sources are sealed sources that behave essentially as point sources, and for point sources the dose rate reduces by the square of the distance from the source. Because no additional shielding credit is taken for items outside the package, the dose rate at the occupied location cannot exceed $10*(281.38/713.84)^2 = 1.6$ mrem/hr. Therefore, the occupied location dose rate limit is met if the 10 mrem/hr at 2 m dose rate limit is met.

Co-60 Analysis

The analysis is performed first for Co-60, as Co-60 is the limiting gamma emitter due to the high energy gammas emitted and the large activity to be transported. Observations may be made based on the Co-60 analysis to reduce the number of runs required for the remaining isotopes.

Two cases are developed for the source in the top corner. Two cases are needed because the inner cover prevents the source from simply locating in the corner immediately adjacent to the lid. The two source locations are illustrated in Figure . When the source is in the "top right" position, there is a streaming path through the lid/body interface gap, but radially the gamma must traverse lead to exit the package. In the "top left" position there is no lid gap streaming but there is a path through the joint that does not include lead.

The "side" location is also illustrated in Figure . When the source is in the side location it is near the mid-height of the package cavity.

Five bottom locations for the source are investigated, as shown in Figure . Because of potential streaming through the lead shrinkage gap, source locations slightly higher than the corner could be bounding. Location 1 is the bottom corner, and successive sources are located in +Z in 1 cm increments.

The mesh tally outputs are pasted into Excel for processing. The mesh tally results are organized by the spreadsheet, and the maximum for each tally location is listed. The 1 Ci dose rates are then scaled until 95% of the limiting dose rate limit is met (i.e., 950 mrem/hr on the inaccessible package surface beneath the personnel barrier, 190 mrem/hr on the accessible package surface, and 9.5 mrem/hr 2 m from the vehicle surface). For Co-60, the inaccessible package surface dose rate is limiting, and the results are scaled by 7,702 Ci.

Note that the mesh tallies cannot form to the contour of the conical impact limiter surfaces, and these conical surfaces also form the outer boundary of the package. Therefore, these dose rates are determined using F2 surface tallies. For both the top and bottom impact limiters, the dose rate is tallied in 5 equal segments on the conical surface (see Figure for the bottom impact limiter; the top impact limiter is similar). The $\pm Y$ segmenting surfaces are located at ± 5 cm. Although the impact limiter surface is curved, the tally area of each segment is estimated as 134.08 cm^2 by approximating the area as a flat rectangle with a width of 10 cm. This approximation is reasonable because the tally is relatively narrow. This approximation will slightly overestimate the dose rate result because the flux is divided by the input segment area, which is slightly lower than the actual area due to this curvature.

The maximum mesh tally results for the 8 source locations are summarized in Table . Dose rates are listed as "NA" if the detector is too far from the source for the dose rate estimate to be statistically meaningful (i.e., it is not necessary to report dose rates on the top of the upper impact limiter if the source is at the bottom of the cask). The limiting dose rate location occurs at the inaccessible cask surface beneath the personnel barrier, with a dose rate of 950 mrem/hr. The maximum dose rate on the accessible package surface is 138.5 mrem/hr and occurs with the source at location "Bottom 1" due to reduced lead thickness at this location, as shown in Figure .

The conical surface tally results are provided in Table . All conical surface dose rates are bounded by the 138.5 mrem/hr dose rate on the accessible package surfaces computed using mesh tallies. Note that for the "Bottom 1" position, the bottom impact limiter tally result using the mesh tally is 121.9 mrem/hr ($R_{mid} = 59.69$ cm), while the dose rate at the position "Conical 1" is 121.4 mrem/hr ($R_{mid} = 73.17$ cm). These tallies are at different physical locations but are in close proximity (approximately 10 cm apart), and the agreement is reasonable. All accessible package surface dose rates are below the limit of 200 mrem/hr. Because the conical tally results are bounded by the mesh tally results, only mesh tally results are reported for the remaining source isotopes.

The maximum dose rate 2 m from the side of the vehicle is 6.8 mrem/hr and occurs with the source in the "Bottom 1" position due to reduced lead thickness at that location. The path to the maximum 2 m dose rate follows a similar path as shown on Figure . This dose rate is higher than the dose rate when the source is at the mid-height of the package cavity because the lead is thinner at the joints. The 2 m dose rates are below the limit of 10 mrem/hr.

Comparing the dose rates for the "Bottom 1" through "Bottom 5" positions, the "Bottom 1" is limiting. Therefore, subsequent bottom models for other isotopes are developed only for this location.

The impact limiters feature a large recess on each end that is seal welded with thin sheet metal to both serve as a rain cover and prevent access to a potentially elevated dose rate region (these sheet metal covers are not modeled in MCNP). Although these regions are permanently inaccessible, additional runs are developed using point detector tallies to determine the

maximum dose rate locations in these regions. When the source is located in the upper right location near the lid gap, the maximum dose rate within this region is 279 mrem/hr. Likewise, when the source is in the bottom corner, the maximum dose rate within this region is 259 mrem/hr. If a dose rate limit of 1,000 mrem/hr is conservatively applied, the dose rates do not exceed the limit.

Cs-137 Analysis

A limited analysis is performed for Cs-137 because the 380-B packaging is overdesigned for this isotope in regards to shielding, which has much weaker energies compared to Co-60. Therefore, this isotope is limited by decay heat rather than dose rate. From Table , the activity limit is 40,675 Ci.

Cases are run for the "top right", "side", and "bottom 1" locations. The dose rates reported in Table indicate that dose rates are far below the limits.

Sr-90 Analysis

A limited analysis is performed for Sr-90 because the 380-B packaging is overdesigned for this isotope in regards to shielding, which has much weaker energies compared to Co-60. Therefore, this isotope is limited by decay heat rather than dose rate. From Table , the activity limit is 30,606 Ci.

Cases are run for the "top right", "side", and "bottom 1" locations. The dose rates reported in Table indicate that dose rates are far below the limits.

Ir-192 Analysis

A limited analysis is performed for Ir-192 because the 380-B packaging is overdesigned for this isotope in regards to shielding, which has much weaker energies compared to Co-60. Therefore, this isotope is limited by decay heat rather than dose rate. From Table , the activity limit is 33,333 Ci.

Cases are run for the "top right", "side", and "bottom 1" locations. The dose rates reported in Table indicate that dose rates are far below the limits.

Ra-226 (no beryllium, chlorine target) Analysis

Ra-226 is the only nuclide listed in Table that generates both neutrons (via (α,n) reactions) and gammas. The quantity of neutrons generated is related to the target material with which Ra-226 is mixed. If beryllium is excluded from the list of allowable target material, $RaCl_2$ is the bounding compound. Separate neutron and gamma input files are generated and the results are summed.

Input files are generated for the "top right", "top left", "side", and "bottom 1" locations. Although Ra-226 is a strong gamma emitter, the isotope is limited by heat load rather than dose rate when beryllium is excluded. From Table , the activity limit is 1,101 Ci.

Dose rates are reported in Table . Dose rates are not negligible, although the Ra-226 dose rates are bounded by the Co-60 dose rates. However, the system is behaving differently due to the neutron source. Because steel and lead are poor neutron shields, the neutron dose rate is at a maximum in a direct line with the source. For $RaCl_2$, the neutron and gamma dose rates are roughly equal. Therefore, the peak total dose rate occurs when the source is at the side location, and the dose rate peaks in a direct line with the source.

Ra-226 (with beryllium) Analysis

Ra-226 is the only nuclide listed in Table that generates both neutrons (via (α,n) reactions) and gammas. If beryllium is the target material a large neutron source is generated. Separate neutron and gamma input files are generated and the results are summed.

Input files are generated for the "top right", "top left", "side", and "bottom 1" locations. The dose rate is dominated almost completely by neutron radiation; the primary gamma component is negligible (<1% of the total dose rate).

Dose rates are computed for a 1 Ci source and are scaled until 95% of a regulatory dose rate limit is met. For this source, the inaccessible cask surface dose rate is limiting (950 mrem/hr). Dose rates are reported in Table for 4.67 Ci Ra-226 mixed with beryllium. The accessible maximum surface dose rate is 122.1 mrem/hr, and the maximum dose rate 2 m from the side of the vehicle is 7.9 mrem/hr. Because the dose rate is almost entirely due to neutron radiation, the dose rates peak next to the source location.

As with the Co-60 source, the dose rates inside the inaccessible recesses within the top and bottom impact limiters are computed. The maximum dose rates in the top and bottom impact limiter recesses are 70.2 mrem/hr and 86.9 mrem/hr, respectively. The dose rate at the centerline is also investigated in addition to the corners, although the corners are limiting. If a dose rate limit of 1,000 mrem/hr is conservatively applied, the dose rates do not exceed the limit.

Single Source Activity Limits

Based on the analysis above, if the 380-B packaging is limited to a single source type, the activity limits are summarized in Table . Note that Co-60 and Ra (with Be) are limited by dose rate, while the remaining isotopes are limited by heat load.

Multiple Source Activity Limits

While each analysis is performed using only a single source isotope type, there may be scenarios in which different source isotopes are mixed in the same package (e.g., 5,000 Ci Co-60 and 10,000 Ci Cs-137). Such mixing is acceptable as long as both dose rate and decay heat limits are met.

When mixing source isotopes, the total decay heat of the mixture may be determined using the "watt per Ci" decay heat values summarized in Table . The total heat load is summed to ensure the total does not exceed 205 watts. For dose rates, a total dose rate may be computed using a "sum of fractions" rule:

$$\sum_{i=1}^{n} \frac{S_i}{A_i} \leq 1$$

where:

S_i is the activity of each source in Ci

A_i is an activity limit that results in achieving 95% of the dose rate limit

A_i values for each source isotope must be determined. For Co-60 and Ra-226 (with beryllium), these values are simply 7,702 Ci and 4.67 Ci, respectively, as these isotopes are dose rate limited. For isotopes that are heat rate limited, A_i values must be determined.

The limiting dose rates on the inaccessible package surface, accessible package surface, and 2 m from the vehicle side surface are summarized in Table . For the isotopes limited by heat load,

there is margin to the dose rate limit. The activity of each isotope is scaled up until the inaccessible package surface dose rate is 950 mrem/hr (activity #1), the accessible package surface dose rate is 190 mrem/hr (activity #2), and the 2 m vehicle dose rate is 9.5 mrem/hr (activity #3). The minimum of these three activities is the A_i value. For Cs-137, Sr-90, and Ir-192, the activities are so high to reach the dose rate limits (~10^6 Ci) that the A_i values are conservatively scaled down an order of magnitude and set equal to 3.0E+05 Ci to account for the higher uncertainties of the MCNP calculations for these isotopes.

5.4.4.2 HAC Analysis

Very little damage to the steel and lead shielding occurs as a result of HAC of transport. For HAC, all impact limiter foam is modeled as a void to simulate potential fire damage (see Figure). The inner cover is assumed to be damaged and is omitted from the model. This assumption allows the source to move to the top corner of the lid where lid streaming is the most severe (see Figure).

HAC models are developed only for the two isotopes that are dose rate limited, Co-60 and Ra-226 (with beryllium), at their maximum activities of 7,702 Ci and 4.67 Ci, respectively. Because the NCT dose rate analysis for Ra-226 (with beryllium) showed the dose rate to be 99% due to neutron radiation, only Ra-226 neutron models are developed for the HAC analysis. Dose rates are computed with mesh tallies 1 m from the surface of the cask body. The source is modeled in 3 positions, "top corner", "side", and "bottom corner." HAC dose rate results are provided in Table . The maximum dose rate is 215.1 mrem/hr and occurs 1 m from the top of the package when the Co-60 source is in the top corner. This dose rate is due to both streaming through the lid gap and the reduced lead thickness at this location. The dose rate regulatory limit of 1,000 mrem/hr is not exceeded.

Note that Co-60 dose rates bound the Ra-226 (with beryllium) dose rates by a large margin at the top and bottom. The reason is that gamma shielding is reduced at these locations in the axial direction, both due to reduced lead thickness and the lid to cask gap. The Ra-226 (with beryllium) source is predominantly a neutron source and hence is much less affected by a steel/lead interface or lid gaps.

5.4.5 Loading Methodology

The following is a concise summary of how to apply the results of this shielding evaulation when loading a 380-B. A final summary table of key information is provided in Table . This information is included in Chapter 7, *Package Operations*.

1. **Radionuclide Limits.** Verify that the total activity of each isotope to be transported does not exceed the activity limits given in Table .

2. **Decay Heat Limit.** Verify that the total heat load is less than or equal to 205 watts. If only a single isotope is to be shipped, this is ensured by step 1 above. If multiple isotopes are to be transported, the total watts shall be calculated by multiplying the activity of each isotope by the heat generation rate found in Table .

3. **Dose Rate Limits for Multiple Source Isotopes.** If more than one isotope is loaded, verify the selected loading does not violate the dose rate limits using the following equation:

$$\sum_{i=1}^{n} \frac{S_i}{A_i} \leq 1$$

where:

S_i is the activity of each source in Ci
A_i is the appropriate value from Table .

Examples for multiple source isotopes are provided below.

Example #1: Is 5,000 Ci Co-60 and 15,000 Ci Cs-137 acceptable for transport?

1. Based on Table , the activity limits are not exceeded.

2. Based on Table , the decay heat is (5000)(1.542E-02)+(15000)(5.04E-03) = 152.7 watts $\leq$ 205 watts.

3. Based on Table , the dose rate sum of fractions is 5000/7702+15000/3.0E+05 = 0.7 $\leq$ 1.0.

Therefore, payload #1 is acceptable for transport.

Example #2: Is 5,000 Ci Co-60 and 30,000 Ci Cs-137 acceptable for transport?

1. Based on Table , the activity limits are not exceeded.

2. Based on Table , the decay heat is (5000)(1.542E-02)+(30000)(5.04E-03) = 228.3 watts > 205 watts.

Therefore, payload #2 is not acceptable for transport because the heat load exceeds 205 watts.

Example #3: Is 5,000 Ci Co-60 and 4.0 Ci Ra-226 (with beryllium) acceptable for transport?

1. Based on Table , the activity limits are not exceeded.

2. Based on Table , the decay heat is (5000)(1.542E-02)+(4)(1.862E-01) = 77.8 watts $\leq$ 205 watts.

3. Based on Table , the dose rate sum of fractions is 5000/7702+4/4.67 = 1.5 > 1.0.

Therefore, payload #3 is not acceptable for transport because the dose rate limits could be exceeded.

Table 5.4-1 – Flux-to-Dose Rate Conversion Factors

E (MeV)	Neutron Factors (mrem/hr)/(n/cm^2/s)	E (MeV)	Neutron Factors (mrem/hr)/(n/cm^2/s)
2.50E-08	3.67E-03	0.5	9.26E-02
1.00E-07	3.67E-03	1.0	1.32E-01
1.00E-06	4.46E-03	2.5	1.25E-01
1.00E-05	4.54E-03	5.0	1.56E-01
1.00E-04	4.18E-03	7.0	1.47E-01
0.001	3.76E-03	10.0	1.47E-01
0.01	3.56E-03	14.0	2.08E-01
0.1	2.17E-02	20.0	2.27E-01

E (MeV)	Gamma Factors (mrem/hr)/(γ/cm^2/s)	E (MeV)	Gamma Factors (mrem/hr)/(γ/cm^2/s)
0.01	3.96E-03	1.4	2.51E-03
0.03	5.82E-04	1.8	2.99E-03
0.05	2.90E-04	2.2	3.42E-03
0.07	2.58E-04	2.6	3.82E-03
0.1	2.83E-04	2.8	4.01E-03
0.15	3.79E-04	3.25	4.41E-03
0.2	5.01E-04	3.75	4.83E-03
0.25	6.31E-04	4.25	5.23E-03
0.3	7.59E-04	4.75	5.60E-03
0.35	8.78E-04	5.0	5.80E-03
0.4	9.85E-04	5.25	6.01E-03
0.45	1.08E-03	5.75	6.37E-03
0.5	1.17E-03	6.25	6.74E-03
0.55	1.27E-03	6.75	7.11E-03
0.6	1.36E-03	7.5	7.66E-03
0.65	1.44E-03	9.0	8.77E-03
0.7	1.52E-03	11.0	1.03E-02
0.8	1.68E-03	13.0	1.18E-02
1.0	1.98E-03	15.0	1.33E-02

Table 5.4-2 – NCT Dose Rate Results (mrem/hr), 7,702 Ci Co-60

Mesh Tally Results						
	Source Location					
Tally Location	**Top L**	**Top R**	**Bot1**	**Side**	**Max**	**Limit**
Package side (inaccessible)	NA	NA	NA	**950**	950	1,000
Side at Impact Limiter Radius	49.4	131.4	**138.5**	86.1	138.5	200
Top Impact Limiter (flat)	52.4	**66.2**	NA	NA	66.2	200
Bottom Impact Limiter (flat)	NA	NA	**121.9**	NA	121.9	200
2 m from Vehicle Side	2.5	6.1	**6.8**	4.9	6.8	10
	Source Location					
Tally Location	**Bot1**	**Bot2**	**Bot3**	**Bot4**	**Bot5**	**Limit**
Package side (inaccessible)	NA	NA	NA	NA	NA	1,000
Side at Impact Limiter Radius	138.5	109.7	65.7	54.0	48.2	200
Top Impact Limiter (flat)	NA	NA	NA	NA	NA	200
Bottom Impact Limiter (flat)	121.9	114.9	94.3	79.0	67.4	200
2 m from Vehicle Side	6.8	5.1	3.2	2.8	2.7	10
Conical Tally Results						
	Source Location					
Tally Location	**Top L**	**Top R**	**Bot1**	**Side**	**Max**	**Limit**
Conical 1	49.9	51.1	121.4	NA	121.4	200
Conical 2	44.3	43.5	120.7	NA	120.7	200
Conical 3	30.8	27.7	98.7	NA	98.7	200
Conical 4	21.6	24.1	61.3	NA	61.3	200
Conical 5	27.8	38.7	70.3	NA	70.3	200
	Source Location					
Tally Location	**Bot1**	**Bot2**	**Bot3**	**Bot4**	**Bot5**	**Limit**
Conical 1	121.4	115.9	88.2	68.3	52.3	200
Conical 2	120.7	108.6	81.9	62.8	48.0	200
Conical 3	98.7	80.4	55.2	42.9	29.3	200
Conical 4	61.3	50.0	34.9	24.9	19.0	200
Conical 5	70.3	53.0	40.8	28.3	19.1	200

Table 5.4-3 – NCT Dose Rate Results (mrem/hr), 40,675 Ci Cs-137

Tally Location	Source Location					
	Top L	Top R	Bot1	Side	Max	Limit
Package side (inaccessible)	NA	NA	NA	**0.1**	0.1	1,000
Side at Impact Limiter Radius	NA	0.1	**2.5**	0.01	2.5	200
Top Impact Limiter (flat)	NA	**0.4**	NA	NA	0.4	200
Bottom Impact Limiter (flat)	NA	NA	**0.8**	NA	0.8	200
2 m from Vehicle Side	NA	0.01	**0.09**	0.001	0.09	10

Table 5.4-4 – NCT Dose Rate Results (mrem/hr), 30,606 Ci Sr-90

Tally Location	Source Location					
	Top L	Top R	Bot1	Side	Max	Limit
Package side (inaccessible)	NA	NA	NA	**8.2**	8.2	1,000
Side at Impact Limiter Radius	NA	1.1	**1.3**	0.8	1.3	200
Top Impact Limiter (flat)	NA	**0.9**	NA	NA	0.9	200
Bottom Impact Limiter (flat)	NA	NA	**1.1**	NA	1.1	200
2 m from Vehicle Side	NA	0.06	**0.06**	0.04	0.06	10

Table 5.4-5 – NCT Dose Rate Results (mrem/hr), 33,333 Ci Ir-192

Tally Location	Source Location					
	Top L	Top R	Bot1	Side	Max	Limit
Package side (inaccessible)	NA	NA	NA	**0.7**	0.7	1,000
Side at Impact Limiter Radius	NA	0.2	**0.9**	0.1	0.9	200
Top Impact Limiter (flat)	NA	**0.3**	NA	NA	0.3	200
Bottom Impact Limiter (flat)	NA	NA	**0.3**	NA	0.3	200
2 m from Vehicle Side	NA	0.01	**0.06**	0.01	0.06	10

Table 5.4-6 – NCT Dose Rate Results (mrem/hr), 1,101 Ci Ra-226 (with Cl)

Tally Location	Source Location					
	Top L	Top R	Bot1	Side	Max	Limit
Package side (inaccessible)	NA	NA	NA	**840.9**	840.9	1,000
Side at Impact Limiter Radius	32.8	77.8	80.0	**92.2**	92.2	200
Top Impact Limiter (flat)	36.8	**52.7**	NA	NA	52.7	200
Bottom Impact Limiter (flat)	NA	NA	**67.0**	NA	67.0	200
2 m from Vehicle Side	2.3	4.4	4.4	**5.7**	5.7	10

Table 5.4-7 – NCT Dose Rate Results (mrem/hr), 4.67 Ci Ra-226 (with Be)

Tally Location	Source Location					
	Top L	Top R	Bot1	Side	Max	Limit
Package side (inaccessible)	NA	NA	NA	**950**	950	1,000
Side at Impact Limiter Radius	48.8	74.0	65.3	**122.1**	122.1	200
Top Impact Limiter (flat)	**28.6**	20.3	NA	NA	28.6	200
Bottom Impact Limiter (flat)	NA	NA	**35.0**	NA	35.0	200
2 m from Vehicle Side	3.3	4.4	3.9	**7.9**	7.9	10

Table 5.4-8 – Activity Limits, Single Source Isotope

Nuclide	Maximum Activity (Ci)	Limited by
Co-60	7,702	Package Side (Inaccessible) Dose Rate (950 mrem/hr)
Cs-137	40,675	Heat Load
Sr-90	30,606	Heat Load
Ir-192	33,333	Heat Load
Ra-226 (no Be, Cl target)	1,101	Heat Load
Ra-226 (with Be)	4.67	Package Side (Inaccessible) Dose Rate (950 mrem/hr)

Table 5.4-9 – A$_i$ Values (Ci) for Multiple Source Isotopes

	A	B	C	D	E = 950*A/B	F = 190*A/C	G = 9.5*A/D	H = MIN (E,F,G)
Isotope	Activity (Ci)	Inaccessible Surface Dose Rate (mrem/hr)	Accessible Surface Dose Rate (mrem/hr)	2m Dose Rate (mrem/hr)	Activity for 950 mrem/hr Inaccessible Surface Dose Rate (Ci)	Activity for 190 mrem/hr Accessible Surface Dose Rate (Ci)	Activity for 9.5 mrem/hr 2m Dose Rate (Ci)	A$_i$ (Ci)
Co-60	7,702	950	138.5	6.8	7,702	10,569	10,706	7,702
Cs-137	40,675	0.1	2.5	0.09	5.97E+08	3.04E+06	4.10E+06	3.00E+05①
Sr-90	30,606	8.2	1.3	0.06	3.55E+06	4.52E+06	4.75E+06	3.00E+05①
Ir-192	33,333	0.7	0.9	0.06	4.40E+07	7.18E+06	4.92E+06	3.00E+05①
Ra-226 (with Cl)	1,101	840.9	92.2	5.7	1,244	2,269	1,832	1,244
Ra-226 (with Be)	4.67	950	122.1	7.9	4.67	7.26	5.61	4.67

①Set to 3.00E+05 Ci, which bounds MIN (E,F,G) by a large margin

Table 5.4-10 – Bounding HAC Dose Rate Results (mrem/hr)

Tally Location	7,702 Ci Co-60			
	Source Location			
	Top	**Bottom**	**Side**	**Max**
1m from Cask Side	**158.6**	67.1	26.5	158.6
1m from Cask Top	**215.1**	NA	NA	215.1
1m from Cask Bottom	NA	**84.2**	NA	84.2
Tally Location	4.67 Ci Ra-226 (with beryllium)			
	Source Location			
	Top	**Bottom**	**Side**	**Max**
1m from Cask Side	36.6	39.9	**41.4**	41.4
1m from Cask Top	**30.7**	NA	NA	30.7
1m from Cask Bottom	NA	**32.9**	NA	32.9

Table 5.4-11 – Final Summary Table

Nuclide	Activity Limit (Ci)	A_i (Ci)	Decay Heat (watt/Ci)[1]
Co-60	7,702	7,702	1.542E-02
Cs-137	40,675	3×10^5	5.040E-03
Sr-90	30,606	3×10^5	6.698E-03
Ir-192	33,333	3×10^5	6.150E-03
Ra-226 (no Be, Cl target)[2]	1,101	1,244	1.862E-01
Ra-226 (with Be)	4.67	4.67	1.862E-01

[1] Includes all decay products.
[2] Excludes beryllium. Impurities may include oxygen, carbon, sulfur, bromine (hydrous), and chlorine (hydrous or anhydrous).

Figure 5.4-1 – MCNP Gamma Model Showing Cell Importances

NCT, Top right location

NCT, Top left location

HAC, Top location

NCT/HAC Side location
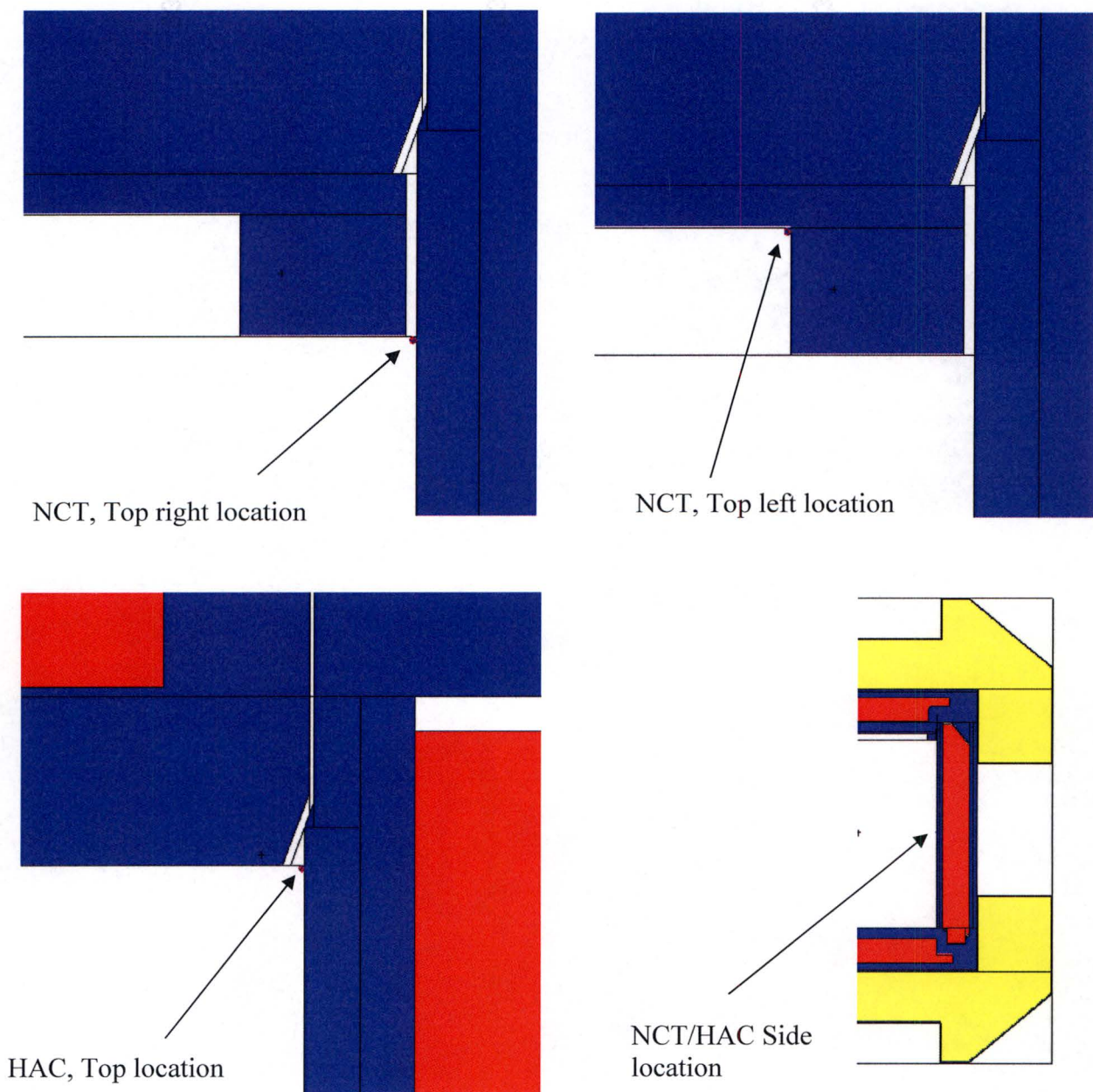
Point source models illustrated; Co-60 source is modeled as a small cylindrical volume at the same locations

Figure 5.4-2 – Top and Side Source Locations
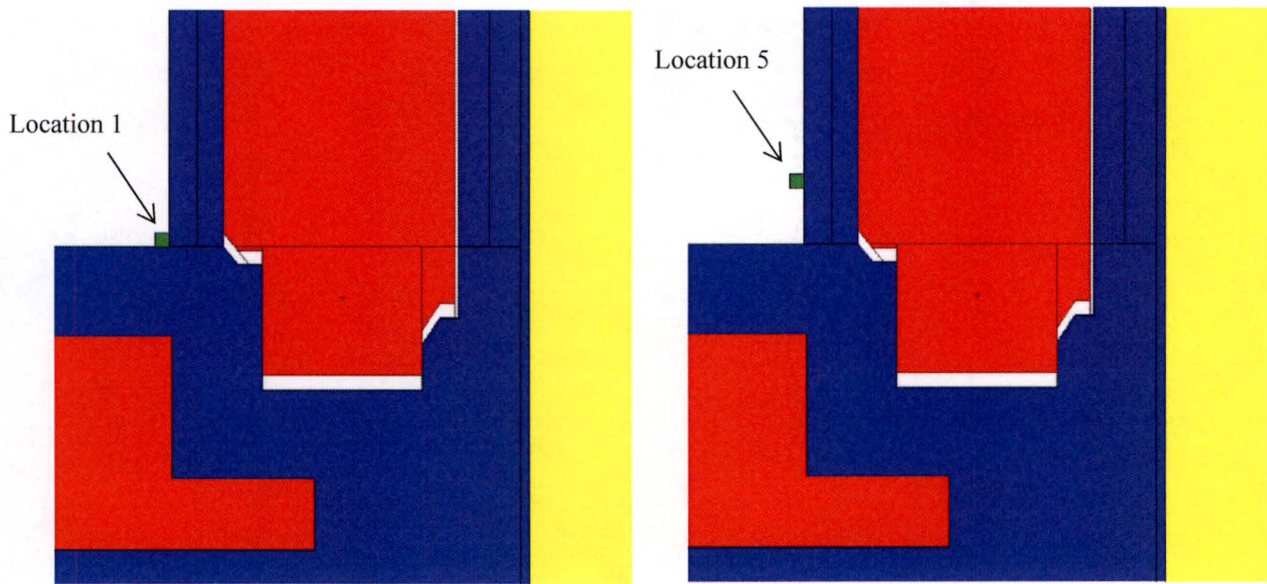
Bottom locations 1 and 5 shown for a Co-60 source (locations 2 through 4 not shown).
Locations 1 through 5 are each 1 cm apart axially

Figure 5.4-3 – Bottom Source Locations
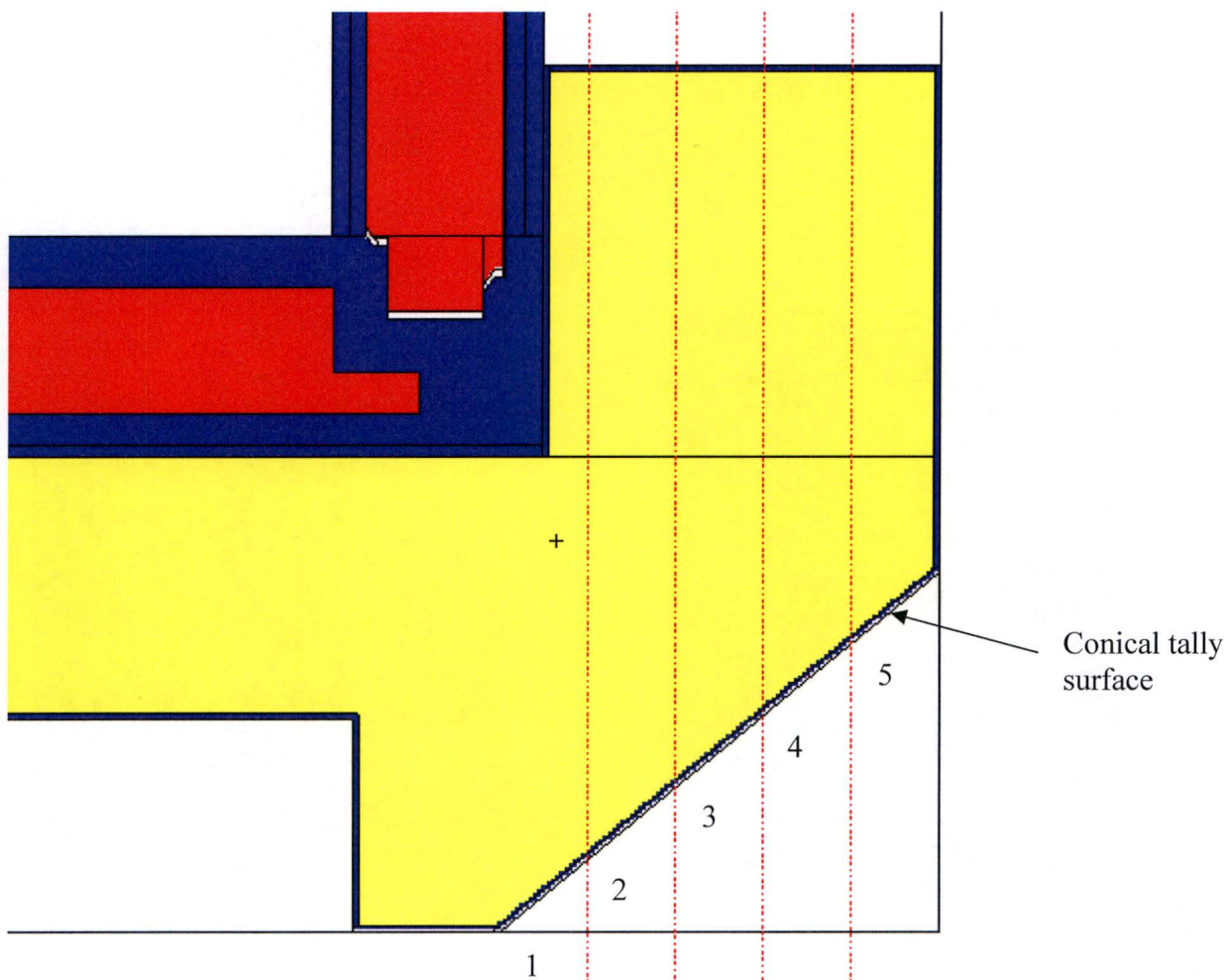
Figure 5.4-4 – Conical Tally Segments

The maximum surface dose rate occurs through the minimum lead shielding. The maximum Co-60 2 m dose rate follows a similar path.
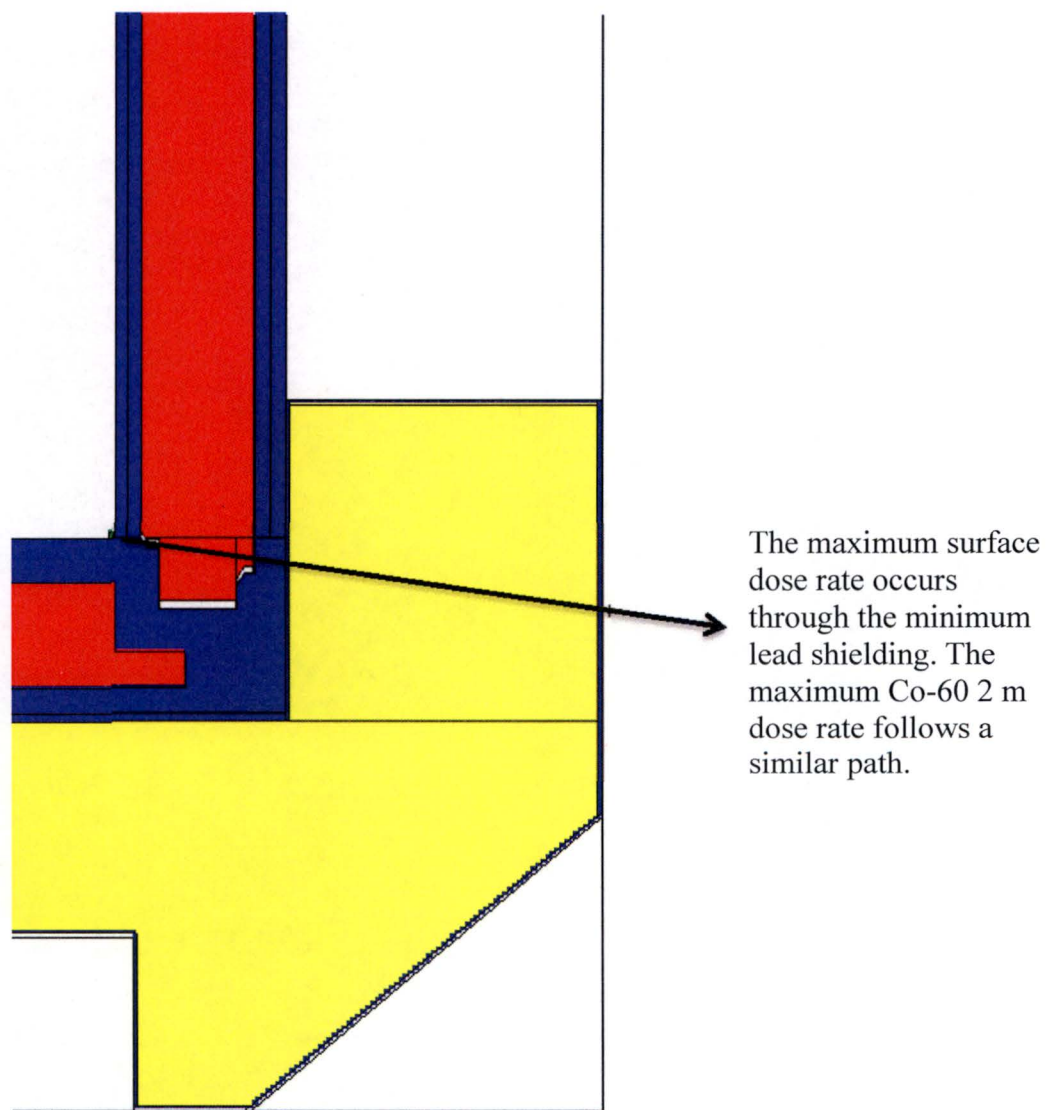
Figure 5.4-5 – Location of Maximum Surface Dose Rate, Co-60

5.5 Appendices

List of Appendices

5.5.1 References

1. Glenn F. Knoll, *Radiation Detection and Measurement*, Second Edition, John Wiley & Sons, 1989.

2. LA-UR-03-1987, *MCNP – A General Monte Carlo N-Particle Transport Code, Version 5*, Los Alamos National Laboratory, April 24, 2003 (Revised 2/1/2008).

3. ORNL/TM-2005/39, Version 6, Vols. I-III, *SCALE: A Modular Code System for Performing Standardized Computer Analyses for Licensing Evaluations*, January 2009.

4. SCALE4.4, *Modular Code System for Performing Standardized Computer Analyses for Licensing Evaluation for Workstations and Personal Computers*, Oak Ridge National Laboratory, September 1998.

5. NUREG-1609, *Standard Review Plan for Transportation Packages for Radioactive Material*.

6. *CH-TRU Payload Appendices*, Revision 3, December 2007.

7. ORNL/TM-2006/15, *Radiolytic Degradation of Urethane Foam Used for Encapsulation of Contaminated Components*, Oak Ridge National Laboratory, March 2006.

5.5.2 Sample Input Files

Sample ORIGEN-S input file for RaBe neutron source:

Note: This input file is developed for 20 Ci of Ra-226 (20.22 g in the input file). The output is divided by 20 to generate the source per Ci in Table .

```
'This SCALE input file was generated by
'OrigenArp Version  6.0.13.12 January 12, 2010
#origens
0$$ al1 71 e t
Decay Case
3$$ 21 1 1 27 a16 2 a33 0 e t
35$$ 0 t
54$$ a8 1 al1 2  e
56$$ a2 10 a10 0 a13 2 a14 5 a15 3 a17 2 e
57** 0 a3 0 e
95$$ 0 t
Case 1
0 MTU
60** 0.001 0.003 0.01 0.03 0.1 0.3 1 3 9 30
61** f0.05
65$$
'Gram-Atoms    Grams    Curies    Watts-All    Watts-Gamma
 21z
 3z    3z    1    0    0    3z    3z    6z
 21z
81$$ a7 200 e
84**
  2.0000000e+07 6.3763000e+06 3.0119000e+06 1.8268000e+06
  1.4227000e+06 9.0718000e+05 4.0762000e+05 1.1109000e+05 1.5034000e+04
  3.0354000e+03 5.8295000e+02 1.0130000e+02 2.9023000e+01 1.0677000e+01
  3.0590000e+00 1.8554000e+00 1.3000000e+00 1.1253000e+00 1.0000000e+00
  8.0000000e-01 4.1399000e-01 3.2500000e-01 2.2500000e-01 1.0000000e-01
  5.0000000e-02 3.0000000e-02 1.0000000e-02 1.0000000e-05 e
73$$ 882260 40000
74** 20.22 20000
75$$ 2 4
t
54$$ a8 1 al1 2  e
56$$ a2 10 a10 10 a14 5 a15 3 a17 2 e
57** 30 a3 0 e
95$$ 0 t
Case 2
0 MTU
60** 40 50 60 70 80 90 100 110 120 130
61** f0.05
65$$
'Gram-Atoms    Grams    Curies    Watts-All    Watts-Gamma
 21z
 3z    3z    1    0    0    3z    3z    6z .
 21z
81$$ a7 200 e
84**
  2.0000000e+07 6.3763000e+06 3.0119000e+06 1.8268000e+06
  1.4227000e+06 9.0718000e+05 4.0762000e+05 1.1109000e+05 1.5034000e+04
  3.0354000e+03 5.8295000e+02 1.0130000e+02 2.9023000e+01 1.0677000e+01
  3.0590000e+00 1.8554000e+00 1.3000000e+00 1.1253000e+00 1.0000000e+00
  8.0000000e-01 4.1399000e-01 3.2500000e-01 2.2500000e-01 1.0000000e-01
  5.0000000e-02 3.0000000e-02 1.0000000e-02 1.0000000e-05 e
t
56$$ f0 t
```

end

Sample MCNP input file for a Co-60 source in the bottom corner:

```
380-B
10    0           55 -47 -11        #100         imp:p=1 fill=3 $ cavity
100   4 -8.9    151 -152 -150                    imp:p=1
c
c    Cask Radial
c
11    2 -7.94   11 -200 55 -45                   imp:p=1 fill=1 $ inner ss
12    2 -7.94   200 -12 55 -59                   imp:p=1 fill=1 $ inner ss
13    1 -11.35  12 -202 55 -159 -130 165         imp:p=1 fill=2 $ side lead
14    0          202 -15 55 -30                  imp:p=1        $ 0.08" gap
15    2 -7.94   15 -201 55 -59                   imp:p=1 fill=1 $ outer ss
16    2 -7.94   201 -16 55 -59                   imp:p=1 fill=1 $ outer ss
c
c    Bottom end of cask
c
20    2 -7.94   50 -55 -16  #21 #22 #23
                #24 #25 #26 #27 #28 #29          imp:p=1 fill=1 $ bottom steel
21    1 -11.35  (52 -54 -53):(51 -52 -31)        imp:p=1 fill=2 $ bot lead
22    1 -11.35  -55 165 168 -67                  imp:p=1 fill=2 $ bot lead
23    1 -11.35  67 -69 194 -55                   imp:p=1 fill=2 $ bot lead
24    1 -11.35  (69 -202 -55 -195):
                (135 -202 195)                   imp:p=1 fill=2 $ bot lead
25    0          202 -15 35 -55                  imp:p=1        $ side lead 0.08" gap
26    0          65 -165 68 12                   imp:p=1        $ bot lead slump
27    0          68 -168 -67 165                 imp:p=1        $ bot lead slump
28    0          67 -69 94 -194                  imp:p=1        $ bot lead slump
29    0          (-95:35) 69 195 -135 -202       imp:p=1        $ bot lead slump
c
c    Lid and top end
c
30    2 -7.94   -16 59 -62 #31 #32               imp:p=1 fill=1 $ steel lid
31    1 -11.35  (-10 58 -60):(-13 60 -61):
                (10 -60 -39)                     imp:p=1 fill=2 $ lid lead
32    0          42 -43 59 -44                   imp:p=1        $ lid radial gap
33    2 -7.94   49 -59 -40 -42                   imp:p=1 fill=1 $ steel lid underside
34    2 -7.94   -15 -59 30                       imp:p=1 fill=1 $ steel body
35    0          159 -59 12 -130                 imp:p=1        $ top lead slump
36    0          130 -30 -202 -59                imp:p=1        $ top lead slump
c
40    0          49 -11 41                       imp:p=1        $ lid radial gap
41    2 -7.94   43 -200 45 -59                   imp:p=1 fill=1 $ lid by radial gap
42    2 -7.94   45 -43 41 11                     imp:p=1 fill=1 $ lid by radial gap
43    0          42 -43 -59 -41                  imp:p=1        $ lid radial gap
44    0          49 -42 -41 40                   imp:p=1        $ lid radial gap
c
51    0          64 -11 47 -49                   imp:p=1        $ inner cover cells
52    2 -7.94   48 -49 -64                       imp:p=1 fill=1 $ inner cover cells
53    2 -7.94   47 -48 63 -64                    imp:p=1 fill=1 $ inner cover cells
54    0          47 -48 -63                      imp:p=1 fill=3 $ inner cover cells
c
c    Top IL
c
60    2 -7.94   -16 62 -75                       imp:p=1     fill=1 $ Top IL steel
61    2 -7.94   16 -70 73 -75                    imp:p=1     fill=1 $ Top IL steel
62    2 -7.94   70 -71 73 -74                    imp:p=16000        $ Top IL steel
63    2 -7.94   71 -72 73 -78                    imp:p=16000        $ Top IL steel
64    2 -7.94   -77 -72 78 -79                   imp:p=16000        $ Top IL steel
65    2 -7.94   76 -77 -78 36                    imp:p=16000        $ Top IL steel
66    2 -7.94   (36:-138) 38 -136 -76            imp:p=16000        $ Top IL steel
```

```
67    3  -0.224    70 -71 74 -75            imp:p=16000          $ foam
68    3  -0.224    (-38:136) 75 -76 -71 -78 imp:p=16000          $ foam
69    0            138 -77 -36              imp:p=1              $ Top IL recess
70    0            -72 -77 79               imp:p=1              $ Top IL corner void
c
c       Bottom IL
c
80    2  -7.94     -16 82 -50               imp:p=1     fill=1   $ Bot IL Steel
81    2  -7.94     16 -70 82 -84            imp:p=1     fill=1   $ Bot IL Steel
82    2  -7.94     70 -71 83 -84            imp:p=8192           $ Bot IL Steel
83    2  -7.94     71 -72 -84 -85           imp:p=8192           $ Bot IL Steel
84    2  -7.94     -72 80 -86 85            imp:p=8192           $ Bot IL Steel
85    2  -7.94     80 -81 -85 36            imp:p=8192           $ Bot IL Steel
86    2  -7.94     (137:36) -37 -136 81     imp:p=8192           $ Bot IL Steel
87    3  -0.224    70 -71 82 -83            imp:p=8192           $ foam
88    3  -0.224    (136:37) 81 -82 -71 -85  imp:p=8192           $ foam
89    0            80 -137 -36              imp:p=1              $ Bot IL recess
90    0            80 -72 86                imp:p=1              $ Bot IL corner void
c
95    0            16 -72 84 -73            imp:p=1              $ axial void between IL
96    0            (77:72:-80) -90 -91 93   imp:p=1              $ outside package
c
999   0            91:90:-93                imp:p=0
c
c       Universe 1: Steel splitting
c
1000  2  -7.94     -1000          u=1 imp:p=1
1001  2  -7.94     1000 -1001 u=1 imp:p=2
1002  2  -7.94     1001 -1002 u=1 imp:p=4
1003  2  -7.94     1002 -1003 u=1 imp:p=8
1004  2  -7.94     1003 -1004 u=1 imp:p=16
1005  2  -7.94     1004 -1005 u=1 imp:p=32
1006  2  -7.94     1005 -1006 u=1 imp:p=64
1007  2  -7.94     1006 -1007 u=1 imp:p=128
1008  2  -7.94     1007 -1008 u=1 imp:p=256
1009  2  -7.94     1008 -1009 u=1 imp:p=512
1010  2  -7.94     1009 -1010 u=1 imp:p=1024
1011  2  -7.94     1010 -1011 u=1 imp:p=2048
1012  2  -7.94     1011 -1012 u=1 imp:p=4096
1013  2  -7.94     1012 -1013 u=1 imp:p=8192
1014  2  -7.94     1013 -1014 u=1 imp:p=1.6e4
1015  2  -7.94     1014 -1015 u=1 imp:p=3.2e4
1016  2  -7.94     1015          u=1 imp:p=6.6e4
c 1017 2 -7.94     1016 -1017 u=1 imp:p=1.3e5
c 1018 2 -7.94     1017 -1018 u=1 imp:p=2.6e5
c 1019 2 -7.94     1018 -1019 u=1 imp:p=5.2e5
c 1020 2 -7.94     1019 -1020 u=1 imp:p=1e6
c 1021 2 -7.94     1020          u=1 imp:p=1
c
c       Universe 2: Lead splitting
c
2000  1  -11.35    -1000          u=2 imp:p=1
2001  1  -11.35    1000 -1001 u=2 imp:p=2
2002  1  -11.35    1001 -1002 u=2 imp:p=4
2003  1  -11.35    1002 -1003 u=2 imp:p=8
2004  1  -11.35    1003 -1004 u=2 imp:p=16
2005  1  -11.35    1004 -1005 u=2 imp:p=32
2006  1  -11.35    1005 -1006 u=2 imp:p=64
2007  1  -11.35    1006 -1007 u=2 imp:p=128
2008  1  -11.35    1007 -1008 u=2 imp:p=256
2009  1  -11.35    1008 -1009 u=2 imp:p=512
2010  1  -11.35    1009 -1010 u=2 imp:p=1024
2011  1  -11.35    1010 -1011 u=2 imp:p=2048
```

```
2012 1 -11.35    1011 -1012  u=2 imp:p=4096
2013 1 -11.35    1012 -1013  u=2 imp:p=8192
2014 1 -11.35    1013 -1014  u=2 imp:p=1.6e4
2015 1 -11.35    1014 -1015  u=2 imp:p=3.2e4
2016 1 -11.35    1015        u=2 imp:p=6.6e4
c 2017 1 -11.35    1016 -1017  u=2 imp:p=1.3e5
c 2018 1 -11.35    1017 -1018  u=2 imp:p=2.6e5
c 2019 1 -11.35    1018 -1019  u=2 imp:p=5.2e5
c 2020 1 -11.35    1019 -1020  u=2 imp:p=1e6
c 2021 1 -11.35    1020        u=2 imp:p=1
c
c    Universe 3: Lead killer
c
3000 0          -1004       u=3 imp:p=1
3001 1 -11.35    1004        u=3 imp:p=1

10      cz 43.3451
11      cz 48.26
200     cz 50.2
12      cz 52.07
13      cz 55.88
15      cz 68.58
201     cz 70.8
202     cz 68.3768
16      cz 73.025
c
30      kz 226.4269  0.62414 -1
130 3   kz 226.4269  0.62414 -1
31      cz 58.42
35      pz 20.32
135 2   pz 20.32
36      cz 50.8
136     cz 51.435
37      pz -32.385
137     pz -33.02
38      pz 205.4225
138     pz 206.0575
39      kz 118.5799          1   1
40      kz 17.1416   0.13250  1
41      kz 16.4079   0.13250  1
42      cz 48.4251
43      cz 48.5775
44      pz 158.75
45      pz 148.9878
47      pz 142.5575
48      pz 146.3675
49      pz 147.6375
c
50      pz 0
51      pz 3.81
52      pz 8.89
53      cz 48.4200
54      pz 19.05
55      pz 25.4
58      pz 153.9875
59      pz 153.67
159 3   pz 153.67
60      pz 163.83
61      pz 169.2275
62      pz 173.0375
63      cz 42.8625
64      cz 47.9425
65      kz 90.8300 0.63330 -1
```

```
165 2  kz 90.8300 0.63330 -1
67     cz 54.7701
68     pz 24.13
168 2  pz 24.13
69     cz 66.0401
c
70     cz 73.66
71     cz 118.745                $ 3" crush
72     cz 119.38                 $ 3" crush
73     pz 127.3175
74     pz 127.9525
75     pz 174.3075
76     pz 230.8225               $ 2" crush top
77     pz 231.4575               $ 2" crush top
78     kz 287.7111 1.42029 -1 $ 3.6" crush
79     kz 288.5400 1.42029 -1 $ 3.6" crush
80     pz -58.42                 $ 2" crush
81     pz -57.785                $ 2" crush
82     pz -1.27
83     pz 45.085
84     pz 45.72
85     kz -114.6736 1.42029 1 $ 3.6" crush
86     kz -115.5025 1.42029 1 $ 3.6" crush
c
90     cz 500
91     pz 400
92     c/z 48.16 0 10
93     pz -250
94     pz 15.24
194 2  pz 15.24
95     kz -80.6452 0.44444 1
195 2  kz -80.6452 0.44444 1
c
150    c/z 47.76 0 0.49
151    pz  25.401
152    pz  26.381
c
1000 1 so 2.54
1001 1 so 5.08
1002 1 so 7.62
1003 1 so 10.16
1004 1 so 12.7
1005 1 so 15.24
1006 1 so 17.78
1007 1 so 20.32
1008 1 so 22.86
1009 1 so 25.4
1010 1 so 27.94
1011 1 so 30.48
1012 1 so 33.02
1013 1 so 35.56
1014 1 so 38.1
1015 1 so 40.64
c 1016 1 so 43.18
c 1017 1 so 45.72
c 1018 1 so 48.26
c 1019 1 so 50.8
c 1020 1 so 53.34
c
1050 py -5
1051 py  5
1052 px 68.03
1054 px 78.3
```

```
1056 px 88.57
1058 px 98.84
1060 px 109.11

mode p
m1      82000    1      $ Lead
m2      6000    -0.08   $ SS304
        14000   -1.0
        15000   -0.045
        24000   -19
        25000   -2
        26000   -68.375
        28000   -9.5
m3      6000    -0.6    $ foam
        8000    -0.24
        7000    -0.12
        1000    -0.04
m4      27000    1      $ Co
c
tr1     48.16  0  25.5
tr2     0       0   1.016 $ bottom lead slump shift, crashes for tr2 >= 1.27
tr3     0       0  -1.016 $ top lead slump shift
c
sdef    cell=100 pos=47.76 0 25.891 erg=d3 rad=d1 ext=d2 axs=0 0 1 wgt=7.4e10 $ 1 Ci Co-
60
si1     0.49
si2     0.49
#       si3     sp3
        L       d
        1.173 3.7e10
        1.332 3.7e10
c
c    Tallies
c
c       ansi/ans-6.1.1-1977 flux-to-dose, photons (mrem/hr)/(p/cm**2/s)
de0         0.01    0.03    0.05    0.07    0.10    0.15    0.20    0.25    0.30
            0.35    0.40    0.45    0.50    0.55    0.60    0.65    0.70    0.80
            1.00    1.40    1.80    2.20    2.60    2.80    3.25    3.75    4.25
            4.75    5.00    5.25    5.75    6.25    6.75    7.50    9.00    11.0
            13.0    15.0
df0         3.96-3 5.82-4 2.90-4 2.58-4 2.83-4 3.79-4 5.01-4 6.31-4 7.59-4
            8.78-4 9.85-4 1.08-3 1.17-3 1.27-3 1.36-3 1.44-3 1.52-3 1.68-3
            1.98-3 2.51-3 2.99-3 3.42-3 3.82-3 4.01-3 4.41-3 4.83-3 5.23-3
            5.60-3 5.80-3 6.01-3 6.37-3 6.74-3 7.11-3 7.66-3 8.77-3 1.03-2
            1.18-2 1.33-2
c
fc2         IL Top Check
f2:p        77
fs2         -92
sd2         314.16 1
c
fc12        IL Bot Check
f12:p       80
fs12        -92
sd12        314.16 1
c
fc22        IL Bot Conical (first 3 junk)
f22:p       86
fs22        -1050 1051 -1052 -1054 -1056 -1058 -1060
sd22        1 1 1 134.08 134.08 134.08 134.08 134.08
c
fc32        IL Top Conical (first 3 junk)
f32:p       79
```

```
fs32        -1050 1051 -1052 -1054 -1056 -1058 -1060
sd32        1 1 1 134.08 134.08 134.08 134.08 134.08
c
c     .     A cylindrical mesh tally is placed around the package.
c           The circumferential tally is 10 degrees wide, with the
c           vector origin 5 degrees below the x axis.
c
c           radius=i
c           axial=j
c           circumferential=k
c
c           IL Side and personnel barrier/bounds vehicle side
fmesh14:p   geom=cyl origin=0 0 -60 axs=0 0 1 vec=0.99619 -0.087156 0
            imesh=119.38 121.38
            iints=1 1
            jmesh=340
            jints=34
            kmesh=0.0277778 1
            kints=1 1
c
c           IL top
fmesh24:p   geom=cyl origin=0 0 231.46 axs=0 0 1 vec=0.99619 -0.087156 0
            imesh=119.38
            iints=13
            jmesh=2.0
            jints=1
            kmesh=0.0277778 1
            kints=1 1
c
c           IL bottom
fmesh34:p   geom=cyl origin=0 0 -60.42 axs=0 0 1 vec=0.99619 -0.087156 0
            imesh=119.38
            iints=13
            jmesh=2.0
            jints=1
            kmesh=0.0277778 1
            kints=1 1
c
c           2m from vehicle side
fmesh44:p   geom=cyl origin=0 0 -150 axs=0 0 1 vec=0.99619 -0.087156 0
            imesh=328.54 330.54
            iints=1 1
            jmesh=540
            jints=27
            kmesh=0.0277778 1
            kints=1 1
c
c           Cask side
fmesh54:p   geom=cyl origin=0 0 45.72 axs=0 0 1 vec=0.99619 -0.087156 0
            imesh=73.025 74.025
            iints=1 1
            jmesh=81.5975
            jints=9
            kmesh=0.0277778 1
            kints=1 1
c
prdmp    j j 1 2
ctme     2940
```

5.5.3 A_2 Calculation

Based on the single source activity limits, the maximum number of A_2 per package may be computed. The A_2 values for each isotope (in TBq) are obtained from Table A-1 of 10 CFR 71. The maximum number of A_2 is 16,431 based on 1,101 Ci of Ra-226. The A_2 calculations are summarized in Table and Table .

The A_2 values listed in 10 CFR 71 include daughter products with half-lives less than 10 minutes. Therefore, Ba-137m is included with Cs-137 and Y-90 is included with Sr-90. However, Ra-226 has two longer-lived daughters in the decay chain, Pb-210 and Po-210, that must be included in the A_2 calculation. A bounding A_2 calculation is performed in which the activities of Pb-210 and Po-210 are equal to the Ra-226 activity of 1,101 Ci.

Table 5.5-1 – A_2 Values, Co-60, Cs-137, Sr-90, Ir-192

Nuclide	Maximum Activity (Ci)	A_2 (TBq)	A_2 (Ci)	Number of A_2
Co-60	7,702	0.4	1.08E+01	712
Cs-137	40,675	0.6	1.62E+01	2,508
Sr-90	30,606	0.3	8.11E+00	3,775
Ir-192	33,333	0.6	1.62E+01	2,056

Table 5.5-2 – A_2 Values, Ra-226

Nuclide	Maximum Activity (Ci)	A_2 (TBq)	A_2 (Ci)	Number of A_2
Ra-226	1,101	0.003	8.11E-02	13,579
Po-210	1,101	0.02	5.41E-01	2,037
Pb-210	1,101	0.05	1.35E+00	815
			Total	16,431

5.5.4 Gas Generation due to Radiolysis

The devices will be shored within the 380-B using either wood, polyurethane foam, or metallic dunnage. Due to the radiation field within the 380-B, hydrogen and other gases may be generated due to radiolysis of non-metallic dunnage. Per Section 3.5.4.2 of NUREG-1609 [5], during a time period of 1 year, hydrogen and other flammable gases shall comprise less than 5% by volume of the total gas inventory within any confined volume. Gas generation must also be factored into the maximum normal operating pressure (MNOP). Therefore, the purpose of this appendix is to estimate both the flammable and total gas generation due to radiolysis of non-metallic dunnage.

The 380-B packaging provides a level of biological shielding independent of the shielding included in the devices themselves to protect public health against the unlikely possibility that the radioactive source could come out of the shielded device. To demonstrate the effectiveness of the shielding components of the 380-B, it is assumed in the shielding analysis in Section 5.3.1, *Configuration of Source and Shielding*, that the source is loose in the payload cavity in the worst location. However, bare sources will not be transported in the 380-B, and loss or exposure of the source from the shielded device is not a routine condition of transport. Therefore, in the gas generation calculations presented in this appendix, credit is taken for shielding provided by the device.

Gas generation due to radiolysis may be estimated using the G-value for gamma, beta, or alpha radiation. A G-value represents 1 molecule of gas generated for every 100 eV of energy absorbed. For the 380-B, a source is transported within a shielded device so that only gamma radiation is of concern (i.e., beta and alpha radiation do not escape the device). Neutron radiation does not directly produce ionizing radiation in matter, although the products of neutron interactions can produce ionization and give rise to radiation-induced chemical changes. G-values are not available for neutron radiation. The only neutron emitter transported in the 380-B is Ra-226 mixed with an (α,n) target isotope. It is assumed that a gas generation analysis performed with Co-60, a strong gamma emitter, is representative of the other radioactive isotopes that may be transported within the package.

It is stated in [7] that urethane foam results in minimal gas generation when subjected to a large Co-60 dose. Therefore, for the purposes of estimating gas generation, wood bounds polyurethane foam and all calculations in this appendix are performed for wood dunnage.

G-values are available from a variety of experimental data. A detailed summary of known experimental results is provided in the CH-TRU Payload Appendices [6]. G(H_2) for gammas in liquid water is 0.45 (from Table 3.1-6 of [6]). Because 0.5 mole of oxygen will be produced for every mole of hydrogen gas for radiolysis of water, G(gas) is 0.45*1.5 = 0.675.

G-values for "wood" are not directly provided, although "cotton cellulose I" is assumed to be a reasonable approximation for wood. Four different sets of data are provided in Table 3.1-30 of [6]. Bounding values are G(H_2) = 1.3 and G(gas) = 4.5.

The G-values for water and wood are summarized in Table 5.5-3. Because the G-values for wood exceed the G-values for water, it may be conservatively assumed that the wood dunnage is dry, although the actual wood dunnage will retain some moisture.

The energy absorption in the wood is computed using MCNP. The exact type of wood to be used as dunnage is not defined, although the wood dunnage to be used would be a softer variety, such as pine, and a reasonably high density of 40 lb/ft³, or 0.641 g/cm³, is utilized. This density includes the mass of any residual moisture, although the entire mass of wood plus water is conservatively modeled only as wood. The wood is modeled in MCNP as cellulose ($C_6H_{10}O_5$).

The dose rate on the surface of a device is assumed to be 200 mrem/hr because the devices are designed to be used in a normal working environment. The actual dose rate on the surface of a device is typically much less than 200 mrem/hr. Because the device geometry is arbitrary, the device is modeled as a simple sphere of pure lead with a point source of Co-60 in the center. Three different device geometries are considered: small, medium, and large. A large device minimizes the volume of wood while a small device maximizes the volume of wood. However, a large device has a larger surface area, and the 200 mrem/hr dose rate on the surface of the device is essentially a surface source. Therefore, it is expected that for a constant surface dose rate, larger devices will result in larger gas generation than a smaller device.

Three device geometries are considered:

1. Small device: The lead radius is fixed at 8 cm, and the Co-60 activity is determined that results in a surface dose rate ≥ 200 mrem/hr.
2. Medium device: The lead radius is fixed at 16 cm, and the Co-60 activity is determined that results in a surface dose rate ≥ 200 mrem/hr.
3. Large device: The maximum allowed Co-60 source activity is used (7702 Ci), and the radius of lead is selected to give a surface dose rate ≥ 200 mrem/hr.

Combinations of source activity and device radius are determined to provide the desired surface dose rate, and the results are summarized in Table 5.5-4. In these preliminary cases, the devices are modeled without the 380-B.

Once the device geometry and appropriate Co-60 source strengths are determined, the device is modeled within the center of the 380-B. The remainder of the package cavity is filled with wood. The mass of wood varies with the size of the device. The wood masses for the three device sizes are summarized in Table 5.5-5.

Energy deposition is calculated in MCNP using an F6 tally. The default output unit is MeV/g per second. The molecules of gas are calculated based on the following formula:

$$\text{Moles of Gas} = G/100 \times (E \times 10^6) \times T \times M / A$$

Where,

G = appropriate G-value (molecules per 100 eV of absorbed energy)

E = energy deposition in MeV/g per second (from MCNP)

T = seconds in 1 year (3.154×10^7 s)

M = mass of wood (grams)

A = Avogadro's number (6.022×10^{23} molecules per mole)

The results are summarized in Table 5.5-6. The G-value for total gas generation is conservatively used to bound flammable gas generation. The large device results in significantly more gas generation than either the medium or small devices even though the volume of wood is

minimized. The volume of gas is computed from the moles of gas based on the ideal gas law (1 mole = 22.4 L). If all of the gas is assumed to be flammable, the minimum void (air) volume may be computed as $V_{gas}/0.05$ because the flammable component is limited to 5% of the void volume. For the large device, the minimum required void volume is 0.4 L. The 0.25-in gap between the inner cover and the lid has a volume of approximately 4.6 L (based on the cavity inner diameter of 38-in), and the total void volume of the 380-B will typically be much larger than 4.6 L. Therefore, the flammable gas generated in 1 year will remain well below 5%. The volume ratio of hydrogen to air is independent of the temperature or pressure inside the cask because the quantities of gas are fixed.

The largest volume of gas generated is 2.01×10^{-2} L (~20 cm^3), which is too small of a volume to affect the MNOP of 10 psig.

Table 5.5-3 – G-Values

Material	G(gas)	G(H$_2$)
Water	0.675	0.45
Wood	4.5	1.3

Table 5.5-4 – Device Geometry and Source Strength

Device	Co-60 Activity (Ci)	Device Radius (cm)	Device Surface Dose Rate (mrem/hr)
Small	0.06	8.0	209
Medium	25	16.0	203
Large	7702	24.1	214

Table 5.5-5 – Wood Mass

Parameter	Small	Medium	Large
Cavity Volume (cm^3)	857,225	857,225	857,225
Device Radius (cm)	8	16	24.1
Device Volume (cm^3)	2,145	17,157	58,633
Wood Volume (cm^3)	855,080	840,067	798,592
Wood density (g/cm^3)	0.641	0.641	0.641
Wood Mass (g)	547,789	538,171	511,601

Table 5.5-6 – Gas Generation

Parameter	Small	Medium	Large
G(gas) (molecules/100 eV)	4.5	4.5	4.5
E (MeV/g per s)*	98.456	346.826	745.697
T (s)	31,536,000	31,536,000	31,536,000
M (g)	547,789	538,171	511,601
Moles of gas	1.27E-04	4.40E-04	8.99E-04
Gas Volume (L)	2.85E-03	9.85E-03	2.01E-02
Minimum void volume to remain below 5% flammable gas in 1 year (L)	0.057	0.20	0.40

* Energy deposition is calculated in MCNP using an F6 tally.

This page left intentionally blank.

6.0 CRITICALITY EVALUATION

Since the 380-B contents do not include any fissile material, a criticality evaluation is not required.

This page left intentionally blank.

7.0 PACKAGE OPERATIONS

This section delineates the procedural outlines for operating the 380-B packaging. Operating procedures shall conform to the requirements identified in the following sections. Reference to specific 380-B packaging components may be found in Appendix 1.3.3, *Packaging General Arrangement Drawings*.

7.1 Procedures for Loading the Package

This section delineates the procedures for loading a payload into the 380-B packaging. Deactivation of electronic security/tracking devices should occur before starting this procedure.

7.1.1 Preparation for Loading

1. Position the conveyance appropriately for loading operations. The cask will remain on the conveyance during all operations.

2. Remove tie-downs from the upper impact limiter.

3. Remove both halves of the personnel barrier. The personnel barrier is attached using eight fasteners (such as bolts, retaining pins, or security locks) on each side.

4. Remove the security cable from the upper impact limiter attachment blocks, if present, which allows access to the impact limiter attachment bolts.

5. Remove the set screw from each of the three 5/8–11 UNC threaded holes marked as impact limiter lift points. Attach rigging to the upper impact limiter using these holes.

6. Remove the twelve, 1-1/4-7 UNC bolts to release the upper impact limiter.

7. Lift and remove the upper impact limiter from the cask body.

7.1.2 Loading of Contents

NOTE: The visual inspections of packaging components delineated in the following steps may be performed at any time during the loading sequence.

1. Remove the 36, 1–1/2–6 UNC bolts that retain the closure lid.

2. Attach rigging to the three, 5/8–11 UNC threaded holes in the closure lid.

3. Lift and remove the closure lid from the cask body. Store the closure lid in a manner to minimize potential damage to the O–ring seals and sealing surfaces.

4. Protect the cask body from entry of precipitation.

5. Install and secure the sealing surface protector to the cask body.

6. Attach rigging to the center, or to the three outer, 5/8-11 UNC threaded holes in the inner cover located in the cask opening, and unfasten and remove the inner cover.

7. Verify that the cask cavity is clean and dry.

8. Identify the shielded device or source container for transport and verify that it meets the payload limits for isotope, activity, heat generation, and weight, as delineated in Section

7.1.4, *Qualifying the Payload for Transport.* More than one device may be placed in the cask, as long as none of the stated payload limits are exceeded for the total payload.

9. Before moving the shielded device, immobilize the source exposure mechanism, or any other mechanism or condition which could allow the source to become exposed during handling.

10. Remove, to the extent practical, any non-essential components or hardware from the shielded device. Verify that the payload will fit completely within the cavity of the 380-B, with adequate clearance below the inner cover.

11. Prepare blocking/dunnage for use within the cask. Dunnage may be made from wood, rigid, closed cell polyurethane foam, or welded or bolted metallic structures.

    a. The maximum weight for all dunnage used in the 380-B package is 2,000 lb.

    b. If using non-metallic dunnage, verify that at least 50% of the side axial height of the device(s) is not covered by dunnage material.

    c. Dunnage shall be configured to allow a minimum of one-half inch of free space between the inner diameter of the cask and the materials of the payload or dunnage, and a minimum of one-half inch of free space between the top of the payload or dunnage and any part of the inner cover.

12. Prior to placing the shielded device into the cask, verify that the device and the cask cavity are dry.

13. Lower the shielded device into the cask, along with dunnage as necessary. As an option, lifting slings made of steel, nylon, polyester, or Kevlar© may be left inside the cask during transport.

14. Lower the inner cover into the cask and fasten in place.

15. Visually inspect both main O–ring seals and the mating surfaces on the cask body. If damage is present which is sufficient to impair containment integrity (e.g., cuts, tears, and/or joint separation in the O–ring, or scratches or dents in the sealing surfaces), replace the seals and/or repair the damaged surfaces per Section 8.2.3.2, *Sealing Area Routine Inspection and Repair.*

16. As an option, remove and sparingly apply vacuum grease to the O–ring seals and/or sealing surfaces, and reinstall the O–rings into the grooves in the closure lid. NOTE: If the O-rings are removed, perform a visual surface finish inspection of the O-ring grooves for scratches or dents that could impair containment integrity. If necessary, repair the damaged surfaces per Section 8.2.3.2, *Sealing Area Routine Inspection and Repair.*

17. Remove and visually inspect the vent port and seal test port plugs and associated sealing washers and mating surfaces in the closure lid. If damage is present which is sufficient to impair containment integrity (e.g., cuts, tears, and/or separation of the O–ring from the metal washer, or scratches or dents in the sealing surfaces), replace the sealing washers and/or repair the damaged surfaces per Section 8.2.3.2, *Sealing Area Routine Inspection and Repair.*

18. Reinstall the vent port and seal test port plugs and sealing washers. Do not tighten at this time.

19. Remove the sealing surface protector.

20. Install the closure lid on the cask body, using the alignment pins to guide the closure lid into position.

21. Visually inspect the closure bolts for wear or damage that could impair their function and, if necessary, replace or repair per the requirements of the drawings in Appendix 1.3.3, *Packaging General Arrangement Drawings*.

22. Coat closure bolt threads, and optionally the washer surfaces, with a low halogen, nickel-based, nuclear grade lubricant prior to assembly. Re-coating is not required if an adequate coat exists. Install the 36, 1–1/2–6 UNC bolts to secure the closure lid to the cask body. Using a crossing pattern, tighten the closure bolts to 850 – 950 ft-lb torque (lubricated).

23. Preshipment leakage rate testing of the containment O-ring seal and the vent port sealing washer shall be performed according to the following criteria:

    a. If the containment (inner) O-ring seal has been replaced or the corresponding sealing surface repaired, or if the vent port plug or sealing washer has been replaced or the mating sealing surface repaired, the preshipment leakage rate tests shall be performed according to Section 8.2.2, *Maintenance/Periodic Leakage Rate Tests*.

    b. If the criteria of step (a) above do not apply, preshipment leakage rate testing shall be performed either according to Section 7.4, *Preshipment Leakage Rate Test*, or according to Section 8.2.2, *Maintenance/Periodic Leakage Rate Tests*.

24. At the conclusion of all leakage rate testing, install the vent port dust cover and seal test port dust cover.

7.1.3   Preparation of the Package for Transport

1. Using rigging attached to the upper impact limiter using the three (3) 5/8–11 UNC threaded holes marked as impact limiter lift points, lower the impact limiter over the cask. Align the attachment holes to the impact limiter attachment blocks.

2. Coat impact limiter attachment bolt threads, and optionally the washer surfaces, with a low halogen, nickel-based, nuclear grade lubricant prior to assembly. Recoating is not required if an adequate coat exists. Install 12, 1–1/4–7 UNC bolts and tighten, using a crossing pattern, to 280 – 340 ft-lb.

3. Install a set screw into each of the three 5/8–11 UNC threaded holes marked as impact limiter lift points.

4. Install a security cable through the holes in the upper impact limiter attachment brackets. Alternatively, install a tamper-indicating lockwire across at least one of the upper impact limiter attachment brackets.

5. Install both halves of the personnel barrier, using bolts, pins, or security locks (a total of eight items per barrier half) as shown on the drawings located in Appendix 1.3.3, *Packaging General Arrangement Drawings*.

6. Install tie-downs over the upper impact limiter and attach to the conveyance.

7. Monitor external radiation for the package per the requirements of 49 CFR §173.441 [2].

8. Determine that surface contamination level for the package and conveyance is per the requirements of 10 CFR §71.87(i) [1] and 49 CFR §173.443 [2].

9. Complete all necessary shipping papers in accordance with Subpart C of 49 CFR 172 [3].

10. 380-B package marking shall be in accordance with 10 CFR §71.85(c) [1] and Subpart D of 49 CFR 172 [3]. Package labeling shall be in accordance with Subpart E of 49 CFR 172. Package placarding shall be in accordance with Subpart F of 49 CFR 172.

7.1.4 Qualifying the Payload for Transport

The following steps ensure that the device(s) placed in the 380-B comply with the limits established in Section 1.2.2, *Contents*, and Section 5.4.5, *Loading Methodology*.

1. The total weight of all device(s) and/or source container(s) shall not exceed 10,000 lb.

2. To meet radionuclide limits, verify that the total activity of each isotope to be transported does not exceed the activity limits given in Table 7.1-1.

3. To meet the decay heat limit, verify that the total heat load is less than or equal to 205 watts. If only a single isotope is to be shipped, this is ensured by step 1 above. If multiple isotopes are to be transported, the total watts shall be calculated by multiplying the activity of each isotope by the heat generation rate found in Table 7.1-1 and summing the results.

4. To meet the decay heat density limit, the decay heat shall not exceed 0.1 W per pound of device weight.

5. To meet the dose rate limits for multiple source isotopes, if more than one isotope is loaded, verify the selected loading does not violate the dose rate limits using the following equation:

$$\sum_{i=1}^{n} \frac{S_i}{A_i} \leq 1$$

where:

      S_i is the activity of each source in Ci
      A_i is the appropriate value from Table 7.1-1.

Examples for multiple source isotopes are provided below.

Example #1: Is 5,000 Ci Co-60 and 15,000 Ci Cs-137 acceptable for transport?

   1. Based on Table 7.1-1, the activity limits are not exceeded.

   2. Based on Table 7.1-1, the decay heat is:

      $(5{,}000)(1.542 \times 10^{-2}) + (15{,}000)(5.04 \times 10^{-3}) = 152.7$ watts ≤ 205 watts.

   3. Based on Table 7.1-1, the dose rate sum of fractions is:

      $5{,}000/7{,}702 + 15{,}000/3.0 \times 10^{5} = 0.7 \leq 1.0$.

Therefore, payload #1 is acceptable for transport.

Example #2: Is 5,000 Ci Co-60 and 30,000 Ci Cs-137 acceptable for transport?

   1. Based on Table 7.1-1, the activity limits are not exceeded.

2. Based on Table 7.1-1, the decay heat is:

$$(5,000)(1.542\times10^{-2}) + (30,000)(5.04\times10^{-3}) = 228.3 \text{ watts} > 205 \text{ watts.}$$

Therefore, payload #2 is not acceptable for transport because the heat load exceeds 205 watts.

Example #3: Is 5,000 Ci Co-60 and 4.0 Ci Ra-226 (with beryllium) acceptable for transport?

1. Based on Table 7.1-1, the activity limits are not exceeded.
2. Based on Table 7.1-1, the decay heat is:

$$(5,000)(1.542\times10^{-2}) + (4)(1.862\times10^{-1}) = 77.8 \text{ watts} \leq 205 \text{ watts.}$$

3. Based on Table 7.1-1, the dose rate sum of fractions is:

$$5,000/7,702 + 4/4.67 = 1.5 > 1.0.$$

Therefore, payload #3 is not acceptable for transport because the dose rate limits could be exceeded.

Table 7.1-1 – Payload Qualification Table

Nuclide	Activity Limit (Ci)	A_i (Ci)	Decay Heat (watt/Ci)[1]
Co-60	7,702	7,702	1.542E-02
Cs-137	40,675	3×10^5	5.040E-03
Sr-90	30,606	3×10^5	6.698E-03
Ir-192	33,333	3×10^5	6.150E-03
Ra-226 (no Be, Cl target)[2]	1,101	1,244	1.862E-01
Ra-226 (with Be)	4.67	4.67	1.862E-01

[1] Includes all decay products.
[2] Excludes beryllium. Impurities may include oxygen, carbon, sulfur, bromine (hydrous), and chlorine (hydrous or anhydrous).

7.2 Procedures for Unloading the Package

This section delineates the procedures for unloading a payload from the 380-B packaging.

7.2.1 Receipt of Package from Carrier

1. Record the condition of the tamper-indicating devices.

2. Deactivate any electronic security/tracking devices.

3. Perform the steps listed in Section 7.1.1, *Preparation for Loading.*

7.2.2 Removal of Contents

1. Remove the vent port cover, and loosen the vent port plug to vent the cask cavity.

2. Remove the 36, 1–1/2–6 UNC bolts that retain the closure lid.

3. Attach rigging to the three, 5/8–11 UNC threaded holes in the closure lid.

4. Lift and remove the closure lid from the cask body. Store the closure lid in a manner to minimize potential damage to the O–ring seals and sealing surfaces.

5. Protect the cask body from entry of precipitation.

6. Install and secure the sealing surface protector to the cask body.

7. Attach rigging to the center, or to the three outer, 5/8-11 UNC threaded holes in the inner cover located in the cask opening, and unfasten and remove the inner cover.

8. Remove, as necessary, sufficient dunnage to allow the shielded device to be removed from the cask.

9. Remove the shielded device from the cask.

10. Lower the inner cover into the cask and fasten in place.

11. Remove the sealing surface protector.

12. Install the closure lid on the cask body, using the alignment pins to guide the closure lid into position.

13. Coat closure bolt threads, and optionally the washer surfaces, with a low halogen, nickel-based, nuclear grade lubricant prior to assembly. Re-coating is not required if an adequate coat exists. Install the 36, 1–1/2–6 UNC bolts to secure the closure lid to the cask body. Using a crossing pattern, tighten the closure bolts to a minimum of 300 ft-lb torque (lubricated). Note: this tightening torque value applies to empty shipment only.

14. Install the vent port and seal test port plugs, with their associated sealing washers, and tighten to 48 – 60 in-lb torque, and install the seal test port dust cover and vent port dust cover.

15. Prepare the packaging for transport according to steps 1 through 6 of Section 7.1.3, *Preparation of the 380-B Package for Transport.* A security cable or tamper-indicating device is not required.

7.3   Preparation of an Empty Package for Transport

Previously used and empty 380-B packagings shall be prepared and transported per the requirements of 49 CFR §173.428 [2].

7.4 Preshipment Leakage Rate Test

After the 380-B package is assembled and prior to shipment, leakage rate testing shall be performed to confirm proper assembly of the package following the guidelines of Section 7.6, *Preshipment Leakage Rate Test*, of ANSI N14.5 [4]. Preshipment leakage rate testing shall be performed according to Section 8.2.2, *Maintenance/Periodic Leakage Rate Tests*. Optionally, preshipment leakage rate testing may be performed using the gas pressure rise method. Using this method, no leakage shall be detected when tested to a sensitivity of 1×10^{-3} reference cubic centimeters per second (ref–cm^3/s) air, or less, per Appendix A.5.2, *Gas Pressure Rise*, of [4].

7.5 Appendix

7.5.1 References

1. Title 10, Code of Federal Regulations, Part 71 (10 CFR 71), *Packaging and Transportation of Radioactive Material*, 01–01–11 Edition.

2. Title 49, Code of Federal Regulations, Part 173 (49 CFR 173), *Shippers–General Requirements for Shipments and Packagings*, 10–01–11 Edition

3. Title 49, Code of Federal Regulations, Part 172 (49 CFR 172), *Hazardous Materials Table, Special Provisions, Hazardous Materials, Communication, Emergency Response Information, Training Requirements, and Security Plans*, 10–01–11 Edition.

4. ANSI N14.5–2014, *American National Standard for Radioactive Materials – Leakage Tests on Packages for Shipment*, American National Standards Institute (ANSI), Inc.

This page left intentionally blank.

8.0 ACCEPTANCE TESTS AND MAINTENANCE PROGRAM

This section describes the acceptance tests and the maintenance program that shall be used on the 380-B package in compliance with Subpart G of 10 CFR 71 [1].

8.1 Acceptance Tests

Per the requirements of 10 CFR §71.85, this section discusses the inspections and tests to be performed prior to first use of the 380-B packaging. Successful completion of these tests will ensure that the requirements of 10 CFR §71.85(a) have been met. Acceptance criteria for all inspections and tests are found either on the drawings in Appendix 1.3.3, *Packaging General Arrangement Drawings*, or in the sections that follow. Deviations from requirements will be recorded and dispositioned in accordance with the cognizant quality assurance program.

8.1.1 Visual Inspection and Measurements

Each 380-B packaging will be visually inspected and measured to ensure that all of the requirements delineated on the drawings in Appendix 1.3.3, *Packaging General Arrangement Drawings*, are satisfied. This includes but is not limited to such items as materials, physical arrangement of components, quantities, dimensions, welds, and measurements.

8.1.2 Weld Examinations

The locations, types, and sizes of all welds will be identified and recorded to ensure compliance with the drawings in Appendix 1.3.3, *Packaging General Arrangement Drawings*. All welds are subject to visual examination per AWS D1.6 [2]. A summary of weld examinations performed on each 380-B packaging is given in Table 8.1-1.

8.1.3 Structural and Pressure Tests

8.1.3.1 Lifting Device Load Testing

The 380-B package has no provisions for lifting when fully assembled, and thus does not contain any lifting devices that require load testing.

8.1.3.2 Containment Boundary Pressure Testing

The MNOP equals 10 psig as stated in Section 3.3.2, *Maximum Normal Operating Pressure*. Per 10 CFR §71.85(b), the containment boundary must be pressure tested to 150% of this pressure, or a test pressure of 15 psig. Conservatively, the 380-B package containment boundary is pressure tested to 125% of the design pressure of 25 psig per the requirements of ASME B&PV Code, Subsection NB, Article NB-6220 [6], or a test pressure of 31.25 psig.

Following pressure testing of the containment boundary, welds directly related to the pressure testing and accessible base material adjacent to the welds shall be visually inspected for plastic deformation or cracking in accordance with AWS D1.6, and liquid penetrant inspected per ASME B&PV Code, Subsection NB, Article NB–5000, and Section V, Article 6, as delineated on the drawings in Appendix 1.3.3, *Packaging General Arrangement Drawings*. Indications of cracking or distortion shall be recorded and evaluated in accordance with the cognizant quality assurance program.

Except for the leakage rate testing of the containment structures prior to lead pour, leakage rate testing per Section 8.1.4, *Fabrication Leakage Rate Tests*, shall be performed after completion of pressure testing to verify package configuration and performance to design criteria.

8.1.4 Fabrication Leakage Rate Tests

This section provides the generalized procedure for fabrication leakage rate testing of the containment vessel boundary and vent port penetration during fabrication. Fabrication leakage rate testing shall follow the guidelines of Section 7.3, *Fabrication Leakage Rate Test*, of ANSI N14.5 [7]. Fabrication leakage rate testing of the containment structure integrity is performed in two stages: prior to, and following, lead installation. These two stages are necessitated by potential of the lead to prevent helium gas from reaching the surface of the containment boundary. Four separate tests comprise the series: containment body structure prior to lead installation, closure lid structure prior to lead installation, containment boundary and containment O-ring seal after lead installation, and the vent port sealing washer. Each test shall meet the acceptance criteria delineated in Section 8.1.4.1, *Fabrication Leakage Rate Test Acceptance Criteria*.

8.1.4.1 Fabrication Leakage Rate Test Acceptance Criteria

1. To be acceptable, each leakage rate test shall demonstrate a "leaktight" leakage rate of 1×10^{-7} reference cubic centimeters per second (ref–cm^3/s), air, or less, per Section 6.3, *Application of Reference Air Leakage Rate (L$_R$)*, of [7]. The final leakage rate shall be adjusted for the helium concentration in the envelope as applicable.

2. In order to demonstrate the leaktight leakage rate, the sensitivity of the leakage rate test procedure shall be 5×10^{-8} cm^3/s, air, or less, per Section 8.4, *Sensitivity*, of [7].

3. Failure to meet the stated leakage rate shall be recorded and evaluated in accordance with the cognizant quality assurance program.

8.1.4.2 Containment Body Structure (Prior to Lead Installation)

This leakage rate test verifies the leak tightness of the upper and lower end structures, and the inner shell that comprise the primary metallic containment boundary of the 380-B packaging.

1. The fabrication leakage rate test shall be performed following the guidelines of Section A.5.3, *Gas Filled Envelope – Gas Detector*, of [7].

2. The 380-B packaging fabrication shall consist of the body weldment (upper and lower end structures, the inner containment shell, and the outer structural shell) and a test lid. The fabrication shall not include the bottom outer plate.

3. Connect a mass spectrometer leakage detector (MSLD) to the body weldment cavity.

4. Evacuate the cavity until the vacuum is sufficient to operate the MSLD.

5. Surround the outer surface of the containment body with an envelope filled with an adequate concentration of helium gas. Verify that the lead cavity on the side and bottom of the cask is open to the helium atmosphere.

6. Perform the helium leakage rate test to the requirements of Section 8.1.4.1, *Fabrication Leakage Rate Test Acceptance Criteria*. If, after repeated attempts, the containment structure fails to pass the leakage rate test, isolate the leak path and, prior to repairing the leak path and

repeating the leakage rate test, record on a nonconformance report and disposition prior to final acceptance in accordance with the cognizant quality assurance program.

8.1.4.3 Closure Lid Structure (Prior to Lead Installation)

This leakage rate test verifies the leak tightness of the part of the containment boundary comprised by the closure lid.

1. The fabrication leakage rate test shall be performed following the guidelines of Section A.5.3, *Gas Filled Envelope – Gas Detector*, of [7].

2. The closure lid shall consist of the main structure, without the lead sheets or outer plate, and shall be mated to a test body.

3. Connect a mass spectrometer leakage detector (MSLD) to the cavity within the test body.

4. Evacuate the cavity until the vacuum is sufficient to operate the MSLD.

5. Surround the outer surface of the closure lid with an envelope filled with an adequate concentration of helium gas.

6. Perform the helium leakage rate test to the requirements of Section 8.1.4.1, *Fabrication Leakage Rate Test Acceptance Criteria.* If, after repeated attempts, the closure lid structure fails to pass the leakage rate test, isolate the leak path and, prior to repairing the leak path and repeating the leakage rate test, record on a nonconformance report and disposition prior to final acceptance in accordance with the cognizant quality assurance program.

8.1.4.4 Containment Boundary and Containment O-ring Seal (After Lead Installation)

This leakage rate test verifies the leak tightness of the final configuration of the containment boundary of the 380-B packaging.

1. The fabrication leakage rate test shall be performed following the guidelines of Section A.5.3, *Gas Filled Envelope – Gas Detector*, of [7].

2. The 380-B packaging shall be assembled with only the inner O-ring seal installed in the closure lid, and the vent port plug installed with its associated sealing washer. If not previously tightened, tighten the closure lid bolts to 850 – 950 ft-lb torque (lubricated), using a crossing pattern. Assembly is as shown in Appendix 1.3.3, *Packaging General Arrangement Drawings.*

3. Connect a port tool to the vent port in the closure lid.

4. Install a helium mass spectrometer leak detector (MSLD) to the port tool. Evacuate through the vent port until the vacuum is sufficient to operate the MSLD.

5. Surround at least the upper end structure and the closure lid with an envelope filled with an adequate concentration of helium gas.

6. Perform the helium leakage rate test to the requirements of Section 8.1.4.1, *Fabrication Leakage Rate Test Acceptance Criteria.* If, after repeated attempts, the containment boundary fails to pass the leakage rate test, isolate the leak path and, prior to repairing the leak path and repeating the leakage rate test, record on a nonconformance report and

disposition prior to final acceptance in accordance with the cognizant quality assurance program.

8.1.4.5 Helium Leakage Rate Testing the Vent Port Sealing Washer

1. The fabrication leakage rate test of the vent port plug sealing washer integrity shall be performed following the guidelines of Section A.5.4, *Evacuated Envelope – Gas Detector*, of [7]. If this test immediately follows the test of Section 8.1.4.4, *Containment Boundary and Containment O-ring Seal (After Lead Installation)*, skip to step no. 3.

2. Assemble the 380-B package with the configuration specified in Section 8.1.4.4, *Containment Boundary and Containment O-ring Seal (After Lead Installation)*. Install the vent port plug with its associated sealing washer.

3. Attach a vacuum pump and a source of helium gas to the vent port. Evacuate the cavity and provide a helium atmosphere inside the cavity by backfilling with helium gas to ambient pressure.

4. Using the vent port tool, close the vent port plug and tighten to 48 – 60 in-lb torque.

5. Install a clean (helium-free) port tool into the vent port.

6. Attach a helium MSLD to the port tool.

7. Evacuate the cavity above the vent port plug sealing washer until the vacuum is sufficient to operate the leak detector per the manufacturer's recommendations.

8. Perform the helium leakage rate test to the requirements of Section 8.1.4.1, *Fabrication Leakage Rate Test Acceptance Criteria*. If, after repeated attempts, the vent port plug sealing washer fails to pass the leakage rate test, isolate the leak path and, prior to repairing the leak path and repeating the leak test, record on a nonconformance report and disposition prior to final acceptance in accordance with the cognizant quality assurance program.

8.1.5   Component and Material Tests

8.1.5.1   Polyurethane Foam

This section establishes the requirements and acceptance criteria for installation, inspection, and testing of the rigid, closed–cell polyurethane foam utilized within the 380-B packaging impact limiters.

8.1.5.1.1   Introduction and General Requirements

The polyurethane foam used within the 380-B packaging is comprised of a specific "formulation" of foam constituents that, when properly apportioned, mixed, and reacted, produce a polyurethane foam material with physical characteristics consistent with the requirements given in Section 8.1.5.1.2, *Physical Characteristics*. In practice, the chemical constituents are batched into multiple parts (e.g., parts A and B) for later mixing in accordance with a formulation. Therefore, a foam "batch" is considered to be a specific grouping and apportionment of chemical constituents into separate and controlled vats or bins for each foam formulation part. Portions from each batch part are combined in accordance with the foam formulation requirements to produce the liquid foam material for pouring into a component or box. Thus, a foam "pour" is defined as apportioning and mixing the

batch parts into a desired quantity for subsequent installation (pouring). Finally, all contiguous pours into a single mold are termed a component part.

The following sections describe the general requirements for constituent storage, and foam pour and test data records. The major chemical constituents of the foam are approximately: carbon, 50% - 70%, oxygen, 14% - 34%, nitrogen, 4% - 12%, and hydrogen, 4% - 10%.

8.1.5.1.1.1 Polyurethane Foam Constituent Storage

The foam supplier shall certify that the polyurethane foam constituents have been properly stored prior to use, and that the polyurethane foam constituents have been used within their shelf life.

8.1.5.1.1.2 Impact Limiter Shell Preparation

Prior to installing foam into the impact limiter shells, the interior surfaces of the shells shall be treated with an antibonding agent, such as a paste wax.

8.1.5.1.1.3 Polyurethane Foam Installation

The foam shall be installed while the longitudinal axis of the impact limiter shell is vertical. The walls of the shell where the liquid foam material is to be installed shall be between 55 °F and 95 °F prior to foam installation. Measure and record the shell temperature to an accuracy of ±2 °F.

In the case of multiple pours into a single impact limiter, the cured level of each pour shall be measured and recorded to an accuracy of ±1 inch.

Measure and record the weight of liquid foam material installed during each pour to an accuracy of ±10 pounds.

All test samples shall be poured into disposable containers at the same time as the actual pour it represents, clearly marking the test sample container with the pour date and a unique pour identification number. All test samples shall be cut from a larger block to obtain freshly cut faces. Prior to physical testing, each test sample shall be cleaned of superfluous foam dust.

8.1.5.1.1.4 Polyurethane Foam Pour and Test Data Records

A production pour and testing record shall be compiled by the foam supplier during the foam pouring operation and subsequent physical testing. Upon completion of production and testing, the foam supplier shall issue a certification referencing the production record data and test data pertaining to each foamed component. At a minimum, relevant pour and test data shall include:

- formulation, batch, and pour numbers, with foam material traceability, and pour date,
- instrumentation description, serial number, and calibration due date,
- pour and test data (e.g., date, temperature, dimensional, and/or weight measurements, compressive stress, etc., as applicable), and
- technician and Quality Assurance/Quality Control (QA/QC) sign–off.

8.1.5.1.2 Physical Characteristics

The following subsections define the required physical characteristics of the polyurethane foam material.

Testing for the various polyurethane foam physical characteristics is based on a "formulation", "batch", or "pour", as appropriate, as defined in Section 8.1.5.1.1, *Introduction and General Requirements*. The physical characteristics determined for a specific foam formulation are relatively insensitive to small variations in chemical constituents and/or environmental conditions, and therefore include physical testing only for leachable chlorides, thermal conductivity, and specific heat. Similarly, the physical characteristics determined for a batch are only slightly sensitive to small changes in formulation and/or environmental conditions during batch mixing, and therefore include physical testing only for flame retardancy. Finally, the physical characteristics determined for a pour are also only slightly sensitive to small changes in formulation and slightly more sensitive to variations in environmental conditions during pour mixing, and therefore include physical testing for density and compressive stress.

8.1.5.1.2.1 Physical Characteristics Determined for a Foam Formulation

The following physical characteristics shall be determined once for a particular foam formulation. If multiple components are to utilize a specific foam formulation, then additional physical testing, as defined below, need not be performed.

8.1.5.1.2.1.1 Leachable Chlorides

1. The leachable chlorides test shall be performed using an ion chromatograph (IC) apparatus. The IC measures inorganic anions of interest (i.e., chlorides) in water. Description of a typical IC is provided in EPA Method 300.0 [8]. The IC shall be calibrated against a traceable reference specimen per the IC manufacturer's operating instructions.

2. One test sample shall be taken from a pour for each foam formulation. The test sample shall be a cube with dimensions of 2.00 ±0.06 in.

3. Place the test sample in a room (ambient) temperature environment (i.e., 65 °F to 85 °F) for sufficient time to thermally stabilize the test sample. Measure and record the room temperature to an accuracy of ±2 °F.

4. Obtain a minimum of 550 mL of distilled or de–ionized water for testing. The test water shall be from a single source to ensure consistent anionic properties for testing control.

5. Obtain a 400 mL, or larger, contaminant free container that is capable of being sealed. Fill the container with 262 ±3 mL of test water. Fully immerse the test sample inside the container for a duration of 72 ±3 hours. If necessary, use an inert standoff to ensure the test sample is completely immersed for the full test duration. Seal the container prior to the 72–hour duration.

6. Obtain a second, identical container to use as a "control". Fill the control container with 262 ±3 mL of the same test water. Seal the control container prior to the 72–hour duration.

7. At the end of the test period, measure and record the leachable chlorides in the test water per the IC manufacturer's operating instructions. The leachable chlorides in the test water shall not exceed one part per million (1 ppm).

8. Should leachable chlorides in the test water exceed 1 ppm, measure and record the leachable chlorides in the test water from the "control" container. The difference in leachable chlorides from the test water and "control" water sample shall not exceed 1 ppm.

8.1.5.1.2.1.2 Thermal Conductivity

1. The thermal conductivity test shall be performed using a heat flow meter (HFM) apparatus. The HFM establishes steady state unidirectional heat flux through a test specimen between two parallel plates at constant but different temperatures. By measurement of the plate temperatures and plate separation, Fourier's law of heat conduction is used by the HFM to automatically calculate thermal conductivity. Description of a typical HFM test method is provided in ASTM C518 [9]. The HFM shall be calibrated against a traceable reference specimen per the HFM manufacturer's operating instructions.

2. Three test samples shall be taken from the sample pour. Each test sample shall be of sufficient size to enable testing per the HFM manufacturer's operating instructions.

3. Place the test samples in a room (ambient) temperature environment (i.e., 65 °F to 85 °F) for sufficient time to thermally stabilize the test samples.

4. Measure and record the necessary test sample parameters as input data to the HFM apparatus per the HFM manufacturer's operating instructions.

5. Perform thermal conductivity testing and record the measured thermal conductivity for each test sample following the HFM manufacturer's operating instructions.

6. Determine and record the average thermal conductivity of the three test samples. The numerically averaged thermal conductivity of the three test samples shall be within the range between 0.24 and 0.36 (BTU–in)/(hr–ft^2–°F).

8.1.5.1.2.1.3 Specific Heat

1. The specific heat test shall be performed using a differential scanning calorimeter (DSC) apparatus. The DSC establishes a constant heating rate and measures the differential heat flow into both a test specimen and a reference specimen. Description of a typical DSC is provided in ASTM E1269 [10]. The DSC shall be calibrated against a traceable reference specimen per the DSC manufacturer's operating instructions.

2. Three test samples shall be taken from the sample pour. Each test sample shall be of sufficient size to enable testing per the DSC manufacturer's operating instructions.

3. Place the test samples in a room (ambient) temperature environment (i.e., 65 °F to 85 °F) for sufficient time to thermally stabilize the test samples.

4. Measure and record the necessary test sample parameters as input data to the DSC per the DSC manufacturer's operating instructions.

5. Perform specific heat testing and record the measured specific heat for each test sample following the DSC manufacturer's operating instructions.

6. Determine and record the average specific heat of the three test specimens. The numerically averaged specific heat of the three test samples shall be within the range between 0.28 and 0.42 Btu/lb$_m$–°F.

8.1.5.1.2.2 Physical Characteristics Determined for a Foam Batch

Polyurethane foam material physical characteristics for flame retardancy shall be determined once for a particular foam batch based on the batch definition in Section 8.1.5.1.1, *Introduction*

and General Requirements. If single or multiple components are to utilize a single foam batch, then additional flame retardancy testing, as defined below, need not be performed for each foam pour.

Polyurethane foam shall be tested for flame retardancy as follows:

1. Three test samples shall be taken from a pour from each foam batch. Each test sample shall be a rectangular prism with nominal dimensions of 0.5 inches thick, 3.0 inches wide, and a minimum length of 8.0 inches. In addition, individual sample lengths must not be less than the total burn length observed for the sample when tested.

2. Place the test samples in a room (ambient) temperature environment (i.e., 65 °F to 85 °F) for sufficient time to thermally stabilize the test samples. Measure and record the room temperature to an accuracy of ±2 °F.

3. Install an approximately 3/8–inch, or larger, Bunsen or Tirrill burner inside an enclosure of sufficient size to perform flame retardancy testing. Adjust the burner flame height to 1½ ±1/4 inch. Verify that the burner flame temperature is 1,550 °F, minimum.

4. Support the test sample with the long axis oriented vertically within the enclosure such that the test sample's bottom edge will be 3/4 ±1/8 inch (see adjacent figure) above the top edge of the burner.

5. Move the burner flame under the test sample for an elapsed time of 60 ±2 seconds. As illustrated, align the burner flame with the front edge of the test sample thickness and the center of the test sample width.

6. Immediately after removal of the test sample from the burner flame, measure and record the following data:

   a. Measure and record, to the nearest second, the elapsed time until flames from the test sample extinguish.

   b. Measure and record, to the nearest second, the elapsed time from the occurrence of drips, if any, until drips from the test sample extinguish.

   c. Measure and record, to the nearest 0.15 inch, the burn length following cessation of all visible burning and smoking.

7. Flame retardancy testing acceptance is based on the following criteria:

   a. The numerically averaged flame extinguishment time of the three test samples shall not exceed fifteen seconds.

   b. The numerically averaged flame extinguishment time of drips from the three test samples shall not exceed three seconds.

   c. The numerically averaged burn length of the three test samples shall not exceed 6.0 in.

8.1-8
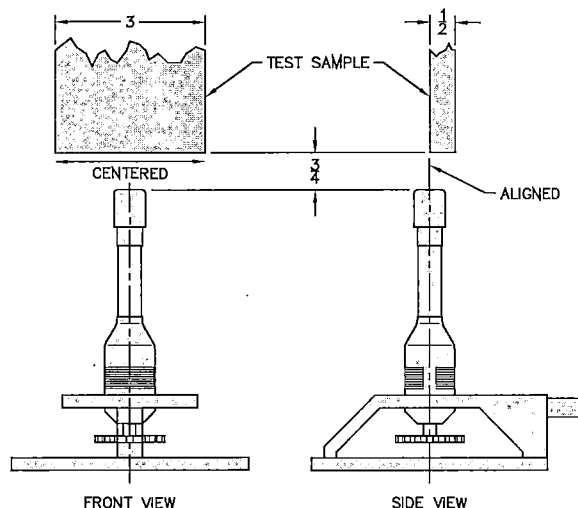
8.1.5.1.2.3 Physical Characteristics Determined for a Foam Pour

Polyurethane foam material physical characteristics for density and compressive stress shall be determined for each foam pour based on the pour definition in Section 8.1.5.1.1, *Introduction and General Requirements*.

8.1.5.1.2.3.1 Density

1. Three test samples shall be taken from the foam pour. Each test sample shall be a rectangular prism with minimum nominal dimensions of 1.0 inch thick (T) × 2.0 inch wide (W) × 2.0 inch long (L).

2. Place the test samples in a room (ambient) temperature environment (i.e., 65 °F to 85 °F) for sufficient time to thermally stabilize the test samples. Measure and record the room temperature to an accuracy of ±2 °F.

3. Measure and record the weight of each test sample to an accuracy of ±1 gram.

4. Measure and record the thickness, width, and length of each test sample to an accuracy of ±0.03 in.

5. Determine and record the room temperature density of each test sample utilizing the following formula:

$$\rho_{foam} = \frac{\text{Weight, g}}{453.6 \text{ g/lb}_m} \times \frac{1,728 \text{ in}^3/\text{ft}^3}{T \times W \times L, \text{ in}^3} \text{ , lb}_m/\text{ft}^3$$

6. Determine and record the average density of the three test samples. The numerically averaged density of the three test samples shall be within ±15% of the specified nominal foam density, i.e., within the range of 13.6 to 18.4 lb_m/ft^3 for a nominal 16 lb_m/ft^3 foam.

8.1.5.1.2.3.2 Compressive Stress

1. Test samples taken from each foam pour shall be tested according to ASTM D1621, *Standard Test Method for Compressive Properties of Rigid Cellular Plastics* [19]. The direction of compressive loading shall be parallel to the foam rise direction (for the perpendicular–to–rise direction, see below).

2. Determine and record the average parallel–to–rise compressive stress of the test samples from each batch pour for each foam density. As shown in Table 8.1-2, the average parallel–to–rise compressive stress for each foam pour shall be the nominal compressive stress ±15% at strains of 10%, 40%, and 70%.

3. Determine and record the average parallel–to–rise compressive stress of all test samples from each foamed component. As shown in Table 8.1-2, the average parallel–to–rise compressive stress for all foam pours used in a single foamed component shall be the nominal compressive stress ±10% at strains of 10%, 40%, and 70%.

4. Additional samples taken from each foam pour shall be tested according to ASTM D1621, *Standard Test Method for Compressive Properties of Rigid Cellular Plastics* [19]. The direction of compressive loading shall be perpendicular to the foam rise direction.

5. Determine and record the average perpendicular–to–rise compressive stress of the test samples from each batch pour for each foam density. As shown in Table 8.1-3, the average

perpendicular–to–rise compressive stress for each foam pour shall be the nominal compressive stress ±15% at strains of 10%, 40%, and 70%.

6. Determine and record the average perpendicular–to–rise compressive stress of all test samples from each foamed component. As shown in Table 8.1-3, the average perpendicular–to–rise compressive stress for all foam pours used in a single foamed component shall be the nominal compressive stress ±10% at strains of 10%, 40%, and 70%.

8.1.5.2 Butyl Rubber O-rings

Physical characteristics of the butyl rubber containment O-ring seals and sealing washers for the following parameters shall be determined for each lot based on the following acceptance tests. All material shall conform to the following ASTM D2000 [11] designation:

M4AA710 A13 B13 F17 F48 Z Trace Element.

8.1.5.2.1 Durometer

The durometer of each lot of the butyl rubber material shall be determined in accordance with ASTM D2240 [12]. Each lot of butyl rubber material shall have a hardness of 70 ±5 Shore A durometer (i.e., within the range of 65 to 75 Shore A durometer).

8.1.5.2.2 Tensile Strength and Elongation

The tensile strength of each lot of the butyl rubber material shall be determined in accordance with ASTM D412 [13]. Each lot of butyl rubber material shall have a minimum tensile strength of 10 MPa and a minimum elongation of 250%.

8.1.5.2.3 Heat Resistance

The heat resistance of each lot of the butyl rubber material shall be determined in accordance with ASTM D573 [14]. Each lot of butyl rubber material shall experience a maximum 10 Shore A durometer hardness increase, a maximum reduction in tensile strength of 25%, and a maximum reduction in ultimate elongation of 25%, when tested at 70 °C.

8.1.5.2.4 Compression Set

The compression set of each lot of the butyl rubber material shall be determined in accordance with Method B of ASTM D395 [15]. After 22 hours at 70 °C, each lot of butyl rubber material shall have a maximum compression set of 25%.

8.1.5.2.5 Cold Temperature Resistance

The cold temperature resistance of each lot of the butyl rubber material shall be determined in accordance with Method A, Section 9.3.2 of ASTM D2137 [16]. After 3 minutes at -40 °C, each lot of butyl rubber material shall be non–brittle.

8.1.5.2.6 Cold Temperature Resiliency

The cold temperature resiliency of each lot of the butyl rubber material shall be determined in accordance with the TR–10 test of ASTM D1329 [17]. Each lot of butyl rubber material shall be resilient at a test temperature of -50 °C or less.

8.1.6   Shielding Integrity Tests

8.1.6.1   Poured Lead Shielding

The poured lead shielding shall be tested to confirm its integrity. The shop test procedure shall include the following elements and requirements:

1. The test technique shall be a gamma scan using a hand held surface probe.
2. The gamma source shall be Co-60. Source strength shall be sufficient to provide a dose reading on the cask surface which is sufficiently above the background dose and is within the calibrated range of the measuring equipment.
3. The source strength shall be recorded at the time of the test.
4. The grid pattern shall be a maximum of four inches square.
5. The type of gamma sensor used for measurements shall be recorded. All equipment shall be calibrated per manufacturer's instructions.
6. The gamma scan test shall be performed according to a written procedure. The cask outer surface shall be marked with a grid which extends over the length of the side lead shield. A chart shall be made corresponding to the gridded surface, where each row of the table represents a circumferential ring of grid squares. The source shall be placed at one end of the cask cavity while the surface is scanned around its circumference. The source shall then be moved to the next axial grid position and the corresponding circumference scanned again. This sequence shall be repeated until the entire cask outer surface is scanned. The maximum dose rate from each grid square shall be recorded on the chart.
7. Acceptance criteria for each grid square will be established using the dose rate results of the analytical shielding model from Chapter 5, *Shielding Evaluation.* The analytical model will be revised to account for the presence of a test lid and test base shielding, but the poured lead thickness shall be the same as in Chapter 5. The model dose rate results shall be calibrated to the actual test source and detector characteristics using a calibration fixture. A computer model of the calibration fixture shall be created, and a ratio of the predicted dose rate to the measured dose rate of the fixture shall be used to adjust the analytical model dose rate results and create the acceptance criteria for the test measurements. Optionally, the un-collided gamma count may be used instead of the dose rate.

8.1.6.2   Plate or Sheet Lead Shielding

Plate or sheet lead is used in the lower end structure of the cask body and in the closure lid. Ultrasonic examination of each plate or sheet is performed prior to installation to ensure that no voids exist in excess of 10% of the lead plate or sheet thickness.

8.1.7   Thermal Tests

Tests to demonstrate the heat transfer capability of the packaging are not required because the thermal evaluations presented in Chapter 3, *Thermal Evaluation,* are based on well-established

heat transfer properties and methodologies and demonstrate relatively large thermal margins for all components. As such, the uncertainties in the predicted temperature levels are small. Further, since the thermal modeling incorporates several conservative assumptions, it is expected that the peak temperatures achieved will be less than predicted. See Chapter 3, *Thermal Evaluation,* for further discussions.

Table 8.1-1 – Weld Examinations

Component Weld	Weld Inspection
Containment	
Inner and outer shell longitudinal seams and inner shell to lower end structure	Radiograph (RT) per ASME B&PV Code, Subsection NB, Article NB-5000, and Section V, Article 2 [3] and liquid penetrant (PT) on final pass per ASME B&PV Code, Subsection NB, Article NB-5000, and Section V, Article 6 [4]
Inner shell to upper end structure	Ultrasonic (UT) per ASME B&PV Code, Subsection NB, Article NB-5000, and Section V, Article 4 [18] and liquid penetrant (PT) on final pass per ASME B&PV Code, Subsection NB, Article NB-5000, and Section V, Article 6 [4]
Vent port drill access hole plug in closure lid and lead pour access hole plugs in upper end structure	Liquid penetrant (PT) on final pass per ASME B&PV Code, Subsection NB, Article NB-5000, and Section V, Article 6 [4]
Non-containment	
Outer shell to upper and lower end structures	Ultrasonic (UT) per ASME B&PV Code, Subsection NB, Article NB-5000, and Section V, Article 4 [18] and liquid penetrant (PT) on final pass per ASME B&PV Code, Subsection NB, Article NB-5000, and Section V, Article 6 [4]
Bottom outer plate and lid outer plate	Liquid penetrant (PT) on final pass per ASME B&PV Code, Subsection NB, Article NB-5000, and Section V, Article 6 [4]
All other non-containment, except seal welds	Liquid penetrant (PT) on final pass per ASME B&PV Code, Subsection NF, Article NB-5000, and Section V, Article 6 [5]

Table 8.1-2 – Compressive Strength (psi) Parallel–to–Foam Rise at 65°F to 85°F

Strain	Minimum		Nominal	Maximum	
	Nom. −15%	Nom. −10%		Nom. +10%	Nom. +15%
10%	604	639	710	781	816
40%	733	776	862	948	991
70%	2,598	2,751	3,056	3,361	3,514

Table 8.1-3 – Compressive Strength (psi) Perpendicular–to–Foam Rise at 65°F to 85°F

Strain	Minimum		Nominal	Maximum	
	Nom. −15%	Nom. −10%		Nom. +10%	Nom. +15%
10%	579	613	681	749	783
40%	748	792	880	968	1,012
70%	2,642	2,798	3,108	3,418	3,574

8.2 Maintenance Program

This section describes the maintenance program used to ensure continued performance of the 380-B packaging.

8.2.1 Structural and Pressure Tests

No structural or pressure tests are necessary to ensure continued performance of the packaging.

8.2.2 Maintenance/Periodic Leakage Rate Tests

This section provides the generalized procedure for maintenance/periodic leakage rate testing of the containment boundary penetrations during routine maintenance, or at the time of seal replacement or sealing area repair. Maintenance leakage rate testing shall follow the guidelines of Section 7.4, *Maintenance Leakage Rate Test*, and Section 7.5, *Periodic Leakage Rate Test*, of [7].

Maintenance/periodic leakage rate testing shall be performed on the main O-ring seal and the vent port sealing washer in accordance with Section 8.2.2.1, *Helium Leakage Rate Testing the Containment O-ring Seal* and 8.2.2.2, *Helium Leakage Rate Testing the Vent Port Sealing Washer*. Each leakage rate test shall meet the acceptance criteria delineated in Section 8.1.4.1, *Fabrication Leakage Rate Test Acceptance Criteria.*

8.2.2.1 Helium Leakage Rate Testing the Containment O-ring Seal

1. The maintenance/periodic leakage rate test of the 380-B package containment O-ring seal integrity shall be performed following the guidelines of Section A.5.4, *Evacuated Envelope – Gas Detector*, of [7].

2. Assemble the 380-B package with the two O-ring seals installed in the closure lid. Tighten the closure lid bolts to 850 – 950 ft-lb torque (lubricated). Assembly is shown in Appendix 1.3.3, *Packaging General Arrangement Drawings*.

3. Attach a vacuum pump and a source of helium gas to the vent port.

4. Evacuate the cavity and provide a helium atmosphere inside the cavity by backfilling with helium gas to ambient pressure.

5. Install a clean (helium–free) port tool into the seal test port.

6. Attach a MSLD to the port tool.

7. Utilizing the port tool, rotate the seal test port to the open position.

8. Evacuate the cavity between the containment O-ring seal and the test O-ring seal until the vacuum is sufficient to operate the leak detector per the manufacturer's recommendations.

9. Perform the helium leakage rate test to the requirements of Section 8.1.4.1, *Fabrication Leakage Rate Test Acceptance Criteria*. If, after repeated attempts, the 380-B package containment O–ring seal fails to pass the leakage rate test, isolate the leak path and, prior to repairing the leak path and repeating the leak test, record on a nonconformance report and disposition prior to final acceptance in accordance with the cognizant quality assurance program.

10. Install the vent port and seal test port plugs, with their associated sealing washers, and tighten to 48 – 60 in-lb torque.

8.2.2.2 Helium Leakage Rate Testing the Vent Port Sealing Washer

1. The maintenance/periodic leakage rate test of the vent port plug sealing washer integrity shall be performed following the guidelines of Section A.5.4, *Evacuated Envelope – Gas Detector*, of [7]. If this test immediately follows the containment O-ring test of Section 8.2.2.1, *Helium Leakage Rate Testing the Containment O-ring Seal*, skip to step no. 4.

2. Assemble the 380-B package with the two O-ring seals installed in the closure lid. Tighten the closure lid bolts to 850 – 950 ft-lb torque (lubricated). Assembly is shown in Appendix 1.3.3, *Packaging General Arrangement Drawings*. Install the vent port and test port plugs, with their associated sealing washers, and tighten to 48 – 60 in-lb torque.

3. Verify the presence of a helium atmosphere below the vent port plug sealing washer, as specified above in Steps 3 – 4 of Section 8.2.2.1, *Helium Leakage Rate Testing the Containment O-ring Seal*.

4. Install a clean (helium-free) port tool into the vent port.

5. Attach a helium MSLD to the port tool.

6. Evacuate the cavity above the vent port plug sealing washer until the vacuum is sufficient to operate the leak detector per the manufacturer's recommendations.

7. Perform the helium leakage rate test to the requirements of Section 8.1.4.1, *Fabrication Leakage Rate Test Acceptance Criteria*. If, after repeated attempts, the vent port plug sealing washer fails to pass the leakage rate test, isolate the leak path and, prior to repairing the leak path and repeating the leak test, record on a nonconformance report and disposition prior to final acceptance in accordance with the cognizant quality assurance program.

8. At the conclusion of all leakage rate testing, install the vent port dust cover and seal test port dust cover.

8.2.3 Component and Material Tests

8.2.3.1 Fasteners

All threaded components shall be visually inspected before installation for deformed or stripped threads. Damaged threaded components shall be repaired or replaced prior to further use. The threaded components to be visually inspected include the closure lid bolts, vent port plug, the test port plug, the port covers, and the impact limiter attachment bolts.

Each closure lid bolt shall be replaced every 400 package service cycles consistent with the fatigue calculations in Section 2.1.2.3.2.1, *Normal Operating Cycles*, number *(6) Mechanical Loads*. A service cycle consists of two lid closure/bolt tightening operations.

8.2.3.2 Sealing Area Routine Inspection and Repair

Before each use and at the time of seal replacement, containment sealing surfaces shall be visually inspected for damage that could impair the sealing capabilities of the packaging. Perform visual surface finish inspections for the closure lid O-ring grooves, the mating sealing area on the cask body, and the surfaces that mate with the sealing washer in the vent port. Damage shall be repaired prior to further use (e.g., using emery cloth or other surface finishing

techniques) to restore the sealing surfaces to the value specified on the drawings in Appendix 1.3.3, *Packaging General Arrangement Drawings*.

Upon completion of any surface finish repairs, perform a leakage rate test per Section 8.2.2, *Maintenance/Periodic Leakage Rate Tests*.

8.2.3.3 Impact Limiter

Before each use, the impact limiters shall be inspected for tears or perforations in the stainless steel sheets, and for the presence of the fire–consumable plastic plugs. Any damage shall be repaired prior to further use.

8.2.3.4 Seals

The containment boundary O-ring seal and the vent port sealing washer shall be replaced within the 12–month period prior to shipment or when damaged (whichever is sooner), per the size and material requirements delineated on the drawings in Appendix 1.3.3, *Packaging General Arrangement Drawings*. Following seal replacement and prior to a loaded shipment, the new seals shall be leakage rate tested to the requirements of Section 8.2.2, *Maintenance/Periodic Leakage Rate Tests*.

8.2.4 Thermal Tests

No thermal tests are necessary to ensure continued performance of the 380-B packaging.

8.3 Appendix

8.3.1 References

1. Title 10, Code of Federal Regulations, Part 71 (10 CFR 71), *Packaging and Transportation of Radioactive Material*, 01–01–11 Edition.

2. ANSI/AWS D1.6/D1.6M:2007, *Structural Welding Code–Stainless Steel*, American Welding Society (AWS).

3. American Society of Mechanical Engineers (ASME) Boiler and Pressure Vessel Code, Section III, *Rules for Construction of Nuclear Facility Components*, Division 1 – Subsection NB, *Class 1 Components*, and Section V, *Nondestructive Examination*, Article 2, *Radiographic Examination*, 2010 Edition.

4. American Society of Mechanical Engineers (ASME) Boiler and Pressure Vessel Code, Section III, *Rules for Construction of Nuclear Facility Components*, Division 1 – Subsection NB, *Class 1 Components*, and Section V, *Nondestructive Examination*, Article 6, *Liquid Penetrant Examination*, 2010 Edition.

5. American Society of Mechanical Engineers (ASME) Boiler and Pressure Vessel Code, Section III, *Rules for Construction of Nuclear Facility Components*, Division 1 – Subsection NF, *Supports*, and Section V, *Nondestructive Examination*, Article 6, *Liquid Penetrant Examination*, 2010 Edition.

6. American Society of Mechanical Engineers (ASME) Boiler and Pressure Vessel Code, Section III, *Rules for Construction of Nuclear Facility Components*, Division 1 – Subsection NB, *Class 1 Components*, Article NB–6220, 2010 Edition.

7. ANSI N14.5–2014, *American National Standard for Radioactive Materials – Leakage Tests on Packages for Shipment*, American National Standards Institute (ANSI), Inc.

8. EPA Method 300.0, Revision 2.1 (October 1993), *Determination of Inorganic Anions by Ion Chromatography*, U.S. Environmental Protection Agency.

9. ASTM C518–10, *Standard Test Method for Steady–State Thermal Transmission Properties by Means of the Heat Flow Meter Apparatus*, American Society for Testing and Materials (ASTM).

10. ASTM E1269-11, *Standard Test Method for Determining Specific Heat Capacity by Differential Scanning Calorimetry*, American Society for Testing and Materials (ASTM).

11. ASTM D2000–12, *Standard Classification System for Rubber Products in Automotive Applications*, American Society for Testing and Materials (ASTM).

12. ASTM D2240–05 (2010), *Standard Test Method for Rubber Property – Durometer Hardness,* American Society for Testing and Materials (ASTM).

13. ASTM D412–06a (2013), *Standard Test Methods for Vulcanized Rubber and Thermoplastic Rubbers and Thermoplastic Elastomers – Tension,* American Society for Testing and Materials (ASTM).

14. ASTM D573–10, *Standard Test Method for Rubber – Deterioration in an Air Oven,* American Society for Testing and Materials (ASTM).

15. ASTM D395–14, *Standard Test Methods for Rubber Property – Compression Set,* American Society for Testing and Materials (ASTM).

16. ASTM D2137–11, *Standard Test Methods for Rubber Property – Brittleness Point of Flexible Polymers and Coated Fabrics,* American Society for Testing and Materials (ASTM).

17. ASTM D1329–08, *Standard Test Method for Evaluating Rubber Property – Retraction at Lower Temperatures (TR Test),* American Society for Testing and Materials (ASTM).

18. American Society of Mechanical Engineers (ASME) Boiler and Pressure Vessel Code, Section III, *Rules for Construction of Nuclear Facility Components,* Division 1 – Subsection NB, *Class 1 Components,* and Section V, *Nondestructive Examination,* Article 4, *Ultrasonic Examination Methods for Welds,* 2010 Edition.

19. ASTM D1621–16, *Standard Test Method for Compressive Properties of Rigid Cellular Plastics,* American Society for Testing and Materials (ASTM).